Investigations of Ternary Complexes Relevant to the Nuclear Fuel Cycle

A thesis submitted to The University of Manchester for the degree of Doctor of Philosophy in the Faculty of Engineering and Physical Sciences

2012

Tamara Lloyd Griffiths

School of Chemistry

Contents

Final Word Count: 60622

List of Tables

List of Figures

List of Symbols and Units

α	Alpha
β	Beta; used to denote the overall stability constant
δ	Chemical shift
ε	Extinction coefficient
γ	Gamma
λ	Wavelength
λ_{max}	Wavelength of maximum absorption
τ	Luminescence lifetime
^{o}C	degrees Celsius
%	Percentage
Å	Ångström
cm	centimetre
g	gram
K	Kelvin
kg	kilogram
M	mol dm^{-3}
m	metre
MBq	MegaBecquerel
MHz	MegaHertz
mL	milliLitre
mM	milliMolar
mm	millimetre
ms	millisecond
mV	milliVolt
nm	nanometre
ns	nanosecond
ppm	Parts per million
μm	micrometre
MΩ	Megaohm

1D	One-dimensional

List of Abbreviations

AHA	Acetohydroxamic acid
An	Actinide
AnO_2^{n+}	Actinyl unit
aq	aqueous
a.u.	arbituary units
CCD	Charge Coupled Device
cf.	*confer*, Latin: "compare"
CMPO	Octyl(phenyl)-N, N-dibutyl carbamoylmethyl phosphine oxide
CO_3^{2-}	Carbonate ion
DIAMEX	DIAMide Extraction
DMDOHEMA	*N, N*-dimethyl-*N, N*-dioctylhexylethoxymalonamide
$DO3A^{3-}$	1, 4, 7, 10- tetraazacyclododecane-1,4,7- triacetate
DSS	3-(trimethylsilyl)-1-propanesulfonic acid
$DTPA^{5-}$	Diethylenetriamine pentaacetate
E	Energy
EARP	Enhanced Actinide Removal Plant
$EDTA^{4-}$	Ethylenediamine tetraacetate
e.g.	*exempli gratia*, Latin: "for example"
E_h	Redox
EMF	Electromotive force
et al.	*et alii*, Latin: "and others"
EXAFS	Extended X-Ray Absorption Fine Structure
FA	Fulvic Acid
GANEX	Group ActiNide Extraction
GHGs	Green House Gases
H_3DO3A	1, 4, 7, 10- tetraazacyclododecane-1,4,7- triacetic acid
H_5DTPA	Diethylenetriamine pentaacetic acid

HA	Humic acid
HDEHP	Di(2-ethylhexyl) phosphoric acid
HEDTA	N-(-hydroxyethyl)ethylenedinitrilotriacetic acid
H_4EDTA	Ethylenediamine tetraacetic acid
HS	Humic substances
HWR	Heavy Water Reactor
I	Ionic strength
ICP-AES	Inductively Coupled Plasma-Atomic Emission Spectroscopy
IDA	Iminodiacetic acid
i.e.	*id est*, Latin: "that is"
J	Total angular momentum
K	Equilibrium constant
K_a	Acid dissociation constant
K_{sp}	Solubility product
K_w	Self ionisation of water constant
L	Orbital quantum number
log	logarithm
Ln	Lanthanide
LWCC	Liquid Waveguide Capillary Cell
LWR	Light Water Reactor
MCP	Micro Channel Plate
MRP	Magnox Reprocessing Plant
MSDF	Magnox Storage and Decanning Facility
MW	Molecular weight
N_{H_2O}	Number of water molecules
NMR	Nuclear Magnetic Resonance
NO_3^-	Nitrate ion
NOM	Natural Organic Matter
Non-HS	Non-humic substances
NpO_2^{n+}	Neptunyl
NTA	Nitrilotriacetic acid

OH^-	Hydroxide ion
OTf	Trifluoromethanesulfonate
Ph_2acac	Diphenylacetylacetate
Phgly	Phenylglyoxalate
PuO_2^{n+}	Plutonyl
PUREX	Plutonium URanium Extraction
pzc	Point of zero charge
S	Spin quantum number
SNF	Spent Nuclear Fuel
TALSPEAK	Trivalent Actinide-Lanthanide Separation by Phosphorus Reagent Extraction from Aqueous Komplexes
TBP	Tributyl phosphate
Tpen	N, N, N', N'-tetrakis(2-pyridyl-methyl)ethylenediamine
TRLIFS	Time Resolved Laser Induced Fluorescence Spectroscopy
TRUEX	TRans-URanic Extraction
U.K.	United Kingdom
UNEX	UNiversal Extraction
UO_2^{n+}	Uranyl
UREX	URanium Extraction
UV-Vis	Ultraviolet-Visible
XRD	X-ray diffraction
V^o	Initial volume
vs.	*versus*, Latin: "against"
VT	Variable Temperature
YAG	Yttrium Aluminium Garnet

The University of Manchester
Tamara Lloyd Griffiths
Doctor of Philosophy
Investigations of Ternary Complexes Relevant to the Nuclear Fuel Cycle
2011

Understanding the behaviour of actinide species is of importance when removing and processing all nuclear waste. Examples include the safe clean-up of contaminated waste ponds and aspects of the TALSPEAK (Trivalent Actinide-Lanthanide Separation by Phosphorus Reagent Extraction from Aqueous Komplexes) process.

The chemistry of the ponds and the TALSPEAK process has been studied by probing the aqueous solution behaviour of Ln^{III}, Am^{III}, Cm^{III} and Th^{IV} ions in the presence of organic ($EDTA^{4-}$ (ethylenediamine tetraacetate), $DTPA^{5-}$ (diethylenetriamine pentaacetate) and lactate) and inorganic (CO_3^{2-} (carbonate) and OH^- (hydroxide)) ligands by a variety of techniques including Nuclear Magnetic Resonance (NMR), Ultra Violet-Visible (UV-Vis) and luminescence spectroscopies, as well as potentiometry.

Various ternary complexes have been shown to exist, including $[M(EDTA)(CO_3)]^{3-}_{(aq)}$, (where M = Ln^{III}, Am^{III} or Cm^{III}) and $[Th(EDTA)(CO_3)_2]^{4-}_{(aq)}$, which form approximately over the pH range 8 to 11, and also $[M(EDTA)(lactate)]^{2-}_{(aq)}$ (where M = Ln^{III} or Am^{III}) and $[Th(EDTA)(lactate)]^{-}_{(aq),}$ which predominantly occur over the pH range 4 to 6. The nature of lactate interaction with $[M(DTPA)]^{2-}_{(aq)}$ complexes (where M = Ln^{III} or Am^{III}) is unclear, as it may be possible that lactate can coordinate directly to the metal ion or to the acetate groups of $DTPA^{5-}$ (*via* a H-bonding interaction).

The knowledge gained in this research has given a deeper insight into the nature of lanthanide and actinide coordination chemistry in mixed-ligand environments. For example, the increasing solubility of actinide metal ions in the contaminated waste ponds is probably due to the ability of organic ligands present in the ponds to solubilise metal ions at high pH, and also under TALSPEAK conditions of pH 3.5, there is likely to be minimal interaction of lactate with the $[Ln(DTPA)]^{2-}_{(aq)}$ complexes.

The determination of metal ion speciation using a combination of NMR, UV-Vis and luminescence spectroscopies, coupled with potentiometry, could be applied to new characterisation challenges faced in the future of the nuclear industry.

Declaration

No portion of the work referred to in this thesis has been submitted in support of an application for another degree or qualification of this or any other university or other institute of learning.

Copyright Statement

i. The author of this thesis (including any appendices and/or schedules to this thesis) owns certain copyright or related rights in it (the "Copyright") and s/he has given The University of Manchester certain rights to use such Copyright, including for administrative purposes.

ii. Copies of this thesis, either in full or in extracts and whether in hard or electronic copy, may be made only in accordance with the Copyright, Designs and Patents Act 1988 (as amended) and regulations issued under it or, where appropriate, in accordance with licensing agreements which the University has from time to time. This page must form part of any such copies made.

iii. The ownership of certain Copyright, patents, designs, trade marks and other intellectual property (the "Intellectual Property") and any reproductions of copyright works in the thesis, for example graphs and tables ("Reproductions"), which may be described in this thesis, may not be owned by the author and may be owned by third parties. Such Intellectual Property and Reproductions cannot and must not be made available for use without the prior written permission of the owner(s) of the relevant Intellectual Property and/or Reproductions.

iv. Further information on the conditions under which disclosure, publication and commercialisation of this thesis, the Copyright and any Intellectual Property and/or Reproductions described in it may take place is available in the University IP Policy (see: http://documents.manchester.ac.uk/DocuInfo.aspx?DocID=487), in any relevant Thesis restriction declarations deposited in the University Library, The University Library's regulations (see: http://www.manchester.ac.uk/library/aboutus/regulations) and in The University's policy on Presentation of Theses.

Acknowledgements

I would like to thank my supervisor, Dr. Clint Sharrad, for all of his help, guidance and enthusiasm over the past three years. Also, thank you for sending me to some very interesting and exciting places (Idaho, San Francisco and Anaheim), and for throwing some tasty BBQ's!

Thank you very much to Dr. Leigh Martin for all of his support working whilst working at Idaho National Laboratory (INL). Thank you to you and your lovely wife, Marie, for making my time in the US wonderful! Thank you to other workers in the lab at INL, including Peter (Yoda), Rocky, Dean, Bruce, Steve and Chris for many fascinating conversations. Thank you to the Van Sickle family for allowing me to stop in their lovely home, and introducing me to lots of 'firsts', such as snow mobiling and cross-country skiing.

Thank you to staff at Manchester University for lots of help along the way: Dr. Louise Natrajan, Dr. Adam Swinburne, Dr. Nick Bryan, Prof. Francis Livens and Prof. Simon Pimblott. Thank you very much to Dr. Mark Sarsfield, Dr. Robin Taylor, Dr. Charles Potter, John Rawcliffe and Glen Charlesworth for a successful Sellafield placement at National Nuclear Laboratory (NNL).

Thank you to all of the Manchester University Radiochemistry Group (past and present) for jolly times! Thank you to Ryan (Mavis) and Carlos (C-dog) for being part of so many fun memories in the laboratory. The Friday Pints crew (best part of the week), including Sean, Simon, Jen Jen, Maddie, Mark (Team Humic), Alex, James, Louise, Greg, Tom, Nigel and Dan. Everyone else around the office (Rich, Rick, Chris, Dave, Steph, Katie, Lucy, Kate, Kurt, Raj) for making radiochemistry a great place to work. Not to forget Bina (Mint) Hotchip and Ric Hart for merry undergraduate times.

Thank you to the lovely Rebecca, Joanne, Katie, Deborah and Kayleigh for fun lunch times at Sellafield.

Thank you to all past housemates for all the good times and glinners! ‘Gleeful’ thanks to Lizzie Boreham, Jessie Fairfield, Emily Crompton, Hannah Sevenoaks and Caroline Topham.

Thank you to my wonderful and amazing family for being so supportive and understanding over the years, but especially 2011. Special thanks to Mum, Dad, Natalie, Giovanni, Auntie Pauline, Uncle Ray, Plug, and the late Joan and Percy Griffiths for being *smashing*!!
Thank you to the Nuclear Decommissioning Authority, the University of Manchester Alumni Fund, the Dalton Nuclear Institute and the Fuel Cycle Research and Development initiative (part of the United States Department of Energy) for providing the generous funding that has made all of the research possible.

And last but not least, thank you to Sean Woodall for putting up with me! Thank you for everything… from reading my thesis to carrying the heavy shopping, but most of all for putting a smile on my face! The last two years have been the best two years. I hope there’s many more in the future!

Chapter 1

Introduction

1.1 Nuclear Fuel Cycle Background

1.1.1 Energy Production

Fossil fuels have been the prime source of energy production for over 200 years.[1] Coal, oil and natural gas provide society with the ability of electricity generation, heat production and fuel for transport.[1] In 2007, 81.6 % of the world's energy supply came from fossil fuels.[1] A high dependence on fossil fuels is not sustainable because of decreasing amounts of resources and the critical effects of global warming.[1]

The four main Green House Gases (GHGs) present in the atmosphere are water vapour (H_2O), carbon dioxide (CO_2), methane (CH_4) and nitrous oxide (N_2O).[1] At normal concentrations, GHGs allow the average temperature of the earth to be moderated to 15 ^oC.[1] However, mean elevated GHG concentrations have caused the average temperature of the earth to increase to 17 ^oC.[1] This temperature increase contributes to detrimental effects on the environment such as Antarctic glaciers melting and CO_2 release from oceans.[1] The amount of CO_2 emitted into the environment must be reduced, and a change of focus to 'clean' energy production rather than 'dirty' energy production.[1]

Nuclear energy production is considered to be a 'clean' energy supply.[1] It is predicted that if nuclear methods were the prime source of energy supply for the next 50 years, then the earth's CO_2 levels could be halved.[1] However, there are many issues concerned with nuclear power such as, exhaustion of uranium reserves, management of spent nuclear fuel and nuclear proliferation.[1]

1.1.2 The Nuclear Fuel Cycle

The nuclear fuel cycle begins with the mining of uranium (U) from ores. On average, one tonne of rock and soil on the earth's surface contains 1 to 5 g of uranium.[2] Natural uranium

ore consists of two isotopes: ^{235}U and ^{238}U.[2] Natural uranium contains only 0.7 % of the fissile isotope ^{235}U, but ^{238}U can be used for breeding fissile plutonium (Pu; *i.e.* ^{239}Pu and ^{241}Pu).[2]

After uranium ore has been mined, it is crushed and dissolved in acidic or alkaline solution. The resulting solid is a uranium ore precipitate called 'yellowcake' (U_3O_8).[2]

The U_3O_8 must be converted into gaseous uranium hexafluoride (UF_6) in order for enrichment to occur.[2] This is the process that increases the concentration of ^{235}U. The first step of UF_6 production is the reduction of U_3O_8 to uranium dioxide (UO_2).[2] The UO_2 is reacted with hydrogen fluoride (HF) to form uranium tetrafluoride (UF_4), which is subsequently reacted with fluorine gas (F_2) to form UF_6.[2]

In order to sustain a nuclear chain reaction in a nuclear reactor, the concentration of ^{235}U must be increased from 0.7 % to approximately 3 %.[2] This can be achieved by utilising techniques that will separate ^{235}U and ^{238}U on the basis of mass. Gaseous diffusion, gas centrifugation and preferential ionisation of one U isotope using a laser are all methods of enrichment.[2] Following enrichment, UF_6 is converted to UO_2.[2]

The UO_2 produced must be fabricated into a form suitable for nuclear reactor fuel, such as enriched UO_2 or mixed UO_2 and plutonium dioxide (PuO_2) fuel pellets.[2] The pellets are stacked and encased in an alloy, which has low neutron absorption, such as zirconium (Zr). This takes the form of a fuel rod, and one hundred of these fuel rods are grouped together to create a fuel bundle.[2]

Inside a nuclear reactor the fuel rods are irradiated. A controlled nuclear chain reaction is maintained by the use of neutron moderator material, which converts the fast neutrons released from nuclear fission into slow neutrons.[2] Control rods are also used to control the rate of nuclear fission.[2] The heat released from nuclear fission is used to produce steam, which can be used to drive turbines and power electrical generators.[2]

Following neutron irradiation, the fuel is called spent nuclear fuel (SNF).[2] SNF typically consists of 95 % ^{238}U, 1 % ^{235}U, 1-2 % Pu isotopes, 2-3 % radioactive fission products and less than 0.1 % of other trans-uranic elements.[2] There are two routes for SNF: 1) reprocessing or 2) waste disposal.[2] Nuclear reprocessing has many advantages including the re-use of fissile material as fuel and reducing both the volume and radiotoxicity of nuclear waste. Before nuclear waste is to be disposed of in a nuclear waste repository, it can be vitrified, covered in concrete or metal and stored in ponds to allow short-lived isotopes to decay. These

will further reduce the risk of radiotoxicity from nuclear waste emanating into the open environent.[2]

1.1.3 Magnox Nuclear Reactors

The Sellafield site is the United Kingdom's (U.K.'s) largest nuclear site.[3] It covers two square miles and contains over 1000 buildings.[4] Sellafield used to be an electricity generating site, but the primary focus is now SNF reprocessing.[3]

In the 1950's, the first generation of nuclear reactors were built at Sellafield.[5] They were known as magnox reactors.[5] The term 'magnox' comes from the magnesium alloy cladding used to surround the nuclear fuel, and means magnesium non-oxidising.[5] Initially, the main purpose of the reactors was to produce weapons-grade plutonium for use by the Ministry of Defence.[6] The plutonium was generated by irradiating uranium, which released large amounts of heat.[6] This later became important for producing power for civilians, and the magnox reactors were the first in the world to produce nuclear power commercially.[7]

There are three types of nuclear reactor known as light water reactor (LWR), heavy water reactor (HWR) and gas-graphite reactor.[8] They are classified on the basis of the materials used in their construction, which includes the fuel, the coolant material and the moderator material.[8] The fuel used inside the magnox reactors was in the form of a rod (Figure 1.1).[9] As previously stated, the magnox nuclear reactors were initially used to produce Pu,[6] and so the fuel rods consisted of a natural uranium (^{235}U and ^{238}U) core encased by a magnesium-aluminium (Mg-Al) alloy cladding.[8] The rods measured approximately 1 m long with a 5 cm diameter and weighed 10-12 kg.[10] The coolant used for magnox reactors was carbon dioxide/helium (CO_2/He), and its purpose was to transfer heat away from the core, preventing the melting of core materials.[8] Graphite was used as a moderator in magnox reactors, which controlled the energy of the neutrons inside the core.[8]

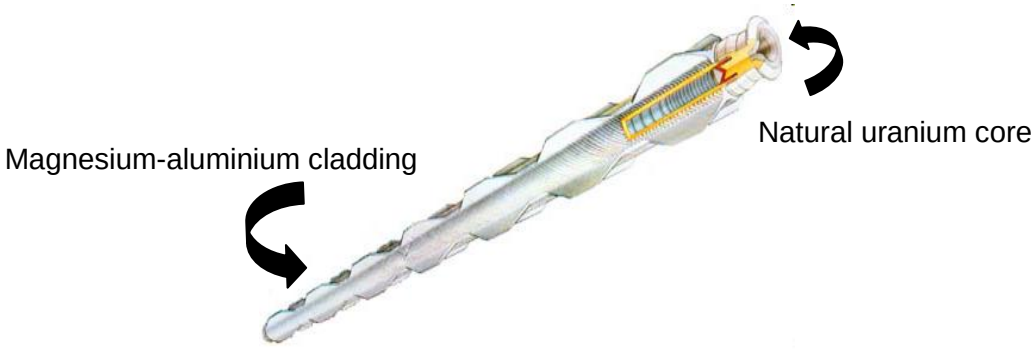

Figure 1.1: Magnox fuel rod. [Taken from Reference 9].

The advantages of using magnox cladding were that it had a low neutron capture cross section, which could minimise irradiation,[5] and that it also could contain the fission material.[5] However, the disadvantages of using magnox cladding were that it had temperature limits and that it reacted readily with water. The temperature limit restricted the thermal efficiency of the plant, and the magnox reaction with water meant that corrosion of the cladding would occur during long-term storage.[9]

1.1.4 Magnox Waste Storage Ponds

After the magnox fuel elements had been irradiated, they were stored in painted steel skips that were put in specially constructed concrete, open air, water ponds.[5,11] Built in the mid 1950s, these ponds formed part of the Magnox Storage and Decanning Facility (MSDF).[12] For almost 30 years, the facility stored and de-clad spent magnox fuel before it was reprocessed elsewhere on the Sellafield site.[12]

Magnox reacts readily in water, therefore the ponds were dosed with sodium hydroxide (NaOH) to keep the pond pH in the alkaline region of approximately pH 11.4.[13] The alkaline pH also meant that magnesium was present as magnesium hydroxide ($Mg(OH)_2$), which formed a protective layer on the cladding surface to reduce magnox corrosion.[13] Magnox was susceptible to corrosion by anions, which would react and attack crevices in the magnox surface area. Therefore, there was a maximum anion level of 1 g m^{-3} of chloride, sulphate and citrate in the ponds.[11] These precautions meant that the spent fuel rods could be stored at

environmental temperatures for a maximum of five years, without the risk of causing a significant increase in corrosion rate.[13]

In 1974, an increased throughput of spent magnox fuel and a shutdown of the Magnox Reprocessing Plant (MRP) meant that the magnox fuel was stored longer than the recommended five year period in the waste ponds and the pH was not maintained at approximately pH 11.4.[12] Consequently, the magnox cladding corroded and the SNF within the rods leaked out into the ponds, which caused radioactive contamination and poor underwater visibility.[14] The ponds are 100 m long, 25 m wide and 7 m deep containing 14 million litres of water and 183 skips.[14] It is thought that there is up to 12000 m^3 of contaminated pond and sludge material in the U.K.[5] The sludge is described as a slurry at the bottom of the ponds consisting of various sized particles,[5] which includes magnesium hydroxide (brucite) and radioactive elements.[5]

1.1.5 Magnox Waste Storage Pond Species

The safe clean-up of the contaminated magnox waste storage ponds is a major issue for the U.K. It is of prime importance to retrieve the radionuclides and process them into a form suitable for storage and disposal.

Before the clean-up operation can begin, understanding the chemistry of radionuclides found in the ponds is vital. It is also important to know how the radionuclides may behave during the retrieval process, if the conditions change. Furthermore, information must be gained on the distribution of metal ion species in the solid, solution and colloidal phases.[5]

Metal ion species present in the ponds include uranium (U), plutonium (Pu), neptunium (Np), americium (Am), technetium (Tc), caesium (Cs) and strontium (Sr). The caesium and strontium present in the ponds are products of fission processes.[15] Plutonium-239, americium-241 and neptunium-237 are considered to be the radionuclides of concern in the ponds.[15] This is because of hazards associated to human health if these actinides are released into the environment.[16] Plutonium-239 is one of the most toxic substances to organisms, and it also has a long half life of 24110 years.[16] There is uncertainty in the true extent of toxicity ^{239}Pu has in the environment. What is known is that work undertaken at Sellafield has caused extensive radioactive pollution. For example, Sellafield is a major contributor to Europe's

collective radiation dose by the discharge of radionuclides into the Irish Sea.[17] Neptunium-237 is also a concern for the environment as it has a very long half life of 2.14 million years.[18] Its concentration in the ponds will continue to increase as it is produced from ^{241}Am decay,[18] which is also a highly radiotoxic element with a half-life of 432 years.[19] The isotopes of ^{239}Pu, ^{237}Np and ^{241}Am are biologically toxic on entrance into the blood stream as they can deposit in the liver and skeleton, and will eventually promote cancerous cell formation.[16]

The chemistry of the metal ion species in the waste ponds is uncertain. This is due to there being many influencing factors, as the ponds are open to the environment (Figure 1.2).[15] At the pond pH of 11.4, CO_2 is able to dissolve into the ponds, which forms carbonate (CO_3^{2-}) anions.[15] This means that carbonate and hydroxide (from NaOH dosing) are considered to be key inorganic complexants of the metal ions. Plant and animal matter are able to deposit in the ponds.[15] The products of organic matter decomposition such as humic acids, fulvic acids and citrate can complex with metal ions.[15] Brucite is a mineral deposit produced from the corrosion of magnox rods.[15] It has formed a sediment sludge at the bottom of the waste ponds, in which metal ions are able to adsorb. Therefore, knowledge must be gained on the chemistry of metal ions with carbonate, hydroxide, organics and mineral surfaces.[15]

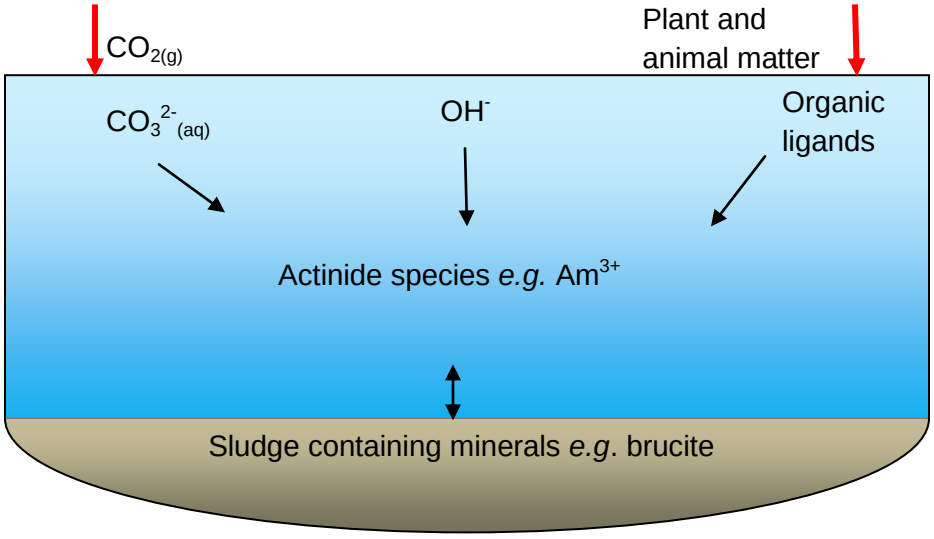

Figure 1.2: Schematic diagram of the nuclear waste storage ponds

1.1.6 The Pond Problem

An assessment of the ponds concluded that most of the actinides in the ponds are likely to be adsorbed to the brucite sludge.[15] However, it has been found that there are more soluble actinide species than expected for the pH, carbonate and oxygen concentrations, plus the probability of adsorption to brucite.[15] It has been hypothesised that the formation of actinide mixed hydroxy-carbonate or mixed organic-inorganic complexes could be increasing the amount of soluble actinide species, rather than the independent formation of pure actinide hydroxide or pure actinide carbonate species.[15]

1.1.7 Nuclear Reprocessing

The reprocessing of SNF is subject to much debate because of the high costs and political controversy. However, advantages of reprocessing include reducing the radiotoxicity of nuclear waste and the recycling of U and Pu back into the fuel cycle.[20] Around 30 % of all SNF produced worldwide has been reprocessed to recover U and Pu.[21] Summarised below are some of the most commonly used solvent extraction techniques that are used to recover U and Pu from SNF.

There are many different technologies that are used to extract radionuclides from nuclear waste but the PUREX process (Plutonium URanium EXtraction) is the most established.[22] This solvent extraction technique uses 30 % tributyl phosphate (TBP) in kerosene to selectively extract hexavalent U and tetravalent Pu from the acidic, aqueous nuclear waste.[22] Trivalent metals, such as Am and Cm, and pentavalent Np remain in the aqueous phase but they can be extracted by other separation techniques.[22]

UREX (URanium EXtraction) is a modified version of the PUREX process and involves the extraction of U and Tc from the nitric acid solution of the dissolved fuel.[23] Acetohydroxamic acid (AHA) is added to nuclear waste, which reduces both Np and Pu and forms hydrophilic complexes. These hydrophilic complexes remain in the aqueous phase, whilst U can be extracted into the organic phase by TBP.[24]

The main contributor of alpha (α) activity in nuclear waste is ^{241}Am, therefore it is of interest to remove it before waste disposal. The TRUEX process (TRans-URanic EXtraction), which

involves the addition of octyl(phenyl)-N, N-dibutyl carbamoylmethyl phosphine oxide (CMPO) in PUREX process solvent (TBP in kerosene), is successful at extracting trivalent lanthanides and actinides.[25] An alternative process for the removal of trivalent actinides and lanthanides from the high acidity PUREX raffinate is the DIAMEX process (DIAMide EXtraction).[26] This process uses a combustible diamide as an extractant.[26]

The UNEX process (UNiversal EXtraction) has the ability to simultaneously extract caesium, strontium and actinides from acidic nuclear waste solutions.[27] The process consists of chlorinated cobalt dicarbollide for ^{137}Cs extraction, polyethylene glycol for ^{90}Sr extraction and CMPO for lanthanide and actinide extraction.[27] The organic phase used is a non-nitro aromatic polar solvent containing phenyltrifluoromethyl sulfone.[27]

1.1.8 The TALSPEAK Process

One of the most challenging features of nuclear waste extraction methods is the separation of trivalent actinides from fission product lanthanide ions.[28] It is necessary to separate trivalent actinides from lanthanides for the strategy of transmutation, which involves irradiating highly radioactive actinide ions with neutrons to convert them into fission products with a much shorter half-life, thus reducing the radiotoxicity of nuclear waste.[28] The lanthanide ions have a larger neutron cross-section and are present in nuclear waste in a 100 fold excess compared to the actinide ions. The lanthanide ions effectively compete with the actinide ions for the neutrons therefore, it is advantageous to separate the trivalent actinides from the trivalent lanthanide ions.[28] The TALSPEAK Process (Trivalent Actinide-Lanthanide Separation by Phosphorus Reagent Extraction from Aqueous Komplexes) retains trivalent actinides in an aqueous phase containing H_5DTPA (diethylenetriamine pentaacetic acid; Figure 1.3) and lactic acid, whilst the trivalent lanthanides are exctracted into an organic phase containing HDEHP (di(2-ethylhexyl) phosphoric acid; Figure 1.4). The process may work by relying on the difference in the 'hardness' (*i.e.* hard = high charge density) of the lanthanide and actinide cations.[28] Actinide ions are 'softer' than lanthanides and so will have a stronger interaction with ligands containing 'softer' donor groups like nitrogen. H_5DTPA contains nitrogen and oxygen donor groups, which form stronger complexes with the 'softer' actinide ions

compared to the 'harder' lanthanide ions, and may be responsible for retaining the actinides in the aqueous phase.[28]

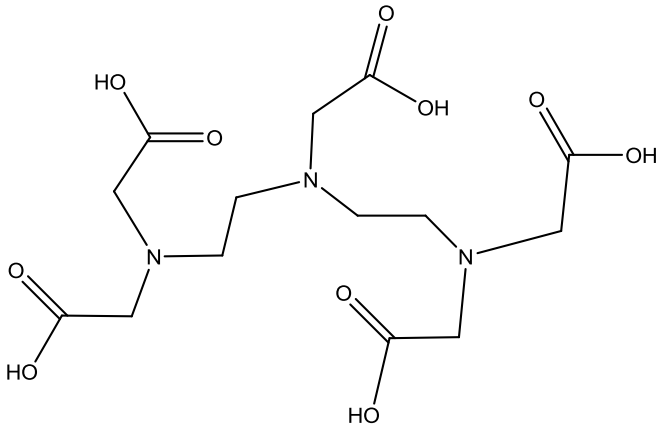

Figure 1.3: Structure of H_5DTPA.

The lanthanides are oxophillic and have a stronger interaction with ligands just containing oxygen donor atoms compared to the actinide ions.[28] Three HDEHP ligands chelate to each lanthanide ion in the organic phase causing three H^+ ions to transfer into the aqueous phase.[28]

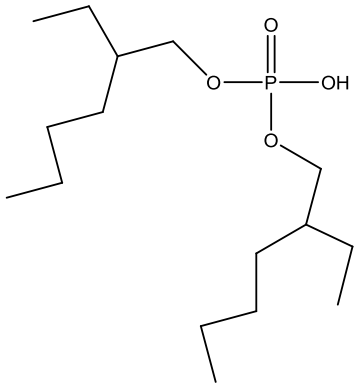

Figure 1.4: Structure of HDEHP.

Lactate (Figure 1.5) is present at high concentrations in the TALSPEAK process and operates as a method of controlling pH.[28] As H^+ ions are transferred into the aqueous phase when HDEHP complexes to Ln ions, lactate is used to buffer the pH in the aqueous phase to pH 3.5.[28] This maintains the efficiency of the TALSPEAK process.[28]

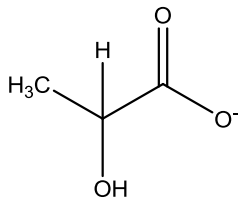

Figure 1.5: Structure of lactate.

1.1.9 Understanding TALSPEAK-The Role of Lactate

The chemistry behind the TALSPEAK process is complicated, and only the behaviour of $DTPA^{5-}$ is understood.[29] The $DTPA^{5-}$ ligand is octadentate and forms 1:1 complexes with actinide ions.[28] Lactate is a weakly coordinating ligand, and its presence in high concentrations in the TALSPEAK process may mean that it is competing with HDEHP and $DTPA^{5-}$ as a complexing ligand.[28] It is possible that the role of lactate in the TALSPEAK process is more complicated than just acting as a pH buffer, as its presence also improves metal extraction kinetics, increases both H_5DTPA solubility and radiation stability and also increases the separation factors of the lanthanides and actinides.[28,29] It is still uncertain exactly how lactate enhances the process, but a lactate containing complex has been postulated to be formed in the TALSPEAK process, such as $[M(DTPA)(lactate)]^{3-}$ (Figure 1.6; where M is a trivalent actinide).[28] It is thought that the formation of these aqueous ternary complexes may be enhancing the TALSPEAK process, but there is no evidence in the literature of their existence.[28]

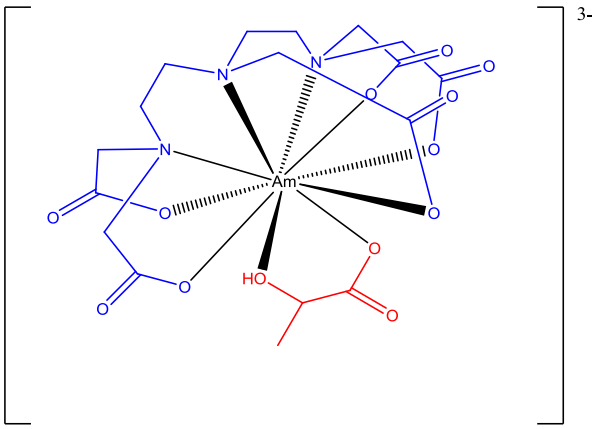

Figure 1.6: Suggestion for the structure of the $[Am(DTPA)(lactate)]^{3-}_{(aq)}$ ternary complex.

1.2 The *f* Elements

1.2.1 Lanthanides and Actinides

The *f* elements comprise of the lanthanide and actinide series. The lanthanides are the elements from cerium (Ce, A_n=58) to lutetium (Lu, A_n=71), and the actinides are the elements from thorium (Th, A_n=90) to lawrencium (Lr, A_n=103).[30] When discussing the lanthanide and the actinide series, the shorthand 'Ln' or 'An' is often used to refer to all of the lanthanides and actinides, respectively.[30] The outer sphere electrons in the lanthanide series accommodate the 4*f* orbitals, whilst those of the actinide series occupy the 5*f* orbitals.[30] As the lanthanide and actinides increase in atomic number, there is a gradual filling of the 4*f* and 5*f* orbitals, respectively (Tables 1.1 and 1.2).[30]

Element	Symbol	Atomic Number	Electronic Configuration
Cerium	Ce	58	$[Xe]4f^1 5d^1 6s^2$
Praseodymium	Pr	59	$[Xe]4f^3 6s^2$
Neodymium	Nd	60	$[Xe]4f^4 6s^2$
Promethium	Pm	61	$[Xe]4f^5 6s^2$
Samarium	Sm	62	$[Xe]4f^6 6s^2$
Europium	Eu	63	$[Xe]4f^7 6s^2$
Gadolinium	Gd	64	$[Xe]4f^7 5d^1 6s^2$
Terbium	Tb	65	$[Xe]4f^9 6s^2$
Dysprosium	Dy	66	$[Xe]4f^{10} 6s^2$
Holmium	Ho	67	$[Xe]4f^{11} 6s^2$
Erbium	Er	68	$[Xe]4f^{12} 6s^2$
Thulium	Tm	69	$[Xe]4f^{13} 6s^2$
Ytterbium	Yb	70	$[Xe]4f^{14} 6s^2$
Lutetium	Lu	71	$[Xe]4f^{14} 5d^1 6s^2$

Table 1.1: Ground state electronic configuration of the lanthanides.[30]

Element	Symbol	Atomic Number	Electronic Configuration
Thorium	Th	90	$[Rn]6d^2 7s^2$
Protactinium	Pa	91	$[Rn]5f^2 6d^1 7s^2$
Uranium	U	92	$[Rn]5f^3 6d^1 7s^2$
Neptunium	Np	93	$[Rn]5f^4 6d^1 7s^2$
Plutonium	Pu	94	$[Rn]5f^6 7s^2$
Americium	Am	95	$[Rn]5f^7 7s^2$
Curium	Cm	96	$[Rn]5f^7 6d^1 7s^2$
Berkelium	Bk	97	$[Rn]5f^9 7s^2$
Californium	Cf	98	$[Rn]5f^{10} 7s^2$
Einsteinium	Es	99	$[Rn]5f^{11} 7s^2$
Fermium	Fm	100	$[Rn]5f^{12} 7s^2$
Mendelevium	Md	101	$[Rn]5f^{13} 7s^2$
Nobelium	No	102	$[Rn]5f^{14} 7s^2$
Lawrencium	Lr	103	$[Rn]5f^{14} 6d^1 7s^2$

Table 1.2: Ground state electronic configuration of the actinides.[30]

The most common oxidation state of the lanthanides is the +3 state, which is easily attainable. The 4th ionisation energy (equation 1.1) is greater than the sum of the first three ionisation energies, and so the +4 oxidation state of the lanthanides is predominantly not formed.[30]

$$Ln^{3+}_{(g)} \rightarrow Ln^{4+}_{(g)} + e^-_{(g)}$$

(equation 1.1)

The +4 state can be accessed for Ce, Pr, Nd, Dy and Tb.[30] In addition, the +2 oxidation state can be obtained for Eu and Yb.[30]

There are more accessible oxidation states for the earlier actinides (*i.e.* Pa to Am) than the later actinides (Figure 1.7). This is because the early actinides have valence electrons that are less tightly bound, and so can be removed more easily.[30] The increasing effective nuclear charge across the actinide series causes the electrons to be more tightly bound, resulting in the +3 oxidation states being preferred for the later actinides rather than higher valence states (*cf.* early actinides).[30]

			+7	+7									
		+6	+6	+6	+6								
	+5	+5	+5	+5	+5								
+4	+4	+4	+4	+4	+4	+4	+4	+4					
+3	+3	+3	+3	+3	+3	+3	+3	+3	+3	+3	+3	+3	+3
					+2			+2	+2	+2	+2	+2	
Th	Pa	U	Np	Pu	Am	Cm	Bk	Cf	Es	Fm	Md	No	Lr

An = most stable oxidation state in aqueous solution.

An = oxidation state only found in the solid state.

Figure 1.7: Actinide oxidation states.[30]

The trend of the Ln^{3+} ionic radii (Table 1.3) shows a gradual decrease along the series. This is known as the lanthanide contraction, which occurs because of the poor ability of the 4*f* electrons to shield other valence electrons from the nuclear charge. This causes the effective nuclear charge to slightly increase along the series, causing the lanthanide ion to contract.[30] A similar effect occurs for the actinide ions, called the actinide contraction, where there is a gradual decrease of the ionic radii along the series.[30]

Element	Radius (Ln^{3+}) / pm‡	Element	Radius (An^{4+}) / pm*	Radius (An^{3+}) / pm*
Cerium	114	Thorium	108	-
Praseodymium	113	Uranium	103	117
Neodymium	111	Plutonium	100	114
Promethium	109	Americium	99	112
Samarium	108	Curium	-	111
Europium	107	Berkelium	-	110
Gadolinium	105			
Terbium	104			
Dysprosium	103			
Holmium	102			
Erbium	100			
Thulium	99			
Ytterbium	99			
Lutetium	98			

Table 1.3: Ionic radii of ‡8 coordinate and *6 coordinate metal ions.[30,31]

An important difference between the lanthanides and actinides is that the actinide 5*f* orbitals are more destabilised than the lanthanide 4*f* orbitals.[30] This causes the 5*f* orbitals to be more radially expanded and the electrons in these orbitals are weakly bound to the nucleus.[30] Consequently, the coordination chemistry of the *f* elements is influenced by these properties.[30] The contracted nature of the 4*f* orbitals causes the lanthanides to participate predominantly in ionic bonding.[30] They are hard Lewis acids and so favour binding to hard Lewis bases *e.g.* oxygen donor atoms.[30] The 5*f* orbitals prefer to participate more in covalent bonding compared to the 4*f* orbitals of the lanthanides.[30] Traversing the lanthanide and actinide series, the charge densities of the ions increase and stronger ionic bonds are favoured.[30]

The lanthanides are large ions and can be coordinated by up to twelve ligands.[30] The Ln^{III} ion coordination number will decrease with decreasing Ln^{III} ionic radius and increasing anion radius.[30] In aqueous solution, Ln^{III} ions will be coordinated by water. The resulting solvated ion is $[Ln(H_2O)_x]^{3+}$ (x = 8 or 9), with the hydration number changing from nine to eight between the Eu^{III} and Tb^{III} ions.[30] The geometry of the water molecules around the Ln^{III} ions is tricapped, trigonal prismatic for nine coordinate, and bicapped, trigonal prismatic for eight coordinate.[30] Actinide coordination number also decreases with decreasing ionic radii. For

example, solid AnF_3 (An = U-Cm) is nine coordinate in a tricapped, trigonal prismatic geometry, whereas the later actinide halides, BkF_3 and CfF_3, are eight coordinate.[30]

The +5 and +6 oxidation states of U, Np, Pu and Am form the actinyl ions, AnO_2^{n+} (n = 1, 2).[30] The actinyl ions arise because of overlap between the O^{2-} *p* orbitals and the 5*f* orbitals.[30] The two oxygen ligands arrange in a thermodynamically strong linear manner (*i.e.* $[O=An=O]^{n+}$), which causes other coordinated ligands to the actinyl ion to occupy the equatorial plane.[30] Four, five and six donor atoms can occupy this plane to give octahedral, pentagonal bipyramidal and hexagonal bipyramidal geometries, respectively.[30] Hexagonal bipyramidal structures tend to form when three bidentate ligands (*e.g.* CO_3^{2-}) are coordinated. UO_2^{2+} is the most stable actinyl ion and tends to be the favoured form of uranium in the environment.[30]

Coordination chemistry can be used to understand how the metal ions in waste nuclear fuel will behave in the environment.

1.2.2 Actinides and the Environment

Water is the main method of transport for metals in the environment.[32] The behaviour of actinide ions in environmental waters is difficult to predict due to the conditions in which they are present. Factors such as pH, temperature, redox (E_h), chemical speciation, oxidation state, ligand concentration, ionic strength and sorption characteristics can all influence actinide behaviour.[33] All of these conditions determine the actinide oxidation state and the nature of the actinide species in water. For example, all of the accessible oxidation states of plutonium (III, IV, V and VI) can co-exist in certain solution conditions, due to the reduction potentials having similar values (equations 1.2 to 1.4).[30,33] Disproportionation and conproportionation reactions cause changes in Pu redox speciation.[30] Consequently, it can be difficult to isolate a single oxidation state of Pu in solution. The Pu^{III} and Pu^{IV} oxidation states are generally stabilised in acidic media, whilst the Pu^{V} and Pu^{VI} oxidation states are more stable at alkaline pH values.[33]

Pu^{IV}/Pu^{III} $E^o = 0.982$ V

(equation 1.2)

$Pu^{V}O_2/Pu^{IV}$ $E^o = 1.17$ V

(equation 1.3)

$Pu^{VI}O_2/Pu^{V}O_2$ $E^o = 0.916$ V

(equation 1.4)

The E^o values show that the more positive the redox potential, then the greater the species' affinity to gain electrons and its tendency to be reduced.[30]

Uranium and neptunium also show a variety of oxidation states in water. In reducing conditions, U^{IV} is prevalent, whilst in oxidising conditions, UO_2^{2+} is dominant.[33] In aerated waters, NpO_2^{+} is found and in strongly oxidising conditions, NpO_2^{2+} occurs.[33]

The effective charge of the actinides is +3 for An^{III} ions, +4 for An^{IV} ions, +2.2 for $An^{V}O_2^{+}$ ions and +3.3 for $An^{VI}O_2^{2+}$ ions.[33] The tetravalent actinide oxidation state has the greatest effective charge density, and so it is most acidic and most susceptible to hydrolysis.[30]

1.2.3 Hydrolysis

1.2.3.1 Trivalent Lanthanide Hydrolysis

The hydrolysis of trivalent lanthanides has been observed by many techniques in the literature, such as potentiometry, solvent extraction and solubility studies.[34] Deducing the hydrolysis constants of metal ions is important for understanding their chemical behaviour in natural environments. In the absence of organic ligands and in low carbonate concentrations, hydrolysis of metal ions dominates in aqueous solution (equation 1.5).[34]

The effect of hydrolysis increases across the series due to the increasing charge density of the lanthanide ions (*i.e.* the Lu^{III} ion is more susceptible to hydrolysis than the La^{III} ion).[31]

$$[Ln(H_2O)_n]^{3+} + H_2O \rightleftharpoons [Ln(OH)(H_2O)_{n-1}]^{2+} + H_3O^+$$

(equation 1.5)[31]

Or for simplication:

$$Ln^{3+} + H_2O \overset{K_1}{\rightleftharpoons} Ln(OH)^{2+} + H^+$$

(equation 1.6)[31]

K_1 is the first hydrolysis constant and can be written as:

$$K_1 = \frac{[Ln(OH)^{2+}][H^+]}{[Ln^{3+}][H_2O]}$$

(equation 1.7)[31]

Or, it can be written as a stepwise stability constant using the self ionisation of water constant, K_w:

$$K_1 = \frac{[Ln(OH)^{2+}][H^+]}{[Ln^{3+}]K_w}$$

(equation 1.8)[31]

K_2 is the second step wise stability constant and can be written as:

$$K_2 = \frac{[Ln(OH)_2{}^+][H^+]}{[Ln(OH)^{2+}]K_w}$$

(equation 1.9)[31]

The overall stability constant is given the symbol 'β', and is the product of the stepwise stability constants. Therefore, the formation of the second lanthanide hydrolysis constant, denoted $\beta_{1\text{-}2}$, can be expressed as:

$$\beta_{1-2} = K_1 K_2$$

(equation 1.10)[31]

Likewise, the formation of the third and fourth hydrolysis constants, denoted $\beta_{1\text{-}3}$ and $\beta_{1\text{-}4}$ respectively, can be expressed as:

$$\beta_{1-3} = K_1 K_2 K_3$$

(equation 1.11)[31]

$$\beta_{1-4} = K_1 K_2 K_3 K_4$$

(equation 1.12)[31]

For the formation of solids, the equilibrium constant is given in terms of the equilibrium concentrations of the dissolved ions, and is called the solubility product (K_{sp}).[31] The solubility product is often quoted as log K_{sp}, and it follows that the more negative the log K_{sp} value, then the lower the solubility of the solid.[31]

For example, for $La(OH)_{3(s)}$:

$La(OH)_{3(s)} \rightleftharpoons La^{III}_{(aq)} + 3\ OH^-_{(aq)}$ *(equation 1.13)*

$K_{sp} = [La^{III}][OH^-]^3$ $\log K_{sp} = -20.3$ *(equation 1.14)*[37]

The hydrolysis of trivalent lanthanides begins at approximately pH 6 in aqueous solutions.[35] A variety of hydroxide species can be formed, such as $Ln(OH)^{2+}$, $Ln(OH)_2^+$, $Ln(OH)_3$, $Ln(OH)_4^-$, $Ln_2(OH)_2^{4+}$, $Ln_3(OH)_5^{4+}$, $Ln_5(OH)_9^{6+}$ and $Ln_6(OH)_{10}^{8+}$.[35,36] Table 1.4 shows hydrolysis constants for selected lanthanide ions.

					Ionic Strength
La^{3+} +	OH^-	$\rightleftharpoons$	$La(OH)^{2+}$	log β_{1-1} -9.1	0.5 M $NaClO_4$
La^{3+} +	2 OH^-	$\rightleftharpoons$	$La(OH)_2^+$	log β_{1-2} -17.9	1 M $NaClO_4$
$La(OH)_{3(s)}$	$\rightleftharpoons$	La^{3+} +	3 OH^-	log K_{sp} -20.3	1 M $NaClO_4$
2 La^{3+} +	3 OH^-	$\rightleftharpoons$	$La_2(OH)_3^{3+}$	log β_{2-3} -10.0	Not stated
5 La^{3+} +	9 OH^-	$\rightleftharpoons$	$La_5(OH)_9^{6+}$	log β_{5-9} -71.4	Not stated
6 La^{3+} +	10 OH^-	$\rightleftharpoons$	$La_6(OH)_{10}^{8+}$	log β_{6-10} -78.8	Not stated
Ce^{3+} +	OH^-	$\rightleftharpoons$	$Ce(OH)^{2+}$	log β_{1-1} -8.7	0.7 M $NaClO_4$
$Ce(OH)_{3(s)}$	$\rightleftharpoons$	Ce^{3+} +	3 OH^-	log K_{sp} -22.1	Not stated
Ce^{3+} +	4 OH^-	$\rightleftharpoons$	$Ce(OH)_4^-$	log β_{1-4} -28.9	Not stated
2 Ce^{3+} +	3 OH^-	$\rightleftharpoons$	$Ce_2(OH)_3^{3+}$	log β_{2-3} -15.9	Not stated
2 Ce^{3+} +	7 OH^-	$\rightleftharpoons$	$Ce_2(OH)_7^-$	log β_{2-7} -44.7	Not stated
Pr^{3+} +	OH^-	$\rightleftharpoons$	$Pr(OH)^{2+}$	log β_{1-1} -8.6	0.5 M $NaClO_4$
$Pr(OH)_{3(s)}$	$\rightleftharpoons$	Pr^{3+} +	3 OH^-	log K_{sp} -22.3	Not stated
Pr^{3+} +	4 OH^-	$\rightleftharpoons$	$Pr(OH)_4^-$	log β_{1-4} -29.8	Not stated
2 Pr^{3+} +	3 OH^-	$\rightleftharpoons$	$Pr_2(OH)_3^{3+}$	log β_{2-3} -15.6	Not stated
2 Pr^{3+} +	5 OH^-	$\rightleftharpoons$	$Pr_2(OH)_5^+$	log β_{2-5} -29.4	Not stated
Nd^{3+} +	OH^-	$\rightleftharpoons$	$Nd(OH)^{2+}$	log β_{1-1} -8.5	0.5 M $NaClO_4$
Nd^{3+} +	2 OH^-	$\rightleftharpoons$	$Nd(OH)_2^+$	log β_{1-2} -12.8	Not stated
$Nd(OH)_{3(s)}$	$\rightleftharpoons$	Nd^{3+} +	3 OH^-	log K_{sp} -23.2	Not stated
Nd^{3+} +	4 OH^-	$\rightleftharpoons$	$Nd(OH)_4^-$	log β_{1-4} -26.8	Not stated
Sm^{3+} +	OH^-	$\rightleftharpoons$	$Sm(OH)^{2+}$	log β_{1-1} -8.4	0.5 M $NaClO_4$
$Sm(OH)_{3(s)}$	$\rightleftharpoons$	Sm^{3+} +	3 OH^-	log K_{sp} -23.9	Not stated
Sm^{3+} +	4 OH^-	$\rightleftharpoons$	$Sm(OH)_4^-$	log β_{1-4} -26.1	Not stated
2 Sm^{3+} +	3 OH^-	$\rightleftharpoons$	$Sm_2(OH)_3^{3+}$	log β_{2-3} -15.3	Not stated
Eu^{3+} +	OH^-	$\rightleftharpoons$	$Eu(OH)^{2+}$	log β_{1-1} -8.4	0.5 M $NaClO_4$
$Eu(OH)_{3(s)}$	$\rightleftharpoons$	Eu^{3+} +	3 OH^-	log K_{sp} -24.5	Not stated
Eu^{3+} +	4 OH^-	$\rightleftharpoons$	$Eu(OH)_4^-$	log β_{1-4} -26.2	Not stated
2 Eu^{3+} +	3 OH^-	$\rightleftharpoons$	$Eu_2(OH)_3^{3+}$	log β_{2-3} -15.4	Not stated
Tb^{3+} +	OH^-	$\rightleftharpoons$	$Tb(OH)^{2+}$	log β_{1-1} -8.2	0.5 M $NaClO_4$
$Tb(OH)_{3(s)}$	$\rightleftharpoons$	Tb^{3+} +	3 OH^-	log K_{sp} -24.3	0
Ho^{3+} +	OH^-	$\rightleftharpoons$	$Ho(OH)^{2+}$	log β_{1-1} -8.1	0.5 M $NaClO_4$
$Ho(OH)_{3(s)}$	$\rightleftharpoons$	Ho^{3+} +	3 OH^-	log K_{sp} -24.5	0
Lu^{3+} +	OH^-	$\rightleftharpoons$	$Lu(OH)^{2+}$	log β_{1-1} -8.0	0.5 M $NaClO_4$
$Lu(OH)_{3(s)}$	$\rightleftharpoons$	Lu^{3+} +	3 OH^-	log K_{sp} -25.1	0

Table 1.4: Hydrolysis constants for selected lanthanides.[35,37]

1.2.3.2 Trivalent Actinide Hydrolysis

The dominant oxidation state of Am in environmental waters is +3.[38] The Am^{III} cation forms the hydrolysis species of $Am(OH)^{2+}$, $Am(OH)_2^{+}$ and $Am(OH)_3$ (Figure 1.8 and Table 1.5).[38] However, in concentrated chloride solutions (greater than 3 M) and above pH 7, α radiolysis from the Am^{III} source can cause chloride to oxidise to chlorine, which can consequently oxidise Am^{III} to Am^{V}.[38]

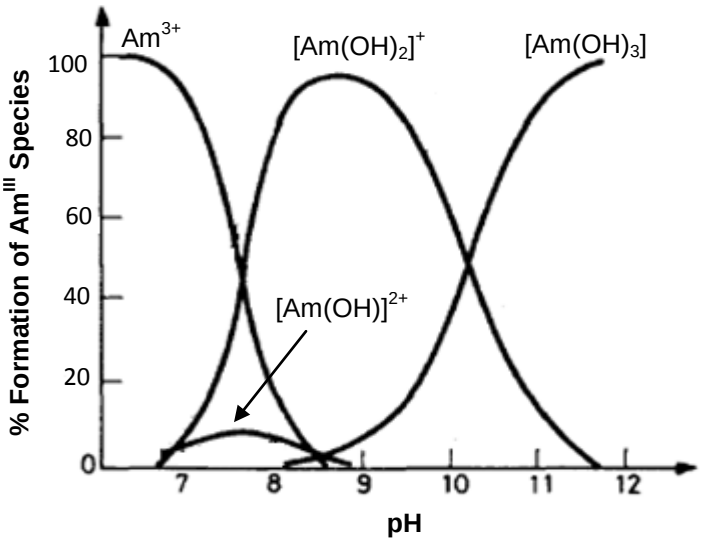

Figure 1.8: Distribution of Am^{III} species in aqueous solution as a function of pH. [Adapted from Reference 39].

Trivalent Cm is the only available oxidation state for Cm in natural waters and the hydrolysis species of $Cm(OH)^{2+}$, $Cm(OH)_2^{+}$ and $Cm(OH)_3$ have been shown to exist (Table 1.5).[38]

						Ionic Strength
Am^{3+}	OH^-	⇌	$Am(OH)^{2+}$	$\log \beta_{1-1}$	-7.4	0.7 M NaCl
Am^{3+}	$2\ OH^-$	⇌	$Am(OH)_2^{+}$	$\log \beta_{1-2}$	-14.96	1 M $NaClO_4$
$Am(OH)_{3(s)}$	⇌	Am^{3+}	$+\ 3\ OH^-$	$\log K_{sp}$	-26.2	0.7 M NaCl
Cm^{3+}	OH^-	⇌	$Cm(OH)^{+}$	$\log \beta_{1-1}$	-6.98	0.1 M electrolyte
Cm^{3+}	$2\ OH^-$	⇌	$Cm(OH)_2^{+}$	$\log \beta_{1-2}$	-15.2	0.1 M electrolyte

Table 1.5: Hydrolysis constants for Am^{III} and Cm^{III}.[37]

1.2.3.3 Tetravalent Actinide Hydrolysis

Tetravalent actinides are susceptible to hydrolysis because of their high charge density. Hydrolysis begins at pH below 1, and polynucleation reactions or colloid formation can subsequently occur.[40,41] Thorium^{IV} hydrolysis is complicated because of the presence of extensive polymerisation reactions that occur within a narrow pH range. It is thought that a variety of mono- and multimetallic species exist such as, $Th(OH)^{3+}$, $Th(OH)_2^{2+}$, $Th_2(OH)_3^{5+}$, $Th_4(OH)_8^{8+}$ and $Th_6(OH)_{15}^{9+}$ (Table 1.6).[37,42] Ekberg *et al*. found that $Th(OH)^{3+}$, $Th(OH)_2^{2+}$, $Th_4(OH)_8^{8+}$ and $Th_6(OH)_{15}^{9+}$ exist between the pH range 2.0 to 4.5, and the species of $Th(OH)_3^{+}$ and $Th(OH)_4$ were present at higher pH.[42]

Th^{4+}	+	OH^-	$\rightleftharpoons$	$Th(OH)^{3+}$	$\log \beta_{1-1}$	-3.3
Th^{4+}	+	$2\ OH^-$	$\rightleftharpoons$	$Th(OH)_2^{2+}$	$\log \beta_{1-2}$	-8.6
Th^{4+}	+	$3\ OH^-$	$\rightleftharpoons$	$Th(OH)_3^{+}$	$\log \beta_{1-3}$	-14.2
$Th(OH)_{4(s)}$		$\rightleftharpoons$	Th^{4+}	+ $4\ OH^-$	$\log K_{sp}$	-50.7
$2\ Th^{4+}$	+	$3\ OH^-$	$\rightleftharpoons$	$Th_2(OH)_3^{5+}$	$\log \beta_{2-3}$	-33.8
$2\ Th^{4+}$	+	$5\ OH^-$	$\rightleftharpoons$	$Th_2(OH)_5^{3+}$	$\log \beta_{2-5}$	-53.7
$4\ Th^{4+}$	+	$8\ OH^-$	$\rightleftharpoons$	$Th_4(OH)_8^{8+}$	$\log \beta_{4-8}$	-19.1
$6\ Th^{4+}$	+	$15\ OH^-$	$\rightleftharpoons$	$Th_6(OH)_{15}^{9+}$	$\log \beta_{6-15}$	-39.5

Table 1.6: Hydrolysis constants for Th^{IV} at 1 M $NaClO_4$ ionic strength.[37,42]

For plutonium, Pu^{IV} is the most stable solution oxidation state and is readily hydrolysed. Hydrolysis forms the following species depending on pH: Pu^{4+}, $Pu(OH)^{3+}$, $Pu(OH)_2^{2+}$, $Pu(OH)_3^{+}$ and $Pu(OH)_4$ (Figure 1.9 and Table 1.7).[43]

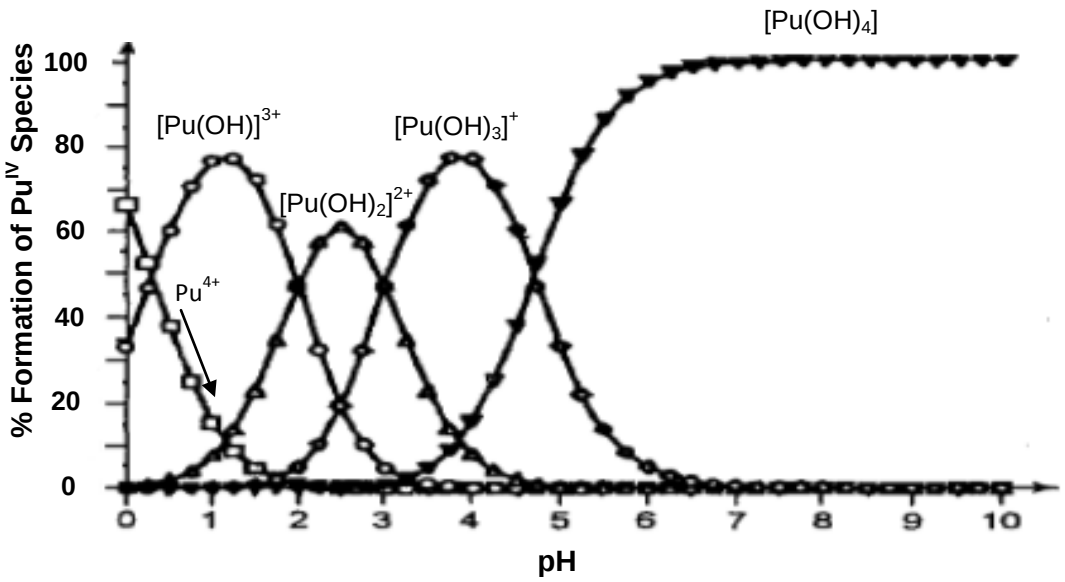

Figure 1.9: Pu^{IV} speciation as a function of pH. [Adapted from Reference 44].

In typical fuel storage pond conditions of pH 11, it is expected that most An^{IV} would be complexed by hydroxide as an $An(OH)_4$ species.[44] It is predicted that there is less than 1 % of free An^{IV} metal ions in the ponds.[15]

Pu^{4+}	+	OH^-	$\rightleftharpoons$	$Pu(OH)^{3+}$	$\log \beta_{1-1}$	-1.22
Pu^{4+}	+	2 OH^-	$\rightleftharpoons$	$Pu(OH)_2^{2+}$	$\log \beta_{1-2}$	-3.12
Pu^{4+}	+	3 OH^-	$\rightleftharpoons$	$Pu(OH)_3^{+}$	$\log \beta_{1-3}$	-5.57
Pu^{4+}	+	4 OH^-	$\rightleftharpoons$	$Pu(OH)_4$	$\log \beta_{1-4}$	-8.37

Table 1.7: Hydrolysis constants for Pu^{IV} at 3 M ionic strength.[32,45]

Charged hydrolytic colloids of An^{IV} oxide, hydroxide and hydroxo-carbonato can form in aqueous solution.[43] Colloidal suspensions consist of particles between a nanometre (nm) and micrometre (μm) in size.[46] The characteristic features of colloids are related to their particle size, particle shape, flexibility, surface properties, particle-particle interactions and particle–solvent interactions.[46] In solution, colloidal particles are solvated to about one molecular layer thickness. This tightly bound solvent is treated as part of the colloid.[46]

The colloid growth of Pu^{IV} oxyhydroxide has been investigated by Rothe *et al.*[47] They proposed that Pu colloids are formed from the polymerisation of $Pu(OH)_2(H_2O)_6^{2+}$ units (equation 1.15), and that the Pu colloids may be measured between the range 12 to 25 nm depending on solution conditions.[47]

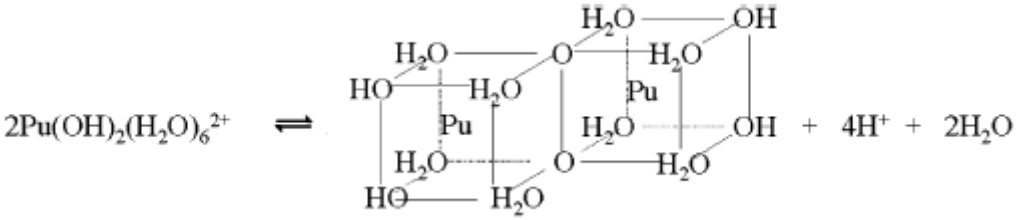

(equation 1.15)

[Taken from Reference 47].

where $Pu(OH)_{4(coll)}$ represents $Pu_nO_p(OH)_{4n-2p}(H_2O)_z$ ($0 \leq p \geq 2n$).[47]

The formation of An^{IV} colloids is important to consider as they may increase the solubility of actinide ions in the ponds, or they may aggregate and form solid actinide species that may become incorporated into the brucite sludge.

1.2.3.4 Pentavalent Actinide Hydrolysis

Pentavalent actinides such as $Np^VO_2^+$ and $Pu^VO_2^+$ hydrolyse above pH 9 to form Pu^VO_2OH, Np^VO_2OH and $Np^VO_2(OH)_2^-$ (Table 1.8).[38] Pentavalent Np is the most common oxidation state of Np in oxygen rich waters.[38] Work in the literature has shown that the oxidised form of Pu can form a major fraction of dissolved Pu in natural waters, but there is debate as to whether this is Pu^V or Pu^{VI}. Orlandini *et al*. have proposed that Pu^V is the only or predominant form of oxidised plutonium in natural waters,[48] but Pu^V is unstable with respect to disproportionation (equation 1.16).

$$2\ Pu^VO_2^+ + 2\ H_2O \rightleftharpoons Pu^{VI}O_2^{2+} + Pu^{IV}(OH)_4$$

(equation 1.16)[44]

Although disproportionation may happen, it is thought that the $An^{V}O_2^{+}$ concentrations in the ponds would be too low for this process to occur.[44]

PuO_2^{+}	+	OH^-	$\rightleftharpoons$	PuO_2OH	$\log \beta_{1-1}$	-9.7
NpO_2^{+}	+	OH^-	$\rightleftharpoons$	NpO_2OH	$\log \beta_{1-1}$	-11.3
NpO_2^{+}	+	$2\ OH^-$	$\rightleftharpoons$	$NpO_2(OH)^-$	$\log \beta_{1-2}$	-23.3

Table 1.8: Hydrolysis constants for $Pu^{V}O_2^{+}$ and $Np^{V}O_2^{+}$ in 0.1 M $NaClO_4$.[38]

1.2.3.5 Hexavalent Actinide Hydrolysis

The hexavalent oxidation state of U, Np and Pu can be mobile in certain environments due to the formation of anionic complexes e.g. $An^{VI}O_2(OH)_n^{2-n}$ (n = 3 or 4).[15,32] The hexavalent state of U is the most stable in oxic conditions, whereas the $Pu^{VI}O_2^{2+}$ species must be stabilised by chloride anions or by oxidising agents that have been formed by radiolysis *e.g.* hypochlorite.[45] Selected hydrolysis constants for $Pu^{VI}O_2$ are presented in Table 1.9.

PuO_2^{2+}	+	OH^-	$\rightleftharpoons$	PuO_2OH^+	$\log \beta_{1-1}$	-5.4
PuO_2^{2+}	+	$2\ OH^-$	$\rightleftharpoons$	$PuO_2(OH)_2$	$\log \beta_{1-2}$	-15.2

Table 1.9: Hydrolysis constants for $Pu^{VI}O_2^{2+}$ in 0.1 M $NaClO_4$.[38]

1.2.4 Carbonate Speciation and Modes of Complexation to Metal Ions

The nuclear waste storage ponds described in Section 1.1.5 are open to the atmosphere, which allows the dissolution of carbon dioxide into the pond water to form carbonate anions (equations 1.17 to 1.19).

$$CO_{2(g)} \rightleftharpoons CO_{2(aq)}$$

(equation 1.17)[49]

$$CO_{2(aq)} + H_2O \rightleftharpoons HCO_3^- + H^+$$

(equation 1.18)[49]

$$HCO_3^- \rightleftharpoons CO_3^{2-} + H^+$$

(equation 1.19)[49]

The above process means that the carbonate anion is ubiquitous in nature. It is estimated that the carbonate concentration in the ponds at pH 11 is around 2×10^{-4} M.[15] Therefore, carbonate complexation in solution with actinides is important to understand.[32,50]

The modes of carbonate binding to metal ions are shown in Figure 1.10.

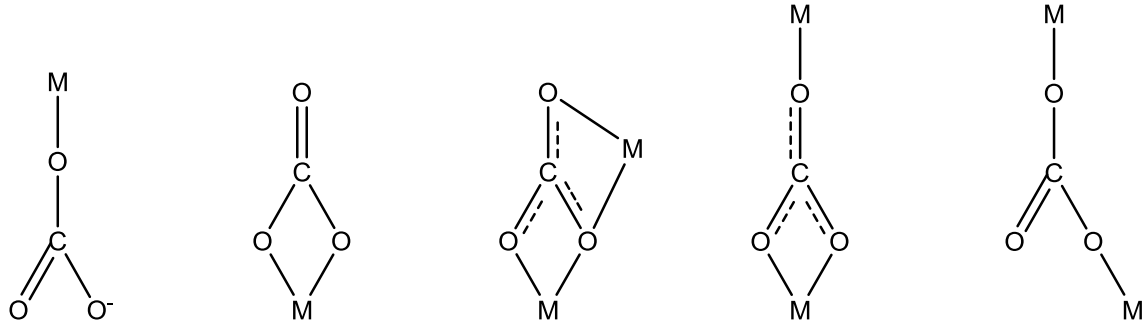

Figure 1.10: The modes of carbonate binding to metal ions.[51]

1.2.4.1 Lanthanide Carbonate Species

Trivalent lanthanides have a strong affinity for carbonate ions. Lanthanide carbonates are very insoluble in water,[52] and can be precipitated from lanthanide ion solutions by the addition of carbonates or bicarbonates.[53] Under alkaline conditions, the precipitation of carbonate complexes tends to be favoured over the hydroxide complexes.[35]

A variety of lanthanide carbonates of different stoichiometry have been identified in the literature including $Ln_2(CO_3)_3.xH_2O$,[52] $Ln(OH)CO_3$[54] and $Ln_2O_2CO_3$.[54] The synthesis of anhydrous $NaLa(CO_3)_2$ is possible under elevated CO_2 pressure at 450 ^oC.[55]

Other lanthanide carbonate formations include the tetra-carbonate complexes of $[C(NH_2)_3]_5[Er(CO_3)_4].11H_2O$ and $[C(NH_2)_3]_4[Dy(CO_3)_4(H_2O)](H_3O).13H_2O$ isolated as single crystals by Goff *et al* (Figure 1.11).[56]

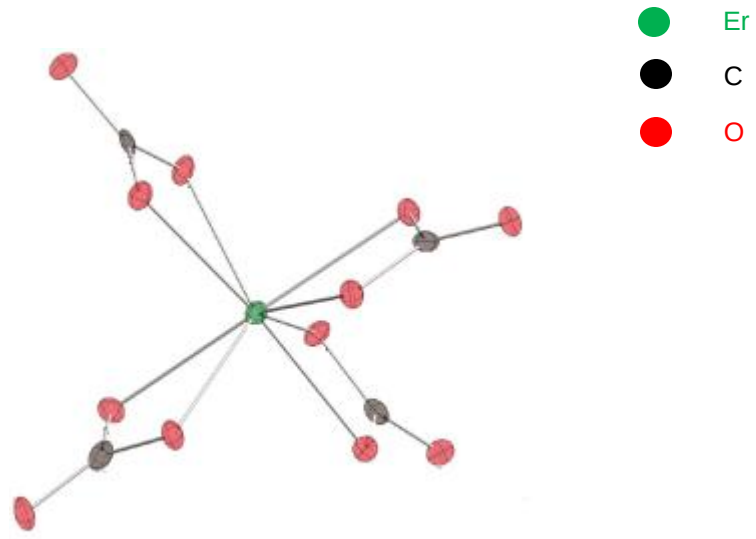

Figure 1.11: Thermal ellipsoid plot illustrating the coordination of carbonate in $[C(NH_2)_3]_5[Er(CO_3)_4].11H_2O$.[56]

At high carbonate concentrations (2.5 M) and using the cobalt hexamine cation, crystals of $[Co(NH_3)_6][Sm(CO_3)_3(H_2O)].4H_2O$ and $[Co(NH_3)_6]_6[K_2(H_2O)_{10}][Nd_2(CO_3)_8]_2.20H_2O$ have been reported by Clark *et al.*[57] and Bond *et al.*,[58] respectively. The Sm^{III} tricarbonate complex has a chain structure of nine coordinate Sm^{III} centres bridged by μ-η^2:η^1 carbonate ligands. The Nd^{III} tetracarbonate complex has a one-dimensional (1D) chainlike structure, and is bound by four chelating and one monodentate carbonate anions (Figure 1.12).

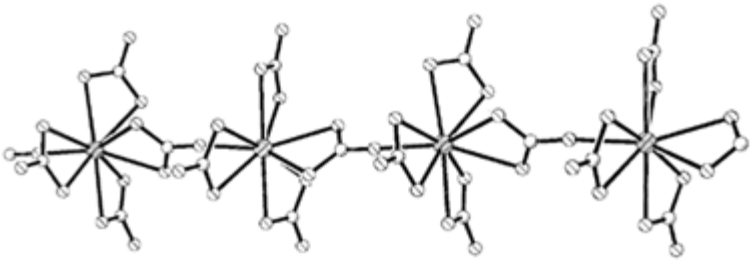

Figure 1.12: Ball and stick view of $[Nd_2(CO_3)_8]_\infty$ 1D chain structure.[58]

Depending on the solution conditions, the limiting solution species for trivalent lanthanides is believed to be $[M(CO_3)_3]^{3-}$ and $[M(CO_3)_4]^{5-}$.[57] A tetravalent Ce pentacarbonate complex can also be synthesised of formula, $Na_6[Ce(CO_3)_5].12H_2O$.[59] All of these species tend to be formed under high carbonate concentrations (molar compared to millimolar in the environment). However, it is still important to understand the various modes of complexation of carbonate to *f* elements.[56]

Table 1.10 presents the stability constants of selected lanthanides with the carbonate anion.

							Ionic Strength
La^{3+}	+	CO_3^{2-}	$\rightleftharpoons$	$La(CO_3)^+$	$\log \beta_{11}$	4.74	0.7 M $NaClO_4$
La^{3+}	+	2 CO_3^{2-}	$\rightleftharpoons$	$La(CO_3)_2^-$	$\log \beta_{12}$	8.78	0.7 M $NaClO_4$
La^{3+}	+	3 CO_3^{2-}	$\rightleftharpoons$	$La(CO_3)_3^{3-}$	$\log \beta_{13}$	8.63	Not stated
Eu^{3+}	+	CO_3^{2-}	$\rightleftharpoons$	$Eu(CO_3)^+$	$\log \beta_{11}$	5.76	0.7 M $NaClO_4$
Eu^{3+}	+	2 CO_3^{2-}	$\rightleftharpoons$	$Eu(CO_3)_2^-$	$\log \beta_{12}$	10.09	0.7 M $NaClO_4$
Lu^{3+}	+	CO_3^{2-}	$\rightleftharpoons$	$Lu(CO_3)^+$	$\log \beta_{11}$	6.02	0.7 M $NaClO_4$
Lu^{3+}	+	2 CO_3^{2-}	$\rightleftharpoons$	$Lu(CO_3)_2^-$	$\log \beta_{12}$	10.85	0.7 M $NaClO_4$

Table 1.10: Carbonate complexation constants for selected lanthanides.[37]

1.2.4.2 Trivalent ActinideCarbonate Species

Trivalent americium carbonates can be synthesised by the same method that trivalent lanthanide carbonates are formed. The addition of $NaHCO_3$ to aqueous Am^{III} solutions yields

$Am_2(CO_3)_3.4H_2O$.[38] If $Am_2(CO_3)_3.4H_2O$ is treated with 0.5 M $NaHCO_3$ or 1.5 M Na_2CO_3, then $NaAm(CO_3)_2.4H_2O$ or $Na_3Am(CO_3)_3.3H_2O$ is formed, respectively.[38] Acidic aqueous Am^{III} solutions under varying CO_2 partial pressures form a mixed hydroxo-carbonato species of $Am(OH)(CO_3)$.[38] In aqueous solutions, $Am(CO_3)^+$ and $Am(CO_3)_2^-$ species have been shown to exist (Figure 1.13 and Table 1.10).[38]

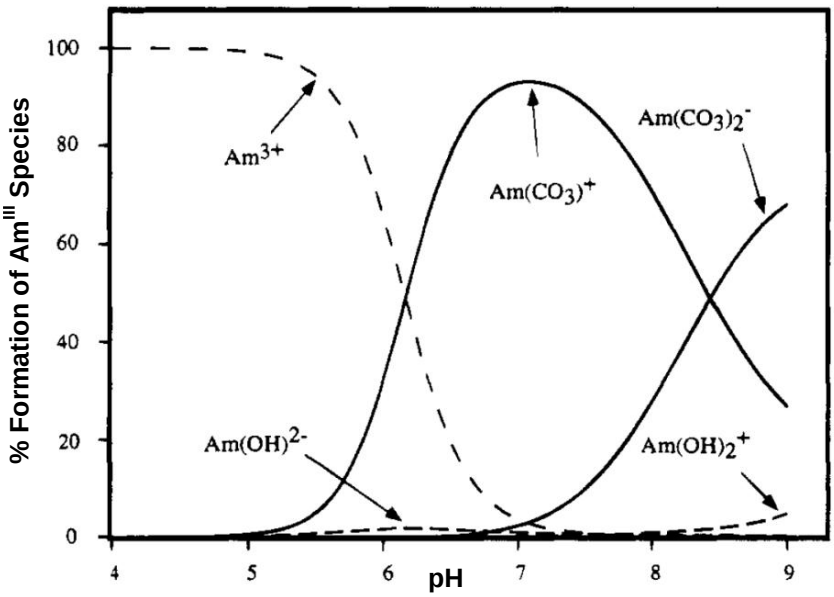

Figure 1.13: Distribution of Am^{III} species in carbonate solution. [Taken from Reference 38].

The speciation diagram illustrates that in aqueous solutions, where hydroxide and carbonate anions are present, Am^{III} will preferentially bind to carbonate ions. It is expected that at higher pH (*i.e.* pH greater than 11) $Am(OH)_2^+$ will dominate.[38] Analogous $Cm_2(CO_3)_3$ solids can be prepared by the addition of carbonate anions to $Cm^{III}_{(aq)}$ solutions.[38] The formation constant of the $Cm(CO_3)^+$ species is shown in Table 1.11.

Am^{3+}	+	CO_3^{2-}	$\rightleftharpoons$	$Am(CO_3)^+$	$\log \beta_{11}$	6.6
Am^{3+}	+	$2\ CO_3^{2-}$	$\rightleftharpoons$	$Am(CO_3)_2^-$	$\log \beta_{12}$	10.5
Am^{3+}	+	$3\ CO_3^{2-}$	$\rightleftharpoons$	$Am(CO_3)_3^{3-}$	$\log \beta_{13}$	12.8
Cm^{3+}	+	CO_3^{2-}	$\rightleftharpoons$	$Cm(CO_3)^+$	$\log \beta_{11}$	6.65

Table 1.11: Carbonate complexation constants for Am^{III} and Cm^{III} at 0.1 M $NaClO_4$ ionic strength.[32,37]

Trivalent plutonium present in the ponds would generally oxidise to tetravalent species.[60] Trivalent Pu carbonate species have been reported in the literature, for example $Pu(CO_3)^+$ and $Pu(CO_3)_2^-$, at ionic strength concentrations between 0.1 to 0.5 M (Table 1.12).[45] A precipitate of $Pu(OH)(CO_3).xH_2O$ can form at high carbonate concentrations and elevated temperatures, which may be represented as $Pu(OH)_3.Pu_2(CO_3)_3.xH_2O$.[61]

Pu^{3+}	+	CO_3^{2-}	$\rightleftharpoons$	$PuCO_3^+$	$\log \beta_{110}$	7.5
Pu^{3+}	+	$2\ CO_3^{2-}$	$\rightleftharpoons$	$Pu(CO_3)_2^-$	$\log \beta_{120}$	12.4

Table 1.12: Carbonate complexation constants for Pu^{III} at 0.3 M $NaClO_4$ ionic strength.[32,37]

1.2.4.3 Tetravalent Thorium and Plutonium Carbonate Species

A tetravalent thorium pentacarbonate complex can be precipitated at high carbonate concentrations (2.5 M) and using the cobalt hexamine cation as a precipitant.[62] The resulting $[Co(NH_3)_6]_2[Th(CO_3)_5].xH_2O$ complex is insoluble in all common solvents. It reacts with dilute acidic solution to evolve CO_2 from the neutralisation of the carbonate anions.[62]

The tetravalent Pu carbonate species of $PuCO_3^{2+}$, $Pu(CO_3)_2$, $Pu(CO_3)_3^{2-}$, $Pu(CO_3)_4^{4-}$ and $Pu(CO_3)_5^{6-}$ have been shown to form, with increase in pH and CO_3^{2-} concentration.[63] The tetravalent Ce, Th and Pu pentacarbonate complexes are analogous. There is also evidence for the formation of a mixed hydroxo-carbonato complex of $[Pu(OH)_m(CO_3)_n]_{4-m-2n}$ (equation 1.20).[63]

$$Pu^{4+}_{(aq)} + nCO_3^{2-} + mOH^- \rightleftharpoons [Pu(OH)_m(CO_3)_n]_{4-m-2n}$$

(equation 1.20)

There has been uncertainty in the literature as to whether the pure carbonate complex or the mixed hydroxo-carbonato species is the most favoured complex. D. Clark *et al*. have shown that the pure carbonate ion, $[Pu(CO_3)_5]^{6-}$, is formed at high carbonate concentrations (3 M) and is preferred in both the solid and solution states.[63] However, Östhols *et al*. have found evidence for the analogous $[Th(CO_3)_5]^{6-}$ complex to be in equilibrium with $[Th(OH)_3(CO_3)]^-$.[64] Anderson *et al*. also found that the simplest carbonate species that would

compete effectively with $Th(OH)_4$ is $Th(CO_3)(OH)_2$.[65] Therefore, Pu^{IV} mixed hydroxo-carbonato complexes could form under conditions of lower carbonate concentrations. Other Pu^{IV} carbonate solids have also been synthesised, for example, $M_4Pu(CO_3)_4$ and $M_6Pu(CO_3)_5$ ($M = Na^+, K^+, NH_4^+$).[45]

Selected stability constants of Th^{IV} and Pu^{IV} carbonate complexes are shown in Table 1.13.

								Ionic Strength
Th^4	+	$5\ CO_3^{2-}$	-	$\rightleftharpoons$	$Th(CO_3)_5^{6-}$	$\log \beta_{150}$	26.3	1 M NH_4NO_3
Th^{4+}	+	CO_3^{2-}	+ $3\ OH^-$	$\rightleftharpoons$	$[Th(OH)_3CO_3]^-$	$\log \beta_{11-3}$	6.8	3 M $NaClO_4$
Pu^{4+}	+	CO_3^{2-}	-	$\rightleftharpoons$	$PuCO_3^{2+}$	$\log \beta_{110}$	17.0	0.3 M $NaClO_4$
Pu^{4+}	+	$4\ CO_3^{2-}$	-	$\rightleftharpoons$	$Pu(CO_3)_4^{4-}$	$\log \beta_{140}$	37.0	0.3 M $NaClO_4$
Pu^{4+}	+	$5\ CO_3^{2-}$	-	$\rightleftharpoons$	$Pu(CO_3)_5^{6-}$	$\log \beta_{150}$	36.7	0.3 M $NaClO_4$
Pu^{4+}	+	$2\ CO_3^{2-}$	+ 2 OH-	$\rightleftharpoons$	$Pu(CO_3)_2(OH)_2^{2-}$	$\log \beta_{12-2}$	44.8	0.1 M $NaClO_4$

Table 1.13: Carbonate complexation constants for Th^{IV} and Pu^{IV}.[32,37]

1.2.4.4 Pentavalent and Hexavalent Actinide Carbonate Species

It is suggested that a key An^V species (where An = U, Np, Pu) at around 10^{-3} M CO_3^{2-} would be $AnO_2(CO_3)^-_{(aq)}$.[15] At higher carbonate concentrations, $[AnO_2(CO_3)_3]^{5-}$ may be observed.[45] There is also evidence of solid An^V carbonate complexes *e.g.* $KAnO_2CO_3$.[45] Mixed hydroxo-carbonato Pu^V species have not been shown to be prevalent, but mixed hydroxo-carbonato species of Np^V can occur.[45]

At high pH and high carbonate concentrations, an An^{VI} carbonate precipitate of $AnO_2CO_{3(s)}$ can occur.[66] Robouch *et al*. suggested that $PuO_2CO_{3(s)}$ may dissolve to form $[PuO_2(CO_3)_2]^{2-}$ and $[PuO_2(CO_3)_3]^{4-}$ complexes.[66] It is thought that a trinuclear complex could then form at higher Pu concentrations (equation 1.21).[66]

$$3\ [PuO_2(CO_3)_3]^{4-} \rightleftharpoons [(PuO_2(CO_3)_2)_3]^{6-} + 3\ CO_3^{2-}$$

(equation 1.21) [66]

There has also been suggestions of mixed hydoxo-carbonato Pu^{VI} complexes, for example, $[PuO_2(OH)(HCO_3)]$ and $[PuO_2(OH)(CO_3)]^-$.[66]

Pu^V and Pu^{VI} stability constants for carbonate complexation are presented in Table 1.14.

							Ionic Strength
PuO_2^+	+	CO_3^{2-}	-	$\rightleftharpoons$	$PuO_2CO_3^-$	$\log \beta_{110}$ 5.1	0
PuO_2^+	+	$3\ CO_3^{2-}$	-	$\rightleftharpoons$	$PuO_2(CO_3)_3^{5-}$	$\log \beta_{130}$ 10.0	1 M Na_2CO_3
PuO_2^{2+}	+	CO_3^{2-}	-	$\rightleftharpoons$	PuO_2CO_3	$\log \beta_{110}$ 8.6	3.5 M $NaClO_4$
PuO_2^{2+}	+	$2\ CO_3^{2-}$	-	$\rightleftharpoons$	$PuO_2(CO_3)_2^{2-}$	$\log \beta_{120}$ 15.1	0
PuO_2^{2+}	+	$3\ CO_3^{2-}$	-	$\rightleftharpoons$	$PuO_2(CO_3)_2^{4-}$	$\log \beta_{130}$ 18.5	0

Table 1.14: Carbonate complexation constants for Pu^V and Pu^{VI}.[32,37]

1.2.5 Organic Ligands in Nuclear Waste Storage Ponds

The nuclear waste ponds are open to the environment allowing plant and animal matter to be deposited. This forms a complex heterogeneous mixture of Natural Organic Matter (NOM).[67] It is possible to separate NOM into two groups, which are humic substances (HS) and non-humic substances (Non-HS).[67] HS account for the largest proportion of NOM and occur in soils and aquatic environments.[68,69] Approximately 80 % of the total carbon in terrestrial media and 60 % of the carbon dissolved in aquatic media are made up of HS.[70] Non-HS include compounds that can show recognisable chemical characteristics.[71] Examples of these compounds include carbohydrates, amino acids and lipids.[71] In general, these compounds are relatively easily attacked by micro-organisms in the soil and water and take a short time to decompose.[71] HS, by comparison, are the unidentifiable components that are resistant to microbial degradation.[71] HS are molecularly heterogeneous substances, which are brown-black in colour.[72] Aquatic HS are less heterogeneous than terrestrial HS, as they have a narrower range of molecular weights (MW) and less variability in physicochemical characteristics among their components.[73] There are three fractions of HS that are classified as follows: a) humin, which is insoluble in aqueous systems at all pH values; b) humic acid (HA), which is soluble in solutions of pH 2 or above; and c) fulvic acid (FA), which is soluble

in water at any pH.[74] The fractions differ in their molecular weight and functional group content.[74] The definitive structure of HS has not been determined. This is due to the heterogeneous nature of the molecules, and because HS can rapidly rearrange their molecular structure as the surrounding conditions change.[75]

A structure of HS was suggested by Stevenson in 1982 (Figure 1.14).[76] It consists of phenolic and benzenecarboxylic acids. As shown in Figure 1.14, the structure is stable because of the large numbers of H-bonds, but it can be broken up by the weakening or breaking of these bonds.[77] The suggested structure is unconstrained and so it would be able to bind metal ions, molecules or compounds.[78]

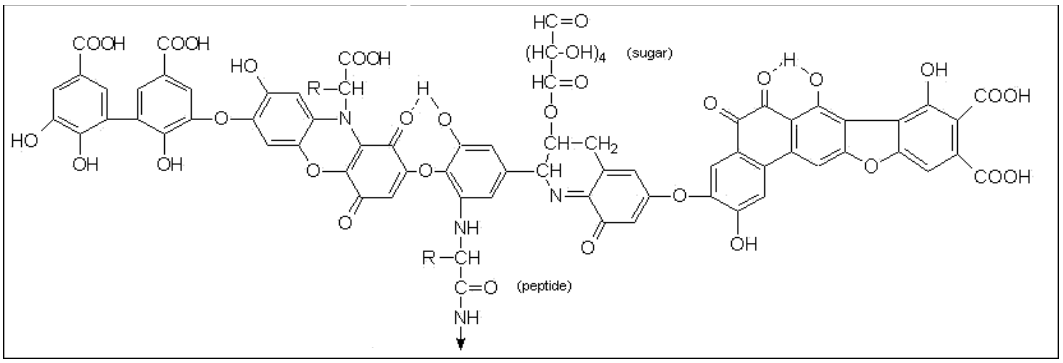

Figure 1.14: Model chemical structure of HA. [Taken from Reference 79].

Almost all metal ions form complexes or chelates with HS.[71] Therefore, it is possible that metal ions, *e.g.* Am^{3+}, could be bound by HS in the ponds. From Figure 1.14 above, it can be seen that HS contain a large number of functional groups, and so may bind large numbers of metal ions.[71]

The donor groups that are most important for HS are COOH, PhOH, C=O and NH_2. A generalised equation for metal ion binding to HS is shown in equation 1.22.

$$x(\text{R-COO}^-) + y(\text{R-PhO}^-) + \text{M}^{n+} \rightleftharpoons (\text{R-COO})_x(\text{R-PhO})_y\text{M}^{(n-x-y)+}$$

(equation 1.22)[80]

HS can be considered as colloids.[71] An important physical property of colloidal dispersions is the tendency of the particles to aggregate.[46] The main cause of aggregation is the Van der Waals forces between the particles.[46] To counteract these and promote stability, equally long

range repulsive forces, *e.g.* electrostatic interactions, are required.[46] The stability of humic colloids in solution is important to understand because if the colloid aggregates and precipitates from solution, then it will carry any bound metal ions with it and so remove them from solution.

It has been found that HS can reduce penta- and hexavalent oxidation states, for example reduction of $Pu^{V}O_2^{+}$ and $Pu^{VI}O_2^{2+}$ to Pu^{IV}, which subsequently would be hydrolysed to $Pu(OH)_4$.[33] The $Pu(OH)_4$ could then either precipitate from the pond solution, adsorb to a solid surface or bind to HS.

1.2.6 Lanthanide and Actinide Complexation with Na_2H_2EDTA and H_5DTPA

Ethylenediamine tetraacetate ($EDTA^{4-}$, Figure 1.15) has been used as a decontaminating agent in the nuclear industry, in defence production of Pu and to process Pu-containing nuclear wastes.[81]

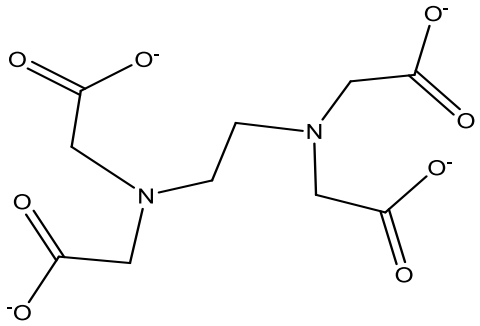

Figure 1.15: Ethylenediamine tetraacetate ($EDTA^{4-}$).

The $EDTA^{4-}$ ligand is a polyaminocarboxylate and can bind to metal ions through four carboxylate O-atoms, and two N-donors. Generally, $EDTA^{4-}$ forms 1:1 complexes with metal ions and can bind hexadentate, pentadentate or tetradentate depending on the size of the coordinated metal ion.[82] The stability of lanthanide-EDTA complexes is due to the large and positive change in entropy during complex formation.[82] Traversing the lanthanide series, the stability constants of the lanthanide-EDTA complexes increases due to the lanthanide contraction.[37] This causes an increase in the charge density of the lanthanide ions and a stronger electrostatic attraction arises between the lanthanides and $EDTA^{4-}$.[37] A range of lanthanide-EDTA salts are quoted in the literature, for example [K][Ln(EDTA)],

[Na][Ln(EDTA)], $[NH_4][Ln(EDTA)]$ and [Ln(EDTAH)], with the remainder of the coordination sphere being filled with water.[82] Trivalent Am and Cm can also form $[An(EDTA)]^-_{(aq)}$ complexes.[37]

Tetravalent thorium has a larger stability constant with $EDTA^{4-}$ compared to the Ln-EDTA complexes.[37] This is because the stability constant for a complex increases with increasing charge and decreasing radius of the metal ion.[30]

Trivalent and tetravalent plutonium-EDTA complexes can be formed under a wide range of conditions. The [Pu(EDTAH)] complex forms in strong acidic solutions, but is deprotonated above pH 3 and can form the mixed $[Pu(EDTA)(OH)]^{2-}$ species.[83] The Pu^{III} ion has a lower affinity for the $EDTA^{4-}$ anion, and so the resulting complex is less stable than the Pu^{IV} ion complex.[45,83] The Pu^{IV}-EDTA complex is so stable that other oxidation states of Pu tend to be oxidised or reduced to the +4 state upon addition of $EDTA^{4-}$.[83] The stoichiometry of Pu^{IV}-EDTA complexes depends on the solution pH and the ratio of Pu^{IV}:$EDTA^{4-}$. In highly acidic conditions (pH less than 1) and equimolar Pu^{IV}:$EDTA^{4-}$ ratios, the $[Pu(EDTAH)]^+$ complex is formed. Over the pH range 1 to 4, the neutral [Pu(EDTA)] complex dominates the Pu^{IV} ion speciation.[83] The Pu^{IV} cation is very susceptible to hydrolysis, even when coordinated to multidentate chelators. At higher pH, $[Pu(EDTA)(OH)]^-$ and $[Pu(EDTA)(OH)_2]^{2-}$ form, eventually resulting in the precipitation of $Pu(OH)_4$.[83] A 1:2 Pu^{IV}:$EDTA^{4-}$ ratio forms the complexes $[Pu(EDTA)(EDTAH)]^{3-}$ and $[Pu(EDTA)_2]^{4-}$, over the pH range 3 to 7 and 7 to 9, respectively.[83] The formation of the bis-$EDTA^{4-}$ Pu^{IV} species illustrates how a single $EDTA^{4-}$ ligand is unable to fill completely the inner coordination sphere of Pu^{IV} , which can be coordinated by 8 to 12 donors (Figure 1.16).[83,84]

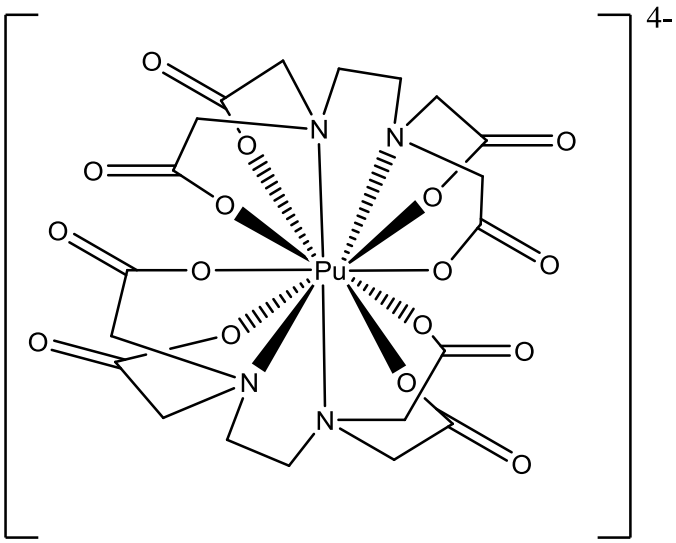

Figure 1.16: Structure of $[Pu(EDTA)_2]^{4-}_{(aq)}$.

Penta- and hexavalent actinide complexes with $EDTA^{4-}$ have been identified. It has been reported that at neutral pH and submicromolar plutonium concentrations, Pu^{V} and Pu^{VI} can exist in the presence of excess $EDTA^{4-}$ for weeks and are resistant to reduction.[45]

Table 1.15 presents stability constants for selected Ln^{III}, Pu^{III}, Am^{III}, Cm^{III}, Th^{IV} and Pu^{IV} $EDTA^{4-}$ species.

								Ionic Strength
La^{3+}	+	$EDTA^{4-}$	-	⇌	$[La(EDTA)]^-$	log β_{110}	14.5	0.5 M Na^+ salt
Ce^{3+}	+	$EDTA^{4-}$	-	⇌	$[Ce(EDTA)]^-$	log β_{110}	15.0	0.5 M Na^+ salt
Pr^{3+}	+	$EDTA^{4-}$	-	⇌	$[Pr(EDTA)]^-$	log β_{110}	15.4	0.5 M Na^+ salt
Nd^{3+}	+	$EDTA^{4-}$	-	⇌	$[Nd(EDTA)]^-$	log β_{110}	15.8	0.5 M Na^+ salt
Sm^{3+}	+	$EDTA^{4-}$	-	⇌	$[Sm(EDTA)]^-$	log β_{110}	16.2	0.5 M Na^+ salt
Eu^{3+}	+	$EDTA^{4-}$	-	⇌	$[Eu(EDTA)]^-$	log β_{110}	16.2	0.5 M Na^+ salt
Tb^{3+}	+	$EDTA^{4-}$	-	⇌	$[Tb(EDTA)]^-$	log β_{110}	16.6	0.5 M Na^+ salt
Ho^{3+}	+	$EDTA^{4-}$	-	⇌	$[Ho(EDTA)]^-$	log β_{110}	17.1	0.5 M Na^+ salt
Er^{3+}	+	$EDTA^{4-}$	-	⇌	$[Er(EDTA)]^-$	log β_{110}	17.5	0.5 M Na^+ salt
Yb^{3+}	+	$EDTA^{4-}$	-	⇌	$[Yb(EDTA)]^-$	log β_{110}	18.0	0.5 M Na^+ salt
Lu^{3+}	+	$EDTA^{4-}$	-	⇌	$[Lu(EDTA)]^-$	log β_{110}	18.2	0.5 M Na^+ salt
Am^{3+}	+	$EDTA^{4-}$	-	⇌	$[Am(EDTA)]^-$	log β_{110}	16.4	0.5 M Na^+ salt
Cm^{3+}	+	$EDTA^{4-}$	-	⇌	$[Cm(EDTA)]^-$	log β_{110}	16.7	0.5 M Na^+ salt
Th^{4+}	+	$EDTA^{4-}$	-	⇌	Th(EDTA)	log β_{110}	22.3	0.5 M Na^+ salt
Th^{4+}	+	$EDTA^{4-}$ +	OH^-	⇌	$[Th(EDTA)(OH)]^-$	log β_{11-1}	15.3	0.1 M electrolyte
Pu^{3+}	+	$EDTA^{4-}$	-	⇌	$[Pu(EDTA)]^-$	log β_{110}	16.0	1 M K^+ salt
Pu^{4+}	+	$EDTA^{4-}$	-	⇌	Pu(EDTA)	log β_{110}	26.4	1 M $NaClO_4$
Pu^{4+}	+	2 $EDTA^{4-}$	-	⇌	$[Pu(EDTA)_2]^{4-}$	log β_{120}	35.4	0.1 M $NaNO_3$
Pu^{4+}	+	$EDTA^{4-}$ +	OH^-	⇌	$[Pu(EDTA)(OH)]^-$	log β_{11-1}	22.0	0.1 M $NaNO_3$
Pu^{4+}	+	$EDTA^{4-}$ +	2 OH^-	⇌	$[Pu(EDTA)(OH)_2]^{2-}$	log B_{11-2}	15.3	0.1 M $NaNO_3$

Table 1.15: Stability constants for selected Ln^{III}, Am^{III}, Cm^{III}, Th^{IV} and $Pu^{III/IV}$-EDTA species.[37,83]

Diethylenetriamine pentaacetic acid (H_5DTPA, $C_{14}H_{23}O_{10}N_3$, Figure 1.17) is a ligand used in the TALSPEAK process.[28] It is an octadentate ligand with three nitrogen and five oxygen donor atoms. When $DTPA^{5-}$ is complexed to lanthanides and actinides, there are one to two coordination sites available for the binding of secondary ligands.[28]

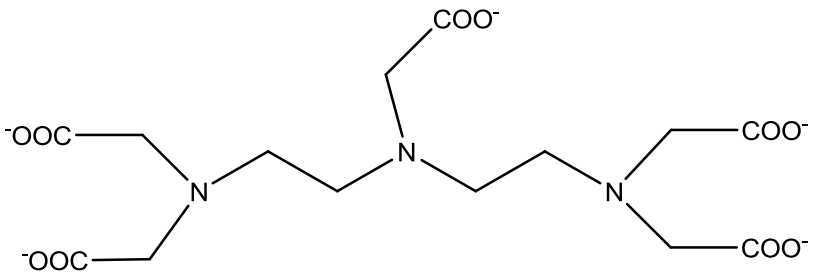

Figure 1.17: Diethylenetriamine pentaacetate ($DTPA^{5-}$).

The $DTPA^{5-}$ ligand can form stable metal complexes in acidic (equations 1.23 and 1.24) and alkaline (equations 1.25 and 1.26) solutions resulting in two species that are present in solution. Examples shown below are for trivalent metal ions.

$$M^{3+} + DTPA^{5-} + H^{+} \rightleftharpoons M(HDTPA)^{-}$$

(equation 1.23)[28]

$$\beta_{111} = \frac{[M(HDTPA)^{-}]}{[M^{3+}].[DTPA^{5-}].[H^{+}]}$$

(equation 1.24)[28]

$$M^{3+} + DTPA^{5-} \rightleftharpoons M(DTPA)^{2-}$$

(equation 1.25)[28]

$$\beta_{110} = \frac{[M(DTPA)^{2-}]}{[M^{3+}].[DTPA^{5-}]}$$

(equation 1.26)[28]

The same trend is observed in the stability constants between Ln^{III} and An^{III}-$DTPA^{5-}$ complexes, which is an increase in charge density causes an increase in the stability constant.[28] Table 1.16 presents stability constants for selected Ln^{III}, Am^{III} and Cm^{III}-$DTPA^{5-}$ species.

La^{3+}	+	$DTPA^{5-}$		-	$\rightleftharpoons$	$[La(DTPA)]^{2-}$	$\log \beta_{110}$	19.49
La^{3+}	+	$DTPA^{5-}$	+	H^{+}	$\rightleftharpoons$	$[La(HDTPA)]^{-}$	$\log \beta_{111}$	22.09
Eu^{3+}	+	$DTPA^{5-}$		-	$\rightleftharpoons$	$[Eu(DTPA)]^{2-}$	$\log \beta_{110}$	22.39
Eu^{3+}	+	$DTPA^{5-}$	+	H^{+}	$\rightleftharpoons$	$[Eu(HDTPA)]^{-}$	$\log \beta_{111}$	24.54
Tb^{3+}	+	$DTPA^{5-}$		-	$\rightleftharpoons$	$[Tb(DTPA)]^{2-}$	$\log \beta_{110}$	22.72
Tb^{3+}	+	$DTPA^{5-}$	+	H^{+}	$\rightleftharpoons$	$[Tb(HDTPA)]^{-}$	$\log \beta_{111}$	24.86
Lu^{3+}	+	$DTPA^{5-}$		-	$\rightleftharpoons$	$[Tb(DTPA)]^{2-}$	$\log \beta_{110}$	22.46
Lu^{3+}	+	$DTPA^{5-}$	+	H^{+}	$\rightleftharpoons$	$[Lu(HDTPA)]^{-}$	$\log \beta_{111}$	24.64
Am^{3+}	+	$DTPA^{5-}$		-	$\rightleftharpoons$	$[Am(DTPA)]^{2-}$	$\log \beta_{110}$	22.9
Am^{3+}	+	$DTPA^{5-}$	+	H^{+}	$\rightleftharpoons$	$[Am(HDTPA)]^{-}$	$\log \beta_{111}$	24.47
Cm^{3+}	+	$DTPA^{5-}$		-	$\rightleftharpoons$	$[Cm(DTPA)]^{2-}$	$\log \beta_{110}$	23.0
Cm^{3+}	+	$DTPA^{5-}$	+	H^{+}	$\rightleftharpoons$	$[Cm(HDTPA)]^{-}$	$\log \beta_{111}$	24.53

Table 1.16: Stability constants for selected Ln^{III}, Am^{III} and Cm^{III}-DTPA species at 0.1 M ionic strength.[28]

1.2.7 Lanthanide and Actinide Mixed Ligand Complexes

There are no solid state mixed ligand complexes of lanthanides or actinides with $EDTA^{4-}/CO_3^{2-}$ reported in the literature. In 1980, work done by Dumonceau *et al.*[85] reported the discovery of $[Ln(EDTA)(CO_3)]^{3-}_{(aq)}$ (Ln= Nd, Ho, Er and Y) species in solution, which were identified spectrophotometrically. There is no English translation of this work and there is some uncertainty as to whether there is still presence of the pure carbonate or pure $EDTA^{4-}$ metal species, *i.e.* $[Ln(CO_3)_4]^{5-}_{(aq)}$ and $[Ln(EDTA)]^{-}_{(aq)}$, respectively. The only actinide mixed ligand complexes to have been reported were by Boukhalfa *et al.*[83] in 2003. The ternary complexes (where ternary means a metal ion complexed by two different non-solvent ligands)[29] of $[Pu(EDTA)(CO_3)]^{2-}_{(aq)}$ and $[Pu(EDTA)(citrate)]^{3-}_{(aq)}$ were formed by the addition of one equivalent of carbonate or citrate to [Pu(EDTA)].[83] The carbonate and citrate anions displace any coordinated H_2O molecules from the Pu^{IV} inner coordination sphere. At near-

neutral pH, the $[Pu(EDTA)(CO_3)]^{2-}_{(aq)}$ species is present in more than 90 % of the reaction mixture.[83] Boukhalfa *et al.* do not report whether more than one CO_3^{2-} anion could complex to the [Pu(EDTA)] species (*i.e.* the formation of a $[Pu(EDTA)(CO_3)_2]^{4-}_{(aq)}$ complex).

Table 1.17 presents stability constants of mixed $EDTA^{4-}$-carbonate/citrate species of Pu^{IV}, determined by potentiometry.

Pu^{4+}	+	$EDTA^{4-}$		Citrate		-	$\rightleftharpoons$	$[Pu(EDTA)(citrate)]^{3-}$	$\log \beta_{1110}$	33.5
Pu^{4+}	+	$EDTA^{4-}$	+	Citrate	+	H^+	$\rightleftharpoons$	$[Pu(EDTAH)(citrate)]^{2-}$	$\log \beta_{1111}$	38.5
Pu^{4+}	+	$EDTA^{4-}$		CO_3^{2-}		-	$\rightleftharpoons$	$[Pu(EDTA)(CO_3)]^{2-}$	$\log \beta_{1110}$	35.5
Pu^{4+}	+	$EDTA^{4-}$	+	CO_3^{2-}	+	H^+	$\rightleftharpoons$	$[Pu(EDTAH)(CO_3)]^-$	$\log \beta_{1111}$	40.4

Table 1.17: Stability constants for Pu^{IV} in an $EDTA^{4-}$-carbonate/citrate mixed ligand system at 0.1 M $NaNO_3$ ionic strength.[83]

A variety of other ternary complexes have been reported in the literature for the lanthanides and actinides, where $EDTA^{4-}$ is the primary organic ligand. For example, Eu^{III}, Am^{III} and Cm^{III}-EDTA ternary complexes using malonate, succinate, glutarate, adipate, oxydiacetate and thiodiacetate as the secondary ligands have been shown to exist by Thakur *et al.*[86] It is interesting to note that they also report the complexation of two oxalate anions to Eu^{III}, Am^{III} and Cm^{III}-EDTA complexes.[86] Limaye *et al.*, have characterised an extensive variety of lanthanide-EDTA ternary complexes where malate, glycolate, salicylic acid, phthalate, catechol, resorcinol, glycine, α/β-alanine, valine, leucine, aspartate and thiomalic acid were used as the secondary ligand.[87]

Table 1.18 presents stability constants for ternary complexes of selected lanthanides and actinides.

					Ionic Strength
Eu^{3+} + $EDTA^{4-}$ + Citrate	$\rightleftharpoons$	$[Eu(EDTA)(citrate)]^{4-}$	$\log \beta_{111}$	20.9	6.6 M $NaClO_4$
Cm^{3+} + $EDTA^{4-}$ + Citrate	$\rightleftharpoons$	$[Cm(EDTA)(citrate)]^{4-}$	$\log \beta_{111}$	21.3	6.6 M $NaClO_4$
Eu^{3+} + $EDTA^{4-}$ + NTA	$\rightleftharpoons$	$[Eu(EDTA)(NTA)]^{4-}$	$\log \beta_{111}$	25.9	6.6 M $NaClO_4$
Pu^{3+} + $EDTA^{4-}$ + NTA	$\rightleftharpoons$	$[Pu(EDTA)(NTA)]^{4-}$	$\log \beta_{111}$	21.8	1 M KCl
Am^{3+} + $EDTA^{4-}$ + NTA	$\rightleftharpoons$	$[Am(EDTA)(NTA)]^{4-}$	$\log \beta_{111}$	25.9	6.6 M $NaClO_4$
Cm^{3+} + $EDTA^{4-}$ + NTA	$\rightleftharpoons$	$[Cm(EDTA)(NTA)]^{4-}$	$\log \beta_{111}$	25.7	6.6 M $NaClO_4$
Eu^{3+} + $EDTA^{4-}$ + HEDTA	$\rightleftharpoons$	$[Eu(EDTA)(HEDTA)]^{4-}$	$\log \beta_{111}$	19.6	1 M KCl
Pu^{3+} + $EDTA^{4-}$ + HEDTA	$\rightleftharpoons$	$[Pu(EDTA)(HEDTA)]^{4-}$	$\log \beta_{111}$	21.4	1 M KCl
Eu^{3+} + $EDTA^{4-}$ + IDA	$\rightleftharpoons$	$[Eu(EDTA)(IDA)]^{3-}$	$\log \beta_{111}$	21.6	0.1 M KNO_3
Pu^{3+} + $EDTA^{4-}$ + IDA	$\rightleftharpoons$	$[Pu(EDTA)(IDA)]^{3-}$	$\log \beta_{111}$	20.7	1 M KCl
Eu^{3+} + $EDTA^{4-}$ + oxalate	$\rightleftharpoons$	$[Eu(EDTA)(oxalate)]^{3-}$	$\log \beta_{111}$	20.2	6.6 M $NaClO_4$
Am^{3+} + $EDTA^{4-}$ + oxalate	$\rightleftharpoons$	$[Am(EDTA)(oxalate)]^{3-}$	$\log \beta_{111}$	20.4	6.6 M $NaClO_4$
Cm^{3+} + $EDTA^{4-}$ + oxalate	$\rightleftharpoons$	$[Cm(EDTA)(oxalate)]^{3-}$	$\log \beta_{111}$	20.4	6.6 M $NaClO_4$
Eu^{3+} + $EDTA^{4-}$ + 2 oxalate	$\rightleftharpoons$	$[Eu(EDTA)(oxalate)_2]^{5-}$	$\log \beta_{112}$	24.0	6.6 M $NaClO_4$
Am^{3+} + $EDTA^{4-}$ + 2 oxalate	$\rightleftharpoons$	$[Am(EDTA)(oxalate)_2]^{5-}$	$\log \beta_{112}$	24.2	6.6 M $NaClO_4$
Cm^{3+} + $EDTA^{4-}$ + 2 oxalate	$\rightleftharpoons$	$[Cm(EDTA)(oxalate)_2]^{5-}$	$\log \beta_{112}$	24.2	6.6 M $NaClO_4$

Table 1.18: Stability constants for selected lanthanide and actinide $EDTA^{4-}$ ternary complexes.[86,88]

Note: NTA = Nitrilotriacetic acid

HEDTA = N-(-hydroxyethyl)ethylenedinitrilotriacetic acid

IDA = Iminodiacetic acid

There are a few reported examples of lanthanide hydroxo complexes fixing CO_2 from the atmosphere. Andrews *et al.*[89] have crystallised a dodecanuclear hydroxo-bridged diphenylacetylacetate (Ph_2acac) La^{III} cluster, templated by CO_3^{2-} and phenylglyoxalate (Phgly), of formula $[La_{12}(OH)_{12}(H_2O)_4(Ph_2acac)_{18}(Phgly)_2(CO_3)_2]$. The structure is interesting because two carbonate anions are trapped in the middle of the La^{III} cage. Each carbonate anion is bound to six La^{III} centres, in both a chelating and bridging manner. Carbonate was not added to the reaction mixture, and so it has been suggested that lanthanide hydroxo

complexes are able to modify their structures to include carbonate.[89] When the reaction is conducted in a CO_2 free atmosphere and a carbonate source added, the dodecanuclear La^{III} cluster is not formed.[89] The fixation of atmospheric CO_2 into a lanthanum hydroxide complex has also been noted by Natrajan *et al*.[90] The $[[La(tpen)(\mu\text{-}OH)]_2(\mu\text{-}\eta^1\text{:}\eta^1OTf)]OTf_3.3MeCN$ complex binds atmospheric CO_2 immediately to form $[[La_6(tpen)_4(CH_3CN)_2(H_2O)_2(\mu_3\text{-}\eta^1\text{:}\eta^2\text{:}\eta^2CO_3)_4(\mu_3\text{-}\eta^1\text{:}\eta^1\text{:}\eta^2CO_3)_2][OTF_3]_6{\cdot}6CH_3CN$, where *tpen=N, N, N', N'-tetrakis(2-pyridyl-methyl)ethylenediamine* and OTf = trifluoromethanesulfonate.[90]

In 2010, Leggett *et al*. conducted an investigation probing for the formation of ternary $[Eu(DTPA)(lactate)]^{3-}$ complexes by UV-Vis and luminescence spectroscopy.[29] They reported that there was an insignificant amount of ternary complex formation for detection at around pH 4.[29] Choppin *et al*. have reported the formation of Eu^{III}, Am^{III} and Cm^{III}-DTPA-IDA ternary complexes.[91] It is thought that IDA is a sufficiently small enough ligand to fill the remainder of the coordination sphere of a metal ion complexed by $DTPA^{5-}$.[91] Figure 1.18 below illustrates the proposed structure of the $[Eu(DTPA)(IDA)]^{4-}_{(aq)}$ ternary complex and Table 1.19 shows the log β_{111} values for the corresponding Eu^{III}, Am^{III}, Cm^{III}-DTPA-IDA ternary complexes.

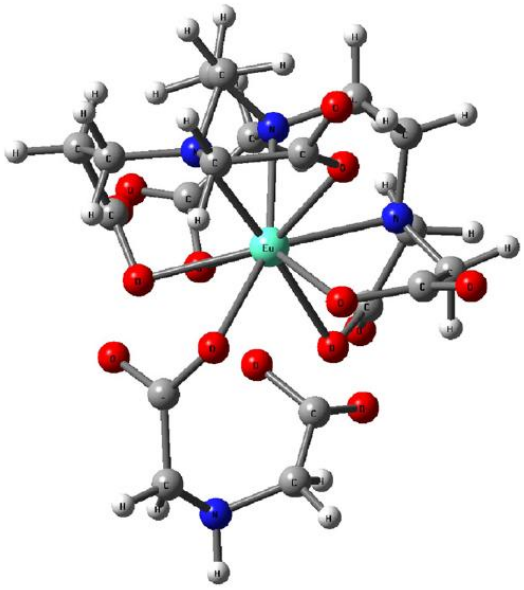

Figure 1.18: Proposed structure of $[Eu(DTPA)(IDA)]^{4-}$. [Taken from Reference 91].

Eu^{3+}	+	$DTPA^{5-}$	+	IDA	$\rightleftharpoons$	$[Eu(DTPA)(IDA)]^{4-}$	$\log \beta_{111}$	27.6
Am^{3+}	+	$DTPA^{5-}$	+	IDA	$\rightleftharpoons$	$[Am(DTPA)(IDA)]^{4-}$	$\log \beta_{111}$	28.0
Cm^{3+}	+	$DTPA^{5-}$	+	IDA	$\rightleftharpoons$	$[Cm(DTPA)(IDA)]^{4-}$	$\log \beta_{111}$	28.1

Table 1.19: Stability constants for Eu^{III}, Am^{III}, Cm^{III}-DTPA-IDA ternary complexes at 6.60 M $NaClO_4$ ionic strength.[91]

1.2.8 Lanthanide and Actinide Sorption to Surfaces

Inorganic oxides or hydroxides are a type of surface found in soils and sediments. When inorganic oxides come into contact with aqueous solution, the surface becomes hydrated.[46] On hydration, the layer of oxygen atoms defines the interface between the solid (or colloid) and the aqueous solution.[46] The arrangement of metal ions and oxides within the solid or colloidal structure and at the surface will be different for each material.[46] A bulk structure of an inorganic oxide can be considered consisting of metal ions (M), and oxides/hydroxides (O), where M will depend on which metal is present in the compound. For example, for brucite ($Mg(OH)_2$), M = Mg.[46]

The protons of the surface OH groups are acidic and may deprotonate:[46]

$$M\text{-}OH \rightleftharpoons M\text{-}O^- + H^+$$

(equation 1.27)

The oxygen atoms of the OH groups may bind protons: [46]

$$M\text{-}OH + H^+ \rightleftharpoons M\text{-}OH_2^+$$

(equation 1.28)

It is important to consider the pK_a values of different mineral surfaces as they can predict the surface speciation. The acid dissociation constants (K_a) for equations 1.27 and 1.28 above can be represented as:

$$K_{a_1} = \frac{[\text{M-O}^-][\text{H}^+]}{[\text{M-OH}]}$$

(equation 1.29)[46]

$$K_{a_2} = \frac{[\text{M-OH}][\text{H}^+]}{[\text{M-OH}_2^+]}$$

(equation 1.30)[46]

The pK_a values can be related to K_a by the following equation:

$$\text{p}K_a = -\log_{10} K_a$$

(equation 1.31)[31]

The pK_a values will vary for different surfaces, whilst the pH will affect the concentrations of M-OH, M-O^- and M-OH_2^+. At a certain pH, the concentrations of M-O^- and M-OH_2^+ will be equivalent, and so the surface charge will be neutral overall. This is the pH for the point of zero charge (pH_{pzc}).[46] When the pH is less than the pH_{pzc}, then the surface will be positively charged *i.e.* M-OH_2^+ is the dominant species. When the pH is greater than pH_{pzc}, then the surface will be negatively charged *i.e.* M-O^- is the dominant species. These negatively charged functional groups can bind metal ions.[46] There are a number of different coordination environments for metal ion binding, which depend on the surface, the charge of the surface and the metal ion.[46,92]

Brucite is the mineral form of magnesium hydroxide ($Mg(OH)_2$). It can be pearly white or pale green in colour (Figure 1.19).[93] It has a layered structure consisting of single sheets of charge-neutral $Mg(OH)_6$ octahedra (Figure 1.20),[93] and a pK_a of 9.24.[94]

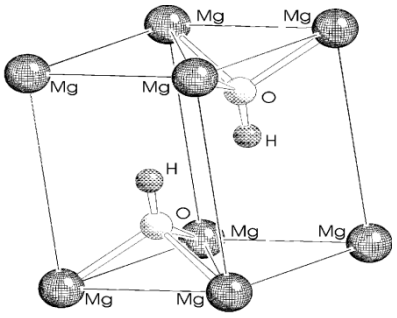

Figures 1.19 and 1.20: Picture of brucite and its chemical structure.
[Taken from References 95 and 96, respectively).

The nuclear waste storage ponds are at an alkaline pH of 11, and so the deprotonation of hydroxyl groups on the brucite surface would cause the surface to be negatively charged.[33] This means that surfaces possess effective binding sites for metal ions because the sorption of metal ions is influenced by the ionic interaction of cations with sorption sites and by sterics.[33] If carbonate has been incorporated into the brucite surface, then this will also provide a surface site for sorption.[33] Research has shown that the majority of actinide species will be adsorbed to mineral sediments because they have strong affinity for surface functional groups. For example, Farr *et al*. found that Pu^{IV} in contact with brucite results in the rapid and almost complete adsorption of Pu^{IV}, in the pH range 8-13.[97] Trivalent and tetravalent Pu is more likely to be adsorbed to mineral surfaces than $Pu^{V}O_2^{+}$ and $Pu^{VI}O_2^{2+}$ species, possibly due to the absence of the dioxo ligands.[33]

1.3 Modelling the Nuclear Waste Storage Ponds and TALSPEAK Process

The aims of this project are to help understand the solubility and stability of radioactive actinide species (*i.e.* Am^{III}, Cm^{III}, Pu^{IV}) in the nuclear waste storage ponds and also in the TALSPEAK process. In the pond scenario, this will entail observing radionuclide complexation by organic ligands (*e.g.* ethylenediamine tetraacetate ($EDTA^{4-}$)) and inorganic ligands (*e.g.* hydroxide and carbonate) in aqueous media. For the TALSPEAK process, this will include understanding lanthanide and actinide complexation by $DTPA^{5-}$ and lactate.

Essentially, this will involve the synthesis of mixed ligand (or ternary) complexes, *i.e.* a metal ion complexed by two different, non-solvent ligands.

Initially, the work will model the actinide ions using lanthanide ions. This is because the actinides are radioactive and so are more difficult to handle in the laboratory. The trivalent lanthanides are generally deemed to be good analogues of the trivalent actinides *e.g.* Am^{III}. The lanthanides can also be analysed using a variety of different spectroscopic techniques. Trivalent lanthanum (La) is not an *f* element but considered to be part of the lanthanoid series. It has the lowest charge density, and is also diamagnetic, which is advantageous when using Nuclear Magnetic Resonance (NMR) spectroscopy.[30] Trivalent Eu and Tb have useful luminescence properties, which can provide information on the number of ligand donor atoms bound to the metal ion, the number of residual waters in the inner coordination sphere and the number of species present. Trivalent Eu is paramagnetic, which can complicate NMR spectroscopy because the resonances are often paramagnetically shifted and broadened. Even though interpretation of NMR spectra can be difficult, NMR spectroscopy of Eu^{III} containing complexes can provide information on the structural characteristics of ligands bound to the metal ion.[33] Trivalent Nd, Ho and Er have absorption spectra that are sensitive to coordination.[30] The changes in the coordination of these lanthanides can be monitored by Ultraviolet-Visible (UV-Vis) spectroscopy. Trivalent Lu, the last element in the lanthanide series, has the smallest ionic charge and highest charge density.[30] It is a diamagnetic lanthanide ion, which like La^{III}, is advantageous for NMR spectroscopy. It is thought by observing the chemistries of the beginning, middle and end of the lanthanide series, then a general understanding of the coordination chemistry of the lanthanide series may be gained. Once knowledge has been gained on the lanthanide systems, it can be applied to actinide containing systems such as Am^{III} and Cm^{III}. Both trivalent Am and Cm have useful absorption and emission properties, which can be monitored to detect changes in coordination of these ions.[30] Luminescence techniques can be applied to both Am^{III} and Cm^{III} to determine the number of water molecules coordinated to the metal ions and also the lifetimes of the excited species in aqueous solution.

Tetravalent thorium could be a useful analogue for Pu^{IV}, as both metal ions have the same oxidation state. A benefit of using Th^{IV} is that the tetravalent state is the most stable state, so

experimental work is not complicated by controlling redox properties.[30] Complexation, and so hydrolysis, is weaker for Th^{IV} than Pu^{IV}, which is beneficial for understanding the solution behaviour of soluble An^{IV} species. There are no UV-Vis or luminescence spectroscopy handles for Th^{IV}, but its complexation with ligands can be studied by ^{1}H and ^{13}C NMR spectroscopy, and also potentiometry.[30]

1.3.1 Thesis Outline

Chapter 2 details the methods and instruments used to conduct the experiments.

Chapter 3 relates lanthanide behaviour to the nuclear waste pond scenario, which involves probing the solution behaviour of the lanthanides with $EDTA^{4-}$, in the presence and absence of carbonate, with spectroscopic techniques. The trivalent lanthanides are used as analogues for the trivalent actinides and so it is important to understand the behaviour of the lanthanides systems before experiments are performed on the radioactive actinides (Chapter 6).

Chapter 4 relates lanthanide behaviour to the TALSPEAK process, which includes the solution behaviour of the lanthanides with $DTPA^{5-}$ in the presence and absence of lactate. This chapter also probes the solution behaviour of the lanthanide-EDTA-lactate and lanthanide-DTPA-carbonate systems to observe how changing the denticity of the primary organic ligand around the metal ion may affect the coordination of the secondary ligand. The binary and ternary systems have been studied using the spectroscopic techniques of NMR and luminescence.

Chapter 5 describes the solution behaviour of Th^{IV} with $EDTA^{4-}$ and $DTPA^{5-}$ in the presence and absence of carbonate and lactate. Tetravalent thorium has a greater charge density than the trivalent lanthanides and actinides. Experiments in this chapter probe the effects of this increase in charge density with respect to the coordination of ligands.

Chapter 6 details the experiments performed using Am^{III} and Cm^{III} with $EDTA^{4-}$ in the presence and absence of carbonate. The binary and ternary systems have been studied using the techniques of UV-Vis and luminescence spectroscopies. The knowledge gained from probing the solution behaviour of these mixed $EDTA^{4-}/CO_3^{2-}$ ligand systems may contribute to an understanding of the chemistry within the nuclear waste ponds and allow for their efficient and safe decommissioning. This chapter also reports the Am^{III} solution behaviour

with $DTPA^{5-}$ in the presence and absence of lactate. This provides information on how the trivalent actinides may behave in the TALSPEAK process. The solution behaviour of the Am-EDTA-lactate, Am-DTPA-carbonate and Am-DO3A-carbonate/lactate systems has also been monitored by luminescence spectroscopy to observe how changing the denticity of the primary organic ligand around the metal ion may affect the coordination of the secondary ligand.

Chapter 7 concludes the work presented in this thesis and future experiments are proposed.

[1] H. Nifenecker, *Rep. Prog. Phys*., 2011, **74**, 12-28.

[2] M. Lenzen, *Energ. Convers. Manag.*, 2008, **49**, 2178-2199.

[3] J. Gray, S. Jones and A. Smith, *J. Radiol. Prot.*, 1995, **15**, 99-131.

[4] N. Baldwin, Remediating Sellafield, WM'03 Conference, Tucson, AZ, 2003.

[5] A. Pitois, P. Ivanov, L. Abrahamsen, N. Bryan, R. Taylor and H. Sims, *J. Environ. Monit.*, 2008, **10**, 315-324.

[6] P. Dore, *End of Alliance : Nuclear Engineering International*; Progressive Media Markets: UK, 2007, 20-21.

[7] *Calder Hall Power Station: The Engineer*; Centaur Media PLC: UK, 1956, 464.

[8] R. Cowan, *J. Econ. Hist.*, 1990, **3**, 541-567.

[9] Cumbrians Opposed to a Radioactive Environment, *Nuclear Transports in Britain: Feeding Sellafield's Pollution*; UK, 1999.

[10] P. Burrow and P. Fish, *Nuclear Fuel Elements;* Caplus, USA, 1998.

[11] C. Kirby, *Corros. Sci.*, 1987, **10**, 567-583.

[12] A. Leigh and N. Routledge, Fuel storage pond clean up, WM'07 Conference, Tucson, AZ, 2007.

[13] D. Albright, *Science and Global Security: Volume 5*, Gordon and Breach Science Publishers, Amsterdam, 1994, 89-97.

[14] D. Mason and A. Buchan, *BNFL Commercial*, 2007.

[15] H. Sims, *BNFL Commercial: Nexia Solutions*, 2005, **7**.

[16] D. Taylor, *Sci. Total Environ.*, 1989, **83**, 217-225.

[17] I. Fairlie, National Radiological Protection Board article, 2004, p. 14.

[18] H. El-Naggar, M. Ezz El-Din and R. Sheha, *J. Radioanal. Nucl. Ch.*, 2000, **246**, 493-504.

[19] E. Martell, Actinides in the Environment and their Uptake by Man, Atmospheric Quality and Modification Division, National Centre for Atmospheric Research, Technical Note, Boulder, Colorado, NCAR, 1975.

[20] M. Bunn, J. Holdren, S. Fetter and B. van der Zwaan, *Nucl. Technol.*, 2005, **150**, 209-230.

[21] L. Giusti, *Waste Manage.*, 2009, **29**, 2227-2239.

[22] J. Mathur, M. Murali and K. Nash, *Solvent Extr. Ion Exc.*, 2001, **19**, 357-390.

[23] F. Poineau, J. Du Mazaubrun, D. Ford, J. Fortner, J. Kropf, G. Silva, N. Smith, K. Long, G. Jarvinen and K. Czerwinski, *Radiochim. Acta*, 2008, **96**, 527-533.

[24] C. Gong, W. Lukens, F. Poineau and K. Czerwinski, *Inorg. Chem.*, 2008, **47**, 6674-6680.

[25] E. Horwitza, D. Kalinaa, H. Diamonda, G. Vandegrifta and W. Schulzb, *Solvent Extr. Ion Exc.*, 1985, **3**, 75-109.

[26] D. Serrano-Purroy, P.Baron, B. Christiansen, R. Malmbeck, C. Sorel and J. Glatz, *Radiochim. Acta*, 2005, **93**, 351-355.

[27] J. Law, S. Herbst, T. Todd, V. Romanovskiy, V. Babainb, V. Esimantovskiy, I. Smirnov and B. Zaitsev, *Solvent Extr. Ion Exc.*, 2001, **19**, 23-36.

[28] M. Nilsson and K. Nash, *Solvent Extr. Ion Exc.*, 2007, **25**, 665–701.

[29] C. Leggett, G. Liu and M. Jensen, *Solvent Extr. Ion Exc.*, 2010, **28**, 313-334.

[30] N. Kaltsoyannis and P. Scott, *The f elements*; Oxford University Press, USA, 1999, 1-67.

[31] C, Housecroft and A. Sharpe, *Inorganic Chemistry*, Second Edition, Pearson Education Ltd., UK, 2005, 741-761.

[32] W. Runde, *Los Alamos Sci.*, 2000, **26**, 392-411.

[33] G. Choppin, *J. Radioanal. Nucl. Ch.*, 2007, **273**, 695-703.

[34] P. Mohapatra and P. Khopkar, *Polyhedron*, 1989, **8**, 2071-2074.

[35] J. Kragten and L. Decnop-Weever, *Talanta*. 1987, **34**, 861-864.

[36] E. Bentouhami , G. Bouet, J. Meullemeestre , F. Vierling and M. Khan, *C. R. Chimie*, 2004, **7**, 537–545.

[37] R. Smith and A. Martell, *Critical Stability Constants*, Volumes 1 and 4: Inorganic Complexes, Plenum Press, New York, 1976.

[38] D. Clark, D. Hobart and M. Neu, *Chem. Rev.* 1995, **95**, 25-48.

[39] A. Pershin and T, Sapozhnikova, *J. Radioanal. Nucl. Ch.*, 1990, **143**, 455-462.

[40] B. Allard, H. Kipatsi and J. Liljenzin, *J. Inorg. Nucl. Chem.*, 1980, **42**, 1015-1027.

[41] V. Neck and J. Kim, *Radiochim. Acta*, 2001, **89**, 1-16.

[42] C. Ekberg, Y. Albinsson, M.Comarmond and P. Brown, *J. Solution Chem.*, 2000, **29**, 63-86.

[43] N. O' Boyle, G. Nicholson, T. Piper, D. Taylor, D. Williams and G.Williams, *Appl. Radiat. Isot.*,1997, **48**, 183-200.

[44] G. Choppin, A. Bond and P. Hromadka, *J. Radioanal. Nucl. Ch.*, 1997, **219**, 203-210.

[45] L. Morss, D. Clark, S. Hecker, G. Jarvinen and M. Neu, *The Chemistry of the Actinide and Transactinide Elements*, 3rd Edition, Wiley, New York, 2006, 813-2103.

[46] D.J. Shaw, *Colloid and Surface Chemistry*, Elsevier science, UK, 4th ed., 1992.

[47] J. Rothe, C. Walther, M. Denecke and T. Fanghanel, *Inorg. Chem.*, 2004, **43**, 4708-4718.

[48] K. Orlandini, W. Penrose and D. Nelson, *Mar. Chem.*, 1986, **18**, 49-57.

[49] S. Reilly, W. Runde and M. Neu, *Geochim. Cosmochim. Ac.*, 2007, **71**, 2672–2679.

[50] K. Cantrell, *Polyhedron*, 1988, **7**, 573-574.

[51] I. Grenthe, P. Robouch and P. Vitorge, *J. Less-Common Met.*, 1986, **122**, 225–231.

[52] F. Firsching and J. Mohammadzadel, *J. Chem. Eng. Data*, 1986, **31**, 40-42.

[53] N. Yanagihara, K. Vemulapalli, Q. Fernando and J. Dyke, *J. Less-Common Met.*, 1991, **167**, 223-232.

[54] T. Tahara, I. Nakai, R. Miyawaki and S. Matsubara, *Z. Kristallogr.*, 2007, **222**, 326–334.

[55] M. Wickleder, *Chem. Rev.*, 2002, **102**, 2011-2087.

[56] G. Goff, M. Cisneros, C. Kluk, K. Williamson, B. Scott, S. Reilly and W. Runde, *Inorg. Chem.*, 2010, **49**, 6558–6564.

[57] D. Clark, R. Donohoe, J. Gordon, P. Gordon, D. Keogh, B. Scott, C. Tait and J. Watkin, *Dalton Trans.*, 2000, 1975–1977.

[58] D. Bond, D. Clark, R. Donohoe, J. Gordon, P. Gordon, D. Keogh, B. Scott, C. Tait and J. Watkin, *Inorg. Chem.*, 2000, **39**, 3934-3937.

[59] S. Voliotis and A. Rimsky, *Acta Cryst.,* 1975, **B31**, 2620.

[60] D. Nelson, K. Orlandini and W. Penrose, *J. Environ. Radioactiv.,* 1989, **9**, 189-198.

[61] P. Hagan, J. Navratil and R. Cichorz, *J. Inorg. Nucl. Chem.,* 1981, **43**, 1054-1055.

[62] K. Ueno and M. Hoshi, *J. Inorg. Nucl. Chem*., 1970, **32**, 3817 - 3822.

[63] D. Clark, S. Conradson, D. Keogh, P. Palmer, B. Scott and C. Tait, *Inorg. Chem.,* 1998, **37**, 2893-2899.

[64] E. Östhols, J. Bruno and I. Grenthe, *Geochim. Cosmochim. Ac.*, 1994, **58**, 613-623.

[65] R. Anderson, M. Bacon and P. Brewer, *Science*, 1982, **216**, 514-516.

[66] P. Robouch and P. Vitorge, *Inorg. Chim. Acta.,* 1987, **140**, 239-242.

[67] P. Warwick, *Environmental Radiochemical Analysis II*, Royal Society of Chemistry, UK, 2003, 230.

[68] E. M. Thurman, *Organic Chemistry of Natural Waters*, Martinus Nijhoff/Junk Publishers, Dordrecht, 1985.

[69] F. J. Stevenson, *Humus Chemistry: Genesis, Composition, Reactions*, Wiley, New York, 1994.

[70] E. M. Peña-Méndez, J. Havel and J. Patočka, *J. Appl. Biomed.,* 2005, **3**, 24.

[71] M. Schnitzer, *Humic Substances in the Environment,* Marcel Dekker, Inc, New York, 1972.

[72] E. Tombàcz, *Soil Sci.,* 1999, **164**, 814.

[73] M. Schnitzer and J. G. Desjardins, *Soil Sci. Soc. Amer. Proc.,* 1962, **26**, 362.

[74] S. Oden, *Zur Kolloidchemie der Humusstoffe. Kolloid Z.*, 1914, **14**, 123-130.

[75] R.S. Swift, *Organic Matter Characterisation: Methods of Soil Analysis part 3*, Soil Science of America, WI, 1996.

[76] F. Stevenson, *Humus Chemistry: Genesis, Composition, Reactions,* Wiley, New York, 1982.

[77] G. Ogner and M. Schnitzer, *Can. J. Chem.,* 1971, **49**, 2302.

[78] H. Kodama and M. Schnitzer, *Fuel,* 1967, **46**, 87.

[79] For the model structure of humic acid obtained October 2007:
www.humintech.com

[80] M. Skinner and S.I.M. Skinner, *Soil Sci.,* 1965, **99**, 278.

[81] D. Rai D. Moore, K. Rosso, A. Felmy and H Bolton, *J. Solution Chem.*, 2008, **37**, 957–986.

[82] G. Kauffman, *Coordination Chemistry: A Century of Progress*, American Chemical Society, 1994, 346-358.

[83] H. Boukhalfa, S. Reilly, W. Smith and M. Neu, *Inorg. Chem.*, 2004, **43**, 5816-5823.

[84] M. Meyer, R. Burgat, S. Faure, B. Batifol, J.-C. Hubinois, H. Chollet and R. Guilard, *C. R. Chimie*, 2007, **10**, 929-947.

[85] J. Dumonceau, S. Bigot, M. Treuil, J. Faucherre and F. Fromage, *Rev. Chim. Minér.*, 1980, **17**, 58-64.

[86] P. Thakur, P. Pathak, T. Gedris and G. Choppin, *J. Solution Chem.*, 2009, **38**, 265-287.

[87] S, Limaye and M. Saxena, *Can. J. Chem.*, 1986, **64**, 865-870.

[88] G. Choppin , P. Thakur and J. Mathur, *Coord. Chem. Rev.*, 2006, **250**, 936–947.

[89] P. Andrews, T. Beck, C. Forsyth, B. Fraser, P. Junk, M. Massi and P. Roesky, *Dalton Trans*., 2007, **48**, 5651-5654.

[90] L. Natrajan, J. Pecaut and M. Mazzanti, *Dalton Trans*., 2006, **8**, 1002-1005.

[91] G. Choppin, P. Thakur and J, Mathur, *C. R. Chimie*, 2007, **10**, 916-928.

[92] O. Pokrovsky, J. Schott and A. Castillo, *Geochim. Cosmochim. Ac.*, 2005, **69**, 905–918.

[93] J. Wang and J. Rustad, *Geochim. Cosmochim. Ac.*, 2006, **70**, 562–582.

[94] J. Parks, Sorption of Boron and Chromium onto solids of environmental significance: implications for sampling and removal in water treatment, *Ph.D Thesis*, submitted to the Faculty of the Virginia Polytechnic Institute and State University, 2005.

[95] Picture of brucite obtained in October 2007 and taken from:
http://www.geology.neab.net/pictures/rock227.jpg

[96] Structure of brucite obtained in October 2007 and taken from:
http://www.cryst.bbk.ac.uk/PPS2/projects/loesel/brucit8.gif

[97] J. Farr, R. Schulze and B. Honeymann, *Radiochim. Acta*, 2000, **88**, 675-679.

Chapter 2

Experimental

2.1 Chemical Reagents

De-ionised 18 MΩ water was used for preparing aqueous solutions in all experimental procedures. The solutions used for the calibration of the pH meters were pH 4.00 (±0.01), 7.00 (± 0.01) and 10.00 (± 0.01) standard buffers (Fisher Scientific).

2.1.1 Trivalent Lanthanide Nitrate Stock Solutions

Stock solutions of lanthanide ions to be studied (*i.e.* La, Ce, Pr, Nd, Sm, Eu, Tb, Ho, Er, Yb and Lu) were prepared by dissolution of the corresponding lanthanide nitrate salts (all 99.99 %, Sigma Aldrich) in de-ionised water. Typical volumes and concentrations of the lanthanide nitrate stock solutions were 5.00 to 100 mL and 0.10 to 1.0 M, respectively.

2.1.2 Ligand Stock Solutions

Na_2H_2EDTA (BDH Chemical), H_5DTPA (Sigma Aldrich), Na_2CO_3, $NaHCO_3$ (Fisher Scientific) and sodium L-lactate (Sigma Aldrich) were used without further purification.
Stock solutions of these ligands were prepared by dissolution of the corresponding ligand in de-ionised water. Typical volumes and concentrations of the ligand solutions were 5.00 to 100 mL and 0.10 to 1.0 M, respectively.

2.1.3 Trivalent Lanthanide Nitrate Secondary Stock Solutions

Lanthanide nitrate secondary stock solutions were made by dilution of the corresponding lanthanide nitrate stock solution. The ionic strength of the solutions were corrected to 0.5 M ionic strength, with sodium nitrate, using the following equation:

$$I = \frac{1}{2}\sum_{i=1}^{n} mz^2$$

(equation 2.1)

Note:- I= ionic strength; *m* = molarity; *z* = charge.

Typical volumes and concentrations of the lanthanide nitrate secondary stock solutions were 3.00 to 20.0 mL and 5.00 to 50.0 mM, respectively.

2.1.4 Ligand Secondary Stock Solutions

Secondary stock solutions of the ligands were made by dilution of the corresponding ligand stock solution. The ionic strength was adjusted with sodium nitrate to 0.5 M. Typical volumes and concentrations of the ligand secondary stock solutions were 3.00 to 20.0 mL and 5.00 to 50.0 mM, respectively.

2.1.5 Trivalent Lanthanide–EDTA/DTPA Binary System Solutions

Experimental solutions of the desired 1:1 lanthanide to multidentate ligand (*i.e.* $EDTA^{4-}$ or $DTPA^{5-}$) ratio were made by mixing of the corresponding lanthanide and ligand secondary stock solutions. Typical volumes and concentrations of lanthanide–EDTA/DTPA experimental solutions were 3.00 to 20.0 mL and 5.00 to 25.0 mM, respectively.

2.1.6 Trivalent Lanthanide-EDTA/DTPA-$NaHCO_3$/Na_2CO_3/Lactate Ternary System Solutions

Experimental solutions of the desired lanthanide to multidentate ligand (*i.e.* $EDTA^{4-}$ or $DTPA^{5-}$) to secondary ligand (*i.e.* carbonate or lactate) ratio were made by mixing of the corresponding lanthanide, multidentate ligand and secondary ligand secondary stock solutions. Solutions that contained $NaHCO_3$ or Na_2CO_3 as the secondary ligand were adjusted to approximately pH 7 with NaOH before the addition of carbonate anions. This was done in order to minimise the conversion of carbonate anions to $CO_{2(aq)}$ in acidic conditions. Typical

volumes of lanthanide-$EDTA^{4-}$/$DTPA^{5-}$-carbonate/lactate experimental solutions were 3.00 to 20.0 mL. These experimental solutions had known lanthanide and multidentate ligand concentrations ranging from 5.00 to 10.0 mM, and known secondary ligand concentrations ranging from 5.00 to 30.0 mM.

The solutions detailed above were analysed by the techniques of UV-Vis spectroscopy and potentiometry.

2.1.7 Nuclear Magnetic Resonance (NMR) Solutions

Experimental solutions for analysis by NMR spectroscopy were prepared as above in sections 2.1.1 to 2.1.4 except lanthanide chloride salts ($LaCl_3$, $EuCl_3$, $LuCl_3$, 99.9 %, Sigma Aldrich) were used and deuterium oxide (D_2O, 99.92 atom % D, Sigma Aldrich) was used as the solvent. NMR spectroscopic titrations of thorium nitrate ($Th(NO_3)_4.6H_2O$, BDH chemicals) were also measured. The ionic strength was not controlled. Typical volumes of NMR experimental solutions were 2.00 to 3.00 mL, of which a 0.7 mL sample was used in a 5 mm glass NMR tube for analysis.

Solutions of sodium deuteroxide (NaOD, 40 wt % solution in D_2O, 99.5 atom % D) and deuterium chloride (DCl, 35 wt % solution in D_2O, 99 atom % D) were used to adjust pD. These solutions had concentrations ranging from 50 mM to 5.00 M.

NMR experiments were performed in deuterium solvents, and so the deuterium ion was substituted for the hydrogen ion in calculations of pH. The value of pD was calculated using equation 2.2:

$$pD = pH + 0.40$$

(equation 2.2)[1]

Note:-

pD = $-\log_{10}$(deuterium ion concentration)

pH is the meter reading from a calibrated pH electrode

This equation accounts for the activity coefficient difference between the different isotopes of the hydrogen ion.

The sodium salt of 3-(trimethylsilyl)-1-propanesulfonic acid (DSS, 97%, Sigma Aldrich) was added to each ^{1}H-NMR sample as an internal chemical shift reference, using the methyl signal (δ_H 0.00 ppm). 1,4-dioxane (Sigma Aldrich) was used as a ^{13}C peak position reference (δ_C 67.19 ppm) for solutions analysed by ^{13}C-NMR spectroscopy.

Carbon-13 labelled $Na_2{}^{13}CO_3$ (99 atom % ^{13}C), $NaH^{13}CO_3$ (98 atom % ^{13}C) and 3-^{13}C-sodium L-lactate (Sigma Aldrich) were used to intensify the ^{13}C-NMR signals of these species.

2.1.8 Standardised Potentiometric Titration Solutions

2.1.8.1 Sodium Hydroxide (NaOH) Standard Solution

A 0.1 M NaOH stock solution was prepared by dilution of a 50 % NaOH standard solution (Sigma Aldrich) to 500 mL with de-ionised water. The ionic strength of this solution was adjusted to 0.5 M with $NaNO_3$. The NaOH solution was standardised by titration with potassium hydrogen phthalate (A.C.S. acidimetric standard, Sigma Aldrich) that had been dried at 70 °C in an oven for over a week.

2.1.8.2 Nitric Acid Standard Solution

A 0.1 M nitric acid stock solution was made from concentrated nitric acid by dilution with de-ionised water. The nitric acid stock solutions were standardised by titration with the standardised sodium hydroxide solution (described above).

2.1.9 pH Electrode Calibration for Potentiometry

The electrode used for acid dissociation constant and stability constant determinations was calibrated by the Gran titration method using a standardised nitric acid solution with a standardised sodium hydroxide solution.[2] The concentration of the hydrogen ion (H^+) was calculated for each titrant addition from the concentrations and volumes of the acid and base solutions, the total volume of the solution and using K_w equal to 13.7.[3] The electrode milliVolt

(mV) readings were plotted against the calculated $-\log_{10}[H^+]$ values, and the straight line of best fit was determined using Microsoft Excel 2007.

The data points between the calculated pH region of 4.5 to 9.5 were excluded from the linear fit of calibration titrations, as is the standard practice.[4] Data in this pH range is excluded because small errors in the concentrations and volumes of reagents could have large effects on the electrode reading. All of the linear fits of the acid-base calibrations had correlation coefficients greater than 0.99. The linear fit from electrode calibration titrations was used to calculate the pH from the electromotive force (EMF, in mV) in titrations of the ligands and the metal-ligand complexes using the equation:

$$pH = (g \times mV) + c$$

(equation 2.3)

where g = gradient of linear fit

c = the y intercept of the linear fit

2.1.10 Trivalent Lanthanide-EDTA Binary System Solutions for Potentiometric Titration

Lanthanide-EDTA solutions for potentiometric titration had a lanthanide and $EDTA^{4-}$ concentration of 5.00 mM and a total volume of 20.0 mL. All solutions were maintained at 0.5 M ionic strength. All lanthanide-EDTA solutions were titrated from acidic to alkaline pH, using standardised 0.1 M NaOH as the titrant. The titrant was added at a rate of 0.01 mL every 45 s.

2.1.11 Trivalent Lanthanide-EDTA-Carbonate Ternary System Solutions for Potentiometric Titration

The lanthanide-EDTA-carbonate solutions for titration were prepared by forming the lanthanide-EDTA complex at alkaline pH (using NaOH to adjust the pH to approximately pH 12), and then adding the sodium bicarbonate to this alkaline solution. This was done in order to minimise the conversion of carbonate anions to $CO_{2(aq)}$, which would happen if carbonate was added to an acidic lanthanide-EDTA solution. All lanthanide-EDTA-carbonate solutions

had a lanthanide, $EDTA^{4-}$ and carbonate concentration of 5.00 mM and a total volume of 20.0 mL. All solutions were maintained at 0.5 M ionic strength. All lanthanide-EDTA-carbonate solutions were titrated from alkaline to acidic pH using standardised 0.1 M HNO_3 as the titrant. The titrant was added at a rate of 0.01 mL every 45 s.

2.1.12 Trivalent Lanthanide Ultraviolet-Visible (UV-Vis) Spectroscopy Solutions

Lanthanide-EDTA binary system and lanthanide-EDTA-carbonate ternary system solutions for analysis by UV-Vis Spectroscopy had a total volume of 3.00 mL and a concentration of all reagents in solution of 5.00 mM. UV-Vis spectroscopic titrations were conducted in H_2O with a constant ionic strength of 0.5 M $NaNO_3$. NaOH and HNO_3 were used for pH adjustment.

2.1.13 Trivalent Lanthanide Luminescence Solutions

Experimental solutions for analysis by luminescence spectroscopy were prepared as above in sections 2.1.1 to 2.1.4 except lanthanide chloride salts ($LaCl_3$, $EuCl_3$, $LuCl_3$, 99.9 %, Sigma Aldrich) were used.

Lanthanide-EDTA/DTPA binary system and lanthanide-EDTA/DTPA-carbonate/lactate ternary system solutions for analysis had a total volume of 3.00 mL and a concentration of all reagents in solution of 10.0 mM. Luminescence spectroscopic titrations were conducted in H_2O and D_2O in order to calculate the number of water molecules (N_{H_2O}) bound to an excited metal ion species. NaOH, HCl, NaOD and DCl were used for pH and pD adjustment. The ionic strength was not controlled.

2.1.14 Trivalent 243-Americium and 248-Curium UV-Vis Spectroscopy Solutions

Experimental solutions of Am^{III} and Cm^{III} were prepared from stock solutions of $Am(NO_3)_3$ and $Cm(NO_3)_3$. The stock solutions had been analysed by Inductively Coupled Plasma-Mass Spectrometry (ICP-MS) to obtain a ^{243}Am concentration of 20.0 mM and ^{248}Cm concentration of 0.67 mM. Americium-EDTA binary system and americium-EDTA-carbonate ternary system solutions for analysis had a total volume of 10.0 mL and a concentration of all

reagents in solution of around 5 x 10^{-5} M. Curium-EDTA binary system and curium-EDTA-carbonate ternary system solutions for analysis had a total volume of 10.0 mL and a concentration of all reagents in solution of around 2 x 10^{-5} M. UV-Vis spectroscopic titrations were conducted in H_2O with a constant ionic strength of 0.5 M $NaNO_3$. NaOH and HNO_3 were used for pH adjustment.

2.1.15 Trivalent 243-Americium Time Resolved Laser Induced Fluorescence Spectroscopy (TRLIFS) Solutions

Experimental solutions of $^{243}Am(NO_3)_3$ were prepared from a 3.54 MBq/mL $^{243}AmCl_3$ stock solution. Converting from the chloride salt to the nitrate salt of Am^{III} was done by diluting the $AmCl_3$ stock solution in H_2O and evaporating to incipient dryness using an infra-red (IR) lamp. This was performed three times before diluting the Am^{III} containing residue in 0.5 M $NaNO_3$ solution. The $^{243}Am^{III}$ concentration of the $Am(NO_3)_3$ solution was measured by gamma spectroscopy. Americium-EDTA binary system and americium-EDTA-carbonate ternary system solutions for analysis had a total volume of 5.00 mL and a concentration of all reagents in solution of approximately 0.4 mM. Luminescence spectroscopic titrations were conducted in H_2O with a constant ionic strength of 0.5 M $NaNO_3$. NaOH and HNO_3 were used for pH adjustment.

2.2 Instruments

NMR measurements were carried out using a Bruker Ultrashield™ 400 spectrometer of operating frequency 400 MHz (^1H) and 101 MHz (^{13}C), with a variable temperature unit set at 295 K, unless otherwise stated. The NMR instrument was controlled remotely using Bruker Topspin 2.1 software. Samples for analysis were pipetted into 5 mm thin wall, 8" length NMR tubes manufactured by Wilmad Lab Glass. ^1H-NMR spectra were collected for 16 scans. ^{13}C-NMR spectra were collected for 128 scans when using ^{13}C labelled sodium carbonate or sodium bicarbonate, 200 scans when using ^{13}C-sodium L-lactate and 1024 scans when using non-^{13}C labelled chemicals. The pD of NMR solutions were measured using a Mini Lab ISFET pH meter Model IQ120 calibrated using pH 7.0 IQ Scientific Instruments Buffer.

Potentiometric titrations were conducted at Idaho National Laboratory on a Mettler Toledo automated burette. Electromotive force (EMF) in mVs was measured with a Metrohm pH meter (Model 713) and a Ross combination pH electrode (Orion Model 8102). The original electrode filling solution (3.0 M KCl) was replaced with 5.0 M NaCl. The potentiometric apparatus consists of a glass cell with a lid. The cell is water-jacketed so that the cell temperature can be maintained at 298 K by water circulating from a constant temperature bath. Continuous stirring throughout the titration is enabled using a Mettler Toledo stirring attachment. All titrations were measured within a nitrogen environment. The apparatus is controlled remotely using Mettler Toledo LabX software. Potentiometric data were analysed using Hyperquad 2006 software.

UV-Vis spectroscopic titrations of Pr^{III}, Nd^{III} and Ho^{III} were conducted at Idaho National Laboratory using a Varian Cary-6000i spectrophotometer equipped with sample holders. Quartz cells of 10 mm pathlength were used.

Steady-state and time-resolved luminescence properties of Eu^{III} and Tb^{III} systems were conducted at Oxford University and were determined using a Perkin-Elmer-LS55 fluorimeter operating in phosphorescence mode. The Eu^{III} and Tb^{III} ions were excited at 397 and 366 nm, respectively. The excitation and emission slit were set to 10 nm, and the gate delay time was fixed to 10 ms increments.

UV-Vis absorption spectra of $^{243}Am^{III}$ and $^{248}Cm^{III}$ were conducted at Idaho National Laboratory using a Liquid Waveguide Capillary Cell (LWCC) (Figure 2.1). The cell had an internal volume of 2 mL, a 1 m pathlength and an effective wavelength range of approximately 300-850 nm. The LWCC was coupled to a Varian Cary 6000i spectrophotometer.

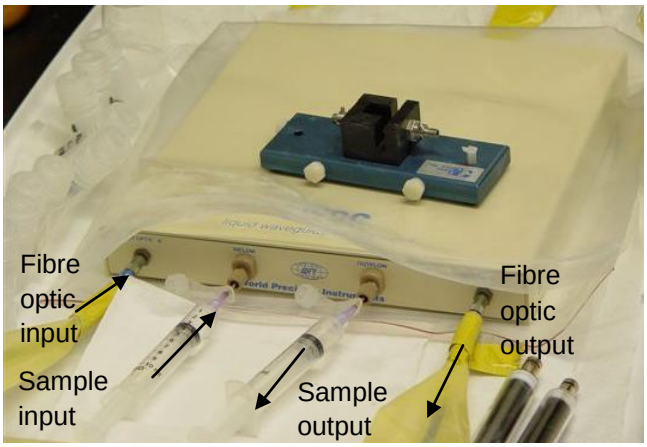

Figure 2.1: Set-up of the Liquid Waveguide Capillary Cell.

Luminescence spectroscopic titrations of $^{243}Am^{III}$ complexes were conducted at National Nuclear Laboratory, Sellafield, Cumbria. A Brilliant B Quantel Nd:YAG laser, which gave an output of 1064 nm, was used to optically pump the TDL90 dye laser after passing through a second harmonic generator (output 532 nm) and third harmonic generator (355 nm). The dye laser was tuned to produce the desired excitation wavelength of 503 nm for $^{243}Am^{III}$ (Figure 2.2). Fibre optics were used to focus the emitted light onto a Micro Channel Plate (MCP), which amplifies the photons before being detected on a Charged Coupled Device (CCD, Acro Spectra Pro 2500i Spectrograph; 0.500 m Imaging Triple Grating Monochromator). A Programming Time Generator (Princeton Instruments) was used to determine the delay width. Data were collected within a gate width of 70 to 120 ns, with a 5.55 ns delay width.

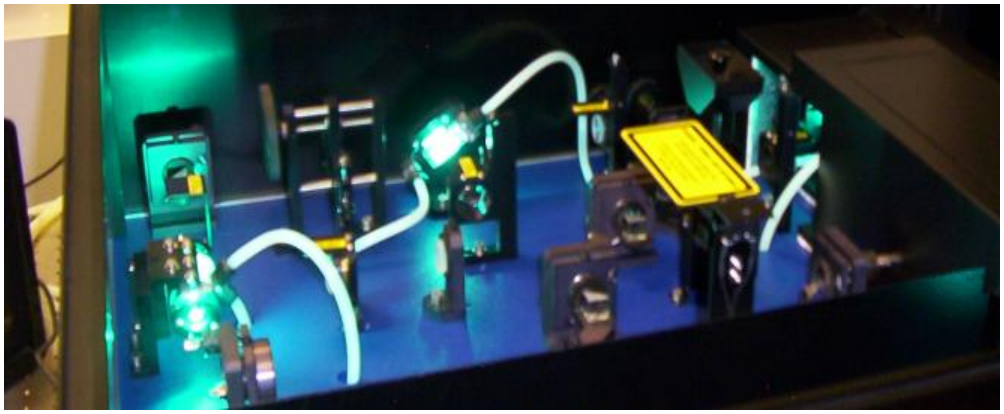

Figure 2.2: Pulsed dye laser set-up.

The instrument was controlled remotely using Winspec software. Data were processed using Grams/AI software and analysed by linear regression on Microsoft Excel 2007. A daily mercury/argon (HgAr) wavelength calibration was performed before Am^{III} measurements were recorded. For maximum power output of the laser, the dye had to be changed weekly. This was done by making a stock dye solution (Fig 2.3) of Coumarin 500 dye (0.5 g) in ethanol (200 mL). The oscillator and amplifier reservoirs were filled with ethanol (750 mL), and the stock dye solution was added to reach maximum power output (approximately 20.0 mL stock dye solution in the amplifier reservoir and 30.0 mL stock dye solution in the oscillator reservoir).

Figure 2.3: Coumarin 500 dye used for the dye laser.

The $^{243}Am^{III}$ containing samples were introduced into the cuvette using a flow system. The sample was prepared in a custom made test-tube, with a four-way head attachment (Figure 2.4). This attachment held the tubes, which pumped the sample around the system.

Figure 2.4: $^{243}Am^{III}$ sample preparation in custom made test tube. The right hand side tube pumped the sample out of the test tube, and the left hand side tube pumped the sample back into the test tube.

The sample was pumped into the flow cell, where the $^{243}Am^{III}$ is excited at 503 nm (Figure 2.5). The lens focuses the emitted light into the fibre optic cables. A pH electrode was also fitted into the flow circuit to allow pH measurements to be taken.

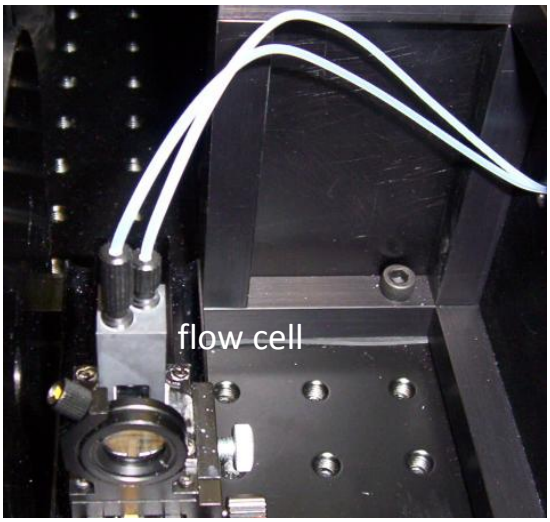

Figure 2.5: Flow cell for $^{243}Am^{III}$ luminescence.

Gamma (γ) Spectroscopy was used at National Nuclear Laboratory, Sellafield to determine the $^{243}Am^{III}$ concentration in prepared samples. A γ-energy spectrum can be produced, which is characteristic of the γ-emitting nuclides in the substance.[5] The detector used was a germanium (Ge) semi-conductor detector (Detector Systems GmbH), which must be cooled to liquid nitrogen temperature (77.4 K) at all times. The instrument was controlled remotely and analysed using Gamma Vision software.

Crystallographic data were collected on a Bruker APEX platform CCD area detector diffractometer. Crystals were cooled to 100 K and were irradiated using Mo-Kα radiation (λ = 0.71071 Å). Data was collected with 20 second frame exposures. The structures were solved by direct methods using SHELXS, and refined using SHELXL software. Hydrogen atoms were included in calculated positions.

Speciation models across the pH range 0 to 14 were calculated using critically selected stability constants for metal ion complexation from Martell and Smith.[6] The calculations were

performed using the speciation programme *JCHESS*[7] and ionic strength corrections were made using the truncated Davies equation.[7]

Accurate volumes were measured using calibrated Fisher Brand Transferpette® S or Eppendorf mechanical pipettes.

[1] R. G. Bates. *Determination of pH: Theory and Practice*, Wiley, New York, 1954.

[2] G. Gran, *Analyst*, 1952, **77**, 661.

[3] H. Boukhalfa, S. Reilly, W. Smith and M. Neu, *Inorg. Chem.*, 2004, **43**, 5816-5823.

[4] A. E. Martell and R. J. Motekaitis, *Determination and Use of Critical Stability Constants*, Wiley, New York, 1992.

[5] R.E. Lapp and H.L. Andrews, *Nuclear Radiation Physics*, Prentice-Hall, Englewood Cliffs, NJ, 1972, 50-54.

[6] R. Smith and A. Martell, *Critical Stability Constants*, Volumes 1 and 4: Inorganic Complexes, Plenum Press, New York, 1976.

[7] J. Van der Lee, A Users Guide to CHESS, Another Speciation and Surface Complexation Computer Code, E´cole des Mi1nes de Paris, Fontainebleau, 1998.

Chapter 3

Lanthanide-EDTA Binary Systems and Lanthanide-EDTA-Carbonate Ternary Systems

3.0 Introduction

As previously mentioned in Section 1.3, one of the aims of this project is to help understand the solubility and stability of radioactive species (*i.e.* Am^{III}, Cm^{III}) in the nuclear waste storage ponds. The chemistry of metal ions in the waste ponds is complicated because they can be coordinated by both organic and inorganic ligands.

Initial work has focused on modelling the pond scenario using the trivalent lanthanide ions as analogues for the trivalent actinides. This is because there is no radiotoxicity associated with the lanthanides, and so they are easier to handle in a laboratory. Organic ligands (*i.e.* humic substances), which are produced from the decomposition of plant and animal matter, are present in the ponds. Humic substances are molecularly heterogeneous,[1] which means that no two metal ion complexes containing humic substances would be identical. The heterogeneous nature of humic substances would complicate the spectroscopic analysis of metal ion binding to humics, for the laboratory models of the ponds. Therefore, the ligand $EDTA^{4-}$ has been chosen to represent organic ligands in the ponds because it is molecularly homogeneous and the complexation of $EDTA^{4-}$ with metal ions is established in the literature.[2] The waste ponds also contain inorganic ligands (*e.g.* hydroxide and carbonate), which are able to coordinate to metal ions. As such, this chapter focuses on probing the solution behaviour of lanthanide-EDTA complexes over a pH range, in the presence and absence of carbonate, using the spectroscopic techniques of NMR, UV-Vis and luminescence.

3.1 Protonation Behaviour and NMR Spectroscopy of Ligands

3.1.1 H_4EDTA

Ethylenediamine tetraacetic acid (H_4EDTA, $C_{10}H_{16}O_8N_2$, Figure 3.1) contains carboxylate and amine functional groups, similar to humic substances,[3] and it predominantly binds to metal ions in a hexadentate mode.[4]

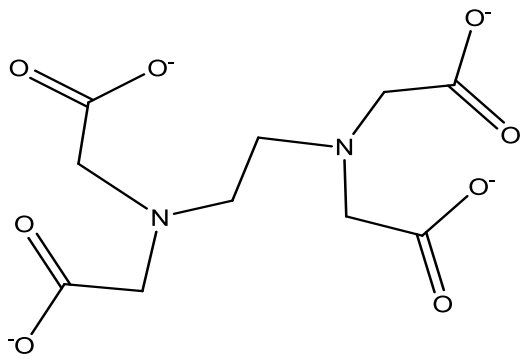

Figure 3.1: Ethylenediamine tetraacetate ($EDTA^{4-}$).

$EDTA^{4-}$ is able to cap a lanthanide ion leaving two to three coordination sites available for the binding of secondary ligands (Figure 3.2).[4] The number of vacant sites of $[Ln(EDTA)]^-_{(aq)}$ complexes can be indicated by the lanthanide hydration number. Evidence in the literature suggests a change in the hydration number from nine to eight in the Eu^{III} to Tb^{III} region of the lanthanides as the 4*f* series is traversed.[5] $EDTA^{4-}$ can form stable metal complexes in acidic and alkaline solutions.[6]

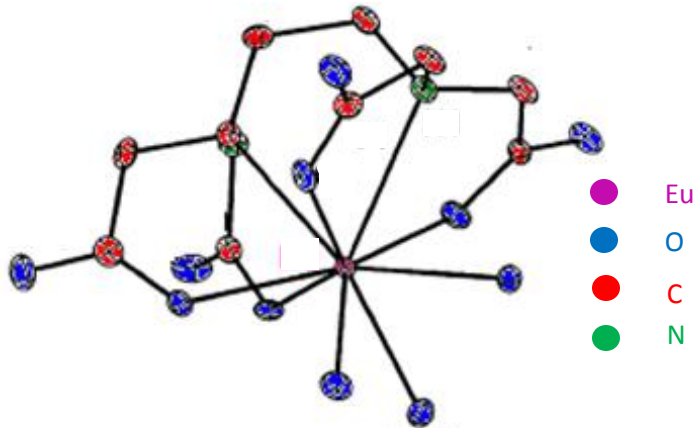

Figure 3.2: Structure of $[Eu(EDTA)(H_2O)_3]^-$. [Adapted from Reference 4].

H_4EDTA forms acidic solutions when dissolved in water (pH neutral) due to the deprotonation of the acetate groups (equations 3.1 to 3.4).[2] The equilibria describing the successive deprotonation of the acetate groups in H_4EDTA at 0.1 M Na^+ ionic strength are shown below.

$$H_4EDTA_{(aq)} \rightleftharpoons H_3EDTA^-_{(aq)} + H^+_{(aq)} \qquad pK_a = 2.00 \qquad \textit{(equation 3.1)}$$

$$H_3EDTA^-_{(aq)} \rightleftharpoons H_2EDTA^{2-}_{(aq)} + H^+_{(aq)} \qquad pK_a = 2.69 \qquad \textit{(equation 3.2)}$$

$$H_2EDTA^{2-}_{(aq)} \rightleftharpoons HEDTA^{3-}_{(aq)} + H^+_{(aq)} \qquad pK_a = 6.13 \qquad \textit{(equation 3.3)}$$

$$HEDTA^{3-}_{(aq)} \rightleftharpoons EDTA^{4-}_{(aq)} + H^+_{(aq)} \qquad pK_a = 9.52 \qquad \textit{(equation 3.4)}$$

The $EDTA^{n-}$ (n = 1 to 4) species present in solution at a certain pH can be determined using the speciation diagram (Figure 3.3), which is derived from known pK_a values (equations 3.1 to 3.4).[2] This shows that as pH is increased, the H_4EDTA ligand is successively deprotonated.

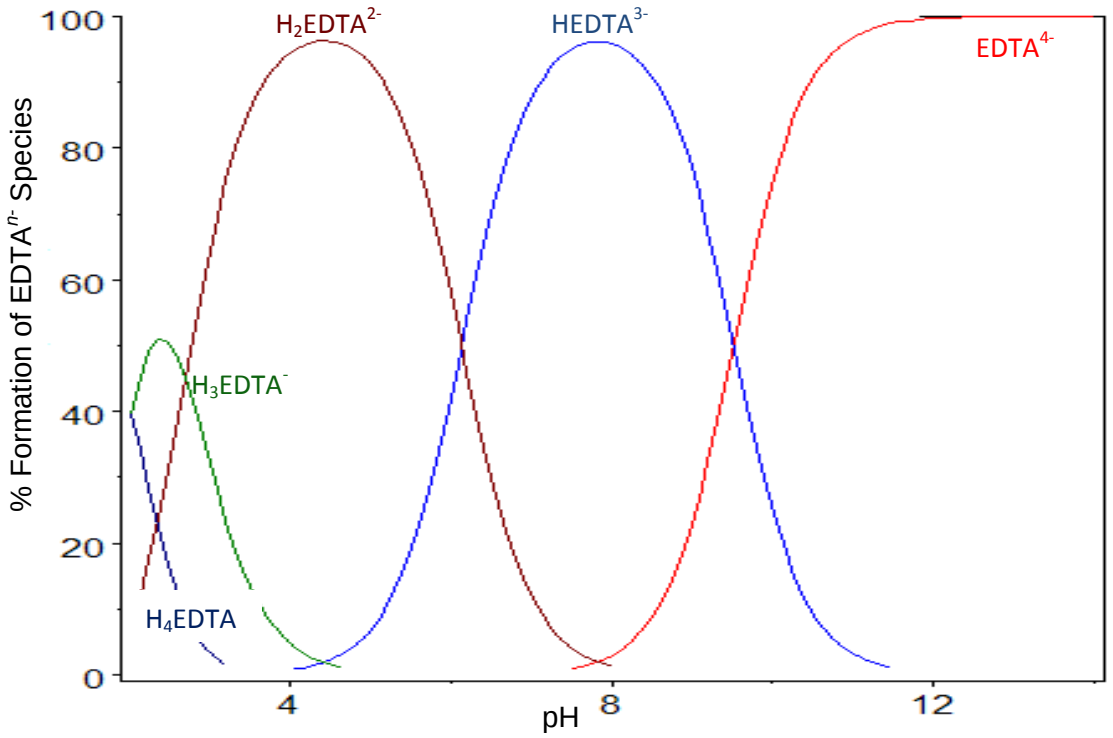

Figure 3.3: Speciation diagram of H_4EDTA (modelled in Hyperquad). The pKa values shown are taken from Martell and Smith for 0.1 M Na^+ ionic strength.[2] Total [$EDTA^{4-}$] = 50 mM.

In order to eliminate confusion and maintain consistency between different types of experiment, acid protons will be described as the ^1H isotope when formulating molecular species, even though the NMR studies are conducted within ^2H environments.

^1H-NMR spectroscopy has been used to monitor how the chemical shifts of $EDTA^{n-}$ species change as a function of pD (Figure 3.4). As pD is increased from 2.9 to 12.7, the ethylene proton resonance shifts from approximately 3.6 ppm to 2.5 ppm and the acetate proton resonance shifts from approximately 3.9 ppm to 3.2 ppm. The inflections of the chemical shifts observed in the NMR titration occur when the pD is equivalent to a pK_a of EDTA. For example, the inflection between pD 5.9 and 7.5 is because of the deprotonation of the H_2EDTA^{2-} species (pK_a = 6.13), and the inflection between pD 8.8 and 10.6 is due to the deprotonation of the $HEDTA^{3-}$ species (pK_a = 9.52). The signals are broadened during the

inflection region, which indicates an exchange process is occurring (*i.e.* deprotonation of $HEDTA^{3-}$ to form $EDTA^{4-}$).

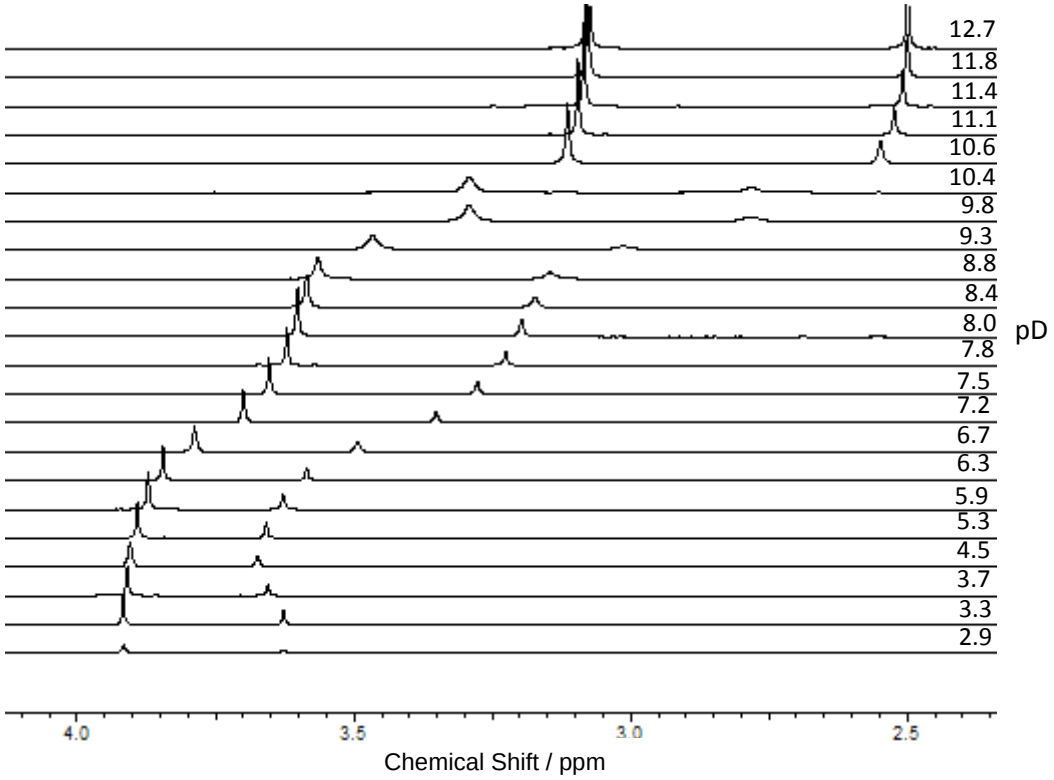

Figure 3.4: ^{1}H-NMR chemical shifts of $EDTA^{n-}$ species as a function of pD; $[0.05\ M]_i$.

3.1.2 Carbonate

Carbonate anions are present in the nuclear waste ponds due to the dissolution of atmospheric $CO_{2(g)}$ (equations 3.5 to 3.8).[7] There are many carbonate equilibria in solution, which are dependent on pH (Figure 3.5 below).[2,8]

$$CO_{2(g)} \rightleftharpoons CO_{2(aq)} \qquad \textit{(equation 3.5)}$$

$$CO_{2(aq)} + H_2O \rightleftharpoons H_2CO_{3(aq)} \qquad \textit{(equation 3.6)}$$

$$H_2CO_{3(aq)} \rightleftharpoons HCO_3^-{}_{(aq)} + H^+ \qquad pK_a = 6.1 \qquad \textit{(equation 3.7)}$$

$$HCO_3^-{}_{(aq)} \rightleftharpoons CO_3^{2-}{}_{(aq)} + H^+ \qquad pK_a = 9.9 \qquad \textit{(equation 3.8)}$$

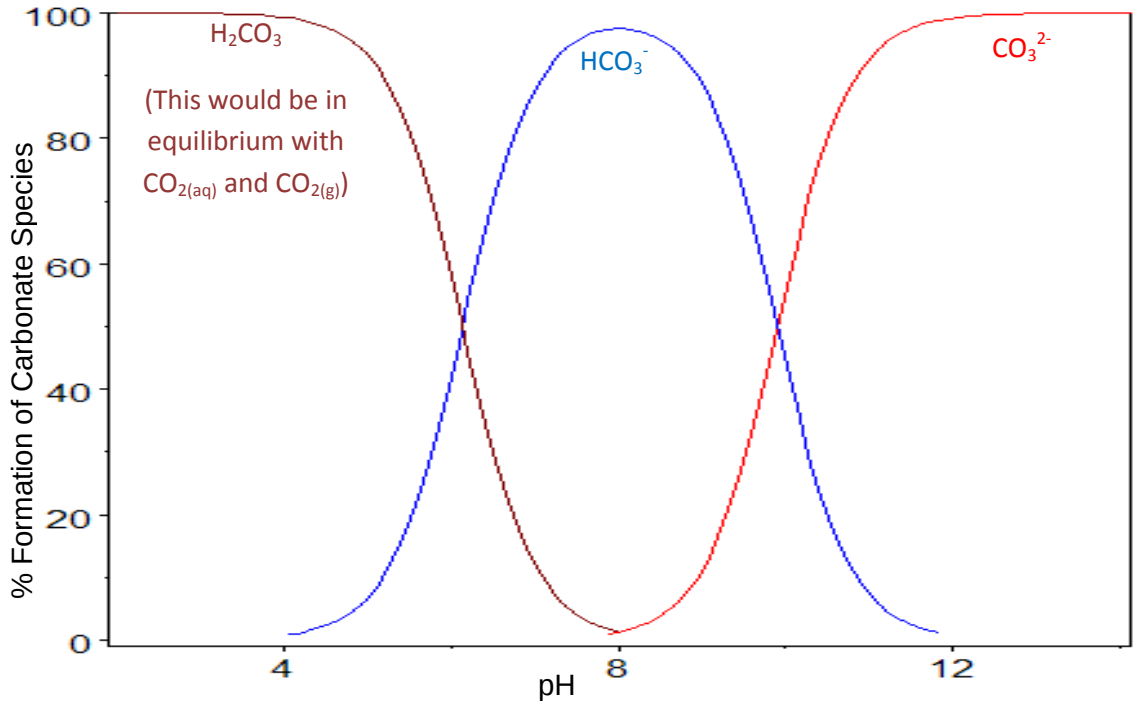

Figure 3.5: Speciation diagram of carbonate (modelled in Hyperquad).

Note: $CO_{2(aq)}$ and $CO_{2(g)}$ formation not included. The pKa values shown are taken from Martell and Smith for 0.1 M Na^+ ionic strength.[2] Total [carbonate] = 50 mM.

^{13}C-NMR spectroscopy has been used to monitor how the chemical shifts of carbonate species change as a function of pD (Figure 3.6). As pD is increased from 7.5 to 13.3, using NaOD, the carbonate resonance shifts from approximately 161.0 ppm to 169.0 ppm. At pD 6.5, the signal at 125.3 ppm is due to the $CO_{2(aq)}$ species.[9] The shift of the carbonate signals over the pD range 7.5 to 13.3 is due to a change in the $HCO_3^-{}_{(aq)}/CO_3^{2-}{}_{(aq)}$ equilibrium (equation 3.8). The signal is broadened at pD 9.9, which indicates an exchange process is occurring (*i.e.* deprotonation of $HCO_3^-{}_{(aq)}$ to $CO_3^{2-}{}_{(aq)}$; pK_a = 9.9).

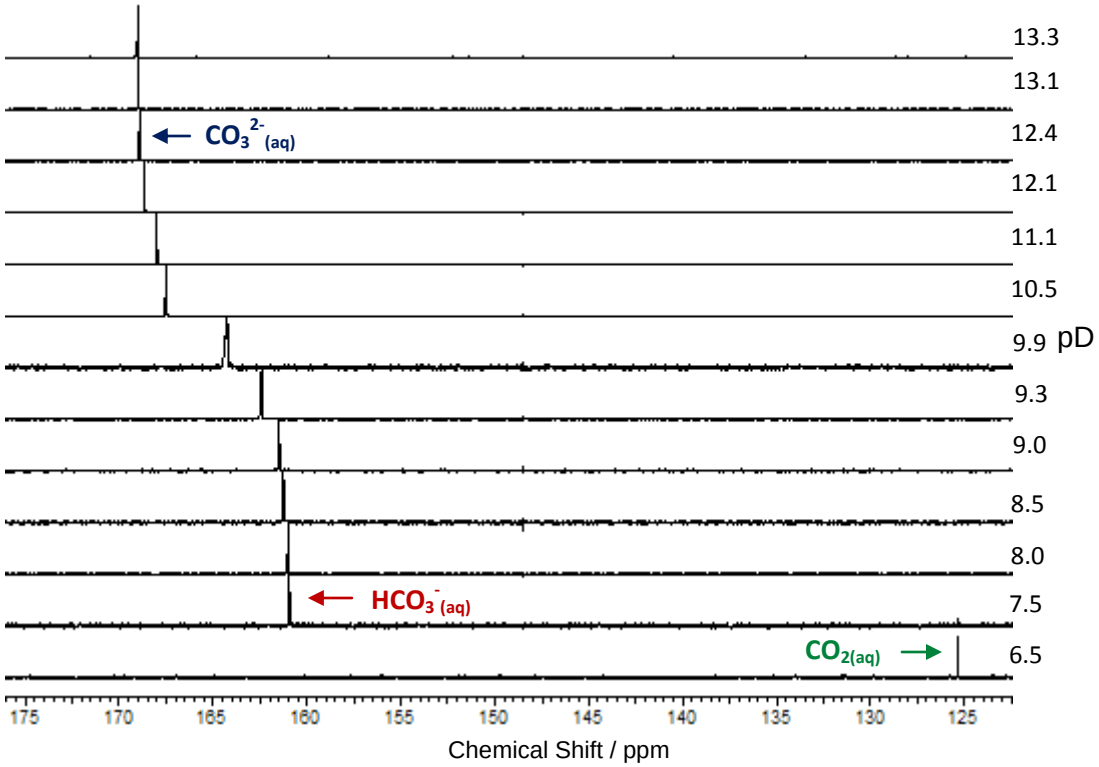

Figure 3.6: ^{13}C-NMR chemical shifts of carbonate species as a function of pD; $[50\ mM]_i$.

3.2 NMR Spectroscopy

3.2.1 Lanthanide-EDTA Binary Systems

3.2.1.1 Diamagnetic Lanthanide Ions (La^{III} and Lu^{III})

Lanthanum and lutetium can form trivalent ions, which have zero *f* electrons and fourteen *f* electrons, respectively. This means that they are both diamagnetic lanthanide ions, which is advantageous for NMR spectroscopy as there are no paramagnetic effects on the signals in a spectrum.

The mixing of equimolar amounts of $LaCl_{3(aq)}$ and $Na_2H_2EDTA_{(aq)}$ produces an acidic solution (pD 2), which contains both the $[Ln(HEDTA)]_{(aq)}$ and $[Ln(EDTA)]^-_{(aq)}$ complexes. The solution is acidic due to the Lewis acidic nature of the lanthanides (equation 3.9), and also from the deprotonation of $Na_2H_2EDTA_{(aq)}$ (see equations 3.1 to 3.4 above).[2]

$$Ln^{III}_{(aq)} + H_2O \rightleftharpoons Ln(OH)^{2+}_{(aq)} + H^+_{(aq)} \qquad \textit{(equation 3.9)}^{10}$$

For a 1:1 La^{III}:$EDTA^{4-}$ system, the aqueous La^{III} species present in solution at a certain pH can be determined using a speciation diagram (Figure 3.7), which is derived from known equilibrium constants (Table 3.1).[2] The speciation diagram shows that at pH less than 1, free $La^{III}_{(aq)}$ dominates the speciation. From pH 1, the $[La(HEDTA)]^{-}_{(aq)}$ species governs the speciation until pH 4, when the the acetate arm is deprotonated and $[La(EDTA)]^{-}_{(aq)}$ species becomes prevalent. Hydrolysis of the La^{III} ion to form $La(OH)_{3(s)}$ is expected to become significant after pH 12.

		Ionic Strength
$La^{III} + HEDTA^{3-} + H^{+} \rightleftharpoons [La(HEDTA)]$	$\log \beta_{111}$ 17.6	0.1 M
$La^{III} + EDTA^{4-} - \rightleftharpoons [La(EDTA)]^{-}$	$\log \beta_{110}$ 15.4	0.1 M
$La(OH)_{3(s)} \rightleftharpoons La^{3+} + 3\ OH^{-}$	$\log K_{sp}$ -20.3	1 M $NaClO_4$

Table 3.1: Stability constants for the complexation of $EDTA^{4-}$ and hydroxide to the La^{III} ion.[2]

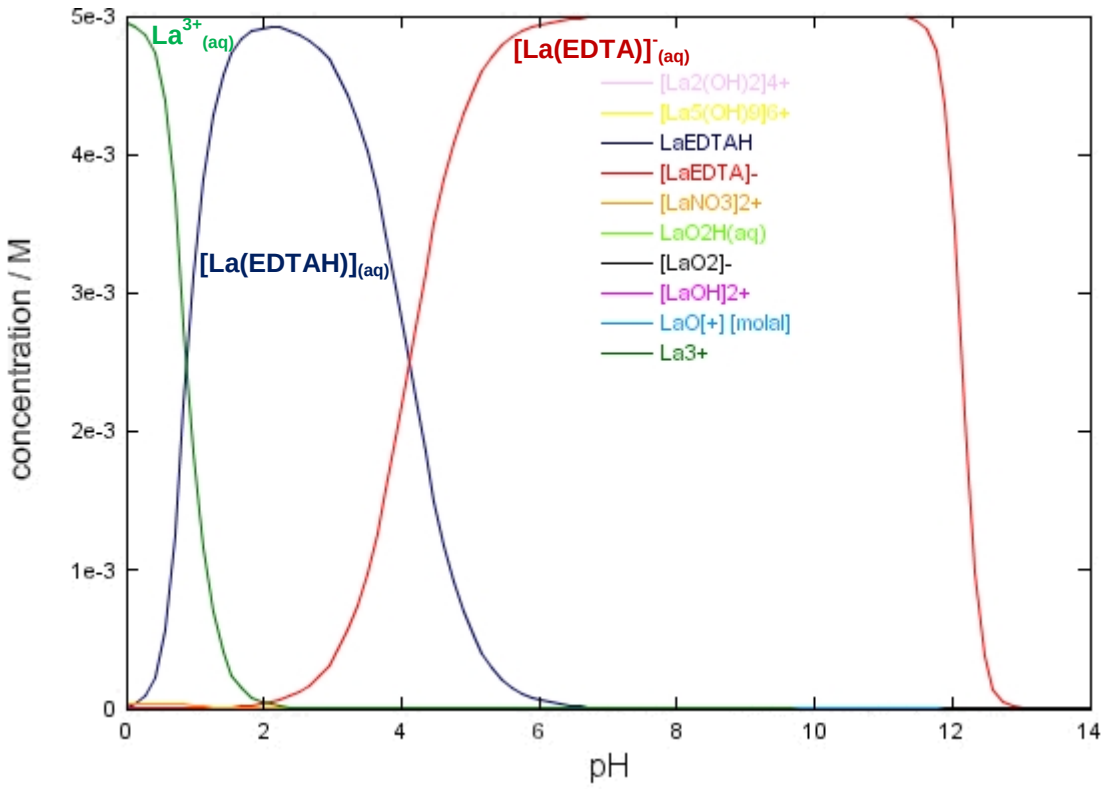

Figure 3.7: Speciation diagram of a 1:1 La^{III}:$EDTA^{4-}$ system as a function of pH using the *JCHESS* code.[11] Total $[La^{III}]$ = total $[EDTA^{4-}]$ = 5 mM. Only aqueous species are shown. Thermodynamic data obtained from the integrated *JCHESS* database and Martell and Smith.[2]

During the preparation of NMR samples for a 1:1 La^{III}:$EDTA^{4-}$ system in this work, crystals of [La(EDTAH)(H_2O)$_4$] were observed to form at pD 2 after one hour (Figure 3.8). The formation of these crystals has previously been reported in the literature,[12] and shows that one of the four acetate arms does not bind to the La^{III} ion, which indicates that this group is protonated. This causes the $HEDTA^{3-}$ ligand to bind to the La^{III} ion in a pentadentate manner, and also means that the dominant solution species at approximately pH 2 can be isolated in the solid phase.

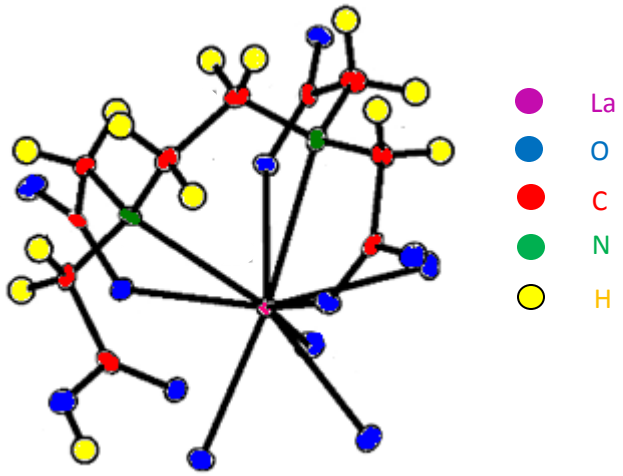

Figure 3.8: Crystal Structure of [La(EDTAH)(H_2O)$_4$].

^{1}H-NMR spectroscopy was used to analyse a 1:1 La^{III}:$EDTA^{4-}$ solution at pD 2 to determine if the pentadentate coordination mode of $HEDTA^{3-}$ could be observed. The ^{1}H-NMR spectrum shows signals at 3.95 and 3.5 ppm (integrates to eight and four protons), which are due to unbound $EDTA^{4-}$ acetate and ethylene protons (Figure 3.9). The spectrum also displays signals at 3.43 and 2.7 ppm (integrates to eight and four protons), which are representative of bound $EDTA^{4-}$ acetate and ethylene protons. Therefore, there is a mixture of bound and unbound $HEDTA^{3-}$/$EDTA^{4-}$ in the system. The signals for the bound $EDTA^{4-}$ protons are broadened, whereas the signals for unbound $EDTA^{4-}$ are more resolved. The broadening of the bound $EDTA^{4-}$ signals may be due to exchange between the hexadentate and pentadentate coordination modes of $HEDTA^{3-}$/$EDTA^{4-}$.

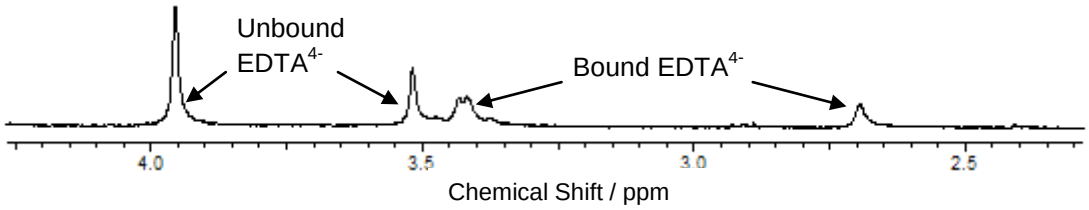

Figure 3.9: ^{1}H-NMR of 1:1 La^{III}:$EDTA^{4-}$ at pD 2; $[50\ mM]_i$.

^{1}H-NMR spectroscopic titrations of the 1:1 Ln^{III}:$EDTA^{4-}$ binary system (where Ln = La or Lu) have been performed to observe the effect of pD, in the alkaline region, on the $EDTA^{4-}$ chemical shifts. The ^{1}H-NMR spectra of the 1:1 La^{III}:$EDTA^{4-}$ system as a function of pD (Figure 3.10) show chemical shifts at 3.37 ppm (AB quartet) and also at 2.7 ppm (singlet). These signals correspond to the methylenic protons of the acetate arms and the ethylene protons of the amine chain, respectively. The presence of the AB quartet and the singlet in the ^{1}H-NMR spectra confirms that $EDTA^{4-}$ is bound to La^{III}. The integration ratio of the AB quartet and the singlet is calculated as 2:1, which is concordant with the 8 methylenic protons and 4 ethylene protons of $EDTA^{4-}$. The $[La(EDTA)]^{-}_{(aq)}$ complex is present in solution from pD 8.6 to 11.2. From pD 11.2, the signals become broadened, indicating that hydrolysis of the $[La(EDTA)]^{-}_{(aq)}$ complex occurs. This hydrolysis species may be a $[La(EDTA)(OH)]^{2-}_{(aq)}$ ternary complex (*i.e.* a water molecule has been replaced by hydroxide in the inner coordination sphere of the La^{III} ion). The speciation diagram (Figure 3.7) shows that $La(OH)_{3(s)}$ forms at pD 10, however, it was not until pD values of 13.2 and above that signals at 3.1 ppm and 2.5 ppm emerge, which are representative of unbound $EDTA^{4-}$. A white precipitate was observed to form at this pD, which is likely to be $La(OH)_{3(s)}$. Therefore, the ^{1}H-NMR spectra suggest that the hydrolysis species, $[La(EDTA)(OH)]^{2-}_{(aq)}$, may form before precipitation of $La(OH)_{3(s)}$.

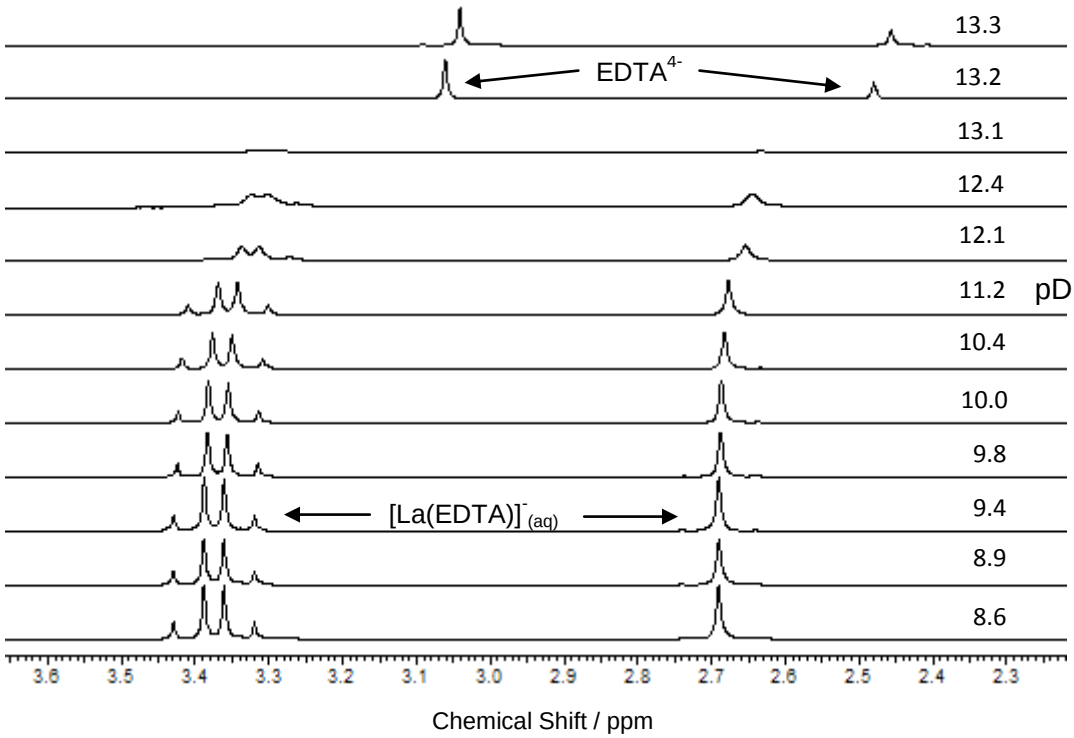

Figure 3.10: ^{1}H-NMR of a 1:1 La^{III}:$EDTA^{4-}$ system as a function of pD; $[50\ mM]_i$.

Similar to the 1:1 La^{III}:$EDTA^{4-}$ system, the aqueous Lu^{III} species present in solution at a certain pH can be determined using a speciation diagram (Figure 3.11), which is derived from known equilibrium constants (Table 3.2).[2] This shows that at pH greater than approximately 2, the $[Lu(EDTA)]^-_{(aq)}$ species dominates. There is no reported log β for formation of the $[Lu(EDTAH)]_{(aq)}$ complex (*cf.* $[La(EDTAH)]_{(aq)}$) and crystals of an analogous $[Lu(EDTAH)(H_2O)_3]$ complex were not observed to form. This difference in the La^{III} and Lu^{III} coordinating behaviour to $EDTA^{4-}$ is likely to arise because the $[Lu(EDTA)]^-_{(aq)}$ complex is more thermodynamically stable than the $[La(EDTA)]^-_{(aq)}$ species, due to the Lu^{III} ion having a higher charge density than La^{III}. Therefore, Lu^{III} may prefer to coordinate to $EDTA^{4-}$ in a hexadentate, rather than pentadentate, manner even at low pH.

		Ionic Strength
$Lu^{III} + EDTA^{4-} \rightleftharpoons [Lu(EDTA)]^-$	$\log \beta_{110}$ 19.7	0.1 M
$Lu(OH)_{3(s)} \rightleftharpoons Lu^{3+} + 3\ OH^-$	$\log K_{sp}$ -25.1	0

Table 3.2: Stability constants for the complexation of $EDTA^{4-}$ and hydroxide to the Lu^{III} ion.[2]

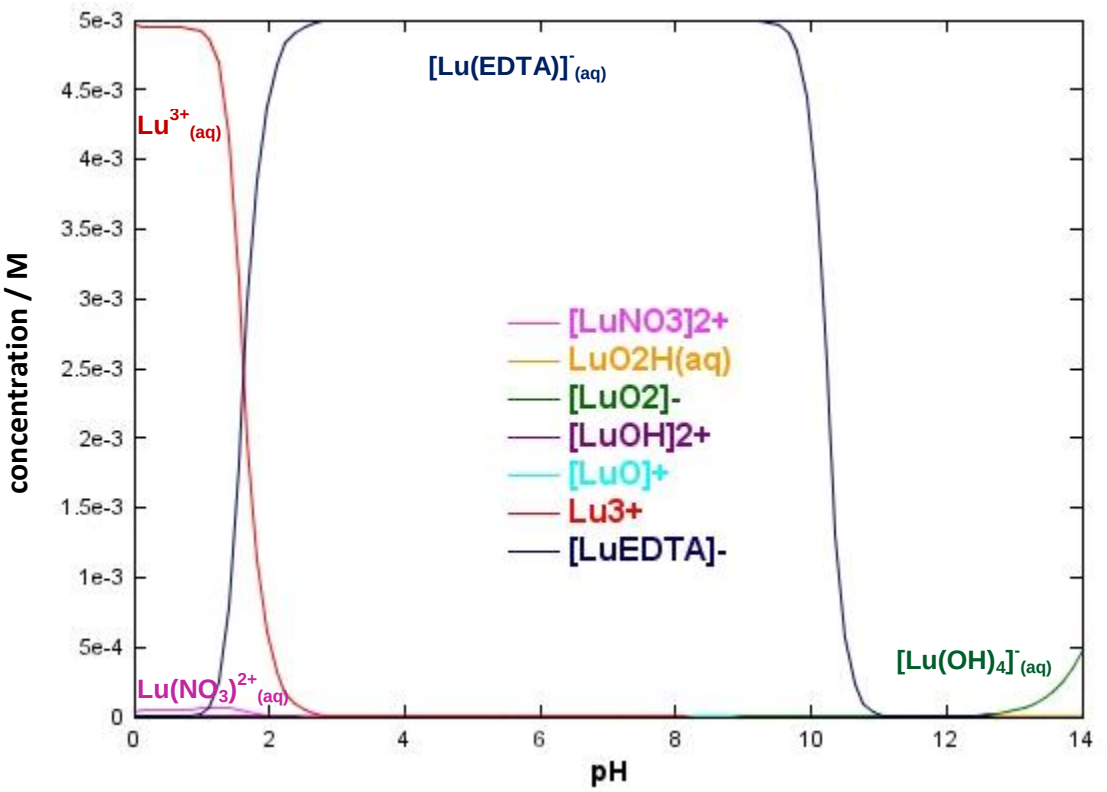

Figure 3.11: Speciation diagram of a 1:1 Lu^{III}:$EDTA^{4-}$ system as a function of pH using the *JCHESS* code.[11] Total [Lu^{III}] = total [$EDTA^{4-}$] = 5 mM. Only aqueous species are shown. Thermodynamic data obtained from the integrated *JCHESS* database and Martell and Smith.[2]

An NMR spectroscopic titration of the 1:1 Lu^{III}:$EDTA^{4-}$ binary system was performed to observe the effect of pD on the $EDTA^{4-}$ chemical shifts. Similar to the ^{1}H-NMR spectra of the 1:1 La^{III}:$EDTA^{4-}$ system shown in Figure 3.10, the ^{1}H-NMR spectra of the 1:1 Lu^{III}:$EDTA^{4-}$ system (Figure 3.12) show chemical shifts at approximately 3.55 and 3.33 ppm (AB quartet) and also at 2.85 ppm (singlet). These chemical shifts correspond to the bound methylenic protons of the acetate arms and the ethylene protons of the amine chain in $EDTA^{4-}$, respectively, and the integration ratio is equal to 2:1. The AB quartet and the singlet resonances confirm that $EDTA^{4-}$ is coordinated to the Lu^{III} ion, approximately over the pD range 2 to 12. At pD greater than 10.1, the signals become broadened, which may be due to hydrolysis of the $[Lu(EDTA)]^{-}_{(aq)}$ complex to form the $[Lu(EDTA)(OH)]^{2-}_{(aq)}$ species. At pD 13.1, signals at 3.1 ppm and 2.5 ppm emerge, which are representative of unbound $EDTA^{4-}$. Similar to the $[La(EDTA)]^{-}_{(aq)}$ complex, hydroxide is able to completely replace $EDTA^{4-}$ in the Lu^{III} coordination sphere. A white precipitate forms, which is likely to be $Lu(OH)_{3(s)}$.

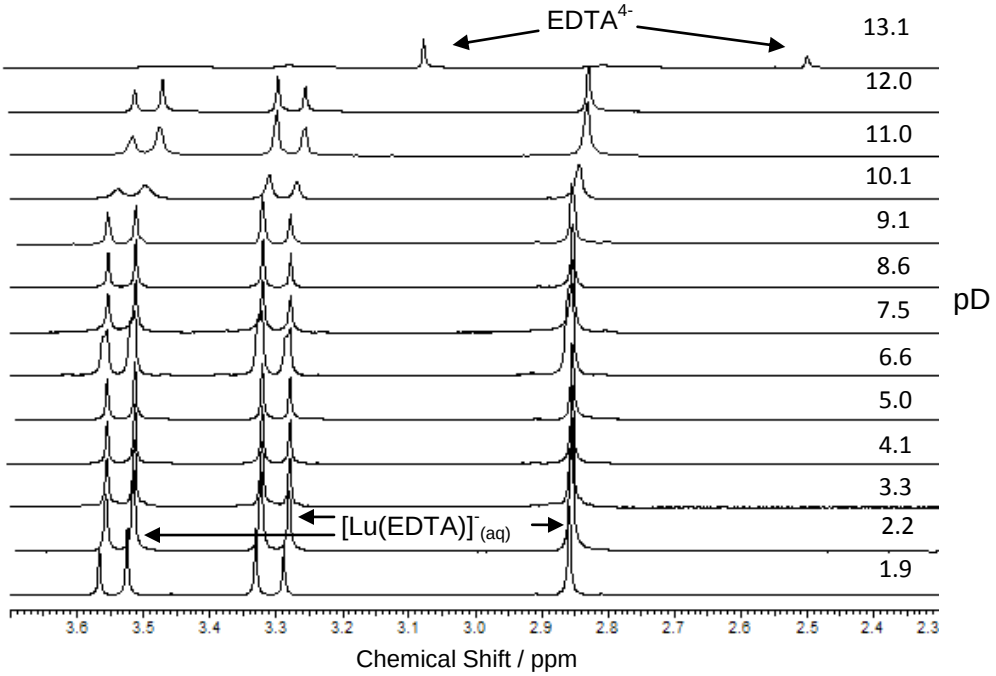

Figure 3.12: ^{1}H-NMR of a 1:1 Lu^{III}:$EDTA^{4-}$ system as a function of pD; $[50\ mM]_i$.

3.2.1.2 Paramagnetic Trivalent Lanthanide Ions (Ce, Pr, Nd, Sm, Eu, Tb, Ho, Er and Yb)

The trivalent lanthanide ions from Ce to Yb have unpaired electrons and so are paramagnetic. Lanthanides that have unpaired electrons cause NMR signals to be paramagnetically shifted and broadened, especially when NMR active nuclei are in close proximity to the paramagnetic ion. Therefore, the effects of paramagnetism on ^{1}H- and ^{13}C-NMR spectra can be useful in determining if a ligand is coordinated to a metal ion.[13]

The mixing of equimolar amounts of $LnCl_{3(aq)}$ (Ln = Ce^{III}, Pr^{III}, Nd^{III}, Sm^{III}, Eu^{III}, Tb^{III}, Ho^{III}, Er^{III}, Yb^{III}) and $Na_2H_2EDTA_{(aq)}$ forms the $[Ln(EDTA)]^-_{(aq)}$ complex in solution. Similar to the La^{III} and Lu^{III} systems, the resulting solutions are acidic due to the Lewis acidic nature of the lanthanides (equation 3.9), and also from the deprotonation of $Na_2H_2EDTA_{(aq)}$ (equations 3.1 to 3.4).[4]

The $[Ln(EDTA)]^-_{(aq)}$ solutions for analysis using NMR spectroscopy were increased to pD 10, using NaOD, to ensure that $[Ln(EDTA)]^-_{(aq)}$ was the dominant species in solution. The ^{1}H-NMR spectrum of the 1:1 Ce^{III}:$EDTA^{4-}$ system shows signals at 1.03 and -3.96 ppm,

which are due to the $EDTA^{4-}$ acetate and ethylene protons, respectively (Figure 3.13). The resonances have been paramagnetically shifted from the free $EDTA^{4-}$ resonances at 3.33 and 2.7 ppm and also broadened. This paramagnetic shift and broadening of the signals indicates $EDTA^{4-}$ is bound to the Ce^{III} ion. Similar observations were obtained for all of the lanthanides studied (Figures A to H, Appendix 1).

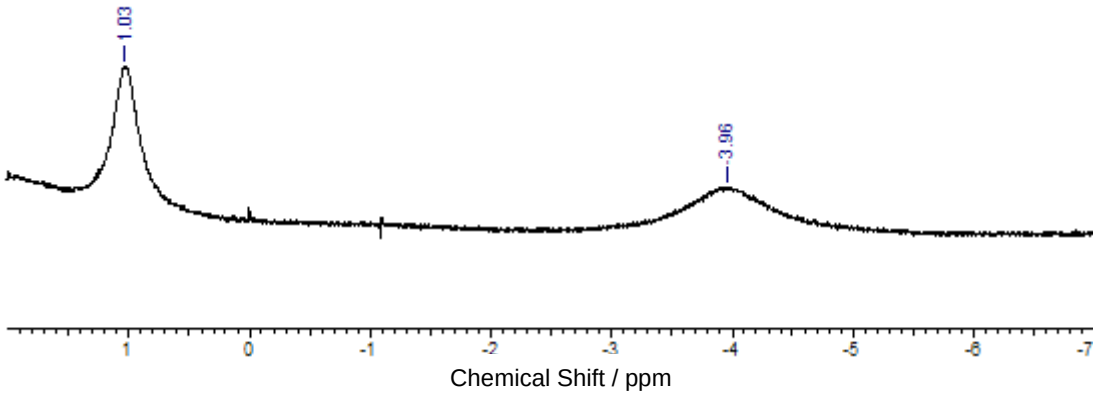

Figure 3.13: ^{1}H-NMR spectrum of a 1:1 Ce^{III}:$EDTA^{4-}$ system at pD 10; $[Ce^{III}]=[EDTA^{4-}] = [5\ mM]_i$.

3.2.2 Lanthanide-EDTA-Carbonate Ternary Systems

3.2.2.1 Diamagnetic Lanthanide Ions (La^{III} and Lu^{III})

Attempts at crystallising $[Ln(EDTA)(CO_3)]^{3-}$ complexes using techniques such as slow diffusion of methanol or ethanol, cation addition of tertiary alkyl ammonium salts (alkyl = methyl, ethyl and propyl) and cobalt hexamine trichloride were not successful.

The interaction of the carbonate anion with the $[Ln(EDTA)]^{-}_{(aq)}$ complex (Ln = La^{III} or Lu^{III}) was analysed by ^{13}C-NMR spectroscopy. In order to probe for ternary $[Ln(EDTA)(CO_3)]^{3-}_{(aq)}$ complexes, an equivalent of carbonate was added to the pre-formed $[Ln(EDTA)]^{-}_{(aq)}$ complex at approximately pD 7, and the pD of the solution was increased with NaOD to approximately pD 13.

The ^{13}C-NMR spectra obtained to study the effect of pD on the 1:1:1 Ln^{III}:$EDTA^{4-}$:CO_3^{2-} system focussed on the chemical shift range 160 to 170 ppm, as this is the region where the carbonate resonance is observed. Labelled (^{13}C) carbonate was used in these experiments in order to increase the intensity of the carbonate signal in the ^{13}C-NMR spectra, allowing for

shorter acquisition times, than if natural carbonate was used. The $EDTA^{4-}$ ligand is not ^{13}C-labelled, and so the reduction in the number of ^{13}C-NMR scans results in the ^{13}C-NMR signals of $EDTA^{4-}$ not being observed. However, ^{1}H-NMR can be used to probe $EDTA^{4-}$ binding for these ternary systems, as shown previously in the binary studies.

The ^{13}C-NMR spectra for the 1:1:1 La^{III}:$EDTA^{4-}$:CO_3^{2-} system shows the shift of the carbonate signal from approximately 161 ppm to 169 ppm over the pD region 8.5 to 13.1 (Figure 3.14). The carbonate signal in the presence of $[La(EDTA)]^-_{(aq)}$ is broadened over the pD range 8.5 to 10.3 compared to that of the free $HCO_3^-{}_{(aq)}$/$CO_3^{2-}{}_{(aq)}$ equilibria (Figure 3.15). This may imply that the carbonate anion is in fast exchange with hydroxide or water for coordination to the $[La(EDTA)]^-_{(aq)}$ complex. After pD 10.3, the carbonate signal becomes more resolved (similar to that of free carbonate in Figure 3.15) and so it is likely that hydroxide is effectively competing for coordination to $[La(EDTA)]^-_{(aq)}$ and replacing any bound carbonate.

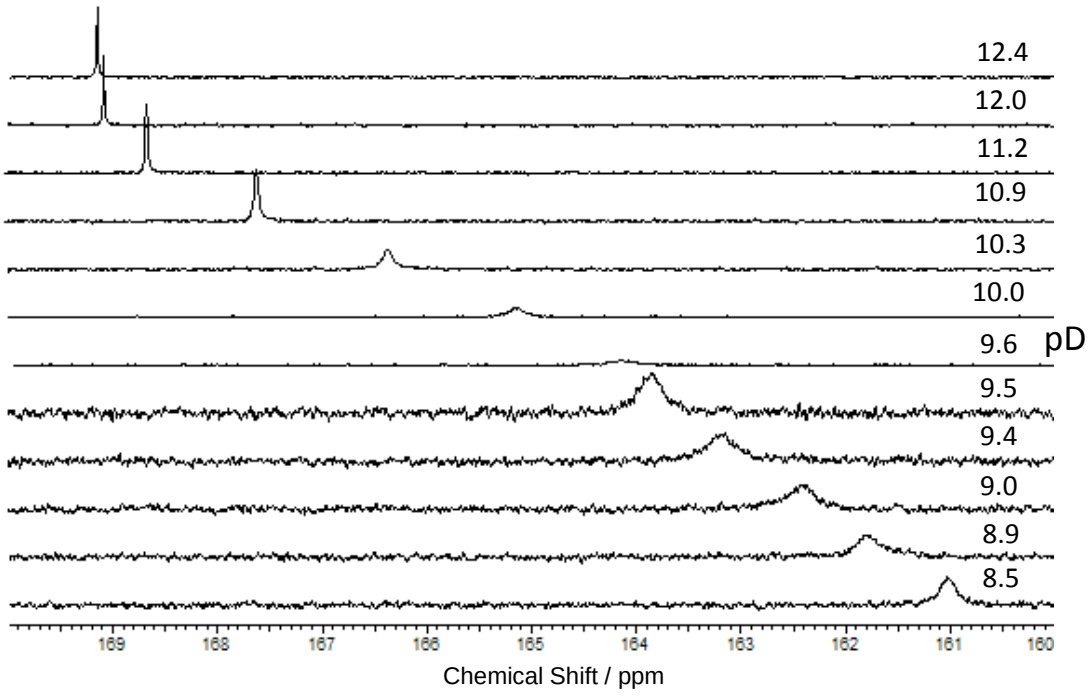

Figure 3.14: ^{13}C-NMR spectra of the effect of pD on a 1:1:1 La^{III}:$EDTA^{4-}$:CO_3^{2-} solution; $[50\ mM]_i$.

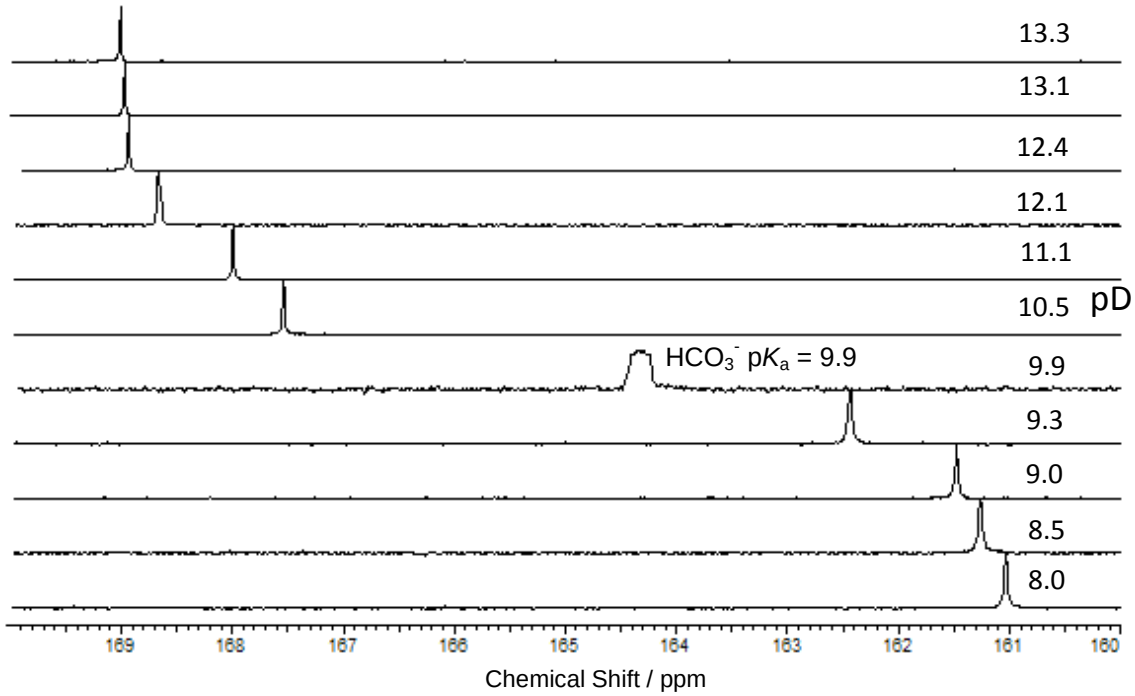

Figure 3.15: ^{13}C-NMR spectra of the effect of pD on a Na$H^{13}CO_3$ solution; $[50\ mM]_i$.

The experiment was repeated for the Lu^{III} ion to observe the effect on carbonate binding when using a lanthanide ion with greater charge density than La^{III}. The ^{13}C-NMR spectra for the effect of pD on the 1:1:1 Lu^{III}:$EDTA^{4-}$:CO_3^{2-} system show a broadened carbonate signal at around 169.4 ppm that becomes better resolved over the pD region 10.3 to 13.2 (Figure 3.16). This signal is due to carbonate that is bound to the $[Lu(EDTA)]^-_{(aq)}$ complex, as the chemical shift of this resonance remains stationary at 169.4 ppm. A second carbonate signal can be observed over the pD range 10.3 to 11.5 when the spectra are expanded (Figure 3.17), which also becomes better resolved over the pD range 12.1 to 13.2 (Figure 3.16). This second carbonate signal shifts from 163.0 ppm to 168.9 ppm over the pD range 10.3 to 13.2, and is assigned to unbound carbonate in the system. The carbonate signals are broadened so it is likely that there is exchange in solution between bound and unbound carbonate to $[Lu(EDTA)]^-_{(aq)}$. As pD is increased, the intensity of the bound CO_3^{2-} signal decreases and the unbound CO_3^{2-} signal increases, until at pD 13.3, only unbound CO_3^{2-} is present at approximately 168.9 ppm. The results presented suggest that there is a stronger interaction between the $[Lu(EDTA)]^-_{(aq)}$ complex and the carbonate ion in solution than the $[La(EDTA)]^-_{(aq)}$ species. The origin of this stronger interaction is likely to be due to the higher charge density of the $Lu^{III}_{(aq)}$ ion than the $La^{III}_{(aq)}$ ion.

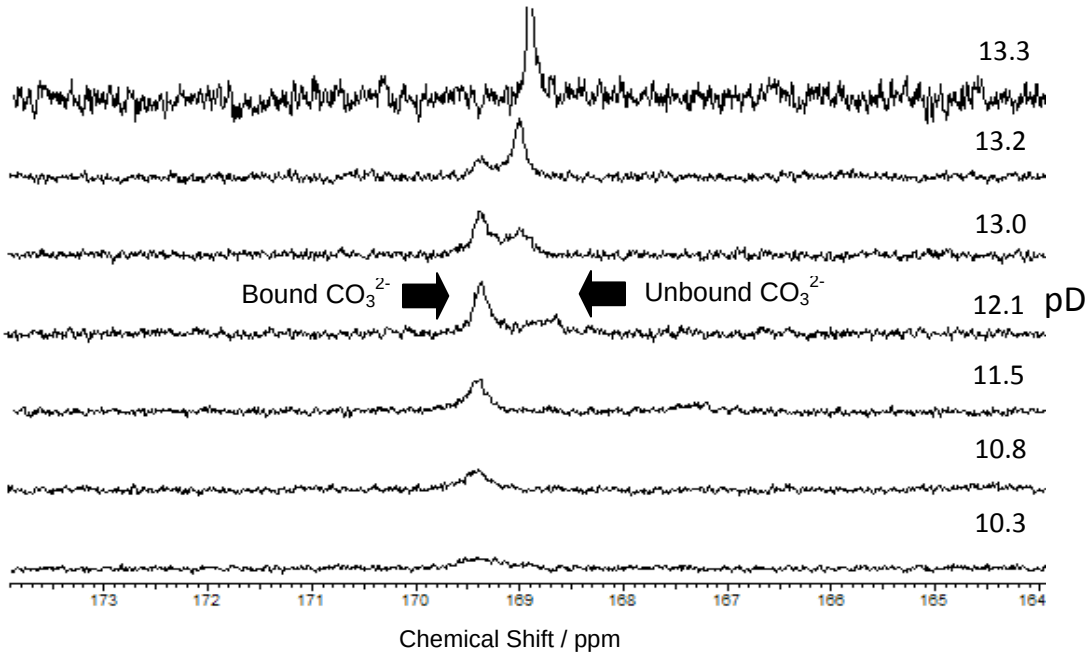

Figure 3.16: ^{13}C-NMR spectra of the effect of pD on a 1:1:1 Lu^{III}:$EDTA^{4-}$:CO_3^{2-} solution; $[50\ mM]_i$.

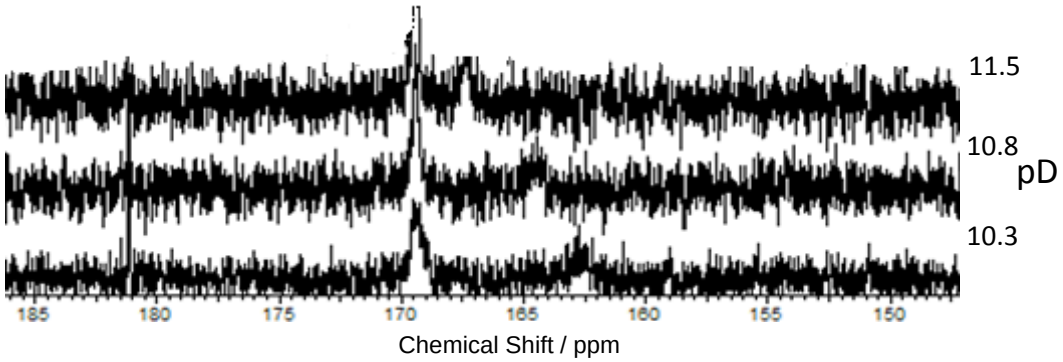

Figure 3.17: Expanded section of Figure 3.16 between pD 10.3 to 11.5.

The ^{1}H-NMR spectra for the effect of pD on the 1:1:1 Ln^{III}:$EDTA^{4-}$:CO_3^{2-} systems (Ln = La^{III} and Lu^{III}) show bound $EDTA^{4-}$ signals up to pD 12.4 and 10.3 in the La^{III} and Lu^{III} systems, respectively, after which unbound $EDTA^{4-}$ signals occur (Figures I and J, in Appendix 1). A white precipitate is observed to form in both systems above pD 13.3, which is likely to be $Ln(OH)_{3(s)}$.

The experiment was repeated using $NaH^{13}CO_{3(aq)}$ (see Figures K (^{13}C-NMR spectra) and L (^{1}H-NMR spectra), in Appendix 1). The results showed that there was no significant difference using $NaH^{13}CO_{3(aq)}$ or $Na_2{}^{13}CO_{3(aq)}$ as the carbonate source.

The percentage of bound $EDTA^{4-}$ and CO_3^{2-} to the Lu^{III} ion (Figure 3.18) was determined by integration of the bound and unbound $EDTA^{4-}$ signals (acetate and ethylene protons) in the ^{1}H-NMR spectra, and by integration of the bound and unbound carbonate signals in the ^{13}C-NMR spectra. At pD 10.3, approximately 70 % of CO_3^{2-} in the system is bound. This stays constant until pD 11.5. Above pD 11.5, the percentage of bound CO_3^{2-} gradually decreases as pD is increased, until at pD 13.3, there is no CO_3^{2-} bound to the Lu^{III} ion. The graph shows that the percentage of $EDTA^{4-}$ bound to Lu^{III} is approximately 100 % at pD 10.3 but this reduces to 90 % at pD 11.5. The percentage of $EDTA^{4-}$ bound remains constant at approximately 90 % from pD 11.5 to 13.2. However, after pD 13.2, the percentage of $EDTA^{4-}$ bound decreases to 0 % as $Lu(OH)_{3(s)}$ is precipitated out of solution. Hydroxide is an effective competitor, and it readily displaces carbonate from the Lu^{III} ion coordination sphere. The $EDTA^{4-}$ ligand can only be removed from the Lu^{III} ion at very high pD, which is due to the $[Lu(EDTA)]^-_{(aq)}$ complex being highly thermodynamically stable ($\log \beta_{[Lu(EDTA)]^-} = 19.7$; $I = 0.1$ M).[2]

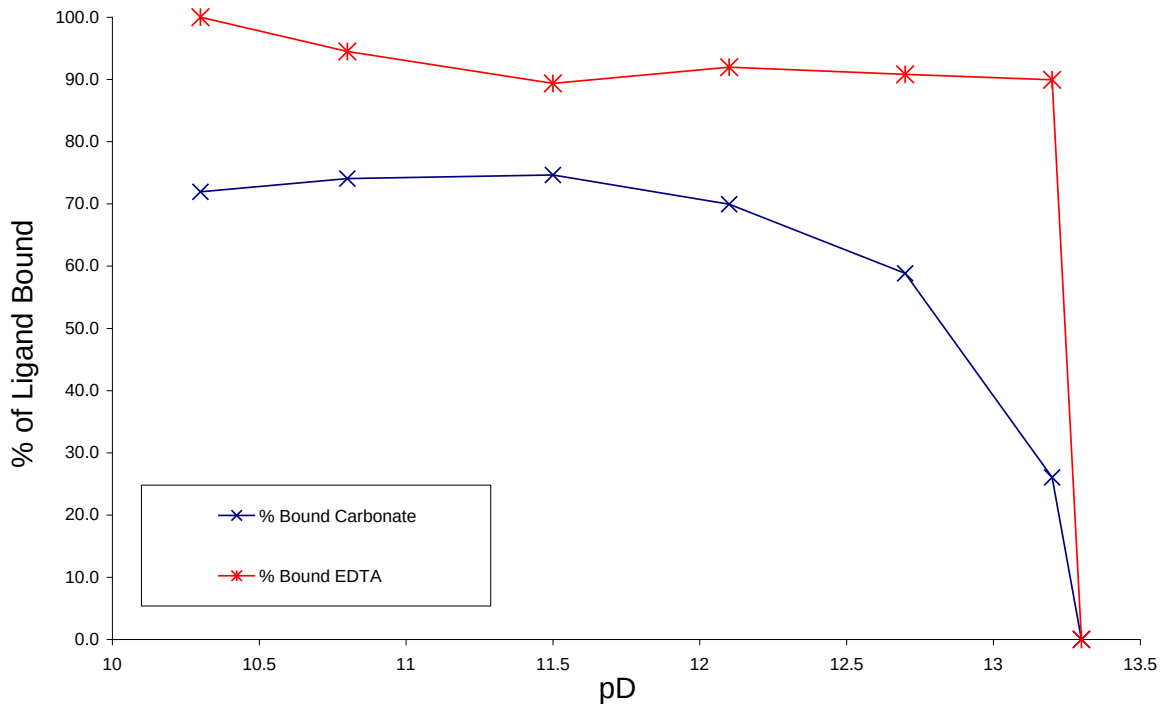

Figure 3.18: Percentage of bound $EDTA^{4-}$ and CO_3^{2-} to the Lu^{III} ion as pD is increased; 1:1:1 Lu^{III}:$EDTA^{4-}$:CO_3^{2-}; $[50\ mM]_i$.

The percentage of bound $EDTA^{4-}$ and CO_3^{2-} to the Lu^{III} ion, using $NaH^{13}CO_3$ as the carbonate source, is shown in Figure 3.19. $NaHCO_{3(aq)}$ is less basic than $Na_2CO_{3(aq)}$ causing the starting pD after the addition of one equivalent of $NaHCO_{3(aq)}$ to the system to be lower compared to adding one equivalent of $Na_2CO_{3(aq)}$ (*i.e.* pD 9.0 *vs.* pD 10.3). At pD 9.0, only 7.2 % of the carbonate is bound, which suggests that HCO_3^- is less likely to bind to $[Lu(EDTA)]^-_{(aq)}$ than CO_3^{2-}. However, as pD is increased (using NaOD) and more HCO_3^- is converted to CO_3^{2-}, then it is more thermodynamically favourable for carbonate to bind to the $[Lu(EDTA)]^-_{(aq)}$ complex. At pD 11.8, there is a maximum of 78 % of carbonate bound to the $[Lu(EDTA)]^-_{(aq)}$ complex, but as pD is increased further then the percentage of carbonate bound begins to decrease as hydrolysis occurs. In both the 1:1:1 Lu^{III}:$EDTA^{4-}$:CO_3^{2-} systems using $Na_2CO_{3(aq)}$ (Figure 3.18) and $NaHCO_{3(aq)}$ (Figure 3.19) as the carbonate source, there is a maximum of 70 to 80 % of carbonate bound to the $[Lu(EDTA)]^-_{(aq)}$ complex. The percentage of carbonate bound to the $[Lu(EDTA)]^-_{(aq)}$ complex may not reach 100 % because of equilibria between carbonate, hydroxide and water molecules in the system. The percentage of $EDTA^{4-}$ bound to the Lu^{III} ion is 98 % at pD 9, decreasing to 91 % at pD 12.3. At pD 13.4, a white precipitate is

observed to form and $Lu(OH)_{3(s)}$ precipitates out of solution. At this pD, both unbound CO_3^{2-} and $EDTA^{4-}$ are present in solution.

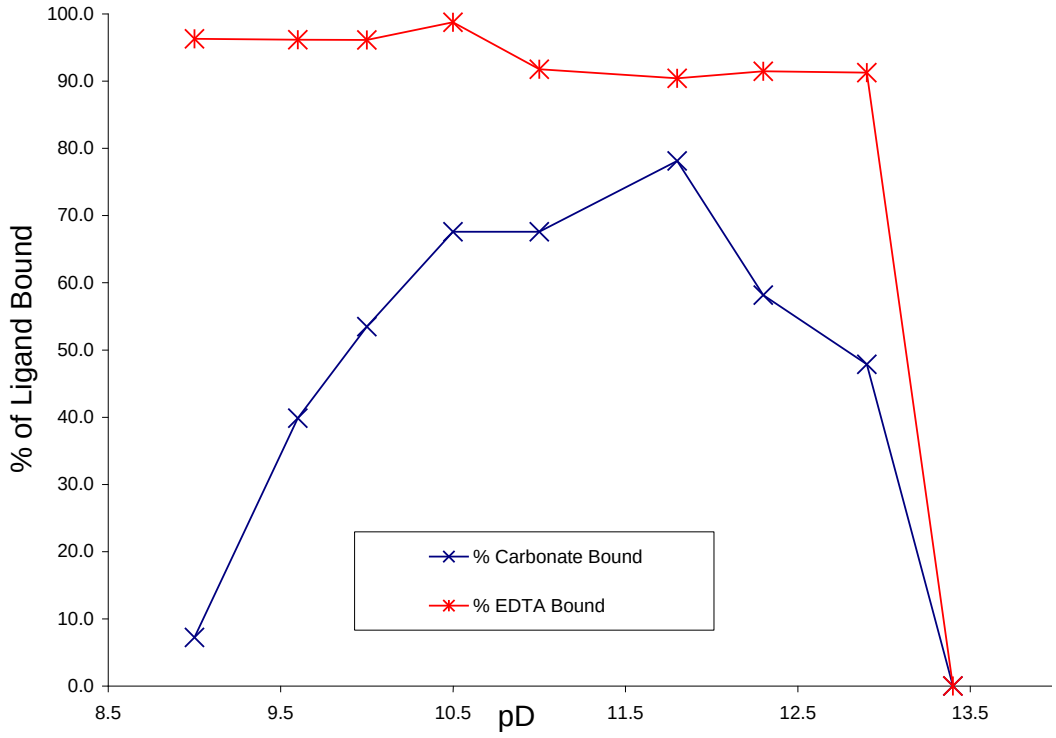

Figure 3.19: Percentage of bound $EDTA^{4-}$ and CO_3^{2-} to the Lu^{III} ion as pD is increased; 1:1:1 Lu^{III}:$EDTA^{4-}$:HCO_3^-; $[50\ mM]_i$.

The stoichiometry of carbonate binding to the $[Lu(EDTA)]^-_{(aq)}$ complex has been investigated to determine whether two carbonate anions are able to bind to the species (Figures M (^{13}C-NMR spectra) and N (^{1}H-NMR spectra) in Appendix 1). The percentage of bound $EDTA^{4-}$ and CO_3^{2-} to the Lu^{III} ion in the 1:1:2 Lu^{III}:$EDTA^{4-}$:CO_3^{2-} system shows that at pD 11.0, approximately 45 % of CO_3^{2-} in the system is bound (Figure 3.20). This gradually decreases to around 35 % at pD 12.8, and as the pD is increased further to 13.2, there is no CO_3^{2-} bound to the Lu^{III} ion. The results suggest that only one carbonate anion is able to bind to the $[Lu(EDTA)]^-_{(aq)}$ complex because at pD 11.0 approximately half of the carbonate in the system is bound. The percentage of $EDTA^{4-}$ bound to the Lu^{III} ion remains constant at around 95 % over the pD range 11.0 to 12.0, but drops to approximately 50 % bound at pD 13.2 and

0 % bound at pD 13.3. There is little difference observed when HCO_3^- is used (Figure O, Appendix 1).

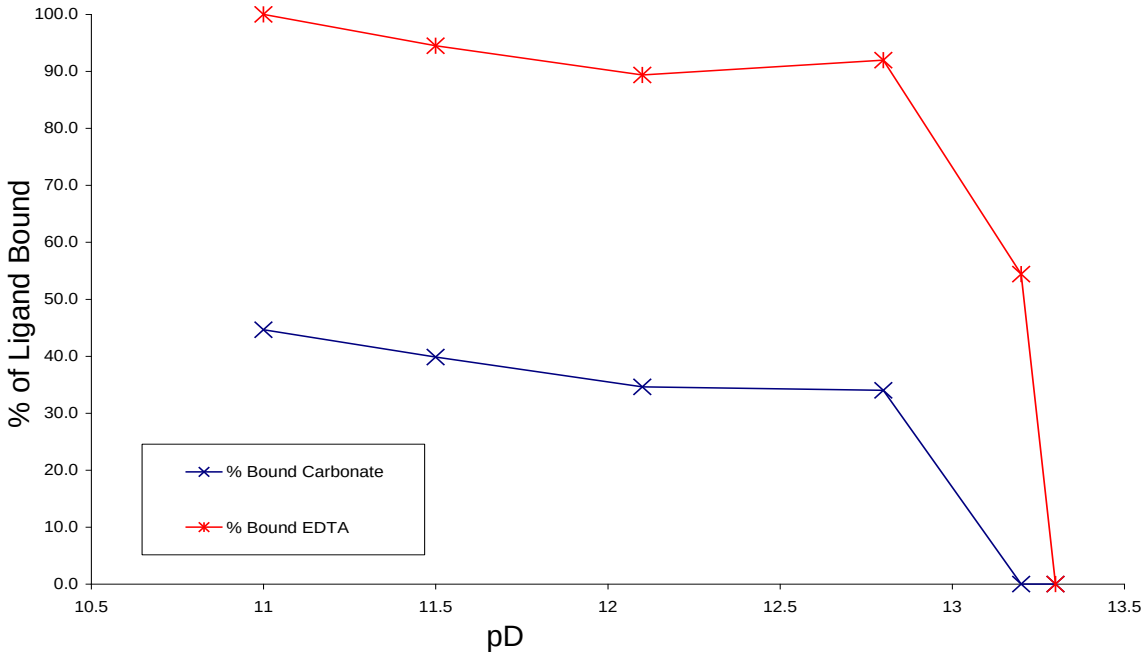

Figure 3.20: Percentage of bound $EDTA^{4-}$ and CO_3^{2-} to Lu^{III} as pD is increased; 1:1:2 Lu^{III}:$EDTA^{4-}$:CO_3^{2-}; $[33\ mM]_i$:$[33\ mM]_i$:$[66\ mM]_i$.

Variable Temperature (VT) NMR spectroscopy was performed on a 1:1:10 La^{III}:$EDTA^{4-}$:CO_3^{2-} solution (Figure 3.21) to attempt to resolve the bound/unbound carbonate signals in the La^{III} system and study any possible exchange processes involving carbonate. The ^{13}C-NMR spectra show a resolved carbonate signal at 167.6 and 167.8 ppm at 40 ^{o}C and 90 ^{o}C, respectively. These spectra indicate that CO_3^{2-} is unbound in the system as there is a single signal. This may be caused by the high temperatures favouring the equilibrium towards unbound carbonate from the $[La(EDTA)]^-_{(aq)}$ complex. By comparison, the low temperature spectrum (*i.e.* 0 ^{o}C) may be showing a splitting of the signal, as it is broadened, indicating bound and unbound CO_3^{2-}.

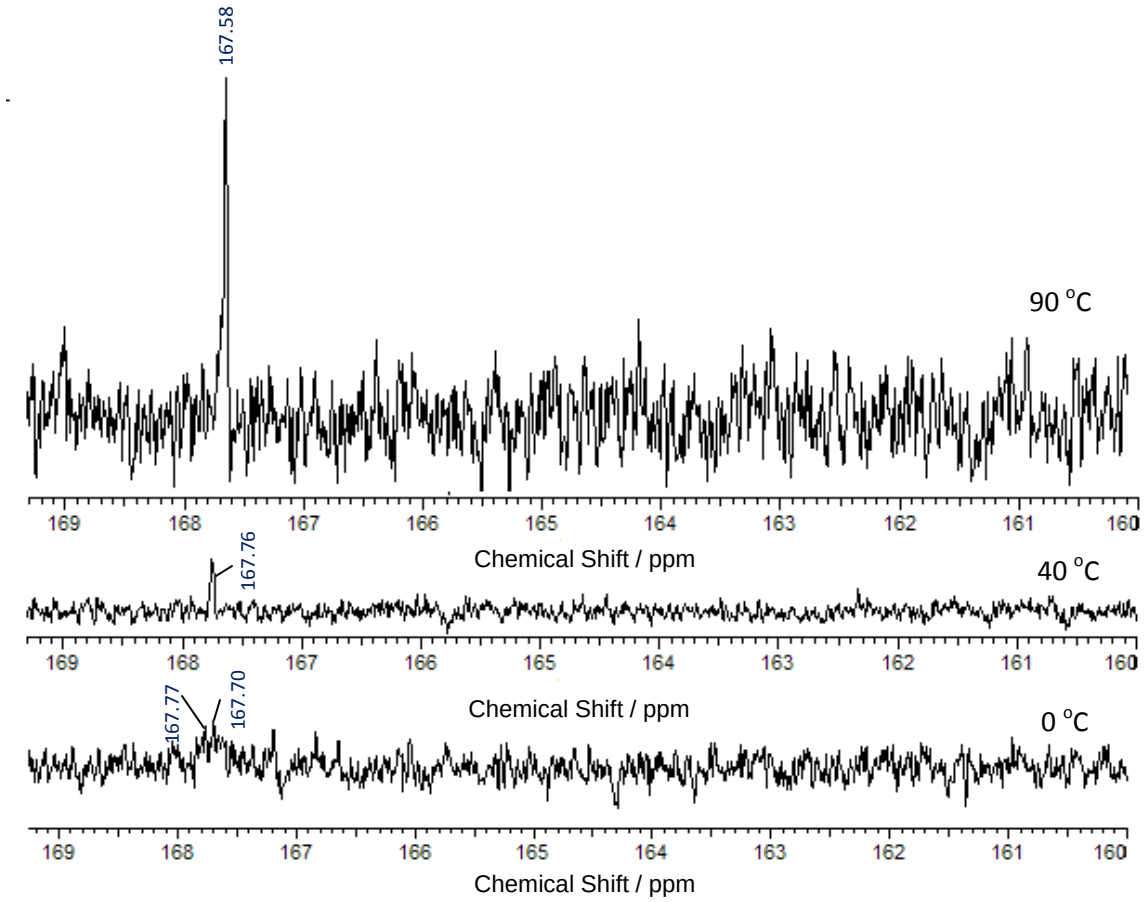

Figure 3.21: ^{13}C-NMR spectra of the effect of temperature on a 1:1:10 La^{III}:$EDTA^{4-}$:CO_3^{2-}; [0.5 M]:[0.5 M]:[5 M], solution; pD 10.5.

[Note: A drop of MeOD was added to the sample at 0 °C in order to prevent the sample freezing].

3.2.2.2 Paramagnetic Trivalent Lanthanide Ions (Ce, Pr, Nd, Sm, Eu, Tb, Ho, Er and Yb)

The 1:1:1 Ln^{III}:$EDTA^{4-}$:CO_3^{2-} systems (where Ln = Ce, Pr, Nd, Sm, Eu, Tb, Ho, Er, Yb) have been analysed by ^{13}C-NMR spectroscopy in order to determine if a paramagnetically shifted or broadened carbonate signal could be observed. All of the systems were analysed at pD 10.0, as it has been established from previous experiments (Section 3.2.2.1) that carbonate is most likely to be bound to $[Ln(EDTA)]^-_{(aq)}$ complexes at this pD (though carbonate interaction may be more favourable in the $[Lu(EDTA)]^-_{(aq)}$ system compared to the $[La(EDTA)]^-_{(aq)}$ system).

The ^{13}C-NMR spectrum for the 1:1:1 Ce^{III}:$EDTA^{4-}$:CO_3^{2-} system at pD 10.0 shows a broadened carbonate signal at approximately 165.7 ppm (Figure 3.22). As the interaction of carbonate with the $[La(EDTA)]^-_{(aq)}$ complex was shown to occur in Section 3.2.2.1, then it is likely that the carbonate signal in the 1:1:1 Ce^{III}:$EDTA^{4-}$:CO_3^{2-} system is broadened due to carbonate interacting with the $[Ce(EDTA)]^-_{(aq)}$ complex, and also due to the free $HCO_3^-{}_{(aq)}$/$CO_3^{2-}{}_{(aq)}$ equilibrium at pD 10.0.

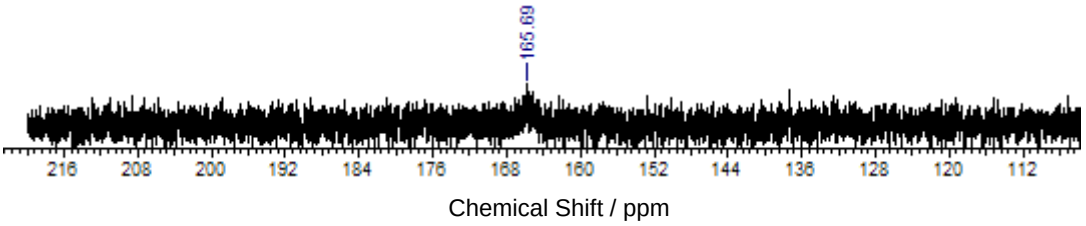

Figure 3.22: ^{13}C-NMR of the 1:1:1 Ce^{III}:$EDTA^{4-}$:CO_3^{2-} system at pD 10.0; $[Ce^{III}]_i$=$[EDTA^{4-}]_i$=$[CO_3^{2-}]_i$ = 5 mM.

The ^{13}C-NMR spectrum for the 1:1:1 Pr^{III}:$EDTA^{4-}$:CO_3^{2-} system at pD 10.0 shows that the carbonate signal is observed neither within its 'normal' 160 to 170 ppm range, nor in the entire spectrum region from 0 to 200 ppm (Figure 3.23). This effect also occurs for the 1:1:1 Ln^{III}:$EDTA^{4-}$:CO_3^{2-} systems (where Ln = Nd, Sm, Eu, Tb, Ho, Er), which are shown as Figures P to U in Appendix 1. It is thought that the carbonate anion is interacting with the paramagnetic $[Ln(EDTA)]^-_{(aq)}$ complexes, which would cause the carbonate signal to be broadened into the baseline.

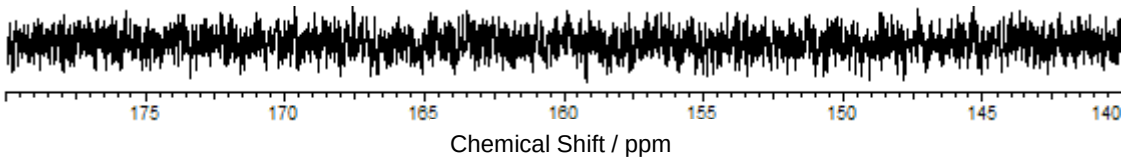

Figure 3.23: ^{13}C-NMR of the 1:1:1 Pr^{III}:$EDTA^{4-}$:CO_3^{2-} system at pD 10; $[Pr^{III}]_i$=$[EDTA^{4-}]_i$=$[CO_3^{2-}]_i$ = 5 mM.

The ^{13}C-NMR spectrum for the 1:1:1 Yb^{III}:$EDTA^{4-}$:CO_3^{2-} system at pD 10.0 shows a broadened carbonate signal at 164.75 ppm and at 7.71 ppm (Figure 3.24). It is likely that the signal at 164.75 ppm corresponds to unbound carbonate and the signal at 7.71 ppm may be the paramagnetically shifted resonance of bound carbonate to $[Yb(EDTA)]^-_{(aq)}$. A paramagnetically shifted carbonate resonance has not been observed for the lanthanides Ce^{III},

Pr^{III}, Nd^{III}, Sm^{III}, Eu^{III}, Tb^{III}, Ho^{III} or Er^{III} over the same chemical shift range (0 to 200 ppm) and also outside of the normal chemical shift range (-100 to 300 ppm).

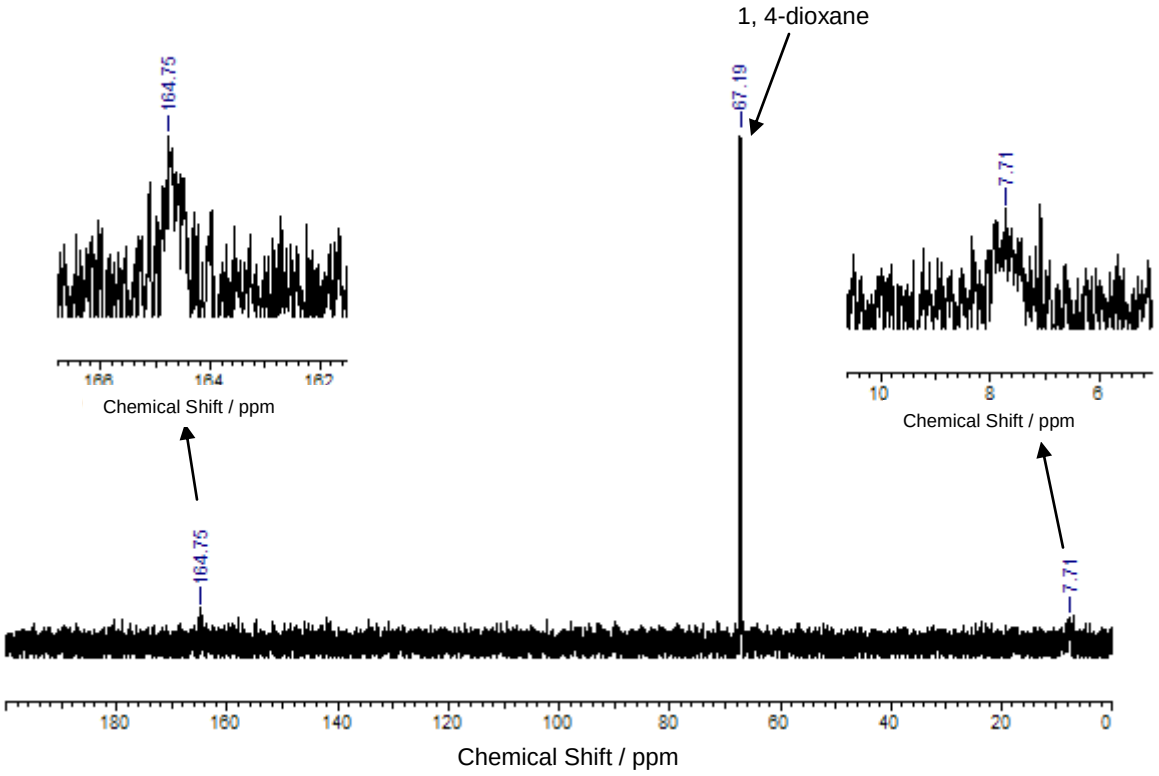

Figure 3.24: ^{13}C-NMR of the 1:1:1 Yb^{III}:$EDTA^{4-}$:CO_3^{2-} system at pD 10.0; $[Yb^{III}]_i$=$[EDTA^{4-}]_i$=$[CO_3^{2-}]_i$ = 5 mM.

3.2.2.3 Summary

^{1}H and ^{13}C-NMR spectroscopy has been a useful technique for understanding the solution behaviour of both the binary Ln^{III}:$EDTA^{4-}$ and ternary Ln^{III}:$EDTA^{4-}$:CO_3^{2-} systems. The $EDTA^{4-}$ ligand is able to complex to all of the lanthanides studied and remains bound to the ions up to high pD (*i.e.* greater than 10), when hydrolysis of the lanthanide ions occur. The ternary $[Ln(EDTA)(CO_3)]^{3-}_{(aq)}$ species are soluble, whereas binary Ln^{III}:CO_3^{2-} systems are not, allowing solution NMR to be used to probe Ln^{III}-CO_3^{2-} interactions. The formation of a ternary $[Ln(EDTA)(CO_3)]^{3-}_{(aq)}$ species has been shown to exist for the lanthanides studied. It is thought that only one carbonate anion can coordinate to the $[Ln(EDTA)]^-_{(aq)}$ complex, and it is preferable for carbonate to bind over the pD region 8 to 11. Below pD 8, HCO_3^- is the dominant carbonate species and the results suggest that it is unfavourable for bicarbonate to

bind to $[Ln(EDTA)]^-_{(aq)}$ as a monodentate ligand. Above pD 11, hydroxide is an effective competitor and is able to replace carbonate in the lanthanide inner coordination sphere.

3.3 UV-Vis Absorption Spectroscopy

The effect of pH on the Ln^{III}:$EDTA^{4-}$ and Ln^{III}:$EDTA^{4-}$:CO_3^{2-} systems has been examined by UV-Vis spectroscopy to observe the formation of these binary and ternary complexes.

3.3.1 Trivalent Lanthanide-EDTA Binary Systems (Pr, Nd and Ho)

The electronic transitions of the Ln^{III} ions involve a redistribution of electrons within the 4*f* shell. As the 4*f* orbitals are much more radially contracted than 5*f* orbitals, the absorption spectra of Ln^{III} ions tend to have comparatively lower intensities and sharp bands.[14] The electronic absorption spectra of the 1:1 Ln^{III}:$EDTA^{4-}$ systems (where Ln = Pr, Nd, Ho) have been analysed as a function of pH at I = 0.5 M $NaNO_3$. The absorption spectra of the 1:1 Pr^{III}:$EDTA^{4-}$ system shows the characteristic absorption bands for Pr^{III} at approximately 445, 465 and 490 nm (Figure 3.25), which correspond to the excitation of electrons from the $^3H_4$ ground state to the $^3P_2$, $^3P_1$ and $^3P_0$ excited state manifold, respectively.[13] The extinction coefficient increases over the pH range 6.6 to 10.2, which may be due to an increase in the formation of the $[Pr(EDTA)]^-_{(aq)}$ species, where $EDTA^{4-}$ is bound in a hexadentate, rather than pentadentate, mode. This effect has also been observed in the literature for a Pu^{IV}:$EDTA^{4-}$ system.[15] In the 1:1 Pr^{III}:$EDTA^{4-}$ system, the extinction coefficient decreases over the pH range 10.2 to 12.1. From the NMR spectra in Section 3.2, it was observed that hydroxide becomes a competitor for lanthanide coordination at high pH (*i.e.* greater than pH 10). Therefore, it is likely that the observed decrease in the extinction coefficient after pH 10.2 is due to hydrolysis of the $[Pr(EDTA)]^-_{(aq)}$ complex to the $[Pr(EDTA)(OH)]^{2-}_{(aq)}$ species, and possibly some $Pr(OH)_{3(s)}$.

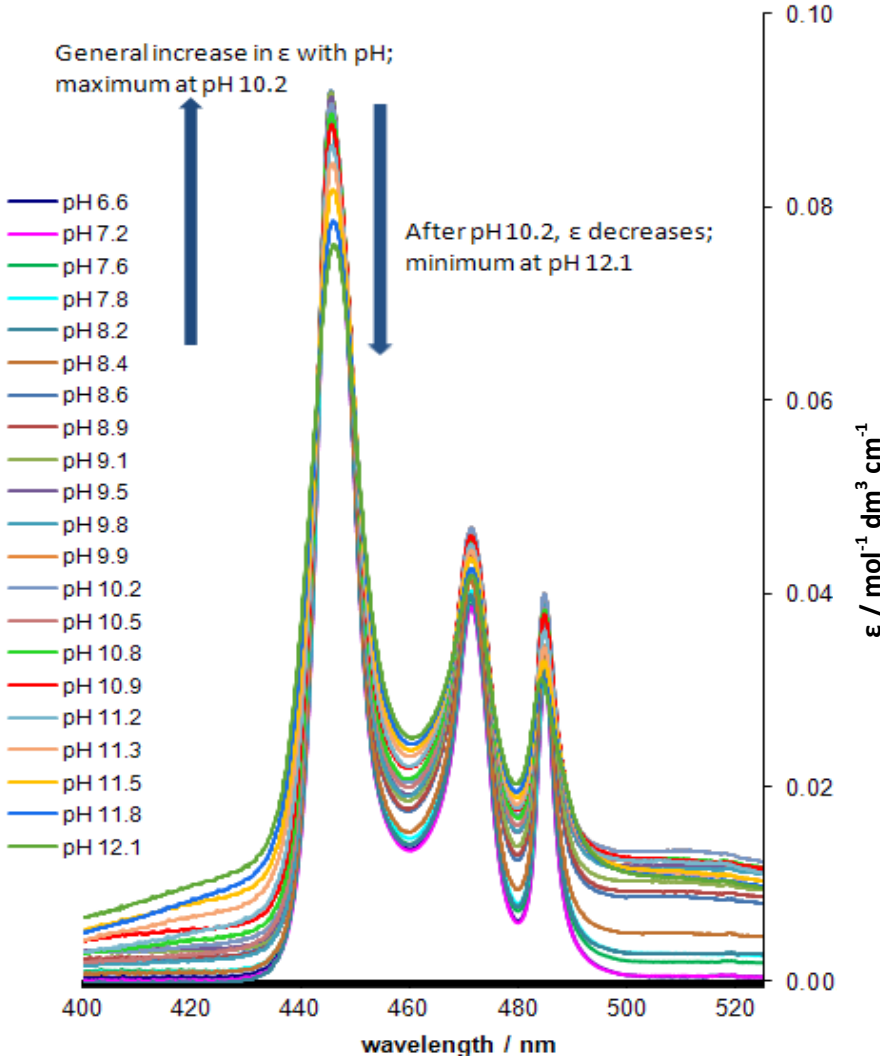

Figure 3.25: Electronic absorption spectra for the effect of pH on a 1:1 Pr^{III}:$EDTA^{4-}$ system; I = 0.5 M $NaNO_3$; $[Pr^{III}]_i = [EDTA^{4-}]_i$ = 10 mM.

The 1:1 Nd^{III}:$EDTA^{4-}$ system has been analysed by UV-Vis absorption spectroscopy as a function of pH at I = 0.5 M $NaNO_3$ (Figure 3.26). The absorption band around 580 nm corresponds to the hypersensitive $^4I_{9/2} \rightarrow {}^4G_{5/2}$ transition of Nd^{III}, which arises because $\Delta J \leq 2$, $\Delta L \leq 2$ and $\Delta S = 0$, where J, L and S are the total angular momentum, orbital quantum number and spin quantum number, respectively.[16] The intensity of the hypersensitive transition is affected the most when changes in the Nd^{III} coordination environment occur.[17] In the binary 1:1 Nd^{III}:$EDTA^{4-}$ system, there is a general red-shift of λ_{max} and an increase in the extinction coefficient as pH is increased from 8.2 to 10.8. Similar

to the 1:1 Pr^{III}:$EDTA^{4-}$ system, the increase in the extinction coefficient may be due to changes in the coordination mode of $EDTA^{4-}$ (*i.e.* the equilibrium between the pentadentate and hexadentate binding modes), and the decrease in the extinction coefficient over the pH range 10.8 to 11.5 is likely to be due to hydrolysis of the $[Nd(EDTA)]^-_{(aq)}$ complex to form the $[Nd(EDTA)(OH)]^{2-}_{(aq)}$ species and possibly some $Nd(OH)_{3(s)}$.

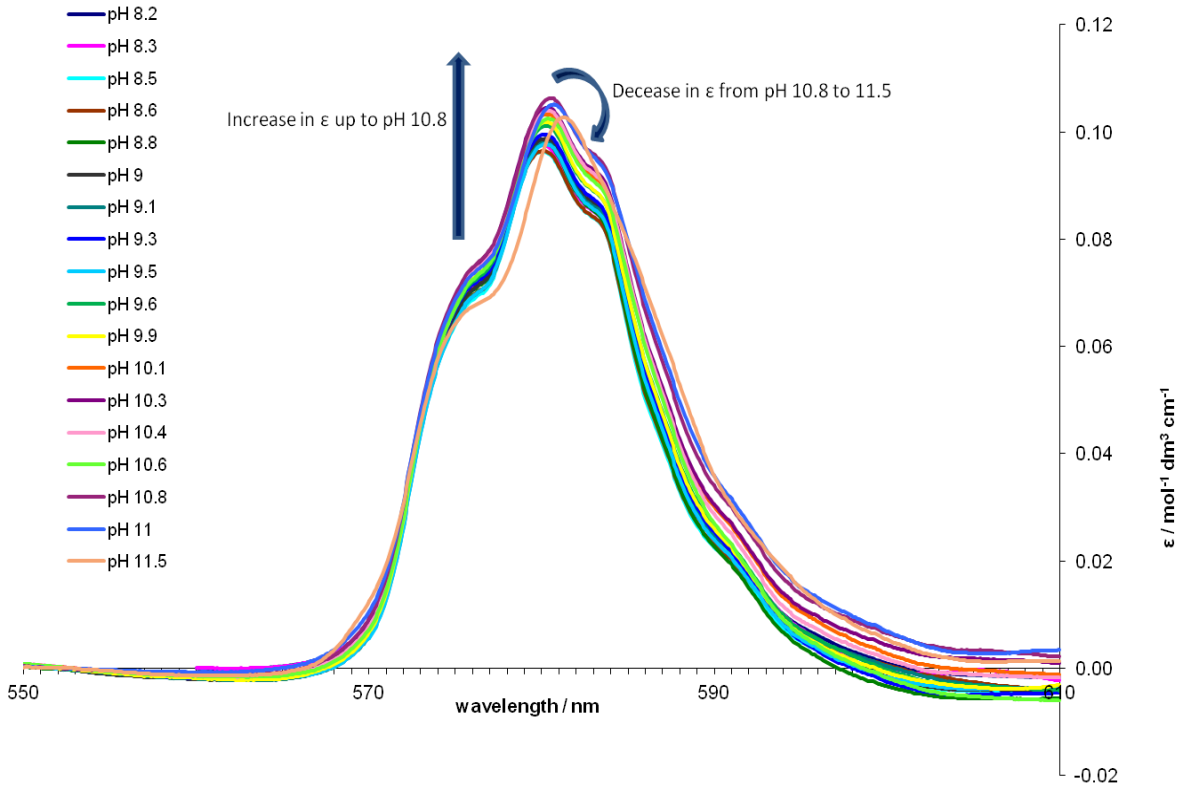

Figure 3.26: Electronic absorption spectra for the effect of pH on a 1:1 Nd^{III}:$EDTA^{4-}$ system; I = 0.5 M $NaNO_3$; $[Nd^{III}]_i = [EDTA^{4-}]_i$ = 10 mM.

The Ho^{III} ion also has a hypersensitive absorption band at around 450 nm, which corresponds to the $^5I_8 \rightarrow {}^5G_6$ transition.[17] The 1:1 Ho^{III}:$EDTA^{4-}$ absorption spectra shows a general increase in the extinction coefficient at 450 nm as pH is increased from 7.5 to 11.5 (Figure 3.27). After pH 11.0, it would be expected that hydrolysis of the $[Ho(EDTA)]^-_{(aq)}$ complex would begin to dominate the speciation. It may be a consequence of the lanthanide contraction that the extinction coefficient begins to decreases at a higher pH in the 1:1 Ho^{III}:$EDTA^{4-}$ system compared to the equivalent Pr^{III} (Figure 3.25) and Nd^{III} (Figure 3.26) systems.

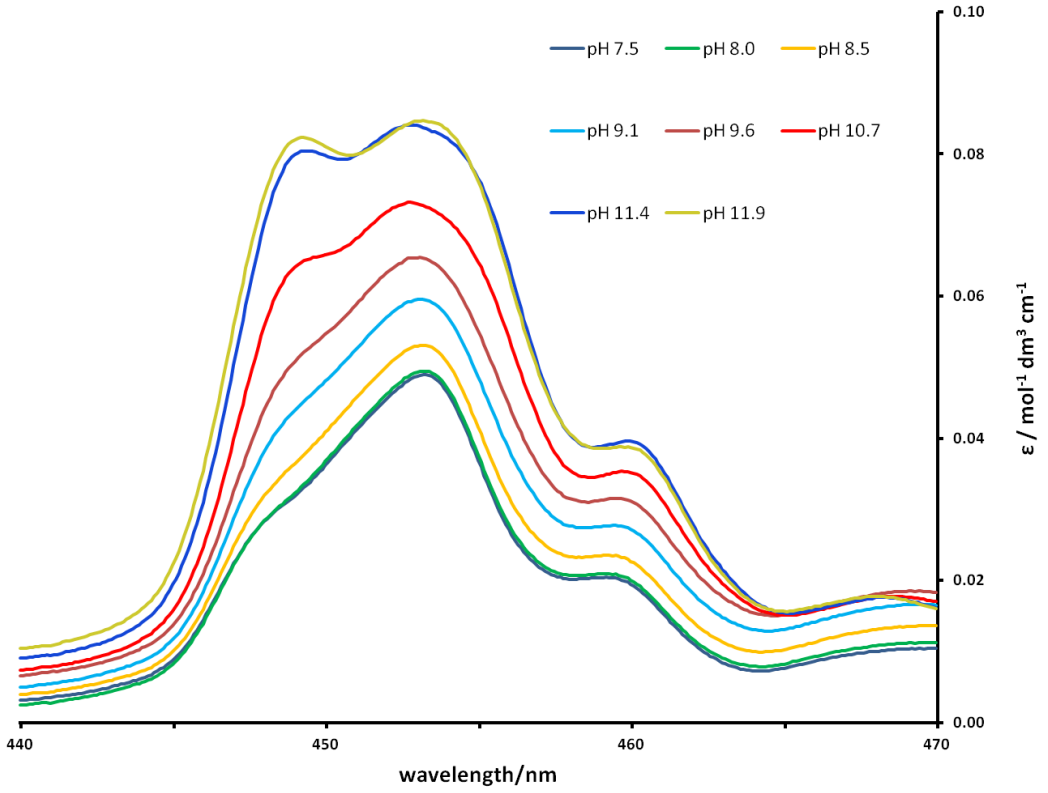

Figure 3.27: Electronic absorption spectra for the effect of pH on a 1:1 Ho^{III}:$EDTA^{4-}$ system; I = 0.5 M $NaNO_3$; $[Ho^{III}]_i = [EDTA^{4-}]_i$ = 10 mM.

In the 1:1 Ln^{III}:$EDTA^{4-}$ systems (Ln = Pr, Nd, Ho) analysed by UV-Vis spectroscopy, the extinction coefficient for the profiles increases approximately over the pH range 6 to 10, suggesting a change in equilibria in solution. By comparison, the NMR spectra for the La^{III} and Lu^{III} systems indicates that the $[Ln(EDTA)]^-_{(aq)}$ complex is the only species in solution over this pH range. This difference between the NMR and UV-Vis results may arise because the UV-Vis results were performed at a constant ionic strength (*i.e.* 0.5 M $NaNO_3$), whereas the ionic strength was not controlled in the NMR experiments.

3.3.2 Trivalent Lanthanide-EDTA-Carbonate Ternary Systems (Pr, Nd and Ho)

The electronic absorption spectra of the 1:1:1 Ln^{III}:$EDTA^{4-}$:CO_3^{2-} ternary systems (where Ln = Pr, Nd, Ho) have been analysed as a function of pH, at I = 0.5 M, to observe if the formation of the $[Ln(EDTA)(CO_3)]^{3-}_{(aq)}$ complex can be detected by UV-Vis spectroscopy. On increasing the pH from 7.7 to 10.6 in the 1:1:1 Pr^{III}:$EDTA^{4-}$:CO_3^{2-} system, there is a general decrease in the extinction coefficient for the absorption bands at approximately 445, 465 and 490 nm (Figure 3.28). By contrast, in the 1:1 Pr^{III}:$EDTA^{4-}$ system, the UV-Vis spectra showed the extinction coefficient to increase up to pH 10.2 and then decrease after pH 10.2 (Figure 3.25). The decrease in the extinction coefficient in the 1:1:1 Pr^{III}:$EDTA^{4-}$:CO_3^{2-} system from pH 7.7 to 10.6 may suggest that the $[Pr(EDTA)(CO_3)]^{3-}_{(aq)}$ species is a weaker light absorbing complex compared to the $[Pr(EDTA)]^{-}_{(aq)}$ species. This may be related to a change in symmetry of the complex when the carbonate anion interacts with the $[Pr(EDTA)]^{-}_{(aq)}$ complex.

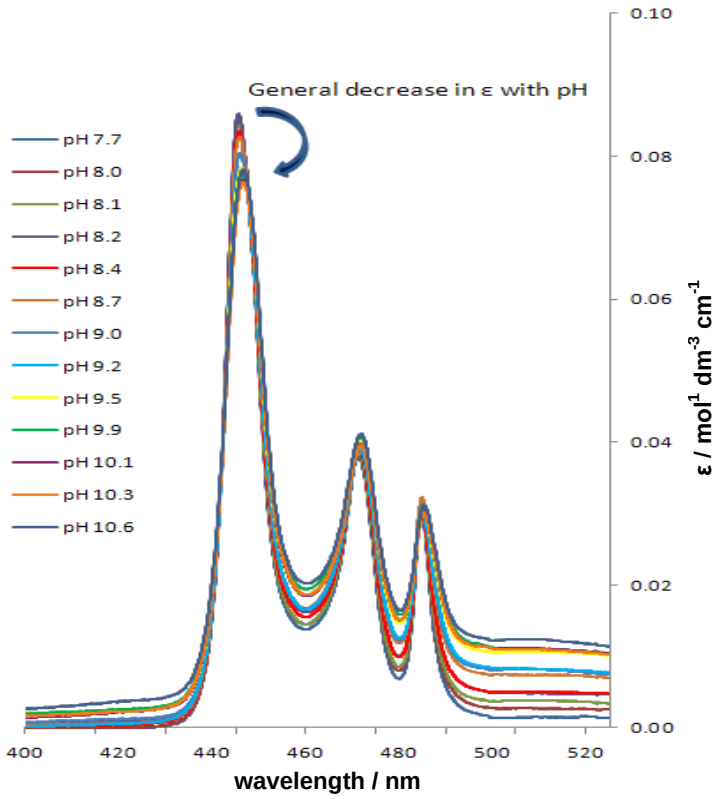

Figure 3.28: Electronic absorption spectra for the effect of pH on a 1:1:1 Pr^{III}:$EDTA^{4-}$:CO_3^{2-} system; I = 0.5 M $NaNO_3$; $[Pr^{III}]_i = [EDTA^{4-}]_i = [CO_3^{2-}]_i$ = 10 mM.

A bathochromic shift of the λ_{max} in both the 1:1 Pr^{III}:$EDTA^{4-}$ and 1:1:1 Pr^{III}:$EDTA^{4-}$:CO_3^{2-} systems can be observed in Figures 3.23 and 3.26. If the λ_{max} for both of these systems is plotted against pH (Figure 3.29), the λ_{max} for the 1:1 Pr^{III}:$EDTA^{4-}$ system remains constant at around 445.7 nm up to pH 11.4, after which it then shifts to 446.3 nm. By contrast, the 1:1:1 Pr^{III}:$EDTA^{4-}$:CO_3^{2-} system shows a gradual shift in λ_{max} from 445.6 to 446.8 nm as pH is increased. The constant λ_{max} in the 1:1 Pr^{III}:$EDTA^{4-}$ system may be due to the $[Pr(EDTA)]^-_{(aq)}$ complex dominating solution speciation up to pH 11.4. The shift of the λ_{max} after pH 11.4 may be due to the coordination mode of $EDTA^{4-}$ alternating between penta- and hexadentate or due to the formation of the $[Pr(EDTA)(OH)]^{2-}_{(aq)}$ species. The gradual shift of λ_{max} in the 1:1:1 Pr^{III}:$EDTA^{4-}$:CO_3^{2-} system may be due to the formation of the $[Pr(EDTA)(CO_3)]^{3-}_{(aq)}$ species.

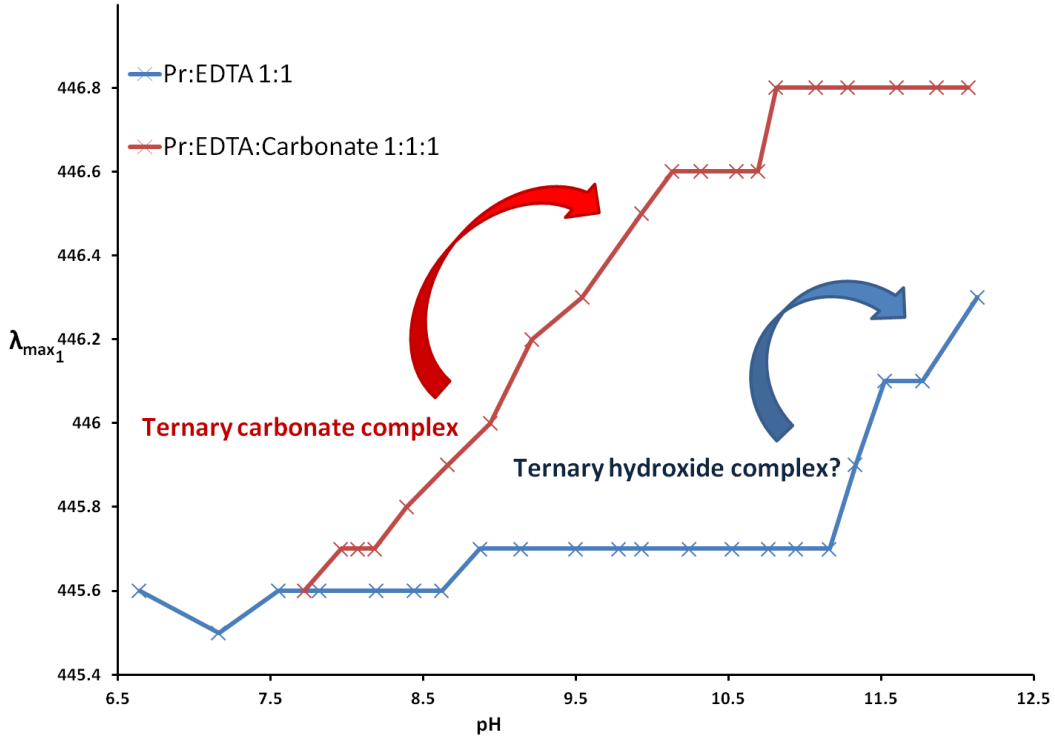

Figure 3.29: Plot of λ_{max} *vs.* pH in the 1:1 Pr^{III}:$EDTA^{4-}$ and 1:1:1 Pr^{III}:$EDTA^{4-}$:CO_3^{2-} systems; I = 0.5 M $NaNO_3$; $[Pr^{III}]_i = [EDTA^{4-}]_i = [CO_3^{2-}]_i$ = 10 mM.

The absorption profiles of the 1:1:1 Nd^{III}:$EDTA^{4-}$:CO_3^{2-} system (Figure 3.30) show a greater increase in the extinction coefficient for the hypersensitive absorption band as pH is

increased, compared to the binary system (Figure 3.26). This increase in intensity of the hypersensitive band, when carbonate is present, indicates that the $[Nd(EDTA)(CO_3)]^{3-}_{(aq)}$ species is forming. The extinction coefficient decreases at pH 11.1, which suggests that carbonate is beginning to be replaced by hydroxide. A gradual red-shift of λ_{max} is also observed as pH is increased.

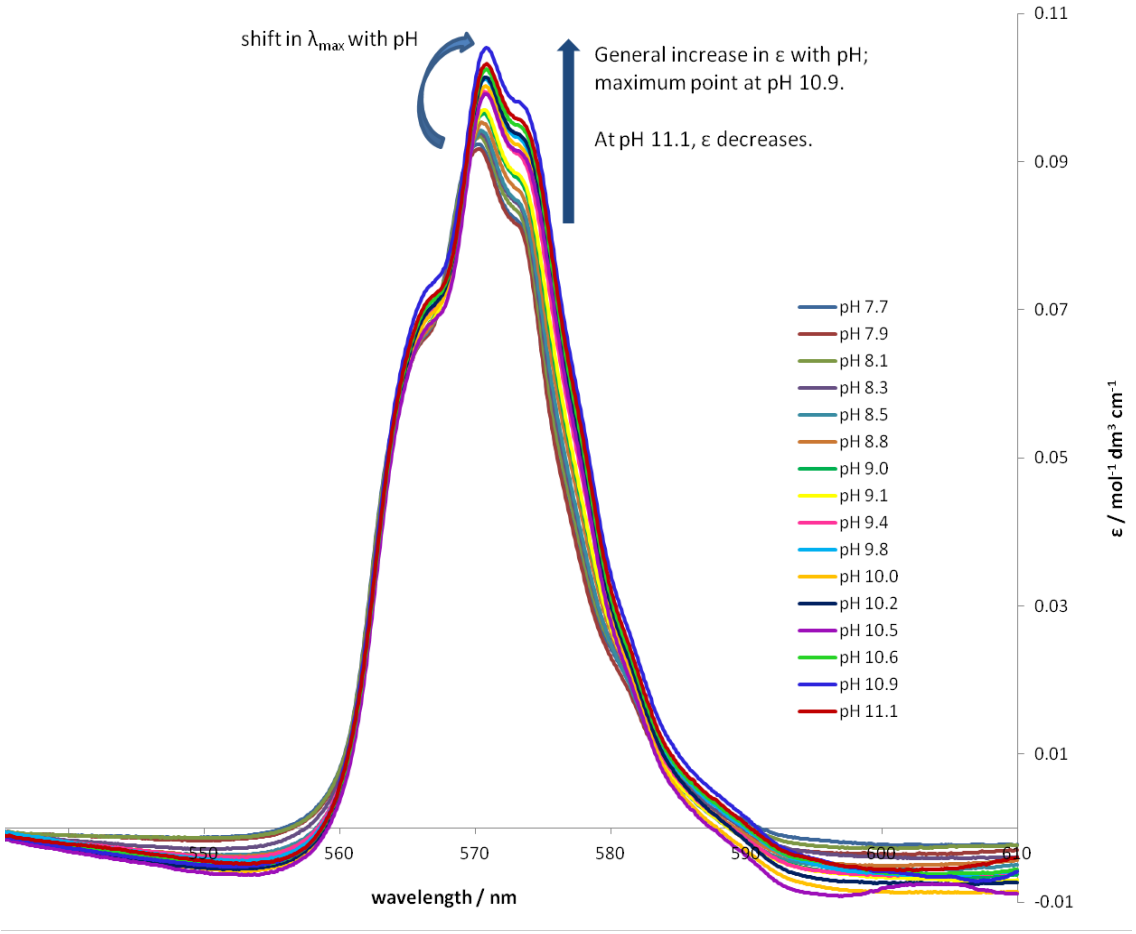

Figure 3.30: Electronic absorption spectra for the effect of pH on a 1:1:1 Nd^{III}:$EDTA^{4-}$:CO_3^{2-} system; I = 0.5 M $NaNO_3$; $[Nd^{III}]_i = [EDTA^{4-}]_i = [CO_3^{2-}]_i$ = 10 mM.

Similar to the 1:1:1 Nd^{III}:$EDTA^{4-}$:CO_3^{2-} ternary system, the absorption profiles of the Ho^{III} ternary system (Figure 3.31) show a greater increase in the extinction coefficient for the hypersensitive absorption band as pH is increased, compared to the binary system (Figure 3.27). This increase in intensity of the Ho^{III} absorption band, in the presence of carbonate, implies the formation of the $[Ho(EDTA)(CO_3)]^{3-}_{(aq)}$ species. The extinction coefficient begins

to decrease at pH 11.7, indicating that carbonate is being replaced by hydroxide in the Ho^{III} inner coordination sphere. This may form the $[Ho(EDTA)(OH)]^{2-}_{(aq)}$ species, and possibly some $Ho(OH)_{3(s)}$.

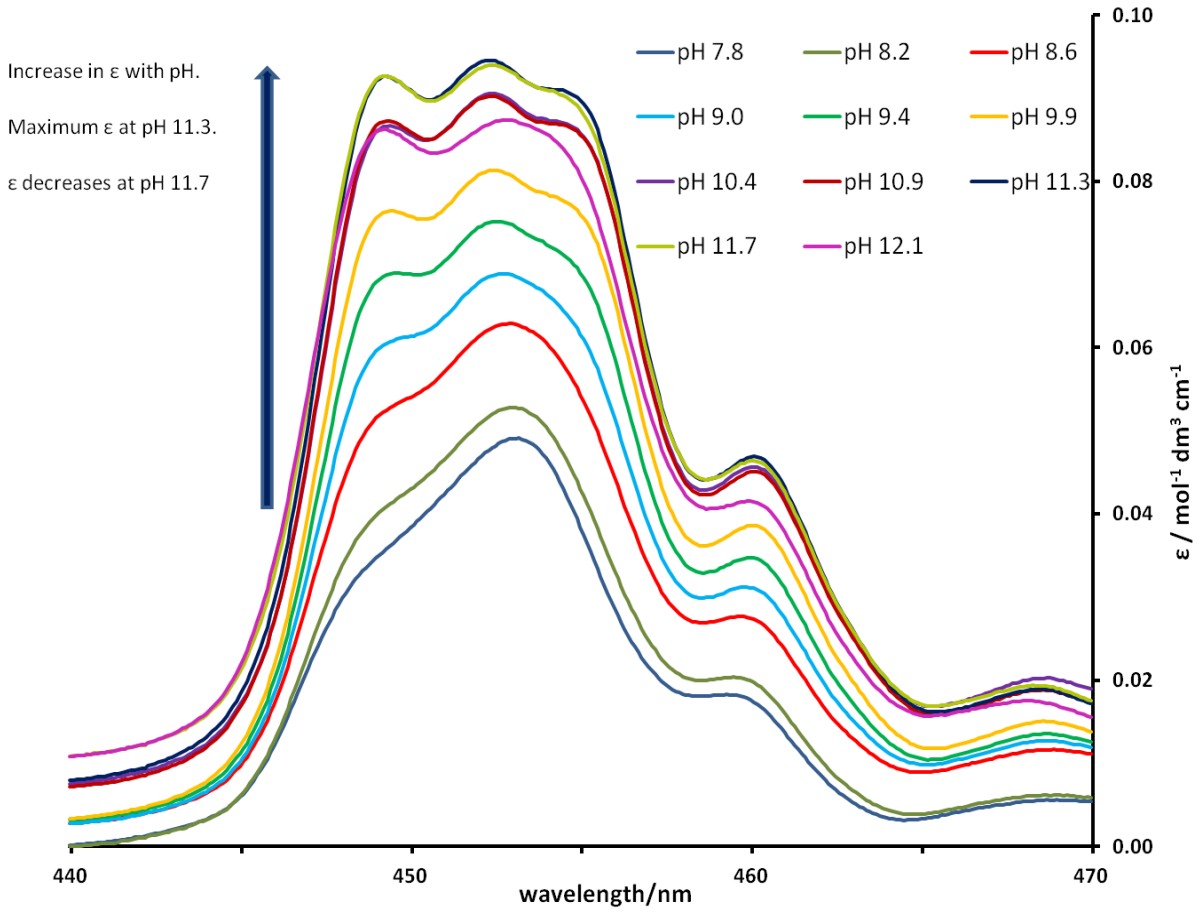

Figure 3.31: Electronic absorption spectra for the effect of pH on a 1:1:1 Ho^{III}:$EDTA^{4-}$:CO_3^{2-} system; I = 0.5 M $NaNO_3$; $[Ho^{III}]_i = [EDTA^{4-}]_i = [CO_3^{2-}]_i$ = 10 mM.

3.3.3 Summary

UV-Vis spectroscopy has been a successful technique for detecting the formation of $[Ln(EDTA)]^-_{(aq)}$, $[Ln(EDTA)(CO_3)]^{3-}_{(aq)}$ species, and possibly a hydrolysis complex of $[Ln(EDTA)(OH)]^{2-}_{(aq)}$ (where Ln = Pr^{III}, Nd^{III}, Ho^{III}). The trivalent lanthanides, Nd^{III} and Ho^{III}, contain hypersensitive electronic transitions that cause significant changes of their

absorption profiles when their inner coordination sphere alters. By contrast, the Pr^{III} ion does not contain hypersensitive transitions and the differences in the absorption profiles of the 1:1 Pr^{III}:$EDTA^{4-}$ binary and 1:1:1 Pr^{III}:$EDTA^{4-}$:CO_3^{2-} ternary systems were subtle. The UV-Vis spectroscopy results indicate carbonate binds to the $[Ln(EDTA)]^-_{(aq)}$ complex over the pH range 8 to 11, after which hydroxide competes with carbonate for coordination to the $[Ln(EDTA)]^-_{(aq)}$ complex. There is general agreement between the UV-Vis absorption results and the NMR results that were obtained in Section 3.2.

3.4 Luminescence Spectroscopy

Luminescence spectroscopy can be used as a method for quantifying the number of bound water molecules to a metal ion.[18] The formation of $[Ln(EDTA)]^-_{(aq)}$, $[Ln(EDTA)(CO_3)]^{3-}_{(aq)}$ and $[Ln(EDTA)(OH)]^{2-}_{(aq)}$ complexes have been indicated to exist by NMR and UV-Vis absorption spectroscopy. Luminescence spectroscopy has been used to analyse these species in order to determine the number of coordinated water molecules, hence providing further information on the coordination environment for these species.

3.4.1 Lanthanide-EDTA Binary Systems (Eu^{III} and Tb^{III})

Luminescence spectroscopic titrations have been performed on the 1:1 Ln^{III}:$EDTA^{4-}$ binary systems (where Ln = Eu or Tb), using H_2O or D_2O as the solvent and NaOH or NaOD for pH/pD adjustment. The Eu^{III} and Tb^{III} ions can be excited directly by absorption of light at 397 nm and 366 nm, respectively.[19] Both the excited Eu^{III} and Tb^{III} species have lifetimes of millisecond order.[20] The excited lanthanide species can either emit light, or they can be quenched non-radiatively by vibrational harmonics of X-H oscillators in the ligands (e.g. N-H) and O-H oscillators in the solvent (Figure 3.32).[20] This is the mechanism of excited state energy lost in the majority of lanthanide complexes.[20]

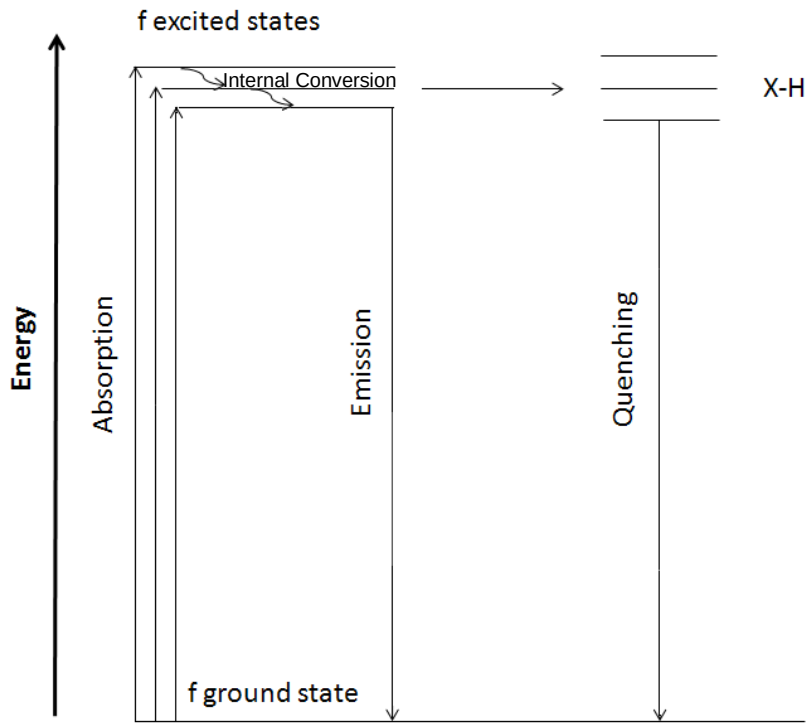

Figure 3.32: Simplified energy level diagram illustrating absorption, emission and quenching pathways. [Adapted from Reference 21].

The luminescence spectra of the 1:1 Eu^{III}:$EDTA^{4-}$ system shows narrow Eu^{III} emission bands at 580, 590, 617, 650 and 690 nm (Figure 3.33). The transitions that are responsible for these emission bands are: $^5D_0 \rightarrow {}^7F_0$ (580 nm); $^5D_0 \rightarrow {}^7F_1$ (590 nm); $^5D_0 \rightarrow {}^7F_2$ (617 nm), $^5D_0 \rightarrow {}^7F_3$ (650 nm) and $^5D_0 \rightarrow {}^7F_4$ (690 nm) (Figure 3.34).[18] The $^5D_0 \rightarrow {}^7F_2$ transition is hypersensitive (*i.e.* $\Delta J = 2$),[22] which will cause significant changes of the emission profile when the Eu^{III} inner coordination sphere alters and the overall symmetry of the complex changes. When the pH of the 1:1 Eu^{III}:$EDTA^{4-}$ system is increased from 7.5 to 10.1, there is a small increase in the emission intensity of the transition at 617 nm. This may be due to possible changes in the coordination mode of $EDTA^{4-}$ (*i.e.* pentadentate *vs.* hexadentate), and also to a small amount of $[Eu(EDTA)(OH)]^{2-}_{(aq)}$ species forming in solution. Hydrolysis of the $[Ln(EDTA)]^{-}_{(aq)}$ complexes was shown to be a more dominant effect after pH 11 (Sections 3.2 and 3.3), therefore at pH 10 there may only be a low concentration of the $[Eu(EDTA)(OH)]^{2-}_{(aq)}$ species.

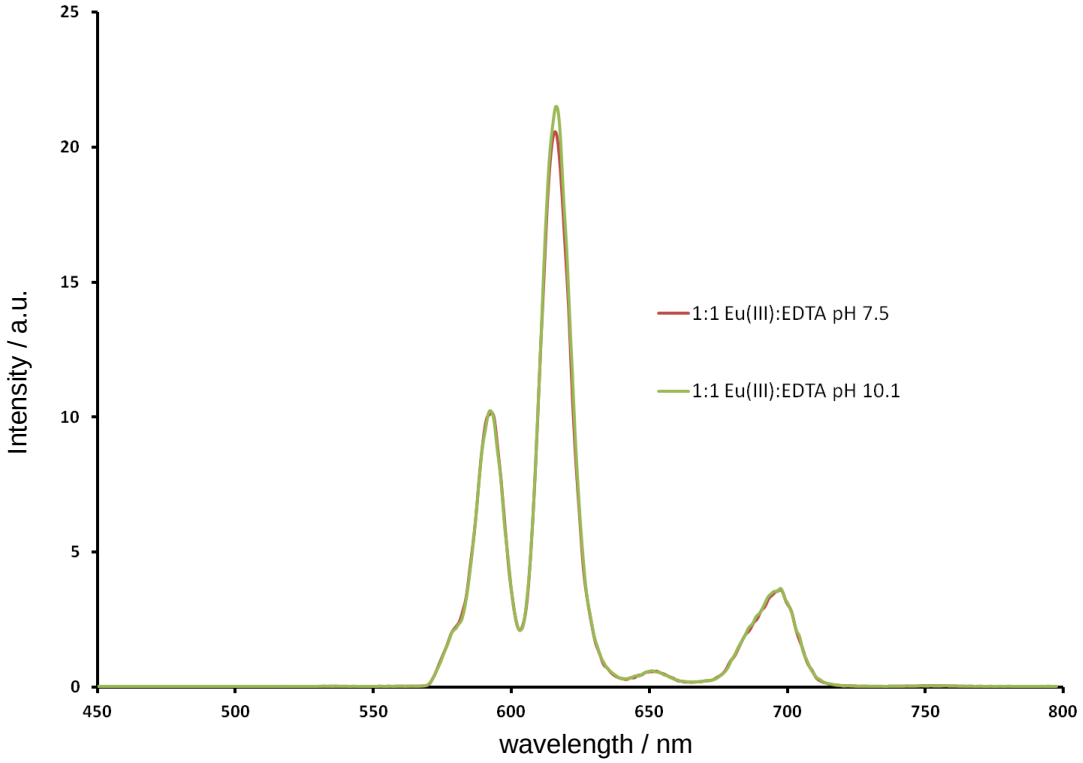

Figure 3.33: Emission spectra for the effect of pH on a 1:1 Eu^{III}:$EDTA^{4-}$ system; $[Eu^{III}]_i = [EDTA^{4-}]_i = 10$ mM; excitation wavelength = 397 nm.

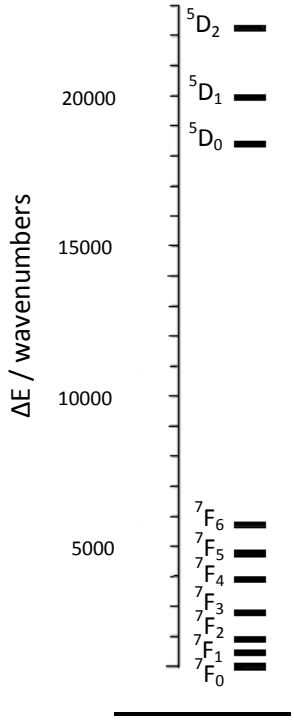

Figure 3.34: Energy level diagram for the Eu^{III} ion. [Adapted from Reference 17].

The luminescence spectra of the 1:1 Tb^{III}:$EDTA^{4-}$ system show narrow emission bands at 490, 545, 590, 620 and 650 nm (Figure 3.35). The transition from the $^5D_4$ emissive state to the $^7F_6$, $^7F_5$, $^7F_4$, $^7F_3$ ground state manifold, plus the $^5D_2 \rightarrow {}^7F_4$ transition, are all responsible for these emission bands, respectively. For the 1:1 Tb^{III}:$EDTA^{4-}$ system, the Tb^{III} emission bands increase in intensity over the pH range 8.6 to 11.6. The initial increase between pH 8.6 to 10.6 may be due to changes in the $EDTA^{4-}$ binding mode, and also due to some $[Tb(EDTA)(OH)]^{2-}_{(aq)}$ complex formation. The largest increase in the emission intensity is observed between pH 10.6 to 11.6 for the 545 nm band, which may indicate an increase in formation of the $[Tb(EDTA)(OH)]^{2-}_{(aq)}$ species. This would support the NMR and UV-Vis results discussed in Sections 3.2 and 3.3.

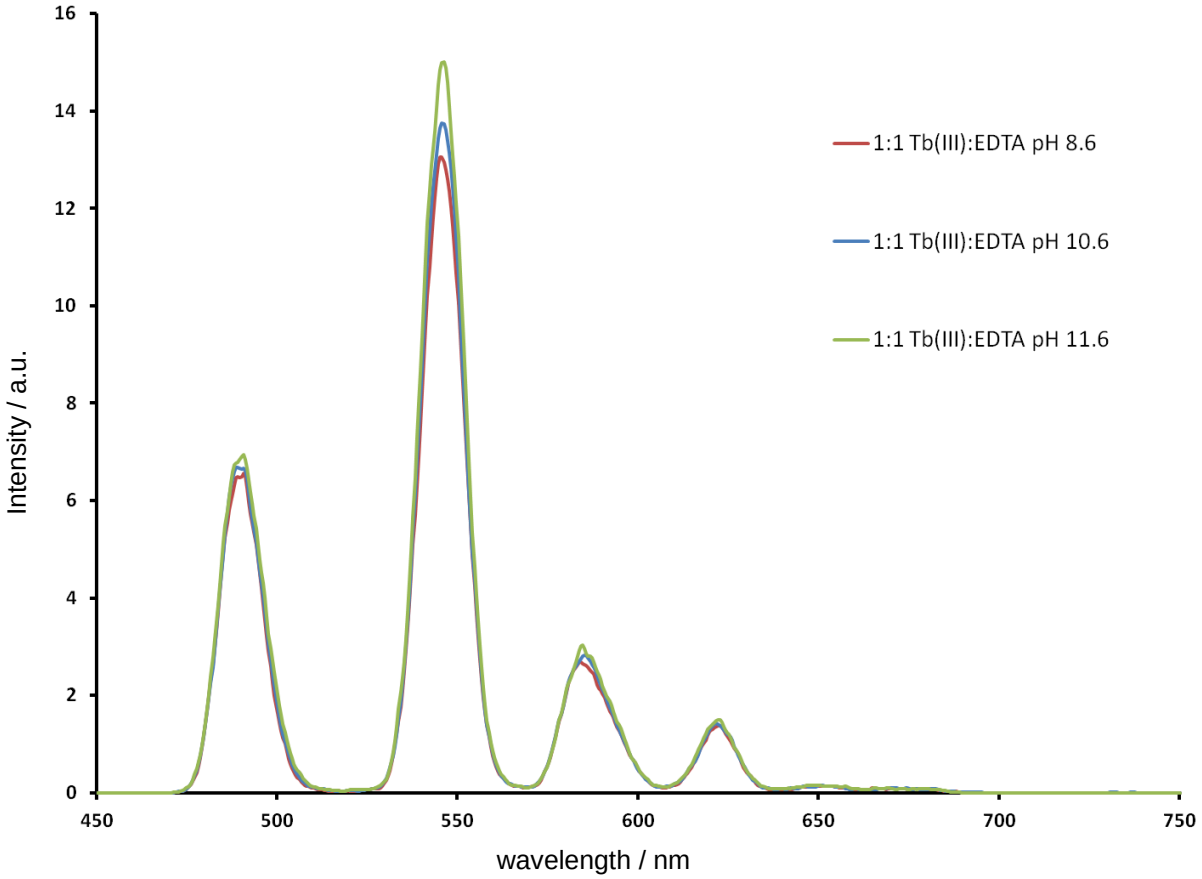

Figure 3.35: Emission spectra for the effect of pH on a 1:1 Tb^{III}:$EDTA^{4-}$ system; $[Tb^{III}]_i = [EDTA^{4-}]_i = 10$ mM; excitation wavelength = 366 nm.

The luminescent lifetimes (τ) have been calculated for the 1:1 Ln^{III}:$EDTA^{4-}$ systems (where Ln = Eu (Table 3.3) or Tb (Table 3.4)). The lifetimes of the excited species are always lower in H_2O, compared to D_2O, as the O-H oscillators are closer in energy to the excited state energy levels of the Eu^{III} and Tb^{III} ions.[20] Therefore, this allows an efficient route for non-radiative energy transfer from the lanthanide metal centre (Figure 3.32).[20] This effect is considerably decreased in deuterated solvents as there is reduced Franck-Condon overlap between the higher harmonics of the O-D oscillator and the Eu^{III} or Tb^{III} excited state.[20] Other oscillators can also quench the luminescence of a lanthanide ion, such as N-H, C-H, and C=O stretching vibrations.[19] The Eu^{III} luminescent lifetimes in H_2O for the pH region of 7.3 to 13.0 are all approximately 0.33 ms, and the lifetimes for the excited Eu^{III} species in D_2O over the pD region 7.5 to 13.0 are approximately 2.30 ms. This suggests that there is little effect of pH/pD on the lifetime of the excited species.

Terbium^{III} luminescent lifetimes are greater than Eu^{III} as there is less prominent Franck-Condon overlap between the Tb^{III} excited state energy levels and the O-H oscillators.[19] The Tb^{III} luminescent lifetimes are approximately 1.20 ms as pH is increased from 8.6 to 11.6. By contrast, there is a decrease in the luminescence lifetime from 3.64 to 2.76 ms as pD is increased from 8.6 to 11.8. This suggests a change in the Tb^{III} coordination sphere that is causing an increase in oscillator quenching in D_2O. This may be due to the functional groups on the $EDTA^{4-}$ ligand (*i.e.* C=O), as C=O will quench luminescence more effectively than O-D functional groups, though still not as effectively as O-H groups that dominate quenching in the H_2O system.

1:1 Eu^{III}:$EDTA^{4-}$	pH	τ / ms	pD	τ / ms
	7.3	0.32 ± 0.03	7.5	2.36 ± 0.02
	10.0	0.34 ± 0.03	10.1	2.39 ± 0.02
	13.0	0.32 ± 0.03	13.0	2.24 ± 0.02

Table 3.3: Luminescent lifetimes (τ) of the 1:1 Eu^{III}:$EDTA^{4-}$ system, at various pH/pD, in H_2O and D_2O.

1:1 Tb^{III}:$EDTA^{4-}$	pH	τ / ms	pD	τ / ms
	8.6	1.17 ± 0.12	8.6	3.64 ± 0.36
	10.5	1.22 ± 0.12	10.5	2.94 ± 0.29
	11.6	1.26 ± 0.13	11.8	2.76 ± 0.28

Table 3.4: Luminescent lifetimes (τ) of the 1:1 Tb^{III}:$EDTA^{4-}$ system, at various pH/pD, in H_2O and D_2O.

The number of water molecules (N_{H_2O}) coordinated to Eu^{III} and Tb^{III} can be calculated using the Horrocks equation,[19,23] where:

$$N_{H_2O} = A\left[\left(\frac{1}{\tau_{H_2O}}\right) - \left(\frac{1}{\tau_{D_2O}}\right) - B\right]$$

(equation 3.10)

For Eu^{III}: [23]

A=1.11 ms

B=0.31 ms^{-1}

For Tb^{III}: [19]

A=5 ms

B=0.06 ms^{-1}

τ = luminescence lifetime in ms

The calculated N_{H_2O} bound to Eu^{III} in the 1:1 Eu^{III}:$EDTA^{4-}$ system at pH 7.4 is 2.7 (Table 3.5). As the hydration number of the $Eu^{III}_{(aq)}$ ion is nine[5] and $EDTA^{4-}$ is a hexadentate ligand, the reduction in N_{H_2O} in the presence of $EDTA^{4-}$ corresponds to the formation of the $[Eu(EDTA)(H_2O)_3]^-_{(aq)}$ species. This also agrees with the single crystal x-ray diffraction (XRD) structure of a $[NH_4][Eu(EDTA)(H_2O)_3]$ complex that was obtained between pH 7 to 9.[24] There is a very small decrease in the N_{H_2O} coordinated to the $[Eu(EDTA)]^-_{(aq)}$ complex at high alkaline pH, which may be caused by some hydroxide interaction with the $[Eu(EDTA)]^-_{(aq)}$ complex. Thakur *et al.*[25] also report a decrease in the N_{H_2O} coordinated to Eu^{III}-ligand complexes at high pH, which they attribute to the formation of hydrolysis species. The N_{H_2O} bound to the Tb^{III} ion in the 1:1 Tb^{III}:$EDTA^{4-}$ system at pH 8.6 is 2.6 (Table 3.5). The hydration number of the Tb^{III} ion has been calculated to be eight,[5] and so on coordination with $EDTA^{4-}$, the N_{H_2O} coordinated to the $[Tb(EDTA)]^-_{(aq)}$ complex would be expected to be

two. The value of 2.6 for the N_{H_2O} coordinated to $[Tb(EDTA)]^-_{(aq)}$ at pH 8.6 may indicate that $EDTA^{4-}$ is alternating between the hexadentate and pentadentate coordination modes. As pH is increased to 10.5, the N_{H_2O} bound to the Tb^{III} ion in this system reduces to 2.1, which suggests that the hexadentate binding mode dominates and corresponds to the $[Tb(EDTA)(H_2O)_2]^-_{(aq)}$ complex. This change in coordination mode of $EDTA^{4-}$ may also be the reason why the lifetimes of the $[Tb(EDTA)]^-_{(aq)}$ excited state would decrease in D_2O as there may be some quenching caused by C=O oscillators of the $EDTA^{4-}$ ligand. At pH 11.7, there is a small reduction in the N_{H_2O} bound to the Tb^{III} ion to 1.8, which may be due to some formation of the $[Tb(EDTA)(OH)(H_2O)]^{2-}_{(aq)}$ complex.[25]

1:1 Eu^{III}:$EDTA^{4-}$	**1:1 Tb^{III}:$EDTA^{4-}$**
pH 7.4, $\boldsymbol{N_{H_2O}}$ **= 2.7 ± 0.5**	pH 8.6, $\boldsymbol{N_{H_2O}}$ **= 2.6 ± 0.5**
pH 10.1, $\boldsymbol{N_{H_2O}}$ **= 2.5 ± 0.5**	pH 10.5, $\boldsymbol{N_{H_2O}}$ **= 2.1 ± 0.5**
pH 13.0, $\boldsymbol{N_{H_2O}}$ **= 2.6 ± 0.5**	pH 11.7, $\boldsymbol{N_{H_2O}}$ **= 1.8 ± 0.5**

Table 3.5: Calculated N_{H_2O} bound to the Ln^{III} ions in the 1:1 Ln^{III}:$EDTA^{4-}$ system (Ln = Eu or Tb), at various pH. The uncertainty in N_{H_2O} calculations is ± 0.5 water molecules.[25]

3.4.2 Lanthanide-EDTA-Carbonate Ternary Systems (Eu^{III} and Tb^{III})

Luminescence spectroscopic titrations have been performed on the 1:1:1 Ln^{III}:$EDTA^{4-}$:CO_3^{2-} ternary systems (where Ln = Eu or Tb), using H_2O or D_2O as the solvent and NaOH or NaOD for pH/pD adjustment. On increasing the pH of the 1:1:1 Eu^{III}:$EDTA^{4-}$:CO_3^{2-} system from pH 7.9 to 10.0, there is a large increase in the emission intensity of the transition at 617 nm (Figure 3.36). This increase in the emission intensity is significantly larger than the increase observed in the 1:1 Eu^{III}:$EDTA^{4-}$ system (Figure 3.33). The luminescence results indicate that carbonate is interacting with the $[Eu(EDTA)]^-_{(aq)}$ complex, and the large increase in emission intensity may suggest that carbonate causes a larger change in the coordination sphere of the $[Eu(EDTA)]^-_{(aq)}$ complex compared to hydroxide.

Similarly, when increasing the pH of the 1:1:1 Tb^{III}:$EDTA^{4-}$:CO_3^{2-} system from pH 8.1 to 10.7, there is a significantly larger increase in the emission intensities of the Tb^{III} transitions (Figure 3.37) compared to that of the 1:1 Tb^{III}:$EDTA^{4-}$ system (Figure 3.34). This suggests carbonate is binding to the $[Tb(EDTA)]^-_{(aq)}$ complex.

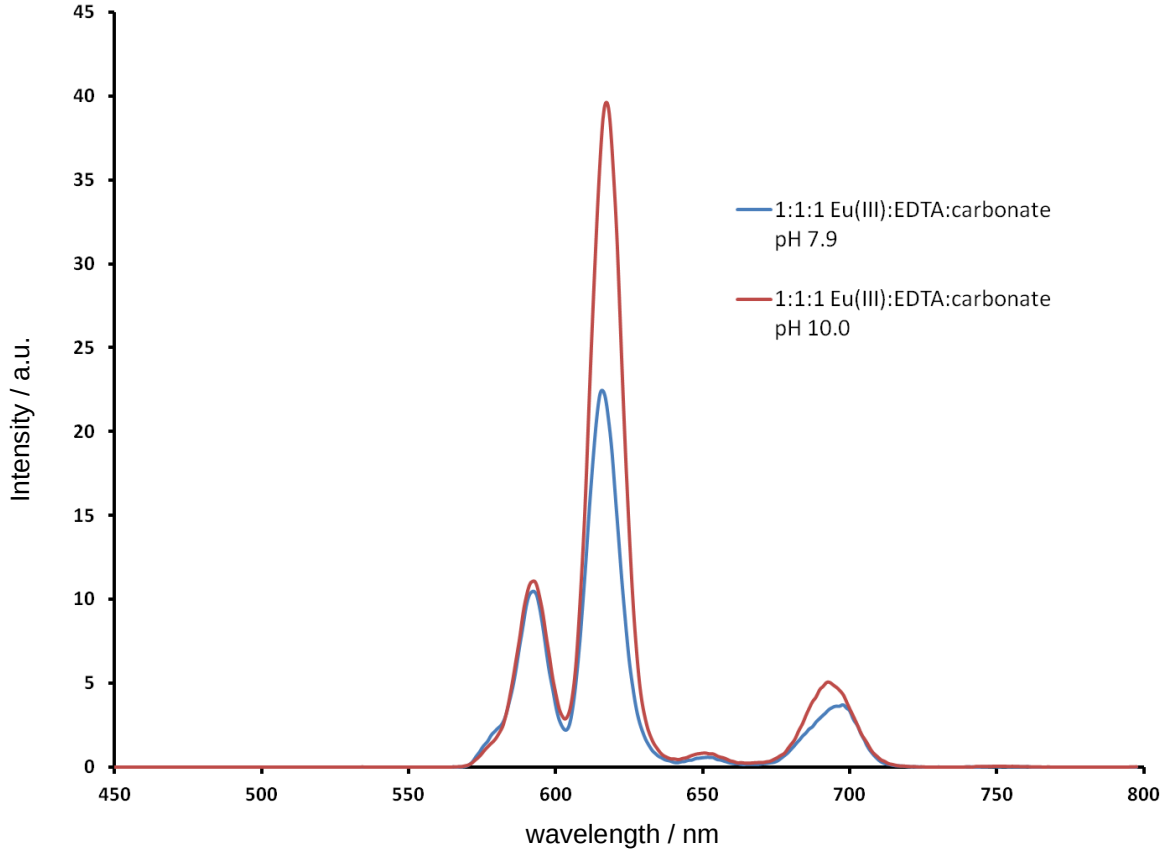

Figure 3.36: Emission spectra for the effect of pH on a 1:1:1 Eu^{III}:$EDTA^{4-}$:CO_3^{2-} system; $[Eu^{III}]_i = [EDTA^{4-}]_i = [CO_3^{2-}]_i = 10$ mM; excitation wavelength = 397 nm.

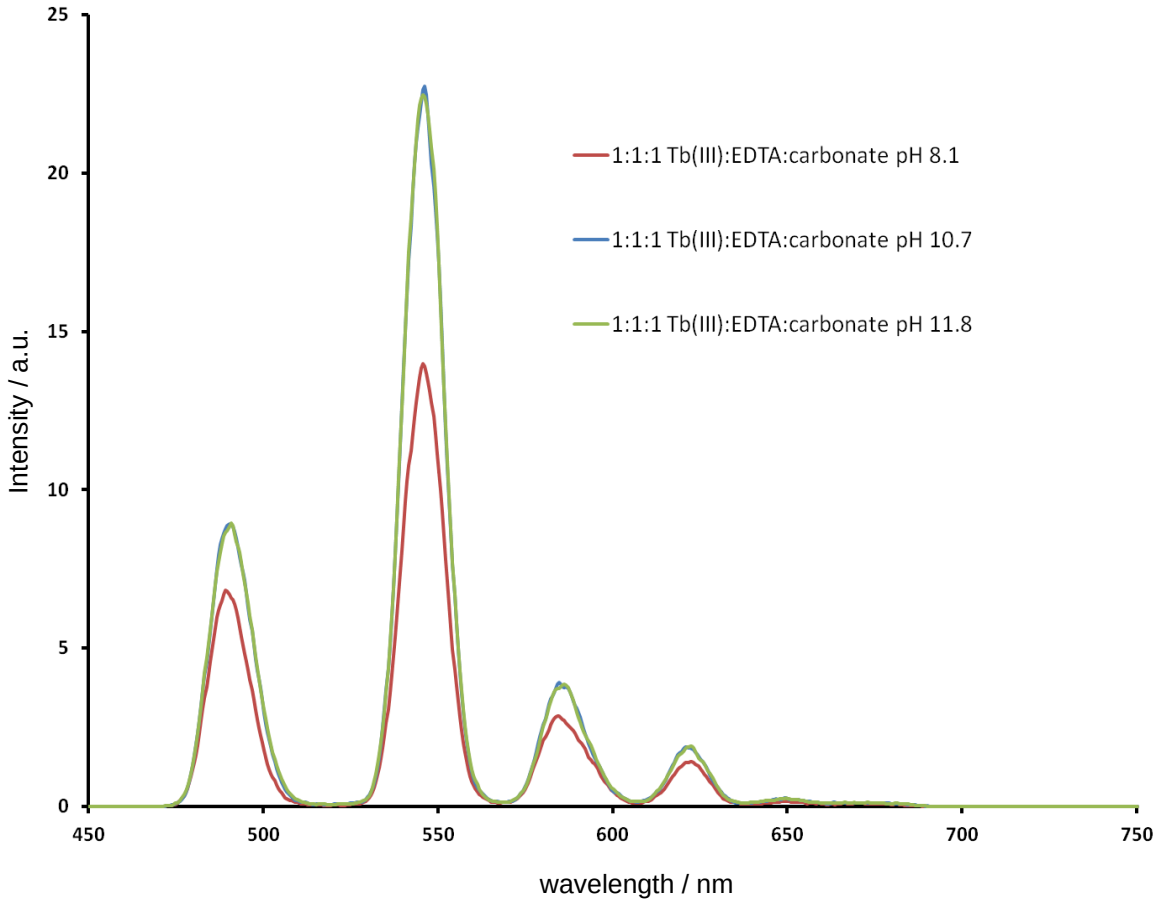

Figure 3.37: Emission spectra for the effect of pH on a 1:1:1 Tb^{III}:$EDTA^{4-}$:CO_3^{2-} system; $[Tb^{III}]_i = [EDTA^{4-}]_i = [CO_3^{2-}]_i$ = 10 mM; excitation wavelength = 366 nm.

The luminescent lifetimes have been calculated for the 1:1:1 Ln^{III}:$EDTA^{4-}$:CO_3^{2-} systems (where Ln = Eu (Table 3.6) or Tb (Table 3.7)). For both the Eu^{III} and Tb^{III} ternary systems with $EDTA^{4-}$ and CO_3^{2-}, there is an increase in the luminescent lifetimes with pH in H_2O environments but a decrease in the lifetimes with pD in D_2O environments. This means that when carbonate binds to Eu- or Tb-EDTA complexes, it causes a reduction in O-H oscillator quenching by H_2O (*i.e.* carbonate replaces water molecules), but an increase in oscillator quenching in D_2O because C=O functional groups of carbonate will quench the excited state better than O-D oscillators.[18]

	pH	τ / ms	pD	τ / ms
1:1:1 Eu^{III}:$EDTA^{4-}$:CO_3^{2-}	7.9	0.33 ± 0.03	7.8	2.39 ± 0.24
	10.0	0.42 ± 0.04	10.1	2.17 ± 0.22
	10.9	0.46 ± 0.05	10.9	2.00 ± 0.20
	12.0	0.43 ± 0.04	12.0	1.97 ± 0.20

Table 3.6: Luminescent lifetimes (τ) of the 1:1:1 Eu^{III}:$EDTA^{4-}$:CO_3^{2-} system, at various pH/pD, in H_2O and D_2O.

	pH	τ / ms	pD	τ / ms
1:1:1 Tb^{III}:$EDTA^{4-}$:CO_3^{2-}	8.1	1.16 ± 0.12	8.4	3.58 ± 0.36
	10.7	1.52 ± 0.15	10.6	2.92 ± 0.29
	11.8	1.56 ± 0.16	11.6	2.80 ± 0.28

Table 3.7: Luminescent lifetimes (τ) of the 1:1:1 Tb^{III}:$EDTA^{4-}$:CO_3^{2-} system, at various pH/pD, in H_2O and D_2O.

The calculated N_{H_2O} bound to the Eu^{III} ion in the 1:1:1 Eu^{III}:$EDTA^{4-}$:CO_3^{2-} system decreases from 2.6 to 1.7 over the pH range 7.9 to 12.0 (Table 3.8). The N_{H_2O} coordinated to the $[Eu(EDTA)]^-_{(aq)}$ complex has reduced in the presence of carbonate compared to when it is absent (Table 3.5). This indicates that the $[Eu(EDTA)(CO_3)(H_2O)]^{3-}_{(aq)}$ species forms, and it is likely that carbonate would bind in a bidentate (rather than monodentate) coordination. Comparable to the 1:1:1 Eu^{III}:$EDTA^{4-}$:CO_3^{2-} system, the calculated N_{H_2O} bound to the Tb^{III} ion in the 1:1:1 Tb^{III}:$EDTA^{4-}$:CO_3^{2-} system decreases from 2.6 to 1.1 over the pH range 8.3 to 11.7 (Table 3.8). The N_{H_2O} coordinated to the $[Tb(EDTA)]^-_{(aq)}$ complex has reduced in the presence of carbonate compared to the 1:1 Tb^{III}:$EDTA^{4-}$ system and so the $[Tb(EDTA)(CO_3)]^{3-}_{(aq)}$ species forms.

The carbonate anion and water molecules may be in fast exchange for coordination to $[Ln(EDTA)]^-_{(aq)}$ complexes (where Ln = Eu^{III} and Tb^{III}), therefore the calculated N_{H_2O} bound to the Ln^{III} ions in these systems will be an average of this exchange process. This is because N_{H_2O} bound to the $[Eu(EDTA)]^-_{(aq)}$ complex in the presence of carbonate is approximately two, which may be an average of three water molecules bound to the $[Eu(EDTA)]^-_{(aq)}$ complex and one water molecule bound to the $[Eu(EDTA)(CO_3)]^{3-}_{(aq)}$ complex (Figure 3.38).

Likewise, the N_{H_2O} bound to the $[Tb(EDTA)]^-_{(aq)}$ complex in the presence of carbonate is approximately one, which may be an average of two water molecules bound to the $[Tb(EDTA)]^-_{(aq)}$ complex and zero water molecules bound to the $[Tb(EDTA)(CO_3)]^{3-}_{(aq)}$ (Figure 3.39). It is also likely that only a fraction of the total carbonate can bind to the $[Eu(EDTA)]^-_{(aq)}$ and $[Tb(EDTA)]^-_{(aq)}$ complexes due to competition with H_2O molecules and OH^- ions, and so the calculated N_{H_2O} bound to the Ln^{III} ions may reflect this speciation.

1:1:1 $Eu^{III}:EDTA^{4-}:CO_3^{2}$	**1:1:1** $Tb^{III}:EDTA^{4-}:CO_3^{2-}$
pH 7.9, N_{H_2O} = **2.6 ± 0.5**	pH 8.3, N_{H_2O} = **2.6 ± 0.5**
pH 10.0, N_{H_2O} = **1.8 ± 0.5**	pH 10.7, N_{H_2O} = **1.3 ± 0.5**
pH 10.9, N_{H_2O} = **1.5 ± 0.5**	pH 11.7, N_{H_2O} = **1.1 ± 0.5**
pH 12.0, N_{H_2O} = **1.7 ± 0.5**	

Table 3.8: Calculated N_{H_2O} bound to the Ln^{III} ions in the 1:1:1 $Ln^{III}:EDTA^{4-}:CO_3^{2-}$ system (Ln = Eu or Tb) at various pH values. The uncertainty in N_{H_2O} calculations is ± 0.5 water molecules.[25]

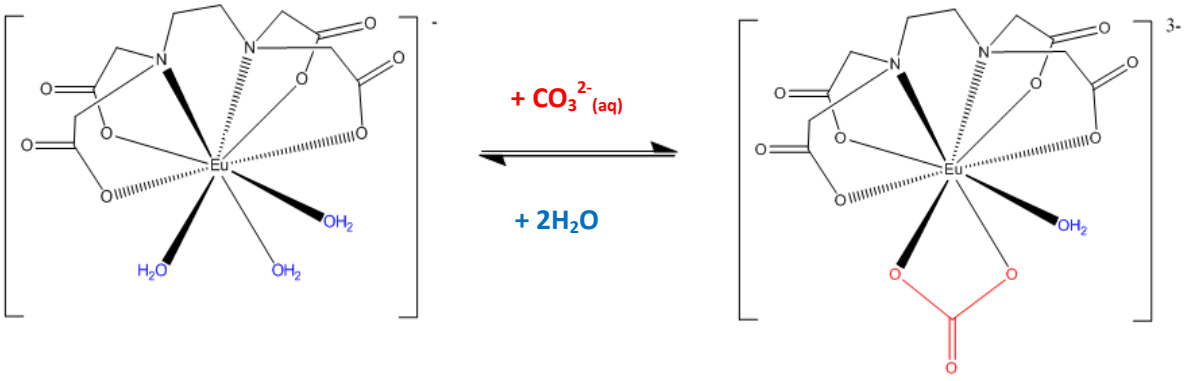

Figure 3.38: Equilibrium between the formation of $[Eu(EDTA)(H_2O)_3]^-_{(aq)}$ and $[Eu(EDTA)(CO_3)(H_2O)]^{3-}_{(aq)}$ species.

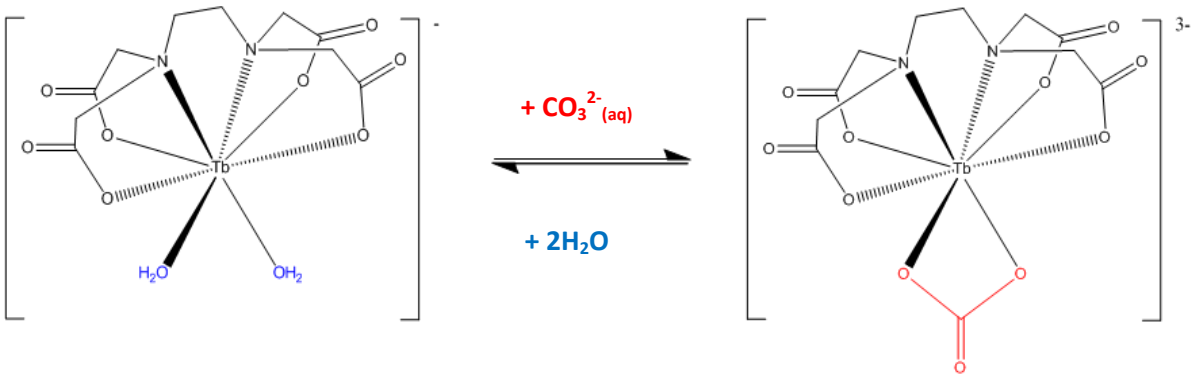

Figure 3.39: Equilibrium between the formation of $[Tb(EDTA)(H_2O)_2]^-_{(aq)}$ and $[Tb(EDTA)(CO_3)]^{3-}_{(aq)}$ species.

3.4.3 Summary

Luminescence spectroscopy of the 1:1 Ln^{III}:$EDTA^{4-}$ binary and 1:1:1 Ln^{III}:$EDTA^{4-}$:CO_3^{2-} ternary systems (where Ln = Eu or Tb) has been advantageous for detecting the formation of $[Ln(EDTA)]^-_{(aq)}$, $[Ln(EDTA)(CO_3)]^{3-}_{(aq)}$ and $[Ln(EDTA)(OH)]^{2-}_{(aq)}$ species. The calculation of the N_{H_2O} bound to the Eu^{III} and Tb^{III} ions in the binary and ternary systems allowed for structures of solution species to be proposed (Figures 3.38 and 3.39). The luminescence spectroscopy results suggest that carbonate can bind to the $[Ln(EDTA)]^-_{(aq)}$ complexes over the pH range 10 to 12. This is consistent with the NMR and UV-Vis absorption results obtained in Sections 3.2 and 3.3.

3.5 Potentiometric Titrations

Potentiometry can be used as a technique for measuring solution equilibria and characterising aqueous species formed as the pH of the system changes.[15] The formation of $[Ln(EDTA)]^-_{(aq)}$, $[Ln(EDTA)(CO_3)]^{3-}_{(aq)}$ and $[Ln(EDTA)(OH)]^{2-}_{(aq)}$ complexes have been shown to exist by NMR, UV-Vis and luminescence spectroscopy (Sections 3.2 to 3.4). Potentiometric titrations of the 1:1 Ln^{III}:$EDTA^{4-}$ binary and 1:1:1 Ln^{III}:$EDTA^{4-}$:CO_3^{2-} ternary systems have been performed in order to determine stability constants for the $[Ln(EDTA)]^-_{(aq)}$, $[Ln(EDTA)(CO_3)]^{3-}_{(aq)}$ and $[Ln(EDTA)(OH)]^{2-}_{(aq)}$ species.

3.5.1 Trivalent Lanthanide-EDTA Binary Systems (La, Ce, Pr, Nd, Eu, Ho and Lu)

Aqueous solutions containing a 1:1 ratio of Ln^{III}:$EDTA^{4-}$ components (where Ln = La, Ce, Pr, Nd, Eu, Ho and Lu) were titrated with NaOH from acidic to alkaline pH. The potentiometric curves for the 1:1 Ln^{III}:$EDTA^{4-}$ binary systems show a steep inflection over the pH region 3 to 11 (Figures 3.40 and 3.41 for La^{III} and Lu^{III}, respectively), which represent a strong acid – strong base titration (*i.e.* HNO_3 – NaOH). This is because the formation of the $[Ln(EDTA)]^-_{(aq)}$ complex over this pH region does not remove or release H^+ ions from or into the solution. The potentiometric curves for Ce^{III} to Ho^{III} binary system are presented as Figures V to Z in Appendix 1.

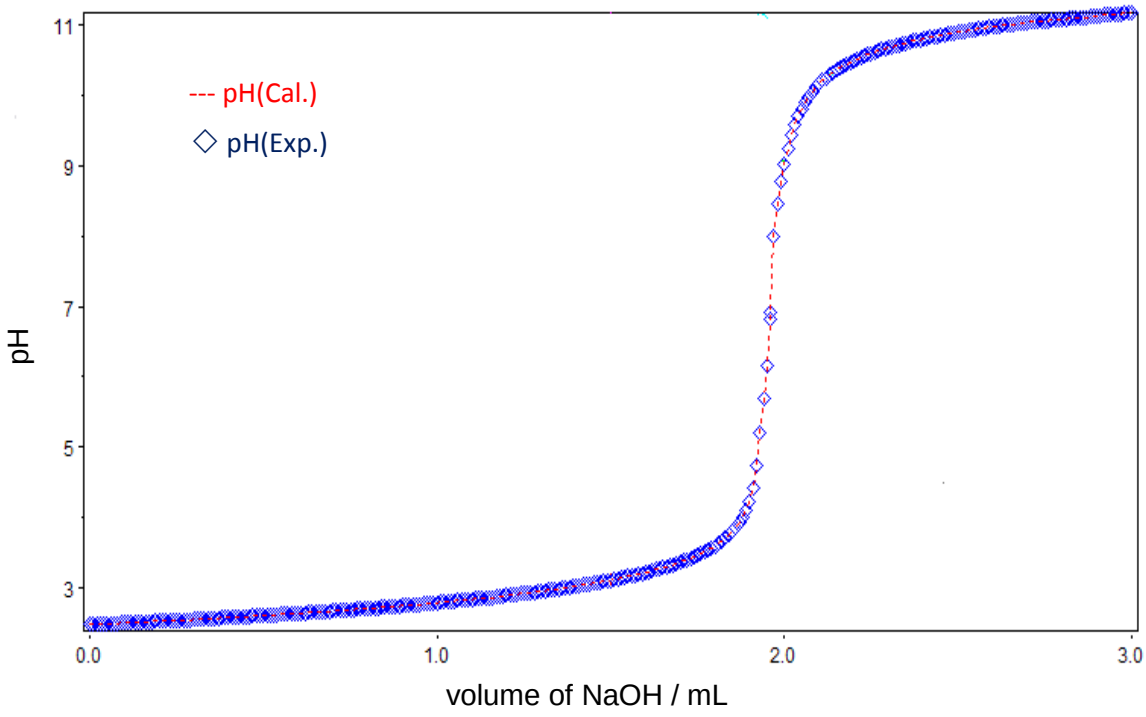

Figure 3.40: Potentiometric titration of the 1:1 La^{III}:$EDTA^{4-}$ system at 25 °C; I = 0.5 M $NaNO_3$; V^0 = 20 mL; $[La^{III}]_i = [EDTA^{4-}]_i$ = 5 mM; Titrant = 0.1 M NaOH.

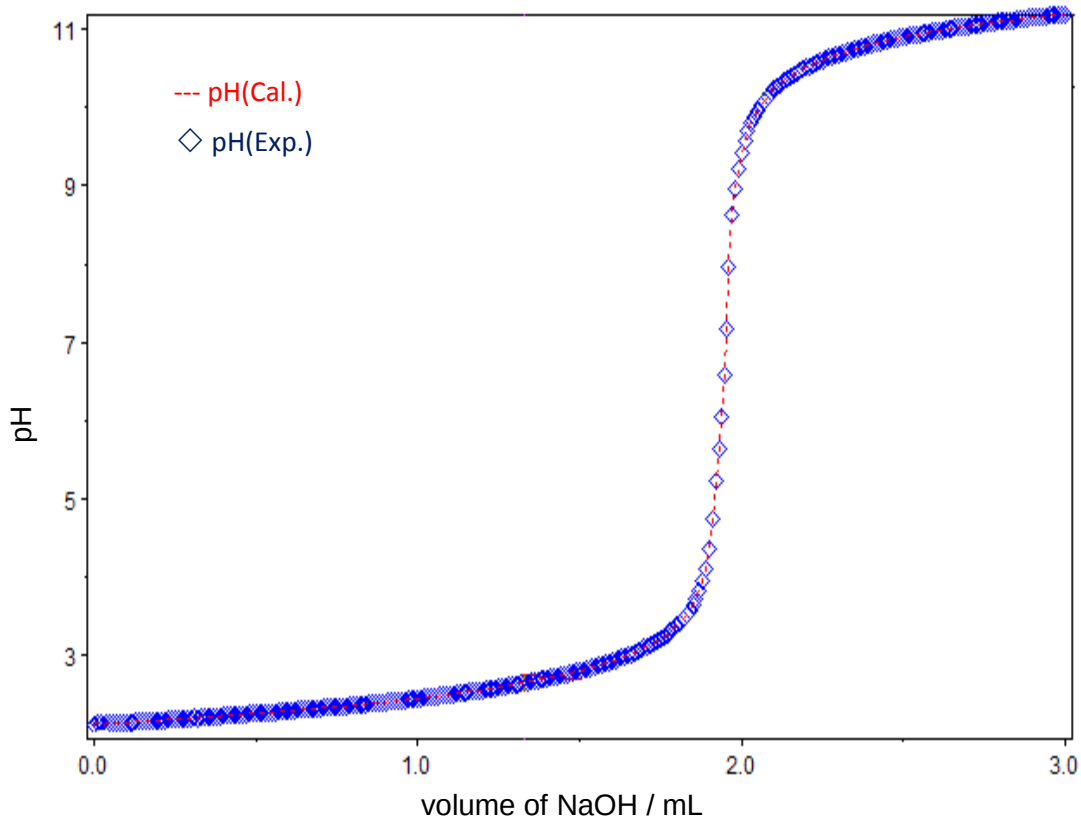

Figure 3.41: Potentiometric titration of the 1:1 Lu^{III}:$EDTA^{4-}$ system at 25 °C; I = 0.5 M $NaNO_3$; V^0 = 20 mL; $[Lu^{III}]_i = [EDTA^{4-}]_i$ = 5 mM; Titrant = 0.1 M NaOH.

Potentiometric data obtained from all of the 1:1 Ln^{III}:$EDTA^{4-}$ binary system titrations were fit using a model that included the $[Ln(EDTA)]^-_{(aq)}$ and $[Ln(EDTA)(OH)]^{2-}_{(aq)}$ complexes, as well as the $Ln(OH)^{2+}_{(aq)}$ and $Ln(NO_3)^{2+}_{(aq)}$ species. The log K values for the formation of the $[Ln(EDTA)]^-_{(aq)}$ and $[Ln(EDTA)(OH)]^{2-}_{(aq)}$ complexes have been calculated (Tables 3.9 and 3.10, respectively). The log $K_{[Ln(EDTA)]^-_{(aq)}}$ values increase along the lanthanide series (Figure 3.42). The interaction of $EDTA^{4-}$ with lanthanide ions is ionic in nature, and so as the lanthanide ionic radii decrease across the series, the lanthanide ions become 'harder'. Hence, the interaction of the lanthanide ions with $EDTA^{4-}$ becomes stronger with increasing charge density (equation 3.11) and the log K values will increase. The log K values are generally in good agreement with the literature values. Conducting experiments (*e.g.* UV-Vis titration) at a lower pH value (*e.g.* pH 1), may better define the cross-over region from free $Ln^{III}_{(aq)}$ to $[Ln(EDTA)]^-_{(aq)}$, allowing for more accurate log $K_{[Ln(EDTA)]^-}$ values to be determined. In

contrast to the trend of increasing log $K_{[Ln(EDTA)]^-}$ values across the lanthanide series, the log K values for the addition of OH^- to the $[Ln(EDTA)]^-_{(aq)}$ complexes are approximately equivalent. The $[Ln(EDTA)]^-_{(aq)}$ complexes are negatively charged, and so there may be some electrostatic repulsion between the lanthanide complex and hydroxide anion, which may dominate the influence of the lanthanide charge density. Therefore, this may cause the log K hydrolysis values to be approximately equivalent.

$$\text{charge density} = \frac{Z^2}{r}$$

(equation 3.11)

where: Z = charge of lanthanide ion; r = radius of lanthanide ion

Reaction	log *K* (this work)	log *K* (literature values)[2]
$La^{III} + EDTA^{4-} \rightleftharpoons [La(EDTA)]^-$	13.47 ± 0.02	14.48
$Ce^{III} + EDTA^{4-} \rightleftharpoons [Ce(EDTA)]^-$	14.37 ± 0.01	15.04
$Pr^{III} + EDTA^{4-} \rightleftharpoons [Pr(EDTA)]^-$	14.97 ± 0.01	15.44
$Nd^{III} + EDTA^{4-} \rightleftharpoons [Nd(EDTA)]^-$	15.51 ± 0.02	15.75
$Eu^{III} + EDTA^{4-} \rightleftharpoons [Eu(EDTA)]^-$	15.30 ± 0.01	16.23
$Ho^{III} + EDTA^{4-} \rightleftharpoons [Ho(EDTA)]^-$	16.00 ± 0.02	17.13
$Lu^{III} + EDTA^{4-} \rightleftharpoons [Lu(EDTA)]^-$	16.09 ± 0.01	18.19

Table 3.9: Stability constants of $Ln^{III}_{(aq)}$ complexation with $EDTA^{4-}$; I = 0.5 M $NaNO_3$ (this work); I = 0.5 M Na^+ salt (literature values).[2]

Reaction	log *K* (this work)
$[La(EDTA)]^- + OH^- \rightleftharpoons [La(EDTA)(OH)]^{2-}$	-11.37 ± 0.01
$[Ce(EDTA)]^- + OH^- \rightleftharpoons [Ce(EDTA)(OH)]^{2-}$	-11.13 ± 0.01
$[Pr(EDTA)]^- + OH^- \rightleftharpoons [Pr(EDTA)(OH)]^{2-}$	-11.23 ± 0.01
$[Nd(EDTA)]^- + OH^- \rightleftharpoons [Nd(EDTA)(OH)]^{2-}$	-11.05 ± 0.02
$[Eu(EDTA)]^- + OH^- \rightleftharpoons [Eu(EDTA)(OH)]^{2-}$	-10.95 ± 0.02
$[Ho(EDTA)]^- + OH^- \rightleftharpoons [Ho(EDTA)(OH)]^{2-}$	-10.94 ± 0.02
$[Lu(EDTA)]^- + OH^- \rightleftharpoons [Lu(EDTA)(OH)]^{2-}$	-11.39 ± 0.01

Table 3.10: Stability constants of $[Ln(EDTA)]^-_{(aq)}$ complexation with hydroxide; I = 0.5 M $NaNO_3$.

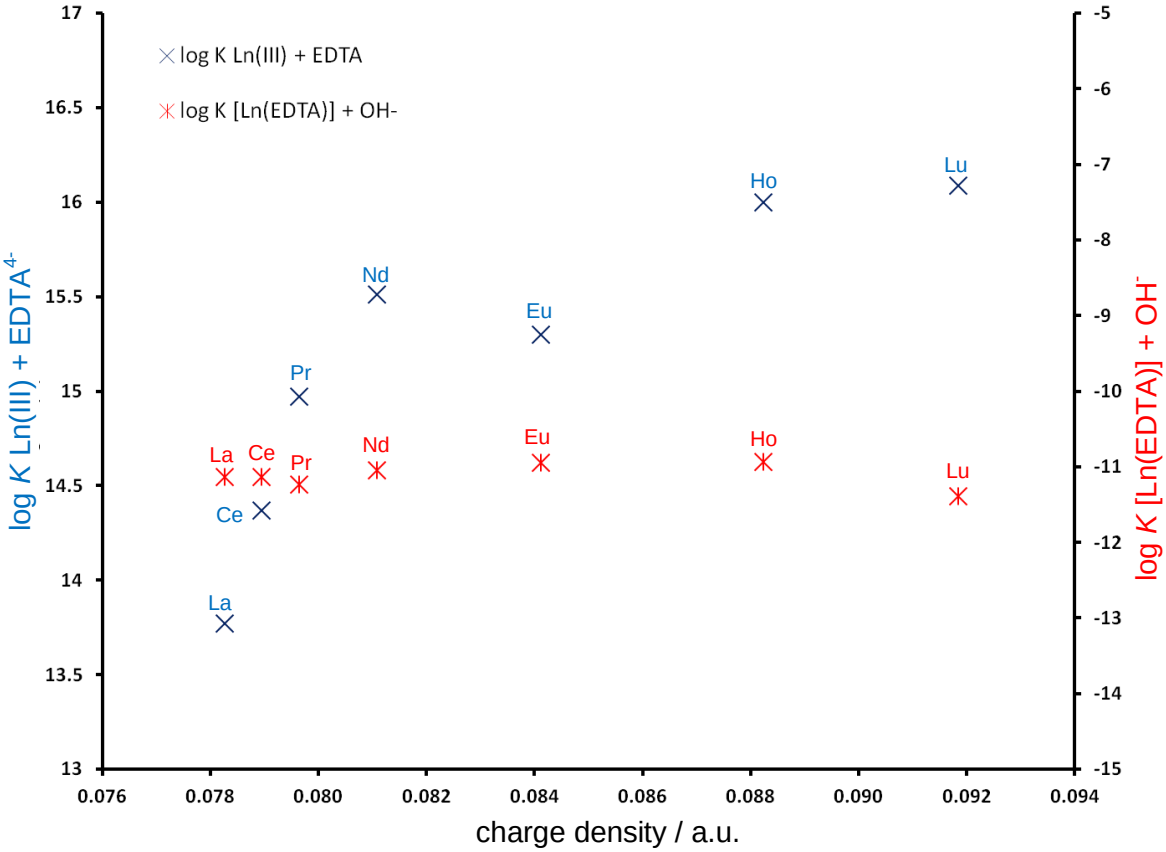

Figure 3.42: Plot of log K Ln^{III} +$EDTA^{4-}$ (left y axis) and log K $[Ln(EDTA)]^-_{(aq)}$ + OH^- (right y axis) as a function of lanthanide charge density.

The speciation diagrams for these lanthanide systems show that the $[Ln(EDTA)]^-_{(aq)}$ complex dominates the solution speciation up to approximately pH 11, after which the $[Ln(EDTA)(OH)]^{2-}_{(aq)}$ complex becomes prevalent (Figure 3.43 and 3.44 for La^{III} and Lu^{III}, respectively). This agrees with the NMR, UV-Vis and luminescence results (Sections 3.2 to 3.4), where hydrolysis was observed to predominantly occur at pH greater than 11. At approximately pH 2, the speciation diagrams show some free $La^{III}_{(aq)}$ ions and $La(NO_3)^{2+}_{(aq)}$ (hence free $EDTA^{4-}$ ligand) but no free $Lu^{III}_{(aq)}$ ions. This is in agreement with the ^{1}H-NMR results that showed free $EDTA^{4-}$ ligand for the 1:1 La^{III}:$EDTA^{4-}$ system at pD 2.0 (Figure 3.9), but not for the Lu^{III} ion system at pD 1.9 (Figure 3.12). The difference in the behaviour of La^{III} and Lu^{III} is likely to be due to a difference in their charge densities. The Lu^{III} ion has a greater charge density than the La^{III} ion and so will have a stronger electrostatic interaction with the $EDTA^{4-}$ ligand.

The species, $[La(EDTAH)(H_2O)_4]_{(aq)}$, which was shown to exist by single crystal x-ray diffraction,[12] could not be modelled from the data. Similarly, the $Ln(OH)_{3(s)}$ complex that was initially modelled in the speciation diagrams derived from known literature values (Figures 3.7 and 3.11), could also not be fitted to the experimental data. It is likely that stability constants could not be determined for the $[La(EDTAH)(H_2O)_4]_{(aq)}$ and $Ln(OH)_{3(s)}$ complexes, because they predominantly exist outside of the pH region that was studied (*i.e.* pH 2 to 11), and so there would not be sufficient potentiometric data to define their formation in solution.

The speciation diagrams obtained for the trivalent lanthanides, Ce, Pr, Nd, Eu and Ho (Figures AA to AE in Appendix 1), also show the $[Ln(EDTA)]^-_{(aq)}$ complex dominates the solution speciation until approximately pH 11, when hydrolysis of the complex occurs.

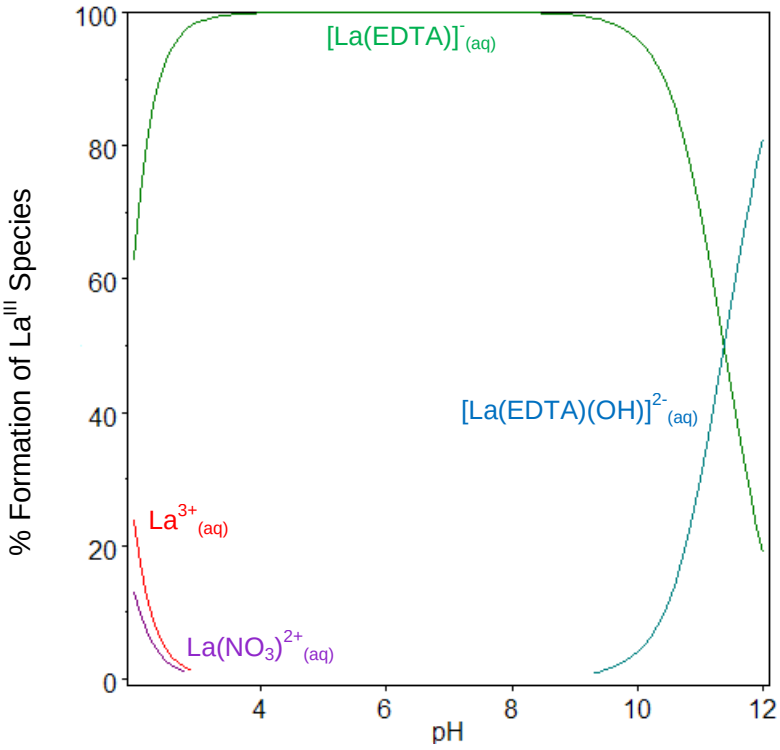

Figure 3.43: Speciation diagram of the 1:1 La^{III}:$EDTA^{4-}$ system.

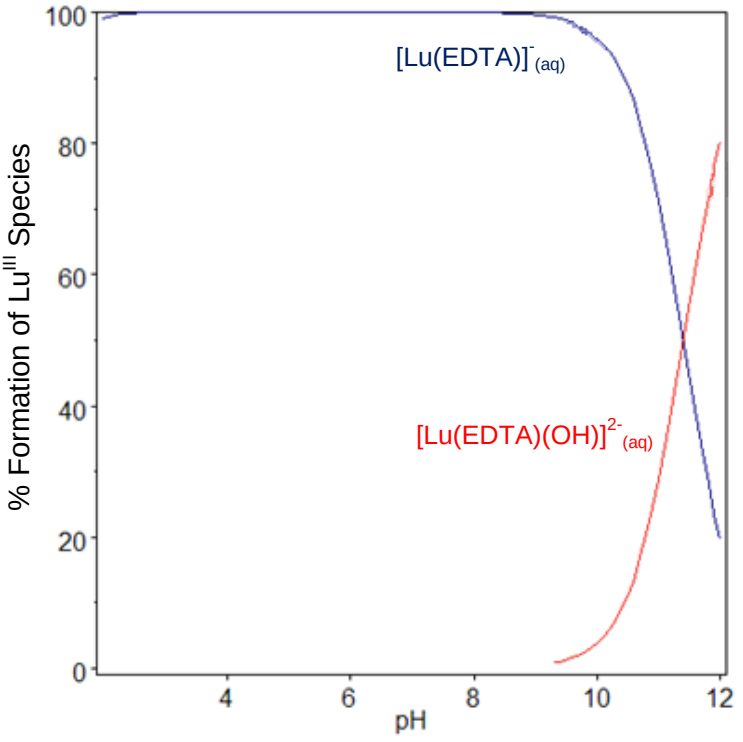

Figure 3.44: Speciation diagram of the 1:1 Lu^{III}:$EDTA^{4-}$ system.

3.5.2 Trivalent Lanthanide-EDTA-Carbonate Ternary Systems (La, Ce, Pr, Nd, Eu, Ho and Lu)

Potentiometric titrations of the 1:1:1 Ln^{III}:$EDTA^{4-}$:CO_3^{2-} systems (where Ln = La, Ce, Pr, Nd, Eu, Ho and Lu) were titrated with HNO_3 from alkaline to neutral pH. Before the titration was performed a 1:1 Ln^{III}:$EDTA^{4-}$ solution was adjusted to approximately pH 12 with NaOH, and an equivalent of carbonate was added to this alkaline solution. The potentiometric curves for all of the 1:1:1 Ln^{III}:$EDTA^{4-}$:CO_3^{2-} ternary systems show two inflections over the pH region 11.5 to 7.0 (Figures 3.45 and 3.46 for La^{III} and Lu^{III}, respectively). The first inflection occurs at approximately pH 10, which corresponds to the formation of the $[Ln(EDTA)(CO_3)]^{3-}_{(aq)}$ complex and the second inflection is present at pH 7.5, which represents the formation of the $[Ln(EDTA)]^{-}_{(aq)}$ species. The potentiometric curves for Ce^{III} to Ho^{III} ternary systems are presented as Figures AF to AJ in Appendix 1.

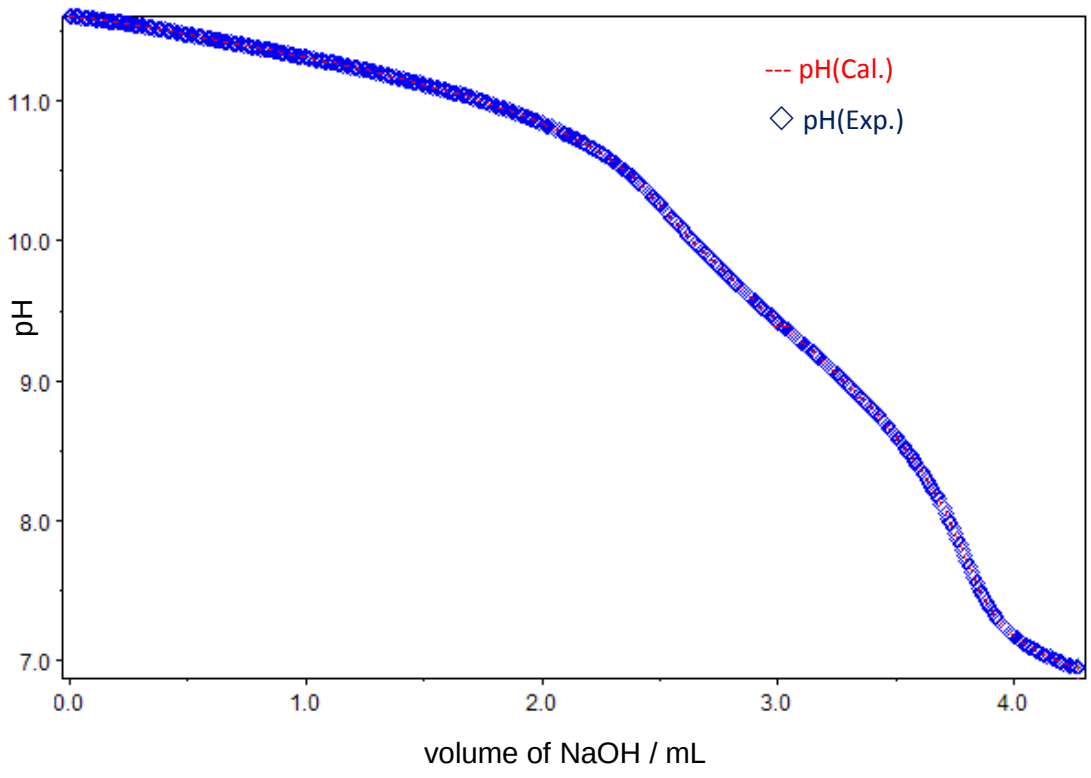

Figure 3.45: Potentiometric titration of a 1:1:1 La^{III}:$EDTA^{4-}$:CO_3^{2-} system at 25 °C; I = 0.5 M $NaNO_3$; V^0 = 20 mL; $[La^{III}]_i$=$[EDTA^{4-}]_i$=$[CO_3^{2-}]_i$=5 mM; Titrant = 0.1 M HNO_3.

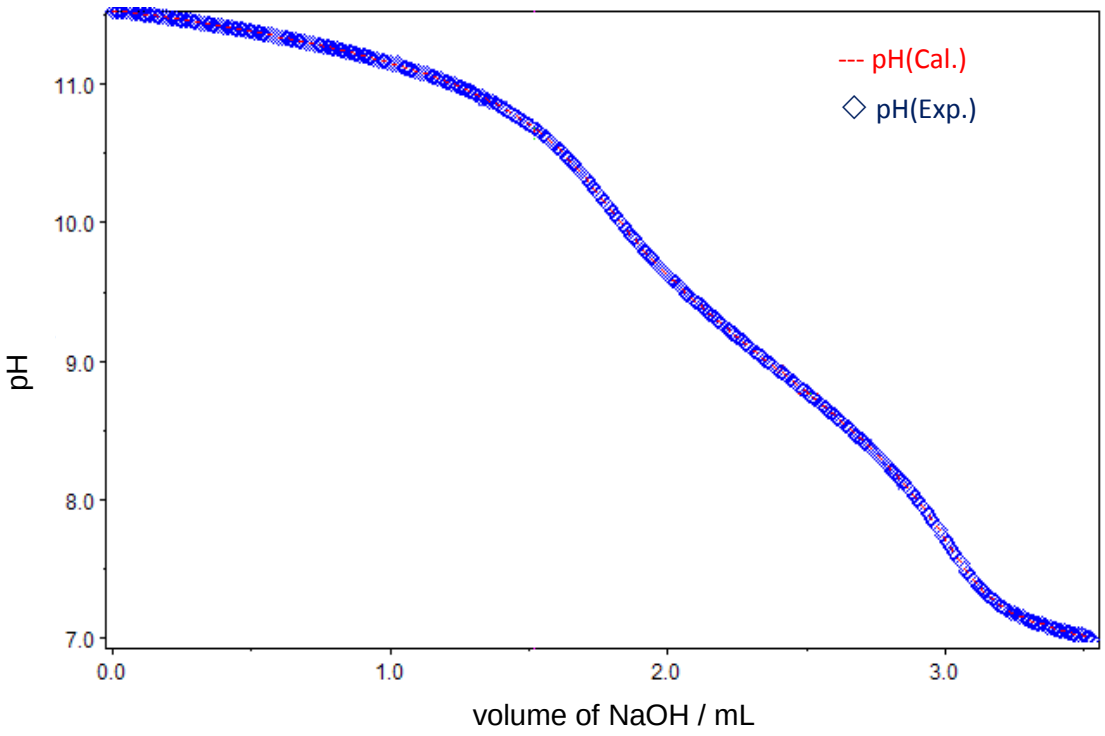

Figure 3.46: Potentiometric titration of a 1:1:1 Lu^{III}:EDTA:CO_3^{2-} system at 25 °C; I = 0.5 M $NaNO_3$; V^0 = 20 mL; $[Lu^{III}]_i = [EDTA^{4-}]_i = [CO_3^{2-}]_i$ = 5 mM; Titrant = 0.1 M HNO_3.

Potentiometric data obtained from all of the 1:1:1 Ln^{III}:$EDTA^{4-}$:CO_3^{2-} ternary system titrations were fit using a model that included the complexes of $[Ln(EDTA)]^-_{(aq)}$, $[Ln(EDTA)(CO_3)]^{3-}_{(aq)}$ and $[Ln(EDTA)(OH)]^{2-}_{(aq)}$, as well as the $Ln(OH)^{2+}_{(aq)}$ and $Ln(NO_3)^{2+}_{(aq)}$ species. The log K values for the addition of carbonate to the $[Ln(EDTA)]^-_{(aq)}$ complex (Table 3.11) are approximately equivalent and show no apparent trend across the series (Figure 3.47). A similar observation was found for the addition of hydroxide to the $[Ln(EDTA)]^-_{(aq)}$ complex, where there was no apparent trend for the log K values across the series (Table 3.10). The anionic $[Ln(EDTA)]^-_{(aq)}$ complex may electrostatically repel the negatively charged carbonate ligand, which could dominate the influence of the lanthanide charge density. This was also the case for the addition of hydroxide to the $[Ln(EDTA)]^-_{(aq)}$ complexes (Section 3.5.1). Therefore, the effects of electrostatic repulsion within the ternary system may cause the log K values for CO_3^{2-} addition to the $[Ln(EDTA)]^-_{(aq)}$ complexes to be approximately equivalent.

The known log K values for carbonate binding to $Ln^{III}_{(aq)}$ ions do increase along the lanthanide series (Table 3.12), which is thought to be dependent on the lanthanide charge densities. The ^{13}C-NMR results indicated that carbonate may have a stronger affinity for

binding to the $[Lu(EDTA)]^-_{(aq)}$ complex than the $[La(EDTA)]^-_{(aq)}$ (Figures 3.16 and 3.14, respectively), as a resolved carbonate signal was observed in the 1:1:1 Lu^{III}:$EDTA^{4-}$:CO_3^{2-} system. However, the calculated log *K* values do not show a significant trend for carbonate binding to the $[Ln(EDTA)]^-_{(aq)}$ across the lanthanide series, as would be expected. This difference between the NMR and potentiometry results may arise because the potentiometric titrations were performed at a constant ionic strength (*i.e.* 0.5 M $NaNO_3$), whereas the ionic strength was not controlled in the NMR experiments and $LnCl_3$ salts (rather than $Ln(NO_3)_3$ salts) were used. Also, there was significant discrepancy between the experimental and calculated pH values when trying to fit the potentiometric data to the models (in both the binary and ternary systems), if the $Ln(NO_3)^{2+}_{(aq)}$ species was not considered. This species may also have an effect on the UV-Vis absorption profiles, where ionic strength was also controlled at 0.5 M $NaNO_3$.

Reaction	**log *K***
$[La(EDTA)]^- + CO_3^{2-} \rightleftharpoons [La(EDTA)(CO_3)]^{3-}$	3.53 ± 0.02
$[Ce(EDTA)]^- + CO_3^{2-} \rightleftharpoons [Ce(EDTA)(CO_3)]^{3-}$	3.51 ± 0.02
$[Pr(EDTA)]^- + CO_3^{2-} \rightleftharpoons [Pr(EDTA)(CO_3)]^{3-}$	3.76 ± 0.03
$[Nd(EDTA)]^- + CO_3^{2-} \rightleftharpoons [Nd(EDTA)(CO_3)]^{3-}$	3.60 ± 0.04
$[Eu(EDTA)]^- + CO_3^{2-} \rightleftharpoons [Eu(EDTA)(CO_3)]^{3-}$	4.14 ± 0.04
$[Ho(EDTA)]^- + CO_3^{2-} \rightleftharpoons [Ho(EDTA)(CO_3)]^{3-}$	3.94 ± 0.06
$[Lu(EDTA)]^- + CO_3^{2-} \rightleftharpoons [Lu(EDTA)(CO_3)]^{3-}$	3.62 ± 0.05

Table 3.11: Stability constants of $[Ln(EDTA)]^-_{(aq)}$ complexation with carbonate; I = 0.5 M $NaNO_3$.

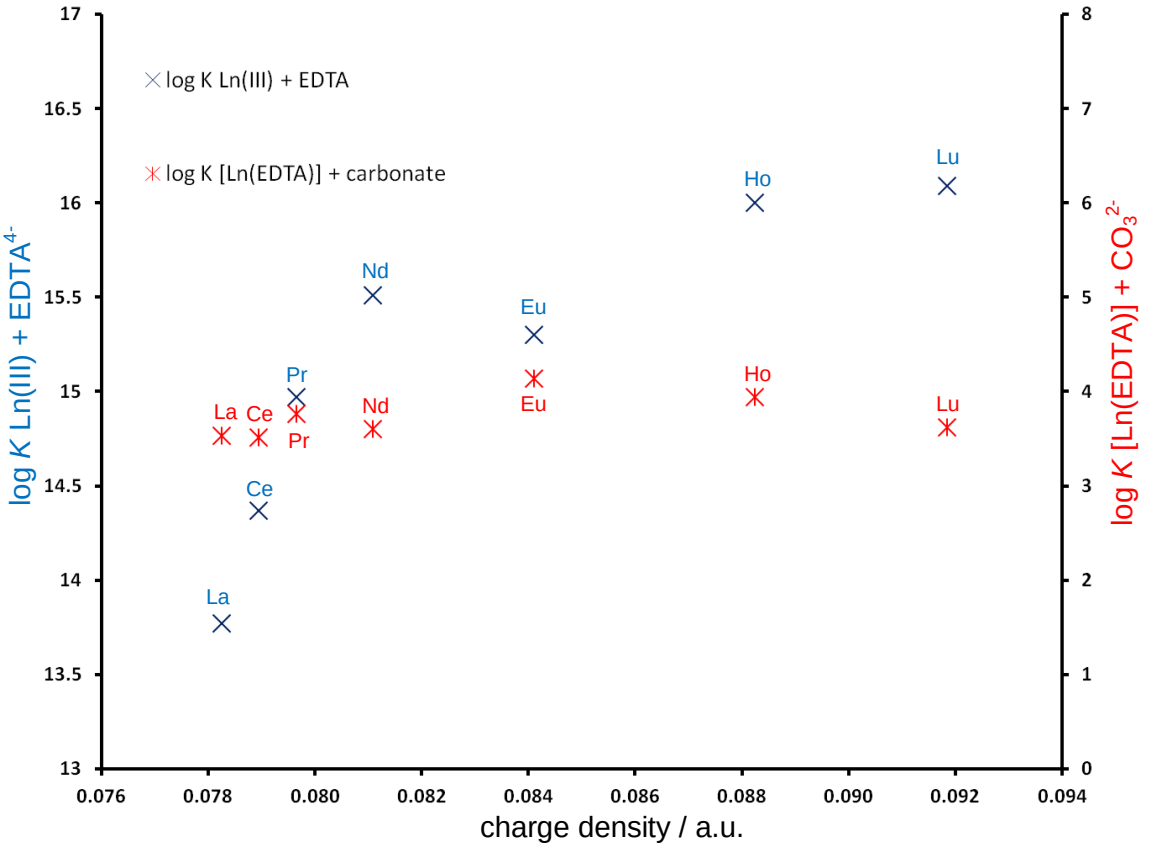

Figure 3.47: Plot of log K Ln^{III} +$EDTA^{4-}$ (left y axis) and log K $[Ln(EDTA)]^{-}_{(aq)}$ + CO_3^{2-} (right y axis) as a function of lanthanide charge density.

Reaction	**log *K*** **(literature values)[2]**
$La^{III} + CO_3^{2-} \rightleftharpoons [La(CO_3)]^+$	5.00
$Ce^{III} + CO_3^{2-} \rightleftharpoons [Ce(CO_3)]^+$	5.34
$Pr^{III} + CO_3^{2-} \rightleftharpoons [Pr(CO_3)]^+$	5.50
$Nd^{III} + CO_3^{2-} \rightleftharpoons [Nd(CO_3)]^+$	5.55
$Eu^{III} + CO_3^{2-} \rightleftharpoons [Eu(CO_3)]^+$	5.76
$Ho^{III} + CO_3^{2-} \rightleftharpoons [Ho(CO_3)]^+$	5.82
$Lu^{III} + CO_3^{2-} \rightleftharpoons [Lu(CO_3)]^+$	6.02

Table 3.12: Stability constants of Ln^{III} complexation with carbonate; I = 0.7 M $NaClO_4$.[2]

The speciation diagrams for these ternary systems show that the $[Ln(EDTA)]^{-}_{(aq)}$ complex dominates the solution speciation up to approximately pH 6.2, after which the $[Ln(EDTA)(CO_3)]^{3-}_{(aq)}$ complex becomes prevalent (Figure 3.48 and 3.49 for La^{III} and Lu^{III}, respectively). At approximately pH 11, the speciation diagrams show that bound carbonate to the $[Ln(EDTA)]^{-}_{(aq)}$ complex begins to be replaced by hydroxide to form the $[Ln(EDTA)(OH)]^{2-}_{(aq)}$ species. The calculated speciation diagrams agree with the NMR, UV-Vis and luminescence results (Sections 3.2 to 3.4) where the $[Ln(EDTA)(CO_3)]^{3-}_{(aq)}$ complex was observed to form over the alkaline region 8 to 11, followed by hydrolysis of this species after pH 11.

The speciation diagrams obtained for the trivalent lanthanides Ce, Pr, Nd, Eu and Ho (Figures AK to AO in Appendix 1) also show similar results to the La^{III} and Lu^{III} ternary systems.

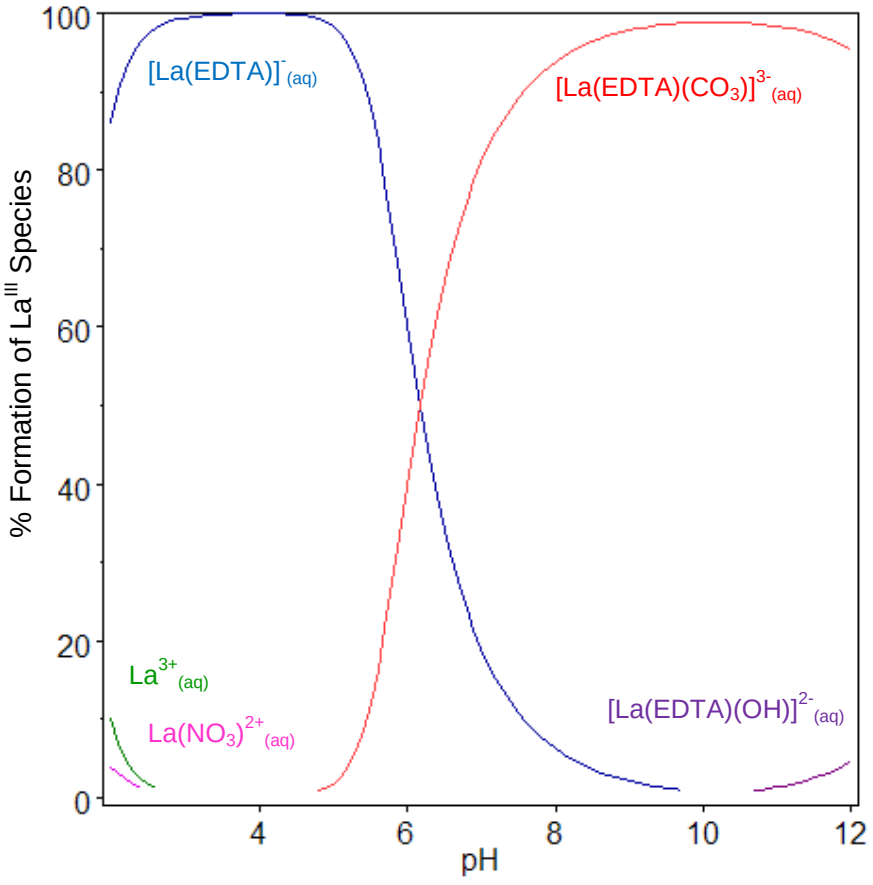

Figure 3.48: Speciation diagram of the 1:1:1 La^{III}:$EDTA^{4-}$:CO_3^{2-} system.

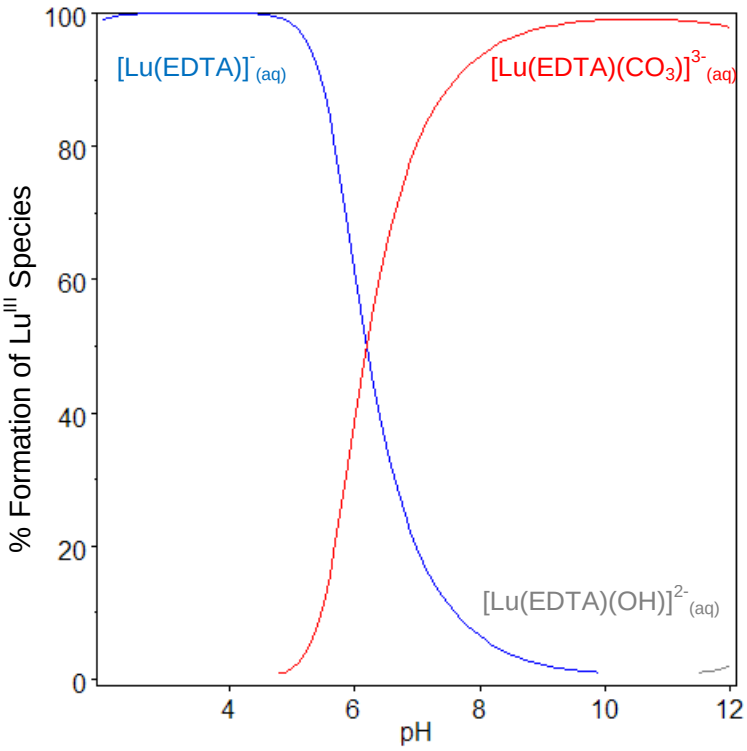

Figure 3.49: Speciation diagram of the 1:1:1 Lu^{III}:$EDTA^{4-}$:CO_3^{2-} system.

3.6 Summary

The formation of $[Ln(EDTA)]^-_{(aq)}$, $[Ln(EDTA)(CO_3)]^{3-}_{(aq)}$ and $[Ln(EDTA)(OH)]^{2-}_{(aq)}$ complexes have been investigated by NMR, UV-Vis and luminescence spectroscopies. In a 1:1 Ln^{III}:$EDTA^{4-}$ system, the $[Ln(EDTA)]^-_{(aq)}$ complex can form in acidic conditions (*i.e.* pH 2) and dominates the solution speciation up to approximately pH 11. At pH 2, the $[Ln(EDTAH)(H_2O)_4]_{(s)}$ complex can be isolated in the solid state for La^{III} but not for Lu^{III}. It is likely that the difference in the coordination chemistry of the La^{III} and Lu^{III} ions with $EDTA^{4-}$ at low pH may be due to the Lu^{III} ion having a higher charge density than the La^{III} ion. This would cause the Lu^{III} ion to be 'harder' resulting in a stronger attraction for $EDTA^{4-}$ than $HEDTA^{3-}$. UV-Vis and luminescence spectroscopies have been able to detect the formation of the $[Ln(EDTA)]^-_{(aq)}$ complex in solution. UV-Vis spectroscopy of the 1:1 Ln^{III}:$EDTA^{4-}$ system (where Ln = Pr, Nd, Ho) showed an increase in the ε of the Ln^{III} profiles, when raising the pH from approximately 7.0 to 10.5. This indicated the formation of the $[Ln(EDTA)]^-_{(aq)}$ complex and possibly a change in the equilibrium between the pentadentate and hexadentate coordination mode of $EDTA^{4-}$. The luminescent lifetime, which can be

calculated using the technique of luminescence spectroscopy, can be used to determine the N_{H_2O} bound to a metal ion using the Horrocks equation (equation 3.10). The hydration number for the Eu^{III} ion is nine in aqueous solution, and for the Tb^{III} ion, the hydration number decreases to eight.[5] On complexation with $EDTA^{4-}$, the N_{H_2O} bound to the Eu^{III} and Tb^{III} ions decreases to approximately three and two, respectively. This indicates that the dominant lanthanide-EDTA complexes in solution approximately over the pH range 7 to 11 have the formulas: $[Eu(EDTA)(H_2O)_3]^-$ and $[Tb(EDTA)(H_2O)_2]^-$.

NMR, UV-Vis and luminescence spectroscopies indicate that hydrolysis of the $[Ln(EDTA)]^-_{(aq)}$ complex to $[Ln(EDTA)(OH)]^{2-}_{(aq)}$ occurs at pH/pD values greater than 10. The ^{1}H-NMR spectra of the 1:1 Ln^{III}:$EDTA^{4-}$ binary systems, for Ln=La or Lu, showed a broadening of the bound $EDTA^{4-}$ resonances at high pD indicating possible exchange processes between $EDTA^{4-}$ and hydroxide within the lanthanide inner coordination sphere. At pD greater than 13, the emergence of unbound $EDTA^{4-}$ resonances can be observed by ^{1}H-NMR and a white precipitate, likely to be $Ln(OH)_{3(s)}$, forms. UV-Vis absorption spectroscopy of the 1:1 Ln^{III}:$EDTA^{4-}$ systems (Ln = Pr, Nd) showed a trend of decreasing extinction coefficient at pH values greater than pH 10.5, which suggested that hydrolysis of the $[Ln(EDTA)]^-_{(aq)}$ complexes was occurring. Luminescence spectroscopy showed an increase in the emission intensity of the 1:1 Ln^{III}:$EDTA^{4-}$ binary system (Ln= Eu or Tb) as pH was increased over the alkaline region. This suggests that there may be some hydroxide interaction with the $[Ln(EDTA)]^-_{(aq)}$ complexes. There is also a very small reduction in the N_{H_2O} bound to the $[Eu(EDTA)]^-_{(aq)}$ and $[Tb(EDTA)]^-_{(aq)}$ complexes at high pH, which Thakur *et al.* attribute to the coordination of hydroxide to metal-ligand complexes.[24]

For the 1:1:1 Ln^{III}:$EDTA^{4-}$:CO_3^{2-} system, the interaction of CO_3^{2-} with the $[Ln(EDTA)]^-_{(aq)}$ complex was observed predominantly over the pH/pD range 8 to 11. ^{13}C-NMR spectroscopy of ternary systems containing diamagnetic lanthanide ions was useful for observing the effect of pD on carbonate binding. In the 1:1:1 La^{III}:$EDTA^{4-}$:CO_3^{2-} system, the carbonate signal is broadened suggesting an exchange process is happening in solution between bound water and carbonate in the inner lanthanide coordination sphere. By contrast, in the Lu^{III} system there are two carbonate signals observed, which represent bound and unbound carbonate in solution. ^{13}C-NMR spectroscopy of ternary systems using paramagnetic lanthanides can be difficult to interpret, but they can be useful for determining if a ligand is bound to the metal

ion as the ligand signals are paramagnetically shifted and broadened. In most cases, the ^{13}C-NMR spectra of paramagnetic lanthanide ternary systems show that the carbonate signal is not observed within the expected region of 160-170 ppm. This implies that carbonate is binding to the $[Ln(EDTA)]^-_{(aq)}$ complex. UV-Vis spectroscopy shows a larger increase in the extinction coefficient for the hypersensitive transitions of the Nd^{III} and Ho^{III} ions in the presence of carbonate compared to those species in the absence of carbonate. The absorption profile of the hypersensitive transitions are affected the most when the inner coordination sphere of the lanthanide ion changes. The Pr^{III} ion does not contain hypersensitive transitions, so the difference between the absorption profiles of the 1:1 Pr^{III}:$EDTA^{4-}$ and the 1:1:1 Pr^{III}:$EDTA^{4-}$:CO_3^{2-} systems is more subtle. Luminescence spectroscopy of the 1:1 Eu^{III} and Tb^{III}:$EDTA^{4-}$ systems show a larger increase in the emission intensity when carbonate is present compared to when it is absent, which indicates that carbonate is binding to these lanthanide-EDTA complexes. The calculated N_{H_2O} bound to the Eu^{III} and Tb^{III} ions is reduced in the 1:1:1 Ln^{III}:$EDTA^{4-}$:CO_3^{2-} system compared to the 1:1 Ln^{III}:$EDTA^{4-}$ system, which suggests equilibria between binary and ternary species exist in solution (Figures 3.38 and 3.39).

The potentiometric titration data for the 1:1 Ln^{III}:$EDTA^{4-}$ and the 1:1:1 Ln^{III}:$EDTA^{4-}$:CO_3^{2-} systems were best fitted to models that contain the $[Ln(EDTA)]^-_{(aq)}$, $[Ln(EDTA)(OH)]^{2-}_{(aq)}$, $Ln(OH)^{2+}_{(aq)}$ and $Ln(NO_3)^{2+}_{(aq)}$ species, and the $[Ln(EDTA)]^-_{(aq)}$, $[Ln(EDTA)(OH)]^{2-}_{(aq)}$, $[Ln(EDTA)(CO_3)]^{3-}_{(aq)}$, $Ln(OH)^{2+}_{(aq)}$ and $Ln(NO_3)^{2+}_{(aq)}$ species, respectively. The calculated log *K* values for $[Ln(EDTA)]^-$ complex formation show an increase in the values as the lanthanide series is crossed, which is due to the lanthanide contraction. This causes stronger electrostatic attractions between the trivalent lanthanides and the $EDTA^{4-}$ ligand. The log *K* values for the addition of hydroxide or carbonate to the $[Ln(EDTA)]^-_{(aq)}$ complex do not show a trend that is dependent on the lanthanide charge density, which may be related to the addition of an anionic ligand to a negatively charged complex. However, ^{13}C-NMR spectroscopy suggests a stronger interaction of carbonate with the $[Lu(EDTA)]^-_{(aq)}$ complex compared to the $[La(EDTA)]^-_{(aq)}$ complex as a resolved bound carbonate signal was observed in the Lu^{III} system but not in the La^{III} system. This difference between the NMR and potentiometry results may arise because the electrolyte concentration was controlled in the potentiometric titrations, whereas it was not controlled in the NMR experiments.

Methodologies for understanding the formation of the Ln^{III} ternary species with $EDTA^{4-}$ and carbonate/hydroxide have been established. The next chapter describes the application of these methods to probe other Ln^{III} ternary systems that are relevant to the nuclear fuel cycle.

[1] E. Tombàcz, *Soil Sci.*, 1999, **164**, 814.

[2] R. Smith and A. Martell, *Critical Stability Constants*, Volumes 1 and 4: Inorganic Complexes, Plenum Press, New York, 1976 (and references therein).

[3] F. Stevenson, *Humus Chemistry:Genesis, Composition, Reactions*, Wiley, New York, 1982.

[4] A. Mondry and R. Janicki, *Dalton Trans.*, 2006, **39**, 4702-4710.

[5] S. Cotton, *C. R. Chimie*, 2005, **8**, 129–145.

[6] K. Ramalingam and C. Krishnamoorthy, *Inorg. Chim. Acta*, 1982, **61**, 167-172.

[7] S. Reilly, W. Runde and M. Neu, *Geochim. Cosmochim. Ac.*, 2007, **71**, 2672–2679.

[8] R. Roy**,** L. Roy**,** K. Vogel**,** C. Porter-Moore**,** T. Pearson**,** C. Good**,** F. Millero and D. Campbell**,** *Mar. Chem.*, 1993, **44**, 249-267.

[9] Y. Fukazawa, *Kenkyu Hokoku - Kanagawa-ken Sangyo Gijutsu Senta*, 2006, **12**, 11-15.

[10] C, Housecroft and A. Sharpe, *Inorganic Chemistry*, Second Edition, Pearson Education Limited, UK, 2005, 741-761.

[11] J. Van der Lee, A Users Guide to CHESS, Another Speciation and Surface Complexation Computer Code, E´cole des Mi1nes de Paris, Fontainebleau, 1998.

[12] J. Hoard, B. Lee and M. Lind, *J. Am. Chem. Soc*., 1965, **87**, 1612-1613.

[13] N. Ouali, B. Bocquet, S. Rigault, P. Morgantini, J. Weber and C. Piguet, *Inorg. Chem.*, 2002, **41**, 1436-1445.

[14] N. Kaltsoyannis and P. Scott, *The f elements*; Oxford University Press, USA, 1999, 1-67.

[15] H. Boukhalfa, S. Reilly, W. Smith and M. Neu, *Inorg. Chem.*, 2004, **43**, 5816-5823.

[16] B. Karmakar, *J. Solid State Chem.*, 2005, **178**, 2663-2672.

[17] D. G. Karraker, *Inorg. Chem.*, 1967, **6,** 1863.

[18] M. Li and P. Selvin, *J. Am. Chem. Soc.*, 1995, **117**, 8132-8138.

[19] S. Faulkner, S. Pope and B. Burton-Pye, *Appl. Spectrosc. Rev.*, 2005, **40**, 1-31.

[20] S. Faulkner, L. Natrajan, W. Perry and D. Sykes, *Dalton Trans.*, 2009, **20**, 3890-3899.

[21] R. Bradshaw, Ph.D. Thesis, University of Oxford, 2010.

[22] P. Solarz and Z. Gajek, *J. Phys. Chem. C.*, 2010, **114**, 10937–10946.

[23] R. Supkowski and W. Horrocks, *Inorg. Chim. Acta*, 2002, **340**, 44-/48.

[24] T. Ternovaya, V. Shelest, N. Gerasimenko and E. Il'nitskaya, *Theor. Exp. Chem.*, 1985, **21**, 418-428.

[25] P. Thakur, J. Conca, L. Van de Burgt and G. Choppin, *J. Coord. Chem.*, 2009, **62**, 3719–3737.

Chapter 4

Lanthanide Binary and Ternary Systems Relevant to the TALSPEAK Process

4.0 Introduction

One of the aims of this project is to help understand the solubility and stability of radioactive actinide species (*i.e.* Am^{III}, Cm^{III}) in the TALSPEAK process. The TALSPEAK process is a technique that separates the trivalent actinides from the trivalent lanthanides.[1] The process uses the ligand H_5DTPA (Figure 4.1) in the aqueous phase, which forms complexes with the trivalent actinides and lanthanides.[1] On contact with an organic phase containing the ligand HDEHP (Figure 4.2), the lanthanides are preferentially extracted into this organic phase whilst the actinides remain in the aqueous phase.[1] When the lanthanides complex to HDEHP in the organic phase, H^+ ions are released into the aqueous phase, and so lactic acid is added to the aqueous phase in order to buffer the solution pH to 3.5.[1]

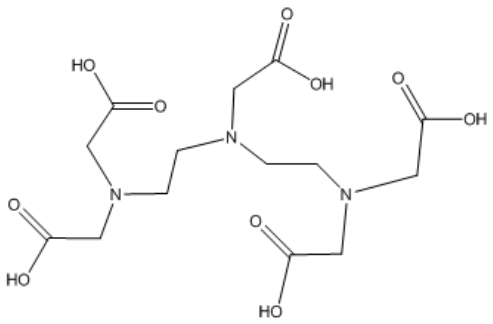

Figure 4.1: Structure of H_5DTPA.

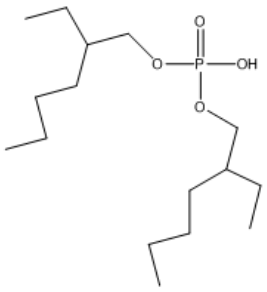

Figure 4.2: Structure of HDEHP.

In the TALSPEAK process, it is known that $[M(DTPA)]^{2-}_{(aq)}$ complexes (where M = Ln^{III} or An^{III}) predominantly form.[1,2] The presence of lactate in the aqueous phase has an effect of improving metal extraction kinetics, increasing both H_5DTPA solubility and radiation stability and also increasing the separation factors of the lanthanides and actinides.[1,2] However, the role of lactate is still not established in the process.[1]

Lactate (Figure 4.3) is a weakly coordinating ligand and its presence in high concentrations in the TALSPEAK process means that it may be competing with H_5DTPA and HDEHP as a complexing ligand.[1] Therefore, this chapter focuses on understanding lanthanide complexation by H_5DTPA and lactate using the spectroscopic techniques of NMR and luminescence. This chapter also probes the solution behaviour of the lanthanide-EDTA-lactate, lanthanide-DTPA-carbonate and lanthanide-DO3A-carbonate systems to observe how changing the denticity of the primary organic ligand around the metal ion may affect the coordination of a secondary ligand.

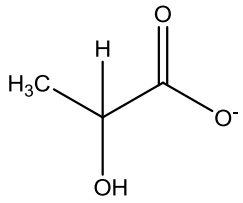

Figure 4.3: Structure of lactate.

4.1 Ligands

4.1.1 H_5DTPA

4.1.1.1 Protonation Behaviour

H_5DTPA is an octadentate ligand that can coordinate to metal ions via its three amine nitrogen atoms and its five carboxylate oxygen atoms. The five carboxylate groups can deprotonate according to the following reactions (equations 4.1 to 4.5 below).

$$H_5DTPA_{(aq)} \rightleftharpoons H_4DTPA^-_{(aq)} + H^+_{(aq)} \qquad pK_a = 2.1\ ^3 \qquad \textit{(equation 4.1)}$$

$$H_4DTPA^-_{(aq)} \rightleftharpoons H_3DTPA^{2-}_{(aq)} + H^+_{(aq)} \qquad pK_a = 2.7\ ^3 \qquad \textit{(equation 4.2)}$$

$$H_3DTPA^{2-}_{(aq)} \rightleftharpoons H_2DTPA^{3-}_{(aq)} + H^+_{(aq)} \qquad pK_a = 4.10\ ^3 \qquad \textit{(equation 4.3)}$$

$$H_2DTPA^{3-}_{(aq)} \rightleftharpoons HDTPA^{4-}_{(aq)} + H^+_{(aq)} \qquad pK_a = 8.09\ ^3 \qquad \textit{(equation 4.4)}$$

$$HDTPA^{4-}_{(aq)} \rightleftharpoons DTPA^{5-}_{(aq)} + H^+_{(aq)} \qquad pK_a = 9.42\ ^3 \qquad \textit{(equation 4.5)}$$

The $DTPA^{n-}$ (n = 1 to 5) species present in solution at a certain pH can be determined using a speciation diagram (Figure 4.4), which is derived from the known pK_a values (equations 4.1 to 4.5).[3] This shows that as pH is increased, the H_5DTPA ligand is successively deprotonated.

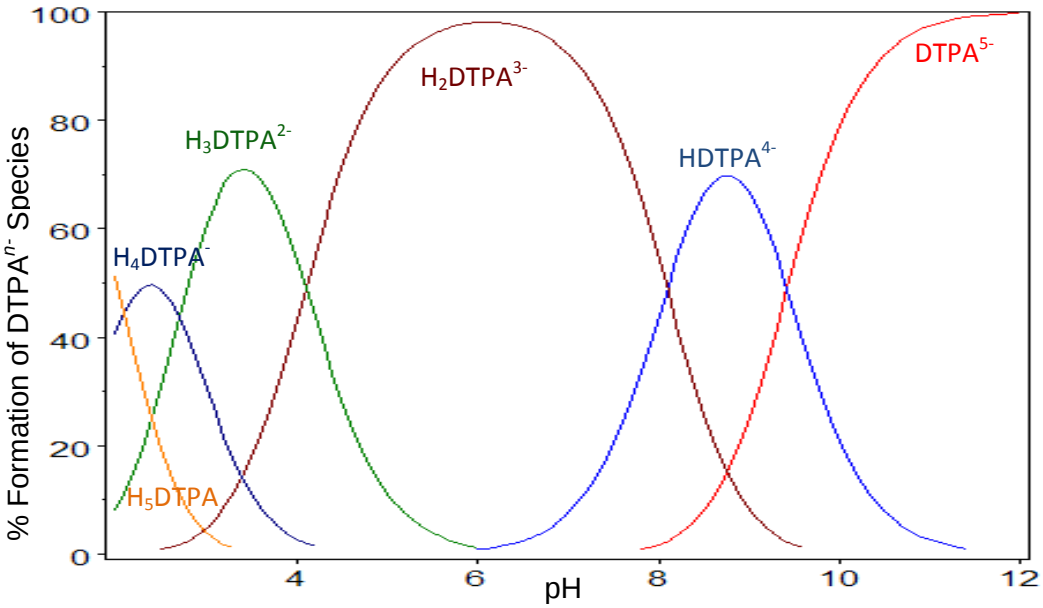

Figure 4.4: Speciation diagram of $DTPA^{n-}$ (modelled in Hyperquad). The pKa values shown are taken from Martell and Smith for 0.1 M Na^+ ionic strength.[3] Total $[DTPA^{5-}]$ = 50 mM.

4.1.1.2 NMR Spectroscopy

For reasons described previously in Section 3.1, acid protons will be described as the ^1H isotope when formulating molecular species in the NMR studies.

^1H-NMR spectroscopy has been used to monitor how the chemical shifts of $DTPA^{n-}$ species change as a function of pD (Figure 4.5). As pD is increased from 1.8 to 12.7, the resonances of the ethylene protons at 3.25 ppm (integrates to 4 protons) and 3.56 ppm (integrates to 4 protons) coalesce to produce a resonance at 2.60 ppm (integrates to 8 protons). The resonance of the terminal acetate protons shifts from 4.18 ppm to 3.15 ppm (integrates to 8 protons), and the resonance of the central acetate protons shifts from 3.74 to 3.09 ppm (integrates to 2 protons). The inflections in the chemical shifts of the observed resonances in the NMR titration occur when the pD is equivalent to a pK_a of DTPA. For example, the inflection

between pD 8.5 and 11.1 is likely to be due to a change in the position of the equilibrium corresponding to equation 4.5 (pK_a = 9.42) with pH.[3]

The signals in the ^{1}H-NMR spectra corresponding to this inflection region are also broadened, which indicates an exchange process is occurring (*i.e.* deprotonation of $HDTPA^{4-}_{(aq)}$ to form $DTPA^{5-}_{(aq)}$).

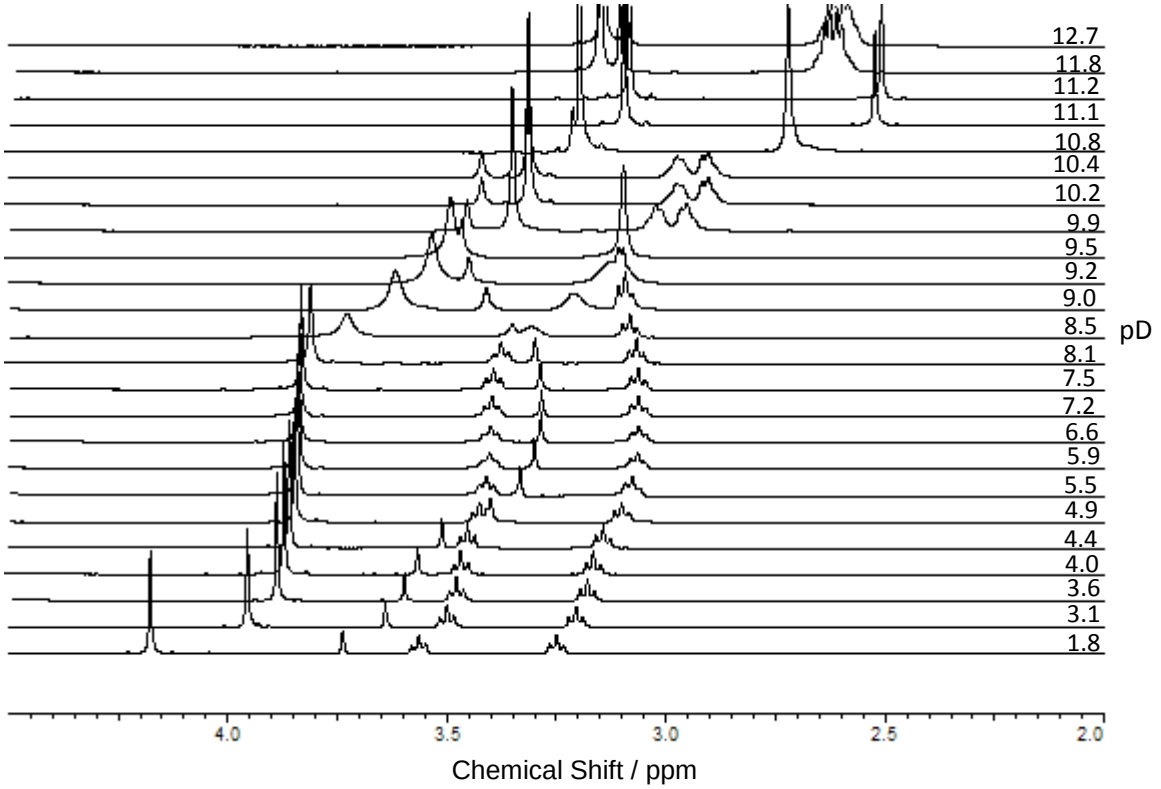

Figure 4.5: ^{1}H-NMR chemical shifts of $DTPA^{n-}$ species as a function of pD; $[50\ mM]_i$.

4.1.2 Lactic Acid

4.1.2.1 Protonation behaviour

Lactic acid ($CH_3C(H)OHCOOH$) can deprotonate according to the following reaction:

$$CH_3C(H)OHCOOH_{(aq)} \rightleftharpoons CH_3C(H)OHCOO^-_{(aq)} + H^+_{(aq)} \qquad pK_a = 3.55\ [3]$$

(equation 4.6)

where: lactate = $CH_3C(H)OHCOO^-$

The percentage of lactic acid or lactate species present in solution at a certain pH can be determined using a speciation diagram (Figure 4.6), which is derived from the known pK_a value (equation 4.6).[3]

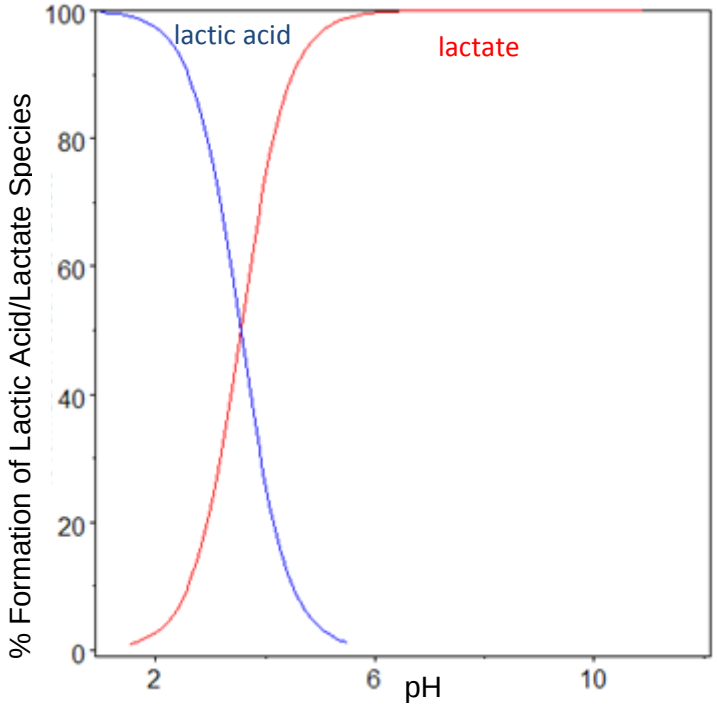

Figure 4.6: Speciation diagram of lactic acid (modelled in Hyperquad). The pKa value shown is taken from Martell and Smith for 0.5 M ionic strength.[3] Total [lactic acid] = 5 mM.

4.1.2.2 NMR Spectroscopy

^{1}H-NMR spectroscopy has been used to monitor the change of the lactate resonances as a function of pD (Figure 4.7). Carbon-13 labelled lactate was used in the experiments, therefore, the -C**H**(OH)- proton resonance has been split into a quartet of doublets (integrates to 1 proton) by coupling to the –C**H$_3$** protons and the ^{13}C atom. Similarly, the resonance for the -C**H$_3$** protons has been split into a doublet of doublets (integrates to 3 protons) by coupling to the -C**H**(OH)- proton and the ^{13}C atom. As pD is increased from 1.6 to 10.9, the -C**H**(OH)- proton resonance shifts from 4.38 to 4.10 ppm and the –C**H$_3$** protons resonance shifts from 1.42 to 1.32 ppm. The inflection occurs when the pD equals the pK_a of lactic acid, which is approximately pD 3.55.[3]

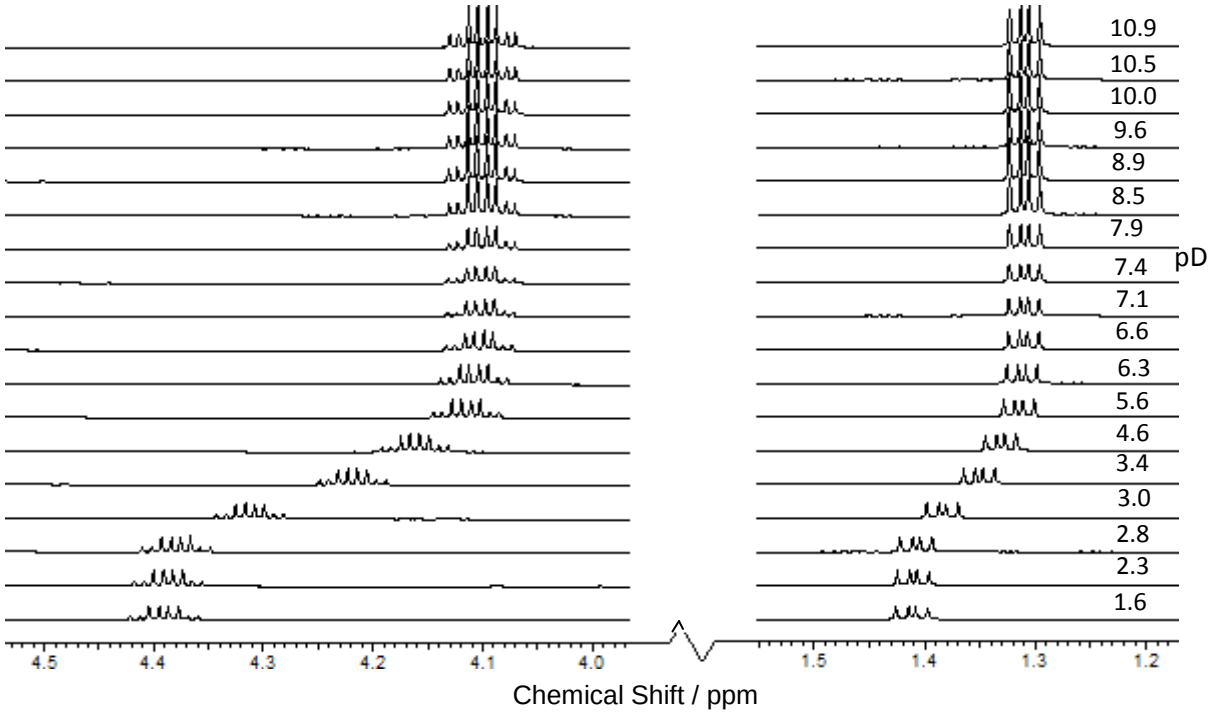

Figure 4.7: ^{1}H-NMR chemical shifts of lactic acid/lactate as a function of pD; $[50\ mM]_i$.

The lactate used in these experiments was ^{13}C-labelled, which allowed for fewer ^{13}C-NMR scans of the system and so a reduction in time of the ^{13}C-NMR experiment. The –**C**H(OH)- and –**C**H$_3$ carbon atoms were not ^{13}C-labelled, and so the reduction in the number of ^{13}C-NMR scans results in these ^{13}C-NMR signals not being observed.

Labelled (^{13}C) lactate on the carboxylate functional group was used in these experiments in order to increase the intensity of the carboxylate signal in the $^{13}C^{-}$NMR spectra, allowing for shorter acquisition times, than if natural lactate was used. The –**C**H$_3$ and the –**C**(H)OH- carbon atoms of lactate were not ^{13}C-labelled, and so the reduction in the number of ^{13}C-NMR scans results in the ^{13}C-NMR signals of these carbon atoms not being observed. However, ^{1}H-NMR can be used to analyse the protons of these functional groups.

The ^{13}C-NMR spectra obtained to probe the effect of pD on the chemical shift of the lactate carboxylate group (Figure 4.8) show that the carboxylate signal shifts from 180.5 to 183.2 ppm as pD is increased from 2.7 to 6.2. This represents the change in the position of the equilibrium between free lactic acid and free lactate. After pD 6.2, the carboxylate signal remains stationary at 183.2 ppm, indicating that lactate is the dominant solution species, which agrees with the lactic acid speciation diagram (Figure 4.6)

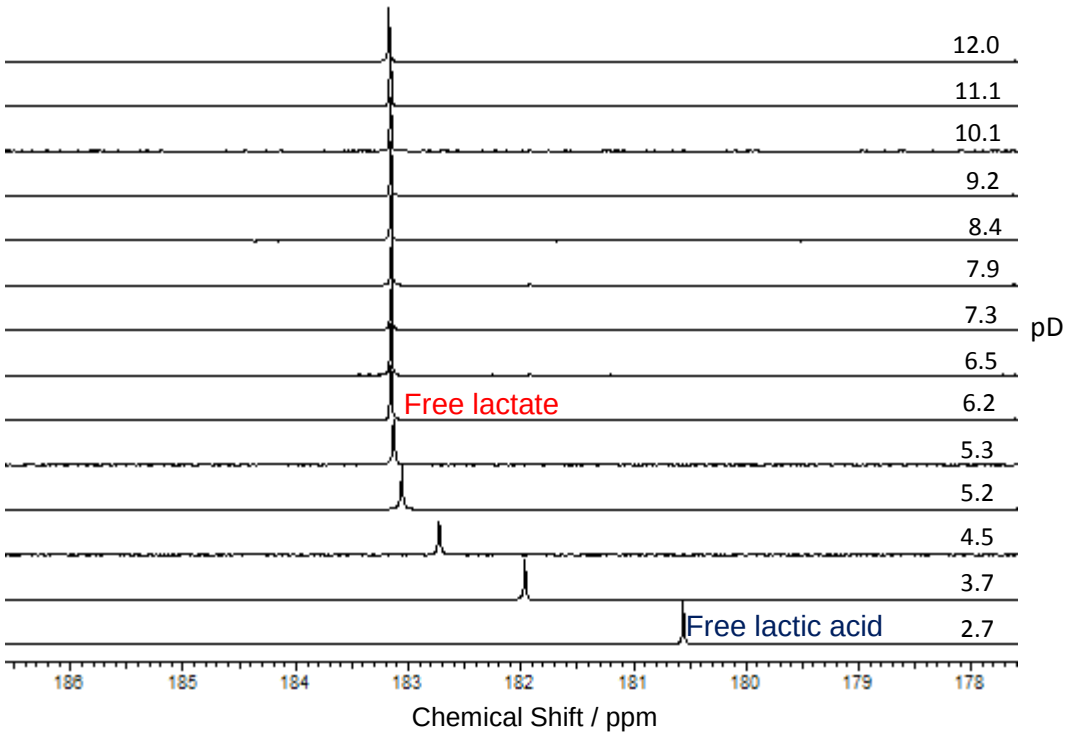

Figure 4.8: ^{13}C-NMR spectra for the effect of pD on the free lactic acid/lactate system; $[lactate]_i$ = 10 mM.

4.1.2.3 Modes of Lactate Coordination to Metal Ions

Lactate is a bidentate ligand that may coordinate via three modes to a metal ion (Figure 4.9).[4]

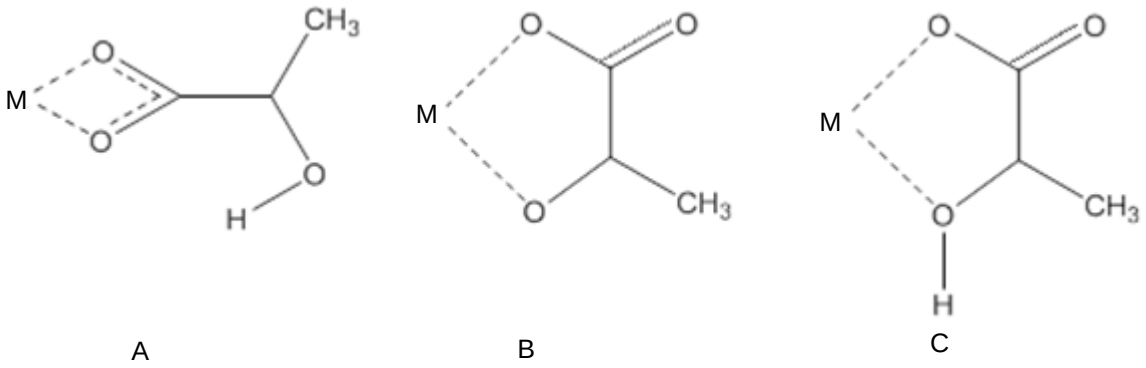

Figure 4.9: Coordination modes of lactate to a metal ion. [Adapted from Reference 4].
A) Bidentate binding with the carboxylate group; B) Bidentate binding with the carboxylate and deprotonated hydroxyl group; C) Bidentate binding with the carboxylate and protonated hydroxyl group.

Tian *et al.* hypothesise that the most likely coordination mode for lactate binding is mode C.[4] This is because metal complexes with lactate seem to have 'enhanced stability'. They suggest that this 'enhanced stability' is likely to be due to the combined interaction of the protonated hydroxyl and carboxylate group with metal ions (5-membered chelate ring) compared to the bidentate coordination of the carboxylate group (4-membered chelate ring).[4] Five-membered chelate rings are considered more thermodynamically stable than four-membered chelate rings due to the bond angles in five-membered chelate rings being more favoured.[5]

4.1.3 H_3DO3A

4.1.3.1 Protonation Behaviour

The H_3DO3A (1,4,7,10-tetraazacyclododecane-1,4,7-triacetic acid) ligand (Figure 4.10) contains four nitrogen donor atoms in an amine ring.[6] It also contains three acetate arms on three of the nitrogen atoms in the amine ring making the H_3DO3A ligand a heptadentate coordinator to metal ions.[6]

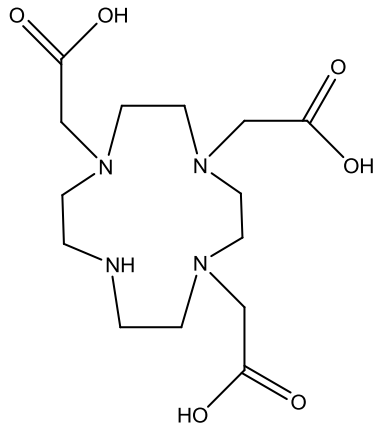

Figure 4.10: Structure of H_3DO3A.

H_3DO3A can deprotonate according to the following equations:

$H_3DO3A_{(aq)} \rightleftharpoons H_2DO3A^-_{(aq)} + H^+_{(aq)}$ $pK_a = 4.43$ [6] *(equation 4.7)*

$H_2DO3A^-_{(aq)} \rightleftharpoons HDO3A^{2-}_{(aq)} + H^+_{(aq)}$ $pK_a = 9.24$ [6] *(equation 4.8)*

$HDO3A^{2-}_{(aq)} \rightleftharpoons DO3A^{3-}_{(aq)} + H^+_{(aq)}$ $pK_a = 11.59$ [6] *(equation 4.9)*

The percentage of $DO3A^{n-}$ (n = 1 to 3) species present in solution at a certain pH can be determined using a speciation diagram (Figure 4.11), which is derived from the known pK_a values (equations 4.7 to 4.9).[6]

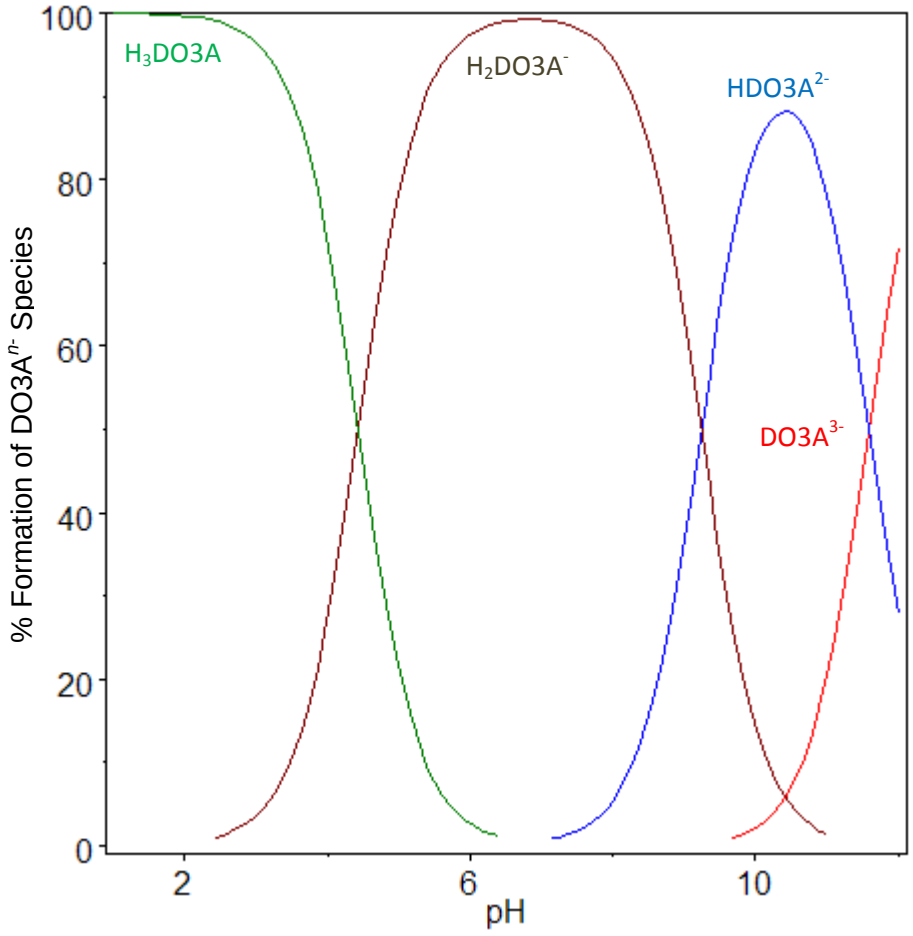

Figure 4.11: Speciation diagram of $DO3A^{n-}$ (modelled in Hyperquad). The pKa values shown are taken from Choppin *et al.*[6] Total $[DO3A^{3-}]$ = 5 mM.

4.2 Lanthanide-DTPA Binary Systems

4.2.1 Speciation Diagram

4.2.1.1 1:1 La^{III}:$DTPA^{5-}$

For a 1:1 La^{III}:$DTPA^{5-}$ system, the aqueous La^{III} species present in solution at a certain pH can be determined using a speciation diagram (Figure 4.12), which is derived from the known equilibrium constants.[3] This shows that from pH 0, the $DTPA^{5-}$ ligand can complex to the La^{III} ion to form the $[La(HDTPA)]^{-}_{(aq)}$ species, in which one of the acetate arms is protonated. As pH is increased, the acetate arm is deprotonated forming the $[La(DTPA)]^{2-}_{(aq)}$ complex, which dominates the speciation until approximately pH 13 when it is expected that $La(OH)_{3(s)}$ becomes prevalent.

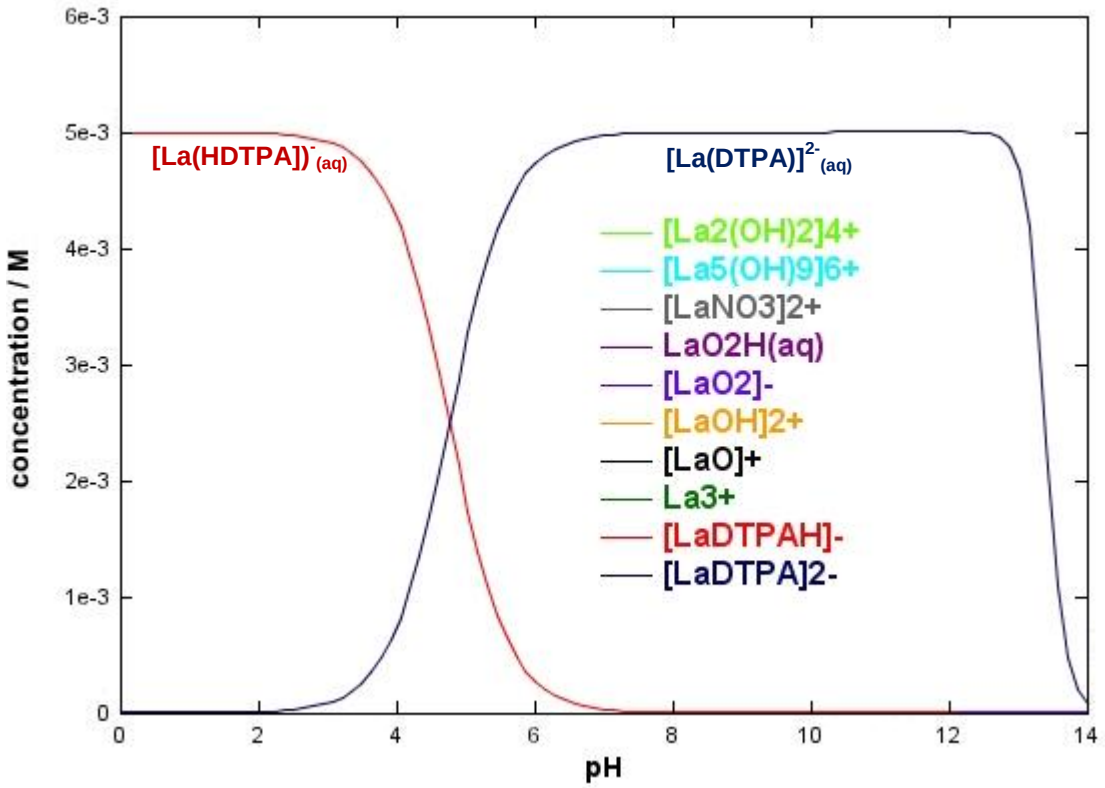

Figure 4.12: Speciation diagram of a 1:1 La^{III}:$DTPA^{5-}$ system as a function of pH using the *JCHESS* code.[7] Total $[La^{III}]$ = total $[DTPA^{5-}]$ = 5 mM. Only aqueous species are shown. Thermodynamic data obtained from the integrated *JCHESS* database and Martell and Smith.[3]

4.2.2 NMR Spectroscopy

4.2.2.1 Diamagnetic Lanthanide Ions (La^{III} and Lu^{III})

^{1}H-NMR spectroscopy was performed on a 1:1 Ln^{III}:$DTPA^{5-}$ binary system (where Ln = La or Lu) to observe the effect of pD on the $DTPA^{5-}$ chemical shifts. The ^{1}H-NMR spectra of the 1:1 La^{III}:$DTPA^{5-}$ system (Figure 4.13) show signals at 2.5, 2.7 and 2.9 ppm (integrates to 2:2:4 protons, respectively), which are due to the ethylene protons of $DTPA^{5-}$. There are also resonances between 3.25 and 3.5 ppm (integrates to 8 protons), which represent the terminal acetate arms of $DTPA^{5-}$. The signal between 3.5 and 3.75 ppm (integrates to 2 protons) is due to the central acetate protons of $DTPA^{5-}$. The ^{1}H-NMR chemical shifts of the $DTPA^{5-}$ ligand in the 1:1 La^{III}:$DTPA^{5-}$ system differ from the free $DTPA^{5-}$ ligand spectra (Figure 4.5) therefore, $DTPA^{5-}$ is bound to the La^{III} ion. The broadening observed in the spectra is likely to be due to an intramolecular re-arrangement of the complex in solution,[8] which may involve the $DTPA^{5-}$ ligand interchanging its coordination mode between octadentate and heptadentate. The ^{1}H-NMR spectra show a small difference in the splitting pattern of the resonance at 3.4 ppm, on going from pD 2.2 to 3.6. This change in the splitting pattern may be due to the deprotonation of the $[La(HDTPA)]^-_{(aq)}$ complex to form the $[La(DTPA)]^{2-}_{(aq)}$ species. There is no significant change in the proton resonances of the 1:1 La^{III}:$DTPA^{5-}$ system over the pD region 3.6 to 12.3, therefore the $DTPA^{5-}$ ligand remains bound to La^{III} over this pD range. However, at pD 13.8, the proton resonances are representative of free $DTPA^{5-}$ ligand (Figure 4.5) and so hydrolysis of the $[La(DTPA)]^{2-}_{(aq)}$ complex occurs. A white precipitate forms, likely to be $La(OH)_{3(s)}$, and $DTPA^{5-}$ is unbound in solution. The speciation observed in the ^{1}H-NMR spectra (obtained from the 1:1 La^{III}:$DTPA^{5-}$ system) are in good agreement with the calculated speciation diagram (Figure 4.12).

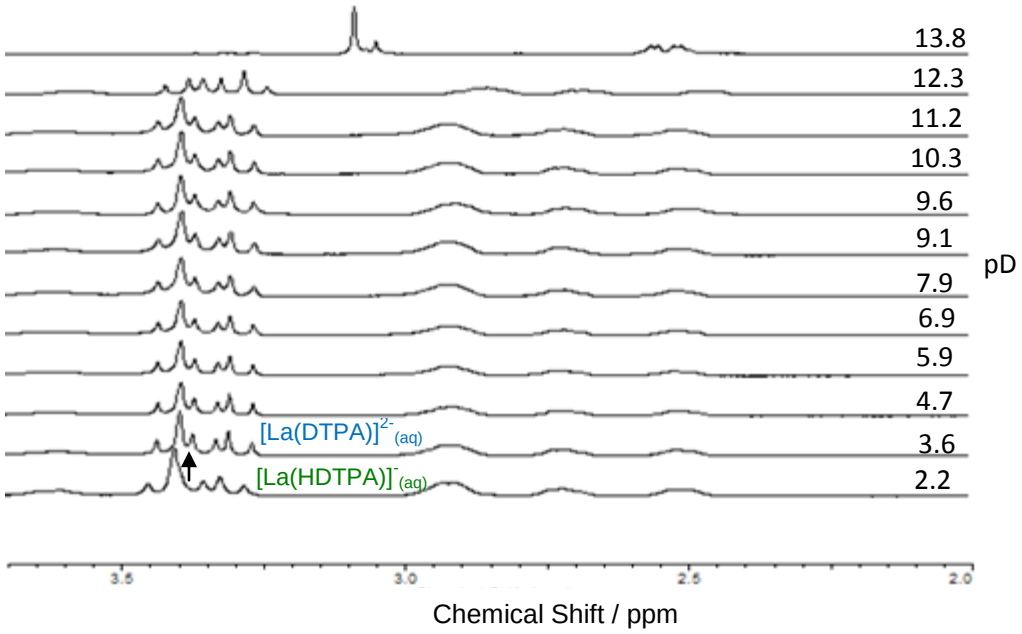

Figure 4.13: ^{1}H-NMR spectra of a 1:1 La^{III}:$DTPA^{5-}$ system as a function of pD; $[La^{III}]_i = [DTPA^{5-}]_i = 50$ mM.

The ^{1}H-NMR spectra examining the effect of pD on a 1:1 Lu^{III}:$DTPA^{5-}$ system (Figure A, Appendix 2) are similar to those of the 1:1 La^{III}:$DTPA^{5-}$ system. The $DTPA^{5-}$ resonances are broadened suggesting that the $DTPA^{5-}$ ligand also alternates between octadentate and heptadentate binding to the Lu^{III} ion. A difference in the splitting pattern of the acetate resonances between 3.3 and 3.5 ppm over the pD range 2.0 to 3.5 indicates the deprotonation of the $[Lu(HDTPA)]^{-}_{(aq)}$ complex to the $[Lu(DTPA)]^{2-}_{(aq)}$ species. The $DTPA^{5-}$ ligand remains bound to the Lu^{III} ion over the pD range 2.0 to 12.2. However, signals that are representative of unbound $DTPA^{5-}$ emerge at pD 12.2 implying that hydrolysis of the $[Lu(DTPA)]^{2-}_{(aq)}$ complex occurs. Hydrolysis of the $[Lu(DTPA)]^{2-}_{(aq)}$ complex begins at a lower pD than the $[La(DTPA)]^{2-}_{(aq)}$ complex, which is likely to be because the Lu^{III} ion has a higher charge density than the La^{III} ion and so would be more susceptible to hydrolysis.

4.2.2.2 Paramagnetic Lanthanide Ions (Eu^{III})

^{1}H-NMR spectroscopy was performed on a 1:1 Eu^{III}:$DTPA^{5-}$ binary system to observe the effects of paramagnetism and pD on the $DTPA^{5-}$ chemical shifts. The ^{1}H-NMR spectra of the 1:1 Eu^{III}:$DTPA^{5-}$ system (Figure 4.14) show signals that range from -17 to +30 ppm. The

paramagnetic shifting of the signals outside of the 'normal' 0 to 10 ppm range means that the $DTPA^{5-}$ ligand is bound to the Eu^{III} ion. The broadening of the signals observed in the spectra are caused by a combination of the Eu^{III} paramagnetism, and also the alternating $DTPA^{5-}$ binding mode between octa-and heptadentate. At pD 13.8, the $DTPA^{5-}$ proton resonances are present at 2.90 and 2.33 ppm, which are representative of the free $DTPA^{5-}$ ligand. The $[Eu(DTPA)]^{2-}_{(aq)}$ complex at this pD hydrolyses to form a white precipitate, which is probably $Eu(OH)_{3(s)}$, and $DTPA^{5-}$ is unbound in solution.

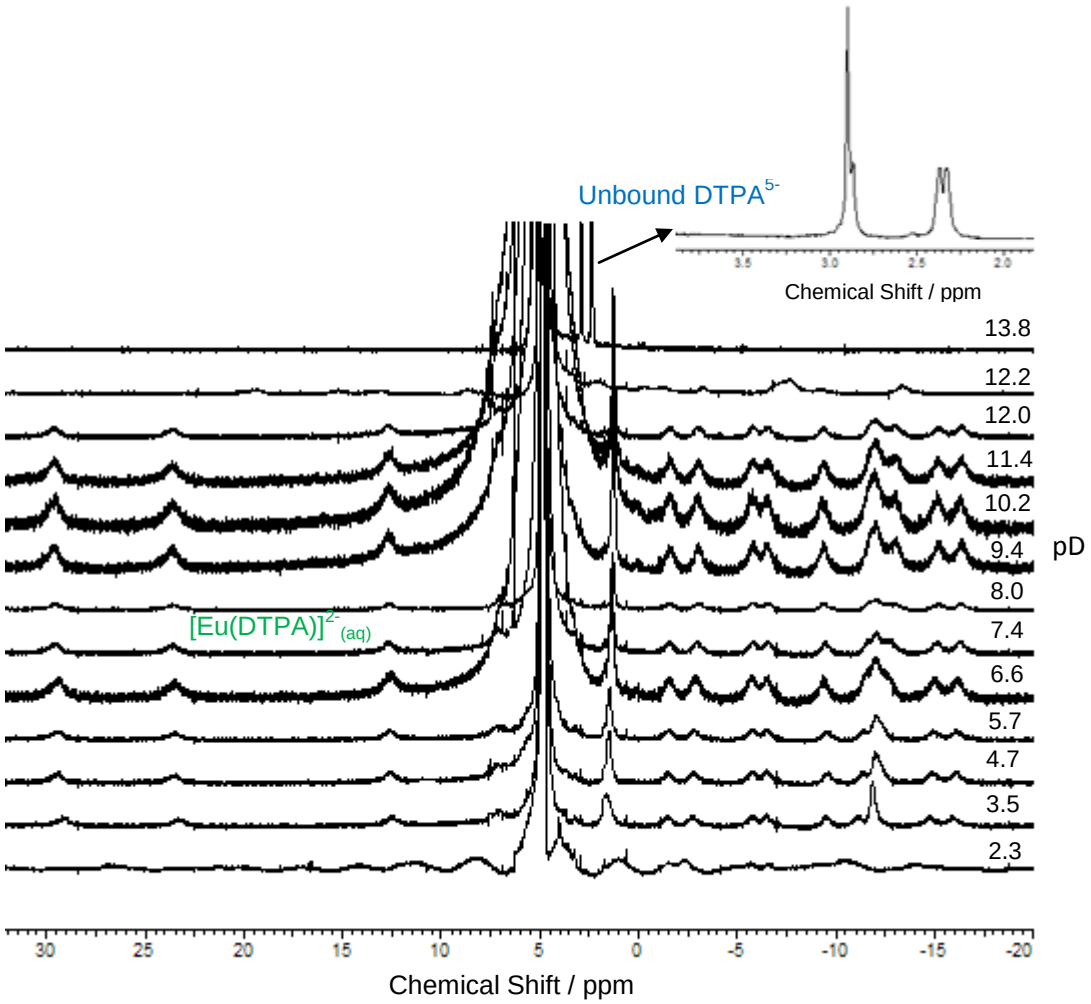

Figure 4.14: ^{1}H-NMR spectra of a 1:1 Eu^{III}:$DTPA^{5-}$ system as a function of pD; $[Eu^{III}]_i = [DTPA^{5-}]_i = 50$ mM.

4.2.3 Luminescence Spectroscopy

4.2.3.1 Eu^{III}

Luminescence spectroscopic titrations have been performed on the 1:1 Eu^{III}:$DTPA^{5-}$ system in H_2O and D_2O using NaOH/NaOD for pH/pD adjustment. The emission spectra of this system show no significant change in the intensity of the emission bands at 580, 590, 617, 650 and 690 nm over the pH range 3.8 to 11.4 (Figure 4.15). This suggests that the $[Eu(DTPA)]^{2-}_{(aq)}$ complex is the dominant solution species within this pH range, and there may be minimal interaction of hydroxide with the complex below pH 11.4.

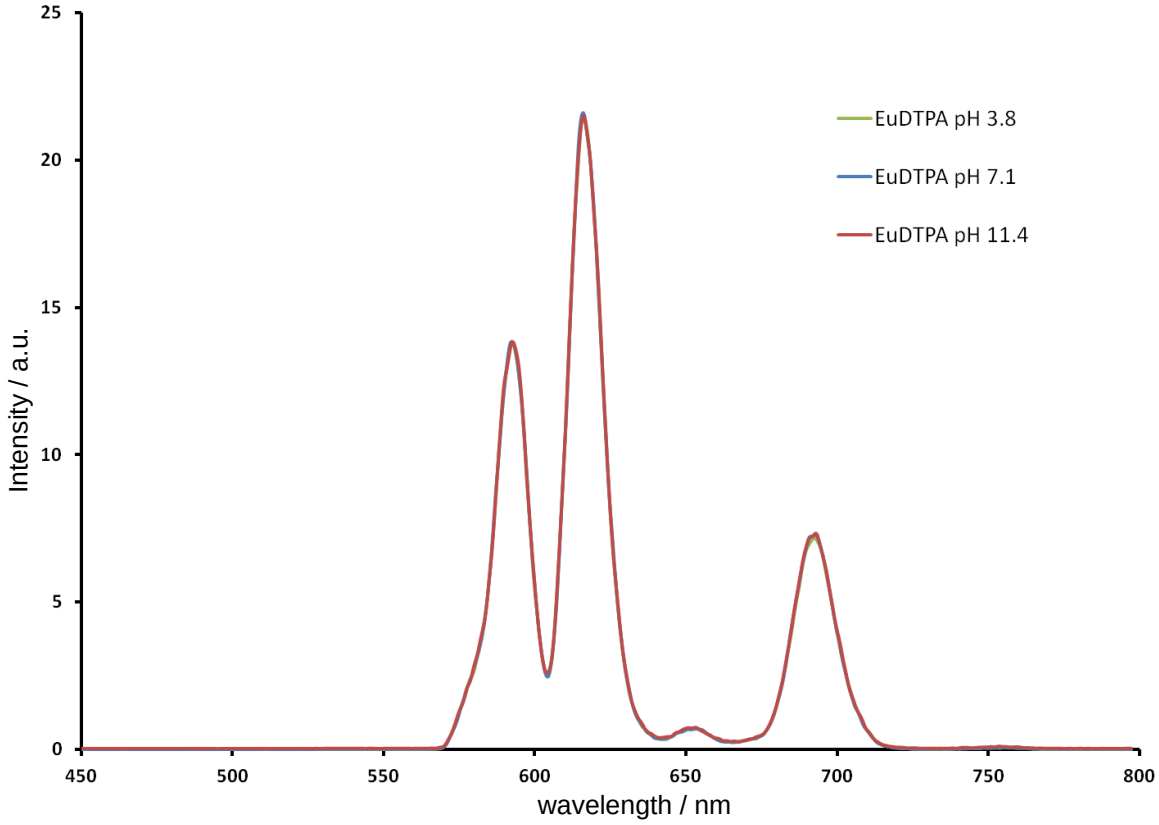

Figure 4.15: Emission spectra of 1:1 Eu^{III}:$DTPA^{5-}$; $[Eu^{III}]_i = [DTPA^{5-}]_i = 10$ mM.

The luminescent lifetimes for the 1:1 Eu^{III}:$DTPA^{5-}$ system in H_2O (Table 4.1) do not significantly change on increasing the pH from 3.8 (τ = 0.61 ms) to 11.4 (τ = 0.63 ms). However, the luminescent lifetimes do increase in D_2O (Table 4.1) from 1.59 to 2.51 ms over the pD range 3.7 to 11.4. This may indicate that there is some exchange process between the

$DTPA^{5-}$ ligand and OD^-/D_2O for Eu^{III} ion coordination. The interaction of OD^-/D_2O with the excited Eu^{III} species would provide a less efficient quenching pathway compared to the C=O functional groups of $DTPA^{5-}$.[9] The lifetimes of the Eu^{III} ion excited states are rapidly quenched in H_2O,[8] and so changes in the Eu^{III} inner coordination sphere may be more noticeable in the D_2O system as the lifetimes are longer.

	pH	τ / ms	pD	τ / ms
1:1 Eu^{III}:$DTPA^{5-}$	3.8	0.61 ± 0.06	3.7	1.59 ± 0.16
	7.1	0.63 ± 0.06	7.3	2.40 ± 0.24
	11.4	0.63 ± 0.06	11.4	2.51 ± 0.25

Table 4.1: Luminescent lifetimes (τ) of a 1:1 Eu^{III}:$DTPA^{5-}$ system at various pH/pD in H_2O and D_2O; $[Eu^{III}]_i = [DTPA^{5-}]_i = 10$ mM.

The N_{H_2O} bound to the Eu^{III} ion in the 1:1 Eu^{III}:$DTPA^{5-}$ system (Table 4.2) does not significantly change over the pH range 3.8 ($N_{H_2O} = 0.9$) to 11.4 ($N_{H_2O} = 1.1$). The hydration number of the Eu^{III} ion is nine,[10] and so if one water molecule is coordinated to the $[Eu(DTPA)]^-_{(aq)}$ complex then the octadentate coordination mode of $DTPA^{5-}$ is primarily observed by luminescence spectroscopy. As the N_{H_2O} bound to the Eu^{III} ion is approximately constant over the pH range 3.8 to 11.4, the effect of hydrolysis in the 1:1 Eu^{III}:$DTPA^{5-}$ system seems to be minimal.

1:1 Eu^{III}:$DTPA^{5-}$
pH 3.8, $\boldsymbol{N_{H_2O}}$ **= 0.9 ± 0.5**
pH 7.1, $\boldsymbol{N_{H_2O}}$ **= 1.1 ± 0.5**
pH 11.4, $\boldsymbol{N_{H_2O}}$ **= 1.1 ± 0.5**

Table 4.2: Calculated N_{H_2O} bound to the Eu^{III} ion in the 1:1 Eu^{III}:$DTPA^{5-}$ system at various pH; $[Eu^{III}]_i = [DTPA^{5-}]_i = 10$ mM. The uncertainty in N_{H_2O} calculations is ± 0.5 water molecules.[11]

4.2.4 Summary

^{1}H-NMR and luminescence spectroscopy have been successfully used to study the solution behaviour of the 1:1 Ln^{III}:$DTPA^{5-}$ systems (where Ln= La, Eu or Lu). The $[Ln(HDTPA)]^{-}_{(aq)}$ complex forms at acidic pH (*i.e.* pH less than 1), where one of the acetate arms of $DTPA^{5-}$ is protonated. As pH is increased, the $[Ln(DTPA)]^{2-}_{(aq)}$ complex dominates the solution speciation from approximately pH 3 to pH greater than 12, when hydrolysis occurs. The ^{1}H-NMR spectra of the 1:1 Ln^{III}:$DTPA^{5-}$ systems (Section 4.2.2) showed broadened $DTPA^{5-}$ signals, which suggested that the $DTPA^{5-}$ ligand was alternating its coordination mode between octa- and heptadentate on the NMR timescale.[8] Luminescence spectroscopy allowed for the determination of the N_{H_2O} bound to the Eu^{III} ion in the 1:1 Eu^{III}:$DTPA^{5-}$ system, which was calculated to be one water molecule. Therefore, the octadentate $DTPA^{5-}$ binding mode was primarily observed on the luminescence timescale, which corresponds to the $[Eu(DTPA)(H_2O)]^{2-}_{(aq)}$ species.

4.3 Lanthanide-Lactate Binary Systems

4.3.1 Speciation Diagram

4.3.1.1 1:1 La^{III}:Lactate

The aqueous La^{III} species present in a 1:1 La^{III}:lactate system at a certain pH can be determined from the speciation diagram (Figure 4.16), which is derived from known equilibrium constants.[3] Free $La^{III}_{(aq)}$ dominates the speciation until pH 5 when the $[La(lactate)]^{2+}_{(aq)}$ species prevails. Lactate is a weakly coordinating ligand, and so it is likely that hydrolysis of the $La^{III}_{(aq)}$ ion to form $La(OH)_{3(s)}$ becomes prevalent after pH 8.

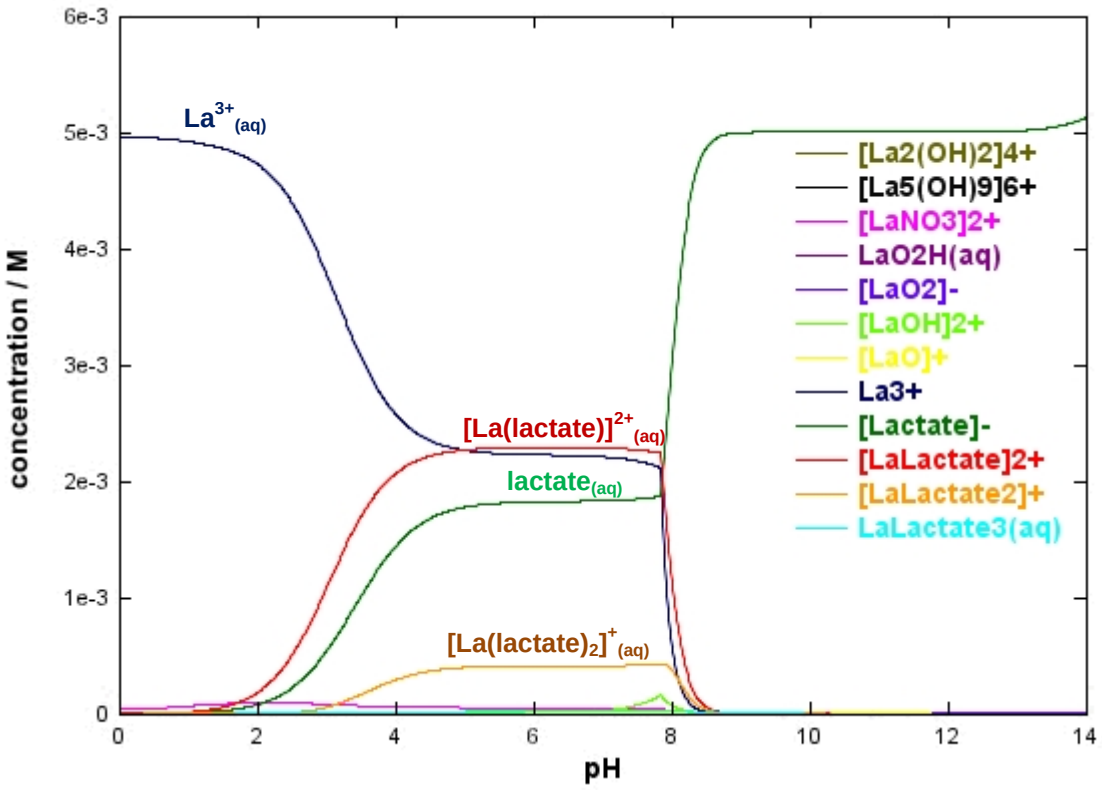

Figure 4.16: Speciation diagram of 1:1 La^{III}:lactate system as a function of pH using the *JCHESS* code.[7] Total [La^{III}] = total [lactate] = 5 mM. Only aqueous species are shown. Thermodynamic data obtained from the integrated *JCHESS* database and Martell and Smith.[3]

4.3.2 NMR Spectroscopy

4.3.2.1 Diamagnetic Lanthanide Ions (La^{III} and Lu^{III})

^{1}H-NMR spectroscopy was performed on a 1:1 Ln^{III}:lactate binary system (where Ln = La or Lu) to observe the effect of pD on the lactate chemical shifts. The ^{1}H-NMR spectra of the 1:1 La^{III}:lactate system (Figure 4.17) show a quartet of doublets (integrates to 1 proton) at approximately 4.37 ppm and a doublet of doublets (integrates to 3 protons) at 1.42 ppm, which are representative of the –C**H**(OH)- and –C$\mathbf{H_3}$ protons of ^{13}C-labelled lactate, respectively. As pD is increased from 3.1 to 13.0, the signals shift from 4.37 to 4.10 ppm and from 1.42 to 1.30 ppm. The shift in the proton resonances from pD 3.1 to 9.9 is initially due to the formation of the $[La(lactate)]^{2+}_{(aq)}$ complex, and then the formation of unbound lactate. This is because at pD 9.9 and above the lactate signals remain stationary in the spectra, implying that only unbound lactate exists. The broadening observed in the spectra between

pD 7.3 to 9.1 is probably due to exchange between bound and unbound lactate. A white precipitate begins to form at pD 7.3, which is likely to be $La(OH)_{3(s)}$.

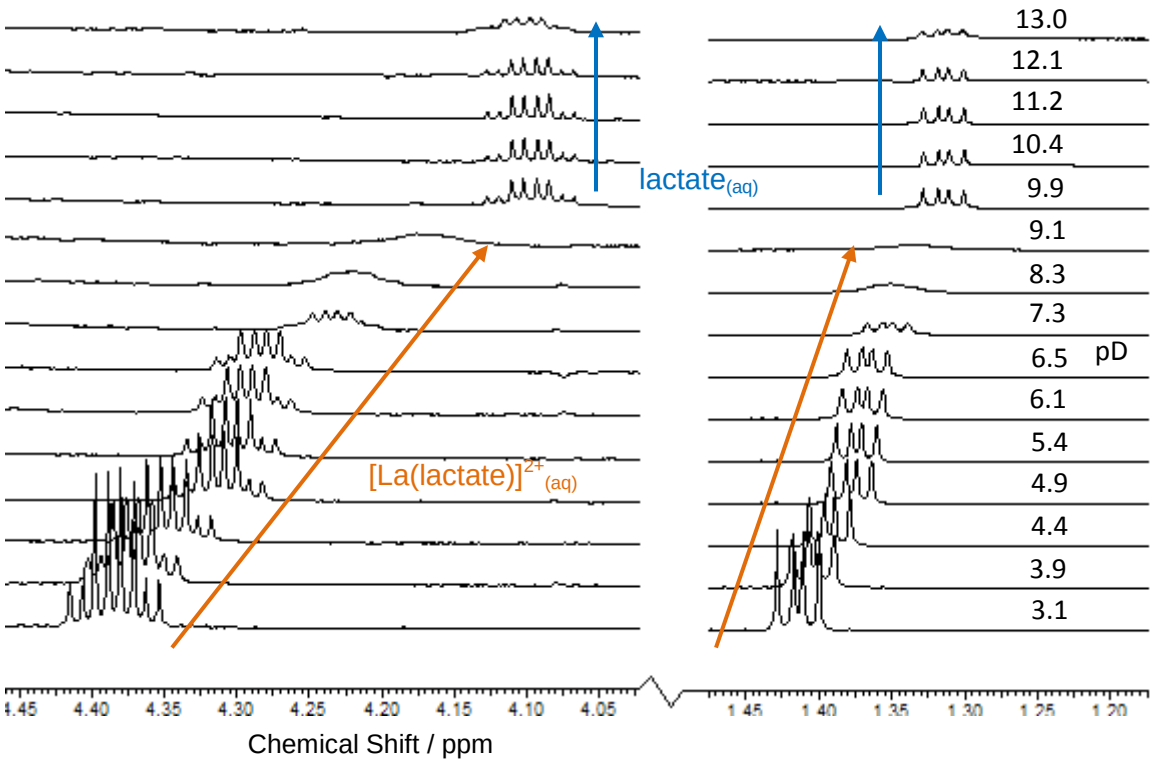

Figure 4.17: ^{1}H-NMR spectra of a 1:1 La^{III}:lactate system as a function of pD; $[La^{III}]_i = [lactate]_i = 50$ mM.

The ^{13}C-NMR spectra obtained for the 1:1 La^{III}:lactate system show a signal for the carboxylate group of lactate at 179.6 ppm that shifts to 183.5 ppm over the pD range 3.1 to 6.8 (Figure 4.18). This change in the chemical shift of the carboxylate signal represents the formation of the $[La(lactate)]^{2+}_{(aq)}$ species. As the pH is increased above 6.8, the carboxylate signal shifts from 183.5 to 183.1 ppm, which corresponds to the formation of free lactate as the $[La(lactate)]^{2+}_{(aq)}$ complex is hydrolysed. There is broadening of the carboxylate signal observed over the pD range 8.3 to 9.1, which is likely to be due to fast exchange between bound and unbound lactate in the system.

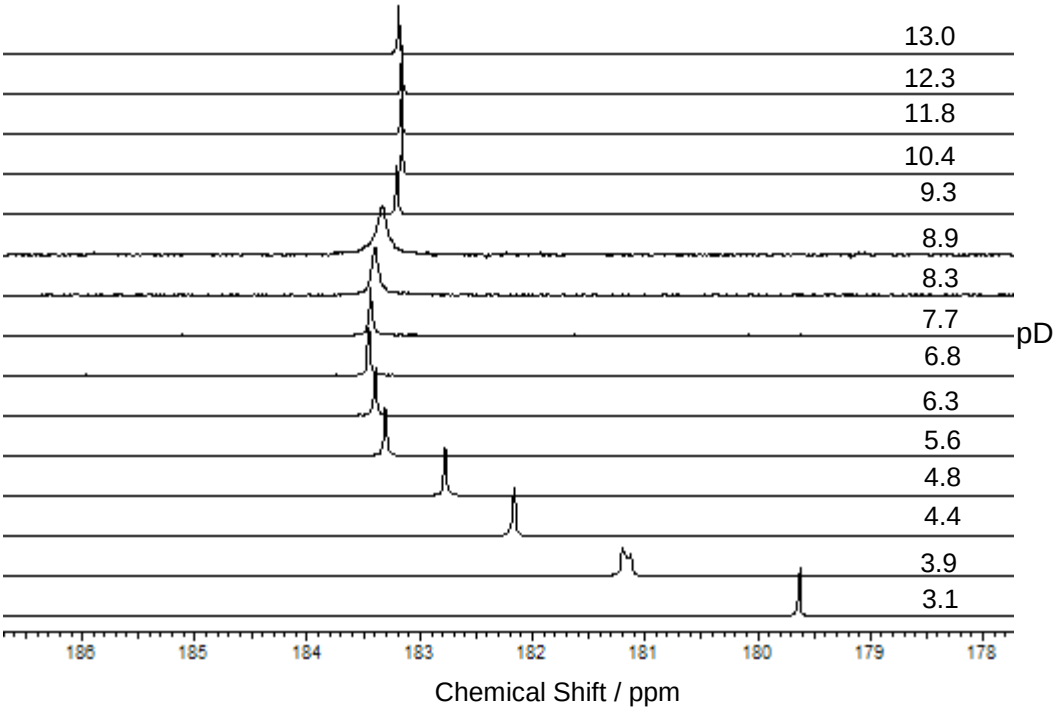

Figure 4.18: ^{13}C-NMR spectra of a 1:1 La^{III}:lactate system as a function of pD; $[La^{III}]_i = [lactate]_i = 50$ mM.

The ^{1}H-NMR spectra obtained to study the effect of pD on the 1:1 Lu^{III}:lactate system (Figure B, Appendix 2) are similar to that of the 1:1 La^{III}:lactate system. The lactate resonances are broadened between pD 3.8 to 6.5, suggesting that there is exchange between bound and unbound lactate. Due to the higher charge density of the Lu^{III} ion compared to the La^{III} ion, hydrolysis of the $[Lu(lactate)]^{2+}_{(aq)}$ complex occurs at a lower pD than the $[La(lactate)]^{2+}_{(aq)}$ complex (approximately pD 5 *vs*. pD 6, respectively).

4.3.2.2 Paramagnetic Lanthanide Ions (Eu^{III})

^{1}H-NMR spectroscopy was performed on a 1:1 Eu^{III}:lactate binary system to observe the effects of paramagnetism and pD on the lactate chemical shifts (Figure 4.19). At pD 3.0, the lactate proton resonances are present at 3.0 and 1.0 ppm, for the –C**H**(OH)- and –C**H$_3$** protons, respectively. At this pD, there has been a paramagnetic shift of the –C**H**(OH)- resonance (compared to the diamagnetic 1:1 La^{III}:lactate system) from 4.4 to 3.0 ppm, and for the –C**H$_3$** protons, there has been a small shift from 1.3 to 1.0 ppm. This paramagnetic shift of

the signal suggests that there is exchange between bound lactate and unbound lactic acid. As pD is increased further from pD 3.0 to 5.9, the -C**H**(OH)- resonance shifts from 3.0 to -2.0 ppm and the -C**H$_3$** protons shift from 1.0 to -0.32 ppm. The paramagnetic shift (and broadening) of the proton resonances means that lactate does bind to the Eu^{III} ion. The -C**H**(OH)- signal is the lactate resonance that shifts the most when lactate is coordinated to the Eu^{III} ion, which may indicate that the protonated hydroxyl group is involved in lactate coordination to metal ions as suggested by Tian *et al*.[4] As pD is increased from pD 5.9 to 8.8, the resonances shift from -2.00 and -0.32 ppm to 4.10 and 1.32 ppm for the -C**H**(OH)- and -C**H$_3$** protons, respectively. This means that at pD 8.8, the lactate resonances are no longer paramagnetically shifted and so lactate is unbound from the Eu^{III} ion. A white precipitate is observed to form, which is likely to be $Eu(OH)_{3(s)}$.

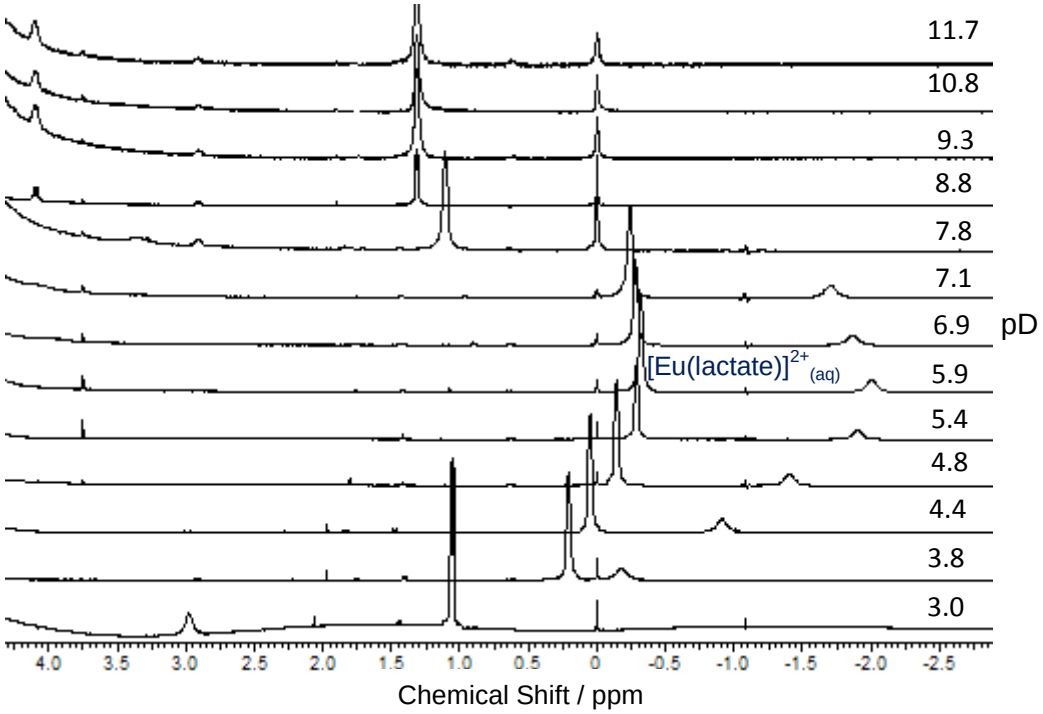

Figure 4.19: ^{1}H-NMR spectra of a 1:1 Eu^{III}:lactate system as a function of pD; $[Eu^{III}]_i = [lactate]_i = 50$ mM.

The ^{13}C-NMR spectra obtained to study the interaction of lactate with the Eu^{III} ion show that the carboxylate signal shifts from 177.8 ppm to 174.0 ppm as pD is increased from pD 3.0 to 5.0 (Figure 4.20). This shift in the carboxylate signal corresponds to the formation of the $[Eu(lactate)]^{2+}_{(aq)}$ complex. As the pD of the system is increased further from 5.0 to 9.2, the

carboxylate signal shifts from 174.0 to 183.0 ppm, which represents the change in equilibrium from the $[Eu(lactate)]^{2+}_{(aq)}$ complex to free lactate and formation of $Eu(OH)_{3(s)}$. The observed broadening of the carboxylate signal over the pD range 3.9 to 7.7 indicates that there is fast exchange between bound and unbound lactate in the system.

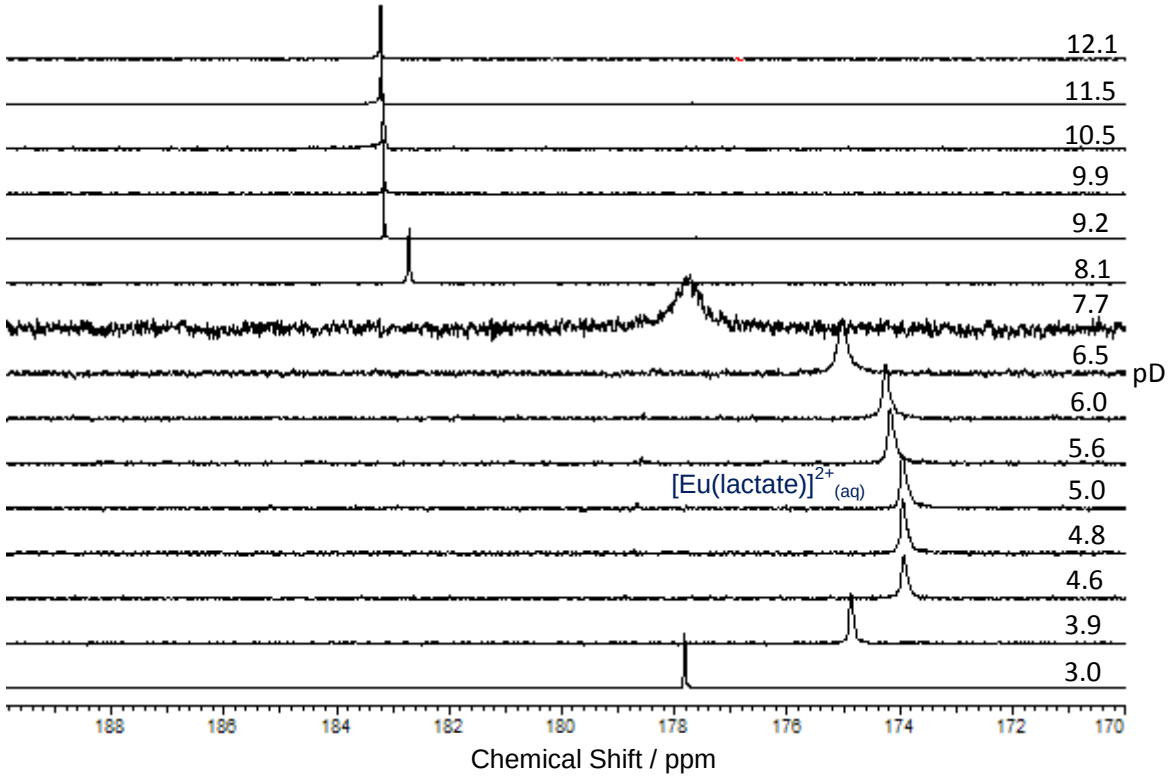

Figure 4.20: ^{13}C-NMR spectra of a 1:1 Eu^{III}:lactate system as a function of pD; $[Eu^{III}]_i = [lactate]_i = 50$ mM.

4.3.3 Summary

NMR spectroscopy has been a valuable technique for probing the solution behaviour of the 1:1 Ln^{III}:lactate systems (where Ln= La, Eu or Lu). Lactate can complex to the lanthanide ions at acidic pH, but as lactate is a weakly coordinating ligand, it is readily replaced by hydroxide over the pH range 5 to 9.

4.4 Lanthanide-DTPA-Lactate Ternary Systems

4.4.1 NMR Spectroscopy

4.4.1.1 Diamagnetic Lanthanide Ions (La^{III} and Lu^{III})

The lanthanide ions (Ln^{III} = La, Eu, Lu) are capable of binding $DTPA^{5-}$ and lactate in the 1:1 Ln:L systems (L= $DTPA^{5-}$ or lactate, in Sections 4.2 and 4.3, respectively). The TALSPEAK process uses $DTPA^{5-}$ and lactate in the aqueous phase, and so the formation of ternary complexes (*i.e.* $[M(DTPA)(lactate)]^{3-}_{(aq)}$; M = An^{III} or Ln^{III}) has been hypothesised to occur in this system.[1]

The potential formation of these ternary complexes in a 1:1:1 Ln^{III}:$DTPA^{5-}$:lactate system has been investigated using NMR spectroscopy. The ^{1}H-NMR spectra of the La^{III} ion ternary system (Figure 4.21) show signals between 2.40 and 3.75 ppm over the pD range 3.8 to 13.2, which correspond to the bound ethylene and acetate protons of $DTPA^{5-}$ that have been observed previously (Figure 4.13). The signals at approximately 4.30 and 1.37 ppm are due to the -C**H**(OH)- and -C$\mathbf{H_3}$ protons of lactate, respectively. These signals shift from 4.30 to 4.10 ppm and from 1.37 to 1.30 ppm as pD is increased from pD 3.8 to 6.0 (Figure 4.22). This pD dependent shift of the lactate signals is likely to be due to the change in equilibrium between lactic acid and lactate. After pD 6.0, the lactate signals remain constant at 4.10 and 1.37 ppm, which is representative of unbound lactate (Figure 4.7) rather than bound lactate (Figure 4.17). There is also no broadening of the lactate signals in the ternary system, which was observed in the 1:1 La^{III}:lactate binary system, and so the ^{1}H-NMR spectra in Figure 4.22 indicate that lactate is not bound to the $[La(DTPA)]^{2-}_{(aq)}$ complex.

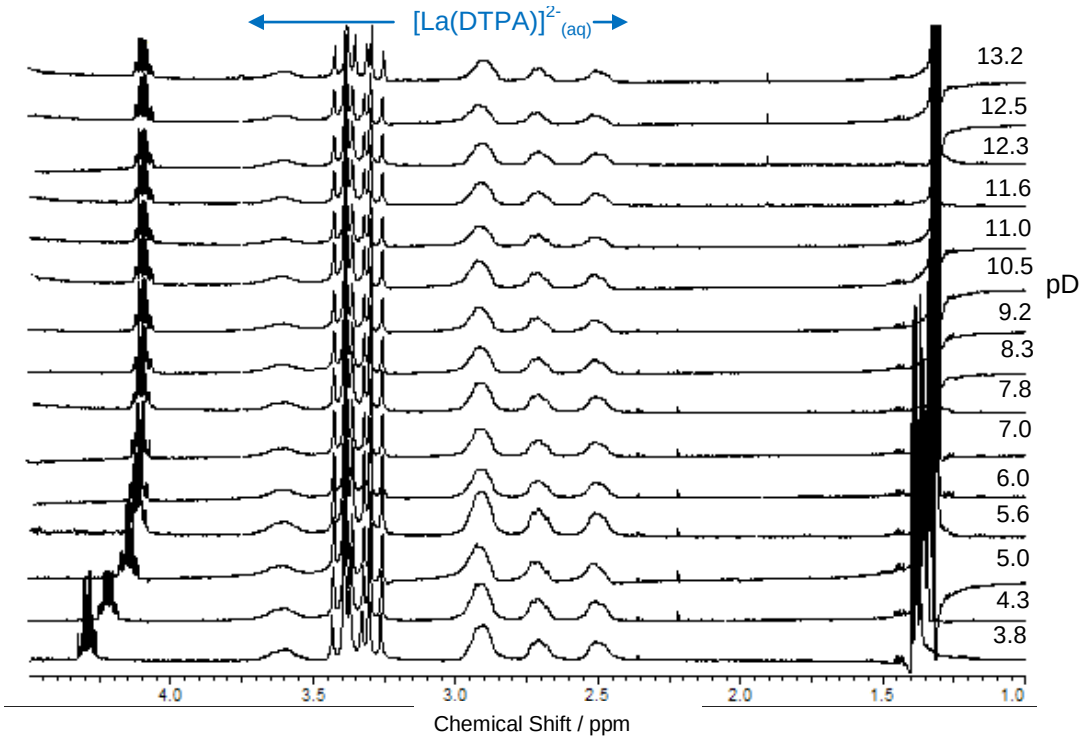

Figure 4.21: ^{1}H-NMR spectra of a 1:1:1 La^{III}:$DTPA^{5-}$:lactate system as a function of pD; $[La^{III}]_i = [DTPA^{5-}]_i = [lactate]_i = 33$ mM.

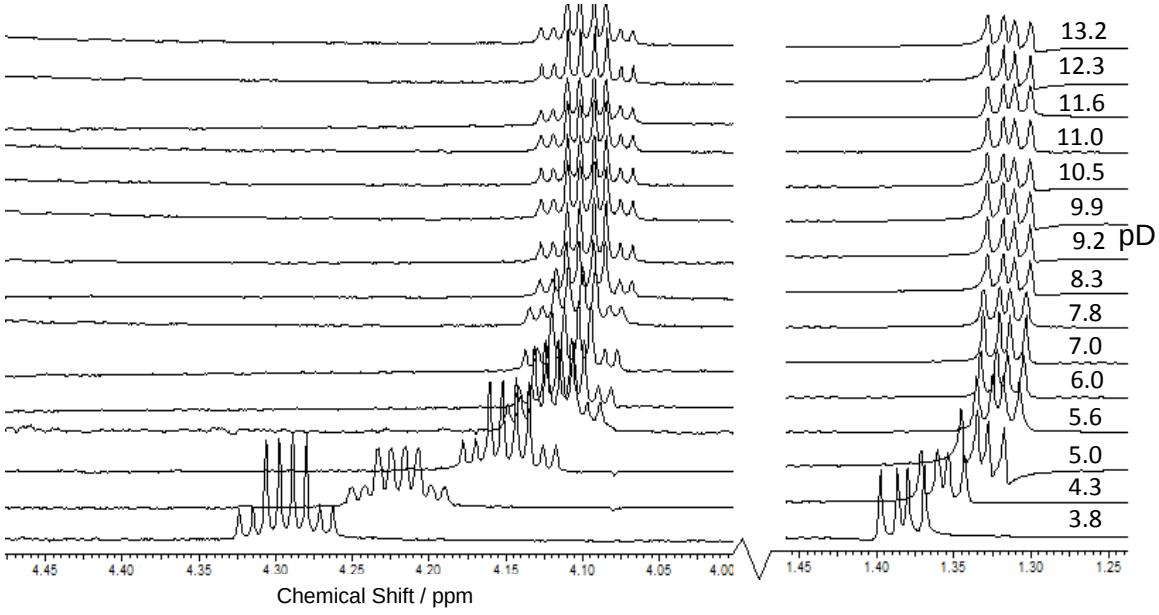

Figure 4.22: 'Zoom in' of lactate signals for the ^{1}H-NMR spectra of a 1:1:1 La^{III}:$DTPA^{5-}$:lactate system as a function of pD; $[La^{III}]_i = [DTPA^{5-}]_i = [lactate]_i = 33$ mM.

The ^{13}C-NMR spectra obtained for the 1:1:1 La^{III}:$DTPA^{5-}$:lactate system show a carboxylate signal at 180.5 ppm that shifts to 183.2 ppm as pD is increased from 3.8 to 5.9 (Figure 4.23). This correlates to the deprotonation of unbound lactic acid to form unbound lactate. The position of the carboxylate signal remains stationary at 183.2 ppm at pH 5.9 and above, suggesting that unbound lactate is the dominant lactate solution species. It is likely that the lactate ligand is predominantly unbound from the $[La(DTPA)]^{2-}_{(aq)}$ complex, as the chemical shift of the carboxylate signal in this system is similar to that of the free lactate ligand (Figure 4.8). There is also no broadening of the lactate signal, which was observed when lactate was coordinated to the La^{III} ion in the binary system (Figure 4.18).

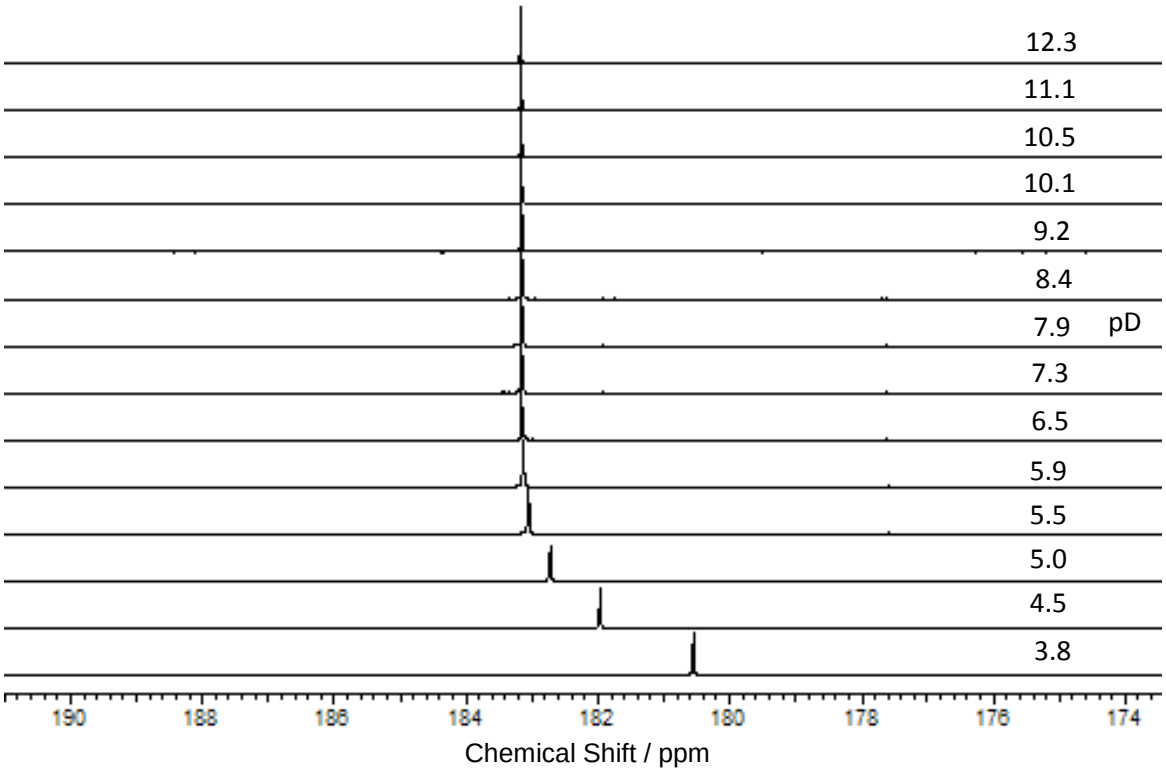

Figure 4.23: ^{13}C-NMR spectra of a 1:1:1 La^{III}:$DTPA^{5-}$:lactate system as a function of pD; $[La^{III}]_i = [DTPA^{5-}]_i = [lactate]_i = 33$ mM.

The ^{1}H- and ^{13}C-NMR spectra obtained to probe the effect of pD on the 1:1:1 Lu^{III}:$DTPA^{5-}$:lactate system (Figures C, D and E, Appendix 2) are in agreement with the La^{III} system, as signals that are representative of bound $DTPA^{5-}$ and unbound lactate are observed.

4.4.1.2 Paramagnetic Lanthanide Ions (Eu^{III})

The interaction of lactate with the $[Eu(DTPA)]^{2-}_{(aq)}$ complex has been investigated using ^{1}H-NMR spectroscopy. The ^{1}H-NMR spectra show signals from around -17 to +30 ppm over the pD range 3.8 to 11.8 (Figure 4.24), which correspond to the $DTPA^{5-}$ ligand being bound to the Eu^{III} ion. There are also signals at 2.19 ppm (integrates to 1 proton) and 0.83 ppm (integrates to 3 protons), which correspond to the -C**H**(OH)- and -C$\mathbf{H_3}$ protons of lactate, respectively. As pD is increased from pD 3.8 to 7.0, these signals shift from 2.19 to 1.44 ppm and 0.83 to 0.59 ppm (Figure 4.25). The lactate signals in the 1:1:1 Eu^{III}:$DTPA^{5-}$:lactate system are observed at a different chemical shift compared to free lactate (*i.e.* 4.1 and 1.3 ppm for -C**H**(OH)- and -C$\mathbf{H_3}$ protons, respectively, in Figure 4.7) and to the $[Eu(lactate)]^{2+}_{(aq)}$ complex (*i.e.* -2.00 and -0.32 ppm for -C**H**(OH)- and -C$\mathbf{H_3}$ protons, respectively, Figure 4.19).

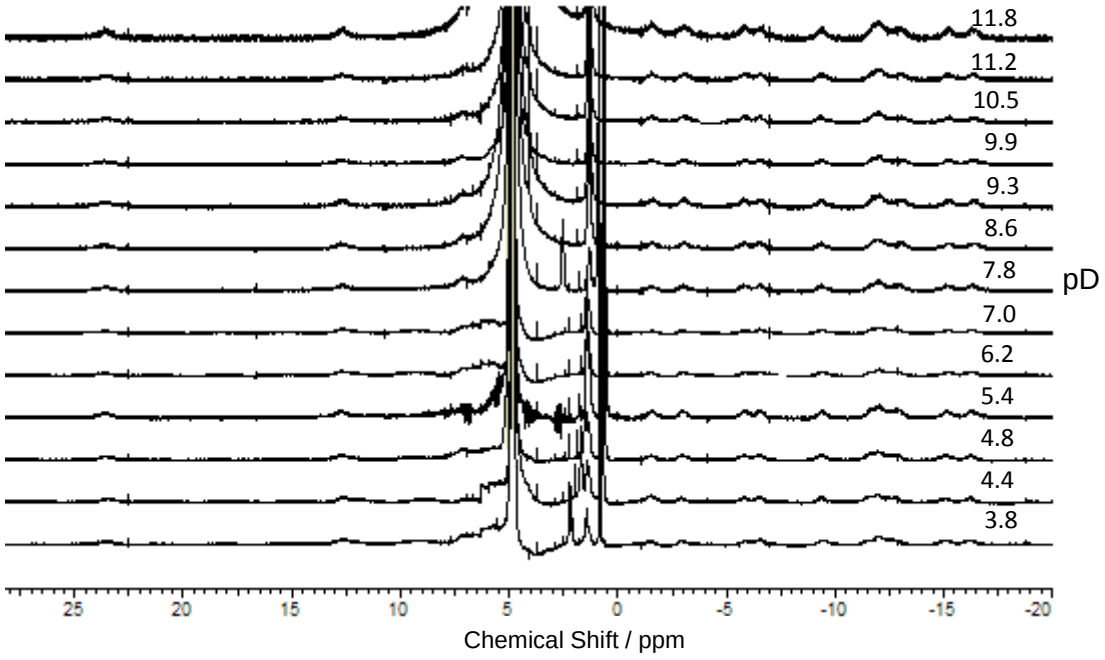

Figure 4.24: ^{1}H-NMR spectra of a 1:1:1 Eu^{III}:$DTPA^{5-}$:lactate system as a function of pD; $[Eu^{III}]_i = [DTPA^{5-}]_i = [lactate]_i = 33$ mM.

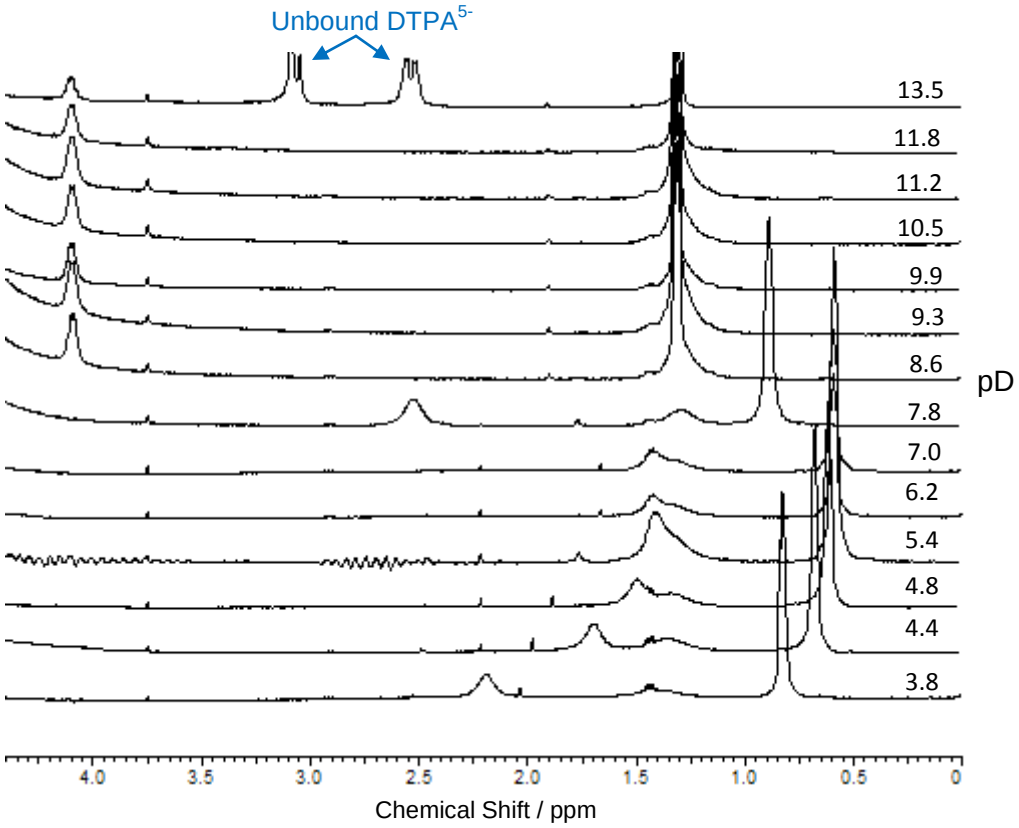

Figure 4.25: 'Zoom in' of lactate signals for the ^{1}H-NMR spectra of a 1:1:1 Eu^{III}:$DTPA^{5-}$:lactate system as a function of pD; $[Eu^{III}]_i = [DTPA^{5-}]_i = [lactate]_i = 33$ mM.

The ^{13}C-NMR spectra obtained to probe the solution behaviour of the 1:1:1 Eu^{III}:$DTPA^{5-}$:lactate system show a shift in the carboxylate signal from 178.0 to 183.5 ppm as pD is increased from 3.8 to 9.4 (Figure 4.26). The observed broadening of the carboxylate signal suggests that there is some interaction with the $[Eu(DTPA)]^{2-}_{(aq)}$ complex over this pD range. From pD 9.4 to 13.4, the lactate signal remains stationary at 183.4 ppm, indicative of unbound lactate.

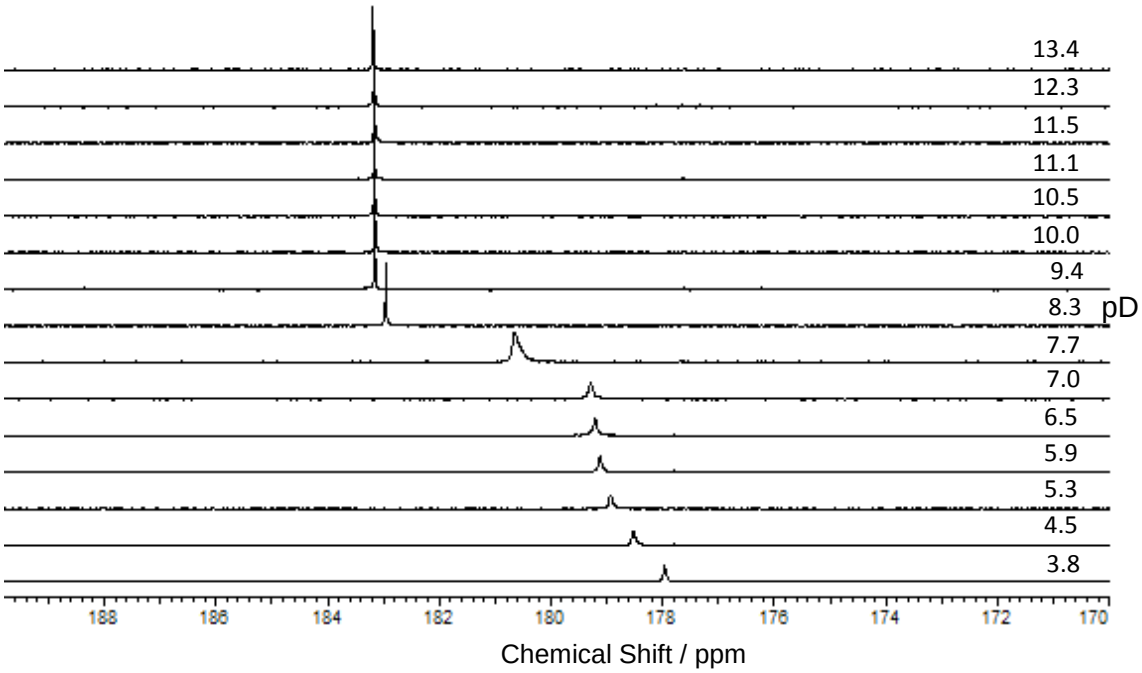

Figure 4.26: ^{13}C-NMR spectra of a 1:1:1 Eu^{III}:$DTPA^{5-}$:lactate system as a function of pD; $[Eu^{III}]_i = [DTPA^{5-}]_i = [lactate]_i = 33$ mM.

The shift of the lactate signals in the NMR spectra obtained for the 1:1:1 Eu^{III}:$DTPA^{5-}$:lactate system indicate that there is some interaction of lactate with the $[Eu(DTPA)]^{2-}_{(aq)}$ complex, but the lactate may be binding in a different manner to the Eu^{III} ion compared to the $[Eu(lactate)]^{2+}_{(aq)}$ complex, as the $DTPA^{5-}$ ligand is restricting access of secondary ligands to the majority of the Eu^{III} coordination sphere. It is also possible that lactate is binding to the $[La(DTPA)]^{2-}_{(aq)}$ and $[Lu(DTPA)]^{2-}_{(aq)}$ complexes, but as the interaction may be weak, it may not be noticeable in the NMR spectra for the diamagnetic systems. There are reports in the literature that hydroxyl groups are able to hydrogen bond to carboxylate groups,[12] so it may also be possible that the hydroxyl group of lactate is hydrogen bonding to the $DTPA^{5-}$ acetate arms rather than directly coordinating to the metal ion. Suggestions for the coordination modes of lactate in the 1:1 Eu^{III}:lactate (Figure 4.27) and 1:1:1 Eu^{III}:$DTPA^{5-}$:lactate systems (Figure 4.28) are presented. It may be possible that lactate is binding directly to the Eu^{III} ion in the $[Eu(DTPA)]^{2-}_{(aq)}$ complex via an oxygen on the lactate carboxylate group, similar to the $[Eu(DTPA)(IDA)]^{4-}_{(aq)}$ complex (Figure 1.18, Section 1.2.7). A suggestion for the mode of hydrogen bonding of the lactate ligand to $DTPA^{5-}$, which is bound to the Eu^{III} ion, is proposed

in Figure 4.29. Any coordinated lactate is likely to be in equilibrium with the octa- and heptadentate $[Eu(DTPA)]^{2-}_{(aq)}$ complexes (Figure 4.29).

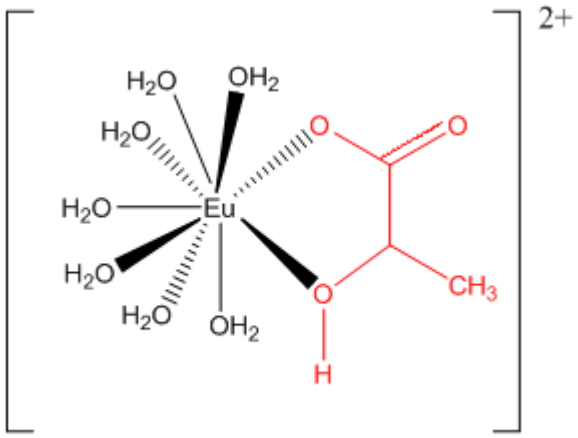

Figure 4.27: Suggested structure of $[Eu(lactate)]^{2+}_{(aq)}$.

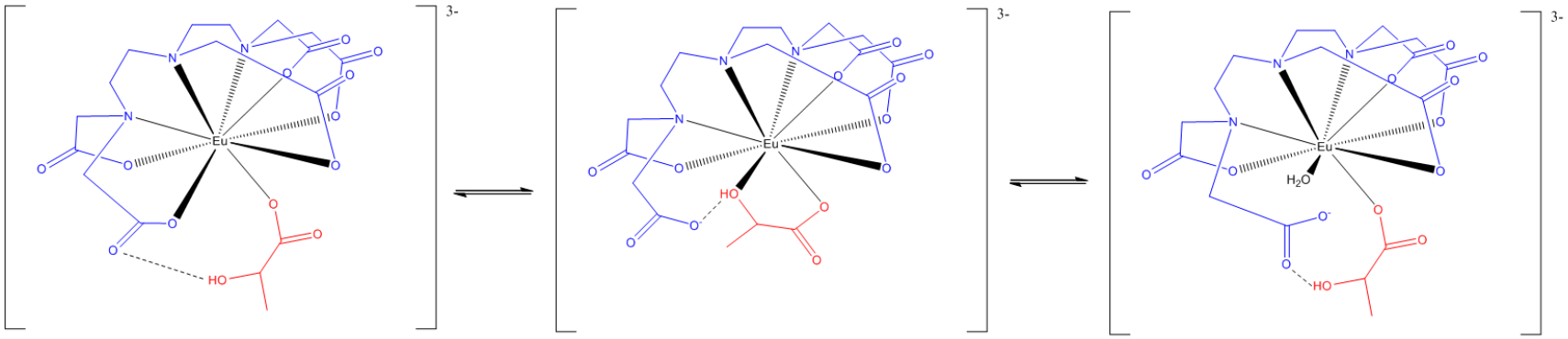

Figure 4.28: Suggested structure of $[Eu(DTPA)(lactate)]^{3-}_{(aq)}$.

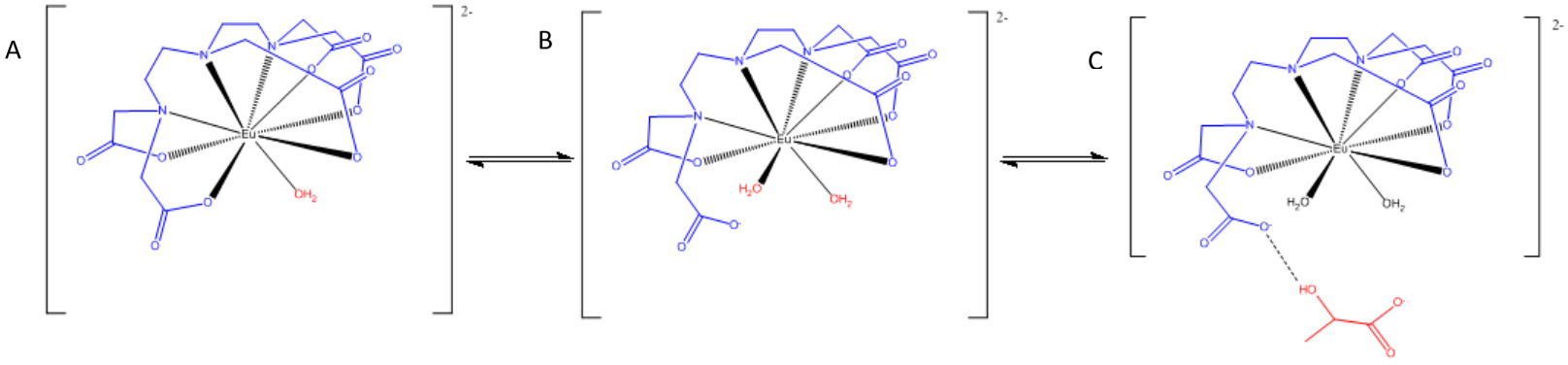

Figure 4.29: Suggested structure of: A) $[Eu(DTPA)(H_2O)]^{2-}$; B) $[Eu(DTPA)(H_2O)_2]^{2-}$ and C) lactate participating in hydrogen bonding with the $[Eu(DTPA)(H_2O)_2]^{2-}$ complex (secondary sphere interaction).

4.4.2 Luminescence Spectroscopy

4.4.2.1 Eu^{III}

Luminescence spectroscopic titrations have been performed on the 1:1:1 Eu^{III}:$DTPA^{5-}$:lactate system in H_2O and D_2O using NaOH/NaOD for pH/pD adjustment. The emission spectra of this system show a decrease in the intensity of the emission bands at 580, 590, 617, 650 and 690 nm on increasing the pH from 3.7 to 7.1 (Figure 4.30). This is then followed by an increase in the emission intensity when the pH is further increased to 11.5. This emission behaviour of the 1:1:1 Eu^{III}:$DTPA^{5-}$:lactate system differs from that of the 1:1 Eu^{III}:$DTPA^{5-}$ system, where no significant change of the emission intensity was observed from pH 3.8 to 11.4 (Figure 4.15). This difference in the emission profiles between the binary and ternary systems may indicate lactate interaction with the $[Eu(DTPA)]^{2-}_{(aq)}$ complex.

The luminescent lifetimes do not significantly change over the pH range 3.7 to 11.5 (Table 4.3), and the N_{H_2O} bound to the Eu^{III} ion is calculated to be 1.1 over the same pH range (Table 4.4). There may be a variety of equilibria possible in the ternary system (Figures 4.28 and 4.29), and so it is likely that the values obtained for the luminescent lifetime and N_{H_2O} bound to the Eu^{III} ion in this system are averages for all of the equilibria. It is apparent that the role of lactate in the 1:1:1 Ln^{III}:$DTPA^{5-}$:lactate system is complicated, and so further luminescence measurements over the pH range 4 to 7 may give more insight into the behaviour of lactate in this system.

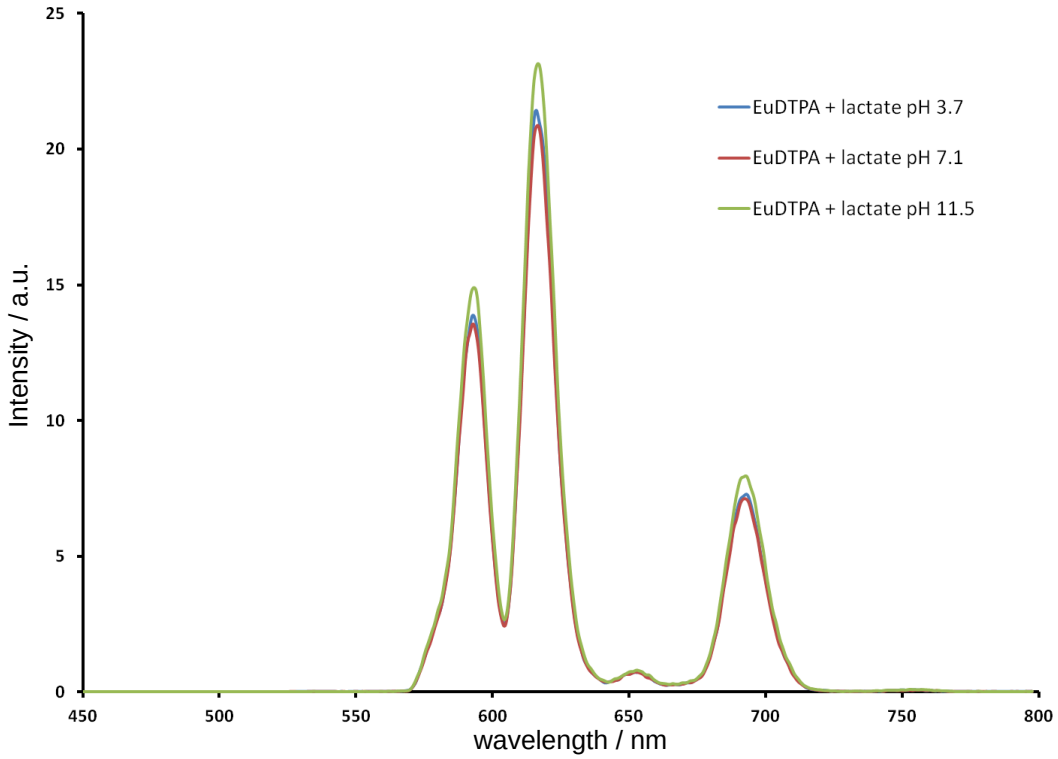

Figure 4.30: Emission spectra of 1:1:1 Eu^{III}:$DTPA^{5-}$:lactate; $[Eu^{III}]_i = [DTPA^{5-}]_i = [lactate]_i = 10$ mM.

1:1:1 Eu^{III}:$DTPA^{5-}$:lactate	**pH**	**τ / ms**	**pD**	**τ / ms**
	3.7	0.63 ± 0.06	3.7	2.44 ± 0.24
	7.1	0.63 ± 0.06	7.3	2.43 ± 0.24
	11.5	0.63 ± 0.06	11.4	2.50 ± 0.25

Table 4.3: Luminescent lifetimes (τ) of 1:1:1 Eu^{III}:$DTPA^{5-}$:lactate at various pH/pD in H_2O and D_2O; $[Eu^{III}]_i = [DTPA^{5-}]_i = [lactate]_i = 10$ mM.

1:1:1 Eu^{III}:$DTPA^{5-}$:lactate
pH 3.5, N_{H_2O} = **1.1 ± 0.5**
pH 7.1, N_{H_2O} = **1.1 ± 0.5**
pH 11.5, N_{H_2O} = **1.1 ± 0.5**

Table 4.4: Calculated N_{H_2O} bound to the Eu^{III} ion in the 1:1:1 Eu^{III}:$DTPA^{5-}$:lactate system at various pH; $[Eu^{III}]_i = [DTPA^{5-}]_i = [lactate]_i = 10$ mM. The uncertainty in N_{H_2O} calculations is ± 0.5 water molecules.[11]

4.4.3 Relevance to the TALSPEAK Process

The TALSPEAK process is concerned with Ln^{III}/$DTPA^{5-}$/lactate systems at approximately pH 3.5 (Section 1.1.8). The ^{1}H-NMR spectroscopic titrations detailed above (Figures 4.13 and 4.14) show that $DTPA^{5-}$ can complex to lanthanides at this pH, and so the $[Ln(DTPA)]^{2-}_{(aq)}$ complex will be present in the aqueous phase of the TALSPEAK process. In a 1:1 Ln^{III}:lactate system at pH 3.5, there is a mixture of the $[Ln(lactate)]^{2+}_{(aq)}$ complex and free lactic acid. The ^{1}H-NMR spectroscopic titration suggests that $[Ln(lactate)]^{2+}_{(aq)}$ complex dominates the speciation of La^{III} over the pH region 5 to 6 (Figure 4.17). In the TALSPEAK process, it is unlikely that there would be significant amounts of the $[Ln(lactate)]^{2+}_{(aq)}$ complex present as the lanthanides would always preferentially bind the higher denticity $DTPA^{5-}$ ligand (Figures 4.21 and 4.24). There may be a weak interaction of lactate with the $[Ln(DTPA)]^{2-}_{(aq)}$ complexes between the pH region 3.8 to 7.8, with the most favourable pH for the interaction of lactate with the $[Ln(DTPA)]^{2-}_{(aq)}$ complex occurring between pH 5.4 to 7.0 (Figure 4.25). At the pH of the TALSPEAK process (*i.e.* pH 3.5), the interaction of lactate with the $[Ln(DTPA)]^{2-}_{(aq)}$ complex may occur, but the interaction is likely to be weak and not favourable, as there will still be approximately 50 % of the lactate species present as lactic acid (pK_a = 3.55).[3]

In summary, the interaction of lactate with the $[Ln(DTPA)]^{2-}_{(aq)}$ complex may occur in the TALSPEAK process. It is expected that the interaction would be weak, and likely to be complicated due to various equilibria in solution (Figures 4.28 and 4.29), where the binding modes of $DTPA^{5-}$ and lactate may interchange in solution. It is also possible that there may be hydrogen bonding between the hydroxyl group of lactate and the carboxylate groups of $DTPA^{5-}$ (Figures 4.28 and 4.29).

4.5 Lanthanide-EDTA-Lactate Ternary System

4.5.1 NMR Spectroscopy

4.5.1.1 Diamagnetic Lanthanides Ions (La^{III} and Lu^{III})

The solution behaviour of the 1:1:1 Ln^{III}:$EDTA^{4-}$:lactate systems (Ln= La, Lu) has been probed to observe the effects on lactate binding when the denticity of the primary organic ligand has been reduced from eight ($DTPA^{5-}$) to six ($EDTA^{4-}$) coordinate. The ^{1}H-NMR spectra for the 1:1:1 La^{III}:$EDTA^{4-}$:lactate (Figure 4.31) show signals at approximately 4.4 and 1.4 ppm, which correspond to the -C**H**(OH)- proton and the -C**H$_3$** protons of lactate, respectively. There are also signals at 3.4 ppm and 2.7 ppm, which have been observed previously (Figure 3.10, Section 3.2.1.1) and are due to the bound acetate and ethylene protons of $EDTA^{4-}$, respectively. As pD is increased from pD 3.0 to 6.0, the –C**H**(OH)- proton signal shifts from 4.4 to 4.1 ppm and the -C**H$_3$** proton signal shifts from 1.4 to 1.3 ppm, which is likely to represent a change in the equilibrium between lactic acid and lactate (Figure 4.32). After pD 6.0, the lactate signals remain constant at 4.1 and 1.3 ppm. The lactate signals in the ^{1}H-NMR of the 1:1:1 La^{III}:$EDTA^{4-}$:lactate system follow the same pD dependent trend for that of free lactate (Figure 4.7).

The AB quartet and singlet signals for the acetate and ethylene $EDTA^{4-}$ protons correspond to $EDTA^{4-}$ being bound to the La^{III} ion. On closer inspection of the acetate signals of $EDTA^{4-}$, the AB quartet splits further into doublets over the pD range 4.5 to 9.7 (Figure 4.33). This splitting effect of the $EDTA^{4-}$ signals did not occur in the 1:1 La^{III}:$EDTA^{4-}$ (Figure 3.10, Section 3.2.1.1) or in the 1:1:1 Ln^{III}:$EDTA^{4-}$:CO_3^{2-} systems (Figure I, Appendix 1). Lactate was shown to interact favourably with lanthanide ions and the $[Ln(DTPA)]^{2-}_{(aq)}$ complex over the pD region 4 to 9 (Figures 4.17 and 4.25, respectively). Although the lactate signals in the ^{1}H-NMR spectra of the 1:1:1 Ln^{III}:$EDTA^{4-}$:lactate system suggest that lactate is unbound, the change in the splitting pattern of the $EDTA^{4-}$ signals over the pD region 4 to 9 indicates that there is some lactate interaction with the $[Ln(EDTA)]^{-}_{(aq)}$ complex. This may be weak coordination to the La^{III} ion or through hydrogen bonding to the $EDTA^{4-}$ carboxylate groups. This may also imply that lactate interacts with the $[Ln(DTPA)]^{2-}_{(aq)}$ complexes (Ln = La or Lu), because the lactate signals do not indicate a direct lactate interaction with the metal ion (Figure 4.22), and it would be difficult to observe a change in the splitting pattern of the

$DTPA^{5-}$ resonances in these systems. This is because the $DTPA^{5-}$ signals are broadened from exchange between the octa- and heptadentate coordination modes. After pD 9.7, the doublet splitting of the AB quartet is not observed in the ^{1}H-NMR spectra of the La^{III}:$EDTA^{4-}$:lactate system, which suggests that lactate is predominantly unbound from the $[La(EDTA)]^{-}_{(aq)}$ complex.

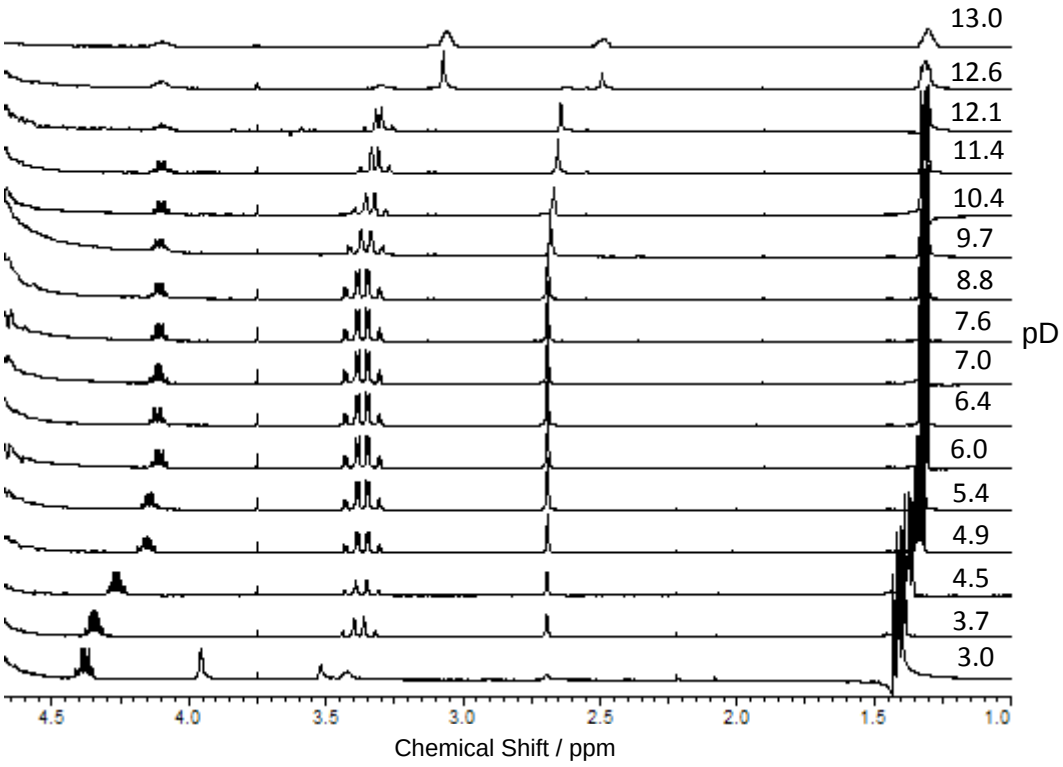

Figure 4.31: ^{1}H-NMR spectra for the effect of pD on a 1:1:1 La^{III}:$EDTA^{4-}$:lactate system; $[La^{III}]_i = [EDTA^{4-}]_i = [lactate]_i = 33$ mM.

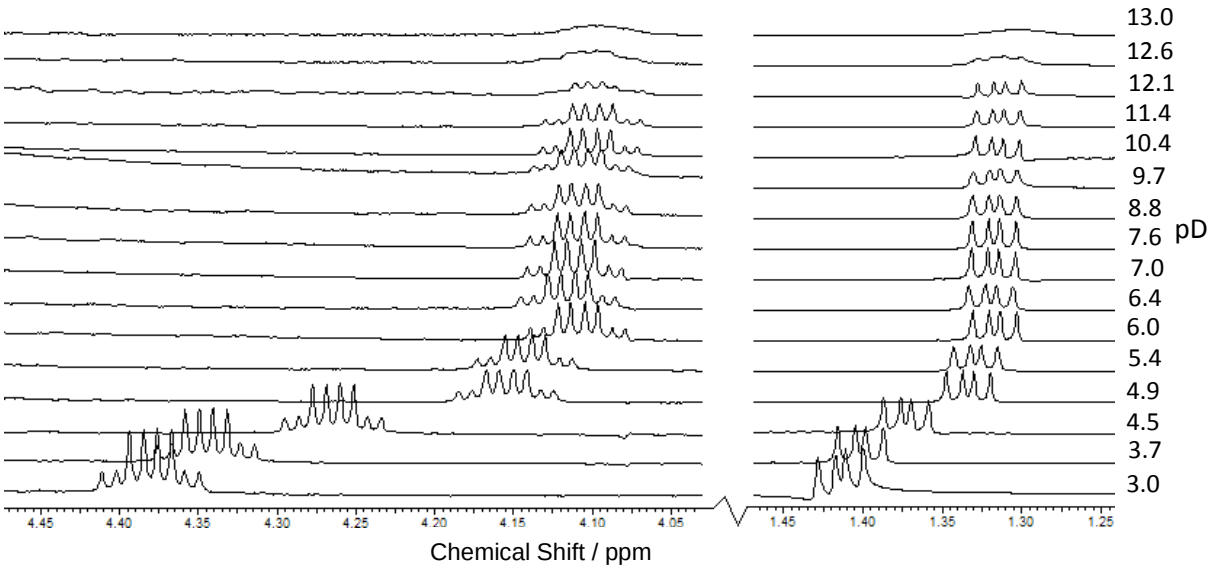

Figure 4.32: 'Zoom in' of the lactate signals in the ^{1}H-NMR spectra for the effect of pD on a 1:1:1 La^{III}:$EDTA^{4-}$:lactate system; $[La^{III}]_i = [EDTA^{4-}]_i = [lactate]_i = 33$ mM.

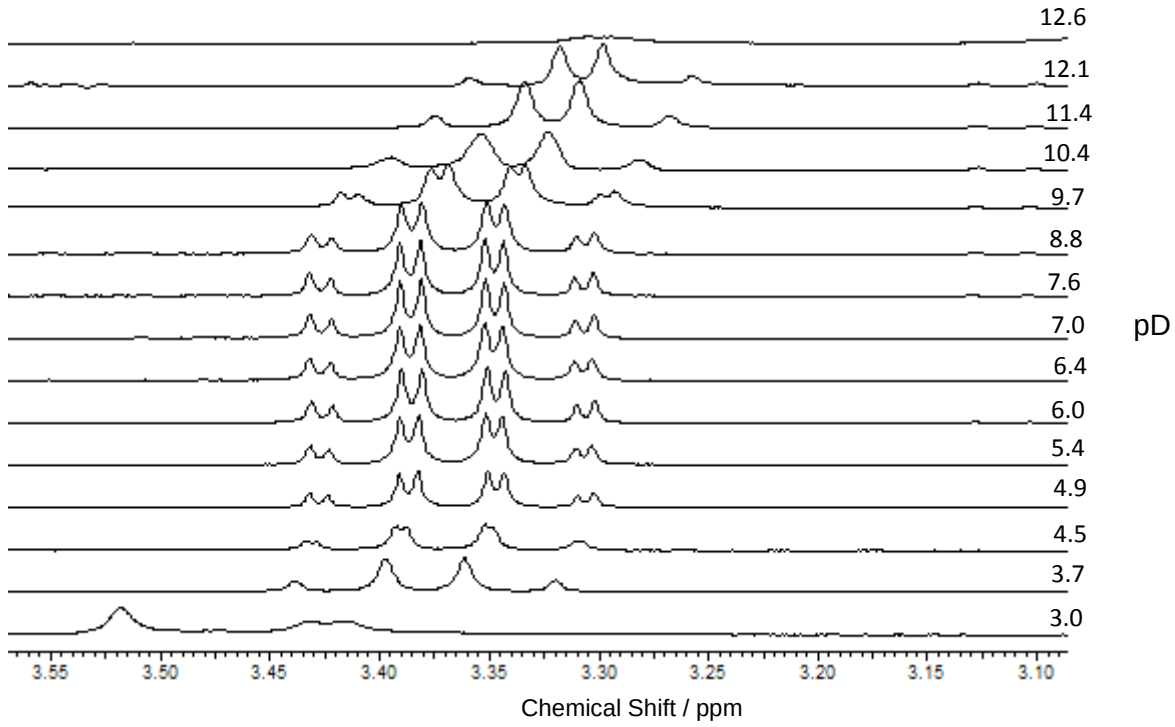

Figure 4.33: 'Zoom in' of the acetate signals of $EDTA^{4-}$ in the ^{1}H-NMR spectra for the effect of pD on a 1:1:1 La^{III}:$EDTA^{4-}$:lactate system; $[La^{III}]_i = [EDTA^{4-}]_i = [lactate]_i = 33$ mM.

The effect of pD on the 1:1:1 Lu^{III}:$EDTA^{4-}$:lactate system do not show the same doublet splitting of the AB quartet for the acetate $EDTA^{4-}$ signals, which was observed for the La^{III} system (Figure 4.33). Instead, the lactate signals shift and broaden over the pD range 4 to 7, which may indicate direct lactate interaction with the Lu^{III} ion inner coordination sphere in the $[Lu(EDTA)]^-_{(aq)}$ complex (Figure F, Appendix 2).

4.5.1.2 Paramagnetic Lanthanide Ions (Eu^{III})

The 1:1:1 Eu^{III}:$EDTA^{4-}$:lactate ternary system has been analysed by ^{1}H-NMR spectroscopy (Figure 4.34) to identify whether a paramagnetic shift of the lactate signals can be observed, which would indicate lactate interaction with the $[Eu(EDTA)]^-_{(aq)}$ complex. The broadened signal at 0.65 ppm, corresponds to the ethylene protons of $EDTA^{4-}$, and a signal at -2.0 ppm (not clearly observed in Figure 4.34), is due to the acetate protons of $EDTA^{4-}$. The $EDTA^{4-}$ signals have been paramagnetically shifted outside of the 'normal' ^{1}H-NMR chemical shift range (0 to 10 ppm), which means that $EDTA^{4-}$ is bound to the Eu^{III} ion over the pD range 2.8 to 13.2. This has been observed previously in Figure D in Appendix 1.

At pD 2.8, signals at 4.4 and 1.4 ppm are observed, which represent the -C**H**(OH)- proton and the -C$\mathbf{H_3}$ protons of lactate, respectively. As pD is increased from pD 2.8 to 5.9, the -C**H**(OH)- proton signal shifts from 4.4 to 2.8 ppm and the -C$\mathbf{H_3}$ proton signal shifts from 1.4 to 1.0 ppm (Figure 4.35). This shift is similar to that observed in the 1:1:1 Eu^{III}:$DTPA^{5-}$:lactate ternary system, and so it is likely that lactate is interacting with the $[Eu(EDTA)]^-_{(aq)}$ complex. In a comparable manner to the 1:1:1 Eu^{III}:$DTPA^{5-}$:lactate system, the lactate anion may be weakly coordinated to the Eu^{III} ion and may participate in hydrogen bonding to the $EDTA^{4-}$ carboxylate groups. As pD is further increased from pD 5.9 to 13.0, the signals shift from 2.8 to 4.09 ppm and 1.0 to 1.09 ppm, which corresponds to a change in the equilibrium between bound and unbound lactate. This suggests that hydroxide is replacing lactate from the $[Eu(EDTA)]^-_{(aq)}$ coordination sphere.

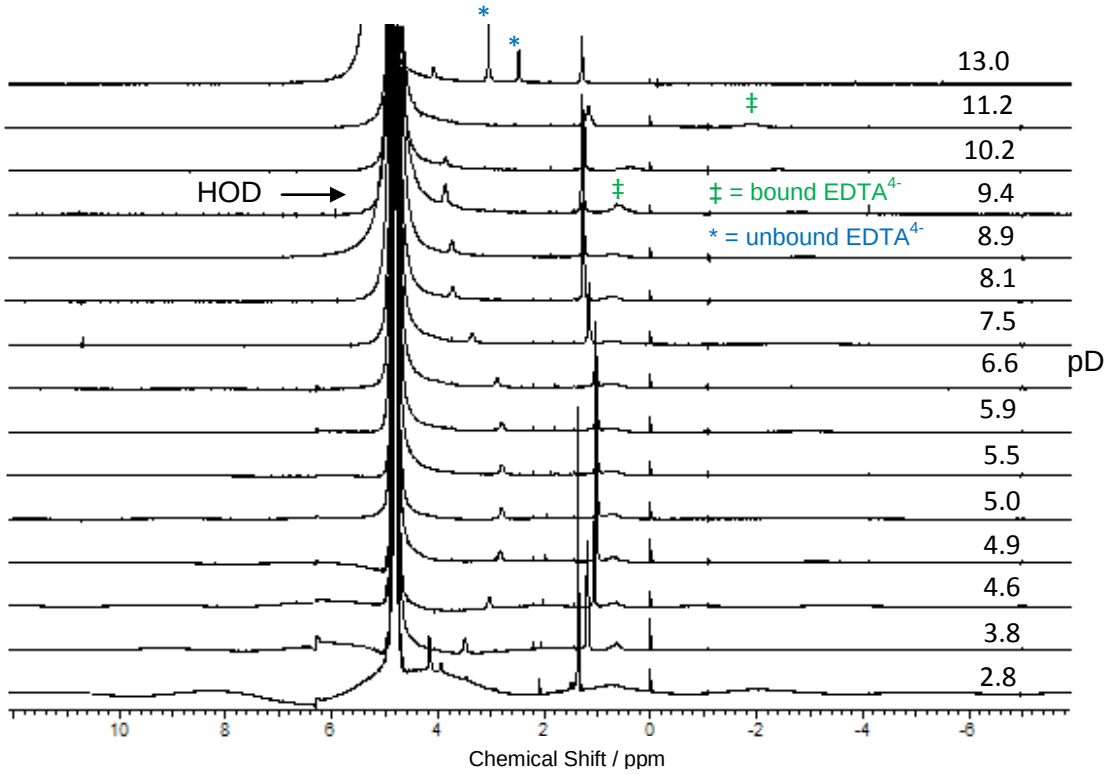

Figure 4.34: ^{1}H-NMR spectra for the effect of pD on a 1:1:1 Eu^{III}:$EDTA^{4-}$:lactate system; $[Eu^{III}]_i = [EDTA^{4-}]_i = [lactate]_i = 33$ mM.

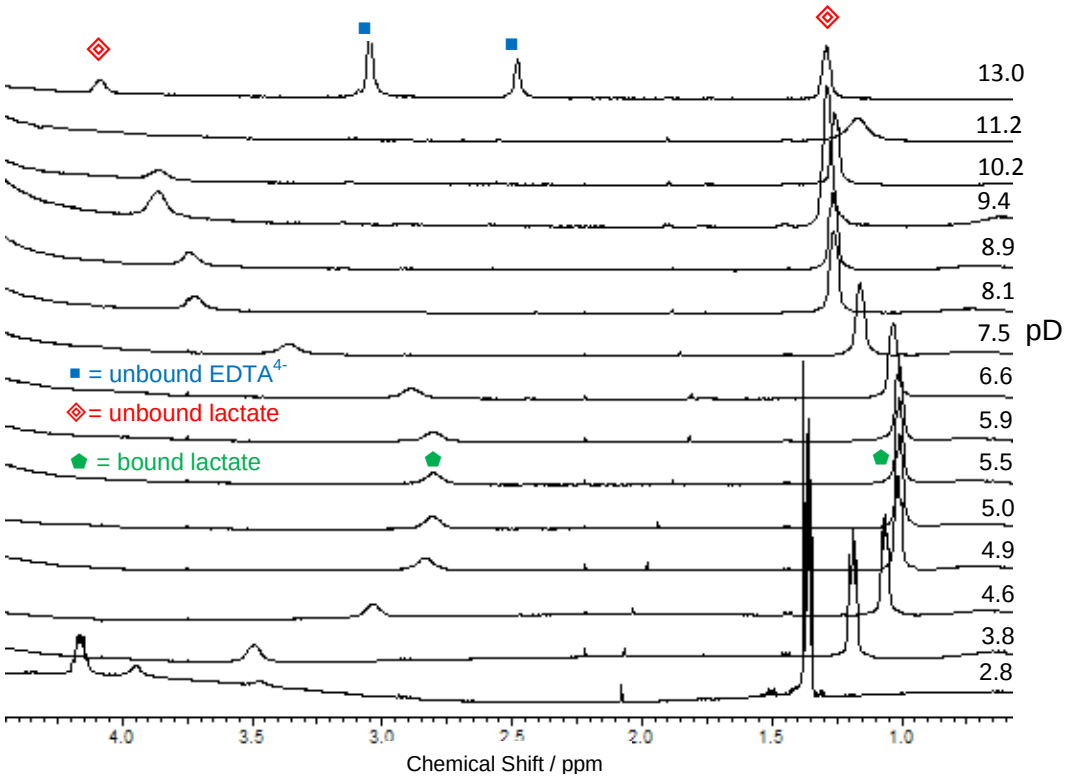

Figure 4.35: 'Zoom in' of the lactate signals in the ^{1}H-NMR spectra for the effect of pD on a 1:1:1 Eu^{III}:$EDTA^{4-}$:lactate system; $[Eu^{III}]_i = [EDTA^{4-}]_i = [lactate]_i = 33$ mM.

4.5.2 Luminescence Spectroscopy

4.5.2.1 Eu^{III}

Luminescence spectroscopic titrations have been performed on the 1:1:1 Eu^{III}:$EDTA^{4-}$:lactate system using H_2O or D_2O as the solvent and NaOH/NaOD for pH/pD adjustment. The luminescence spectra show Eu^{III} emission bands at 580, 590, 617, 650 and 690 nm (Figure 4.36). Over the pH region studied, there is little difference in the emission spectra (Figure 3.30; Figure 4.36), luminescent lifetimes (Table 3.4; Table 4.5) and N_{H_2O} bound to the Eu^{III} ion (Table 3.6; Table 4.6) in the 1:1 Eu^{III}:$EDTA^{4-}$ binary and 1:1:1 Eu^{III}:$EDTA^{4-}$:lactate systems, respectively. ^{1}H-NMR spectroscopy of the 1:1:1 Eu^{III}:$EDTA^{4-}$:lactate system (Figure 4.35) indicated the interaction of lactate with the $[Eu(EDTA)]^-_{(aq)}$ over the pD range 3.8 to 8.1, but the luminescence results do not show this interaction. This may mean that further luminescence titrations need to be performed over the pH region 3.8 to 8.1 to further probe the interaction of lactate with the $[Eu(EDTA)]^-_{(aq)}$ complex. The interaction of lactate with the Eu^{III} inner coordination sphere, in the $[Eu(EDTA)]^-_{(aq)}$ complex, is likely to be weak and may occur faster than the luminescence timescale.

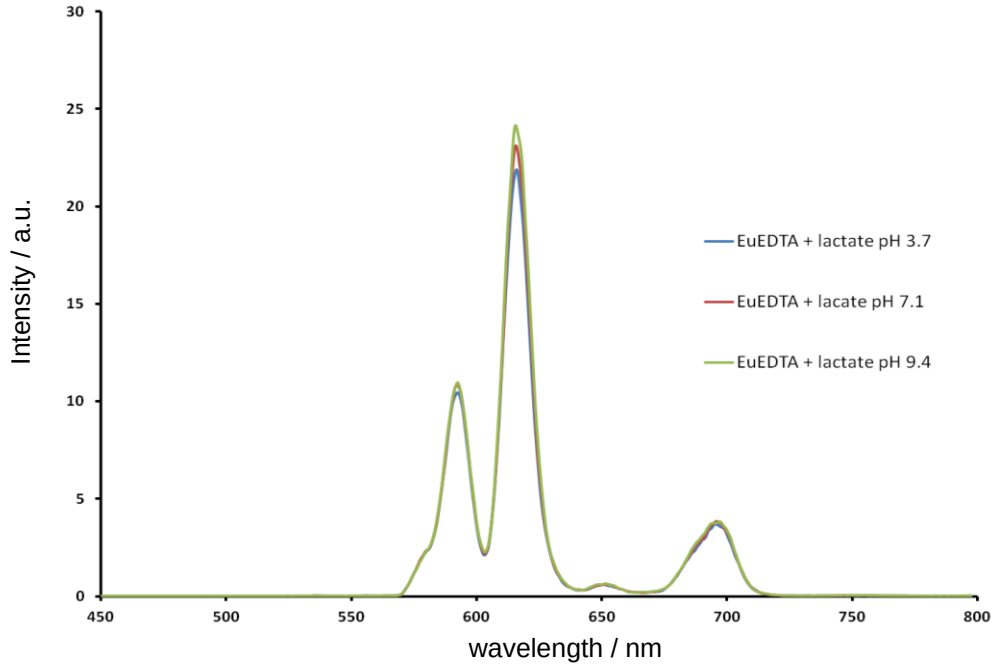

Figure 4.36: Emission spectra for the effect of pH on a 1:1:1 Eu^{III}:$EDTA^{4-}$:lactate system; $[Eu^{III}]_i = [EDTA^{4-}]_i = [lactate]_i = 10$ mM.

1:1:1 Eu^{III}:$EDTA^{4-}$:lactate	pH	τ / ms	pD	τ / ms
	3.7	0.32 ± 0.03	3.7	2.40 ± 0.24
	7.1	0.33 ± 0.03	7.0	2.22 ± 0.22
	9.4	0.34 ± 0.03	9.4	2.26 ± 0.23

Table 4.5: Luminescent lifetimes (τ) of 1:1:1 Eu^{III}:$EDTA^{4-}$:lactate system at various pH/pD in H_2O and D_2O; $[Eu^{III}]_i = [EDTA^{4-}]_i = [lactate]_i = 10$ mM.

1:1:1 Eu^{III}:$EDTA^{4-}$:lactate
pH 3.7, N_{H_2O} = **2.7 ± 0.5**
pH 7.1, N_{H_2O} = **2.5 ± 0.5**
pH 9.4, N_{H_2O} = **2.4 ± 0.5**

Table 4.6: Calculated N_{H_2O} bound to the Eu^{III} ion in the 1:1:1 Eu^{III}:$EDTA^{4-}$:lactate system at various pH; $[Eu^{III}]_i = [EDTA^{4-}]_i = [lactate]_i = 10$ mM. The uncertainty in N_{H_2O} calculations is ± 0.5 water molecules.[11]

4.5.3 Summary

NMR spectroscopy has been a valuable technique for probing the interaction of lactate with $[Ln(EDTA)]^-_{(aq)}$ complexes. The lactate ligand has been shown to interact with the La^{III}, Eu^{III} and Lu^{III}-EDTA complexes. In the 1:1:1 La^{III}:$EDTA^{4-}$:lactate system, the AB quartet resonance for the bound acetate protons of $EDTA^{4-}$ is further split into doublets over the pD region that lactate would be expected to bind to La^{III}. This further splitting pattern is not observed in the ^{1}H-NMR spectra recorded for the 1:1 La^{III}:$EDTA^{4-}$ and the 1:1:1 La^{III}:$EDTA^{4-}$:CO_3^{2-} systems, and so it is likely that lactate and carbonate do have different binding modes to the $[La(EDTA)]^-_{(aq)}$ complex. The hydroxyl group in lactate is probably involved in the coordination of lactate to metal ions, rather than the coordination mode being strictly due to bidentate binding of the carboxylate group (Figure 4.37). The change in the splitting pattern of the $EDTA^{4-}$ acetate resonances may be due to lactate forcing $EDTA^{4-}$ to bind as a pentadentate ligand, rather than hexadentate, or it may be due to hydrogen bonding of the hydroxyl group of lactate to the acetate groups of $EDTA^{4-}$ either as a primary sphere or secondary sphere interaction (Figure 4.38). The interaction of lactate could not be established

using luminescence spectroscopy, and so further luminescence titrations may need to be performed over the pD region 4 to 8 in order to observe this interaction. It is likely that the interaction of lactate with the $[Ln(EDTA)]^-_{(aq)}$ complexes is weak and may occur faster than the luminescence timescale.

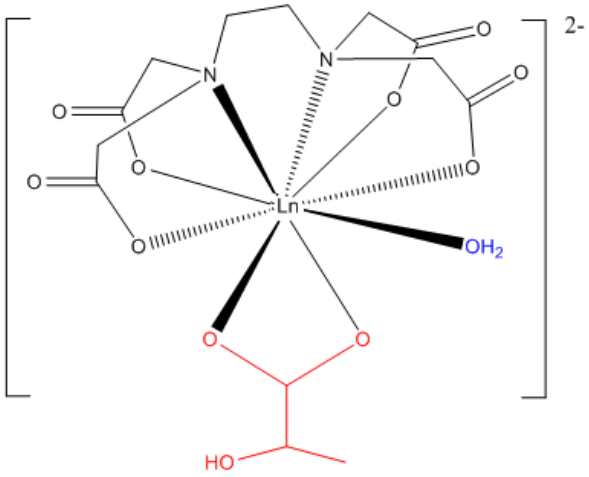

Figure 4.37: The binding of lactate to $[Ln(EDTA)]^-_{(aq)}$ complexes via the carboxylate group.

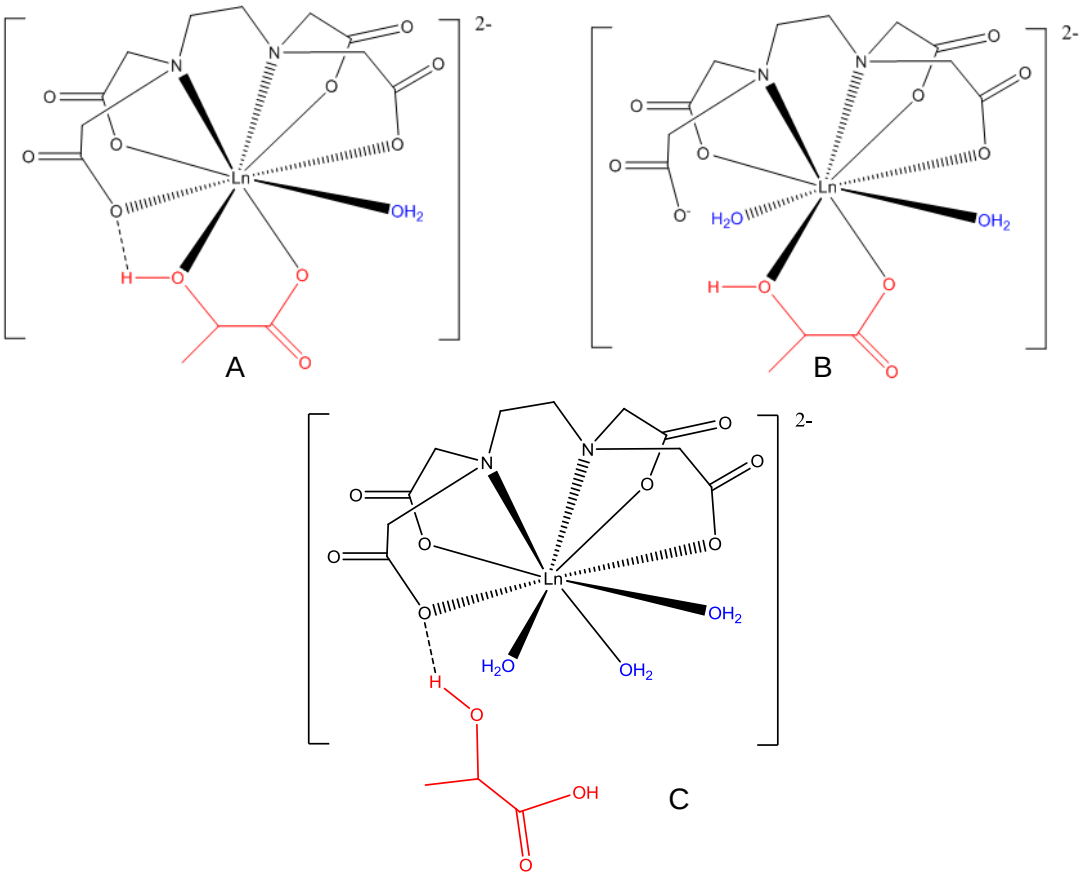

Figure 4.38: A) Hydrogen bonding of the lactate hydroxyl group to $EDTA^{4-}$ acetate groups in the $[Ln(EDTA)(lactate)(H_2O)]^{2-}_{(aq)}$ complex; B) Pentadentate coordination mode of $EDTA^{4-}$ to accommodate the lactate ligand in the $[Ln(EDTA)(lactate)(H_2O)_2]^{2-}_{(aq)}$ and C) lactate participating in hydrogen bonding with the $[Eu(EDTA)(H_2O)_3]^{-}_{(aq)}$ complex (secondary sphere interaction).

4.6 Lanthanide-DTPA-Carbonate Ternary System

4.6.1 NMR Spectroscopy

4.6.1.1 Diamagnetic Lanthanide Ions (La^{III} and Lu^{III})

The formation of $[Ln(EDTA)(CO_3)]^{3-}_{(aq)}$ ternary complexes were shown to exist in Chapter 3. The solution behaviour of the 1:1:1 Ln^{III}:$DTPA^{5-}$:CO_3^{2-} system (Ln= La or Lu) has been probed using ^{13}C-NMR spectroscopy to observe whether carbonate can still bind to the lanthanide ions when the steric hindrance around the lanthanide ion coordination sphere has increased (*i.e.* hexadentate $EDTA^{4-}$ *vs.* octadentate $DTPA^{5-}$). The ^{13}C-NMR spectra obtained to probe the effect of pD on the 1:1:1 Ln^{III}:$DTPA^{5-}$:CO_3^{2-} system focus on the chemical shift

range from 160 to 170 ppm, as this is the region where the carbonate resonance is observed. The carbonate source used in these experiments is ^{13}C-labelled carbonate, as described for the Ln^{III}:$EDTA^{4-}$:CO_3^{2-} systems in Section 3.2.2.

The ^{13}C-NMR spectra of the La^{III} ternary system show a carbonate signal at 162.1 ppm that shifts to 169.1 ppm, over the pD range 9.9 to 13.6 (Figure 4.39). Similarly with the Lu^{III} ternary system, the carbonate signal at 160.9 ppm shifts with pD to 169.0 ppm (Figure 4.40). In the 1:1:1 La^{III}:$DTPA^{5-}$:CO_3^{2-} system ^{13}C-NMR spectra, the shift in the carbonate signal does not correlate to the gradual shift that was observed for the ^{13}C-NMR spectra obtained for the 1:1:1 La^{III}:$EDTA^{4-}$:CO_3^{2-} system (Figure 3.14, Section 3.22) as pH was increased. The carbonate signals are resolved in the ^{13}C-NMR spectra obtained for the 1:1:1 La^{III}:$DTPA^{5-}$:CO_3^{2-} system, and are similar to the free carbonate signals (Figure 3.15, Section 3.22). By contrast, the carbonate signals in the ^{13}C-NMR spectra obtained for the 1:1:1 La^{III}:$EDTA^{4-}$:CO_3^{2-} system (Figure 3.14, Section 3.22) were broadened, which indicated that carbonate was exchanging with water and/or hydroxide for coordination to the $[La(EDTA)]^-_{(aq)}$ complex. Therefore, it is likely that carbonate is predominantly not directly binding to the La^{III} ion inner coordination sphere in the $[La(DTPA)]^{2-}_{(aq)}$ complex. This may be due to the increase in the steric hindrance around the La^{III} coordination sphere in the $[La(DTPA)]^{2-}_{(aq)}$ complex compared to the $[La(EDTA)]^-_{(aq)}$ species.

The 1:1:1 Lu^{III}:$DTPA^{5-}$:CO_3^{2-} ^{13}C-NMR spectra show a broadened carbonate signal over the pH range 8.8 to 11.1, which indicates that carbonate is in exchange with water or hydroxide for coordination to the $[Lu(DTPA)]^{2-}_{(aq)}$ complex. At pD 12.7 and above, the carbonate signal becomes resolved, which suggests that carbonate has been replaced by hydroxide in the Lu^{III} ion inner coordination sphere. The carbonate signal is almost broadened into the baseline at pD 10.6 (Figure 4.41), implying a fast bound/unbound carbonate exchange process. The difference in the carbonate signals between the La^{III} and Lu^{III}:$DTPA^{5-}$:CO_3^{2-} ternary systems may be due to the Lu^{III} ion having a higher charge density than the La^{III} ion.

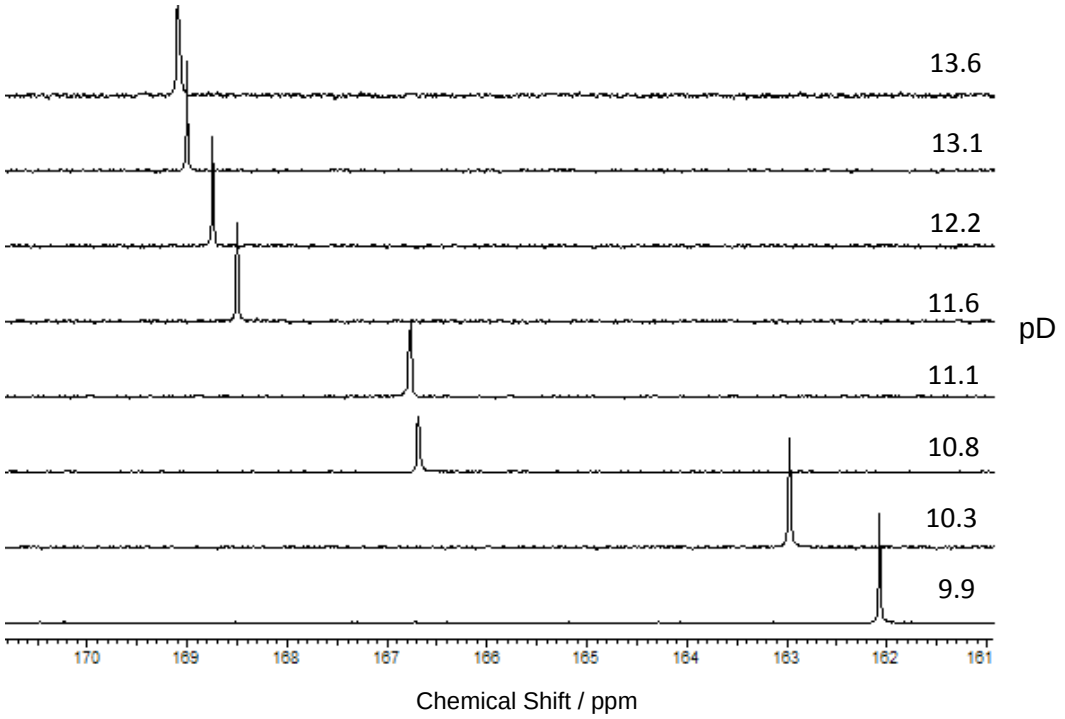

Figure 4.39: ^{13}C-NMR spectra for the effect of pD on the 1:1:1 La^{III}:$DTPA^{5-}$:CO_3^{2-} system; $[La^{III}]_i = [DTPA^{5-}]_i = [CO_3^{2-}]_i = 33$ mM.

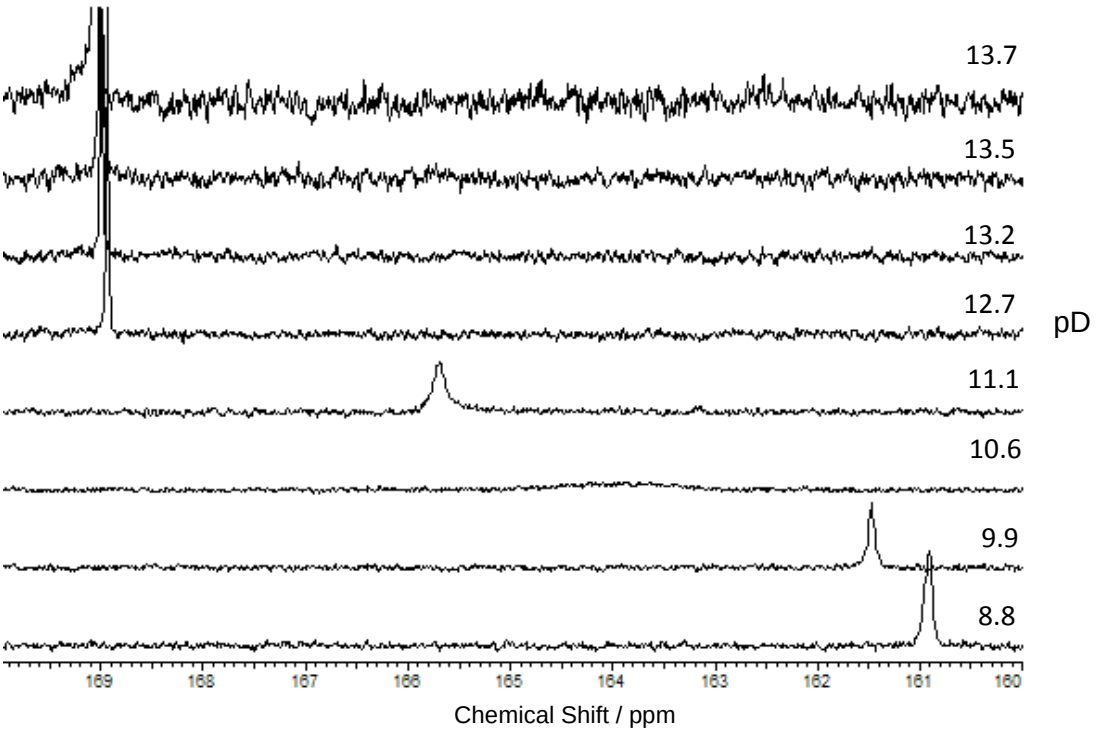

Figure 4.40: ^{13}C-NMR spectra for the effect of pD on the 1:1:1 Lu^{III}:$DTPA^{5-}$:CO_3^{2-} system; $[Lu^{III}]_i = [DTPA^{5-}]_i = [CO_3^{2-}]_i = 33$ mM.

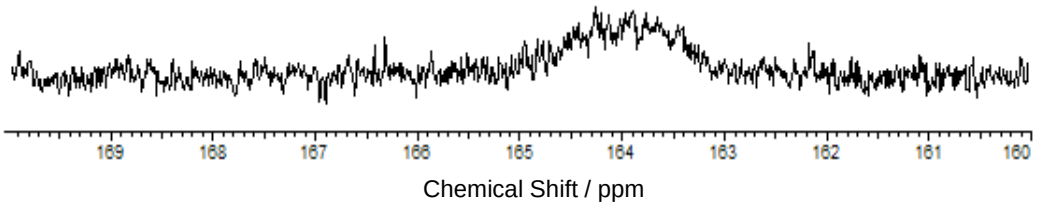

Figure 4.41: 'Zoom-in' of the ^{13}C-NMR spectrum at pD 10.6 for the 1:1:1 Lu^{III}:$DTPA^{5-}$:CO_3^{2-} system; $[Lu^{III}]_i = [DTPA^{5-}]_i = [CO_3^{2-}]_i$ = 33 mM.

A resolved bound carbonate signal is not observed in the ^{13}C-NMR spectra for the 1:1:1 Lu^{III}:$DTPA^{5-}$:CO_3^{2-} system, as was the case for the 1:1:1 Lu^{III}:$EDTA^{4-}$:CO_3^{2-} system (Figure 3.16, Section 3.2.2), which suggests that carbonate binding is weaker to the $[Lu(DTPA)]^{2-}_{(aq)}$ complex than the $[Lu(EDTA)]^{-}_{(aq)}$ complex. This may be because the sterics imposed by the $DTPA^{5-}$ ligand causes carbonate to bind in a monodentate manner, rather than bidentate (Figure 4.42). Carbonate may be able to bind in a bidentate mode if $DTPA^{5-}$ was complexing to the Lu^{III} ion in a heptadentate manner.

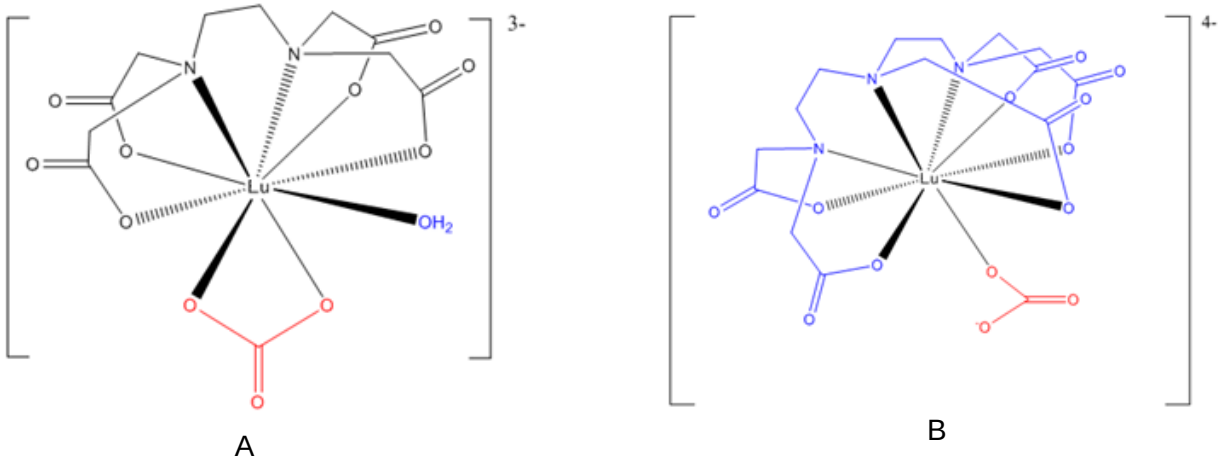

Figure 4.42: A) Carbonate binding in a bidentate mode to the $[Lu(EDTA)]^{-}_{(aq)}$ complex and B) Carbonate binding in a monodentate mode to the $[Lu(DTPA)]^{2-}_{(aq)}$ complex.

4.7 Lanthanide-DO3A-Carbonate Ternary Systems

4.7.1 Luminescence Spectroscopy

4.7.1.1 Eu^{III}

The $DO3A^{3-}$ ligand contains four nitrogen and three oxygen donor atoms, and it can bind to metal ions in a heptadentate coordination mode.[6] The four nitrogen atoms are present in a cyclic amine ring, and so $DO3A^{3-}$ complexes have enhanced stability because of the macrocyclic effect.[13] Lanthanide ions complexed by $DO3A^{3-}$ have one or two coordination sites free depending on the lanthanide hydration number.[14,15] In aqueous solution, H_2O molecules fill these sites completing the coordination sphere of the lanthanide ion.[14,15] Luminescence spectroscopy of the 1:1:1 Eu^{III}:$DO3A^{3-}$:CO_3^{2-} system has been performed to observe if carbonate can replace the water molecules within the Eu^{III} ion inner coordination sphere. $DO3A^{3-}$ is a cyclic ligand, and so there may be some effect on the mode of binding of secondary ligands compared to open chain ligands, such as $EDTA^{4-}$ and $DTPA^{5-}$.

The emission spectra of the 1:1 Eu^{III}:$DO3A^{3-}$ and 1:1:1 Eu^{III}:$DO3A^{3-}$:CO_3^{2-} systems show the Eu^{III} ion emission bands at 580, 590, 617, 650 and 690 nm (Figure 4.43). There is a significant increase in the emission intensity of the bands at 590, 617 and 690 nm when carbonate is added to the $[Eu(DO3A)]_{(aq)}$ complex, which suggests that carbonate does interact with the $[Eu(DO3A)]_{(aq)}$ species. There is a small increase in the luminescent lifetime of the excited Eu^{III} species in the presence of carbonate in the H_2O system, but no significant change in the D_2O system (Tables 4.7 and 4.8). At pH 9, the calculated N_{H_2O} bound to the Eu^{III} ion decreases from 2.0 in the 1:1 Eu^{III}:$DO3A^{3-}$ system to 0.7 in the 1:1:1 Eu^{III}:$DO3A^{3-}$:CO_3^{2-} system (Table 4.9). It is likely that the CO_3^{2-} anion is binding as a bidentate ligand and is either in fast exchange with water molecules (Figure 4.44) or only a fraction of the total carbonate can bind to $[Eu(DO3A)]_{(aq)}$ due to competition with OH^- ions and/or H_2O molecules. An analogous $[Gd(DO3A)(CO_3)]^{2-}{}_{(aq)}$ complex, detected using NMR relaxivity measurements, has been reported to exist in the literature.[16]

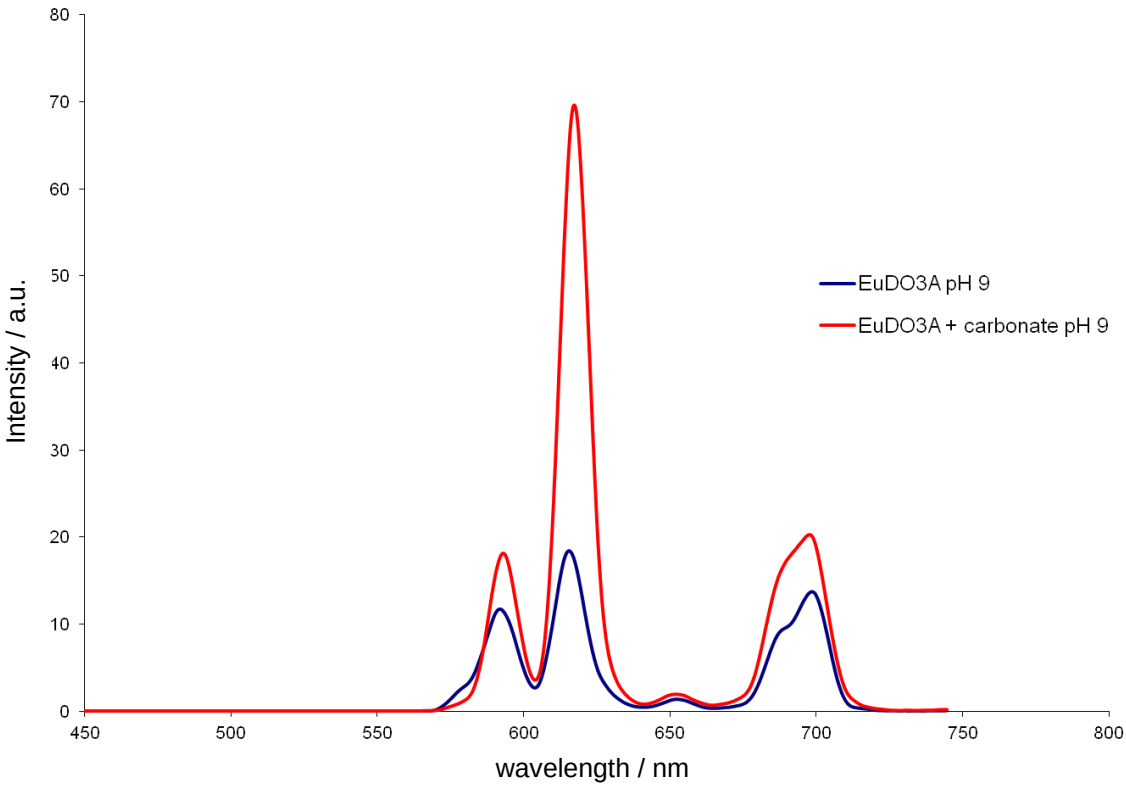

Figure 4.43: Emission spectra for the 1:1 Eu^{III}:$DO3A^{3-}$ and 1:1:1 Eu^{III}:$DO3A^{3-}$:CO_3^{2-} systems; $[Eu^{III}]_i = [DO3A^{3-}]_i = [CO_3^{2-}]_i = 10$ mM.

1:1 Eu^{III}:$DO3A^{3-}$	**pH**	**τ / ms**	**pD**	**τ / ms**
	9	0.28 ± 0.03	9	0.69 ± 0.07

Table 4.7: Luminescent lifetimes (τ) of 1:1 Eu^{III}:$DO3A^{3-}$ system in H_2O and D_2O; $[Eu^{III}]_i = [DO3A^{3-}]_i = 10$ mM.

1:1:1 Eu^{III}:$DO3A^{3-}$:CO_3^{2-}	**pH**	**τ / ms**	**pD**	**τ / ms**
	9	0.41 ± 0.04	9	0.67 ± 0.07

Table 4.8: Luminescent lifetimes (τ) of 1:1:1 Eu^{III}:$DO3A^{3-}$:CO_3^{2-} system in H_2O and D_2O; $[Eu^{III}]_i = [DO3A^{3-}]_i = [CO_3^{2-}]_i = 10$ mM.

1:1 Eu^{III}:$DO3A^{3-}$	1:1:1 Eu^{III}:$DO3A^{3-}$:CO_3^{2-}
pH 9, N_{H_2O} = 2.0 ± 0.5	pH 9, N_{H_2O} = 0.7 ± 0.5

Table 4.9: Calculated N_{H_2O} bound to the Eu^{III} ion in the 1:1 Eu^{III}:$DO3A^{3-}$ and 1:1:1 Eu^{III}:$DO3A^{3-}$:CO_3^{2-} system; $[Eu^{III}]_i = [DO3A^{3-}]_i = [CO_3^{2-}]_i$ = 10 mM. The uncertainty in N_{H_2O} calculations is ± 0.5 water molecules.[11]

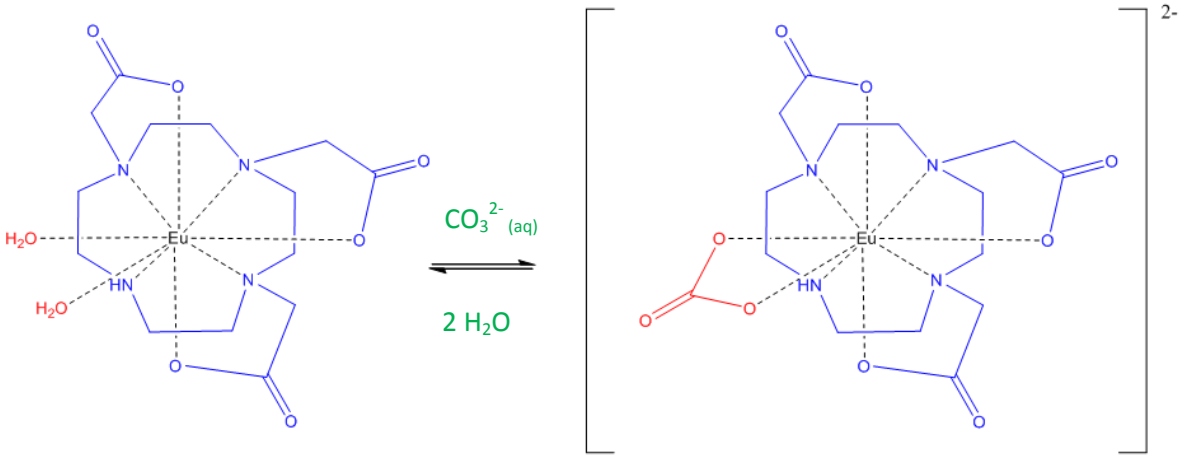

Figure 4.44: The exchange of H_2O and $CO_3^{2-}{}_{(aq)}$ for complexation to $[Eu(DO3A)]_{(aq)}$.

4.8 Summary

This chapter has focussed on lanthanide binary and ternary systems that are relevant to the TALSPEAK process. The TALSPEAK process is concerned with trivalent lanthanide and actinide separation using $DTPA^{5-}$ and lactate ligands in the aqueous phase and HDEHP in the organic phase. It has been hypothesised that the formation of ternary $[M(DTPA)(lactate)]^{3-}{}_{(aq)}$ complexes ($M = Ln^{III}$ or An^{III}) may occur in the TALSPEAK process, which contribute to an increase in the separation factors of actinides and lanthanides. There have been no reports of $[Ln(DTPA)(lactate)]^{3-}{}_{(aq)}$ complexes in the literature.

The role of $DTPA^{5-}$ is well understood in the TALSPEAK process, and it is known that one $DTPA^{5-}$ ligand can complex to a Ln^{III} or An^{III} ion.[1] The $[Ln(DTPA)]^{2-}{}_{(aq)}$ complexes are very stable, and $DTPA^{5-}$ can bind to the Ln^{III} ions over the pD region 1 to 13, after which hydrolysis dominates. The protonated $DTPA^{5-}$ complex, $[Ln(HDTPA)]^{-}{}_{(aq)}$, is present at low

pH (*i.e.* pH less than 3). In solution, it is likely that the $DTPA^{5-}$ ligand is continuously alternating between hepta- and octadentate coordination modes.[8]

Lactate can bind to lanthanide ions from acidic pH (*i.e.* pH 2), but as lactate is a weakly coordinating ligand, it is readily replaced by hydroxide, even at pH values as low as pH 5. Under TALSPEAK conditions of pH 3.5, $[Ln(DTPA)]^{2-}_{(aq)}$ complexes will dominate the lanthanide speciation in the aqueous phase. $[Ln(lactate)]^{2+}_{(aq)}$ complexes are unlikely to exist as the lanthanide ions will always preferentially bind the higher denticity ligand, $DTPA^{5-}$, over lactate. Lactate interaction with the $[Eu(DTPA)]^{2-}_{(aq)}$ species has been shown to occur over the pD range 3.8 to 7.8, with the most favourable pD region for lactate interaction occurring between pD 5.4 to 7.8. The exact nature of lactate interaction with the $[Eu(DTPA)]^{2-}_{(aq)}$ complexes is unclear as it may be a primary or secondary sphere interaction. Under TALSPEAK conditions of pH 3.5, the interaction of lactate with $[Ln(DTPA)]^{2-}_{(aq)}$ complexes is likely to be weak and possibly unfavourable due to the presence of lactic acid ($pK_a = 3.55$), which is unlikely to bind to metal ions.

The interaction of lactate with the $[Ln(EDTA)]^{-}_{(aq)}$ complexes was observed using NMR spectroscopy. Lactate coordinates to the $[Ln(EDTA)]^{-}_{(aq)}$ complex over the pD range 3.7 to 9.7, with the most favourable pD region for lactate binding being from approximately pD 5 to 7. Changes in the acetate proton resonances of $EDTA^{4-}$ in the 1:1:1 La^{III}:$EDTA^{4-}$:lactate system indicate that the coordination mode of lactate is different to carbonate (*i.e.* it is not only dependent on the carboxylate group of lactate binding to a metal ion). It is likely that the hydroxyl group is involved when lactate interacts with the $[Ln(EDTA)]^{-}_{(aq)}$ complex, either by directly binding to the La^{III} ion or hydrogen bonding to the carboxylate groups of $EDTA^{4-}$ (or both).

The interaction of the CO_3^{2-} anion with the $[Lu(DTPA)]^{2-}_{(aq)}$ complex was shown to occur over the pD range 8.8 to 11.1, using NMR spectroscopy. The ^{13}C-NMR spectra acquired to study the 1:1:1 La^{III}:$DTPA^{5-}$:CO_3^{2-} system suggest that there is minimal carbonate interaction with the $[La(DTPA)]^{2-}_{(aq)}$ complex. The difference between the La^{III} and Lu^{III} ions in the DTPA-CO_3^{2-} ternary systems may be because the Lu^{III} ion has a higher charge density than the La^{III} ion. Carbonate complexation is much weaker to the $[Ln(DTPA)]^{2-}_{(aq)}$ complexes compared to the $[Ln(EDTA)]^{-}_{(aq)}$ complexes, because CO_3^{2-} may be forced to bind in a monodentate, rather than bidentate, mode.

The interaction of CO_3^{2-} with the $[Eu(DO3A)]_{(aq)}$ complex was observed using luminescence spectroscopy. It is likely that the CO_3^{2-} ion is binding in a bidentate mode and may be in fast exchange with two water molecules for coordination to the $[Eu(DO3A)]_{(aq)}$ complex. It is also possible that only a fraction of the $[Eu(DO3A)(CO_3)]^{2-}_{(aq)}$ complex forms due to competition with H_2O molecules and OH^- ions.

The next chapter uses the knowledge gained from the lanthanide experiments in Chapters 3 and 4 to probe for actinide ternary complexes. The chemical behaviour of the actinides has been analysed using a variety of techniques, such as NMR, UV-Vis and luminescence spectroscopy to determine if lanthanides can be used to model actinide metal ions in these systems.

[1] M. Nilsson and K. Nash, *Solvent Extr. Ion Exc.*, 2007, **25**, 665–701.

[2] C. Leggett, G. Liu and M. Jensen, *Solvent Extr. Ion Exc.*, 2010, **28**, 313-334.

[3] R. Smith and A. Martell, *Critical Stability Constants*, Volumes 1 and 4: Inorganic Complexes, Plenum Press, New York, 1976.

[4] G. Tian, L. Martin and L. Rao, *Inorg. Chem.*, 2010, **49**, 10598-10605.

[5] R. Hancock, *J. Chem. Ed.*, 1992, **69**, 615-621.

[6] G. Choppin and K. Schaab, *Inorg. Chim. Acta*, 1992, **252**, 299-310.

[7] J. Van der Lee, A Users Guide to CHESS, Another Speciation and Surface Complexation Computer Code, E´cole des Mi1nes de Paris, Fontainebleau, 1998.

[8] S. Aime and M. Botta, *Inorg. Chim. Acta*, 1990, **177**,101-105.

[9] S. Faulkner, L. Natrajan, W. Perry and D. Sykes, *Dalton Trans.*, 2009, **20**, 3890-3899.

[10] S. Cotton, *C. R. Chimie*, 2005, **8**, 129–145.

[11] P. Thakur, J. Conca, L. Van de Burgt and G. Choppin, *J. Coord. Chem.*, 2009, **62**, 3719–3737.

[12] P. Gale, *Coord. Chem. Rev.*, 2003, **240**, 191- 221.

[13] D. Cabbiness and D. Margerum, *J. Am. Chem. Soc.*, 1969, **91**, 6540–6541.

[14] C. Allen Chang, L. Francesconi, M. Malley, K. Kumar, J. Gougoutas, M. Tweedle, D. Lee and L. Wilson, *Inorg. Chem.*, 1993, **32**, 3501-3508.

[15] M. Woods, G. Kiefer, S. Bott, A. Castillo-Muzquiz, C. Eshelbrenner, L. Michaudet, K. McMillan, S. Mudigunda, D. Ogrin, G. Tircsó, S. Zhang, P. Zhao and A. Sherry, *J. Am. Chem. Soc.*, 2004, **126**, 9248-9256.

[16] D. Parker, R. Dickins, H. Puschmann, C. Crossland and J. Howard, *Chem. Rev.*, 2002, **102**, 1977-2010.

Chapter 5

Thorium^{IV} Binary and Ternary Systems Relevant to the Nuclear Fuel Cycle

5.0 Introduction

Thorium is an early actinide, and typically exists in the +4 oxidation state.[1] The Th^{IV} ion is a 'Lewis acid' and preferentially binds to hard donor atoms such as fluorine and oxygen (*e.g.* $Th(NO_3)_4.3H_2O$; Figure 5.1).[1] The coordination numbers of the Th^{IV} ion are high, with fifteen being the largest coordination number reported.[2]

Tetravalent thorium has a greater charge density than the trivalent lanthanides, and so experiments reported in this chapter probe the effects of this increase in charge density with respect to ligand coordination properties. The effect of pD on the Th-EDTA, Th-DTPA and Th-lactate binary systems, as well as the Th-EDTA-carbonate; Th-EDTA-lactate, Th-DTPA-carbonate and Th-DTPA-lactate ternary systems have been analysed by ^{1}H and ^{13}C-NMR spectroscopy.

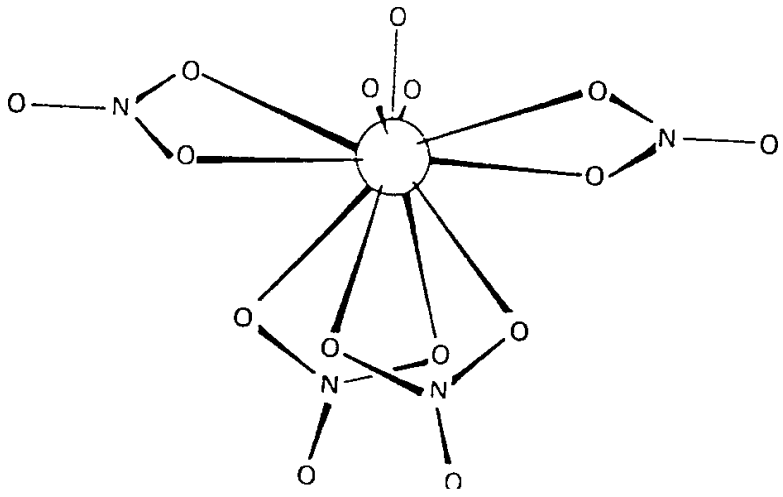

Figure 5.1: Structure of $Th(NO_3)_4.3H_2O$. [Taken from Reference 1].

5.1 Th^{IV}-EDTA Binary System

5.1.1 Speciation Behaviour

For a 1:1 Th^{IV}:$EDTA^{4-}$ system, the aqueous Th^{IV} species present in solution at a certain pH can be determined using a speciation diagram (Figure 5.2), which is derived from known equilibrium constants (Table 5.1).[3] The speciation diagram shows that over the pH range 0 to 4, the $[Th(HEDTA)]^{+}_{(aq)}$ complex is dominant. After pH 4, $[Th(EDTA)]_{(aq)}$ prevails until hydrolysis of the Th^{IV} ion is expected to occur at pH 7, forming the $Th(OH)_{4(s)}$ complex.

						Ionic Strength
Th^{IV} +	$EDTA^{4-}$	$\rightleftharpoons$	[Th(EDTA)]	log β_{110}	22.3	0.5 M Na^{+} salt
$Th(OH)_{4(s)}$	$\rightleftharpoons$	Th^{4+}	+ 4 OH^{-}	log K_{sp}	-50.7	0

Table 5.1: Stability constants for the complexation of $EDTA^{4-}$ and hydroxide to Th^{IV}.[3]

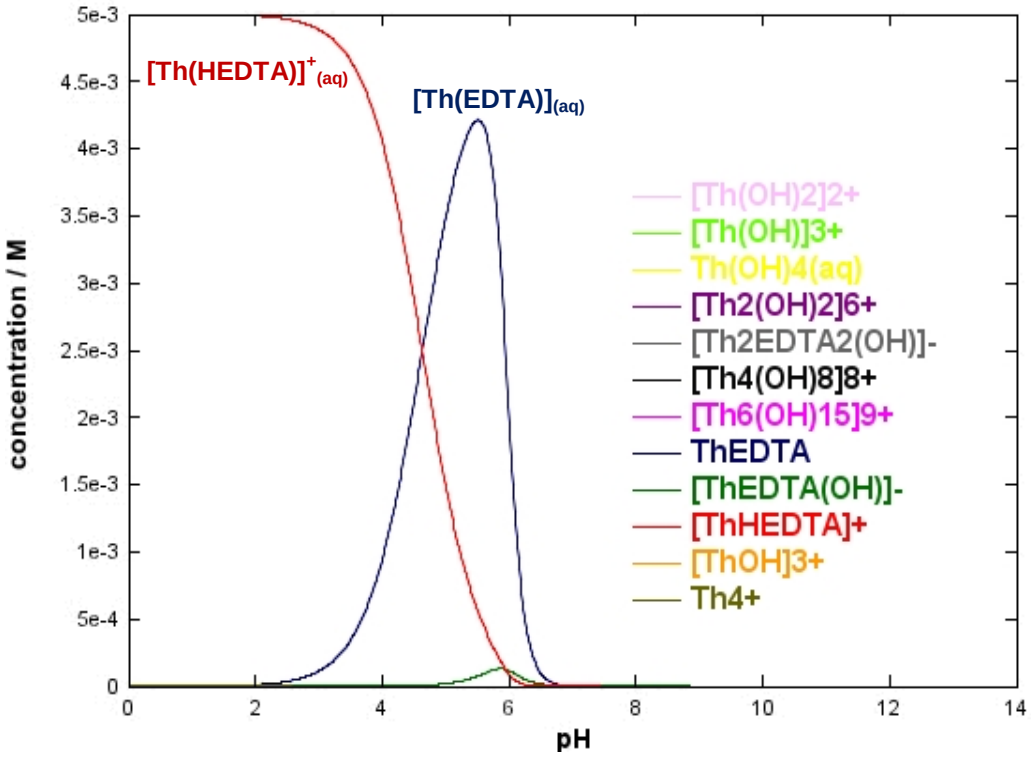

Figure 5.2: Speciation diagram of a 1:1 Th^{IV}:$EDTA^{4-}$ system as a function of pH using the *JCHESS* code.[4] Total $[Th^{IV}]$ = total $[EDTA^{4-}]$ = 5 mM. Only aqueous species are shown. Thermodynamic data obtained from the integrated *JCHESS* database and Martell and Smith.[3]

The acid protons will be described as the ^{1}H isotope when formulating molecular species in the NMR studies, as detailed in Section 3.1.

The mixing of equimolar amounts of $Th(NO_3)_{4(aq)}$ and $Na_2H_2EDTA_{(aq)}$ forms the $[Th(EDTA)]_{(aq)}$ complex in solution. This solution is acidic (pD 1.4) due to the Lewis acidic nature of the Th^{IV} ion, and also from the deprotonation of $Na_2H_2EDTA_{(aq)}$ (equations 3.1 to 3.4, Chapter 3).

^{1}H-NMR spectroscopy of the 1:1 Th^{IV}:$EDTA^{4-}$ system (Figure 5.3) shows signals for the acetate and ethylene protons of $EDTA^{4-}$ at 3.58 ppm (integrates to 8 protons) and 2.85 ppm (integrates to 4 protons), respectively. These signals are shifted from the free $EDTA^{4-}$ acetate and ethylene proton resonances (*e.g.* approximately 3.65 and 3.25 ppm, respectively, at pH 7; Figure 3.4 in Chapter 3), and so are representative of $EDTA^{4-}$ coordinated to Th^{IV}. As pD is increased, there is a small shift of the resonances for the acetate and ethylene protons from 3.58 to 3.48 ppm and 2.85 to 2.78 ppm, respectively, which may be an effect of hydrolysis of the $[Th(EDTA)]_{(aq)}$ complex. The bound $EDTA^{4-}$ signals are broadened compared to unbound $EDTA^{4-}$, which may suggest that the $EDTA^{4-}$ ligand is interchanging between hexadentate and pentadentate coordination modes. At pD 11.1, signals at 3.12 and 2.55 ppm emerge, which correspond to the acetate and ethylene protons of unbound $EDTA^{4-}$, respectively. Therefore, $EDTA^{4-}$ can coordinate to the Th^{IV} ion up to approximately pD 11.1, after which hydrolysis occurs and a white precipitate forms, likely to be $Th(OH)_{4(s)}$.

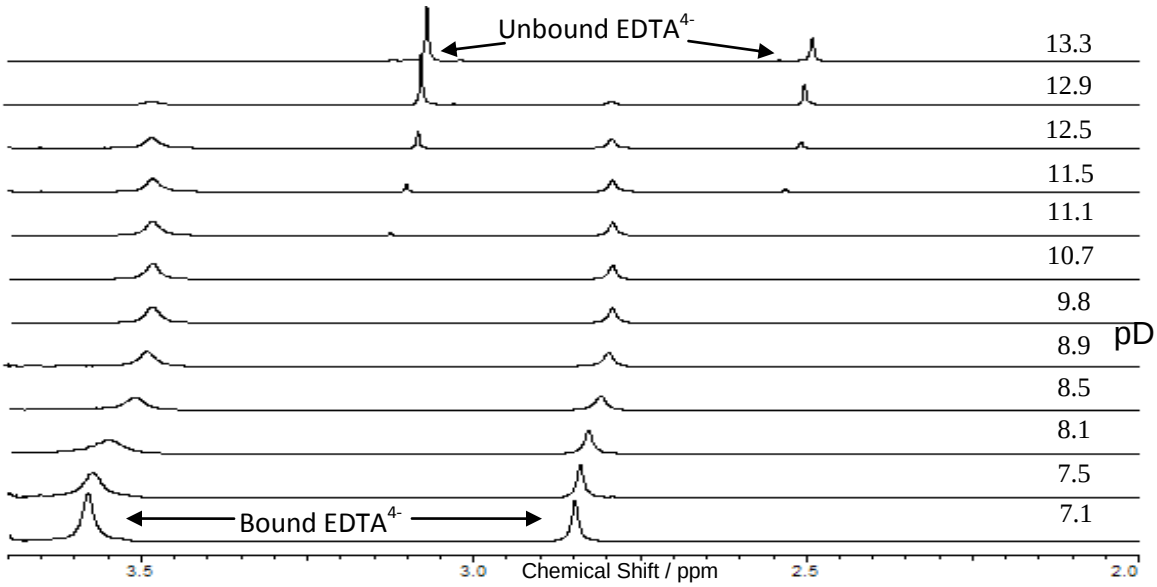

Figure 5.3: ^{1}H-NMR spectra for the effect of pD on a 1:1 Th^{IV}:$EDTA^{4-}$ system; $[Th^{IV}]_i = [EDTA^{4-}]_i = 50$ mM.

5.2 Th^{IV}-EDTA-Carbonate Ternary System

The interaction of carbonate with the $[Th(EDTA)]_{(aq)}$ complex has been analysed using ^{13}C-NMR spectroscopy. The ^{13}C-NMR spectra for the 1:1:1 Th^{IV}:$EDTA^{4-}$:CO_3^{2-} system (Figures 5.4 and 5.5) focus on the chemical shift range 160 to 170 ppm, as this is the region where the carbonate resonance is observed. The carbonate source used in these experiments was ^{13}C-labelled carbonate, as described in Section 3.2.2.

^{13}C-NMR spectroscopy of the 1:1:1 Th^{IV}:$EDTA^{4-}$:CO_3^{2-} system shows a broadened carbonate signal at approximately 167 ppm, over the pD range 7.2 to 8.4 (Figure 5.4). The observed broadening of the carbonate signal is likely to be due to fast exchange between bound CO_3^{2-} to the $[Th(EDTA)]_{(aq)}$ complex and unbound HCO_3^- in solution. As pD is increased further, two resolved carbonate signals are observed in the ^{13}C-NMR spectra at 168.4 and 166.9 ppm (Figure 5.5). The peak at 168.4 ppm is representative of bound carbonate, and the signal at 166.9 ppm corresponds to unbound carbonate. The unbound carbonate signal shifts with pD from 166.9 ppm to 169.1 ppm, and the proportion of unbound carbonate to bound carbonate in solution increases as the pH is raised from pH 11.0 to 12.8. This is likely to be due to the competition of hydroxide with carbonate for coordination to the $[Th(EDTA)]_{(aq)}$ complex. A white precipitate is observed to form at pD 11.0, which is likely to be $Th(OH)_{4(s)}$. Above pD 13.2, there is no bound CO_3^{2-} or $EDTA^{4-}$ (indicated by ^1H-NMR spectroscopy; Figure A in Appendix 3) in the system, and so all Th^{IV} ions are precipitated as $Th(OH)_{4(s)}$.

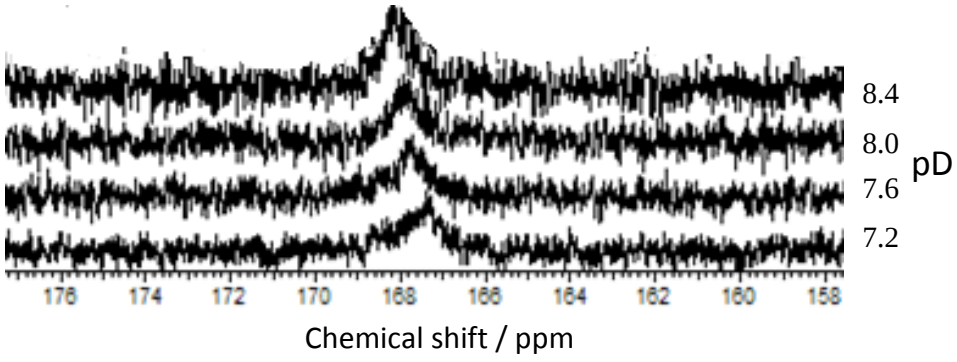

Figure 5.4: ^{13}C-NMR spectra for the effect of pD on a 1:1:1 Th^{IV}:$EDTA^{4-}$:CO_3^{2-} solution; $[Th^{IV}]_i = [EDTA^{4-}]_i = [CO_3^{2-}]_i = 33$ mM.

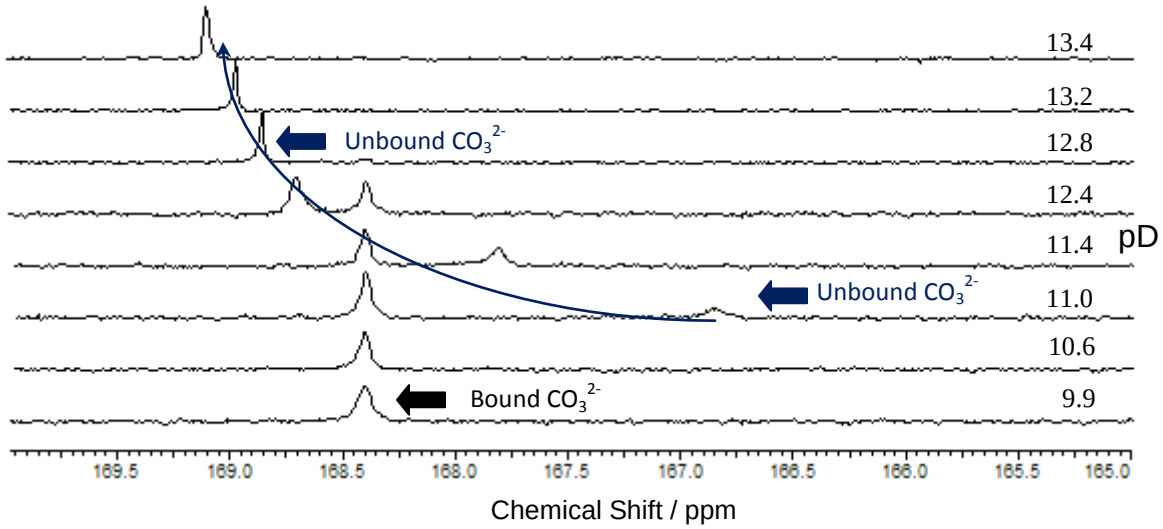

Figure 5.5: ^{13}C-NMR spectra for the effect of pD on a 1:1:1 Th^{IV}:$EDTA^{4-}$:CO_3^{2-} solution; $[Th^{IV}]_i = [EDTA^{4-}]_i = [CO_3^{2-}]_i$ = 33 mM.

The percentage of bound $EDTA^{4-}$ and CO_3^{2-} to the Th^{IV} ion in the 1:1:1 Th^{IV}:$EDTA^{4-}$:CO_3^{2-} system as a function of pD (Figure 5.6) has been calculated from the integration of the relevant NMR signals, as described in Section 3.22. Over the pD region 8.4 to 10.6, all of the carbonate in the system is bound. This differs from the 1:1:1 Lu^{III}:$EDTA^{4-}$:CO_3^{2-} system, where it was found that carbonate binding at approximately pD 9 was unfavourable (Figure 3.19, Chapter 3). At approximately pD 11.0 in the Th^{IV} system, both the percentage of bound CO_3^{2-} and $EDTA^{4-}$ begin to decrease, though the percentage of CO_3^{2-} binding decreases at a higher rate with respect to pD than $EDTA^{4-}$. This is because $EDTA^{4-}$ has a larger stability constant with the Th^{IV} ion than CO_3^{2-}.[3] A comparison of the $[Lu(EDTA)]^-_{(aq)}$ (see Section 3.2.2.1) and $[Th(EDTA)]_{(aq)}$ systems shows that approximately 90 % of $EDTA^{4-}$ remains bound to the Lu^{III} ion up to pD 13.0, whereas only 30 % of $EDTA^{4-}$ remains bound in the Th^{IV} system at the same pD. Despite $EDTA^{4-}$ having a larger stability constant with the Th^{IV} ion than the Lu^{III} ion, Th^{IV} is more susceptible to hydrolysis than Lu^{III}, and so hydrolysis occurs at a lower pD (Table 5.2).

Lu^{3+}	+ $EDTA^{4-}$	$\rightleftharpoons$	$Lu(EDTA)^{-}$	$\log \beta_{11}$	19.7	I = 0.1 M $NaClO_4$
Th^{4+}	+ $EDTA^{4-}$	$\rightleftharpoons$	Th(EDTA)	$\log \beta_{11}$	23.2	I = 0.1 M $NaClO_4$
$Lu(OH)_3$		$\rightleftharpoons$	Lu^{3+} + 3 OH^-	$\log K_{sp}$	-25.1	0
$Th(OH)_{4(s)}$		$\rightleftharpoons$	Th^{4+} + 4 OH^-	$\log K_{sp}$	-50.7	0

Table 5.2: Stability constants for the coordination of $EDTA^{4-}$ and hydroxide to the Lu^{III} and Th^{IV} ions. [3]

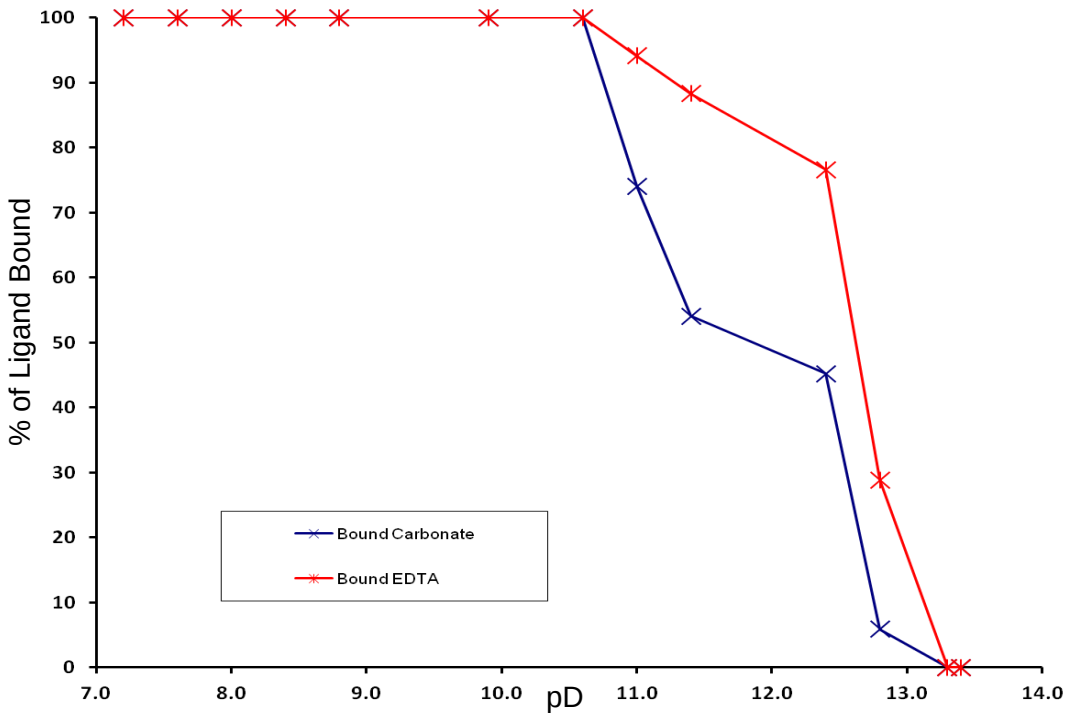

Figure 5.6: Percentage of bound $EDTA^{4-}$ and CO_3^{2-} to Th^{IV} as a function of pD for the 1:1:1 Th^{IV}:$EDTA^{4-}$:CO_3^{2-} system; $[Th^{IV}]_i = [EDTA^{4-}]_i = [CO_3^{2-}] = 33$ mM.

As mentioned previously, the Th^{IV} ion can accommodate a high number of donor atoms, with the most being reported as fifteen.[2] Therefore, the stoichiometry of carbonate binding to the $[Th(EDTA)]_{(aq)}$ complex was investigated by NMR spectroscopy (Figures B and C for the ^{13}C- and ^{1}H-NMR spectra, respectively, Appendix 3) to observe whether two carbonate anions could bind to the $[Th(EDTA)]_{(aq)}$ complex. The percentage of bound $EDTA^{4-}$ and CO_3^{2-} to Th^{IV} as a function of pD in the 1:1:2 Th^{IV}:$EDTA^{4-}$:CO_3^{2-} system is shown in Figure 5.7. All of the carbonate in the system is bound to the Th^{IV} ion over the pD range 9.0 to 10.3, which suggests the formation of the $[Th(EDTA)(CO_3)_2]^{4-}_{(aq)}$ species. From pD 10.3 to 10.7, the percentage of CO_3^{2-} bound decreases from 100 % to 57 %. After pD 10.7, there is a

gradual decrease of the percentage of carbonate bound to the Th^{IV} ion up to pD 13.2, when no carbonate is bound. The initial 'rate' of decrease of carbonate binding with respect to pD is high, which may suggest that one of the carbonate ions is more readily replaced by hydroxide compared to the second carbonate ion. At approximately pD 11, the percentage of $EDTA^{4-}$ bound decreases and a white precipitate forms, which is likely to be $Th(OH)_{4(s)}$. Above pD 13.4, there is no bound CO_3^{2-} or $EDTA^{4-}$ in the system.

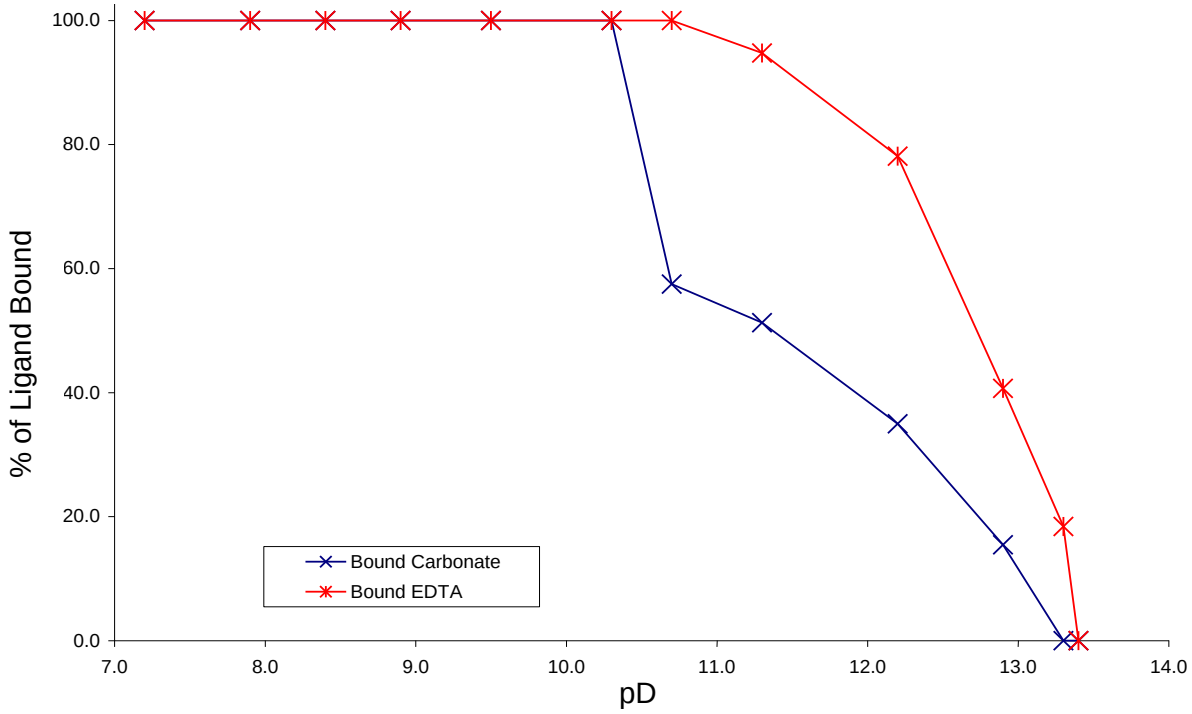

Figure 5.7: Percentage of bound $EDTA^{4-}$ and CO_3^{2-} to the Th^{IV} ion as a function of pD in the 1:1:2 Th^{IV}:$EDTA^{4-}$:CO_3^{2-} system; $[Th^{IV}]_i = [EDTA^{4-}]_i = 33$ mM; $[CO_3^{2-}]_i = 66$ mM.

The stoichiometry of carbonate binding was further investigated by NMR spectroscopy (Figures D and E for ^{13}C- and ^{1}H-NMR spectra, respectively, Appendix 3) to observe whether three carbonate anions could bind to the $[Th(EDTA)]_{(aq)}$ complex. The percentage of bound $EDTA^{4-}$ and CO_3^{2-} to the Th^{IV} ion in the 1:1:3 Th^{IV}:$EDTA^{4-}$:CO_3^{2-} system is shown in Figure 5.8. Over the pD range 7.5 to 9.5, approximately 70 % of the carbonate in the system is bound to the $[Th(EDTA)]_{(aq)}$ complex. This provides further evidence for the formation of the $[Th(EDTA)(CO_3)_2]^{4-}_{(aq)}$ species, as approximately two thirds of the carbonate present in the solution is bound to the $[Th(EDTA)]_{(aq)}$ complex. There is no pD at which all of the carbonate

in the system is bound to the $[Th(EDTA)]_{(aq)}$ complex, therefore formation of the $[Th(EDTA)(CO_3)_3]^{6-}{}_{(aq)}$ species is unlikely. From pD 9.3 to 10.8, there is a gradual decrease in the percentage of carbonate bound to the $[Th(EDTA)]_{(aq)}$ complex from approximately 70 to 40 %. This indicates the loss of a carbonate anion from the Th^{IV} ion coordination sphere, which may form a $[Th(EDTA)(CO_3)(OH)]^{3-}{}_{(aq)}$ species. The 'rate' of decrease for the loss of the first carbonate anion, with respect to pD, is lower in the 1:1:3 Th^{IV}:$EDTA^{4-}$:CO_3^{2-} system when compared to that for the 1:1:2 Th^{IV}:$EDTA^{4-}$:CO_3^{2-} system. This may be because there is more carbonate present in the 1:1:3 Th^{IV}:$EDTA^{4-}$:CO_3^{2-} system, and so the equilibrium may be favoured towards forming the $[Th(EDTA)(CO_3)_2]^{4-}{}_{(aq)}$ species. From pD 10.8 to 13.2, there is a gradual decrease in the percentage of carbonate bound from 40 to 0 %, implying the loss of the second carbonate ion. The percentage of bound $EDTA^{4-}$ decreases at pD 11.0, coinciding with the formation of a white precipitate, which is likely to be $Th(OH)_{4(s)}$. Above pD 13.2, there is no bound CO_3^{2-} or $EDTA^{4-}$ to the Th^{IV} ion in the system.

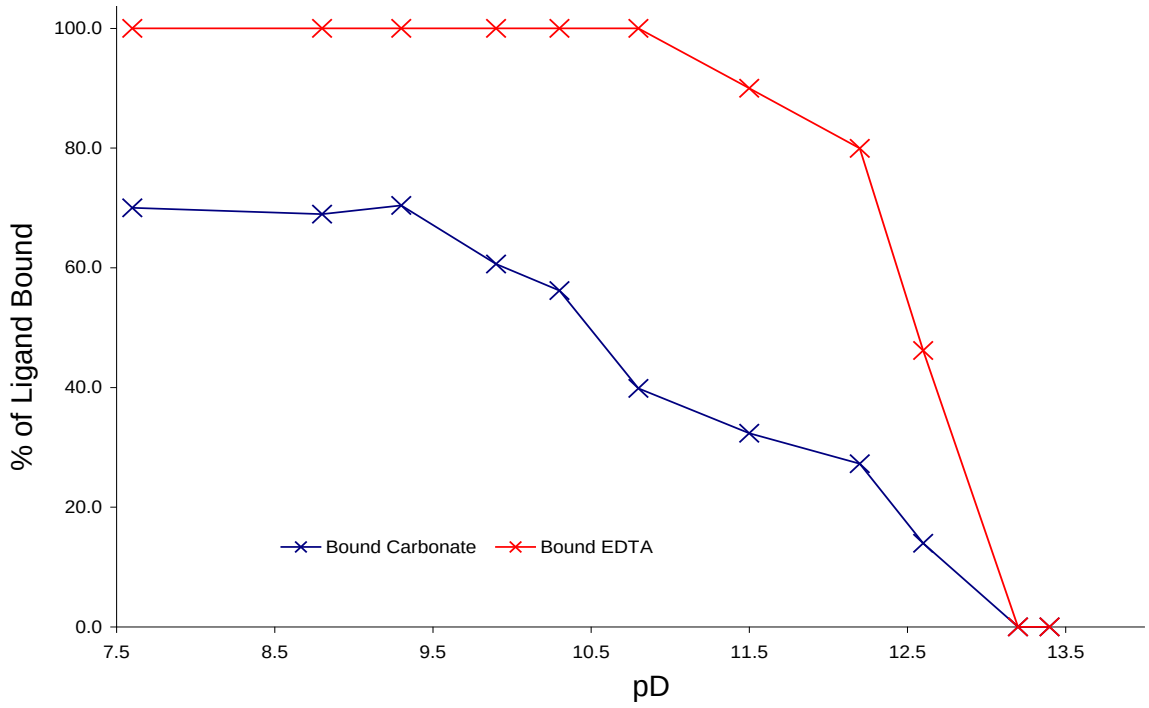

Figure 5.8: Percentage of bound $EDTA^{4-}$ and CO_3^{2-} to the Th^{IV} ion as a function of pD for the 1:1:3 Th^{IV}:$EDTA^{4-}$:CO_3^{2-} system; $[Th^{IV}]_i = [EDTA^{4-}]_i = 25$ mM; $[CO_3^{2-}]_i = 75$ mM.

5.2.1 Summary

NMR spectroscopy has been used to identify the formation of the $[Th(EDTA)(CO_3)]^{2-}_{(aq)}$ and $[Th(EDTA)(CO_3)_2]^{4-}_{(aq)}$ complexes. The Th^{IV} ion has a higher charge density than the trivalent lanthanides, and so will have increased attraction for anionic ligands. The combination of this increased electrostatic attraction for anionic ligands and the tendency of the Th^{IV} ion to coordinate to a high number of donor atoms,[2] enables two carbonate anions to bind to the $[Th(EDTA)]_{(aq)}$ complex. This was not observed for the trivalent lanthanide systems.

Possible structures for the $[Th(EDTA)(CO_3)]^{2-}_{(aq)}$ and $[Th(EDTA)(CO_3)_2]^{4-}_{(aq)}$ species are illustrated in Figure 5.9. It is likely that CO_3^{2-} coordinates in a bidentate mode to the Th^{IV} ion and is in exchange with water molecules. The number of water molecules coordinated to the $[Th(EDTA)(CO_3)]^{2-}_{(aq)}$ and $[Th(EDTA)(CO_3)_2]^{4-}_{(aq)}$ species is unknown, but an approximation would be two water molecules bound to the $[Th(EDTA)(CO_3)]^{2-}_{(aq)}$ complex and zero water molecules bound to the $[Th(EDTA)(CO_3)_2]^{4-}_{(aq)}$ species, which would give an overall coordination number of ten. This is a commonly observed coordination number for the Th^{IV} ion.[5,6] The coordinated water molecules may also be in equilibrium with hydroxide anions, particularly at high pH.

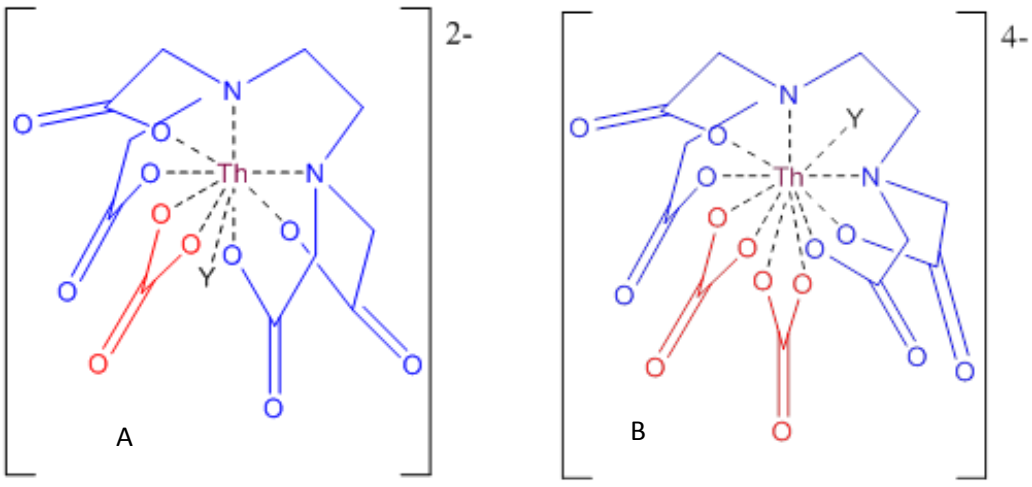

Figure 5.9: Possible structures for: A) $[Th(EDTA)(CO_3)]^{2-}_{(aq)}$ and B) $[Th(EDTA)(CO_3)_2]^{4-}_{(aq)}$ species; Y represents an unknown quantity of water molecules or hydroxide anions that may be coordinated to the complexes.

5.3 Th^{IV}-Lactate Binary System

5.3.1 Speciation Behaviour

In order to observe whether $[Th(EDTA)(lactate)]^{-}_{(aq)}$ or $[Th(DTPA)(lactate)]^{2-}_{(aq)}$ complexes exist, which would be analogous to the $[Ln(EDTA)(lactate)]^{2-}_{(aq)}$ and $[Ln(DTPA)(lactate)]^{3-}_{(aq)}$ species in Chapter 4, the coordination behaviour of lactate to the Th^{IV} ion must first be understood.

The aqueous Th^{IV} species present in a 1:1 Th^{IV}:lactate system at a certain pH can be determined from the speciation diagram (Figure 5.10), which is derived from known equilibrium constants ($\log \beta_{[Th(lactate)]^{3+}} = 4.2$; $I = 1$ M and Table 5.2).[3] The $[Th(lactate)]^{3+}_{(aq)}$ species does not dominate the speciation at any pH due to the low thermodynamic stability of the $[Th(lactate)]^{3+}_{(aq)}$ complex. Hydrolysis of the Th^{IV} ion to form $Th(OH)_{4(s)}$ is expected to prevail from pH 2 .

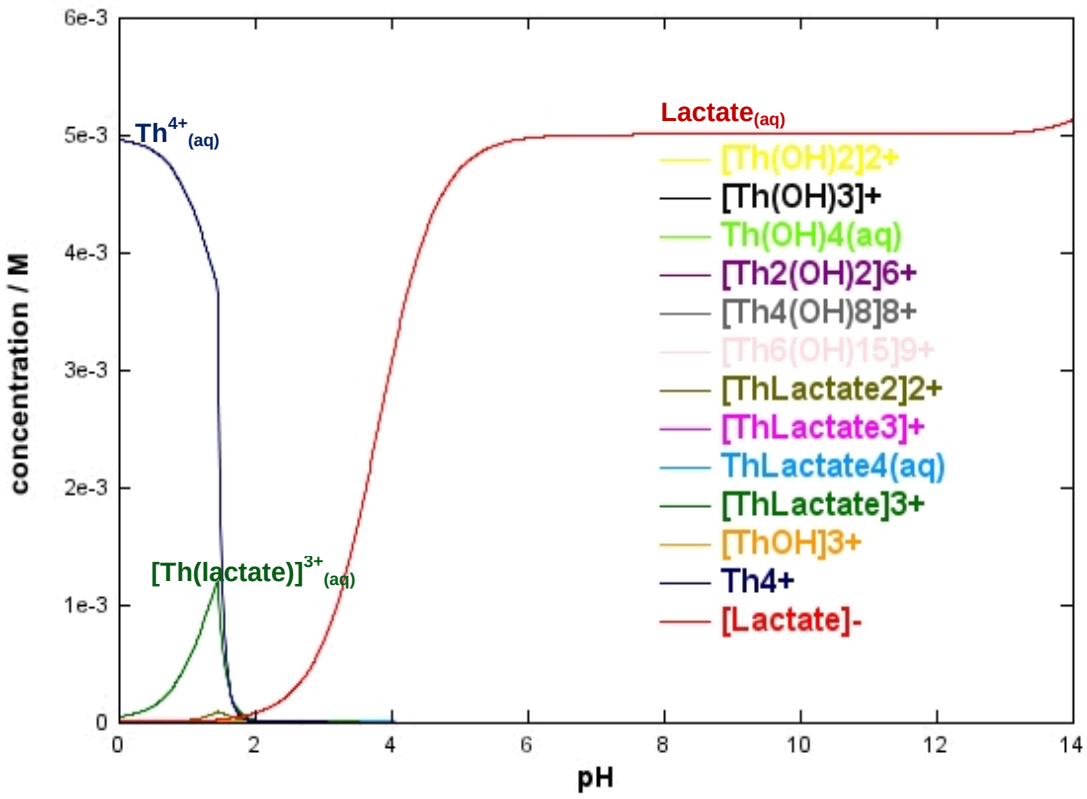

Figure 5.10: Speciation diagram of 1:1 Th^{IV}:lactate system as a function of pH using the *JCHESS* code.[4] Total $[Th^{IV}]$ = total [lactate] = 5 mM. Only aqueous species are shown. Thermodynamic data obtained from the integrated *JCHESS* database and Martell and Smith.[3]

The ^{1}H-NMR spectra obtained for the 1:1 Th^{IV}:lactate system show that the lactate signals for the -C**H**(OH)- proton (approximately 4.1 ppm) and the –C**H$_3$** protons (approximately 1.4 ppm) have been broadened between the pD range 3.5 to 7.4 (Figure 5.11). The signal for the –C**H**(OH)- proton is difficult to observe over the pD range 3.5 to 5.9 in the spectra presented in Figure 5.11, because it has been broadened into the baseline. The broadening of the lactate signals is likely to be due to exchange between bound and unbound lactate in the Th^{IV} system. From pD 8.6 to 12.0, the lactate signals become resolved, and correlate to the NMR spectra of free lactate in this pD range (Figure 4.8, Section 4.1.2.2). Therefore, lactate is unbound from the Th^{IV} ion over this pD region. A white precipitate forms at pD 7.4, which is likely to be $Th(OH)_{4(s)}$.

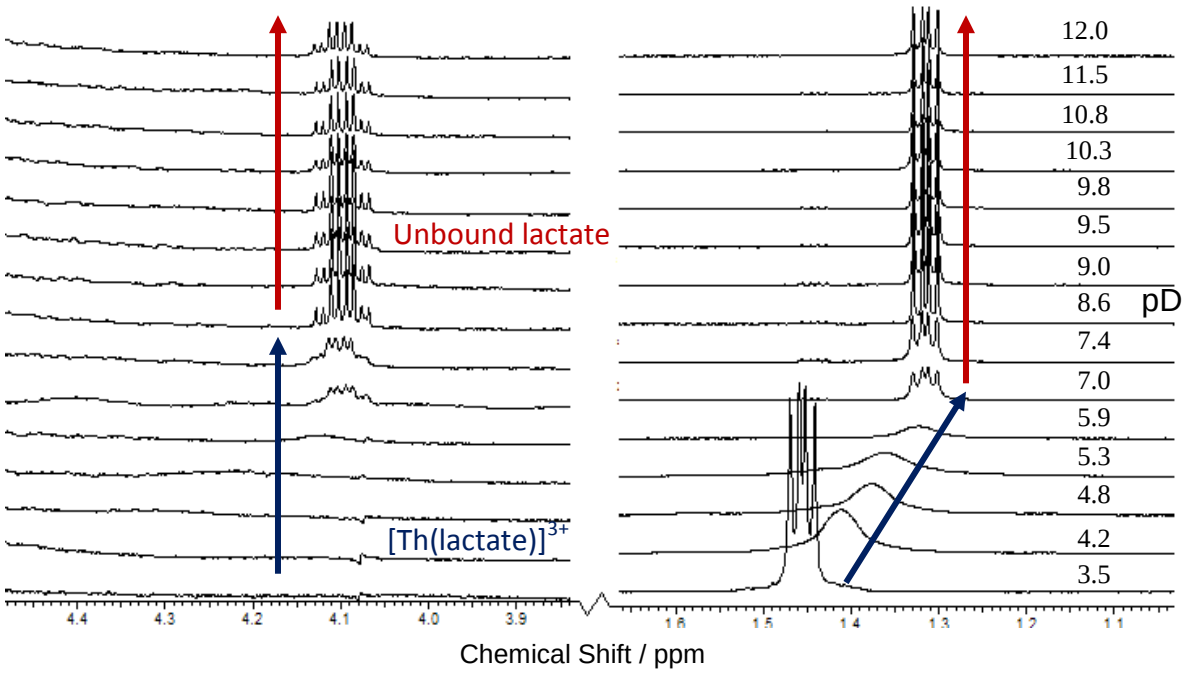

Figure 5.11: ^{1}H-NMR spectra for the effect of pD on the 1:1 Th^{IV}:lactate system; $[Th^{IV}]_i = [lactate]_i = 10$ mM.

The lactate used in these experiments was ^{13}C-labelled on the carboxylate functional group, to increase the intensity of the corresponding ^{13}C-NMR signal, as described in previous ^{13}C-labelled studies (Section 3.2.2). The –**C**H(OH)- and –**C**H_3 carbon atoms were not ^{13}C-labelled, and so the reduction in the number of ^{13}C-NMR scans results in these ^{13}C-NMR signals not being observed. The ^{13}C-NMR spectra for the 1:1 Th^{IV}:lactate system show a signal for the carboxylate group at 183.5 ppm, which is broadened over the pD range 3.5 to

5.8 (Figure 5.12). This broadening of the carboxylate signal is not observed in the free lactate ^{13}C-NMR spectra (Figure 5.13), and so it is likely due to exchange between bound and unbound lactate. This provides further evidence that lactate can bind to the Th^{IV} ion, but the thermodynamic stability related to this binding is likely to be relatively weak (*cf*. CO_3^{2-}, Section 5.2).

To summarise, ^{1}H- and ^{13}C-NMR spectra indicate that lactate can bind to the Th^{IV} ion, which occurs predominantly over the pD region 3.5 to 5.9. After pD 5.9, hydroxide replaces lactate in the Th^{IV} inner coordination sphere and a white precipitate, probably $Th(OH)_{4(s)}$, forms.

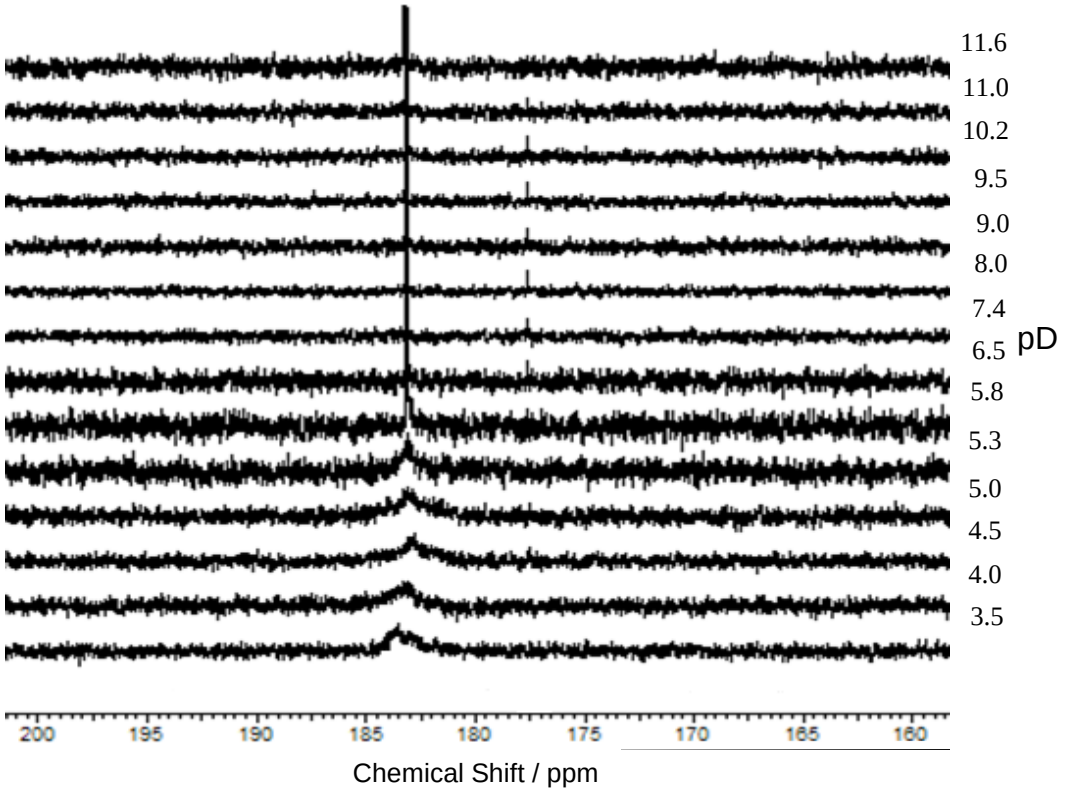

Figure 5.12: ^{13}C-NMR spectra for the effect of pD on the 1:1 Th^{IV}:lactate system; $[Th^{IV}]_i = [lactate]_i = 10$ mM.

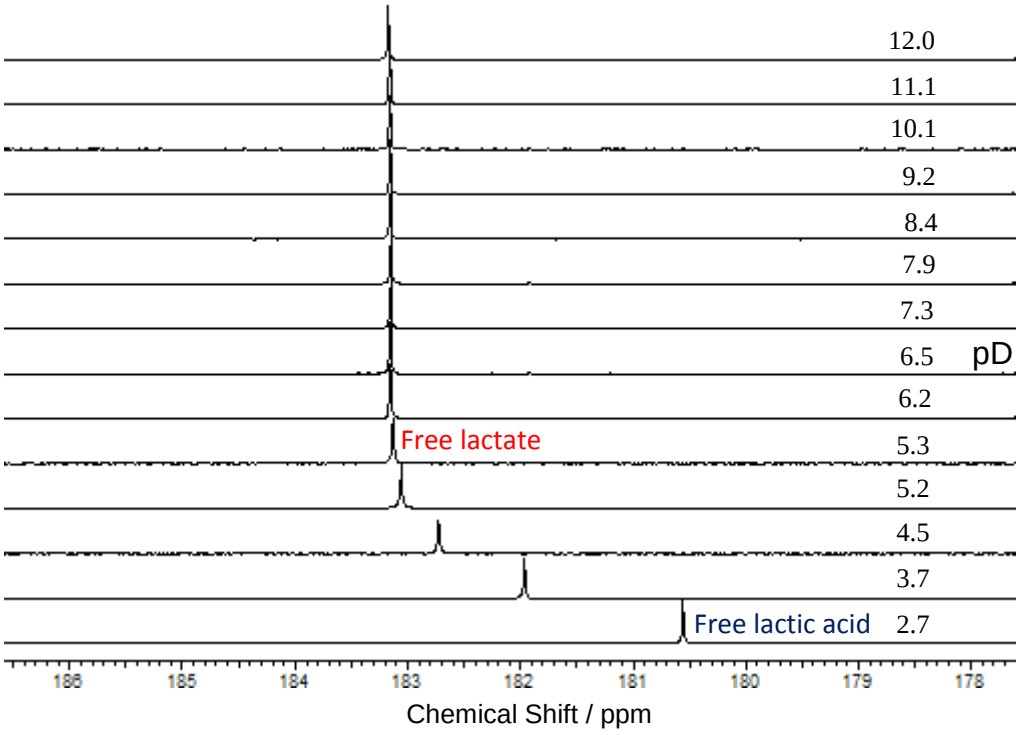

Figure 5.13: ^{13}C-NMR spectra for the effect of pD on the free lactic acid/lactate system; $[lactate]_i$ = 10 mM.

5.4 Th^{IV}-EDTA-Lactate Ternary System

Section 5.3.1 discussed the interaction of lactate with the Th^{IV} ion in the 1:1 Th^{IV}:lactate binary system. NMR spectroscopy has been performed on a 1:1:1 Th^{IV}:$EDTA^{4-}$:lactate system to observe whether lactate can interact with the Th^{IV} ion in the presence of $EDTA^{4-}$. The ^{1}H-NMR spectra of this system as a function of pD show lactate signals at approximately 4.45 and 1.43 ppm for the –C**H**(OH)- proton and -C**H$_3$** protons, respectively (Figure 5.14). As pD is increased from 2.7 to 3.6, the –C**H**(OH)- proton signal shifts from 4.45 to 4.50 ppm, which is representative of a change in the equilibrium between lactic acid and lactate. From pD 3.6 to 8.9, the signal for the -C**H**(OH)- proton shifts from 4.50 to 4.10 ppm and the signal for the -C**H$_3$** protons shift from 1.43 to 1.30 ppm. The -C**H**(OH)- proton signal of lactate is also observed to be broadened over this pD range. This pD dependent shift and broadening of the lactate signals corresponds to the equilibrium between lactate bound to the $[Th(EDTA)]_{(aq)}$ complex and unbound lactate in solution. The lactate signals do not shift with increasing pD after pD 8.9, and the signals are resolved, which implies that lactate is predominantly in the unbound form.

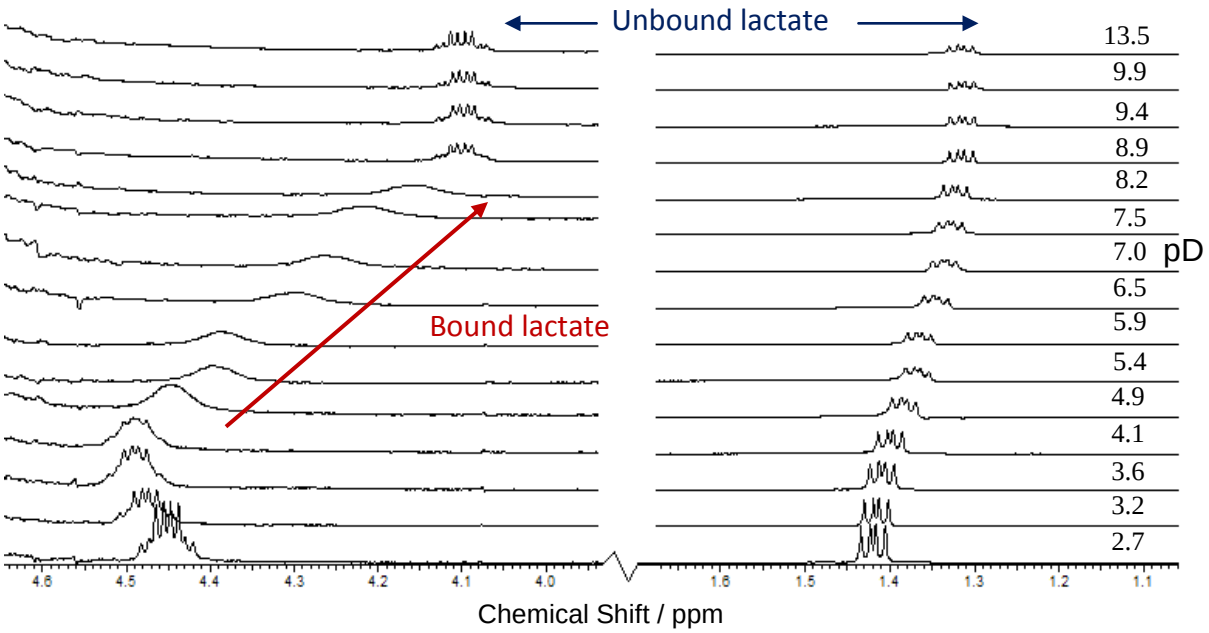

Figure 5.14: 'Zoom-in' of lactate signals in the ^{1}H-NMR spectra for the effect of pD on the 1:1:1 Th^{IV}:$EDTA^{4-}$:lactate system; $[Th^{IV}]_i$= $[EDTA^{4-}]_i$ = $[lactate]_i$ = 10 mM.

The ^{1}H-NMR spectra also show signals at approximately 3.6 and 2.9 ppm (Figure 5.15), which correspond to the acetate and ethylene protons of coordinated $EDTA^{4-}$ (integration ratio of 8:4 protons, respectively). Over the pD range 2.7 to 5.9, the acetate and ethylene proton resonances of bound $EDTA^{4-}$ split into overlapping multiplets. This splitting pattern was not observed for the 1:1 Th^{IV}:$EDTA^{4-}$ binary system (Figure 5.16) or the 1:1:1 Th^{IV}:$EDTA^{4-}$:CO_3^{2-} ternary system (Figure A, Appendix 3), where broadened AB quartets were observed, typical of symmetrical hexadentate coordination of $EDTA^{4-}$. The overlapping multiplets suggest that the coordination mode of $EDTA^{4-}$ is asymmetrical (*i.e.* pentadentate) when lactate binds. This induced asymmetrical binding of $EDTA^{4-}$ to Th^{IV} may occur in order to relieve steric hindrance around the Th^{IV} ion when lactate binds. In the analogous La^{III}:$EDTA^{4-}$:lactate system, the ^{1}H-NMR spectra (Figure 4.34, Section 4.5.1.1) also showed a splitting of the signal for the acetate protons of $EDTA^{4-}$ from an AB quartet to an AB quartet of doublets, over the pD region that lactate was expected to bind to the $[La(EDTA)]^{-}_{(aq)}$ complex. The change in the coordination mode of $EDTA^{4-}$ from hexa- to pentadentate was also suggested to occur in the 1:1:1 La^{III}:$EDTA^{4-}$:lactate system (Section 4.5.1.1). As the bound/unbound lactate equilibrium shifts towards the unbound form from pD 7.0 in the Th^{IV}

system, the acetate and ethylene proton resonances of bound $EDTA^{4-}$ become more broadened, suggesting that the coordination mode of $EDTA^{4-}$ may be alternating between pentadentate and hexadentate. Above pD 8.9, the $EDTA^{4-}$ signals at 3.48 and 2.79 ppm resemble the signals observed in the 1:1 Th^{IV}:$EDTA^{4-}$ system (Figure 5.3), indicative of hexadentate $EDTA^{4-}$ binding to the Th^{IV} ion as a result of the lactate being predominantly unbound. Above pD 9.9, unbound $EDTA^{4-}$ signals are observed in the ^{1}H-NMR spectra (Figure 5.15), and a white precipitate forms, which is likely to be $Th(OH)_{4(s)}$.

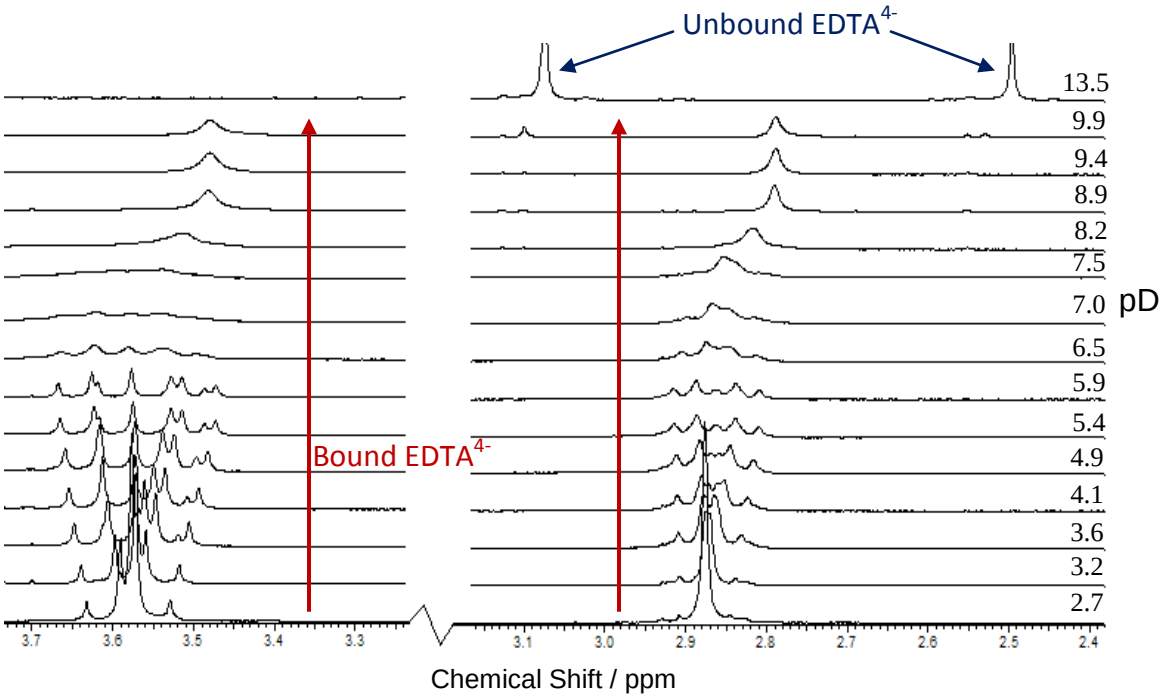

Figure 5.15: 'Zoom-in' of $EDTA^{4-}$ signals in the ^{1}H-NMR spectra for the effect of pD on the 1:1:1 Th^{IV}:$EDTA^{4-}$:lactate system; $[Th^{IV}]_i = [EDTA^{4-}]_i = [lactate]_i = 10$ mM.

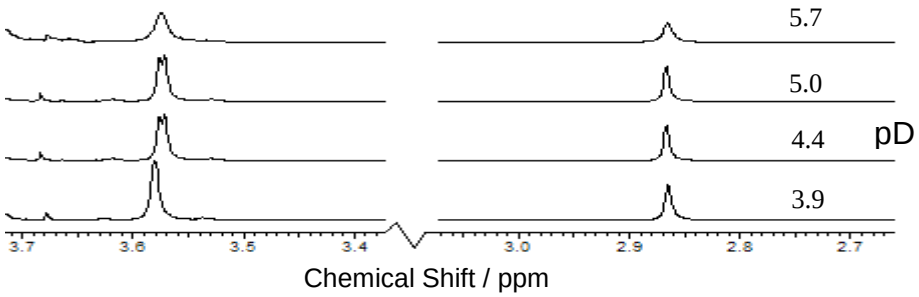

Figure 5.16: 'Zoom-in' of $EDTA^{4-}$ signals in the ^{1}H-NMR spectra for the effect of pD on the 1:1 Th^{IV}:$EDTA^{4-}$ system; $[Th^{IV}]_i = [EDTA^{4-}]_i = 10$ mM.

The shift in the signal for the ^{13}C-labelled carboxylate group of lactate can be monitored by ^{13}C-NMR spectroscopy (Figure 5.17). Over the pD range 2.7 to 5.8, the carboxylate signal of lactate shifts from 180.6 to 184.0 ppm, which corresponds to the deprotonation of lactic acid to form lactate as observed in the free lactate ^{13}C-NMR spectra (Figure 5.13). The broadening of the signal over the pD range 2.7 to 10.2 is likely to be due to an exchange process between uncoordinated lactate and bound lactate to the $[Th(EDTA)]_{(aq)}$ complex. On increasing pD from 5.8 to 11.3, the carboxylate signal shifts from 184.0 to 183.2 ppm, which is representative of the shift in the bound/unbound lactate equilibrium to more unbound lactate. At pD greater than 10.2, the signal at 183.2 ppm becomes better resolved suggesting lactate is predominantly unbound in the system.

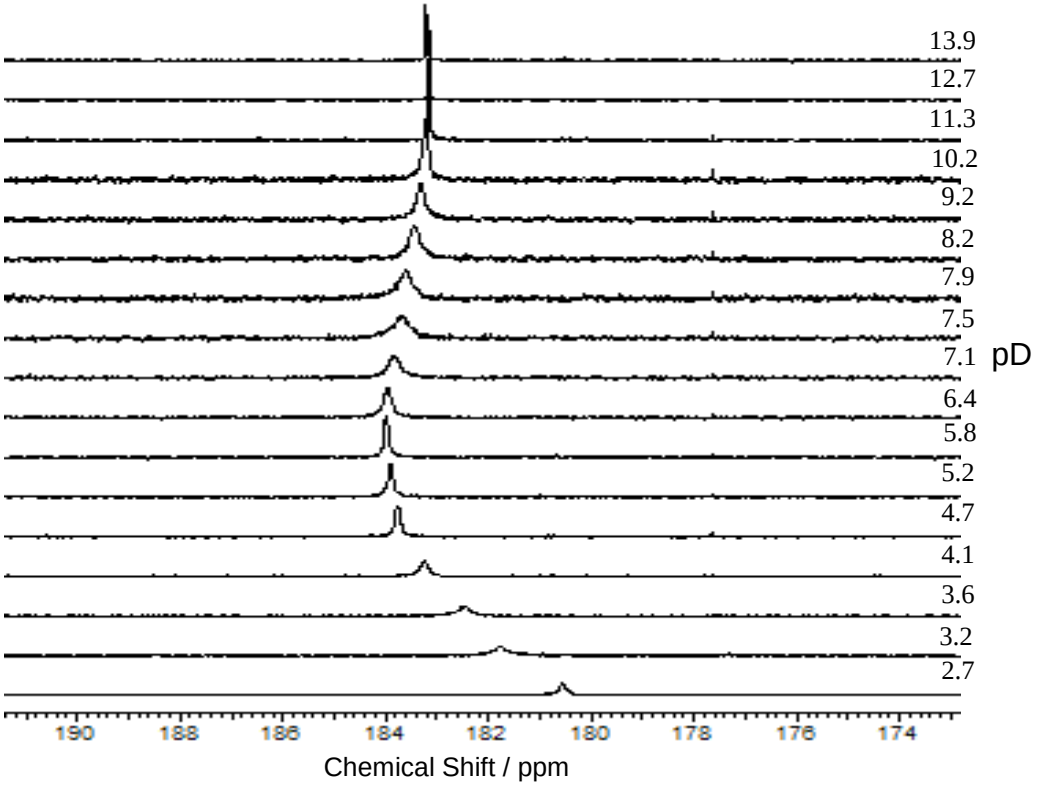

Figure 5.17: ^{13}C-NMR spectra for the effect of pD on the 1:1:1 Th^{IV}:$EDTA^{4-}$:lactate system; $[Th^{IV}]_i = [EDTA^{4-}]_i = [lactate]_i = 10$ mM.

5.4.1 Summary

^{1}H- and ^{13}C-NMR spectroscopy indicate that a $[Th(EDTA)(lactate)]^{-}_{(aq)}$ complex exists over the pD range 2.7 to 8.2, and the bound lactate is likely to be in equilibrium with hydroxide and water molecules. The occurrence of overlapping multiplets for the acetate and ethylene proton resonances of bound $EDTA^{4-}$ over the pD range 2.7 to 5.9, suggests that $EDTA^{4-}$ may alter its binding mode to accommodate the lactate ligand into the Th^{IV} ion inner coordination sphere. As discussed in Section 4.4.1.2, there are reports in the literature that hydroxyl groups are able to hydrogen bond to carboxylate groups,[7] so it may also be possible that the hydroxyl group of lactate is hydrogen bonding to the $EDTA^{4-}$ acetate arms as well as directly coordinating to the metal ion. A suggestion for the structure of the $[Th(EDTA)(lactate)]^{-}_{(aq)}$ ternary complex is illustrated in Figure 5.18. However, it is not known if, or how many, water molecules fill the remaining vacant coordination sites of the Th^{IV} ion. An approximation would be three water molecules bound to the $[Th(EDTA)(lactate)]^{-}_{(aq)}$ complex, which would give an overall coordination number of ten, if $EDTA^{4-}$ was bound as a pentadentate ligand and lactate was bound in a bidentate mode. As previously mentioned, this is a commonly observed Th^{IV} ion coordination number.[5,6] The coordinated water molecules may also be in equilibrium with hydroxide anions, particularly at high pH.

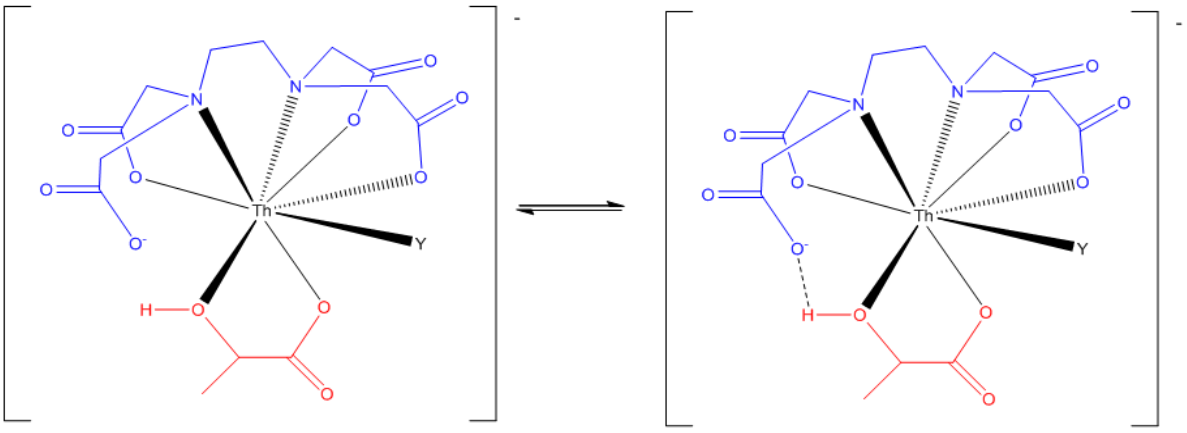

Figure 5.18: Suggestion for the structure of the $[Th(EDTA)(lactate)]^{-}_{(aq)}$ ternary complex; lactate may H-bond to the $EDTA^{4-}$ carboxylate group. Y represents water molecules or hydroxide ions that may be coordinated to the complex.

5.5 Th^{IV}-DTPA Binary System

5.5.1 Speciation Behaviour

The formation of a $[Th(EDTA)(lactate)]^-_{(aq)}$ ternary complex has been shown to exist in Section 5.4. As discussed previously in Section 4.4, the formation of $[M(DTPA)(lactate)]^{3-}_{(aq)}$ complexes (where M = An^{III} or Ln^{III}) may play a role in improving the efficiency of the TALSPEAK process.[8] Experimental work detailed in Section 4.4 explained that lactate may interact with $[Ln(DTPA)]^{2-}_{(aq)}$ complexes, but the nature of the interaction could be primary or secondary sphere. The 1:1 Th^{IV}:$DTPA^{5-}$ and 1:1:1 Th^{IV}:$DTPA^{5-}$:lactate systems will be probed by ^1H- and ^{13}C-NMR spectroscopy to further understand lactate communication with metal ion complexes.

For a 1:1 Th^{IV}:$DTPA^{5-}$ system, the aqueous Th^{IV} species present in solution at a certain pH can be determined using a speciation diagram (Figure 5.19), which is derived from known equilibrium constants (Tables 5.2 and 5.3).[3] The speciation diagram shows that over the pH range 0 to 2, the $[Th(HDTPA)]_{(aq)}$ complex is dominant. As pH is increased further, the acetate arm of $HDTPA^{4-}$ is deprotonated to form the $[Th(DTPA)]^-_{(aq)}$ complex, which is the dominant solution species from pH 2 to 6. Hydrolysis of the Th^{IV} ion is expected to begin at approximately pH 6, forming the $Th(OH)_{4(s)}$ complex.

Th^{4+}	+	$DTPA^{5-}$	+	H^+	$\rightleftharpoons$	Th(HDTPA)	$\log \beta_{111}$ 28.8	I = 0.5 M Na^+ salt
Th^{4+}	+	$DTPA^{5-}$		-	$\rightleftharpoons$	$Th(DTPA)^-$	$\log \beta_{110}$ 26.6	I = 0.5 M Na^+ salt

Table 5.3: Stability constants for the coordination of $DTPA^{5-}$ and $HDTPA^{4-}$ to the Th^{IV} ion.[3]

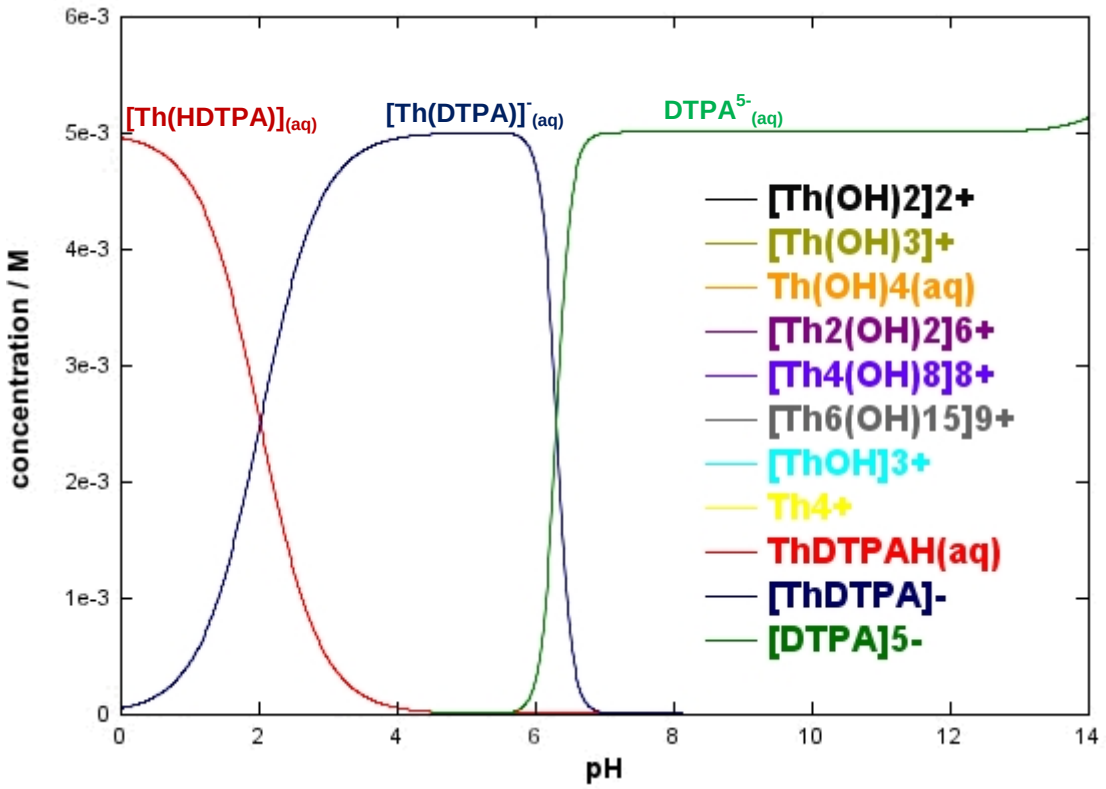

Figure 5.19: Speciation diagram of a 1:1 Th^{IV}:$DTPA^{5-}$ system as a function of pH using the *JCHESS* code.[4] Total [Th^{IV}] = total [$DTPA^{5-}$] = 5 mM. Only aqueous species are shown. Thermodynamic data obtained from the integrated *JCHESS* database and Martell and Smith.[3]

The ^{1}H-NMR spectra obtained for the effect of pD on the 1:1 Th^{IV}:$DTPA^{5-}$ system show signals between 3.55 and 3.75 ppm (integrates to 8 protons) and between 3.4 and 3.55 ppm (integrates to 2 protons), which correspond to the bound terminal acetate arms and the central acetate arm of $DTPA^{5-}$, respectively (Figure 5.20). The signals at 3.1, 2.8 and 2.6 ppm (integrate to 4:2:2 protons, respectively), are representative of the bound ethylene arms of $DTPA^{5-}$. Similar to the $[Ln(DTPA)]^{2-}$ ^{1}H-NMR spectra (Section 4.2), it is likely that the signals are broadened due to the $DTPA^{5-}$ ligand interchanging its coordination mode between octa- and heptadentate.[9] The $DTPA^{5-}$ ligand remains coordinated to the Th^{IV} ion approximately over the pD range 3 to 12. At pD values greater than 13.3, the ^{1}H-NMR signals are representative of unbound $DTPA^{5-}$, and $Th(OH)_{4(s)}$ precipitates out of solution.

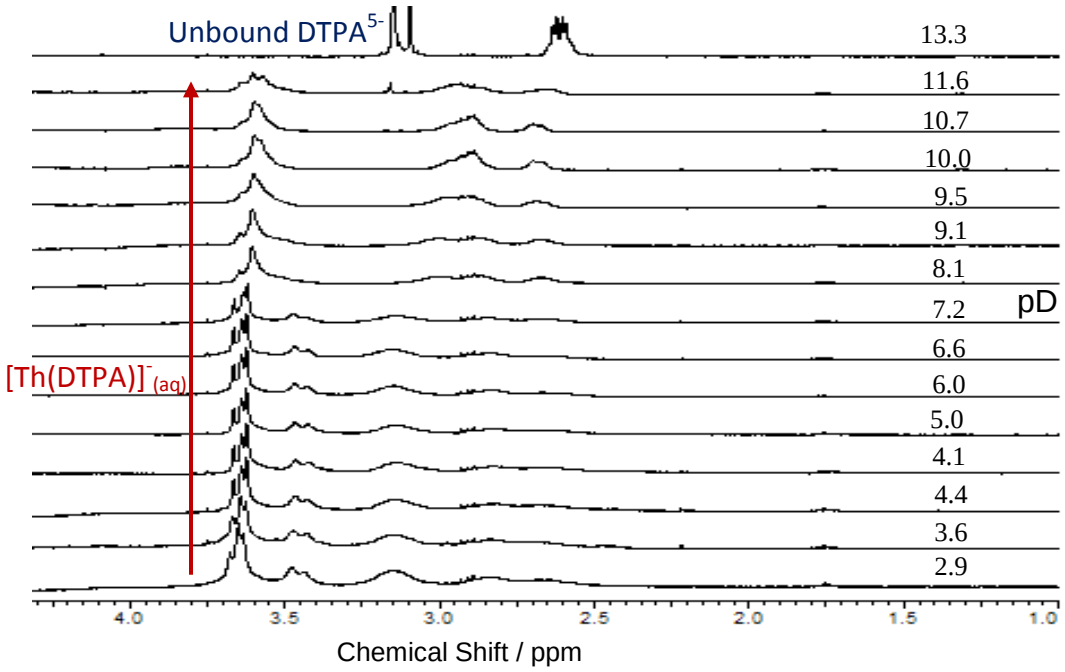

Figure 5.20: ^{1}H-NMR spectra for the effect of pD on the 1:1 Th^{IV}:$DTPA^{5-}$ system; $[Th^{IV}]_i = [DTPA^{5-}]_i = 10$ mM.

5.6 Th^{IV}-DTPA-Lactate Ternary System

The interaction of lactate with the $[Th(DTPA)]^-_{(aq)}$ complex has been probed using NMR spectroscopy. The ^{1}H-NMR spectra of a 1:1:1 Th^{IV}:$DTPA^{5-}$:lactate system show the same chemical shifts for the bound acetate and ethylene protons of $DTPA^{5-}$ (Figure 5.21) as described in Section 5.5. Over the pD range 2.5 to 5.5, the signal at 4.40 ppm shifts to 4.10 ppm and the signal at 1.40 ppm shifts to 1.30 ppm (Figure 5.22). These signals correspond to the –C**H(**OH)- proton and the –C**H$_3$** protons of lactate, and the pD dependent shift of these signals is due to the change in protonation state of lactic acid. The -C**H(**OH)- proton signal at 4.10 ppm is broadened over the pD range 4.2 to 10.7, which may imply that lactate is interacting with the $[Th(DTPA)]^-_{(aq)}$ complex. A change in the $DTPA^{5-}$ splitting pattern is not observed, unlike $EDTA^{4-}$ in the 1:1:1 Th^{IV}:$EDTA^{4-}$:lactate system (Figure 5.15). However, the $DTPA^{5-}$ signals in the ^{1}H-NMR of the 1:1:1 Th^{IV}:$DTPA^{5-}$:lactate system are already broadened due to intramolecular rearrangement of the $[Th(DTPA)]^-_{(aq)}$ complex in solution,[9] so any change of the $DTPA^{5-}$ splitting pattern in the ^{1}H-NMR spectra would be difficult to observe.

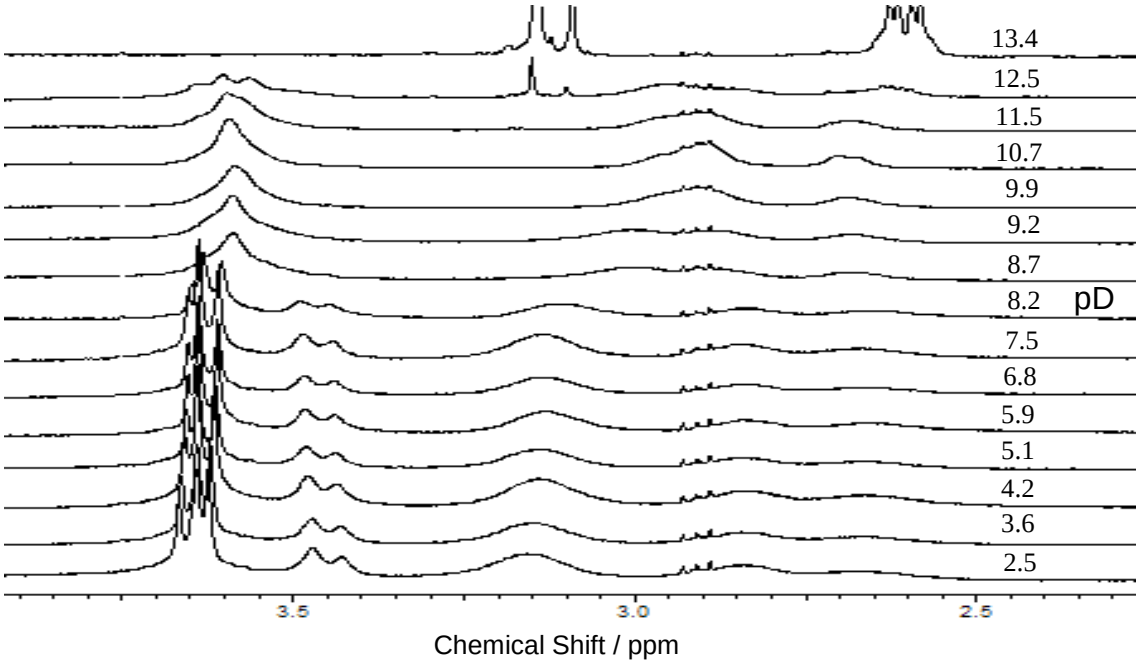

Figure 5.21: ^{1}H-NMR spectra of the $DTPA^{5-}$ signals for the effect of pD on the 1:1:1 Th^{IV}:$DTPA^{5-}$:lactate system; $[Th^{IV}]_i = [DTPA^{5-}]_i = [lactate]_i = 10$ mM.

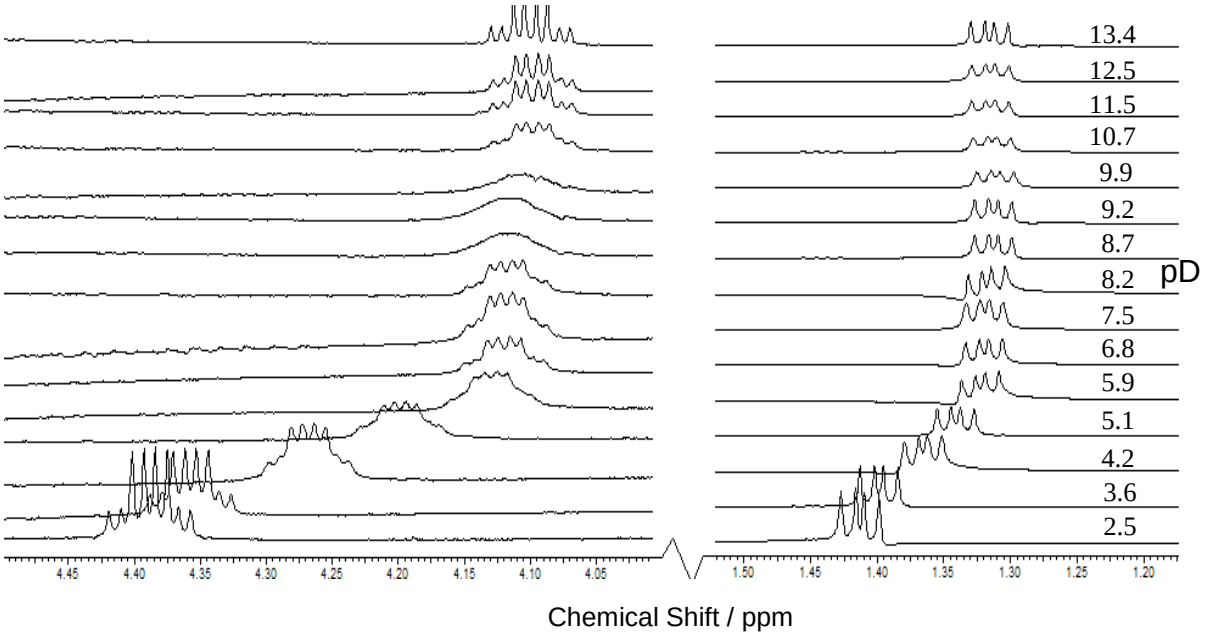

Figure 5.22: ^{1}H-NMR spectra of the lactate signals for the effect of pD on the 1:1:1 Th^{IV}:$DTPA^{5-}$:lactate system; $[Th^{IV}]_i = [DTPA^{5-}]_i = [lactate]_i = 10$ mM.

The corresponding ^{13}C-NMR spectra obtained to study the effect of pD on the 1:1:1 Th^{IV}:$DTPA^{5-}$:lactate system are shown in Figure 5.23. Monitoring the shift of the lactate carboxylate group by ^{13}C-NMR spectroscopy shows a change in the chemical shift from 179.3 to 183.2 ppm over the pD range 2.5 to 8.1. This is likely to be due to the deprotonation of lactic acid to form lactate. The observed broadening of the carboxylate signal between pD 2.5 to 10.0, indicates that lactate interacts with the $[Th(DTPA)]^-_{(aq)}$ complex. Broadening of the carboxylate signal is not observed in the free ligand ^{13}C-NMR spectra (Figure 5.13). At pD 11.6, the carboxylate signal becomes better resolved, similar to that of the free ligand, suggesting lactate has been displaced from the inner sphere of the $[Th(DTPA)]^-_{(aq)}$ complex, probably by hydroxide anions.

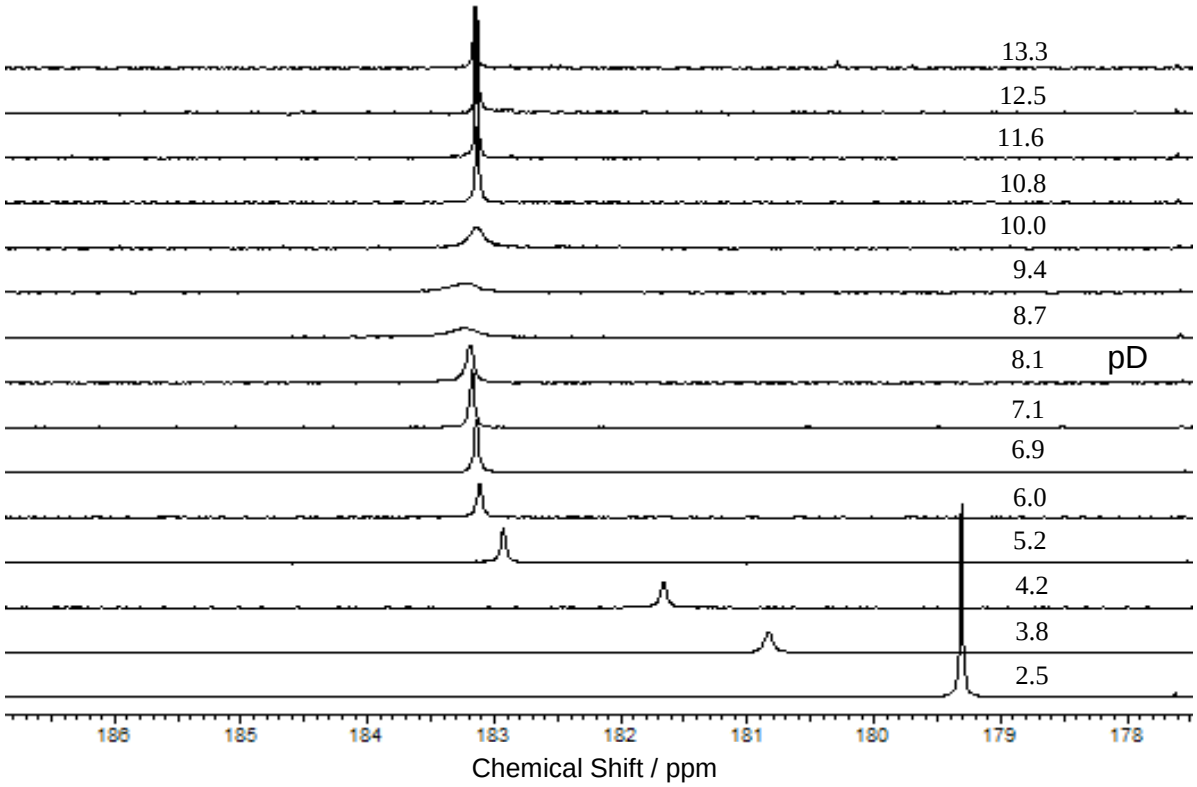

Figure 5.23: ^{13}C-NMR spectra for the effect of pD on the 1:1:1 Th^{IV}:$DTPA^{5-}$:lactate system; $[Th^{IV}]_i = [DTPA^{5-}]_i = [lactate]_i = 10$ mM.

5.6.1 Summary

The interaction of lactate with the $[Th(DTPA)]^{-}_{(aq)}$ has been shown to occur using NMR spectroscopy. Possible structures of the $[Th(DTPA)(lactate)]^{2-}_{(aq)}$ species are shown in Figure 5.24. The structures take into account that $DTPA^{5-}$ may coordinate to the Th^{IV} ion as an octa- and heptadentate ligand, and the lactate hydroxyl group may participate in hydrogen bonding to an acetate group on $DTPA^{5-}$.[7] It is unknown if, or how many, water molecules may complete the inner coordination sphere of the Th^{IV} ion.

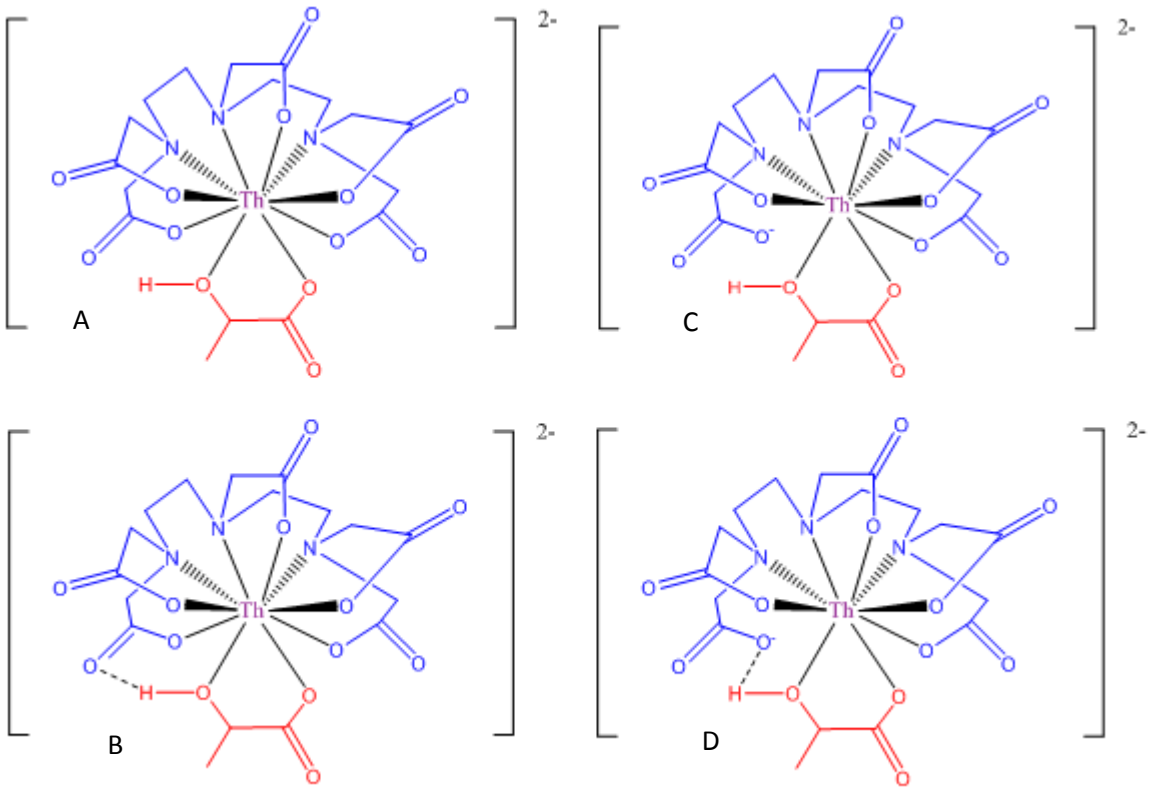

Figure 5.24: Possible structures of the $[Th(DTPA)(lactate)]^{2-}_{(aq)}$ complex where: A) octadentate coordination mode of $DTPA^{5-}$; B) octadentate coordination mode of $DTPA^{5-}$ and H-bonding of lactate to acetate group of $DTPA^{5-}$; C) heptadentate coordination mode of $DTPA^{5-}$ and D) heptadentate coordination mode of $DTPA^{5-}$ and H-bonding of lactate to acetate group of $DTPA^{5-}$.

[Note: coordinated water molecules or hydroxide ions are not shown].

5.7 Th^{IV}-DTPA-Carbonate Ternary System

The formation of the $[Th(EDTA)(CO_3)]^{2-}_{(aq)}$ and $[Th(EDTA)(CO_3)_2]^{4-}_{(aq)}$ complexes were shown to exist in Section 5.2. The possible formation of ternary complexes using $DTPA^{5-}$ as the organic ligand was probed by NMR spectroscopy to observe whether carbonate would still be able to interact with Th^{IV} when encapsulated by a ligand capable of octadentate binding. The ^{1}H-NMR spectra of the 1:1:1 Th^{IV}:$DTPA^{5-}$:CO_3^{2-} system (Figure F, Appendix 3) show that $DTPA^{5-}$ can coordinate to the Th^{IV} ion up to pD 12.8, after which hydrolysis occurs and $DTPA^{5-}$ is observed predominantly in the unbound form.

The carbonate source used in these experiments was ^{13}C-labelled carbonate, as described in Section 3.2.2. ^{13}C-NMR spectra recorded for the 1:1:1 Th^{IV}:$DTPA^{5-}$:CO_3^{2-} system (Figure 5.25) show a carbonate signal at 168 ppm that shifts with pD to 169 ppm. The signal is broadened over the pD range 9.4 to 12.9, indicating that carbonate may be exchanging between being free and bound to the Th^{IV} ion in the $[Th(DTPA)]^-_{(aq)}$ complex. Above pD 12.9, the carbonate signal becomes better resolved, which implies that carbonate has been displaced from the Th^{IV} ion coordination sphere, probably by hydroxide.

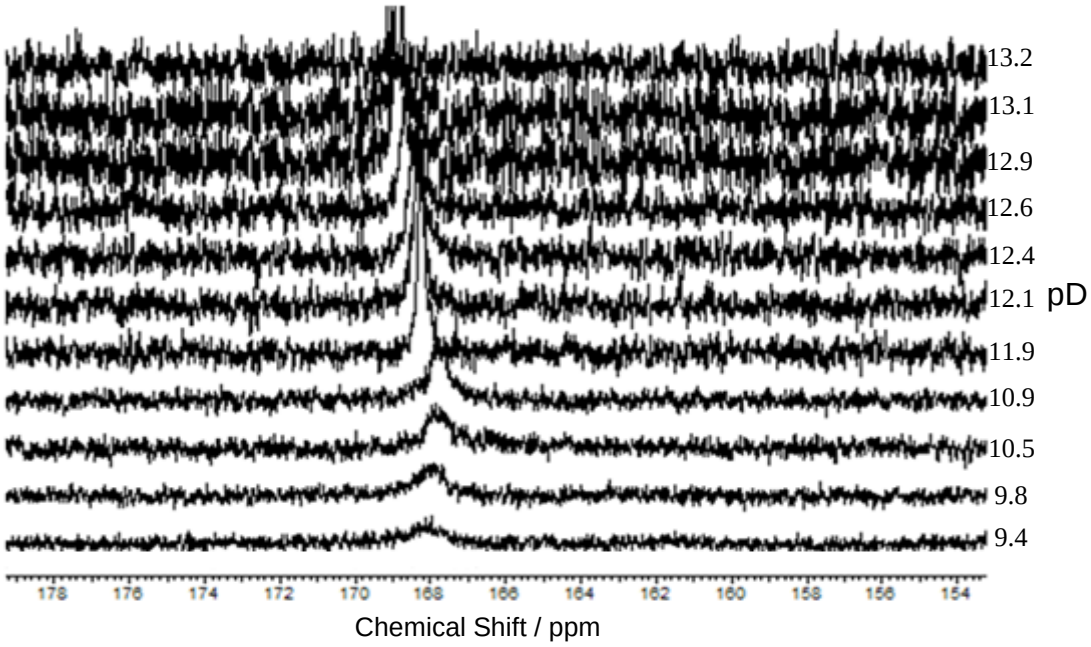

Figure 5.25: ^{13}C-NMR spectra for the effect of pD on the 1:1:1 Th^{IV}:$DTPA^{5-}$:CO_3^{2-} system; $[Th^{IV}]_i = [DTPA^{5-}]_i = [CO_3^{2-}]_i = 10$ mM.

Two carbonate anions were shown to be able to bind to the $[Th(EDTA)]_{(aq)}$ complex in Section 5.2. Therefore, the carbonate coordination behaviour in the 1:1:2 Th^{IV}:$DTPA^{5-}$:CO_3^{2-} system was probed by NMR spectroscopy to observe if two carbonate anions would still be able to coordinate to the Th^{IV} ion, when the steric hindrance imposed by the organic ligand has been increased by changing the denticity from hexa- to octadentate. The ^{1}H-NMR spectra obtained for the 1:1:2 Th^{IV}:$DTPA^{5-}$:CO_3^{2-} system (Figure G, Appendix 3) show that $DTPA^{5-}$ is coordinated to the Th^{IV} ion up to pD 12.2, after which hydrolysis occurs and $DTPA^{5-}$ is observed predominantly unbound in the system.

The ^{13}C-NMR spectrum recorded at pD 9.9 of the 1:1:2 Th^{IV}:$DTPA^{5-}$:CO_3^{2-} system (Figure 5.26) shows two carbonate signals at approximately 168 and 162 ppm. The peak at 168 ppm is characteristic of bound carbonate, whilst the signal at 162 ppm is representative of unbound carbonate. This suggests that a ternary $[Th(DTPA)(CO_3)]^{3-}_{(aq)}$ complex does exist as both bound and unbound carbonate signals are present in the spectra. The observed broadening of the carbonate signals is likely to be caused by an exchange process between the carbonate anion being bound to the $[Th(DTPA)]^-_{(aq)}$ complex and being unbound in solution. It is unlikely that two carbonate anions are bound to the $[Th(DTPA)]^-_{(aq)}$ complex as two separate resonances are observed. As pD is increased, the two carbonate resonances coalesce and become more resolved. This implies that carbonate has been replaced from the $[Th(DTPA)]^-_{(aq)}$ coordination sphere, probably by hydroxide.

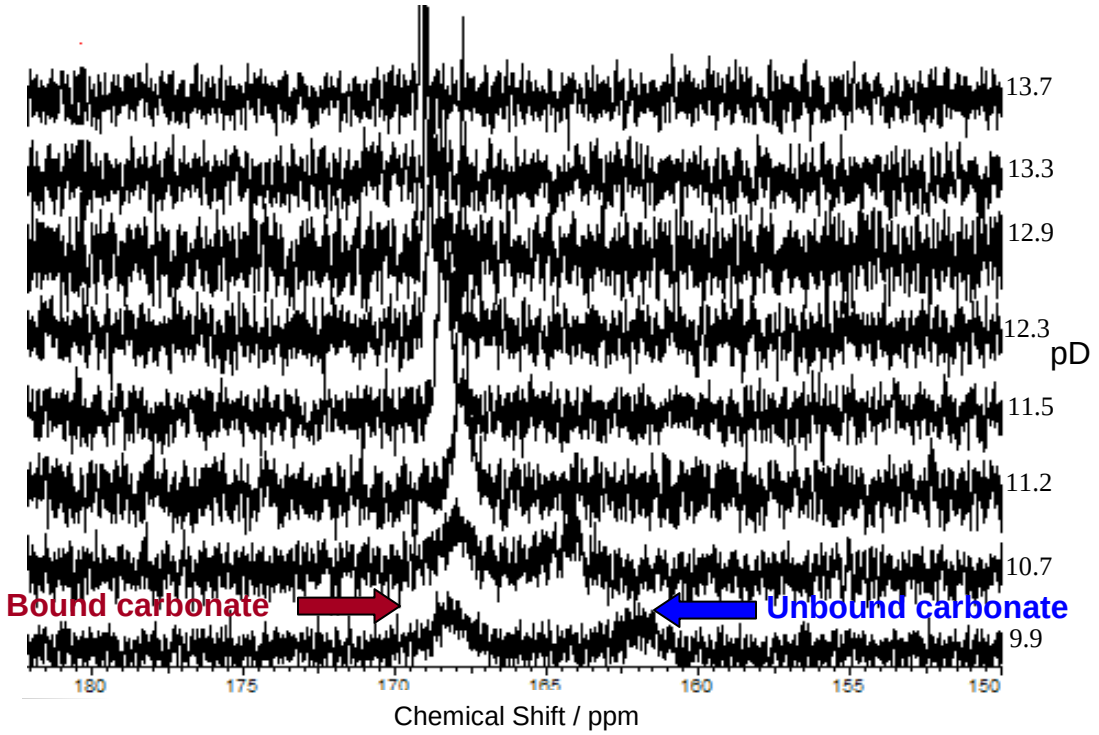

Figure 5.26: 'Zoom-in' of the carbonate signals present in the ^{13}C-NMR spectra for the effect of pD on the 1:1:2 Th^{IV}:$DTPA^{5-}$:CO_3^{2-} system; $[Th^{IV}]_i = [DTPA^{5-}]_i$ =10 mM; $[CO_3^{2-}]_i$ = 20 mM.

Structures for the $[Th(DTPA)(CO_3)]^{3-}_{(aq)}$ species observed by NMR spectroscopy have been postulated and are presented in Figure 5.27. The structures consider that $DTPA^{5-}$ may coordinate to the Th^{IV} ion as an octa- and heptadentate ligand. It is unknown if, or how many, H_2O molecules or OH^- anions may complete the inner coordination sphere of the Th^{IV} ion.

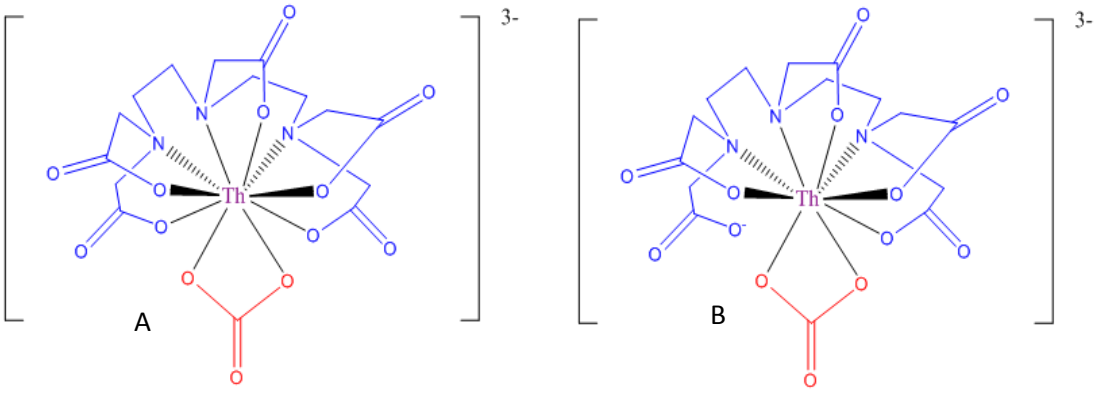

Figure 5.27: Possible structures for the $[Th(DTPA)(CO_3)]^{3-}_{(aq)}$ species where: A) octadentate coordination mode of $DTPA^{5-}$ and B) heptadentate coordination mode of $DTPA^{5-}$.

[Note: coordinated water molecules or hydroxide ions are not shown].

5.8 Summary

Thorium typically exists in the tetravalent oxidation state and also has a smaller ionic radius than the trivalent lanthanide ions.[10] The charge density of the Th^{IV} ion is greater than that of the trivalent lanthanide ions (*i.e.* 0.148 a.u. *vs.* average 0.08 a.u.). This high charge density of the Th^{IV} cation causes it to have an increased electrostatic attraction to hard donor atoms, such as oxygen. The combination of the high charge density of the Th^{IV} ion and its tendency to accommodate a high number of donor atoms allows the formation of the following ternary complexes: $[Th(EDTA)(CO_3)]^{2-}_{(aq)}$; $[Th(EDTA)(CO_3)_2]^{4-}_{(aq)}$; $[Th(EDTA)(lactate)]^{-}_{(aq)}$; $[Th(DTPA)(lactate)]^{2-}_{(aq)}$ and $[Th(DTPA)(CO_3)]^{3-}_{(aq)}$. The analogous Ln^{III} ternary complexes of $[Ln(EDTA)(CO_3)_2]^{5-}_{(aq)}$ may not form as the charge density is not great enough.

On formation of the $[Th(EDTA)(CO_3)]^{2-}_{(aq)}$ and $[Th(EDTA)(CO_3)_2]^{4-}_{(aq)}$ complexes, it is likely that $EDTA^{4-}$ is predominantly bound in a hexadentate manner and the carbonate anions are coordinated in a bidentate mode. When the $[Th(EDTA)(lactate)]^{-}_{(aq)}$ complex forms, the NMR evidence suggests that the coordination mode of lactate is different to carbonate because there are multiple overlapping signals for the $EDTA^{4-}$ resonances, which were not observed in the 1:1 Th^{IV}:$EDTA^{4-}$ or 1:1:x Th^{IV}:$EDTA^{4-}$:CO_3^{2-} systems (where x = 1 to 3). The $EDTA^{4-}$ ligand may alter its binding mode from hexadentate to pentadentate in order to accommodate the larger bite angle of lactate (*cf.* carbonate) into the Th^{IV} ion coordination sphere (Figure 5.28). The hydroxyl group of lactate may also participate in H-bonding to the acetate groups of $EDTA^{4-}$.[7]

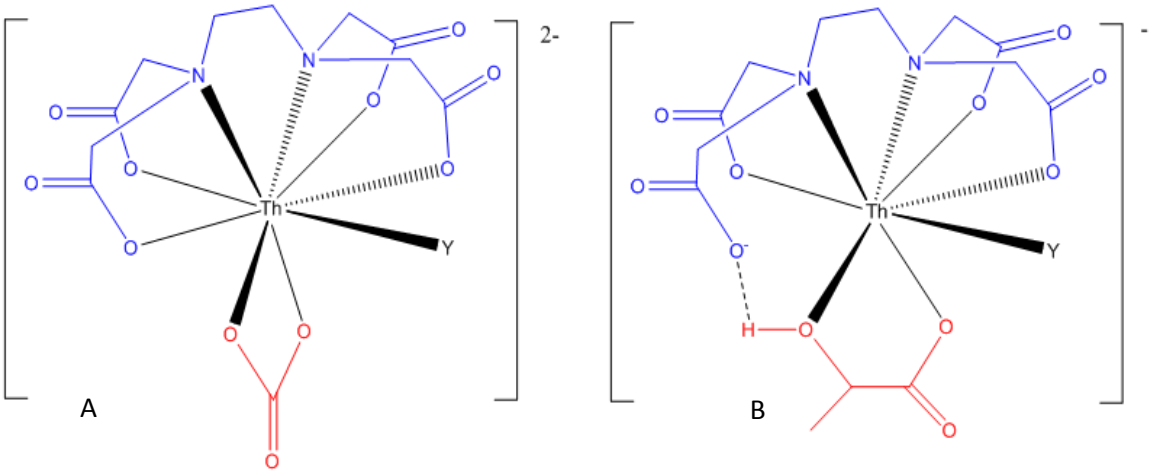

Figure 5.28: Possible structures for the: A) $[Th(EDTA)(CO_3)]^{2-}_{(aq)}$ species and B) $[Th(EDTA)(lactate)]^{-}_{(aq)}$ species. Y represents possible coordinated water molecules or hydroxide ions.

On increasing the denticity of the organic ligand coordinated to the Th^{IV} ion from hexa- to octadentate, the lactate and carbonate ligands can still bind to Th^{IV} to form the $[Th(DTPA)(lactate)]^{2-}_{(aq)}$ and $[Th(DTPA)(CO_3)]^{3-}_{(aq)}$ species. It is likely that the interaction of these secondary ligands is stronger for the Th^{IV} ion than the trivalent lanthanides, which is exemplified by bound and unbound carbonate signals observed in the ^{13}C-NMR spectra of the 1:1:2 Th^{IV}:$DTPA^{5-}$:CO_3^{2-} system but not in the Ln^{III} systems. Even though the Th^{IV} ion has a tendency to coordinate a high number of donor atoms, two carbonate anions were not observed to bind to the $[Th(DTPA)]^{-}_{(aq)}$ complex (*cf.* $[Th(EDTA)]_{(aq)}$). Therefore, the inner coordination sphere of the Th^{IV} ion in the $[Th(DTPA)(CO_3)]^{3-}_{(aq)}$ species is likely to be saturated.

The next chapter will focus on the formation of ternary complexes, with the trivalent minor actinides of americium and curium.

[1] S. Cotton, *Lanthanide and Actinide Chemistry*, John Wiley & Sons, Ltd., U.K., 2006, 173-199.

[2] S. R. Daly, P. M. B. Piccoli, A. J. Schultz, T. K. Todorova, L. Gagliardi and G. S. Girolami, *Angew. Chem. Int. Ed.*, 2010, **49**, 3379–3381.

[3] R. Smith and A. Martell, *Critical Stability Constants*, Volumes 1 and 4: Inorganic Complexes, Plenum Press, New York, 1976.

[4] J. Van der Lee, A Users Guide to CHESS, Another Speciation and Surface Complexation Computer Code, E´cole des Mi1nes de Paris, Fontainebleau, 1998.

[5] R. Agarwal, I. Chakraborti and N. Sharma, *Iran. J. Chem. & Chem. Eng.*, 2002, **21**, 104-109.

[6] L. Zhu, X. Zhu, Y. Zhang, B. Li, Z. Cao and Y. Zhang, *J. Mol. Struct.*, 2003, **657**, 375-380.

[7] P. Gale, *Coord. Chem. Rev.*, 2003, **240**, 191- 221.

[8] M. Nilsson and K. Nash, *Solvent Extr. Ion Exc.*, 2007, **25**, 665–701.

[9] S. Aime and M. Botta, *Inorg. Chim. Acta*, 1990, **177**,101-105.

[10] C. Housecroft and A. Sharpe, *Inorganic Chemistry*, Second Edition, Pearson Education Ltd., UK, 2005, 741-761.

Chapter 6

Minor Actinide Binary and Ternary Systems Relevant to the Nuclear Fuel Cycle

6.0 Introduction

The focus of this project is to help determine actinide speciation (*i.e.* Am^{III}, Cm^{III}) in the nuclear waste storage ponds and in the TALSPEAK process. The speciation of the metal ions in the waste ponds is complicated by many influencing factors such as pH, E_h, carbonate anions, organic ligands and mineral surfaces. The solubility of actinide ions in the ponds is greater than expected for the conditions present,[1] and the formation of ternary complexes (*i.e.* $[An(organic)(inorganic)]^{n-}$ may be responsible for the increased actinide solubility in this aqueous system. Similarly, the formation of ternary complexes (*i.e.* $[M(DTPA)(lactate)]^{3-}_{(aq)}$; M =$An^{III}$/$Ln^{III}$) has been hypothesised to occur in the TALSPEAK process.[2] The formation of these ternary complexes may increase the separation factors of the actinides from the lanthanides.[3]

Chapters 3 and 4 described the solution behaviour of the lanthanide-$EDTA^{4-}$/$DTPA^{5-}$ binary systems and the lanthanide-$EDTA^{4-}$/$DTPA^{5-}$-carbonate/lactate ternary systems, which were analysed by the techniques of NMR, UV-Vis and luminescence spectroscopies. These studies showed that $[Ln(EDTA)]^{-}_{(aq)}$ and $[Ln(DTPA)]^{2-}_{(aq)}$ complexes dominate the Ln^{III} ion speciation over the pH range 2 to 11 in the binary systems. Above pH values of 11, hydrolysis products form (*i.e.* $[Ln(EDTA)(OH)]^{2-}_{(aq)}$ and $Ln(OH)_{3(s)}$). In the presence of carbonate, $[Ln(EDTA)(CO_3)]^{3-}_{(aq)}$ and $[Lu(DTPA)(CO_3)]^{4-}_{(aq)}$ species predominantly exist over the pH range 8 to 11. The coordination of carbonate to these complexes is likely to be in equilibrium with H_2O molecules or OH^- ions. Lactate may interact with $[Ln(EDTA)]^{-}_{(aq)}$ and $[Eu(DTPA)]^{2-}_{(aq)}$ complexes approximately over the pH range 4 to 9, though whether this interaction is primary or secondary sphere has yet to be established. As the trivalent lanthanides are considered to be chemically analogous to the trivalent actinides, it may be expected that similar ternary complexes can be formed with Am^{III} and Cm^{III}. This chapter

details the studies of the binary and ternary systems of Am^{III}, using both UV-Vis and luminescence spectroscopies, and of Cm^{III}, using UV-Vis only.

6.1 UV-Vis Spectroscopy

6.1.1 An^{III}-EDTA Binary Systems

6.1.1.1 Am^{III} and Cm^{III}

The complexation of Am^{III} and Cm^{III} with $EDTA^{4-}$ as a function of pH has been studied by UV-Vis absorption spectroscopy (Figures 6.1, 6.2 and 6.3). The absorption maximum (λ_{max}) of $Am(NO_3)_{3(aq)}$ is found at 503 nm, which corresponds to an electronic transition from the $^7F_0$ ground state to the $^5L_6$ excited state (Figure 6.4).[4,5] On complexation with $EDTA^{4-}$, a bathochromic shift of the λ_{max} for this transition occurs to 507 nm accompanied by an increase in the extinction coefficient. As the pH of this system is increased from approximately 3 to 11, a very small red-shift of the peak maximum occurs coupled with a broadening of the absorption profile. This may be due to a change in denticity of the $EDTA^{4-}$ ligand to the Am^{III} cation as $EDTA^{4-}$ becomes fully deprotonated (*i.e.* conversion from $HEDTA^{3-}$ to $EDTA^{4-}$). At pH values greater than 11, the extinction coefficient begins to decrease, which may be due to the formation of hydrolysis species (*i.e.* $[Am(EDTA)(OH)]^{2-}_{(aq)}$ and $Am(OH)_{3(s)}$). The precipitation of $An(OH)_{3(s)}$ (An = Am^{III} or Cm^{III}) was not directly observed in the experiments, possibly because low metal ion concentrations were used (*i.e.* x 10^{-5} M). However, the precipitation of small amounts of $An(OH)_{3(s)}$ must be considered to occur at high pH in all of the systems studied.

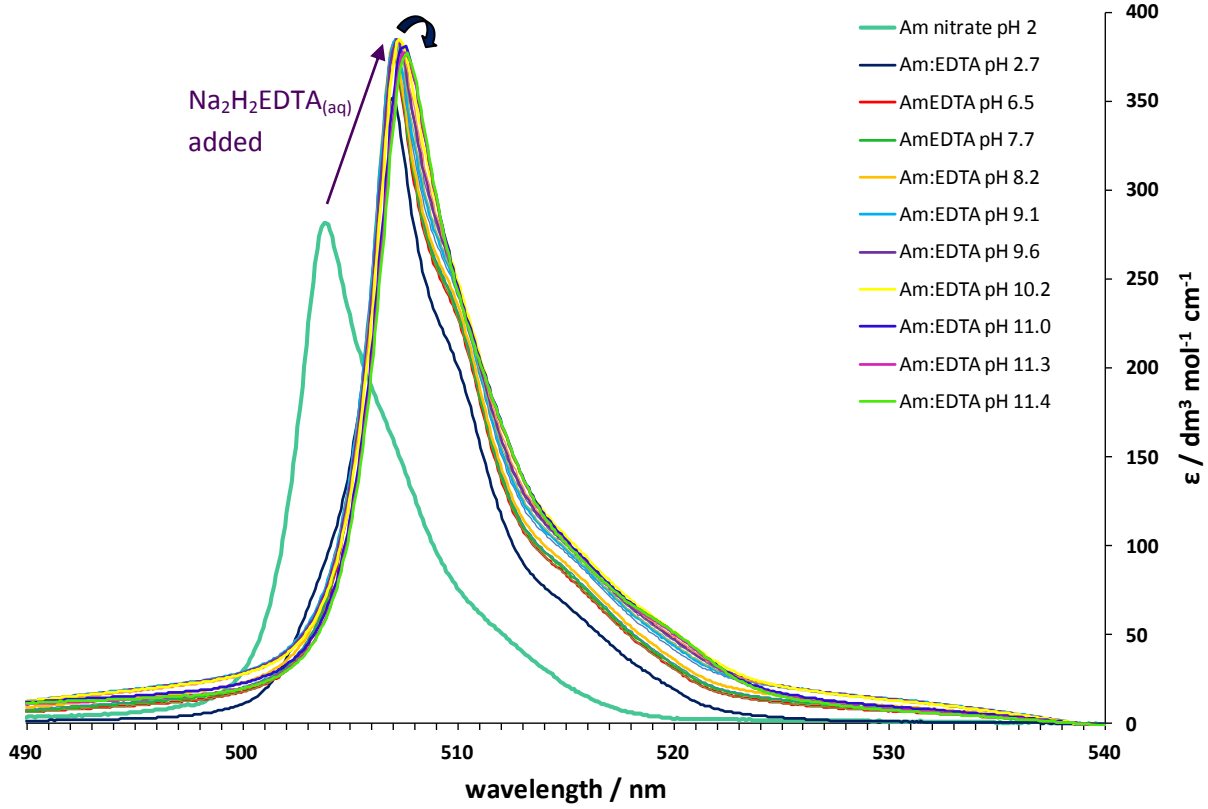

Figure 6.1: UV-Vis absorption spectra for the effect of pH on a 1:1 Am^{III}:$EDTA^{4-}$ system; $[Am^{III}]_i = [EDTA^{4-}]_i = 5 \times 10^{-5}$ M; I = 0.5 M $NaNO_3$.

All of the measured Cm^{III} spectra showed the presence of an absorption band that is broad relative to the individual Cm^{III} bands (Figure 6.2). This broad absorption has been previously observed in the literature, and has been attributed to radiation decomposition of the solvent with time.[6] All Cm^{III} spectra presented have been normalised in order to distinguish between changes in the Cm^{III} absorption profile and solvent decomposition. The Cm^{III} spectra show absorption bands at 377, 382, 397, 434 and 456 nm (Figure 6.3), of which the band at 397 nm corresponds to the electronic transition from the $^8S_{7/2}$ ground state to the $^6I_{17/2}$ excited state (Figure 6.4).[4,5] Raising the pH of the 1:1 Cm^{III}:$EDTA^{4-}$ system from pH 4.2 to 10.8 causes a red-shift, coupled with an increase in the extinction coefficient, of the Cm^{III} absorption profile. This is likely to represent the increase in the formation of the $[Cm(EDTA)]^-_{(aq)}$ complex. Above pH 10.8, the observed decrease in the extinction coefficient of the Cm^{III} spectra is indicative of the formation of Cm hydrolysis species (*e.g.* $[Cm(EDTA)(OH)]^{2-}_{(aq)}$ or $Cm(OH)_{3(s)}$).

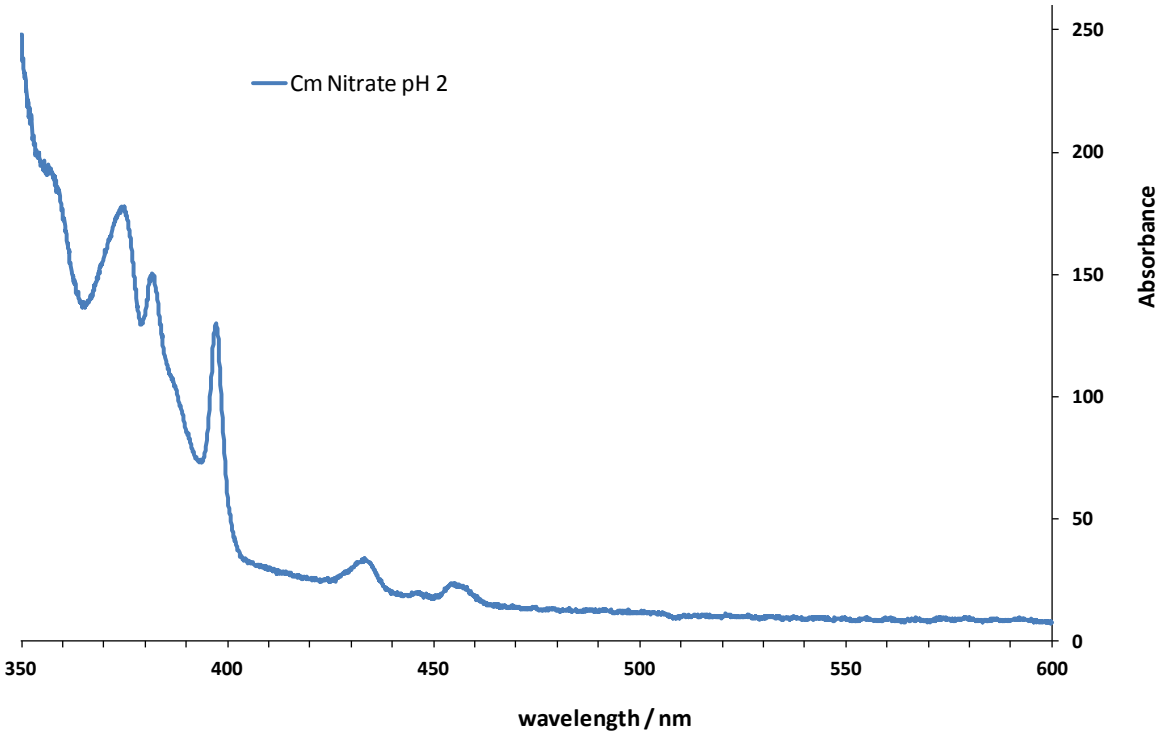

Figure 6.2: UV-Vis absorption spectrum of $Cm(NO_3)_{3(aq)}$ at pH 2; $[Cm^{III}]_i$ = 2 x 10^{-5} M; I = 0.5 M $NaNO_3$.

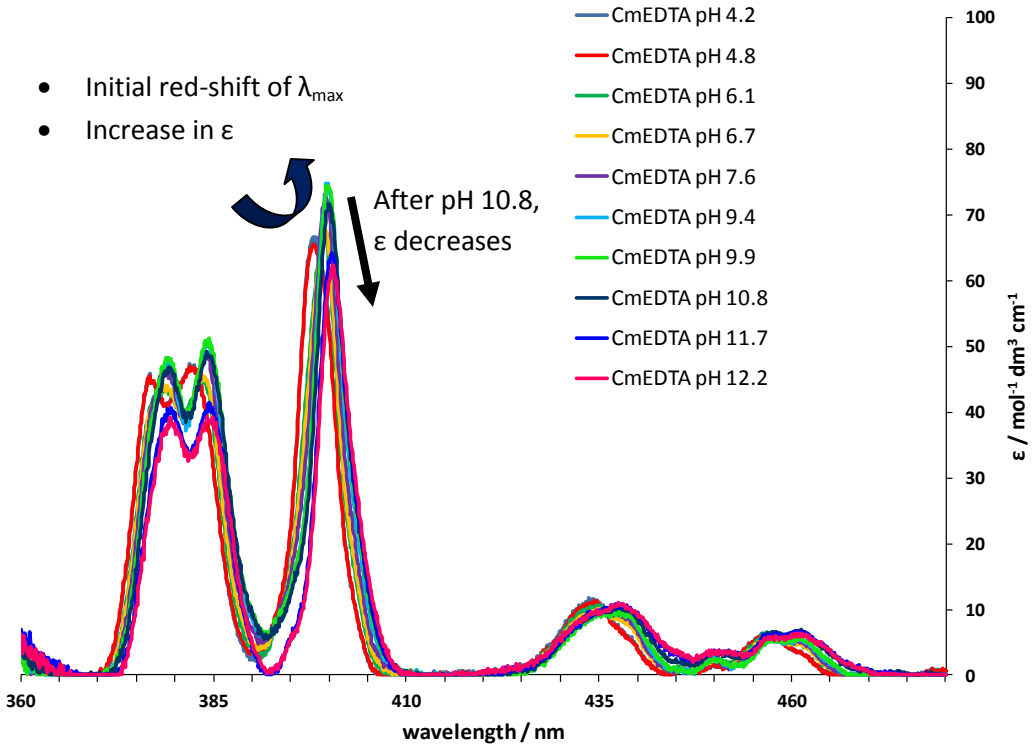

Figure 6.3: Normalised UV-Vis absorption spectra for the effect of pH on a 1:1 Cm^{III}:$EDTA^{4-}$ system; $[Cm^{III}]_i = [EDTA^{4-}]_i$ = 2 x 10^{-5} M; I = 0.5 M $NaNO_3$.

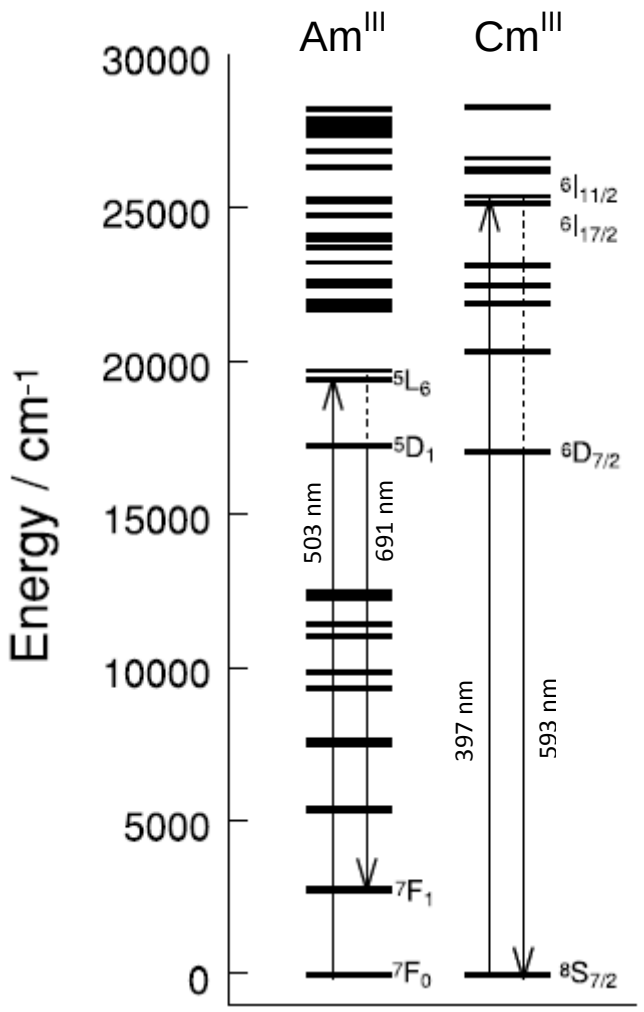

Figure 6.4: Energy-level diagram of Am^{III} and Cm^{III} ions, with their absorption and emission wavelengths. The up and down arrows denote the absorption and emission processes, respectively. [Taken from Reference 5].

6.1.2 An^{III}-EDTA-Carbonate Ternary Systems

6.1.2.1 Am^{III} and Cm^{III}

The UV-Vis absorption spectra of a 1:1 An^{III}:$EDTA^{4-}$ system (where An = Am or Cm) have been measured as a function of carbonate concentration at pH 10 ± 0.5, adjusted using NaOH or HNO_3 (Figures 6.5 and 6.6, respectively). The pH of the 1:1 An^{III}:$EDTA^{4-}$ systems were initially increased to approximately pH 10, using NaOH, before the addition of carbonate ions. This was done in order to prevent the conversion of $CO_3^{2-}{}_{(aq)}$ ions to $CO_{2(aq)}$ in acidic conditions. As the carbonate concentration is increased in the 1:1 An^{III}:$EDTA^{4-}$ systems, there is a growth in the extinction coefficient and a slight shift of the peak maximum. This indicates

the formation of the $[An(EDTA)(CO_3)]^{3-}_{(aq)}$ species, similar to the $[Ln(EDTA)(CO_3)]^{3-}_{(aq)}$ complexes discussed in Chapter 3. The extinction coefficient in the 1:1:X An^{III}:$EDTA^{4-}$:CO_3^{2-} system (where X = 0 to 2) continues to increase up to two equivalents of carbonate. This is likely to reflect the position of the equilibrium being favoured towards the formation of the $[An(EDTA)(CO_3)]^{3-}_{(aq)}$ species.

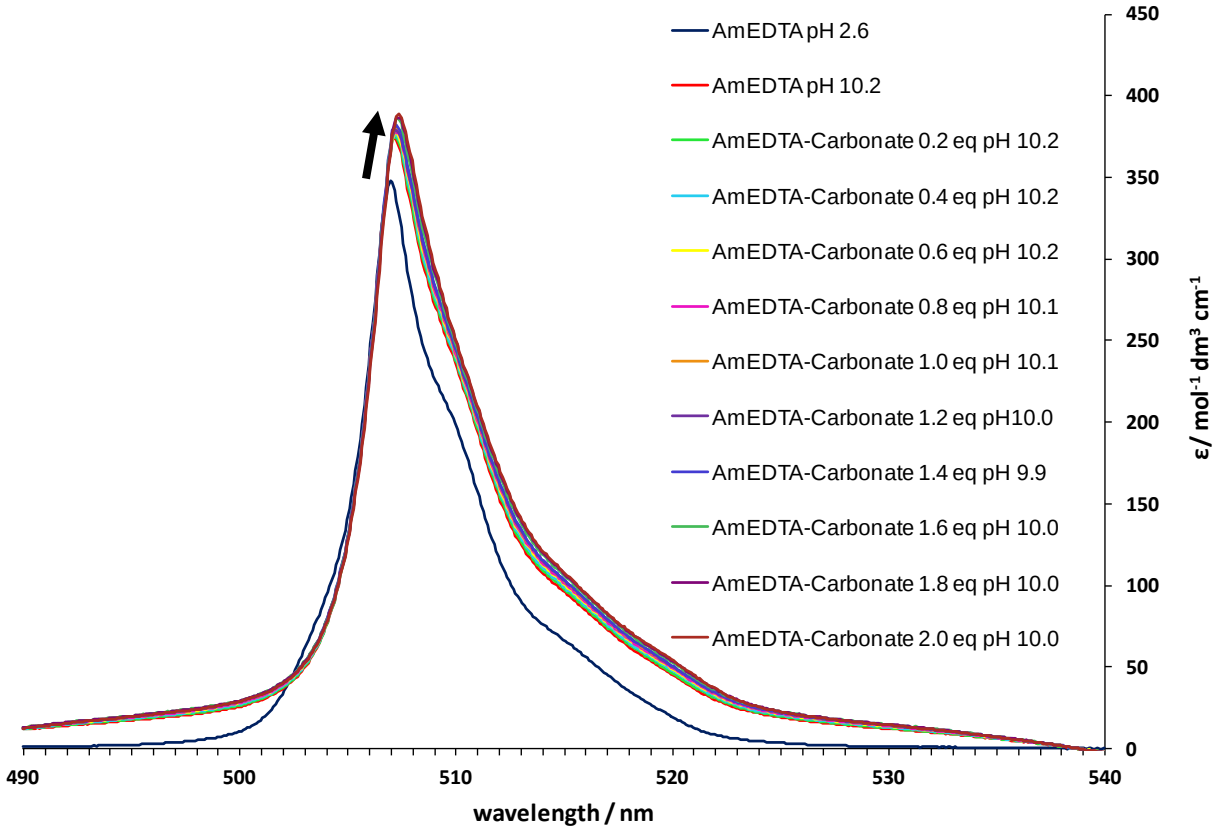

Figure 6.5: UV-Vis absorption spectra for a 1:1:x Am^{III}:$EDTA^{4-}$:CO_3^{2-} system (where x = 0 to 2 equivalents); $[Am^{III}]_i = [EDTA^{4-}]_i = [CO_3^{2-}]_i = 5 \times 10^{-5}$ M; pH = 10 ± 0.5; *I* = 0.5 M $NaNO_3$.

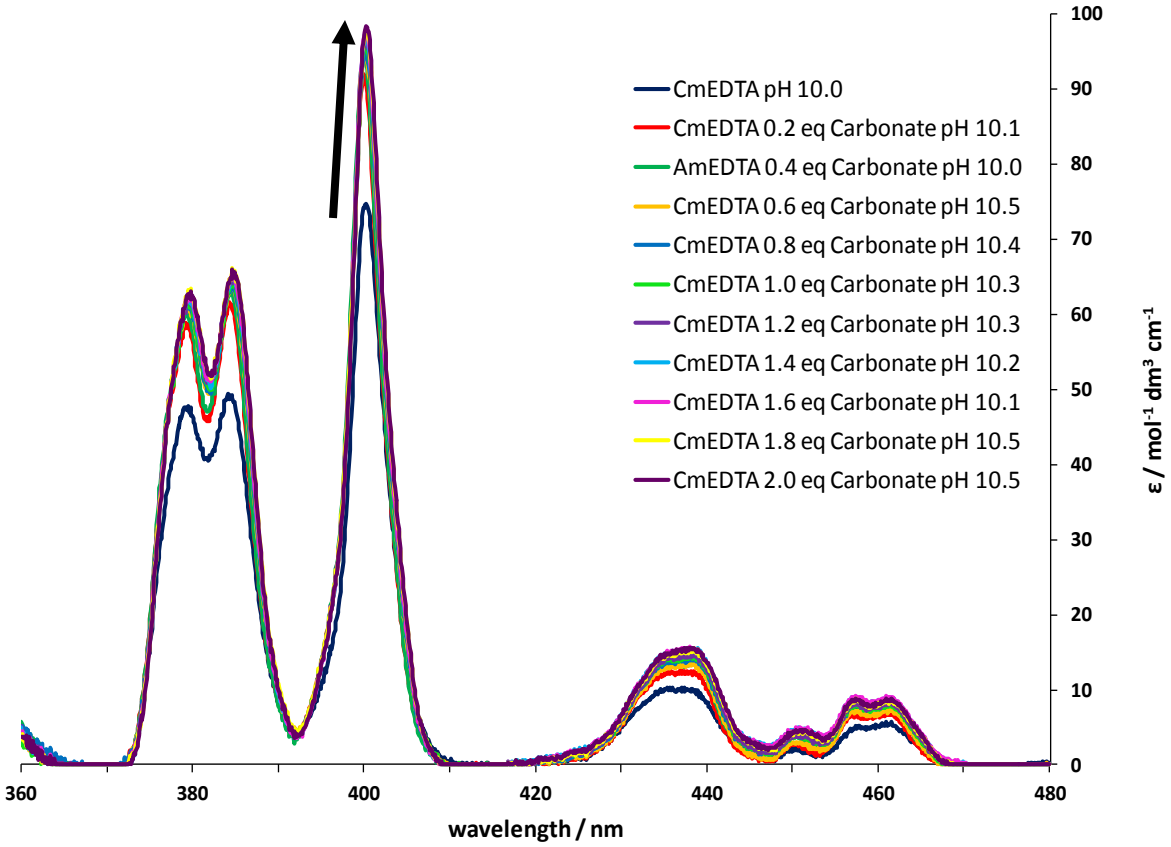

Figure 6.6: UV-Vis absorption spectra for a 1:1:x Cm^{III}:$EDTA^{4-}$:CO_3^{2-} system (where x = 0 to 2 equivalents); $[Cm^{III}]_i = [EDTA^{4-}]_i = [CO_3^{2-}]_i = 2 \times 10^{-5}$ M; pH = 10 ± 0.5; I = 0.5 M $NaNO_3$.

The effects of pH, adjusted using NaOH, on the absorption spectra of the 1:1:2 Am^{III}:$EDTA^{4-}$:CO_3^{2-} are shown in Figure 6.7. As pH is increased from 10 to 12, the extinction coefficient decreases, and a slight red-shift of the peak maximum occurs after pH 11. It is envisaged that the carbonate anion is replaced by hydroxide above pH 11, as observed in the Ln^{III} systems in Chapter 3.

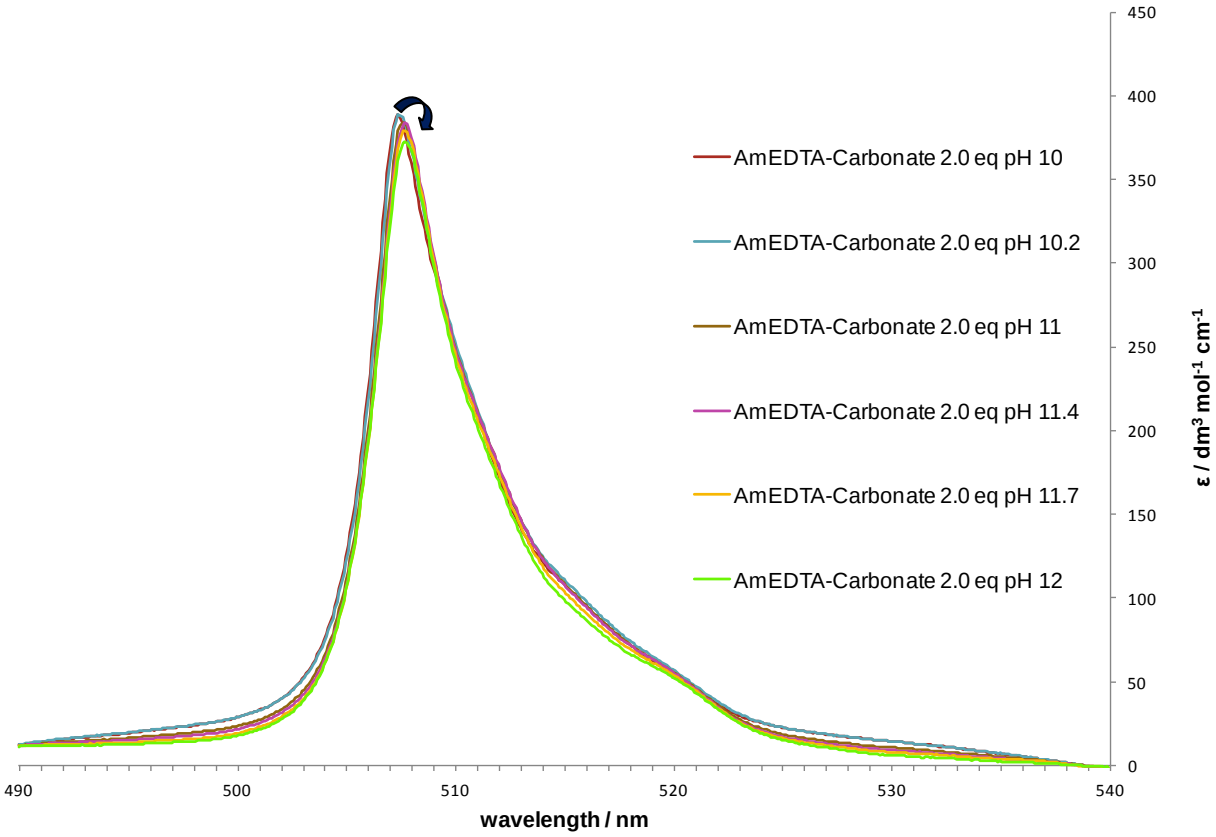

Figure 6.7: UV-Vis absorption spectra for the effect of pH on a 1:1:2 Am^{III}:$EDTA^{4-}$:CO_3^{2-} system; $[Am^{III}]_i = [EDTA^{4-}]_i = 5 \times 10^{-5}$ M; $[CO_3^{2-}]_i = 1 \times 10^{-4}$ M; I = 0.5 M $NaNO_3$.

6.1.3 Time Resolved Laser Induced Fluorescence Spectroscopy

6.1.3.1 Am^{III}

Time-resolved laser induced fluorescence spectroscopy (TRLIFS) can be used to study actinide complexation with ligands at trace metal concentrations.[7] There are few reports in the literature of Am^{III} luminescence. This is because Am^{III} has a lower luminescence intensity and faster luminescent lifetime than Cm^{III},[7] which is the minor actinide that tends to dominate luminescence work in the literature.[8,9]

The energy level diagram of the Am^{III} ion is presented in Figure 6.3. On excitation at 503 nm, the Am^{III} ion emits light of wavelength 691 nm.[10] The time-resolved emission spectra of the $Am^{III}_{(aq)}$ ion, obtained at pH 2 (Figure 6.8), show peaks at 694 nm and 833 nm, which are due to the $^5D_1 \rightarrow {}^7F_1$ and the $^5D_1 \rightarrow {}^7F_2$ transitions, respectively. The literature precedence is to

study the emission at 691 nm, therefore, only this band has been analysed in the work presented here.

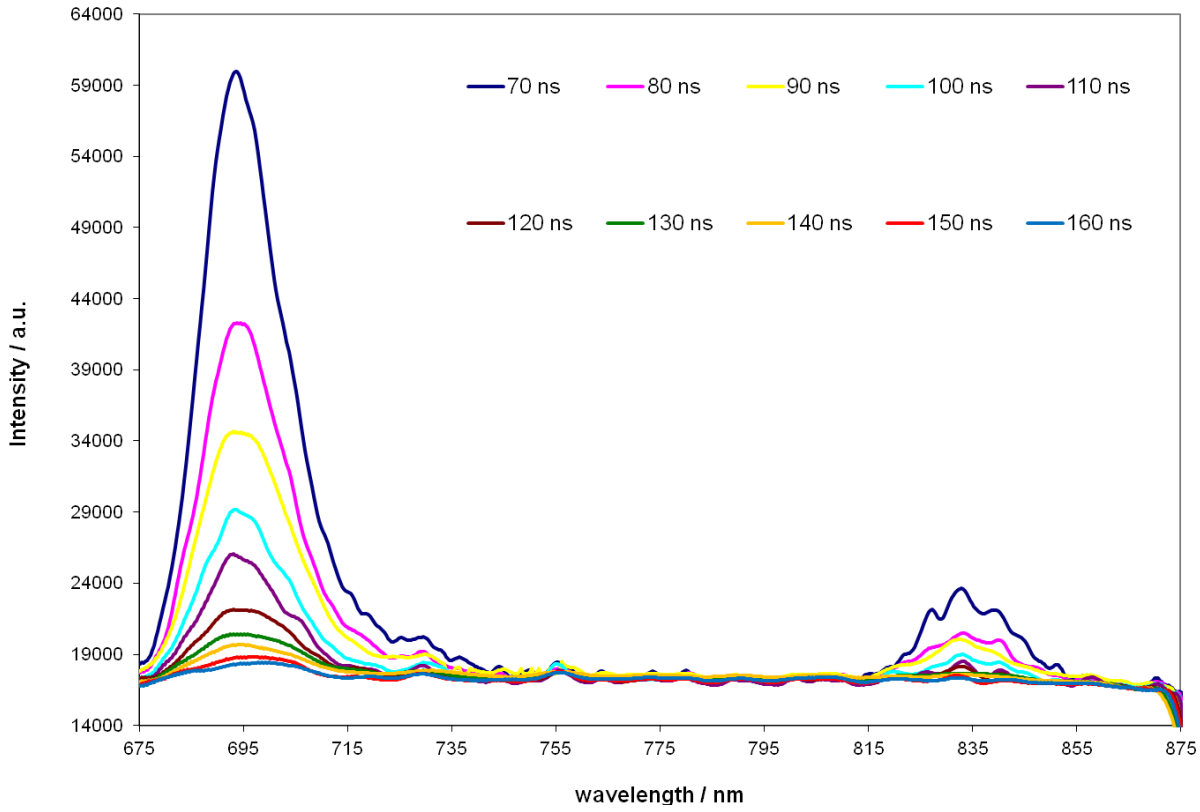

Figure 6.8: The time-resolved emission spectra of the $Am^{III}_{(aq)}$ ion at pH 2; $[Am^{III}] = 4 \times 10^{-4}$ M; I = 0.5 M $NaNO_3$.

A plot of the intensity of the signal at λ_{max} *vs*. the gate delay (Figure 6.9, using the left *y* axis) illustrates the exponential decay of the signal after each 10 ns delay. A plot of ln(intensity) *vs*. the gate delay (Figure 6.9, using the right *y* axis) gives a linear fit, from which the luminescent lifetime can be calculated using equation 6.1.

$$\tau = -\frac{1}{m}$$

(equation 6.1)

where:

τ = luminescent lifetime (ns); m = gradient.

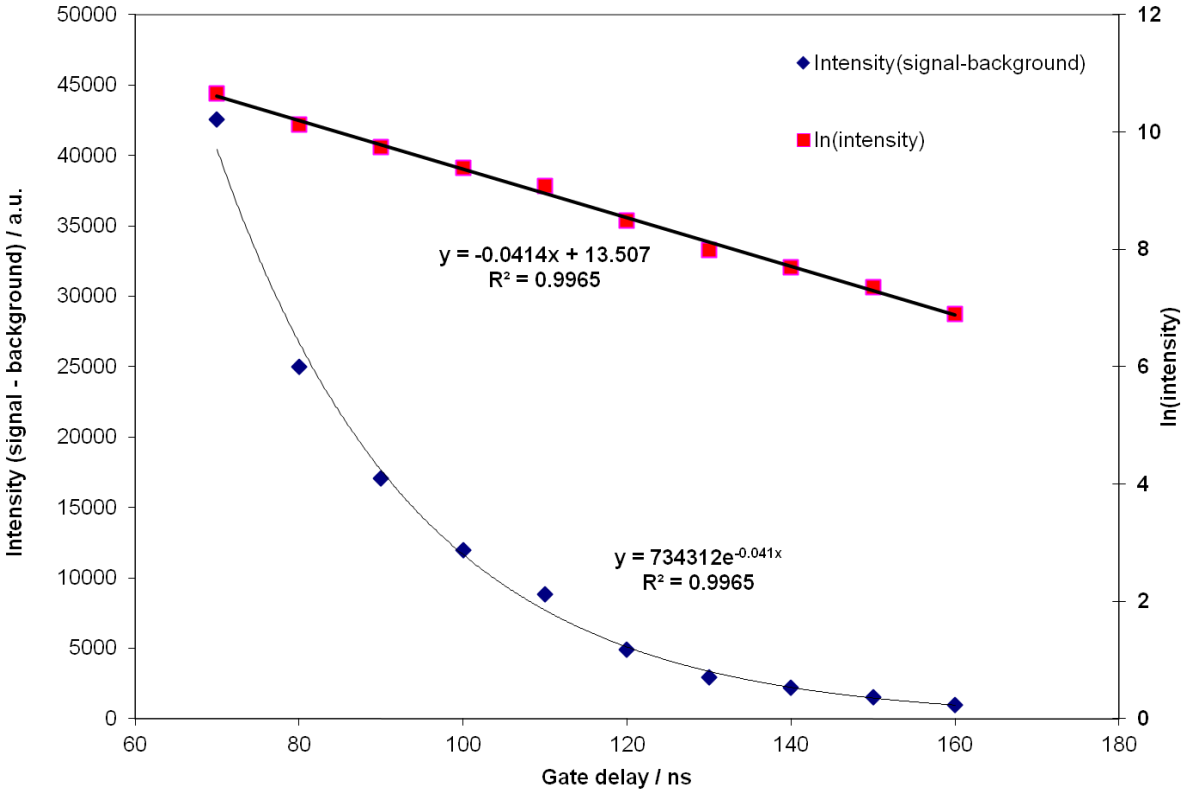

Figure 6.9: Plot of intensity of signal *vs.* gate delay (left *y* axis) and ln(intensity) *vs*. gate delay (right *y* axis).

The luminescent lifetime of the $Am^{III}_{(aq)}$ ion in 0.5 M $NaNO_3$ was calculated to be 24.1 ± 1.2 ns at room temperature (RT). This is in good agreement with literature values, which range from 22 to 25 ns at 22 to 25 ^{o}C in 0.01 M to 0.10 M $HClO_4$ solution.[5,11,12]

The inner-sphere hydration number of a metal ion can provide information on its coordination environment in solution.[5] Separate work performed by Kimura *et al.*[12] and Goodall *et al.*[13] have derived equations to calculate the N_{H_2O} coordinated to the Am^{III} ion from the luminescent lifetime. The ionic strength of the Am^{III} solutions in the Kimura work was 0.01 M $HClO_4$ (T = 25 ^{o}C),[12] and for the Goodall work, the ionic strength was 0.1 M $HClO_4$ (RT).[13] The equations are presented below as equations 6.2 (Kimura) and 6.3 (Goodall).

$$N_{H_2O} = \left(\frac{2.56 \times 10^{-7}}{\tau}\right) - 1.43$$

(*equation 6.2*)[11]

$$N_{H_2O} = \left(\frac{2.47 \times 10^{-7}}{\tau}\right) - 1.59$$

(*equation 6.3*)[12]

The value of the N_{H_2O} coordinated to the $Am^{III}_{(aq)}$ ion, using both equations 6.2 and 6.3, is calculated to be approximately nine (Table 6.1). There are reports in the literature that detail nine inner-sphere water molecules associated with the $Am^{III}_{(aq)}$ ion, characterised using absorption and luminescence spectroscopies, and ten water molecules coordinated to the $Am^{III}_{(aq)}$ ion determined by X-ray Absorption Fine Structure (XAFS) spectroscopy.[14] In 2001, Matonic *et al.* crystallized the $[Am(H_2O)_9]^{3+}_{(aq)}$ species in a tri-capped, trigonal prismatic geometry (Figure 6.10).[14,15] For the purposes of this work, it is assumed that the $Am^{III}_{(aq)}$ coordination number will be nine in 0.5 M $NaNO_3$.

N_{H_2O}	Equation
9.19	6.2
8.66	6.3

Table 6.1: Calculated number of coordinated water molecules to the $Am^{III}_{(aq)}$ ion.

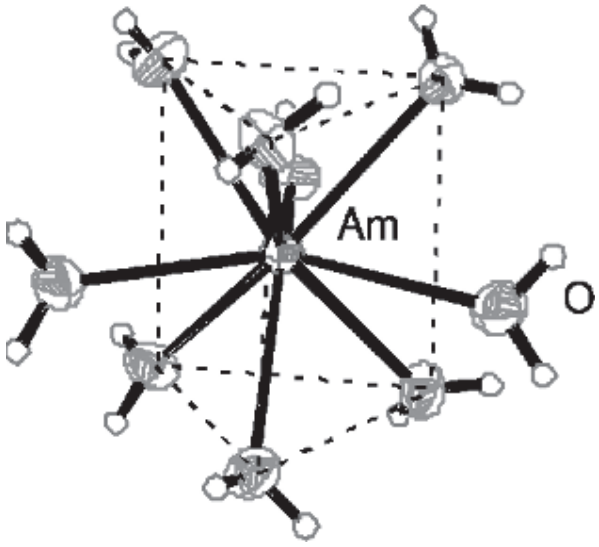

Figure 6.10: Tri-capped, trigonal prismatic structure of the $[Am(H_2O)_9]^{3+}_{(aq)}$ species. [Taken from Reference 14].

6.1.3.2 Am^{III}-EDTA Binary System

The 1:1 Am^{III}:$EDTA^{4-}$ system has been examined using luminescence spectroscopy. The luminescent lifetime is found to increase as pH is raised from approximately pH 1 to 12, and subsequently the N_{H_2O} bound to the Am^{III} ion in this system decreases (Table 6.2 and Figure 6.11, respectively). As pH is increased, the equilibrium between the free $Am^{III}_{(aq)}$ ion and the $EDTA^{4-}$ ligand with the $[Am(EDTA)]^-_{(aq)}$ complex is favoured towards complex formation, therefore, the N_{H_2O} bound to the Am^{III} ion will decrease. This reduction in N_{H_2O} bound to the Am^{III} ion causes the luminescent lifetime to increase as there are fewer OH oscillators to quench the Am^{III} excited state.[12,13] At pH 10, the N_{H_2O} bound to the Am^{III} ion is calculated to be three, which can be represented by the $[Am(EDTA)(H_2O)_3]^-_{(aq)}$ species. Above pH 10, the N_{H_2O} bound to the $[Am(EDTA)]^-_{(aq)}$ species reduces to 1.6, and so hydrolysis species are likely to be formed (*e.g.* $[Am(EDTA)(OH)]^{2-}_{(aq)}$ and $Am(OH)_{3(s)}$). Average percentage error bars have been included for all plots of N_{H_2O} *vs.* pH.

pH	τ / ns
0.5	28.3
1.3	28.3
2.4	33.6
3.5	35.3
5.0	44.1
7.0	48.0
8.8	51.5
9.3	50.7
10.0	51.0
11.7	80.1

Table 6.2: Calculated luminescent lifetimes (τ) of the 1:1 Am^{III}:$EDTA^{4-}$ system as a function of pH; $[Am^{III}]_i = [EDTA^{4-}]_i = 4 \times 10^{-4}$ M; I = 0.5 M $NaNO_3$.

.

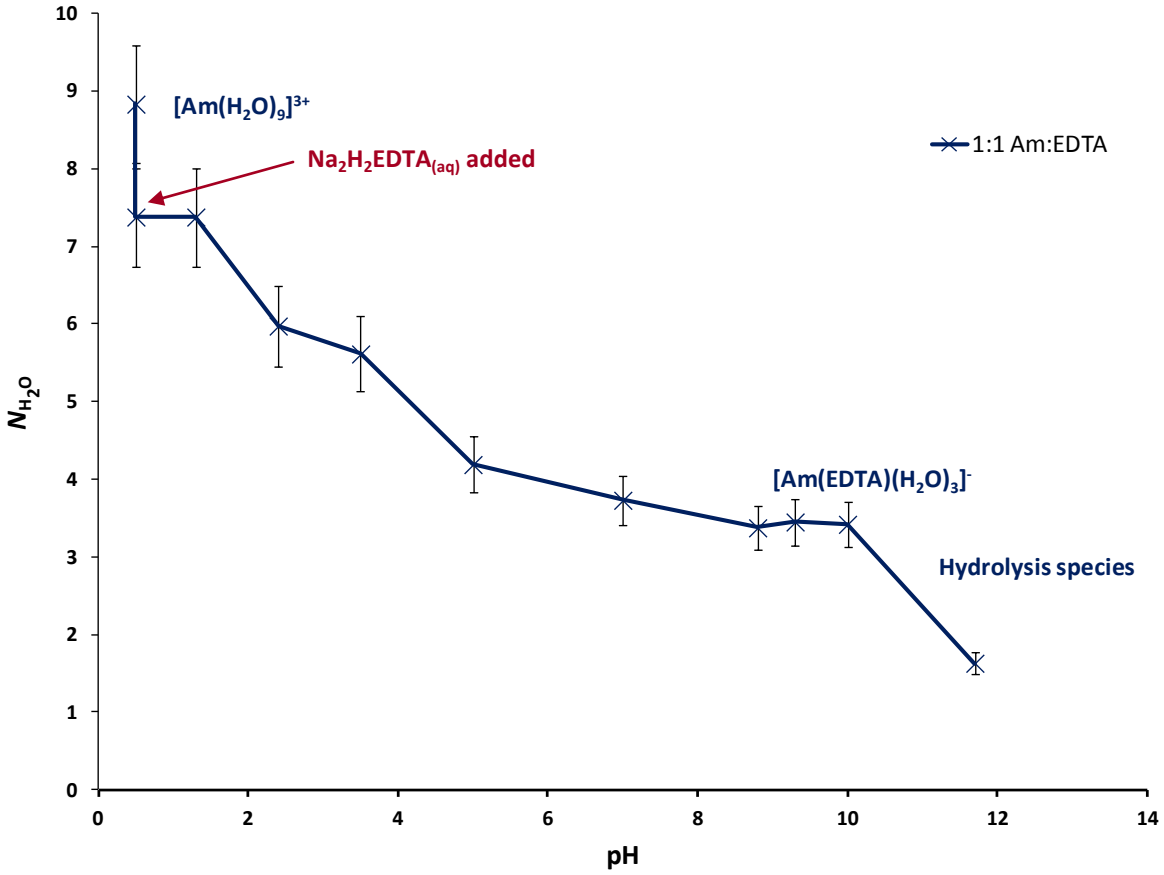

Figure 6.11: The effect of pH on the N_{H_2O} bound to the Am^{III} ion in the 1:1 Am^{III}:$EDTA^{4-}$ system; $[Am^{III}]_i = [EDTA^{4-}]_i = 4 \times 10^{-4}$ M; I = 0.5 M $NaNO_3$.

For a 1:1 Am^{III}:$EDTA^{4-}$ system, the aqueous Am^{III} species present in solution at a certain pH can be determined using a speciation diagram (Figure 6.12), which is derived from known equilibrium constants (Table 6.3).[16] The speciation diagram shows that from pH 1 to 11, the $[Am(EDTA)]^-_{(aq)}$ species is dominant. Hydrolysis of the Am^{III} ion to form $Am(OH)_{3(s)}$ is expected to dominate at approximately pH 11.

						Ionic Strength
Am^{III} +	$EDTA^{4-}$	$\rightleftharpoons$	$[Am(EDTA)]^-$	$\log \beta_{110}$	16.4	0.5 M Na^+ salt
$Am(OH)_{3(s)}$	$\rightleftharpoons$	Am^{3+} +	3 OH^-	K_{sp}	-25.4	0.1 M salt

Table 6.3: Stability constants for the complexation of $EDTA^{4-}$ and hydroxide to Am^{III}.[16]

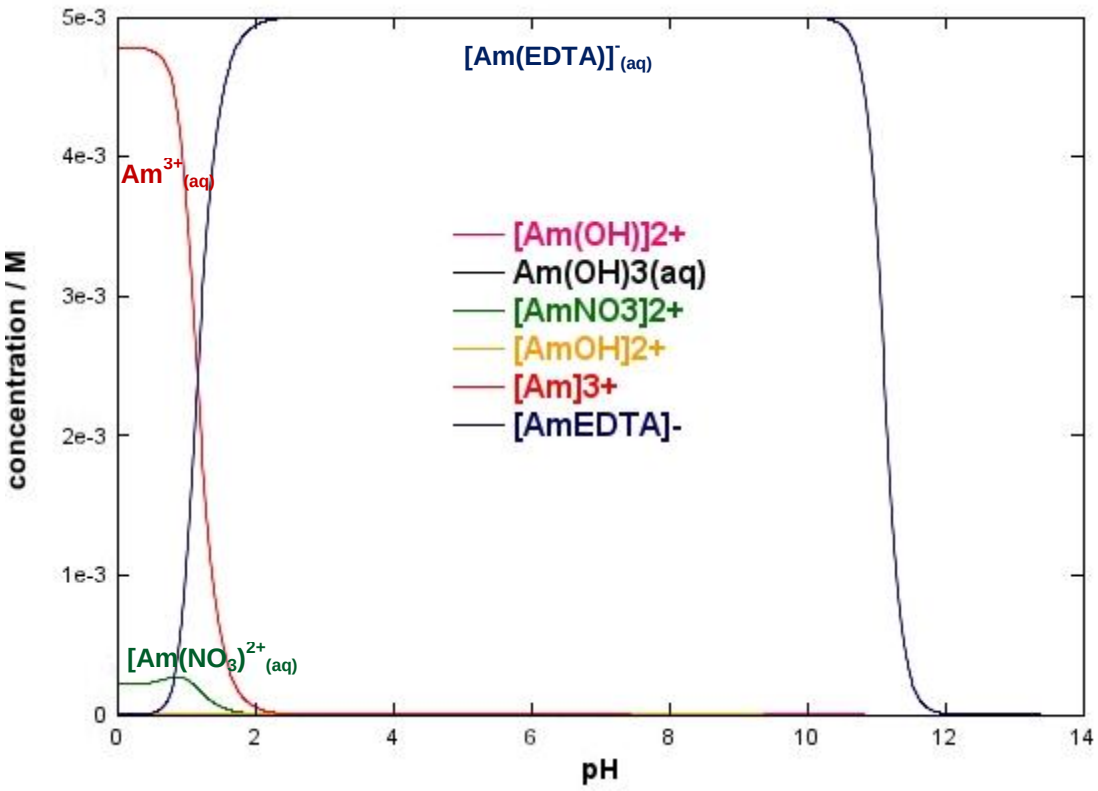

Figure 6.12: Speciation diagram of a 1:1 Am^{III}:$EDTA^{4-}$ system as a function of pH using the *JCHESS* code.[17] Total [Th^{IV}] = total [$EDTA^{4-}$] = 5 mM. Only aqueous species are shown. Thermodynamic data obtained from the integrated *JCHESS* database and Martell and Smith.[16]

A plot for the percentage formation of the $[Am(EDTA)]^{-}_{(aq)}$ complex as a function of pH (Figure 6.13) can be derived from the N_{H_2O} bound to the Am^{III} ion in the 1:1 Am^{III}:$EDTA^{4-}$ system. This speciation diagram shows that the percentage formation of the $[Am(EDTA)]^{-}_{(aq)}$ complex increases from approximately 30 % to 90 % over the pH range 0.5 to 10.0. Differences in the speciation diagrams presented in Figures 6.12 and 6.13 suggest that other equilibria may be present at acidic and alkaline pH. For example, in the acidic pH region, there may be an equilibrium between the $[Am(HEDTA)]_{(aq)}$ and $[Am(EDTA)]^{-}_{(aq)}$ species (*i.e.* pentadentate *vs.* hexadentate $EDTA^{4-}$ coordination), as previously observed in the La^{III} system (Chapter 3). Similarly, at alkaline pH, the $[Am(EDTA)]^{-}_{(aq)}$ complex may be in equilibrium with the hydrolysis species, $[Am(EDTA)(OH)]^{2-}_{(aq)}$. Therefore, as the formation constants of the $[Am(HEDTA)]_{(aq)}$ and $[Am(EDTA)(OH)]^{2-}_{(aq)}$ species are unknown, discrepancies in the calculated speciation diagram may occur (Figure 6.12).

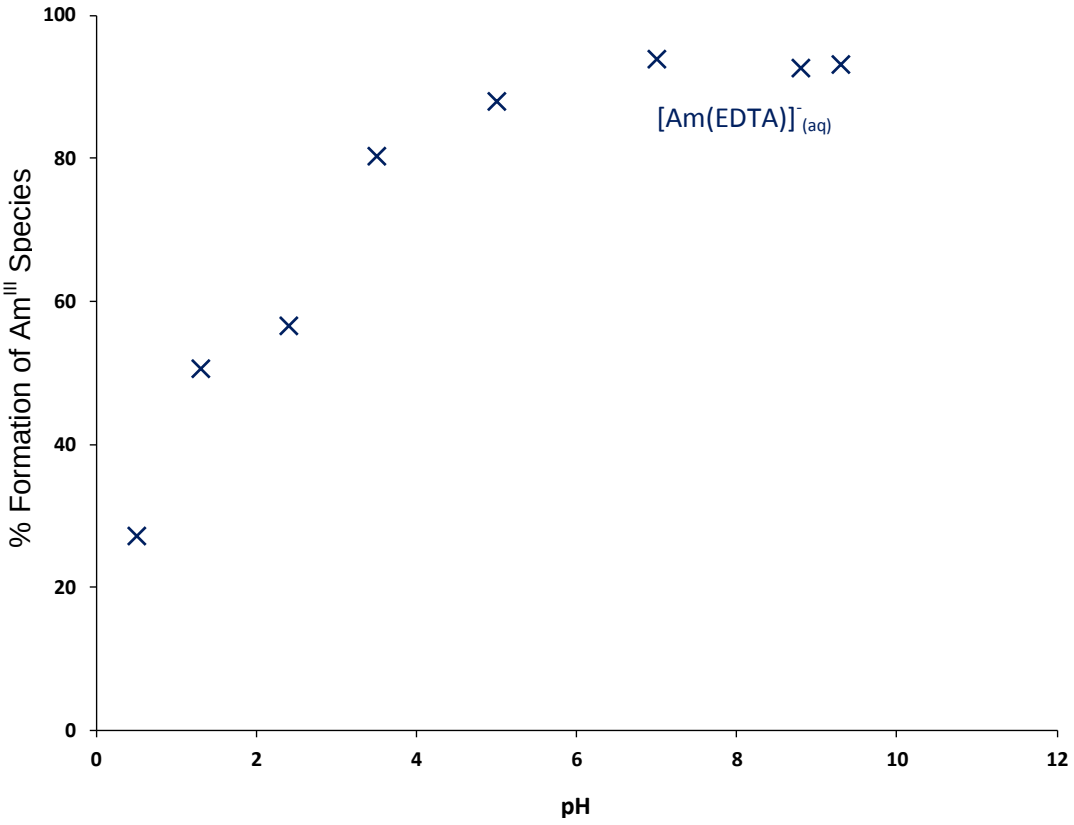

Figure 6.13: Plot of the percentage formation of the $[Am(EDTA)(H_2O)_3]^-_{(aq)}$ species as a function of pH.

The calculation of the N_{H_2O} bound to the Am^{III} ion can give insight into its speciation in the 1:1 Am:$EDTA^{4-}$ system as a function of pH. Possible structures of the solution species in this system are proposed in Figure 6.14.

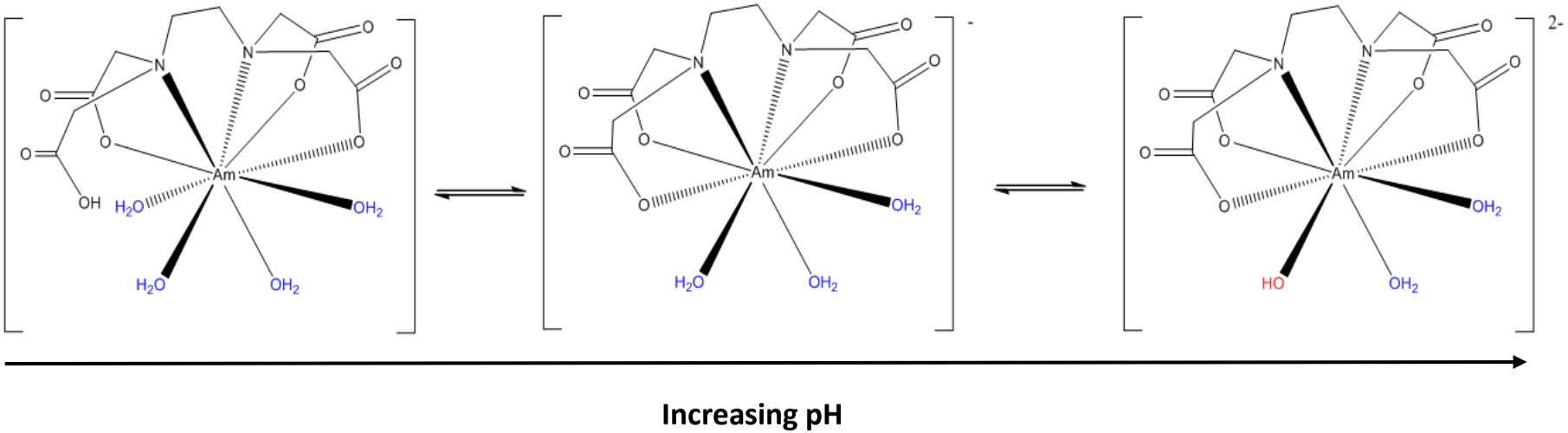

Figure 6.14: Possible structures of; **A**) $[Am(HEDTA)(H_2O)_4]_{(aq)}$; **B**) $[Am(EDTA)(H_2O)_3]^-_{(aq)}$ and **C**) $[Am(EDTA)(OH)(H_2O)_2]^{2-}_{(aq)}$ species.

6.1.3.3 Am^{III}-EDTA-Carbonate Ternary System

Luminescence spectroscopy performed on the 1:1:1 Am^{III}:$EDTA^{4-}$:CO_3^{2-} system as a function of pH, adjusted using NaOH, shows that the luminescent lifetime of the excited Am^{III} species has increased in the presence of carbonate (Table 6.4) compared to when it is absent (Table 6.2). It is likely that the carbonate anion is replacing inner-sphere water molecules in the $[Am(EDTA)]^-_{(aq)}$ complex, and so decreasing the number of OH oscillators that quench Am^{III} luminescence. Overlaying the data for the N_{H_2O} bound to the Am^{III} ion in the 1:1 Am^{III}:$EDTA^{4-}$ and the 1:1:1 Am^{III}:$EDTA^{4-}$:CO_3^{2-} systems shows a decrease in the N_{H_2O} coordinated to the $[Am(EDTA)]^-_{(aq)}$ complex from three to two, approximately over the pH range 8 to 11 (Figure 6.15). This is indicative of the carbonate anion either in exchange with water molecules for coordination to the $[Am(EDTA)]^-_{(aq)}$ complex (Figure 6.16), or a fraction of the $[Am(EDTA)(CO_3)]^{3-}_{(aq)}$ species forming in solution, which is analogous to the Ln^{III} systems discussed in Chapter 3. Above pH 11, the N_{H_2O} coordinated to the $[Am(EDTA)]^-_{(aq)}$ complex decreases to 1.6. Given the observations for the Ln^{III}:$EDTA^{4-}$:CO_3^{2-} systems in Chapter 3, this is likely to correlate to the formation of hydrolysis species (*e.g.* $[Am(EDTA)(OH)]^{2-}_{(aq)}$ and $Am(OH)_{3(s)}$).

pH	τ / ns
7.8	63.7
8.5	61.3
9.3	63.1
9.5	64.6
10	63.2
10.3	59.7
11	59.1
11.4	80.8
11.7	80.1

Table 6.4: Calculated luminescent lifetimes (τ) of the 1:1:1 Am^{III}:$EDTA^{4-}$:CO_3^{2-} system as a function of pH; $[Am^{III}]_i = [EDTA^{4-}]_i = [CO_3^{2-}]_i = 4 \times 10^{-4}$ M; I = 0.5 M $NaNO_3$.

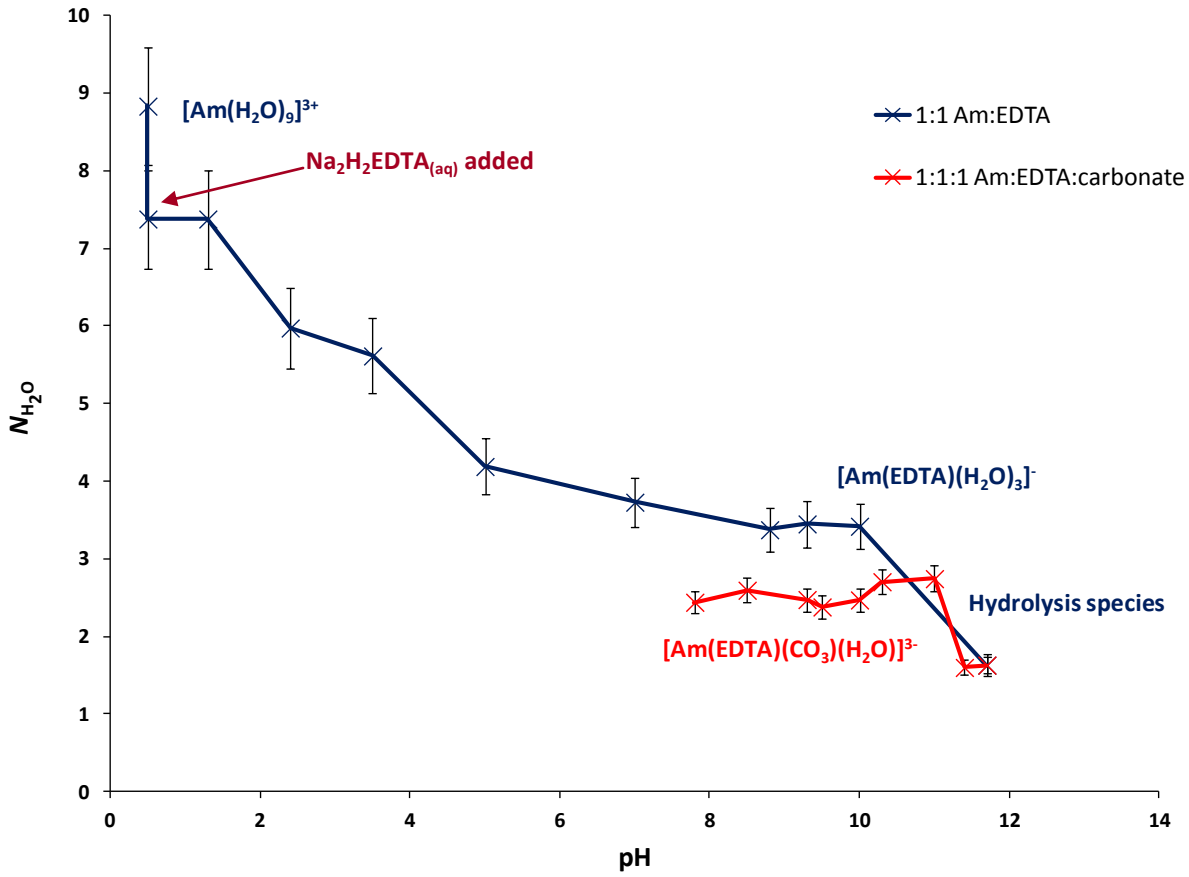

Figure 6.15: The effect of pH on the N_{H_2O} bound to Am^{III} in the 1:1:1 Am^{III}:$EDTA^{4-}$:CO_3^{2-} system; $[Am^{III}]_i = [EDTA^{4-}]_i = [CO_3^{2-}]_i = 4 \times 10^{-4}$ M; I = 0.5 M $NaNO_3$.

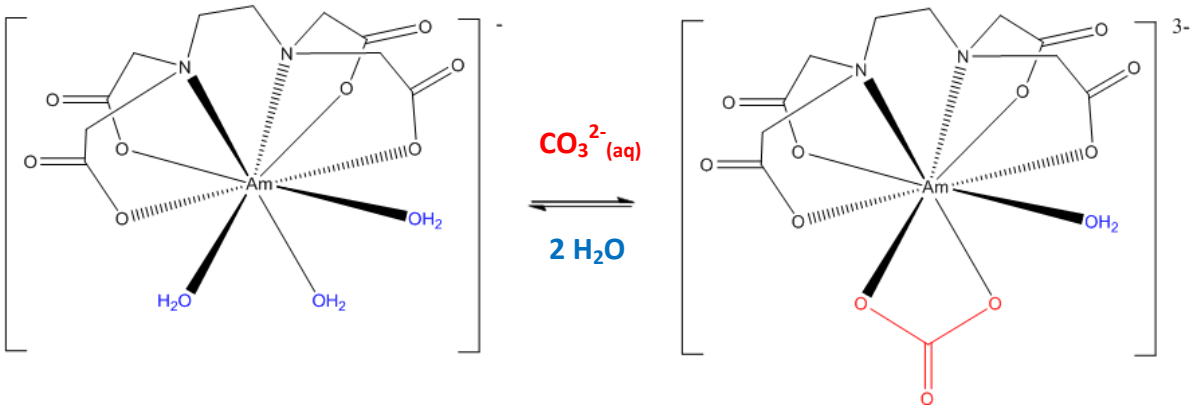

Figure 6.16: The exchange of H_2O and $CO_3^{2-}{}_{(aq)}$ for complexation to $[Am(EDTA)]^-_{(aq)}$.

An excess of carbonate added to the 1:1 Am^{III}:$EDTA^{4-}$ system showed no significant difference in the luminescent lifetime of the $[Am(EDTA)(CO_3)(H_2O)]^{3-}_{(aq)}$ species. Therefore, it is unlikely that two carbonate anions are coordinating to the $[Am(EDTA)]^{-}_{(aq)}$ complex, which is in agreement with the analogous Ln^{III} systems in Chapter 3.

6.1.3.4 Am^{III}-EDTA-Lactate Ternary System

The luminescence results for the 1:1:1 Am^{III}:$EDTA^{4-}$:lactate system show an increase in the luminescent lifetime (Table 6.5) compared to the 1:1 Am^{III}:$EDTA^{4-}$ system (Table 6.2) over the pH range 4.5 to 5.5, adjusted using NaOH. This consequently causes a reduction in the N_{H_2O} coordinated to the Am^{III} ion over the same pH range (Figure 6.17). The ^{1}H-NMR spectra of the 1:1:1 Ln^{III}:$EDTA^{4-}$:lactate systems showed that the AB quartet resonance for the bound acetate protons of $EDTA^{4-}$ was further split into doublets over the pD region approximately 4 to 10 (Section 4.5). It has previously been discussed how the lactate ligand may induce the splitting of the acetate resonance of $EDTA^{4-}$, possibly by causing $EDTA^{4-}$ to bind as a pentadentate ligand, rather than hexadentate, or possibly by hydrogen bonding via the hydroxyl group to the acetate groups of $EDTA^{4-}$, either in a primary sphere or secondary sphere interaction (Section 4.5 and Section 5.4). The reduction in the N_{H_2O} coordinated to the Am^{III} ion over the pH range 4.5 to 5.5 suggests that lactate can directly bind to the $[Am(EDTA)]^{-}_{(aq)}$ complex (Figure 6.16). Above approximately pH 6, the N_{H_2O} bound to the Am^{III} ion follows the same trend as the 1:1 Am^{III}:$EDTA^{4-}$ system. It may be possible that the presence of a small amount of hydroxide anions causes lactate to be removed from the Am^{III} primary coordination sphere. Even though lactate may be predominantly displaced from the Am^{III} inner coordination sphere above pH 6, it may be able to participate in hydrogen bonding with the $EDTA^{4-}$ ligand as a secondary sphere interaction, because the AB quartet resonance of the acetate protons of $EDTA^{4-}$ are still split into doublets up to pH 10.

Possible structures of species that may be present in the Am^{III}:$EDTA^{4-}$:lactate system are proposed in Figure 6.18.

pH	τ / ns
4	39.9
4	41.2
4.5	48.7
5.5	47.2
6	45.2
9.3	49.8
10	52.4
10.4	52.4
10.8	51.3

Table 6.5: Calculated luminescent lifetimes (τ) of the 1:1:1 Am^{III}:$EDTA^{4-}$:lactate system as a function of pH; $[Am^{III}]_i = [EDTA^{4-}]_i = [lactate]_i = 4 \times 10^{-4}$ M; I = 0.5 M $NaNO_3$.

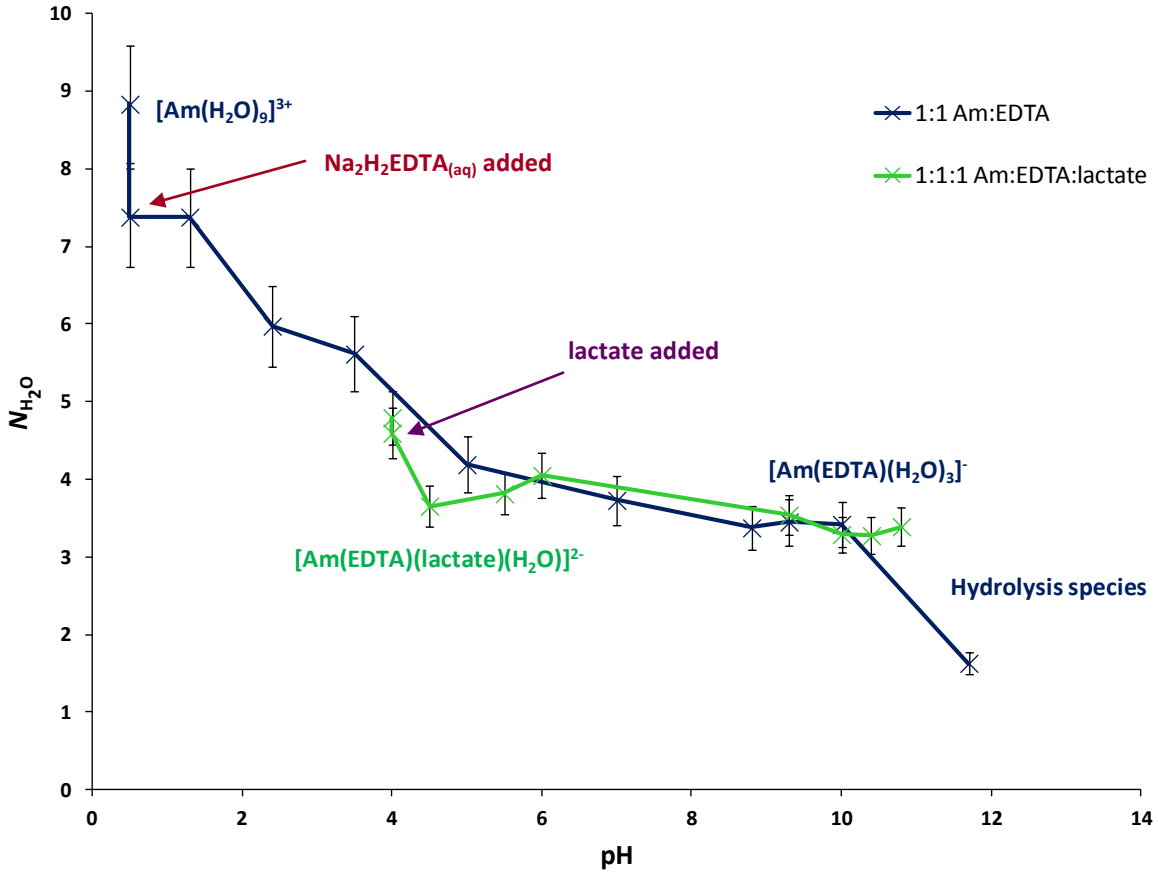

Figure 6.17: The effect of pH on the N_{H_2O} bound to Am^{III} in the 1:1:1 Am^{III}:$EDTA^{4-}$:lactate system; $[Am^{III}]_i = [EDTA^{4-}]_i = [lactate]_i = 4 \times 10^{-4}$ M; I = 0.5 M $NaNO_3$.

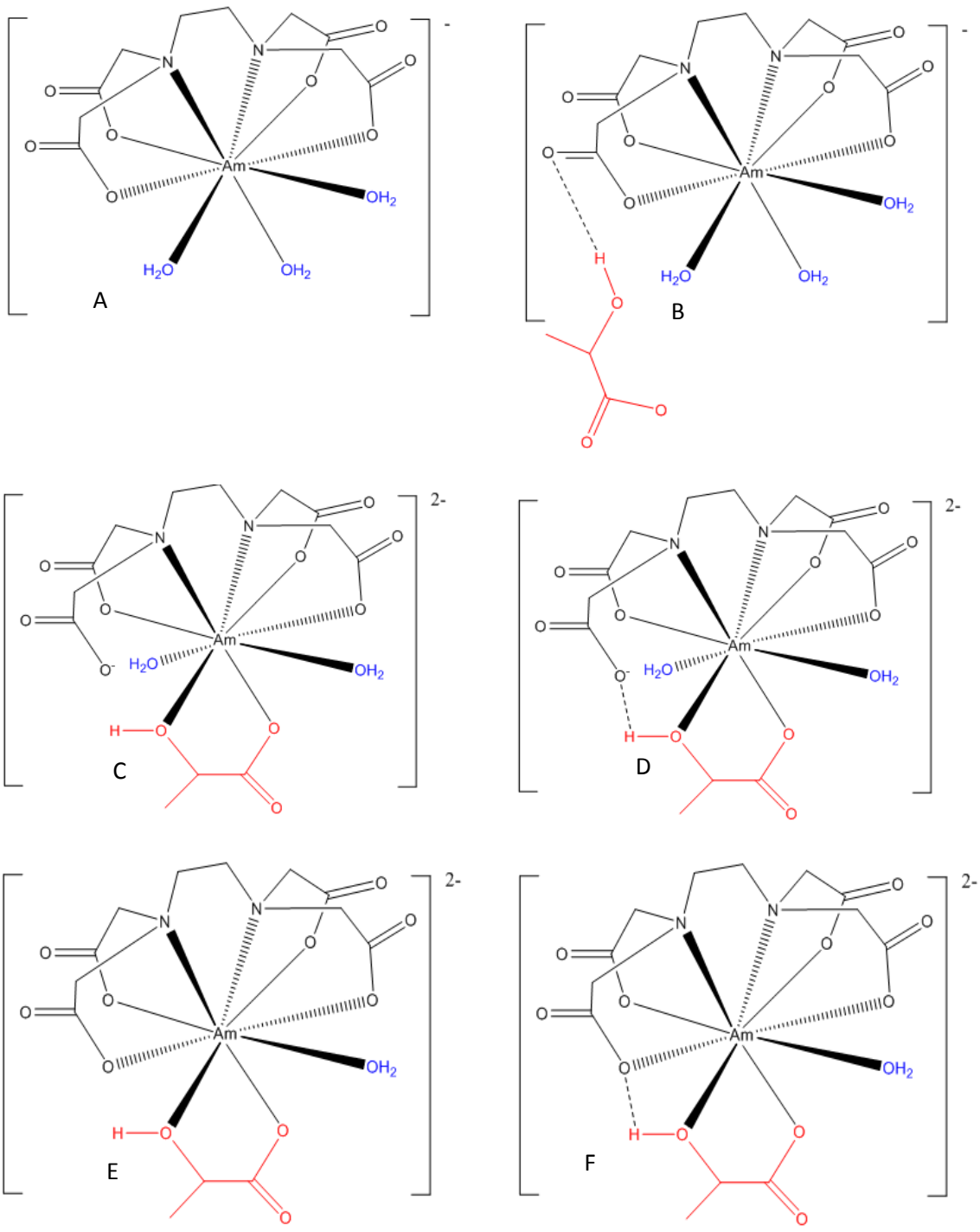

Figure 6.18: Possible structures of; **A**) $[Am(EDTA)(H_2O)_3]^-_{(aq)}$; **B**) $[Am(EDTA)(H_2O)_3]^-_{(aq)}$ with secondary sphere lactate H-bonding interaction; **C**) $[Am(EDTA)(lactate)(H_2O)_2]^{2-}_{(aq)}$ with pentadentate $EDTA^{4-}$ coordination; **D**) $[Am(EDTA)(lactate)(H_2O)_2]^{2-}_{(aq)}$ with pentadentate $EDTA^{4-}$ coordination and lactate H-bond interaction; **E**) $[Am(EDTA)(lactate)(H_2O)]^{2-}_{(aq)}$ with hexadentate $EDTA^{4-}$ coordination and **F**) $[Am(EDTA)(lactate)(H_2O)]^{2-}_{(aq)}$ with hexadentate $EDTA^{4-}$ coordination and lactate H-bond interaction.

6.1.3.5 Am^{III}-DTPA Binary Systems

The effect of pH, using NaOH as the titrant, on the 1:1 Am^{III}:$DTPA^{5-}$ system has been analysed using luminescence spectroscopy. The luminescent lifetime (τ) of the excited Am^{III} ion species is approximately 65 ns over the pH range 7.0 to 11.9 (Table 6.6). This translates into two water molecules bound to the $[Am(DTPA)]^{2-}$ complex over this pH range. In Chapter 4, the ^{1}H-NMR spectra of the $[Ln(DTPA)]^{2-}$ complexes were broadened, and so it was discussed how the $DTPA^{5-}$ ligand can alter its coordination mode in solution to bind either in an octadentate or heptadentate manner to metal ions.[18] Therefore, the heptadentate coordination mode of $DTPA^{5-}$ to the Am^{III} ion seems to be primarily observed when using TRLIFS. The luminescence results of the 1:1 Am^{III}:$DTPA^{5-}$ system show that the $[Am(DTPA)]^{2-}_{(aq)}$ complex is the dominant solution species approximately over the pH range 7 to 12, which agrees with the NMR results for the equivalent lanthanide systems.

pH	τ / ns
7.0	66.8
10.0	65.0
11.0	64.5
11.8	64.7
11.9	65.0

Table 6.6: Calculated luminescent lifetimes (τ) of the 1:1 Am^{III}:$DTPA^{5-}$ system as a function of pH; $[Am^{III}]_i = [DTPA^{5-}]_i = 4 \times 10^{-4}$ M; I = 0.5 M $NaNO_3$.

6.1.3.6 Am^{III}-DTPA-Carbonate Ternary System

Luminescence spectroscopy was utilised to observe if carbonate could interact with the $[Am(DTPA)]^{2-}_{(aq)}$ complex. The luminescent lifetime (τ) at approximately pH 10 (Table 6.7) shows a slight increase in the 1:1:1 Am^{III}:$DTPA^{5-}$:CO_3^{2-} system (τ = 69.1 ns) compared to the 1:1 Am^{III}:$DTPA^{5-}$ system (τ = 65.0 ns). Subsequently, there may be a small decrease in the N_{H_2O} coordinated to the Am^{III} ion in the 1:1:1 Am^{III}:$DTPA^{5-}$:CO_3^{2-} system over the pH range 9.0 to 10.8 (Figure 6.19), which might suggest there is a weak carbonate interaction with the

$[Am(DTPA)]^{2-}_{(aq)}$ complex. This correlates with the ^{1}H-NMR spectra of the 1:1:1 Lu^{III}:$DTPA^{5-}$:CO_3^{2-} systems (Section 4.6), where relatively weak carbonate interactions with the $[Lu(DTPA)]^{2-}_{(aq)}$ complex were shown to occur approximately over the pH range 10 to 11.

pH	τ / ns
7.0	68.4
7.4	67.3
9.0	67.4
9.9	69.1
10.8	66.6
11.9	65.0

Table 6.7: Calculated luminescent lifetimes (τ) of the 1:1:1 Am^{III}:$DTPA^{5-}$:CO_3^{2-} system as a function of pH; $[Am^{III}]_i = [DTPA^{5-}]_i = [CO_3^{2-}]_i = 4 \times 10^{-4}$ M; I = 0.5 M $NaNO_3$.

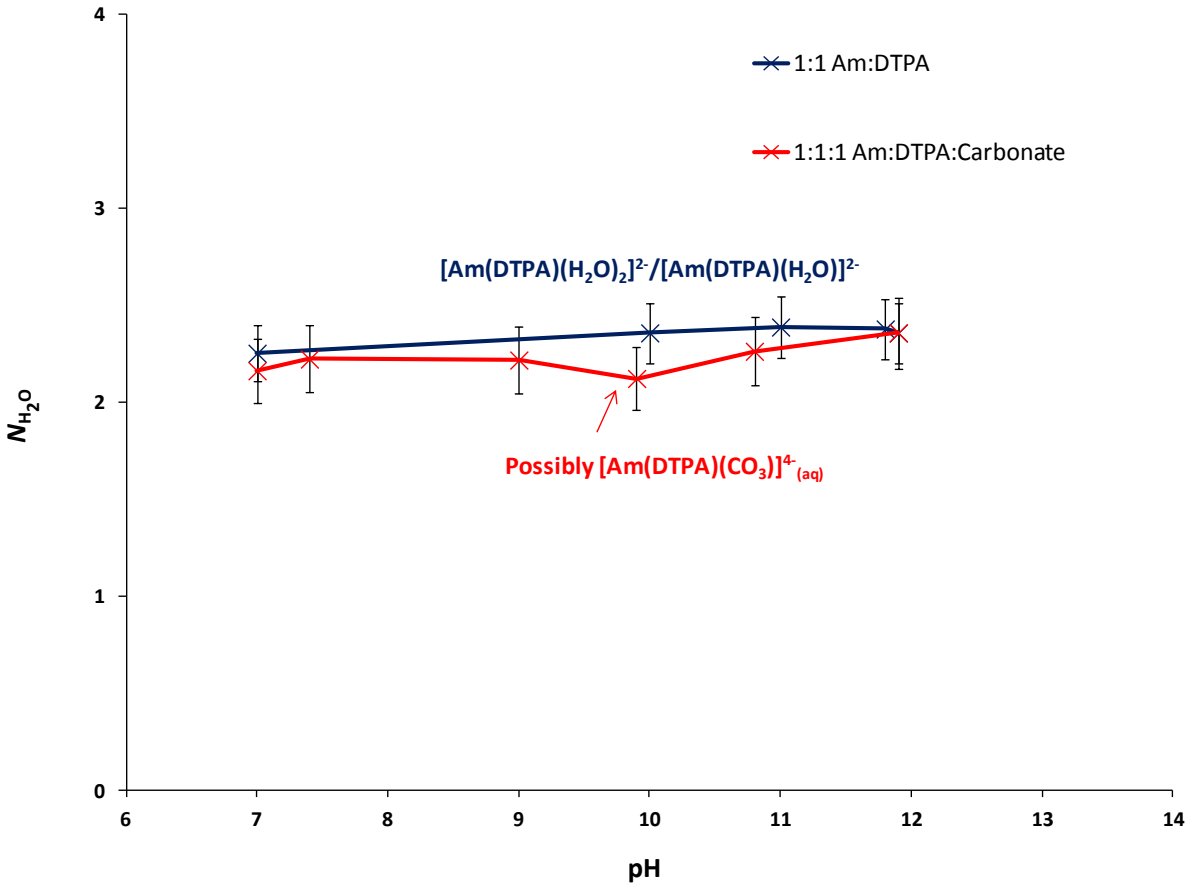

Figure 6.19: The effect of pH on the N_{H_2O} bound to the Am^{III} ion in the 1:1:1 Am^{III}:$DTPA^{5-}$:CO_3^{2-} system as a function of pH; $[Am^{III}]_i = [DTPA^{5-}]_i = [CO_3^{2-}]_i = 4 \times 10^{-4}$ M; I = 0.5 M $NaNO_3$.

6.1.3.7 Am^{III}-DTPA-Lactate Ternary System

The effect of pH on the 1:1:1 Am^{III}:$DTPA^{5-}$:lactate system, using NaOH as the titrant, has been studied using luminescence spectroscopy. Over the pH range 2.8 to 6.8, the N_{H_2O} coordinated to the Am^{III} ion in this system averages at approximately two (Figure 6.20), suggesting that the $[Am(DTPA)]^{2-}_{(aq)}$ complex dominates the speciation over this pH range. There is no observed decrease in the N_{H_2O} bound to the $[Am(DTPA)]^{2-}_{(aq)}$ complex over the pH region that lactate may be expected to directly bind to the Am^{III} ion (*i.e.* pH 4 to 6). Therefore, the formation of the $[Am(DTPA)(lactate)]^{3-}_{(aq)}$ complex may be minimal.

The luminescent lifetime decreases from 68.0 ns to 57.9 ns (Table 6.8) above pH 6.8, resulting in an increase of the N_{H_2O} bound to the $[Am(DTPA)]^{2-}_{(aq)}$ complex from two to three (Figure 6.20). This change is not observed in the binary system. As mentioned previously, the observed broadening of the $DTPA^{5-}$ signals in the ^{1}H-NMR spectra of the $[Ln(DTPA)]^{2-}_{(aq)}$ complexes illustrate the ability of the $DTPA^{5-}$ coordination mode to rapidly interconvert in solution (Section 4.2). The luminescence results of the 1:1:1 Am^{III}:$DTPA^{5-}$:lactate system suggest that lactate may alter the $DTPA^{5-}$ coordination mode in solution after pH 6.8, possibly by hydrogen bonding via the hydroxyl group to a carboxylate group on one of the acetate arms of $DTPA^{5-}$ (Figure 6.21). This may cause $DTPA^{5-}$ to bind in a hexadentate mode to the Am^{III} ion at alkaline pH.

pH	τ / ns
2.8	67.7
3.3	63.7
4.3	67.6
6.8	68.0
7.5	57.9
8.5	59.2
9.6	57.0
10.2	57.9
11	58.3
11.6	63.3

Table 6.8: Calculated luminescent lifetimes (τ) of the 1:1:1 Am^{III}:$DTPA^{5-}$:lactate system as a function of pH; $[Am^{III}]_i = [DTPA^{5-}]_i = [lactate]_i = 4 \times 10^{-4}$ M; I = 0.5 M $NaNO_3$.

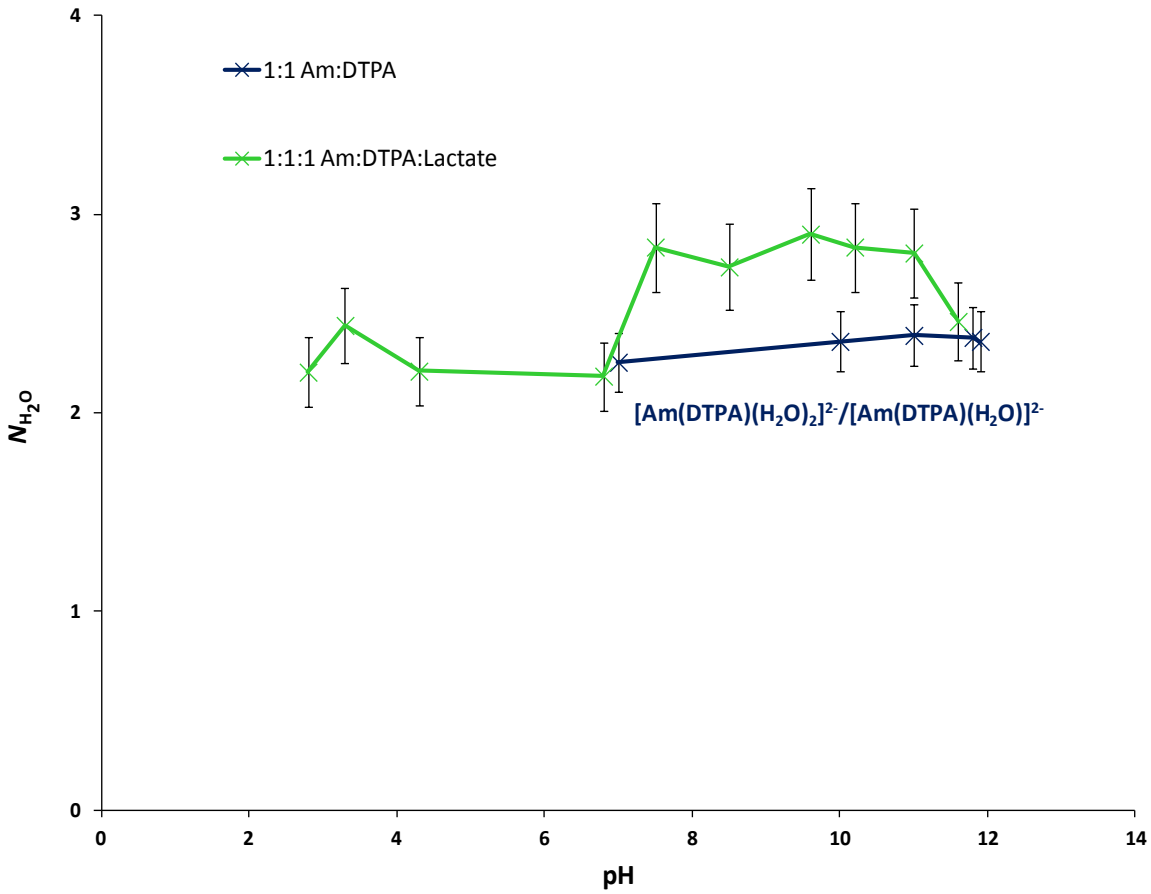

Figure 6.20: The effect of pH on the N_{H_2O} bound to the Am^{III} ion in the 1:1:1 Am^{III}:$DTPA^{5-}$:lactate system as a function of pH; $[Am^{III}]_i = [DTPA^{5-}]_i = [lactate]_i = 4 \times 10^{-4}$ M; I = 0.5 M $NaNO_3$.

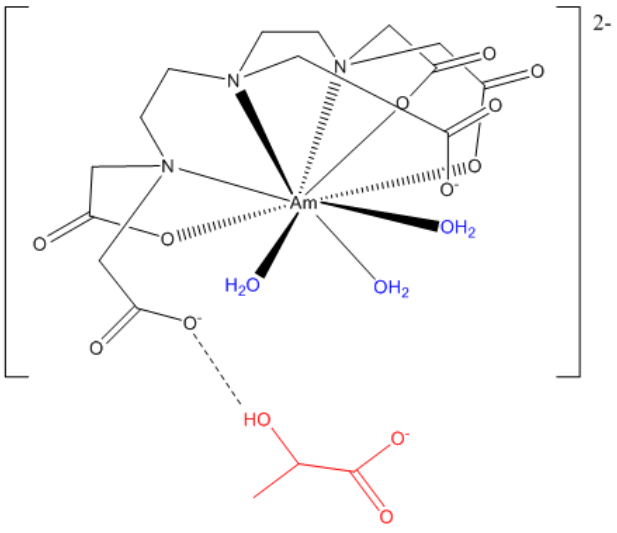

Figure 6.21: Possible hydrogen bonding of lactate to the $[Am(DTPA)]^{2-}_{(aq)}$ complex, illustrating hexadentate $DTPA^{5-}$ coordination mode.

6.1.3.8 Am^{III}-DO3A Binary System

In order to understand the possible coordination behaviour of carbonate and lactate to the $[Am(DO3A)]_{(aq)}$ complex, the luminescence spectroscopic titration of the 1:1 Am^{III}:$DO3A^{3-}$ system must firstly be performed. The experimental determination of the N_{H_2O} bound to the Am^{III} ion in this system is approximately 2.5, over the pH range 2 to 12 (Figure 6.22). The $DO3A^{3-}$ ligand contains seven donor groups, and can display fluctionality in the both the ring conformation and the acetate arms.[19] Therefore, the non-integer value of the N_{H_2O} bound to the $[Am(DO3A)]_{(aq)}$ complex may reflect this process. At pH values above 12, the N_{H_2O} bound to the Am^{III} ion in the 1:1 Am^{III}:$DO3A^{3-}$ system decreases to 1, which may represent the formation of hydrolysis species (*e.g.* $[Am(DO3A)(OH)(H_2O)]_{(aq)}$ and $Am(OH)_{3(s)}$).

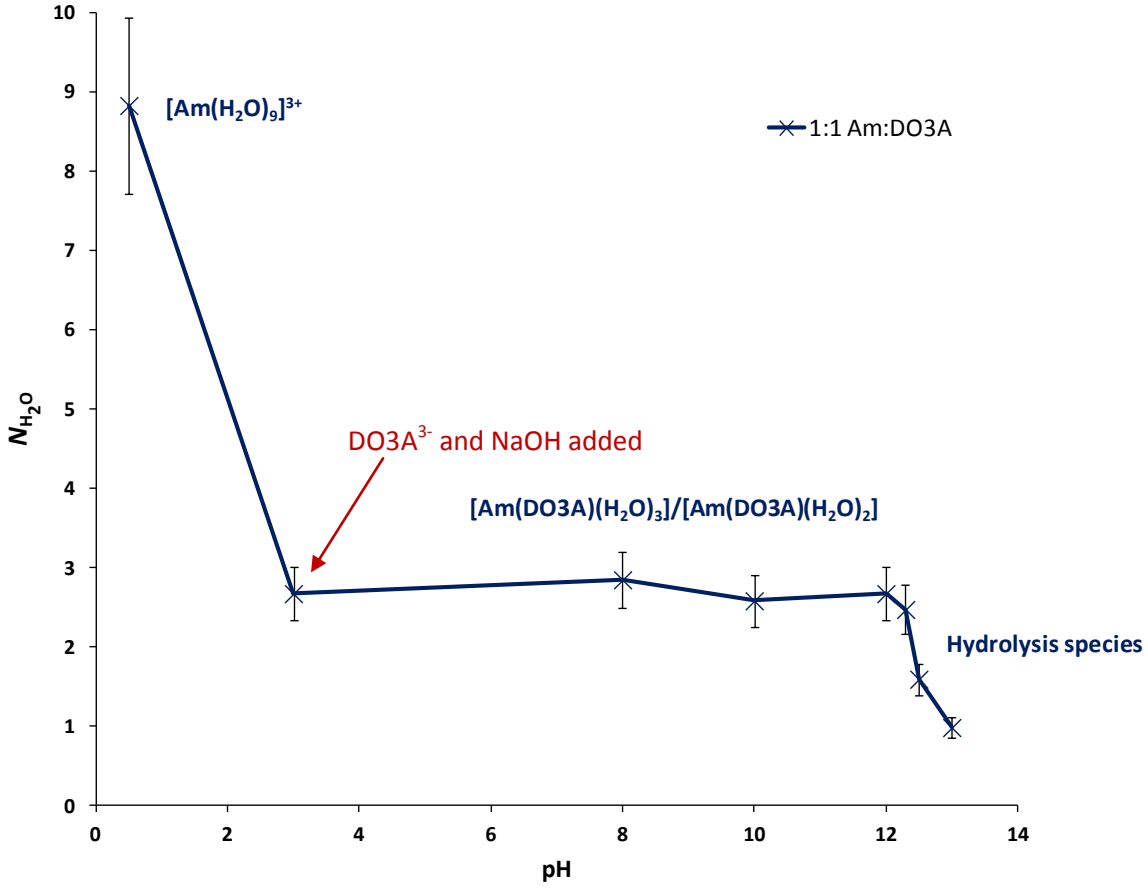

Figure 6.22: The effect of pH on the N_{H_2O} bound to the Am^{III} ion in the 1:1 Am^{III}:$DO3A^{3-}$ system as a function of pH; $[Am^{III}]_i = [D03A^{3-}]_i = 4 \times 10^{-4}$ M; I = 0.5 M $NaNO_3$.

6.1.3.9 Am^{III}-DO3A-Carbonate Ternary System

Carbonate interaction with the $[Am(DO3A]_{(aq)}$ complex has been examined using luminescence spectroscopy. For most of the pH range 7.0 to 11.5 no carbonate interaction is observed, except at pH 10, where there may be a small decrease in the N_{H_2O} bound to the [Am(DO3A)] complex (Figure 6.23). This is the pH where carbonate binding occurs to form similar Ln^{III} and An^{III} ternary complexes, including the $[Eu(DO3A)(CO_3)]^{2-}_{(aq)}$ complex (Section 4.7). Therefore, the formation of the $[Am(DO3A)(CO_3)]^{2-}_{(aq)}$ species may occur at this pH.

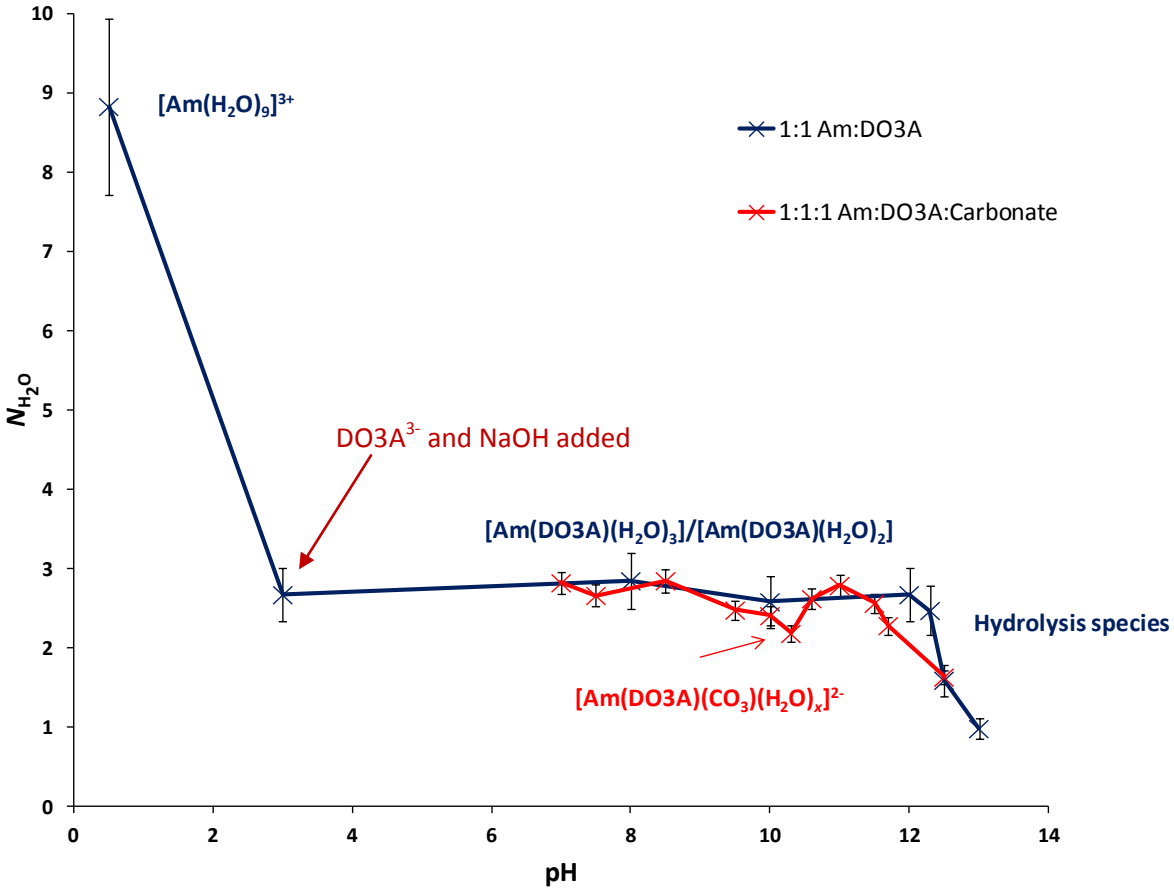

Figure 6.23: The effect of pH on the N_{H_2O} bound to the Am^{III} ion in the 1:1:1 Am^{III}:$DO3A^{3-}$:CO_3^{2-} system as a function of pH; $[Am^{III}]_i = [DO3A^{3-}]_i = [CO_3^{2-}]_i = 4 \times 10^{-4}$ M; I = 0.5 M $NaNO_3$.

6.1.3.10 Am^{III}-DO3A-Lactate Ternary System

Luminescence spectroscopic titrations have been performed on a 1:1:1 Am^{III}:$DO3A^{3-}$:lactate system to observe the possible interaction of lactate with the $[Am(DO3A)]_{(aq)}$ complex. There is no significant difference in the N_{H_2O} bound to the Am^{III} ion in the 1:1 Am^{III}:$DO3A^{3-}$ and the 1:1:1 Am^{III}:$DO3A^{3-}$:lactate systems, approximately over the pH range 4 to 12 (Figure 6.24). Therefore, there is little evidence of inner-sphere lactate coordination to the $[Am(DO3A)]_{(aq)}$ complex. In the literature, $[Ln(DO3A)(lactate)]^-_{(aq)}$ complexes have been reported using NMR spectroscopy (Ln = Pr^{III})[20] and single crystal XRD (Yb^{III} and Ho^{III}).[21] A comparable $[Gd(DO3A)(lactate)]^-$ complex, obtained *in silico*, shows the nine-coordinate Gd^{III} ion enveloped by $DO3A^{3-}$ with bidentate lactate occupying the remaining binding sites (Figure 6.25).[22] The structure provides evidence for lactate coordination *via* the hydroxyl and carboxylate groups. The $[Ln(DO3A)(lactate)]^-_{(aq)}$ complexes were crystallised from, or analysed in, aqueous solutions at pH 6.5 with excess lactate concentrations relative to the $[Ln(DO3A)]_{(aq)}$ complex.

The luminescent lifetimes of the Am^{III}:$DO3A^{3-}$ binary and ternary systems with carbonate and lactate are presented in Tables A to C, Appendix 4.

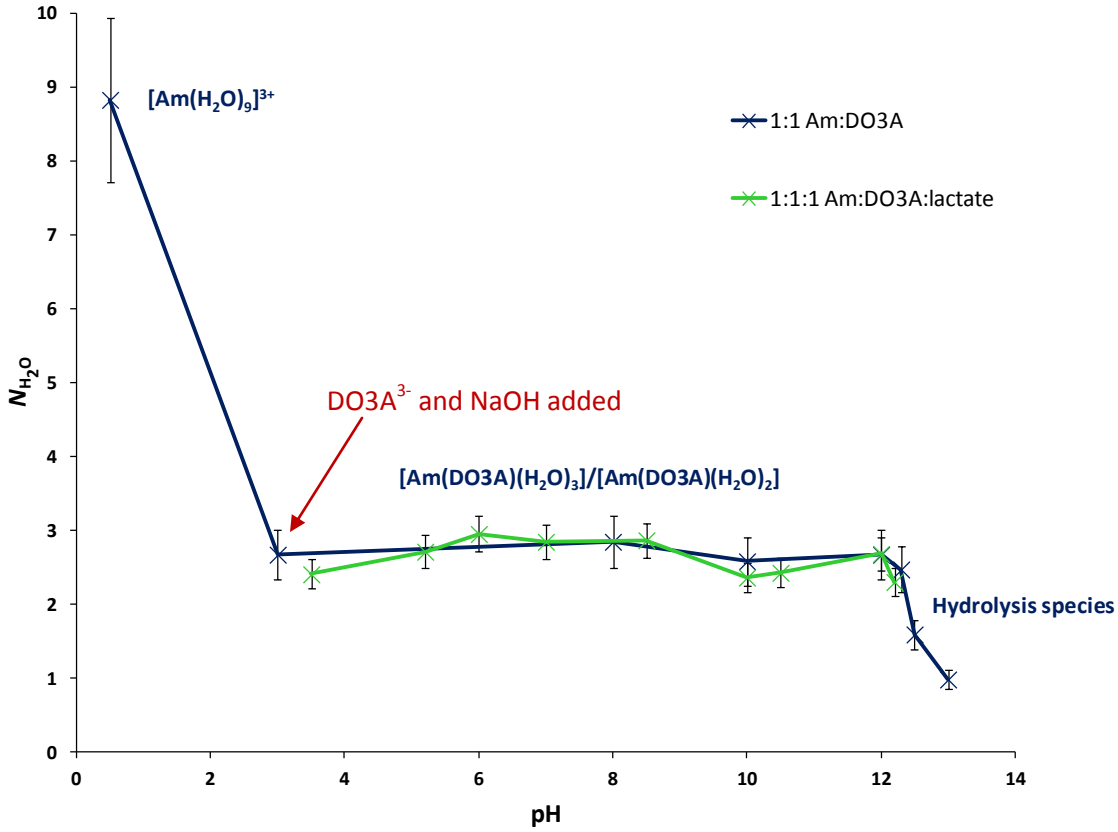

Figure 6.24: The effect of pH on the N_{H_2O} bound to the Am^{III} ion in the 1:1:1 Am^{III}:$DO3A^{3-}$:lactate system as a function of pH; $[Am^{III}]_i = [DO3A^{3-}]_i = [lactate]_i = 4 \times 10^{-4}$ M; I = 0.5 M $NaNO_3$.

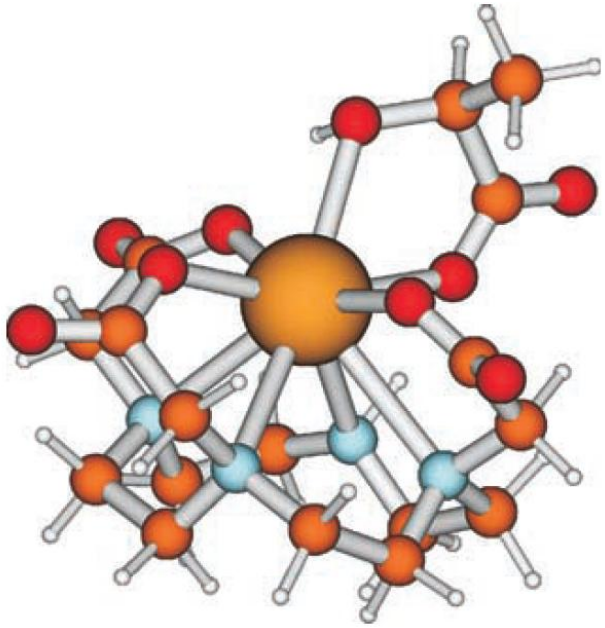

Figure 6.25: Structure of $[Gd(DO3A)(lactate)]^-$ adduct obtained *in silico*. [Taken from Reference 22].

6.2 Summary

UV-Vis spectroscopic titrations have provided evidence for the formation of the $[An(EDTA)]^-_{(aq)}$ and $[An(EDTA)(CO_3)]^{3-}_{(aq)}$ complexes (where An = Am^{III} or Cm^{III}). In both the An^{III}:$EDTA^{4-}$:CO_3^{2-} systems, there is a continuous growth in the extinction coefficient as the concentration of the carbonate in the system increases, representative of CO_3^{2-} interaction with the $[An(EDTA)]^-_{(aq)}$ complex. Above pH 11.0, a decrease in the extinction coefficient in all of the binary and ternary systems studied is indicative of the formation of hydrolysis species (*e.g.* $[An(EDTA)(OH)]^{2-}_{(aq).}$ This is similar to the behaviour observed in the 1:1:1 Ln^{III}:$EDTA^{4-}$:CO_3^{2-} systems (Chapter 3).

TRLIFS has been used to determine the lifetime of excited Am^{III} species, from which the N_{H_2O} bound to the Am^{III} ion in different systems can be calculated. The N_{H_2O} coordinated to the Am^{III} ion was calculated to be nine, which are likely to be arranged in a tri-capped, trigonal prismatic structure.[14] On complexation with $EDTA^{4-}$, the N_{H_2O} bound to the Am^{III} ion decreases to three at pH 10, and so luminescence spectroscopy can be used to detect the formation of the $[Am(EDTA)(H_2O)_3]^-_{(aq)}$ complex. In the presence of carbonate, the N_{H_2O} coordinated to the $[Am(EDTA)]^-_{(aq)}$ species decreases from three to two at alkaline pH. It is likely that carbonate is binding in a bidentate manner and either is in fast exchange with H_2O molecules (Figure 6.16) or only a fraction of the $[Am(EDTA)(CO_3)]^{3-}_{(aq)}$ species will form in solution. In the 1:1:1 Am^{III}:$EDTA^{4-}$:lactate, a decrease in the N_{H_2O} coordinated to the $[Am(EDTA)]^-_{(aq)}$ species occurs over the pH range 4.5 to 5.5, and so it is likely that some $[Am(EDTA)(lactate)]^{2-}_{(aq)}$ complex forms. This is comparable with the analogous Ln^{III} systems, where lactate interaction with the $[Ln(EDTA)]^-_{(aq)}$ complexes was observed over the pH range 4 to 6, using NMR spectroscopy (Section 4.5).

Luminescence spectroscopy indicated the existence of the $[Am(DTPA)]^{2-}_{(aq)}$ complex. The addition of CO_3^{2-} to this system may produce a small reduction in the N_{H_2O} bound to the $[Am(DTPA)]^{2-}_{(aq)}$ species at pH 10 compared to when carbonate is absent. This may suggest a weak carbonate interaction with the $[Am(DTPA)]^{2-}_{(aq)}$ complex, which was also observed in the Lu^{III} system using NMR spectroscopy (Section 4.6). Analysis of the 1:1:1 Am^{III}:$DTPA^{5-}$:lactate system using luminescence spectroscopy did not show a significant decrease in the N_{H_2O} bound to the $[Am(DTPA)]^{2-}_{(aq)}$ species over the pH range where lactate

would be expected to bind (*i.e.* pH 4 to 6). However, above pH 6.8, the N_{H_2O} bound to the $[Am(DTPA)]^{2-}_{(aq)}$ species increases from two to three. This suggests that lactate may alter the $DTPA^{5-}$ coordination mode, possibly by hydrogen bonding to a carboxylate group, which may cause $DTPA^{5-}$ to bind as a hexadentate ligand.

The determination of the N_{H_2O} bound to the Am^{III} ion in the 1:1 Am^{III}:$DO3A^{3-}$ system was calculated to be approximately 2.5, suggesting the flexibility of the $DO3A^{3-}$ binding mode between hepta- and hexadentate. At the pH value where carbonate would be expected to bind (*i.e.* pH 10), there is a small decrease in the N_{H_2O} bound to the $[Am(DO3A)]_{(aq)}$ complex compared to when carbonate is absent. Therefore, there may be some interaction of carbonate with the $[Am(DO3A)]_{(aq)}$ complex. In the analogous Eu^{III} system, carbonate interaction with the $[Eu(DO3A)]_{(aq)}$ complex was observed to occur, and so the Am^{III} results are consistent with the trivalent lanthanides. There was no significant reduction in the N_{H_2O} bound to the Am^{III} ion in the 1:1:1 Am^{III}:$DO3A^{3-}$:lactate, over the pH region that is favourable for lactate binding (*i.e.* pH 4 to 6). Therefore, the formation of $[Am(DO3A)(lactate]_{(aq)}$ complex may be minimal under the conditions studied. In excess lactate concentrations relative to $[Ln(DO3A)]_{(aq)}$ complexes (Ln = Pr^{III}, Yb^{III}, Ho^{III}, Gd^{III}), the discovery of $[Ln(DO3A)(lactate)]^{-}_{(aq)}$ species have been reported in literature using XRD and NMR spectroscopy.[19-21] Future work could use the techniques of NMR, UV-Vis and luminescence spectroscopies to probe the $[Am(DO3A)]_{(aq)}$ system in excess lactate concentrations, to observe whether a $[Am(DO3A)(lactate)]^{-}_{(aq)}$ species can form.

[1] H. Sims, *BNFL Commercial: Nexia Solutions*, 2005, **7**.

[2] M. Nilsson and K. Nash, *Solvent Extr. Ion Exc.*, 2007, **25**, 665–701.

[3] C. Leggett, G. Liu and M. Jensen, *Solvent Extr. Ion Exc.*, 2010, **28**, 313-334.

[4] M. Morgenstern, R. Klenze and J. I. Kim, *Radiochim. Acta.*, 2000, **88**, 7-16.

[5] T. Kimura, R. Nagaishi, Y. Kato and Z. Yoshida, *Radiochim. Acta.*, 2001, **89**, 125-130.

[6] W. Carnell and P. Fields, *J. Am. Chem. Soc.*, 1959, **81**, 4445-4449.

[7] A. Barkleit, G. Geipel, M. Acker, S. Taut and G. Bernhard, *Spectrochim. Acta. A.*, 2011, **78**, 549-552.

[8] P. Thakur, J. Conca, L. Van de Burgt and G. Choppin, *J. Coord. Chem.*, 2009, **62**, 3719-3737.

[9] P. Thakur, P. Pathak, T. Gedis and G. Choppin, *J. Solution Chem.*, 2009, **38**, 265-287.

[10] A. Yusov, *J. Radioanal. Nucl. Ch.*, 1990, **143**, 287-294.

[11] J. Beitz, *J. Alloy. Compd.*, 1994, **207**/**208**, 41-50.

[12] T. Kimura and Y. Kato, *J. Alloy. Compd.*, 1998, **271-273**, 867-871.

[13] P. Goodall, D. Morris and J. Rawcliffe, *Nexia Solutions*, 2008, **1**, 1-74.

[14] W. Runde and W. Schultz, *The Chemistry of the Actinide and Trans-actinide Elements:Chapter 8*, 2011, 1265-1395.

[15] J. Matonic, B. Scott and M. Neu, *Inorg. Chem.*, 2001, **40**, 2638-2639.

[16] R. Smith and A. Martell, *Critical Stability Constants*, Volumes 1 and 4: Inorganic Complexes, Plenum Press, New York, 1976.

[17] J. Van der Lee, A Users Guide to CHESS, Another Speciation and Surface Complexation Computer Code, E´cole des Mi1nes de Paris, Fontainebleau, 1998.

[18] S. Aime and M. Botta, *Inorg. Chim. Acta.*, 1990, **177**,101-105.

[19] É. Csajbók, Z. Baranyai, I. Bányai, E. Brücher, R. Király, A. Müller-Fahrnow, J. Platzek, B. Radüchel and M. Schäfe, *Inorg. Chem.*, 2003, **42**, 2342-2349.

[20] S. Aime, M. Botta, V. Mainero and E. Terreno, *Magnet. Reson, Med.*, 2002, **47**, 10-13.

[21] R. Dickins, S. Aime, A. Batsanov, A. Beeby, M. Botta, J. Bruce, J. Howard, C. Love, D. Parker, R. Peacock and H. Puschmann, *J. Am. Chem. Soc.*, 2002, **124**, 12697-12705.

[22] E. Terreno, M. Botta, P. Boniforte, C. Bracco, L. Milone, B. Mondino, F. Uggeri and S. Aime, *Chem. Eur. J.*, 2005, **11**, 5531 – 5537.

Chapter 7

Conclusions and Future Work

7.1 Conclusions

In both the nuclear waste ponds and the TALSPEAK process it has been hypothesised that ternary complexes may form.[1,2] In the nuclear waste pond scenario, the formation of mixed $[An(organic)(inorganic)]^{n-}_{(aq)}$ complexes (*e.g.* organic = humic substances, and inorganic = OH^-) may be increasing actinide solubility in the ponds, whereas in the TALSPEAK process ternary $[An/Ln(DTPA)(lactate)]^{3-}_{(aq)}$ complexes may be enhancing the separation of trivalent actinides from lanthanides.[1,2]

The aqueous solution behaviour of lanthanide and selected actinide ions in the presence of organic ($EDTA^{4-}$, $DTPA^{5-}$ $DO3A^{3-}$ and lactate) and inorganic (carbonate and hydroxide) ligands has been probed using the techniques of NMR, UV-Vis and/or luminescence spectroscopies. Tables 7.1 and 7.2 below summarise the species that were found to exist at certain intervals within the range of solution conditions studied (variable pH, relative stoichiometries).

Ligand	Metal Ion	Ionic Radii/ pm	Charge density / a.u.	Carbonate Ternary Complex	Lactate Ternary Complex
EDTA	La^{3+}	116‡	0.078	✓	✓
EDTA	Ce^{3+}	114‡	0.079	✓	-
EDTA	Pr^{3+}	113‡	0.080	✓	-
EDTA	Nd^{3+}	111‡	0.081	✓	-
EDTA	Sm^{3+}	108‡	0.083	✓	-
EDTA	Eu^{3+}	107‡	0.084	✓	✓
EDTA	Tb^{3+}	104‡	0.087	✓	-
EDTA	Ho^{3+}	102‡	0.088	✓	-
EDTA	Er^{3+}	100‡	0.090	✓	-
EDTA	Yb^{3+}	99‡	0.091	✓	-
EDTA	Lu^{3+}	98‡	0.092	✓	✓
EDTA	Th^{4+}	108*	0.148	✓	✓
EDTA	Am^{3+}	112*	0.080	✓	✓
EDTA	Cm^{3+}	111*	0.081	✓	-

Table 7.1: Summary of Ln and selected An-$EDTA^{4-}$- carbonate/lactate species that were found to exist, where: - = experiment not performed; ‡ = ionic radii of 8 coordinate and * = 6 coordinate metal ions.

Ligand	Metal Ion	Ionic Radii/ pm	Charge density / a.u.	Carbonate Ternary Complex	Lactate Ternary Complex
DTPA	La^{3+}	116‡	0.078	x	?
DTPA	Eu^{3+}	107‡	0.084	-	?
DTPA	Lu^{3+}	98‡	0.092	✓	?
DTPA	Th^{4+}	108*	0.148	✓	✓
DTPA	Am^{3+}	112*	0.080	?	?
DO3A	Eu^{3+}	107‡	0.084	✓	-
DO3A	Am^{3+}	112*	0.080	?	?

Table 7.2: Summary of Ln and selected An-$DTPA^{5-}$/$DO3A^{3-}$-carbonate/lactate species that were found to exist, where: - = experiment not performed; ? = further work needs to be conducted; ‡ = ionic radii of 8 coordinate and * = 6 coordinate metal ions.

The organic ligands of $EDTA^{4-}$, $DTPA^{5-}$ and $DO3A^{3-}$ were all capable of retaining metal ions in solution up to approximately pH 13. Generally, at pH values above 10, hydrolysis of the metal ion complexes occurs to form ternary hydroxide complexes (*i.e.* $[Ln(EDTA)(OH)]^{2-}_{(aq)}$. As the pH is raised further to pH 13, a white precipitate of the metal ion hydroxide forms, and signals that are representative of unbound ligand can be observed using NMR spectroscopy.

The original hypothesis, that mixed hydroxy-carbonate species are causing actinide species to be more soluble than what would be expected for the current conditions in the Sellafield nuclear waste ponds,[1] is unlikely to be the case. This is because hydroxide was found typically to replace bound carbonate in ternary complexes as pH is raised, rather than forming quarternary complexes with both carbonate and hydroxide. It is proposed that the increasing solubility of actinide metal ions is probably due to the ability of organic ligands present in the ponds to solubilise metal ions at high pH. In the majority of experiments performed, total precipitation of the metal ion from aqueous solution was not achieved until pH values of 13.3 or greater. In all experiments performed, pure metal hydroxide and carbonate compounds were typically insoluble in aqueous solution, unless the species were reacted in, for example, acidic conditions.

For the $M:EDTA^{4-}:CO_3^{2-}$ ternary systems (where M= Ln^{III}, An^{III} or Th^{IV}), the interaction of CO_3^{2-} with the $[M(EDTA)]^-_{(aq)}$ complex was predominantly observed over the pH/pD range 8 to 11. The formation of Ln/An ternary complexes, such as $[Ln(EDTA)(CO_3)]^{3-}_{(aq)}$, is likely to be dependent on electrostatic interactions and favoured by metal ions having a high charge density. For example, in the ^{13}C-NMR spectra of the $Lu^{III}:EDTA^{4-}:CO_3^{2-}$ system, a carbonate signal that represented a definitive bound carbonate species (*i.e.* $[Lu(EDTA)(CO_3)]^{3-}_{(aq)}$) was observed (Figure 3.16, Section 3.22), whereas in the equivalent La^{III} system, the carbonate signal was broadened, indicating an exchange process between bound and unbound carbonate (Figure 3.14, Section 3.22). Thorium is a tetravalent cation and has a small ionic radius, which causes the Th^{IV} cation to have a higher charge density than the trivalent lanthanide and actinide ions. This higher charge density leads to a greater affinity for anionic ligands, and so ternary complexes were more readily formed in the Th^{IV} systems when compared to the trivalent lanthanides and actinides. This is evident by the $[Th(EDTA)]_{(aq)}$ complex, which can bind two carbonate anions (*cf.* one carbonate ligand for trivalent Ln and An), to form the $[Th(EDTA)(CO_3)_2]^{4-}_{(aq)}$ species. Luminescence spectroscopy was used to calculate the N_{H_2O}

bound to Eu^{III}, Tb^{III} and Am^{III}, providing further information on the coordination environment for these species. In the 1:1:1 M^{III}:$EDTA^{4-}$:CO_3^{2-} system (where M= Eu, Tb or Am) approximately over the pH range 8 to 11, the calculated N_{H_2O} bound to the M^{III} ions is reduced when compared to the 1:1 M^{III}:$EDTA^{4-}$ system, which suggests that equilibria between binary and ternary species exist in solution (Figures 3.38 and 3.39).

Potentiometric titrations have been performed for the 1:1 Ln^{III}:$EDTA^{4-}$ and the 1:1:1 Ln^{III}:$EDTA^{4-}$:CO_3^{2-} systems. The data were best fitted to models that contain the $[Ln(EDTA)]^-_{(aq)}$, $[Ln(EDTA)(OH)]^{2-}_{(aq)}$, $Ln(OH)^{2+}_{(aq)}$ and $Ln(NO_3)^{2+}_{(aq)}$ species, and the $[Ln(EDTA)]^-_{(aq)}$, $[Ln(EDTA)(OH)]^{2-}_{(aq)}$, $[Ln(EDTA)(CO_3)]^{3-}_{(aq)}$, $Ln(OH)^{2+}_{(aq)}$ and $Ln(NO_3)^{2+}_{(aq)}$ species, respectively. The $[Ln(EDTA)]^-_{(aq)}$, $[Ln(EDTA)(OH)]^{2-}_{(aq)}$ and $[Ln(EDTA)(CO_3)]^{3-}_{(aq)}$ species were previously established using NMR, UV-Vis and/or luminescence spectroscopy. The calculated log *K* values for $[Ln(EDTA)]^-$ complex formation increase as the lanthanide series is crossed (Table 3.9, Chapter 3), which is due to the lanthanide contraction. This causes stronger electrostatic attractions between the trivalent lanthanides and the $EDTA^{4-}$ ligand. The log *K* values for the addition of hydroxide or carbonate to the $[Ln(EDTA)]^-_{(aq)}$ complexes do not show a trend that is dependent on the lanthanide charge density (Tables 3.10 and 3.11 in Chapter 3, respectively), which may be related to the addition of an anionic ligand to a negatively charged complex. However, ^{13}C-NMR spectroscopy suggests a stronger interaction of carbonate with the $[Lu(EDTA)]^-_{(aq)}$ complex compared to the $[La(EDTA)]^-_{(aq)}$ species. This difference between the NMR and potentiometry results may arise because the electrolyte concentration was controlled in the potentiometric titrations, whereas it was not controlled in the NMR experiments.

When the steric hindrance around a metal ion coordination sphere was increased by changing the denticity of the organic ligand from hexadentate (*i.e.* $EDTA^{4-}$) to octadentate (*i.e.* $DTPA^{5-}$), the interaction of the CO_3^{2-} anion with the $[Lu(DTPA)]^{2-}_{(aq)}$ complex and $[Th(DTPA)]^-_{(aq)}$ was shown to occur approximately over the pD range 9 to 11, when investigated by NMR spectroscopy. By contrast, the ^{13}C-NMR spectra acquired to study the 1:1:1 La^{III}:$DTPA^{5-}$:CO_3^{2-} system suggest that there is minimal carbonate interaction with the $[La(DTPA)]^{2-}_{(aq)}$ complex. The difference between the La^{III} and Lu^{III}/Th^{IV} ions in the $DTPA^{5-}$-CO_3^{2-} ternary systems may be because the Lu^{III} and Th^{IV} ions have a higher charge density than the La^{III} ion. Carbonate complexation is likely to be much weaker to the

$[Lu(DTPA)]^{2-}_{(aq)}$ complex compared to the $[Lu(EDTA)]^{-}_{(aq)}$ complex because CO_3^{2-} may be forced to bind in a monodentate, rather than bidentate, mode.

The TALSPEAK process utilises the ligands $DTPA^{5-}$ and lactate in an aqueous phase (buffered to pH 3.5), and the ligand HDEHP in an organic phase, in order to separate the trivalent lanthanides from the actinides. NMR spectroscopy showed that lactate can bind to metal ions (*i.e.* La^{III}, Eu^{III}, Lu^{III} and Th^{IV}) from acidic pH (*i.e.* pH 2), but as lactate is a weakly coordinating ligand, it is readily replaced by hydroxide, even at pH values as low as pH 5. The analysis of a 1:1:1 Ln^{III}:$DTPA^{5-}$:lactate system at approximately pH 3.5 using NMR spectroscopy showed that $[Ln(DTPA)]^{2-}_{(aq)}$ complexes will dominate the lanthanide speciation in the aqueous phase. The binary $[Ln(lactate)]^{2+}_{(aq)}$ complexes are unlikely to exist at this pH as the lanthanide ions will always preferentially bind the higher denticity ligand, $DTPA^{5-}$, over lactate. Lactate interaction with the $[Eu(DTPA)]^{2-}_{(aq)}$ complex occurs over the pD range 3.8 to 7.8, with the most favourable pD region for lactate interaction occurring between pD 5.4 to 7.8. It is possible that lactate interacts with the $[La(DTPA)]^{2-}_{(aq)}$ and $[Lu(DTPA)]^{2-}_{(aq)}$ complexes, but as the interaction is likely to be weak, it may not be noticeable in the NMR spectra for the diamagnetic systems. The nature of the lactate interaction is unclear, as lactate may be directly binding with the hydroxyl and carboxylate groups to the metal ion, or may be participating in H-bonding *via* the hydroxyl group to the $DTPA^{5-}$ acetate arms.[3] Under TALSPEAK conditions of pH 3.5, there is likely to be minimal interaction of lactate with the $[Ln(DTPA)]^{2-}_{(aq)}$ complexes.

The interaction of lactate with $[M(EDTA)]^{n-}_{(aq)}$ complexes (where M = La^{III}, Eu^{III}, Lu^{III}, Am^{III} and n = 1, or Th^{IV} and n = 0), was shown to occur predominantly over the pH range 4 to 8. Changes in the acetate proton resonances of $EDTA^{4-}$ in the La^{III} and Th^{IV}:$EDTA^{4-}$:lactate systems suggest that the coordination mode of lactate is different to carbonate (*i.e.* it is not only dependent on the carboxylate group of lactate binding to a metal ion). It is likely that the hydroxyl group is also involved in lactate interaction to $[M(EDTA)]^{n-}_{(aq)}$ complexes, either by directly binding to the Ln^{III} or Th^{IV} ions or by hydrogen bonding to the carboxylate groups of $EDTA^{4-}$,[3] or both (Figure 4.38, Section 4.5 and Figure 5.18, Section 5.4). Therefore, $EDTA^{4-}$ may adapt its binding mode (*i.e.* from hexa- to pentadentate) in order to accommodate the larger bite angle of lactate (*cf.* carbonate) into the metal ion coordination sphere. The $DTPA^{5-}$ ligand may also change its coordination mode to allow lactate interaction with a metal ion,

although it is difficult to observe a change in the splitting pattern of the $DTPA^{5-}$ resonances using NMR spectroscopy. This is because the $DTPA^{5-}$ signals are already broadened from exchange between the octa- and heptadentate coordination modes.[4]

In all experiments where ternary complexes were shown to exist, hydroxide replaces the secondary ligand (*i.e.* carbonate or lactate) in preference to the multidentate ligand (*i.e.* $EDTA^{4-}$ or $DTPA^{5-}$). This is because the multidentate ligands form complexes with greater thermodynamic stability compared to carbonate and lactate ligands.[5]

The results of the experiments suggest that trivalent actinide behaviour can generally be modelled on trivalent lanthanide systems, though there are some discrepancies that are likely to be due to An^{III} ions having lower charge densities compared to the Ln^{III} ions. An example of analogous behaviour between Ln^{III} and An^{III} ions is that ternary An^{III} and Ln^{III} complexes with $EDTA^{4-}$/carbonate and $EDTA^{4-}$/lactate were shown to exist. Whereas in the $DTPA^{5-}$/carbonate system, a Lu^{III} ternary complex forms but there is not enough evidence to affirm the formation of a comparable Am^{III} ternary complex. The Lu^{III} ion has a higher charge density than the Am^{III} ion (0.092 a.u. *vs*. 0.08 a.u.), therefore the $[Am(DTPA)(CO_3)]^{4-}_{(aq)}$ complex may not form due to the charge density of the Am^{III} ion not being large enough. An advantage of being able to use lanthanides as analogues for trivalent actinides are that lanthanides are easier to handle in a laboratory as there is no radiotoxicity associated with them. However, it is advantageous to work with trivalent actinides to observe directly how the metal ions behave in the systems studied.

The use of a combination of NMR, UV-Vis and luminescence spectroscopies, coupled with potentiometry, to determine metal ion speciation in the presence of organic and inorganic ligands over a wide pH range (*i.e.* 1 to 14) is unique as there are no reports in the literature, which use all of these techniques together to study metal ion speciation. Similarly, there are few reports on analysing alkaline samples using luminescence spectroscopy, as the majority of literature details luminescence relevant to the pH of biological systems.[6] Also, there is no published work on the examination of Am^{III} luminescence in environmentally relevant systems (*i.e.* containing carbonate), as has been detailed in this work.

7.2 Future Work

Only potentiometric titrations of the 1:1 Ln^{III}:$EDTA^{4-}$ and 1:1:1 Ln^{III}:$EDTA^{4-}$:CO_3^{2-} systems have been performed. It would be advantageous if potentiometric titrations of the equivalent actinide systems (*i.e.* Am^{III}, Cm^{III} and Th^{IV}) were conducted, in order to determine stability constants for the formation of the binary and ternary complexes, thus allowing the generation of speciation diagrams. It is likely that the same Ln^{III} potentiometric model could be applied to the trivalent actinide data, but a new model would have to be constructed for the Th^{IV} systems, in order to account for the $[Th(EDTA)(CO_3)_2]^{4-}_{(aq)}$ species. Potentiometric titrations of M^{n+}:$EDTA^{4-}$:lactate systems (where M = Ln^{III}, An^{III} or Th^{IV}) could also be done, so that formation constants of the $[M(EDTA)(lactate)]^{n-}_{(aq)}$ complexes can be determined and compared with those for the $[M(EDTA)(CO_3)]^{n-}_{(aq)}$ species.

It is most likely that lactate binds directly to metal ions in the M^{n+}:$EDTA^{4-}$:lactate systems (where M = Ln^{III}, An^{III} or Th^{IV}), though there may be some secondary sphere interaction. In the Ln^{III}/An^{III}:$DTPA^{5-}$:lactate systems, it is unclear whether the nature of lactate interaction with $[Ln/An(DTPA)]^{2-}_{(aq)}$ complexes is primary or secondary sphere. The use of Extended X-Ray Absorption Fine Structure (EXAFS) spectroscopy to probe the local coordination environment of the lanthanide ions in the Ln^{III}/An^{III}:$DTPA^{5-}$:lactate systems, plus NMR spectroscopy of the An^{III} systems, may help provide information on the role of lactate, and could be applied to ascertain metal ion speciation in the TALSPEAK process.

As mentioned previously in Section 1.1.6, it is likely that most of the actinides in the ponds are adsorbed to the brucite sludge.[1,7] Future work could involve contacting a known concentration of individual metal ion solutions (*e.g.* La^{III} or Lu^{III}) with brucite at high pH (*i.e.* pH 11), in order to allow the metal ions to adsorb to the brucite. The brucite solid could then be isolated by centrifugation, and the resulting solution characterised by Inductively Coupled Plasma-Atomic Emission Spectroscopy (ICP-AES) to calculate the percentage of metal ion that has adsorbed to the brucite surface. The brucite surface could then be contacted with solutions of $EDTA^{4-}$, $DTPA^{5-}$, mixed solutions of $EDTA^{4-}$/$DTPA^{5-}$, $EDTA^{4-}$/CO_3^{2-}, $DTPA^{5-}$/CO_3^{2-}, $EDTA^{4-}$/lactate and $DTPA^{5-}$/lactate at varying concentrations (*e.g.* 10 mM, 50 mM) and pH values (*e.g.* pH 2 to 13). Over time, samples of the solution could be taken and analysed by spectroscopy. For example, if La^{III}, Lu^{III} or Th^{IV} metal ions were used, and

the solutions were made in D_2O, then NMR spectroscopy could be used to probe for metal complexes (*e.g.* $[Lu(EDTA)]^-_{(aq)}$ or $[Lu(EDTA)(CO_3)]^{3-}_{(aq)}$]. Likewise, UV-Vis spectroscopy could be used to probe for Nd^{III} or Ho^{III} complexes, and luminescence spectroscopy to analyse for Eu^{III}, Tb^{III} or Am^{III} complexes. ICP-AES or γ-spectroscopy (*e.g.* for $^{152}Eu^{III}$ or ^{243}Am) of the solutions could be used to calculate the concentration of metal ions leached into the solution over time. This type of experiment may give an indication of the type of conditions that favour metal ion de-adsorbtion from a surface into a solution. The initial metal ion solutions contacted with brucite could also be mixed-metal systems (*e.g.* Eu^{III}/Am^{III} or Nd^{III}/Am^{III}) to observe whether de-adsorption of a metal ion from a surface can be favoured over another, under different conditions.

Initially, sodium hydroxide was added to the ponds to reduce Magnox corrosion.[8] This alkaline pH is likely to have formed pure metal hydroxide and pure metal carbonate species (through the dissolution of $CO_{2(g)}$ into the ponds).[8] The concentration of organics would have been low when the ponds first came into operation, but overtime, the organic concentration will have risen due to the accumulation of plant and animal deposits. Therefore, experiments could be performed in order to recreate the history of the ponds, in which pure metal ion hydroxides or carbonates were synthesised (*e.g.* $Lu(OH)_{3(s)}$ or $Lu_2(CO_3)_{3(s)}$) and contacted with different organic ligand solutions, as described above, of varying concentrations and pH values. A sample of the solution could be taken at various time points and analysed by spectroscopy (*i.e.* NMR, UV-Vis or luminescence, depending on the metal ion being used). This type of experiment may give an insight into the type of conditions that favour the solubilisation of metal ions from insoluble metal ion precipitates, and may contribute to an understanding of how the chemistry within the Sellafield waste ponds has developed over its history.

The techniques of NMR, UV-Vis and luminescence could be applied in the study of metal ion speciation within real nuclear waste pond samples or groundwater samples in the vicinity of a nuclear waste repository in the environment. This is because radionuclides are capable of migrating into the environment, where they can interact with dissolved components (*e.g.* humic substances) or minerals.[9] Experimental data on the solubility and speciation of metal ion complexes that form in natural systems are needed as a first step in the prediction of metal ion migration in the environment.[6]

The Enhanced Actinide Removal Plant (EARP) at Sellafield was constructed to reduce the activity of discharges to the Irish Sea.[10] The plant operates by the addition of NaOH to the acidic, active, aqueous waste, which also contains iron (Fe).[10] Various iron precipitates are formed including $Fe(OH)_3$, Fe_2O_3 and FeOOH, as well as the co-precipitation of the radionuclides.[10] The resulting suspension is filtered, and the solution in discharged directly to the sea, whilst the solid is encapsulated in cement.[10] The techniques detailed in this work (*i.e.* NMR, UV-Vis and luminescence spectroscopies) could be applied to probe radionuclide speciation, in the presence of Fe^{III}, over an acidic to alkaline pH range.

Other applications for these techniques could be to further investigate metal ion speciation in solvent extraction systems (aqueous and organic phases), including PUREX (Section 1.1.7), GANEX (Group ActiNide Extraction)[11] or outside the field of nuclear reprocessing, such as manufacturing processes[12] and extraction of metals from ores.[13] The GANEX process is the latest strategy that is being developed for the management of radioactive waste in future Generation IV reactors.[11] Generation IV systems are currently theoretical models, but the aims of these new types of reactors are to show improvements in safety, economics, environmental performance and resistance to nuclear proliferation.[14] GANEX focuses on the separation of actinides (U, Np, Pu, Am and Cm) from fission products (including lanthanides), that would then be used to create a new mixed-actinide fuel for future reactors.[11] The GANEX process operates by first extracting the trans-uranic actinides and the lanthanides into an organic phase containing *N*, *N*-dimethyl-*N*, *N*-dioctylhexylethoxymalonamide (DMDOHEMA) and HDEHP.[11] The actinides are then selectively extracted into an acidic aqueous phase containing DTPA.[11] It is envisioned that the research presented could be applied to new technologies and challenges faced in the future of the nuclear industry.

[1] H. Sims, *BNFL Commercial: Nexia Solutions*, 2005, **7**.

[2] M. Nilsson and K. Nash, *Solvent Extr. Ion Exc.*, 2007, **25**, 665–701.

[3] P. Gale, *Coord. Chem. Rev.*, 2003, **240**, 191-/221.

[4] S. Aime and M. Botta, *Inorg. Chim. Acta*, 1990, **177**,101-105.

[5] R. Smith and A. Martell, *Critical Stability Constants*, Volumes 1 and 4: Inorganic Complexes, Plenum Press, New York, 1976.

[6] S. Faulkner, S. Pope and B. Burton-Pye, *Appl. Spectrosc. Rev.*, 2005, **40**, 1–31.

[7] A. Pitois, P. Ivanov, L. Abrahamsen, N. Bryan, R. Taylor and H. Sims, *J. Environ. Monit.*, 2008, **10**, 315-324.

[8] D. Albright, *Science and Global Security: Volume 5*, Gordon and Breach Science Publishers, Amsterdam, 1994, 89-97.

[9] R. Silva, Presentation for the Materials Research Society Annual Meeting, 1983.

[10] K. Hildred, P. Townson, G. Hutson and R. Williams, *Powder Technol.*, 2008, **108**, 164-172.

[11] C. Marie, M. Miguirditchian, D. Guillaneux, J. Bisson, M. Pipelier and D. Dubreuil, *Solvent Extr. Ion Exc.*, 2011, **29**, 292–315.

[12] A. Visser, R. Swatloski, S. Griffin, D. Hartman and Robin D. Rogers, *Separ. Sci. Technol.*, 2001, **36**, 785-804.

[13] I. Wernick and N. Themelis, Annu. *Rev. Energ. Env*., 1998, **23**, 465-97.

[14] J. Marques, *Energ. Convers. Manage.*, 2010, **51**, 1774–1780.

Appendix 1

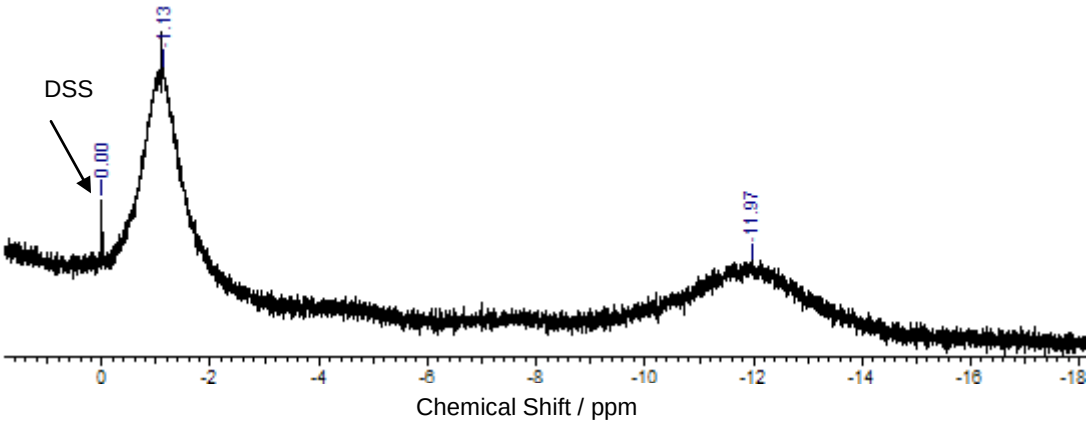

Figure A: ^{1}H-NMR spectrum of 1:1 [Pr^{III}]:[$EDTA^{4-}$] system at pD 10; [Pr^{III}]=[$EDTA^{4-}$]=[5 mM]$_i$.

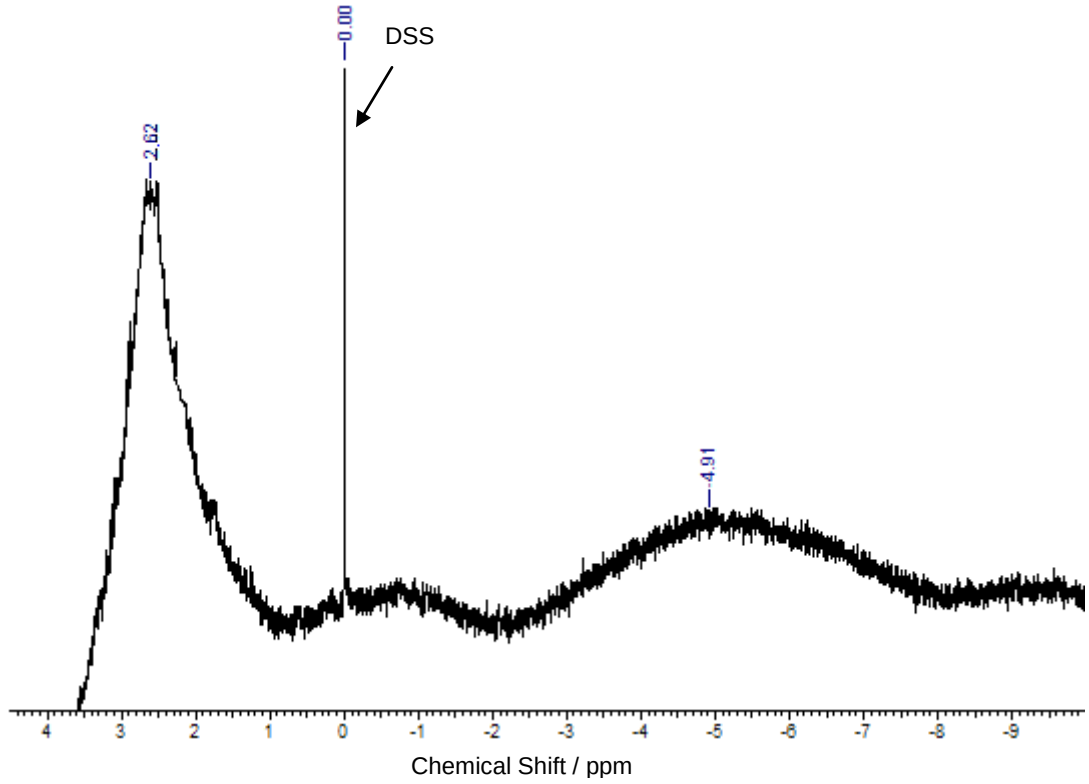

Figure B: ^{1}H-NMR spectrum of 1:1 [Nd^{III}]:[$EDTA^{4-}$] system at pD 10; [Nd^{III}]=[$EDTA^{4-}$]=[5 mM]$_i$.

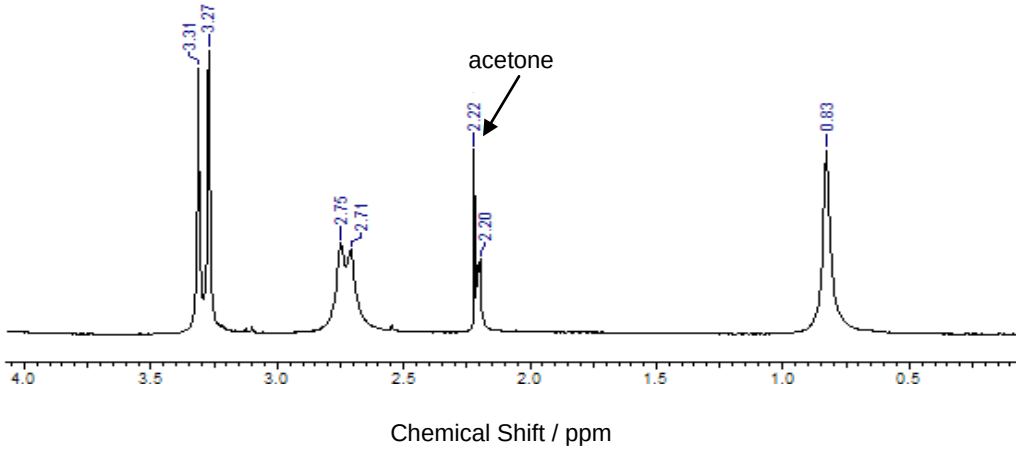

Figure C: ^{1}H-NMR spectrum of 1:1 [Sm^{III}]:[$EDTA^{4-}$] system at pD 10; [Sm^{III}]=[$EDTA^{4-}$]=[5 mM]$_i$.

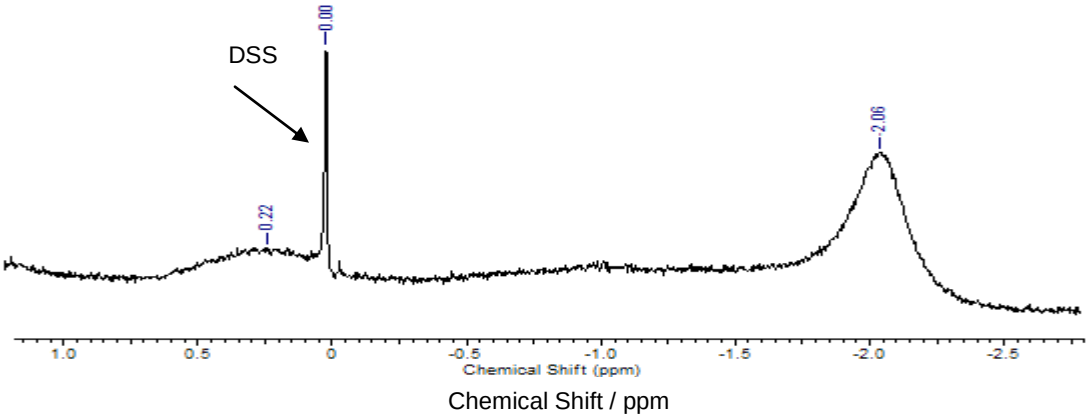

Figure D: ^{1}H-NMR spectrum of 1:1 [Eu^{III}]:[$EDTA^{4-}$] system at pD 10; [Eu^{III}]=[$EDTA^{4-}$]=[5 mM]$_i$.

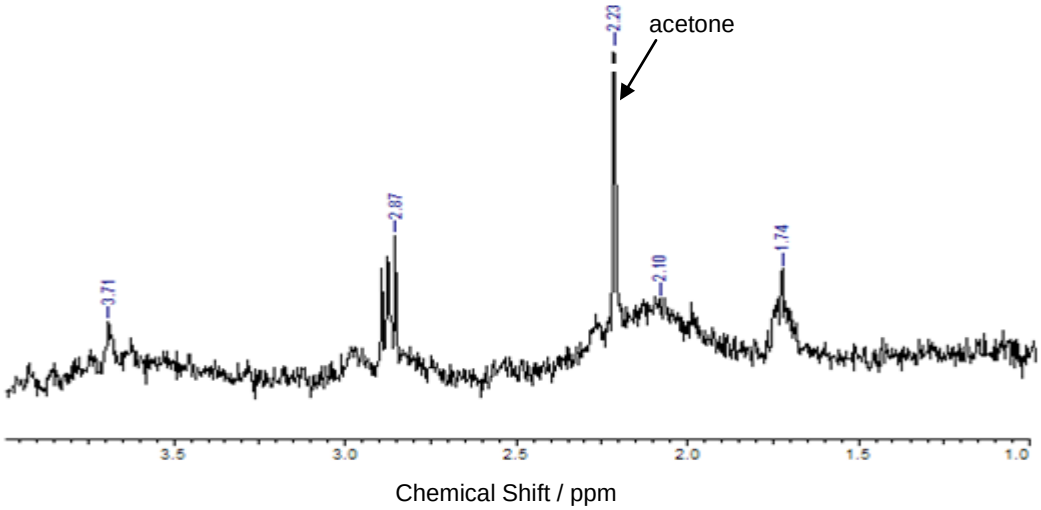

Figure E: ^{1}H-NMR spectrum of 1:1 [Tb^{III}]:[$EDTA^{4-}$] system at pD 7; [Tb^{III}]=[$EDTA^{4-}$]=[5 mM]$_i$.

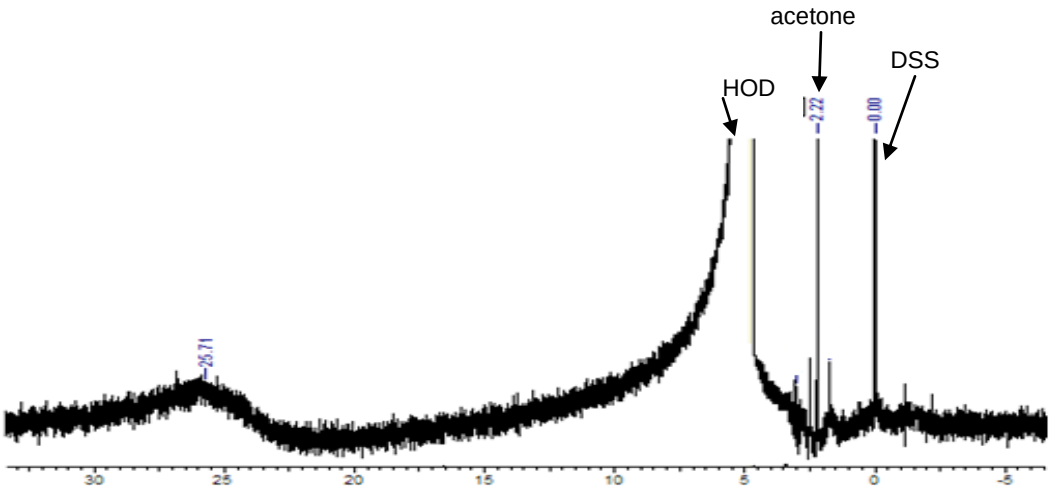

Figure F: ^{1}H-NMR spectrum of 1:1 [Ho^{III}]:[$EDTA^{4-}$] system at pD 10; [Ho^{III}]=[$EDTA^{4-}$]=[5 mM]$_i$.

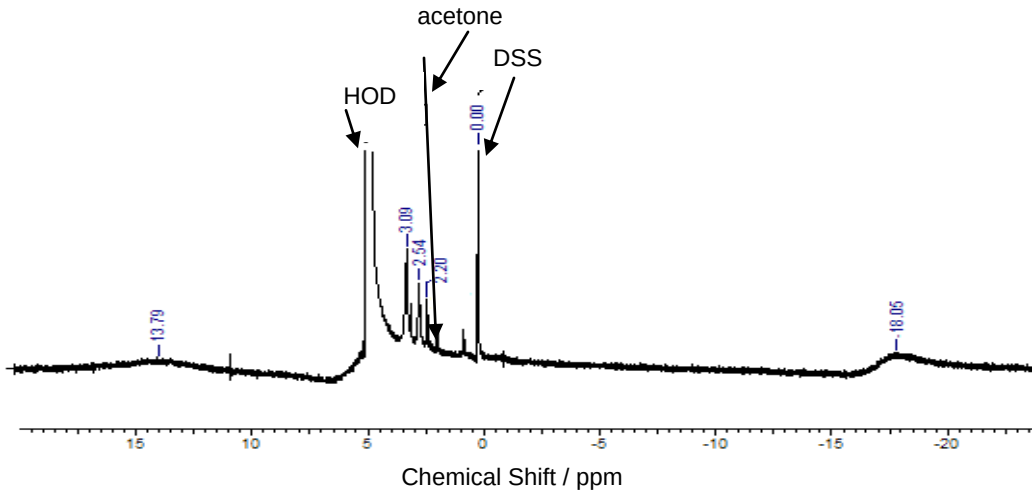

Figure G: ^{1}H-NMR spectrum of 1:1 [Er^{III}]:[$EDTA^{4-}$] system at pD 10; [Er^{III}]=[$EDTA^{4-}$]=[5 mM]$_i$.

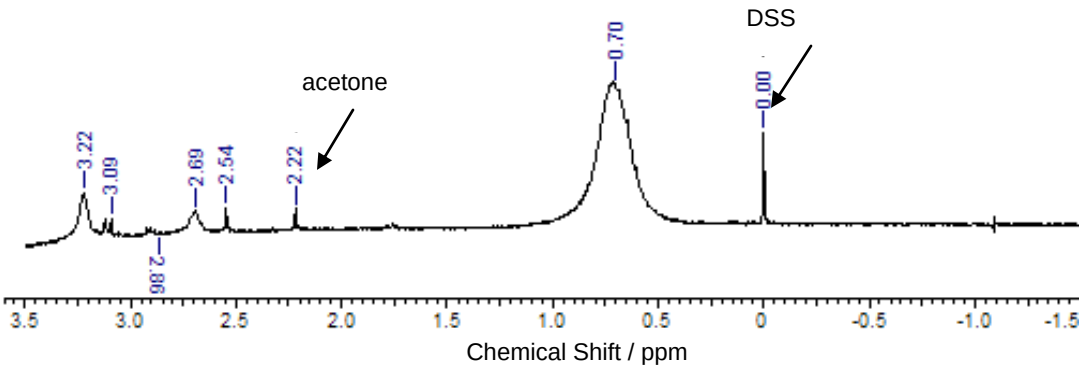

Figure H: ^{1}H-NMR spectrum of 1:1 [Yb^{III}]:[$EDTA^{4-}$] system at pD 10; [Yb^{III}]=[$EDTA^{4-}$]=[5 mM]$_i$.

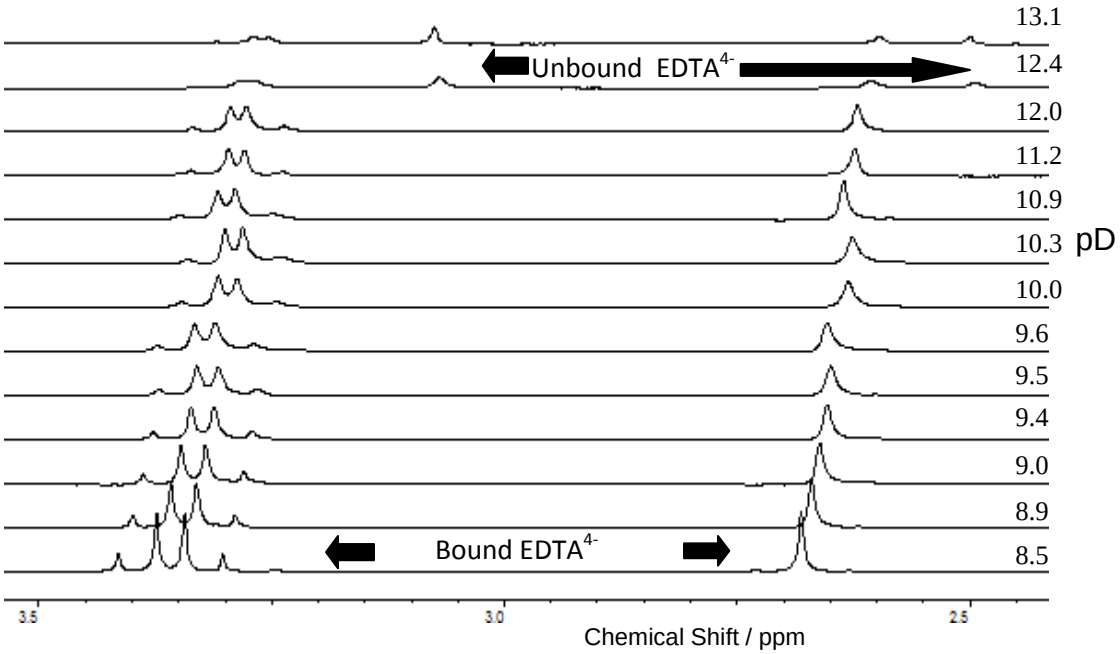

Figure I: ^{1}H-NMR spectra of the effect of pD on a 1:1:1 La^{III}:$EDTA^{4-}$:CO_3^{2-} solution; [50 mM].

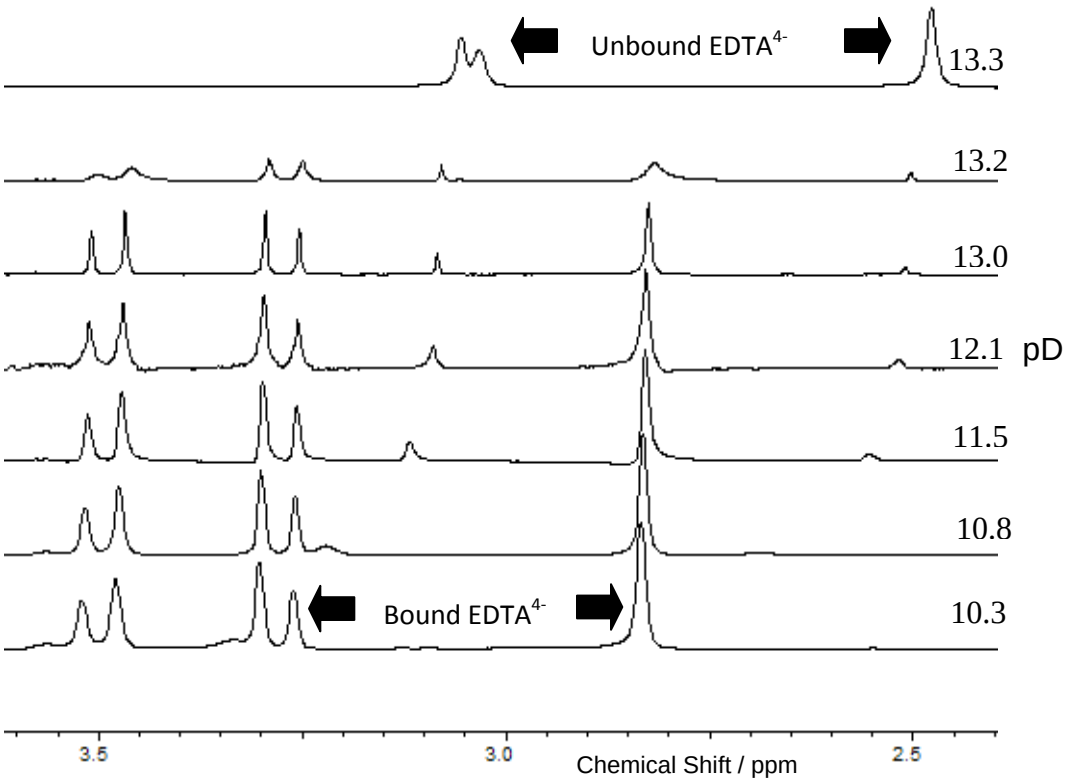

Figure J: ^{1}H-NMR spectra of the effect of pD on a 1:1:1 Lu^{III}:$EDTA^{4-}$:CO_3^{2-} solution; [50 mM].

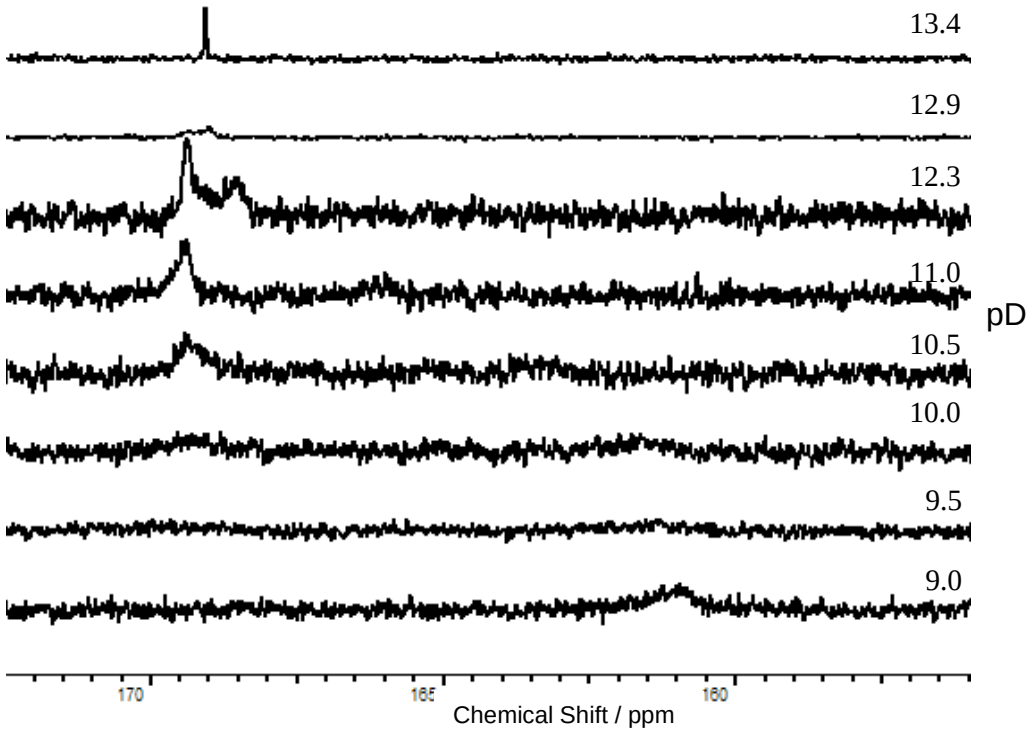

Figure K: ^{13}C-NMR spectra of the effect of pD on a 1:1:1 Lu^{III}:$EDTA^{4-}$:HCO_3^- solution; [50 mM].

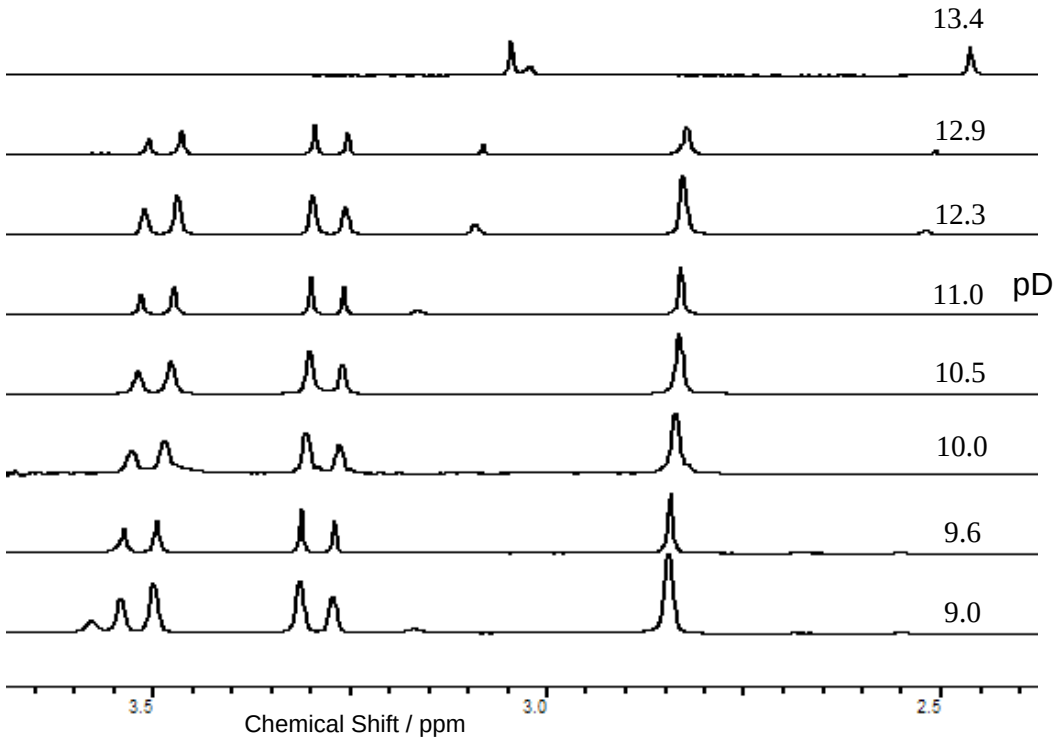

Figure L: ^{1}H-NMR spectra of the effect of pD on a 1:1:1 Lu^{III}:$EDTA^{4-}$:HCO_3^- solution; [50 mM].

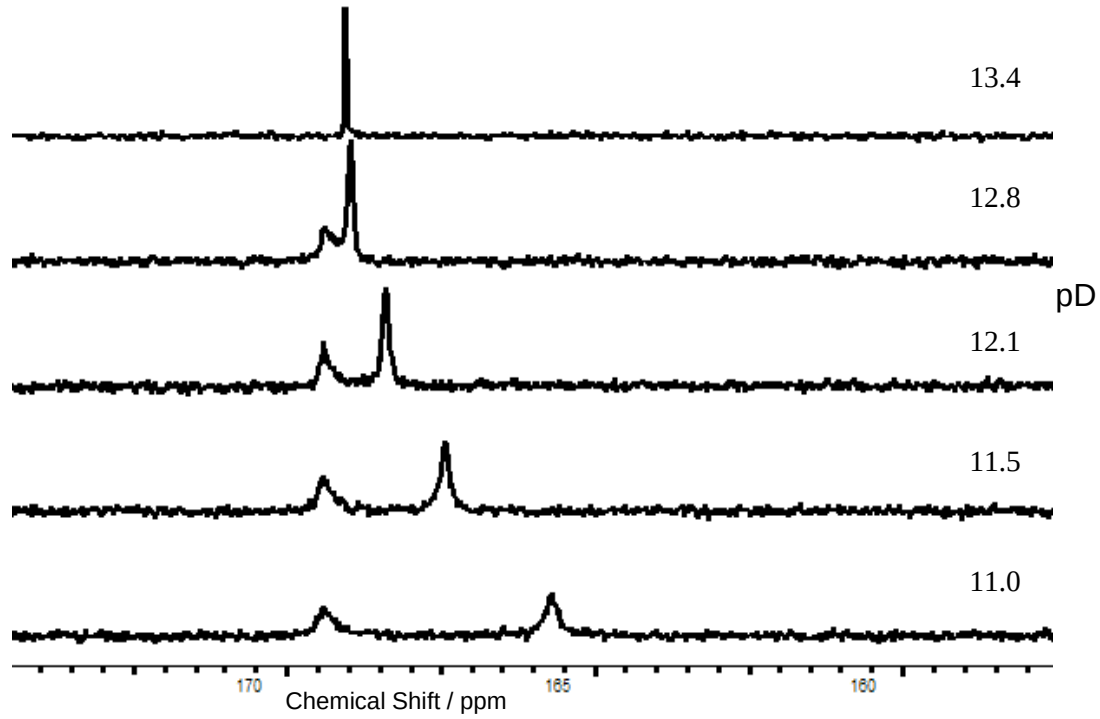

Figure M: ^{13}C-NMR spectra of the effect of pD on a 1:1:2 Lu^{III}:$EDTA^{4-}$:HCO_3^- solution; [33 mM]:[33 mM]:[66 mM].

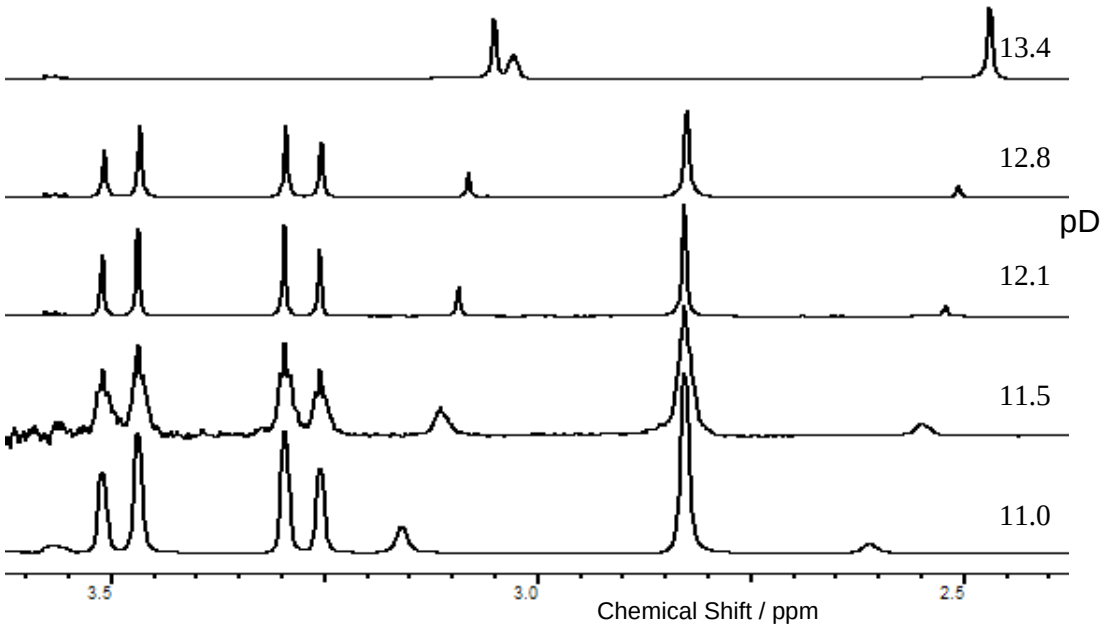

Figure N: ^{1}H-NMR spectra of the effect of pD on a 1:1:2 Lu^{III}:$EDTA^{4-}$:HCO_3^- solution; [33 mM]:[33 mM]:[66 mM].

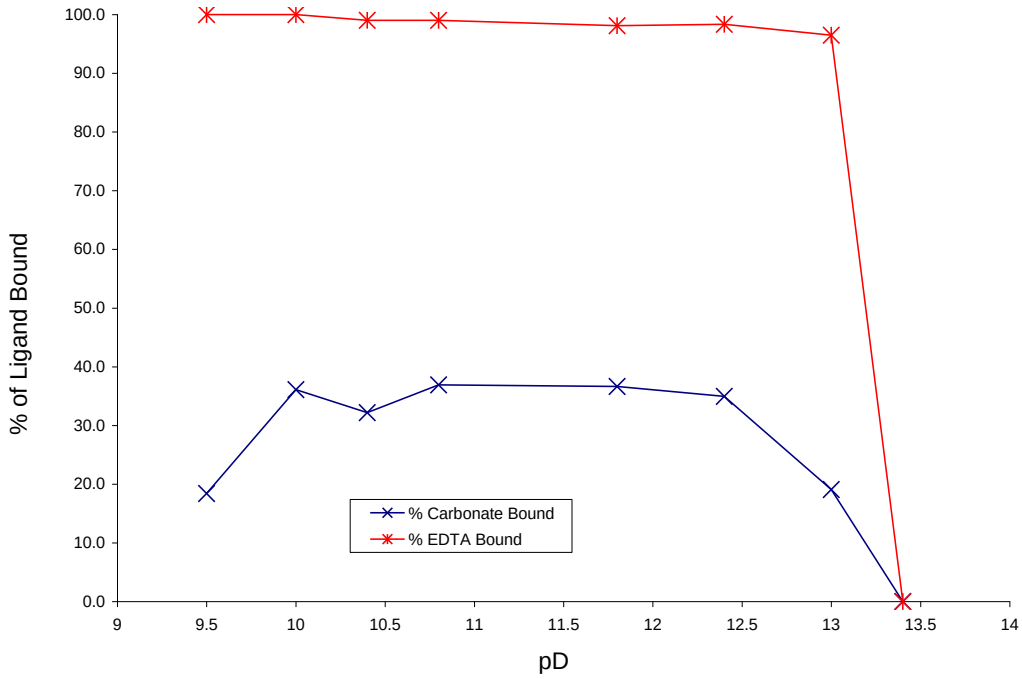

Figure O: Percentage of bound $EDTA^{4-}$ and carbonate to Lu(III) as pD is increased; 1:1:2 Lu^{III}:$EDTA^{4-}$:HCO_3^-; [33 mM]:[33 mM]:[66 mM].

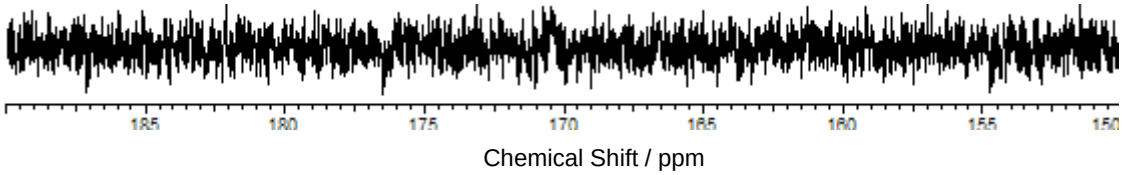

Figure P: ^{13}C-NMR of the 1:1:1 Nd^{III}:$EDTA^{4-}$:CO_3^{2-} system at pD 10; [Nd^{III}]=[$EDTA^{4-}$]=[CO_3^{2-}] = 5 mM.

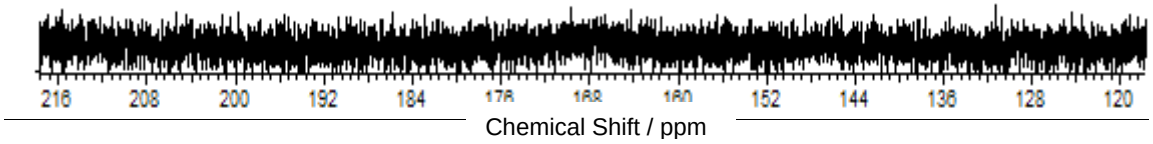

Figure Q: ^{13}C-NMR of the 1:1:1 Sm^{III}:$EDTA^{4-}$:CO_3^{2-} system at pD 10; [Sm^{III}]=[$EDTA^{4-}$]=[CO_3^{2-}] = 5 mM.

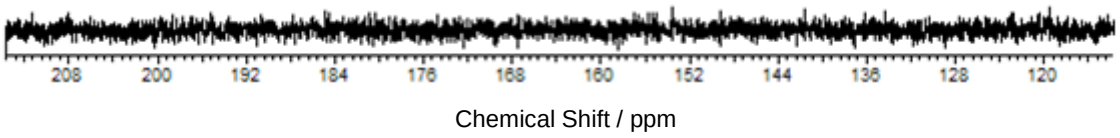

Figure R: ^{13}C-NMR of the 1:1:1 Eu^{III}:$EDTA^{4-}$:CO_3^{2-} system at pD 10; [Eu^{III}]=[$EDTA^{4-}$]=[CO_3^{2-}] = 5 mM.

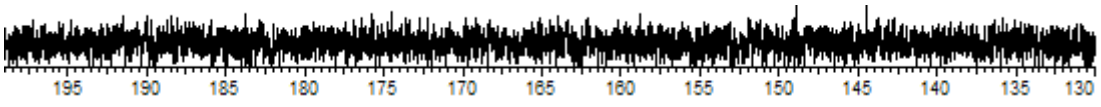

Figure S: ^{13}C-NMR of the 1:1:1 Tb^{III}:$EDTA^{4-}$:CO_3^{2-} system at pD 10; $[Tb^{III}]=[EDTA^{4-}]=[CO_3^{2-}]$ = 5 mM.

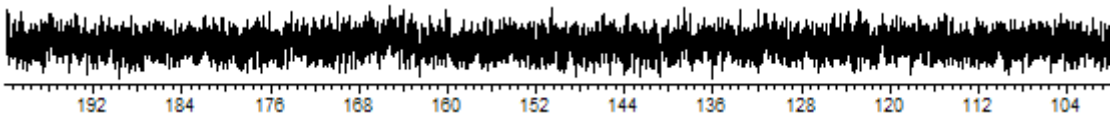

Figure T: ^{13}C-NMR of the 1:1:1 Ho^{III}:$EDTA^{4-}$:CO_3^{2-} system at pD 10; $[Ho^{III}]=[EDTA^{4-}]=[CO_3^{2-}]$ = 5 mM.

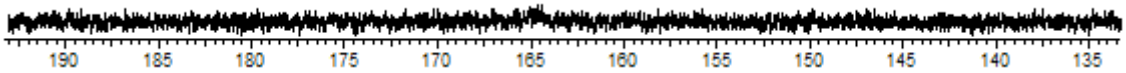

Figure U: ^{13}C-NMR of the 1:1:1 Er^{III}:$EDTA^{4-}$:CO_3^{2-} system at pD 10; $[Er^{III}]=[EDTA^{4-}]=[CO_3^{2-}]$ = 5 mM.

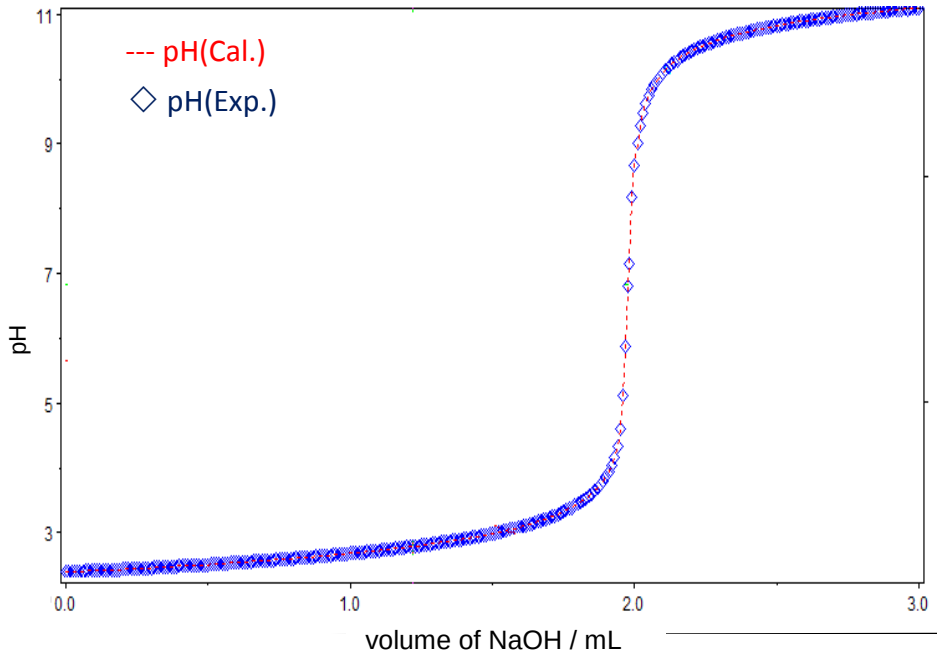

Figure V: Potentiometric titration of the 1:1 Ce^{III}:$EDTA^{4-}$ system at 25 °C; I = 0.5 M $NaNO_3$; V^0 = 20 mL; $[Ce^{III}]_i = [EDTA^{4-}]_i$ = 5 mM; Titrant = 0.1 M NaOH.

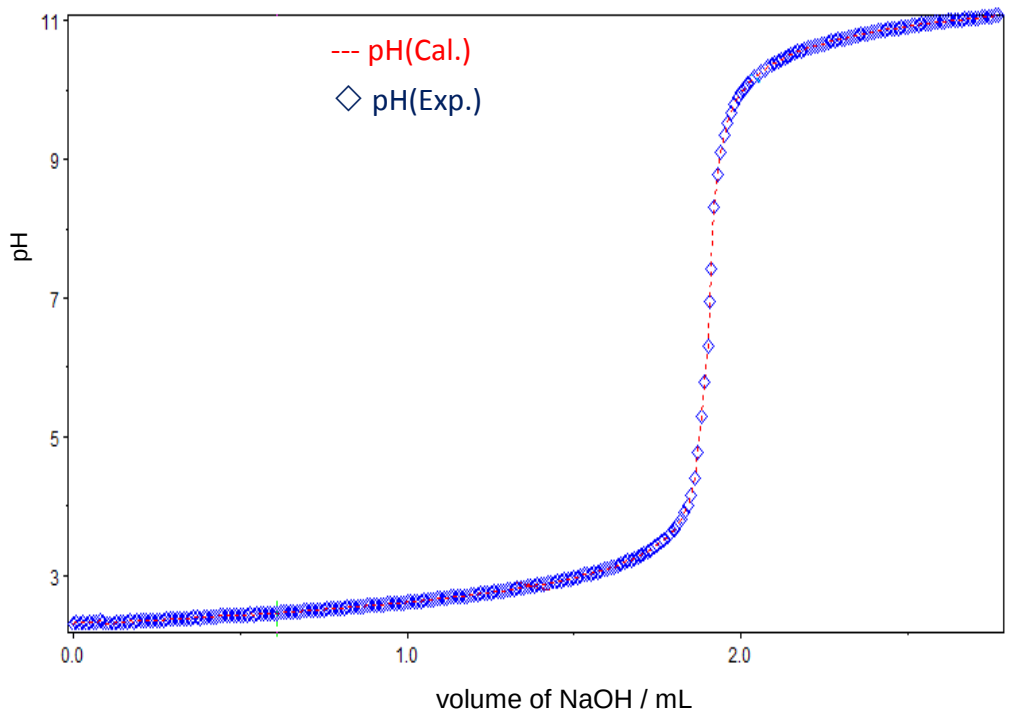

Figure W: Potentiometric titration of the 1:1 Pr^{III}:$EDTA^{4-}$ system at 25 °C; I = 0.5 M $NaNO_3$; V^0 = 20 mL; $[Pr^{III}]_i = [EDTA^{4-}]_i$ = 5 mM; Titrant = 0.1 M NaOH.

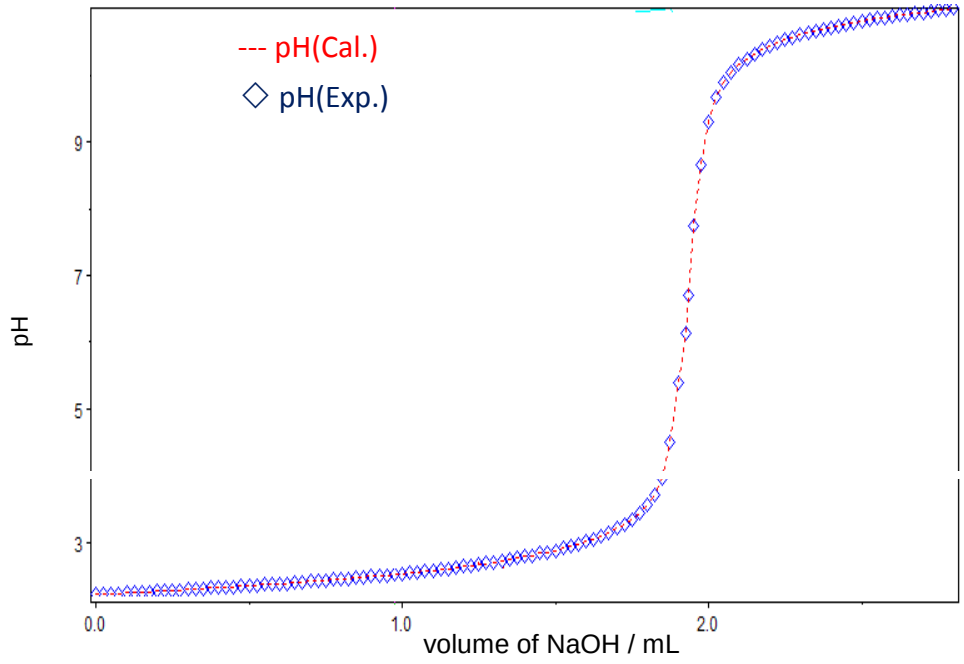

Figure X: Potentiometric titration of the 1:1 Nd^{III}:$EDTA^{4-}$ system at 25 °C; I = 0.5 M $NaNO_3$; V^0 = 20 mL; $[Nd^{III}]_i = [EDTA^{4-}]_i$ = 5 mM; Titrant = 0.1 M NaOH.

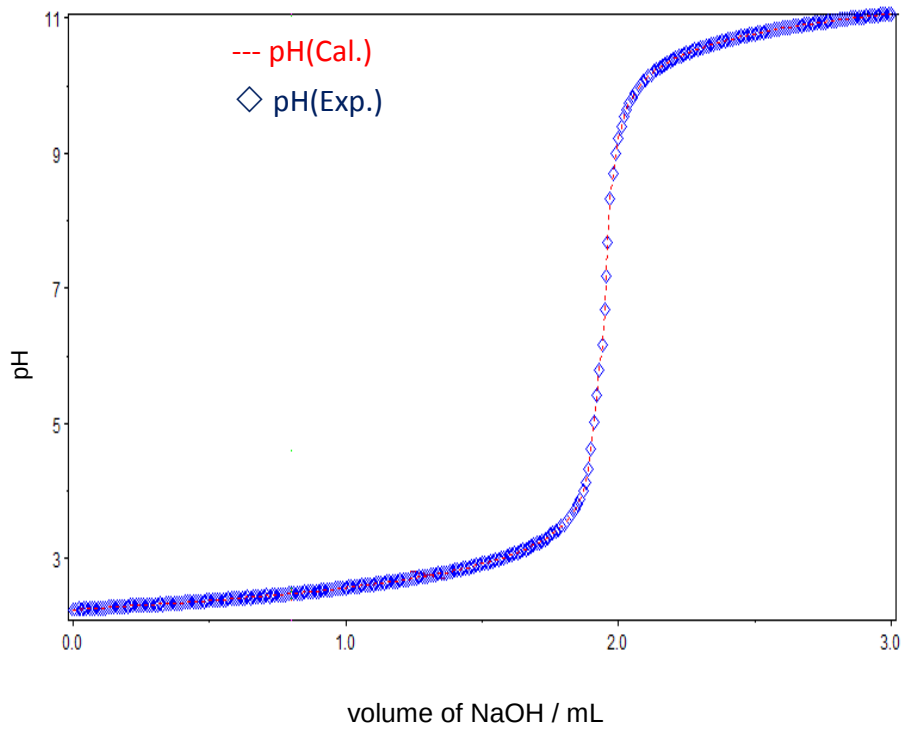

Figure Y: Potentiometric titration of the 1:1 Eu^{III}:$EDTA^{4-}$ system at 25 °C; I = 0.5 M $NaNO_3$; V^0 = 20 mL; $[Eu^{III}]_i = [EDTA^{4-}]_i$ = 5 mM; Titrant = 0.1 M NaOH.

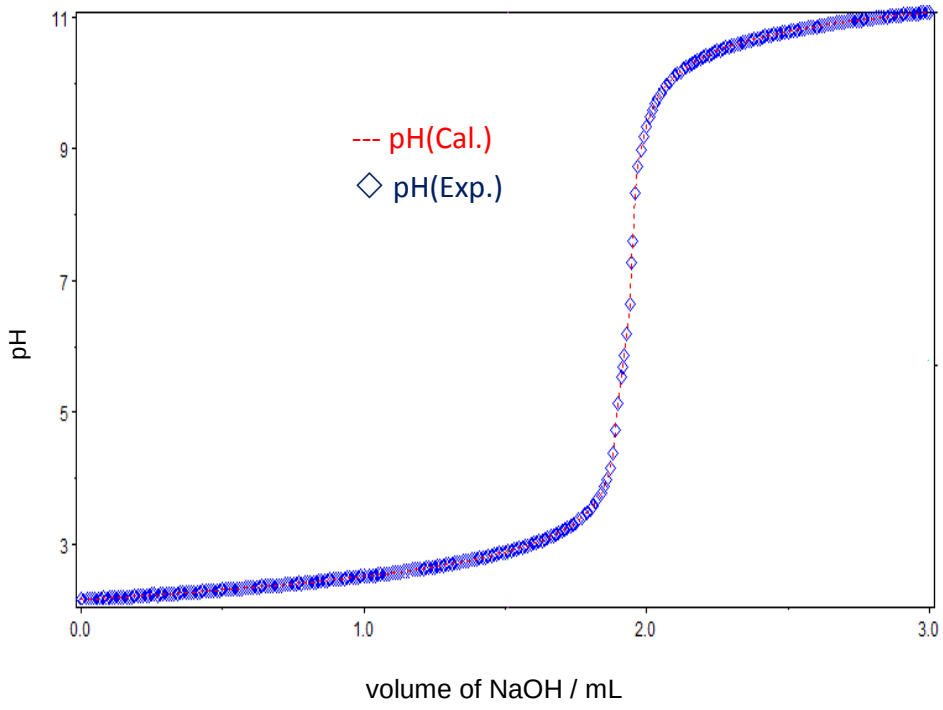

Figure Z: Potentiometric titration of the 1:1 Ho^{III}:$EDTA^{4-}$ system at 25 °C; I = 0.5 M $NaNO_3$; V^0 = 20 mL; $[Ho^{III}]_i = [EDTA^{4-}]_i$ = 5 mM; Titrant = 0.1 M NaOH.

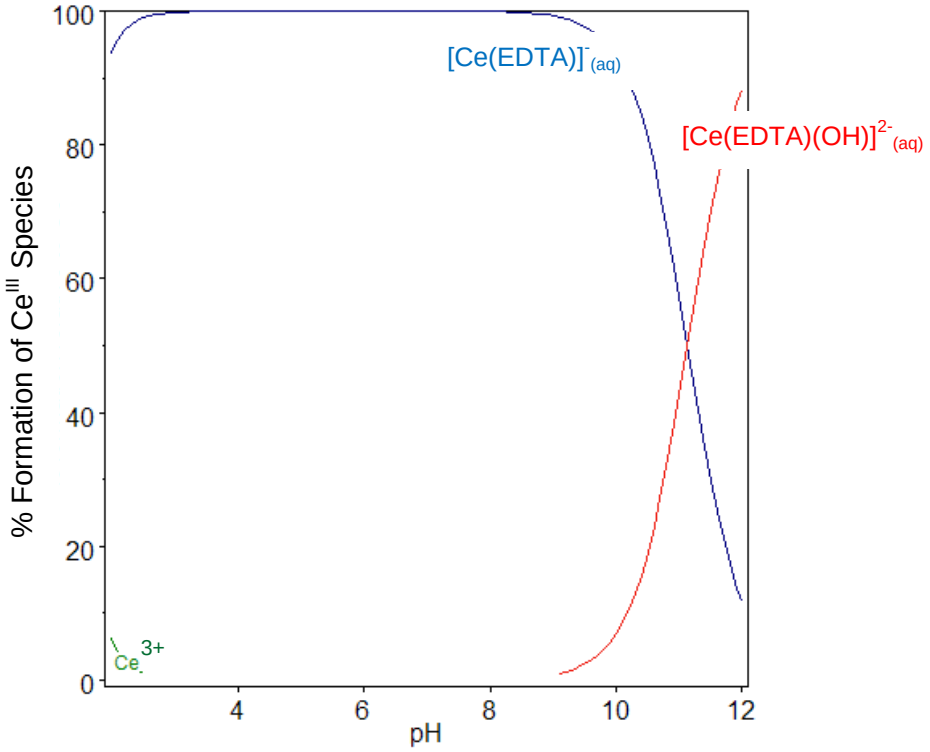

Figure AA: Speciation diagram of the 1:1 Ce^{III}:$EDTA^{4-}$ system.

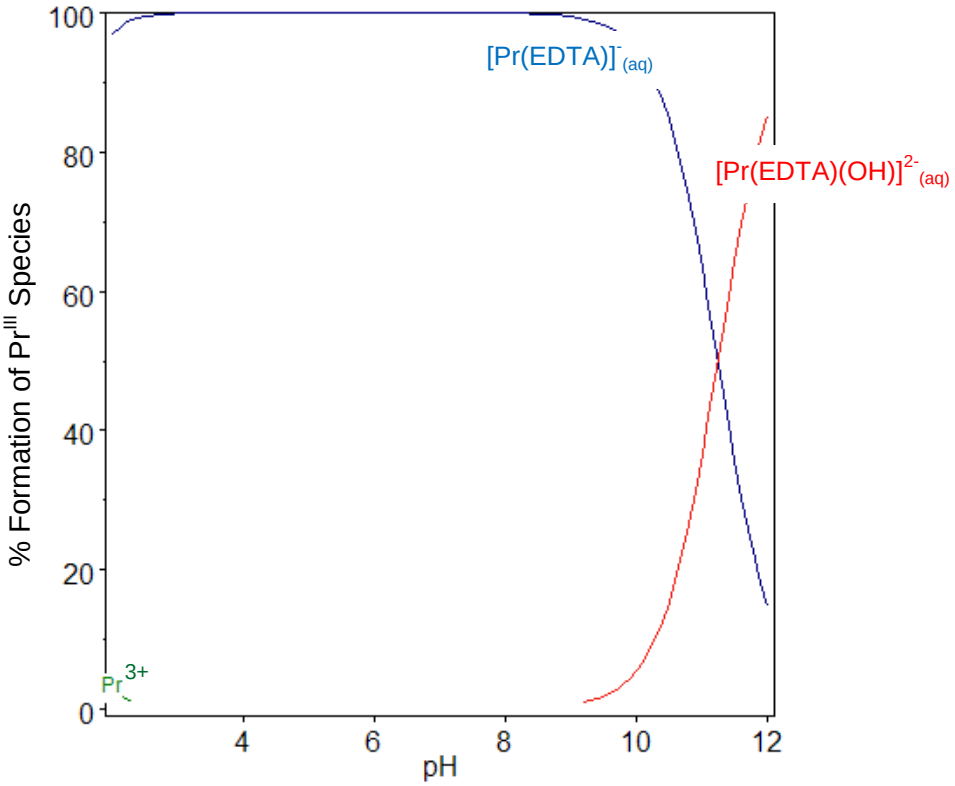

Figure AB: Speciation diagram of the 1:1 Pr^{III}:$EDTA^{4-}$ system.

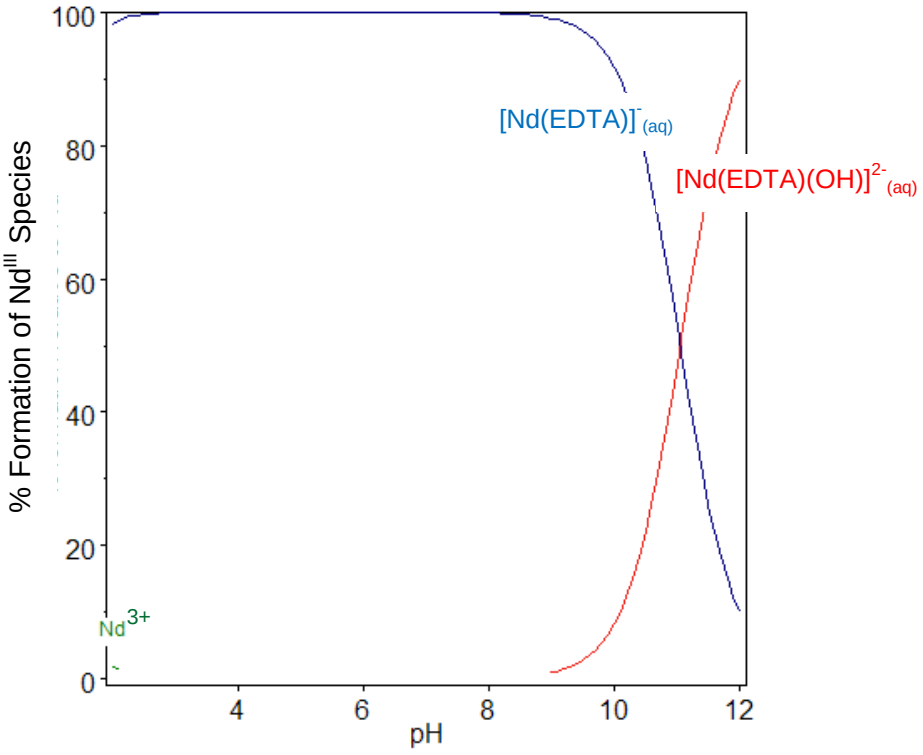

Figure AC: Speciation diagram of the 1:1 Nd^{III}:$EDTA^{4-}$ system.

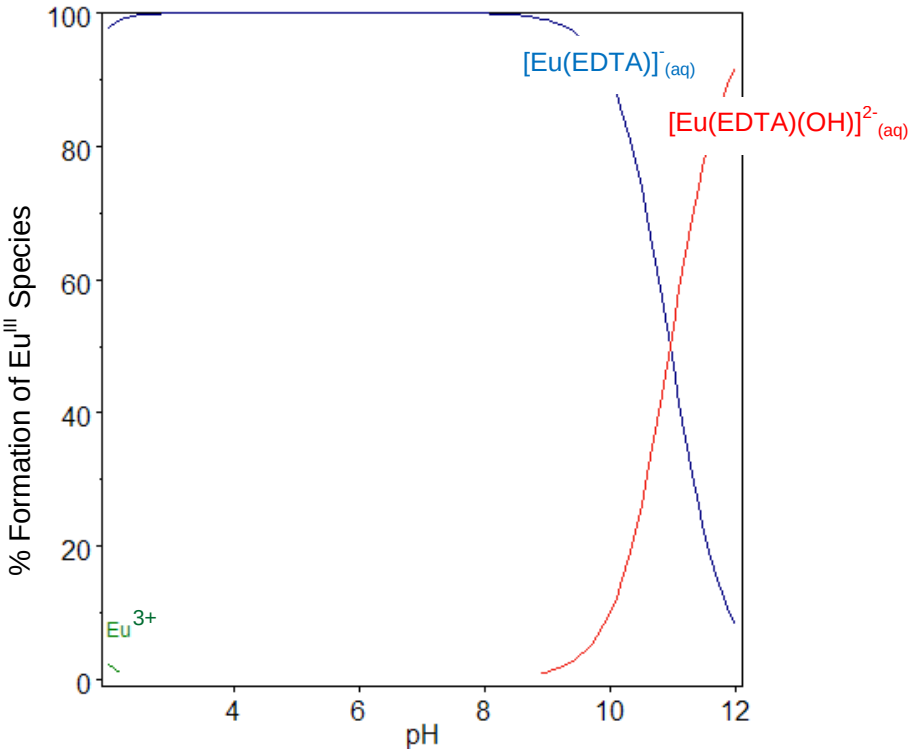

Figure AD: Speciation diagram of the 1:1 Eu^{III}:$EDTA^{4-}$ system.

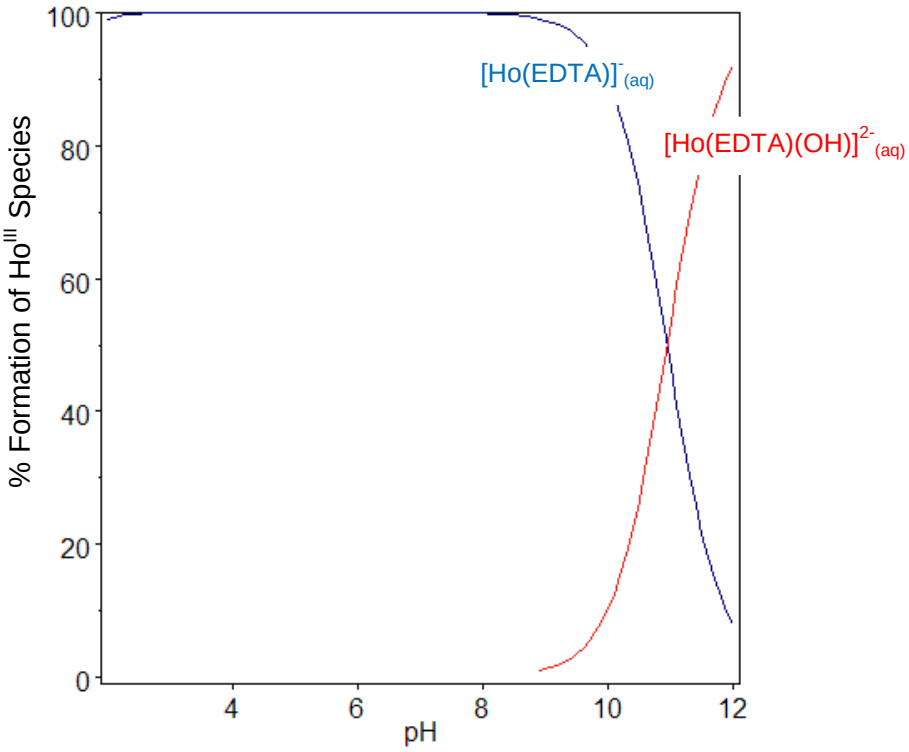

Figure AE: Speciation diagram of the 1:1 Ho^{III}:$EDTA^{4-}$ system.

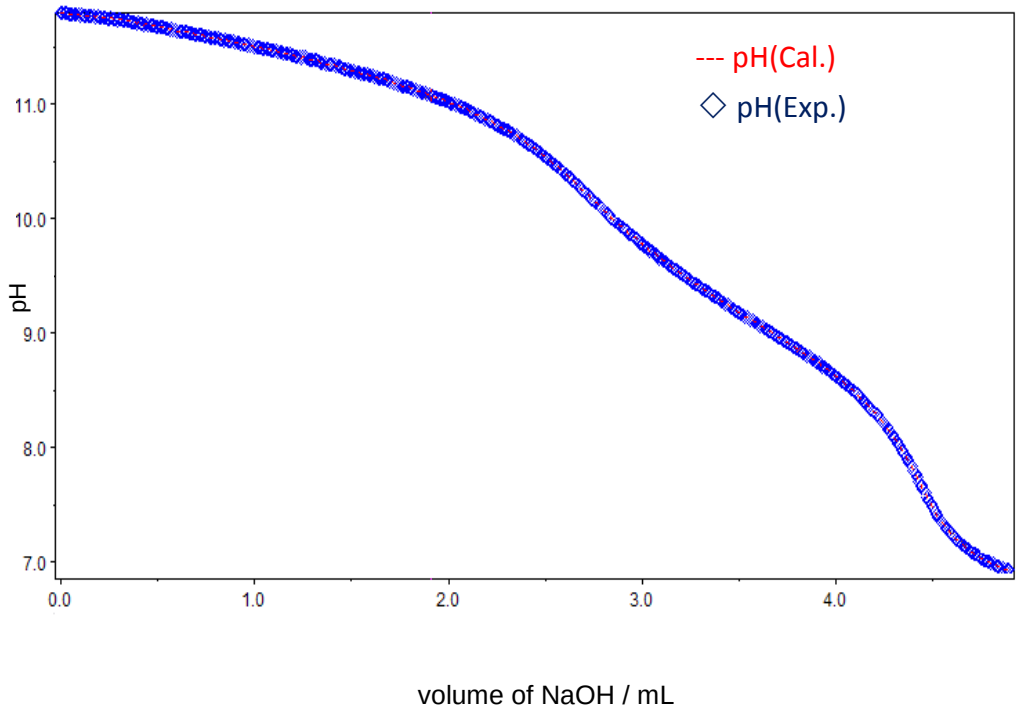

AF: Potentiometric titration of a 1:1:1 Ce^{III}:$EDTA^{4-}$:CO_3^{2-} system at 25 °C; I = 0.5 M $NaNO_3$; V^0 = 20 mL; $[Ce^{III}]_i = [EDTA^{4-}]_i = [CO_3^{2-}]_i$ = 5 mM; Titrant = 0.1 M HNO_3.

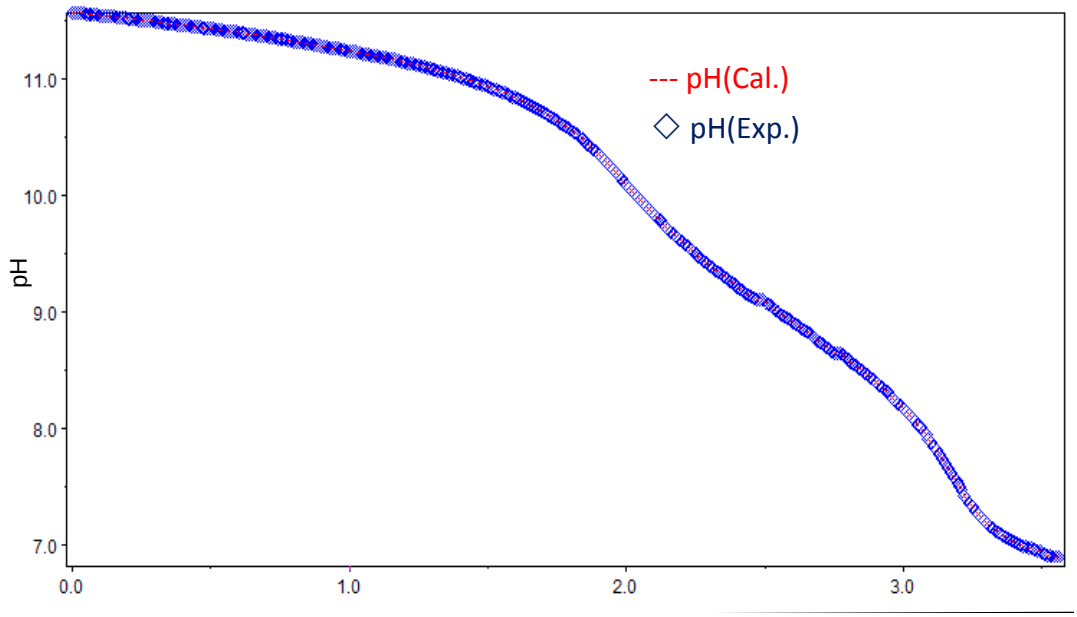

AG: Potentiometric titration of a 1:1:1 Pr^{III}:$EDTA^{4-}$:CO_3^{2-} system at 25 °C; I = 0.5 M $NaNO_3$; V^0 = 20 mL; $[Pr^{III}]_i = [EDTA^{4-}]_i = [CO_3^{2-}]_i$ = 5 mM; Titrant = 0.1 M HNO_3.

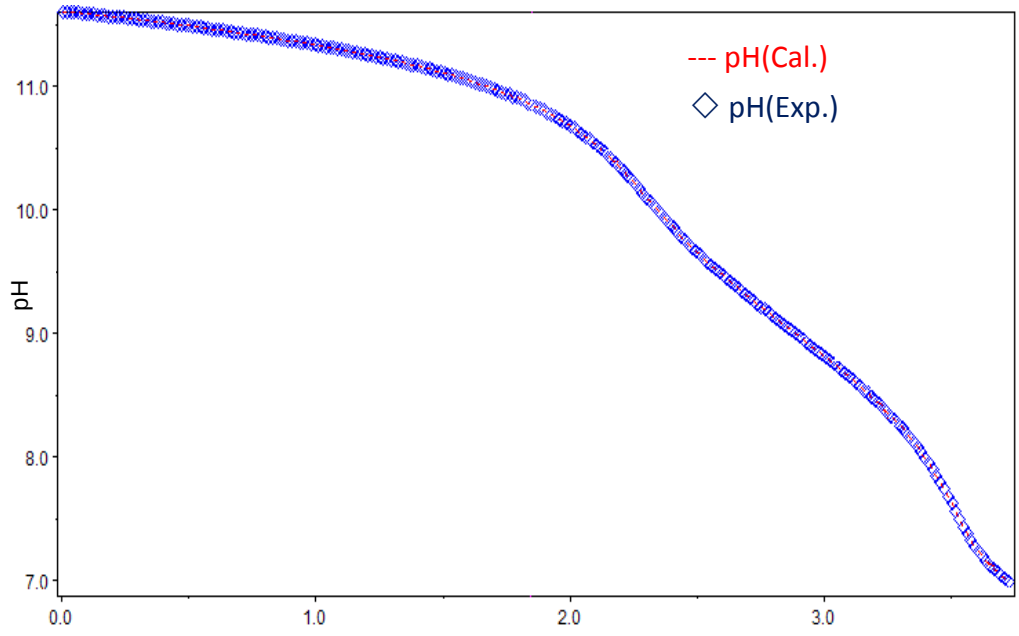

AH: Potentiometric titration of a 1:1:1 Nd^{III}:$EDTA^{4-}$:CO_3^{2-} system at 25 °C; I = 0.5 M $NaNO_3$; V^0 = 20 mL; $[Nd^{III}]_i = [EDTA^{4-}]_i = [CO_3^{2-}]_i$ = 5 mM; Titrant = 0.1 M HNO_3.

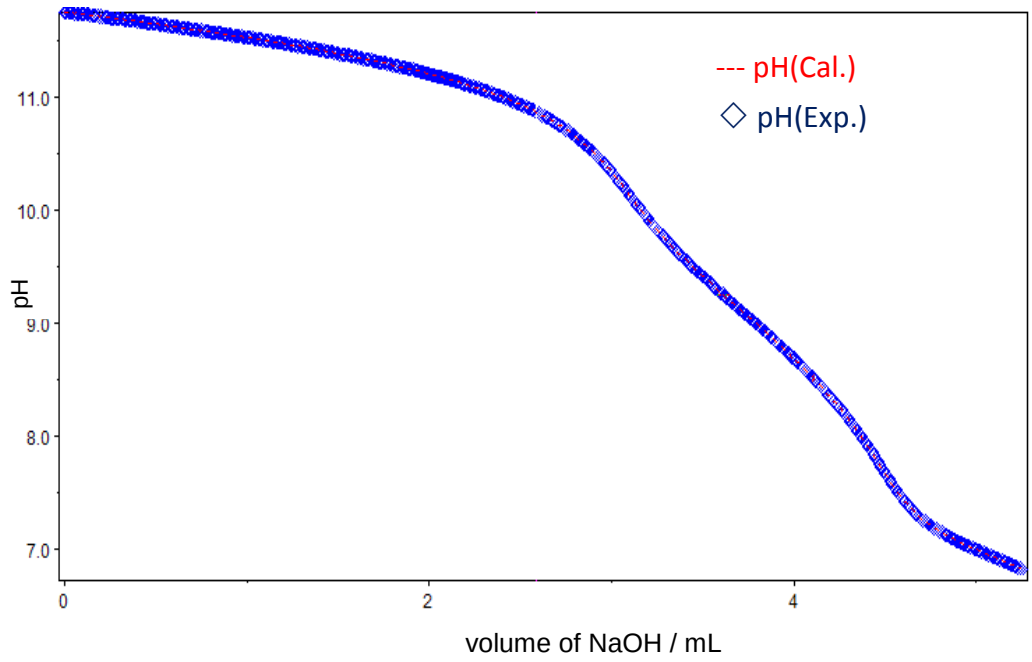

AI: Potentiometric titration of a 1:1:1 Eu^{III}:$EDTA^{4-}$:CO_3^{2-} system at 25 °C; I = 0.5 M $NaNO_3$; V^0 = 20 mL; $[Eu^{III}]_i = [EDTA^{4-}]_i = [CO_3^{2-}]_i$ = 5 mM; Titrant = 0.1 M HNO_3.

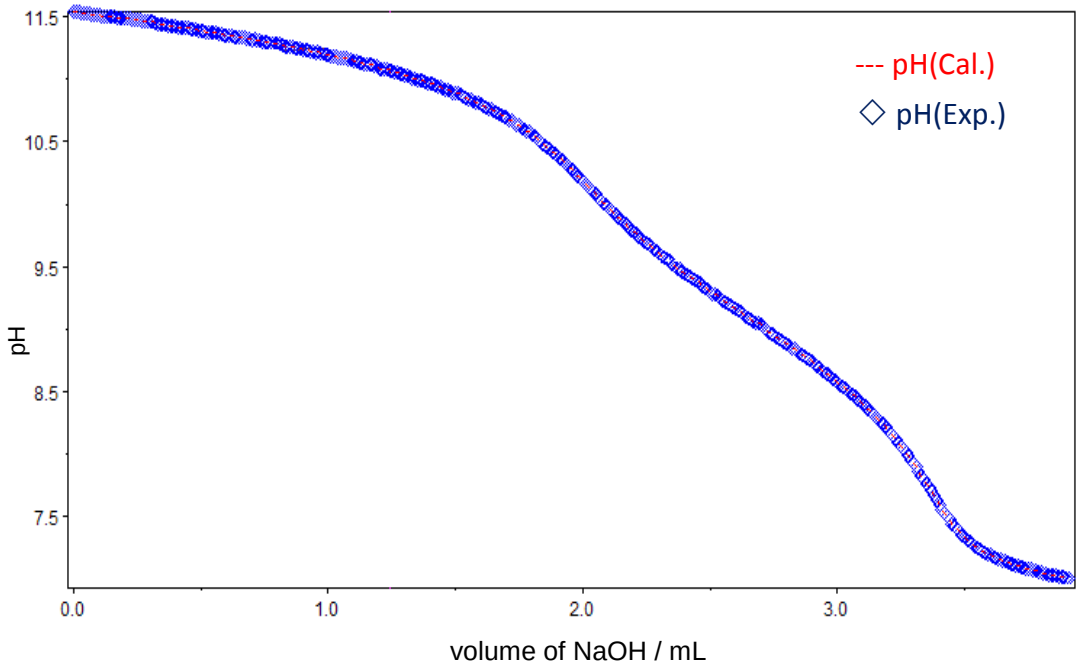

AJ: Potentiometric titration of a 1:1:1 Ho^{III}:$EDTA^{4-}$:CO_3^{2-} system at 25 °C; I = 0.5 M $NaNO_3$; V^0 = 20 mL; $[Ho^{III}]_i = [EDTA^{4-}]_i = [CO_3^{2-}]_i$ = 5 mM; Titrant = 0.1 M HNO_3.

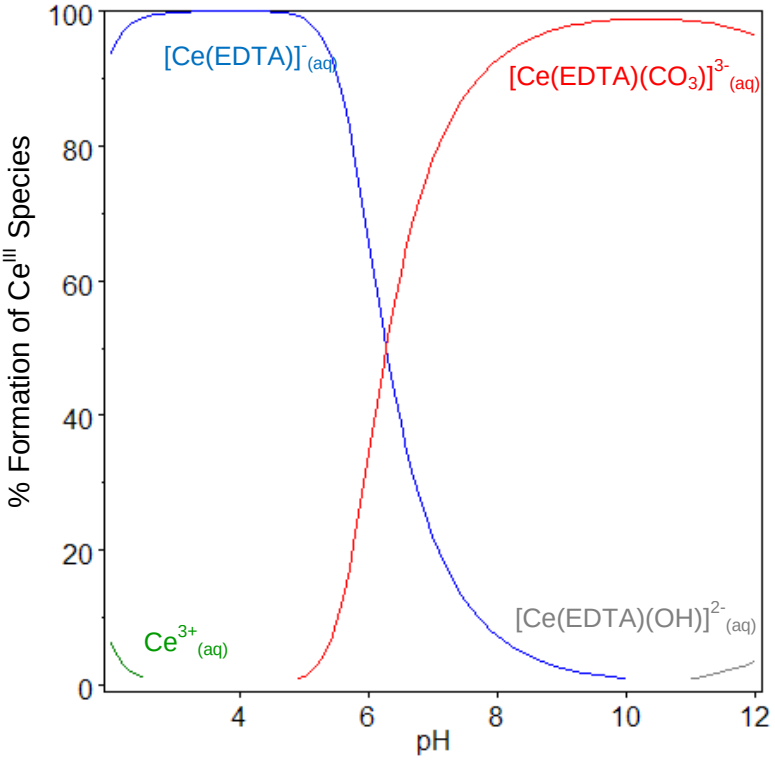

Figure AK: Speciation diagram of the 1:1:1 Ce^{III}:$EDTA^{4-}$:CO_3^{2-} system.

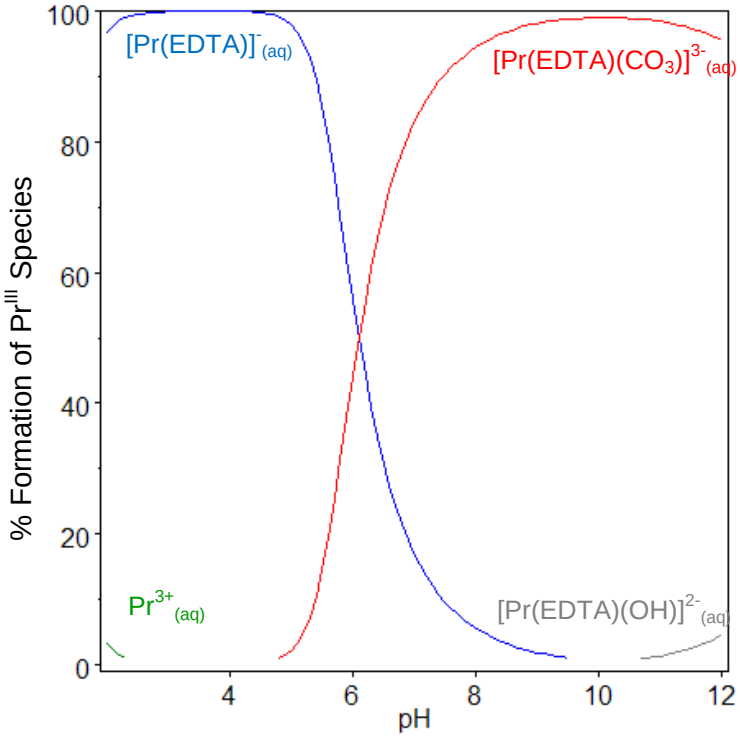

Figure AL: Speciation diagram of the 1:1:1 Pr^{III}:$EDTA^{4-}$:CO_3^{2-} system.

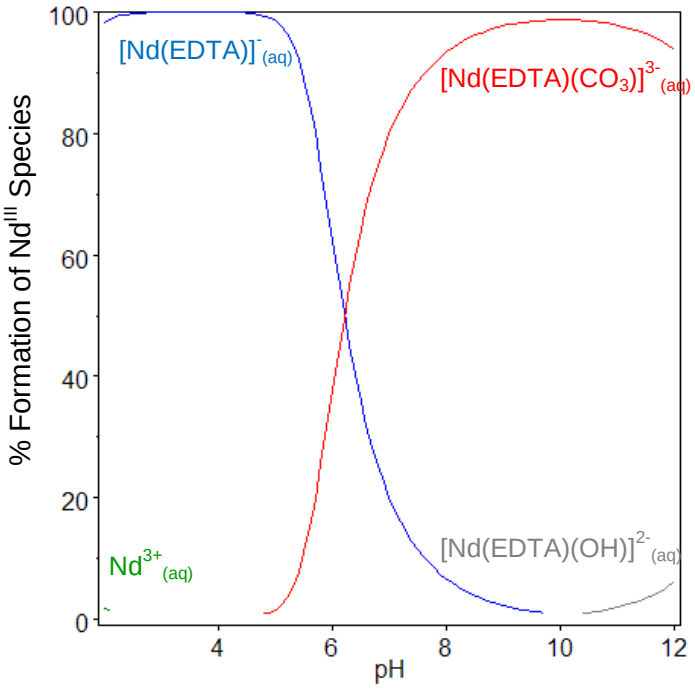

Figure AM: Speciation diagram of the 1:1:1 Nd^{III}:$EDTA^{4-}$:CO_3^{2-} system.

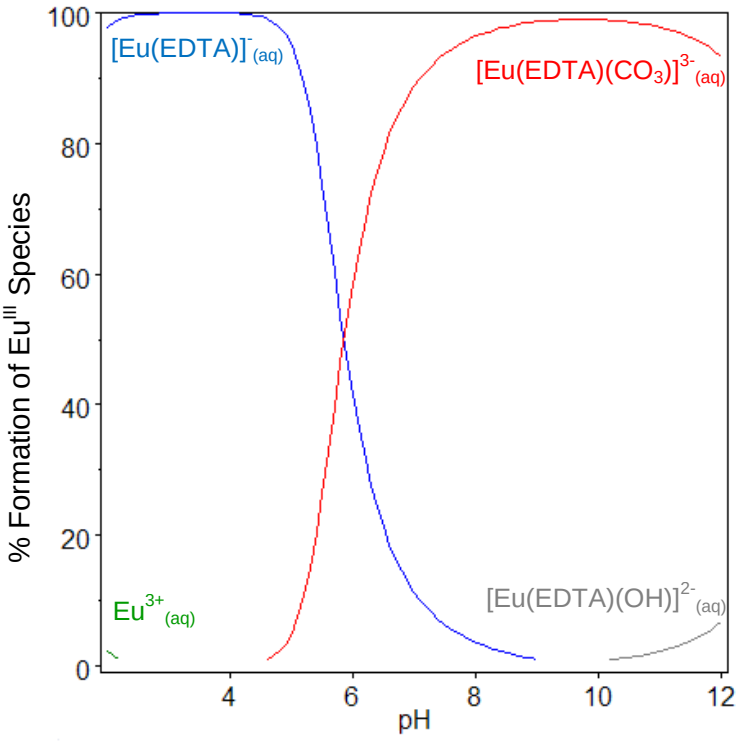

Figure AN: Speciation diagram of the 1:1:1 Eu^{III}:$EDTA^{4-}$:CO_3^{2-} system.

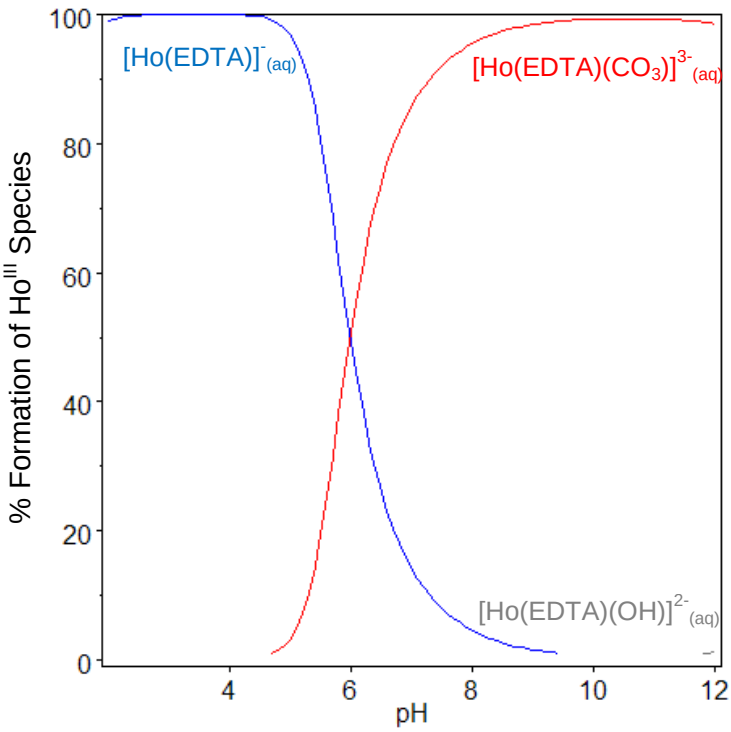

Figure AO: Speciation diagram of the 1:1:1 Ho^{III}:$EDTA^{4-}$:CO_3^{2-} system.

Appendix 2

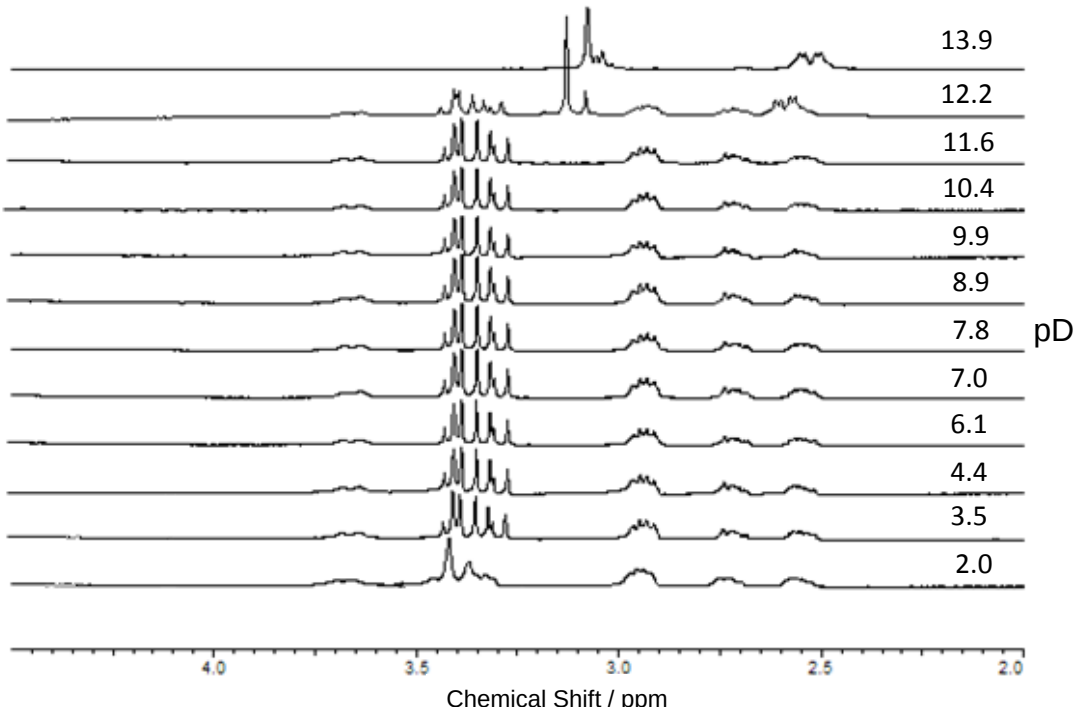

Figure A: ^{1}H-NMR spectra of a 1:1 Lu^{III}:$DTPA^{5-}$ system as a function of pD; $[Lu^{III}]_i=[DTPA^{5-}]_i=50$ mM.

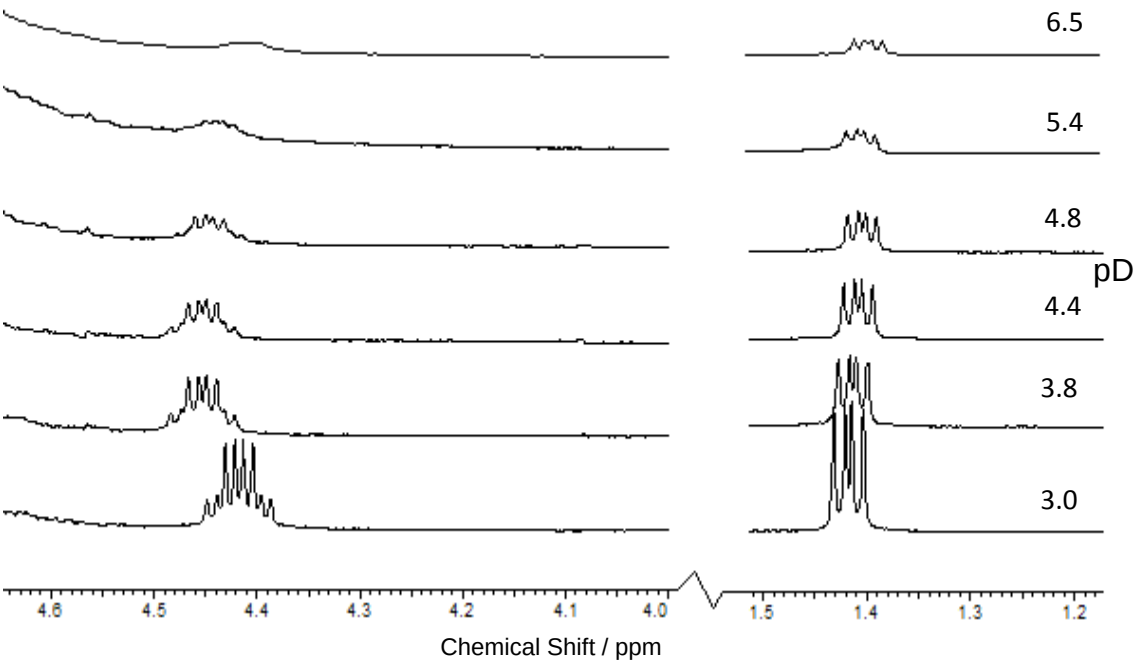

Figure B: ^{1}H-NMR spectra of a 1:1 Lu^{III}:lactate system as a function of pD; $[Lu^{III}]_i=[lactate]_i=50$ mM.

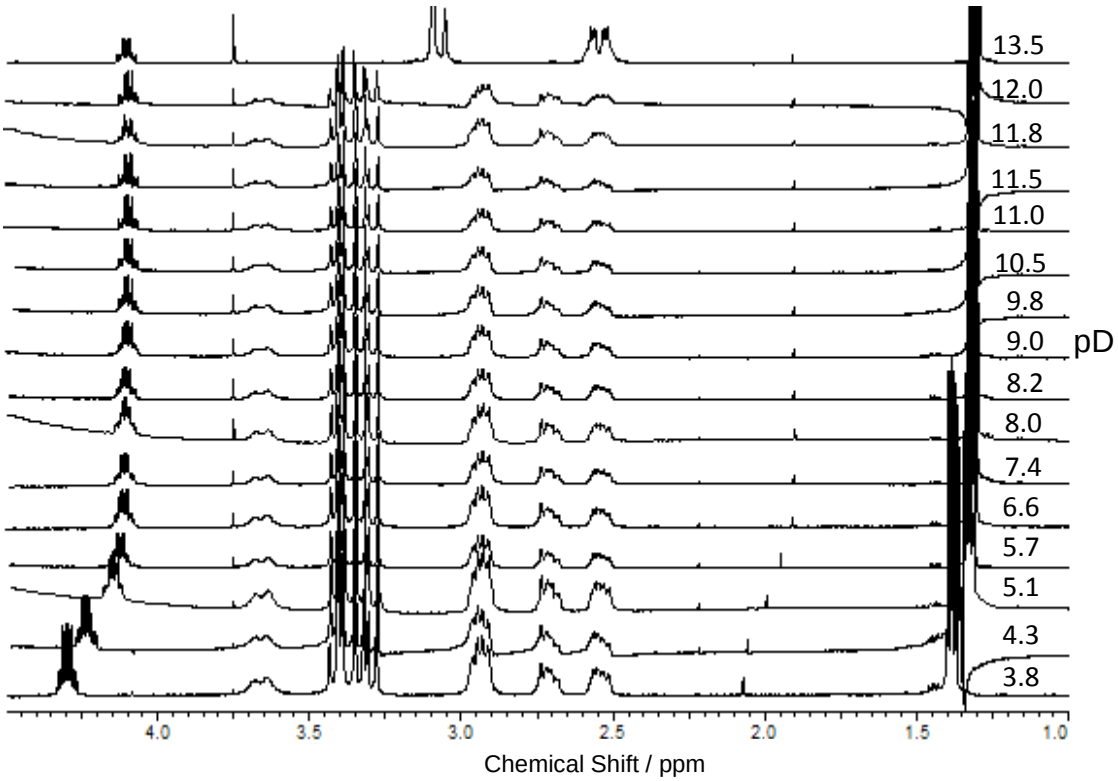

Figure C: ^{1}H-NMR spectra of a 1:1:1 Lu^{III}:$DTPA^{5-}$:lactate system as a function of pD; $[Lu^{III}]_i = [DTPA^{5-}]_i = [lactate]_i = 33$ mM.

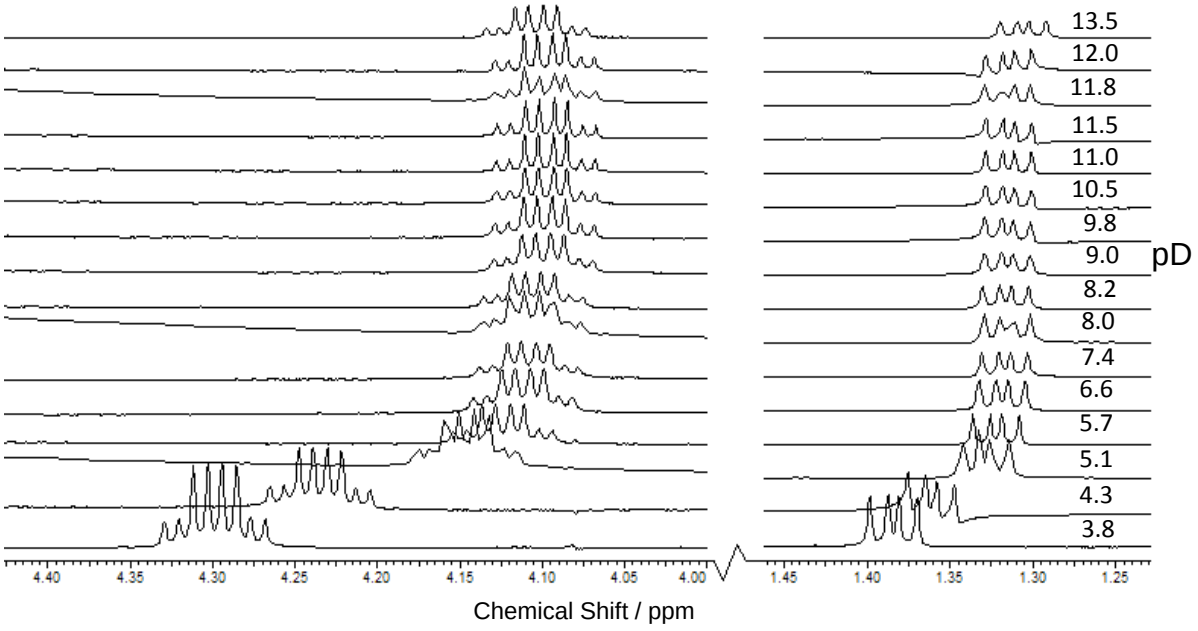

Figure D: 'Zoom in' of lactate signals for the ^{1}H-NMR spectra of a 1:1:1 Lu^{III}:$DTPA^{5-}$:lactate system as a function of pD; $[Lu^{III}]_i = [DTPA^{5-}]_i = [lactate]_i = 33$ mM.

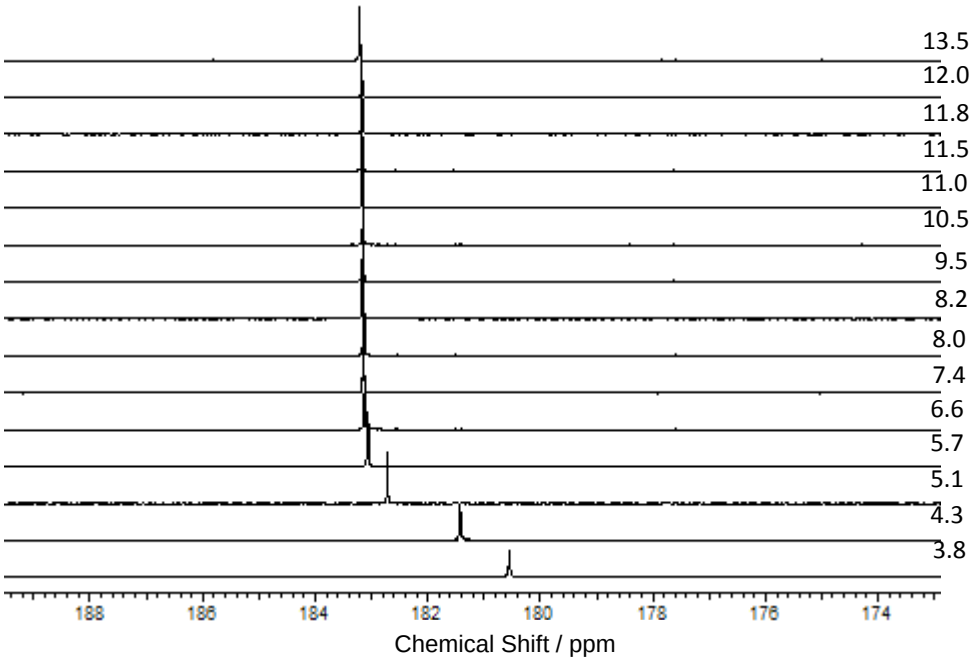

Figure E: ^{13}C-NMR spectra of a 1:1:1 Lu^{III}:$DTPA^{5-}$:lactate system as a function of pD; $[Lu^{III}]_i = [DTPA^{5-}]_i = [lactate]_i = 33$ mM.

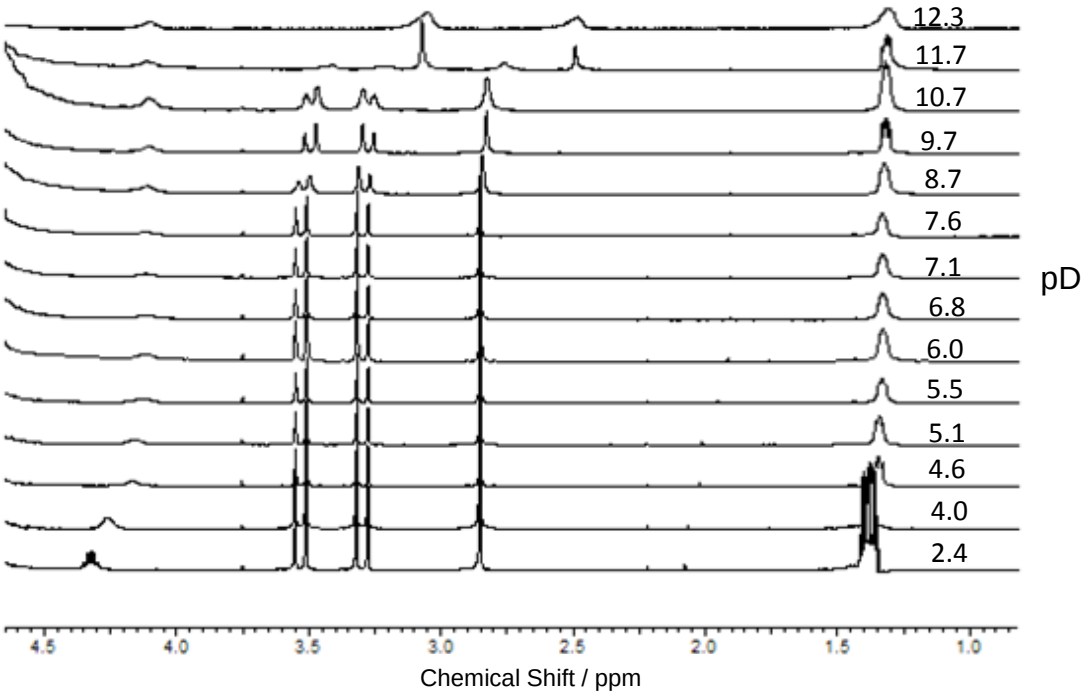

Figure F: ^{1}H-NMR spectra for the effect of pD on a 1:1:1 Lu^{III}:$EDTA^{4-}$:lactate system; $[Lu^{III}]_i = [EDTA^{4-}]_i = [lactate]_i = 33$ mM.

Appendix 3

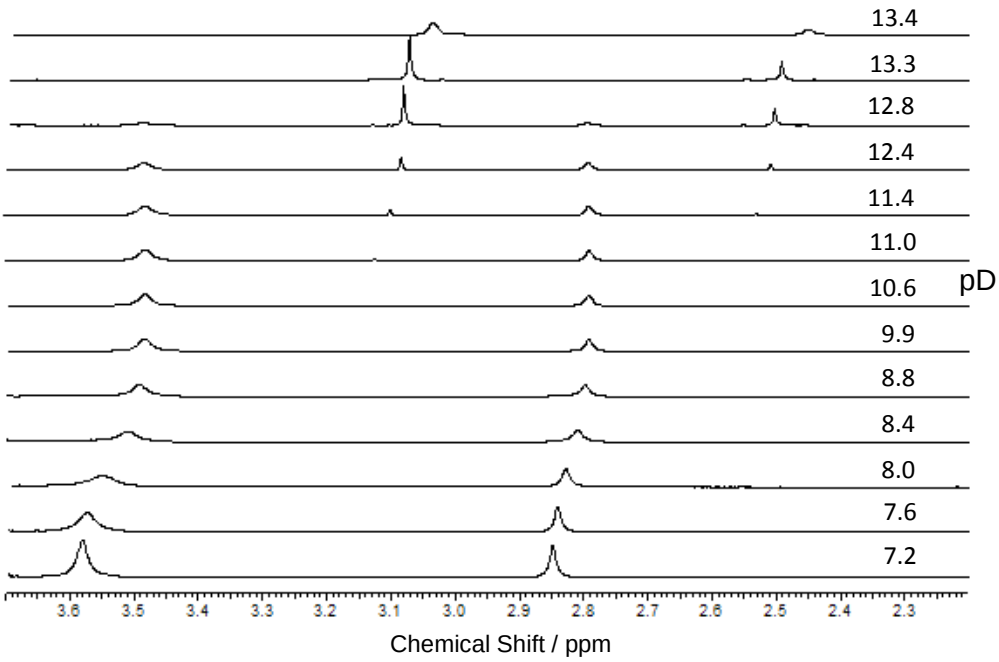

Figure A: ^{1}H-NMR spectra for the effect of pD on the 1:1:1 Th^{IV}:$EDTA^{4-}$:CO_3^{2-} system; $[Th^{IV}]_i = [EDTA^{4-}]_i = [CO_3^{2-}]_i$ = 33 mM.

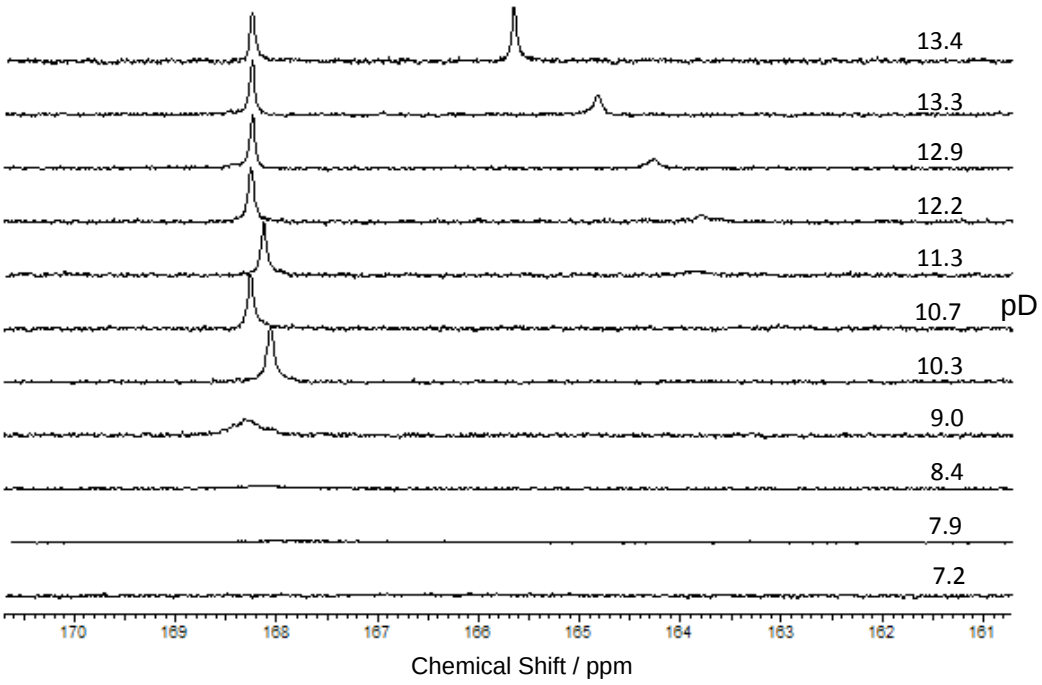

Figure B: ^{13}C-NMR spectra for the effect of pD on the 1:1:2 Th^{IV}:$EDTA^{4-}$:CO_3^{2-} system; $[Th^{IV}]_i = [EDTA^{4-}]_i$ = 33 mM; $[CO_3^{2-}]_i$ = 66 mM.

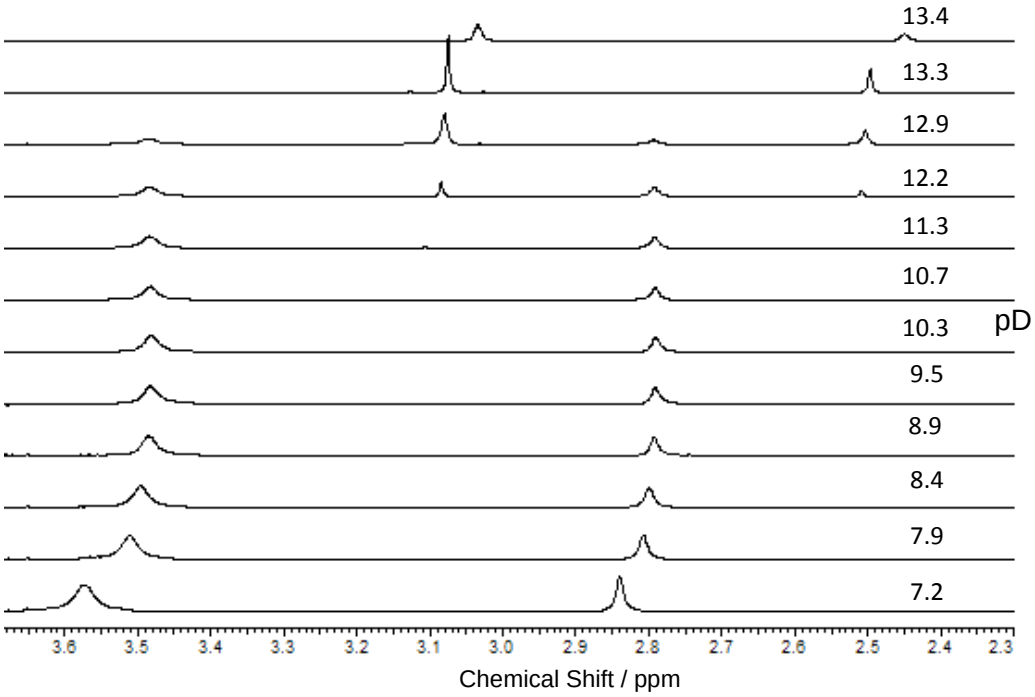

Figure C: ^{1}H-NMR spectra for the effect of pD on the 1:1:2 Th^{IV}:$EDTA^{4-}$:CO_3^{2-} system; $[Th^{IV}]_i = [EDTA^{4-}]_i = 33$ mM; $[CO_3^{2-}]_i = 66$ mM.

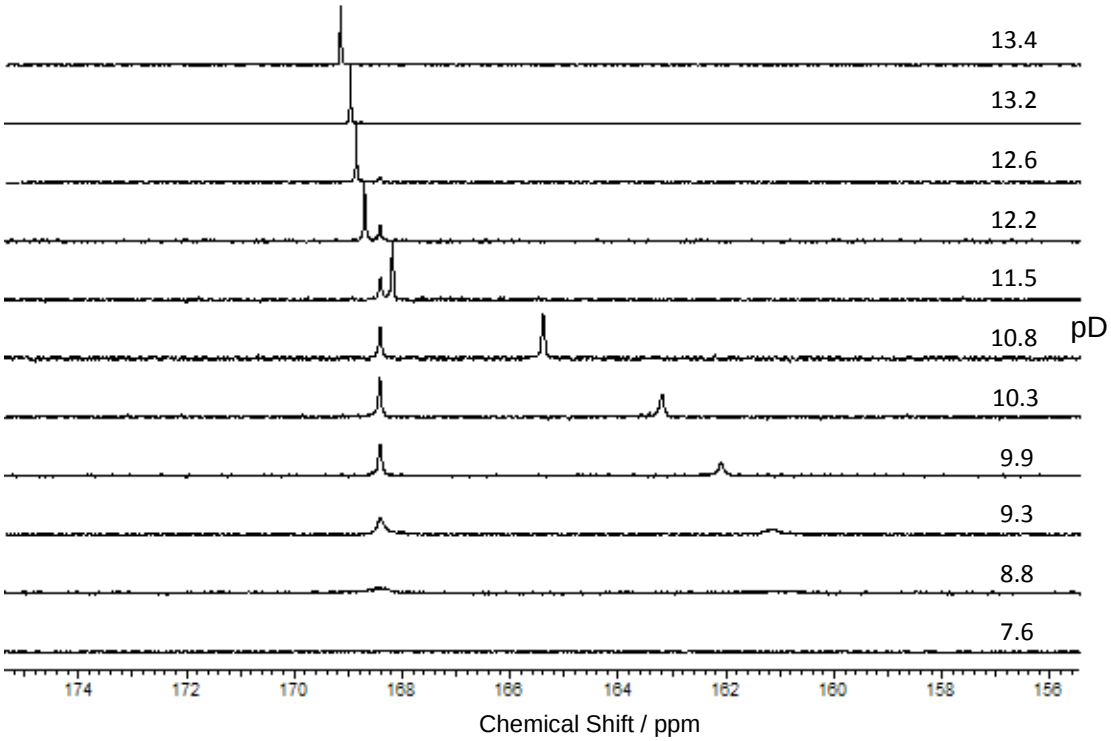

Figure D: ^{13}C-NMR spectra for the effect of pD on a 1:1:3 Th^{IV}:$EDTA^{4-}$:CO_3^{2-} system; $[Th^{IV}]_i = [EDTA^{4-}]_i = 25$ mM; $[CO_3^{2-}]_i = 75$ mM.

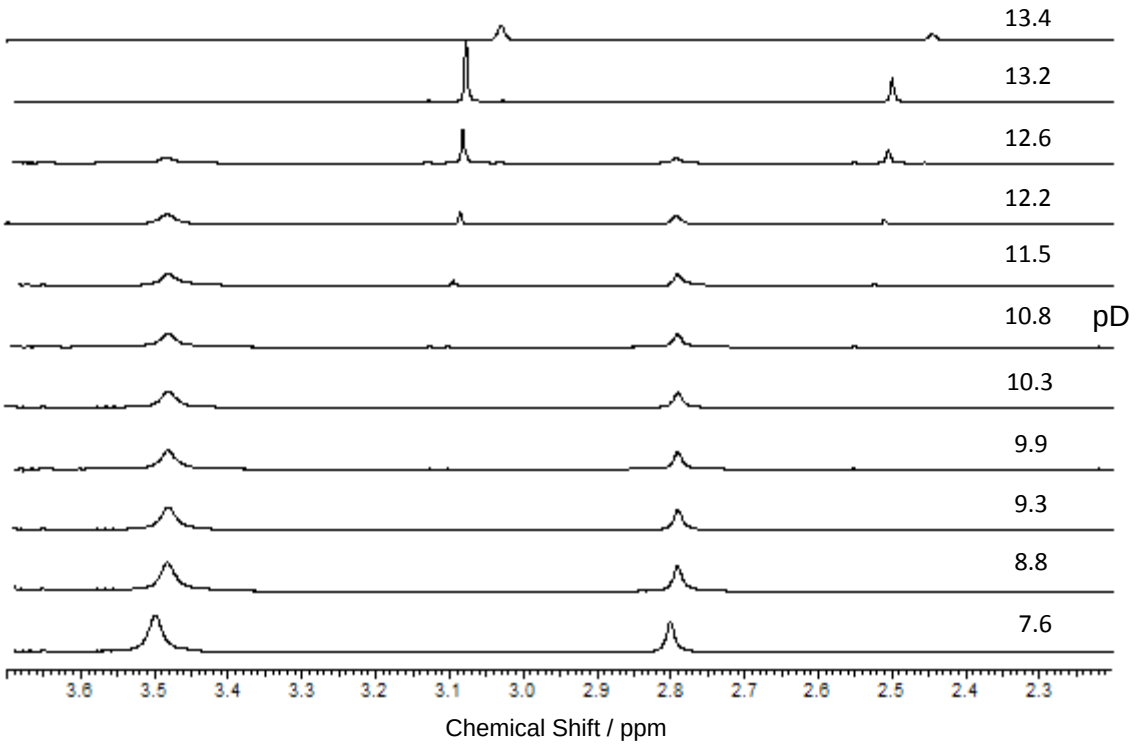

Figure E: ^{1}H-NMR spectra for the effect of pD on a 1:1:3 Th^{IV}:$EDTA^{4-}$:CO_3^{2-} system; $[Th^{IV}]_i = [EDTA^{4-}]_i =$ 25 mM; $[CO_3^{2-}]_i$ = 75 mM.

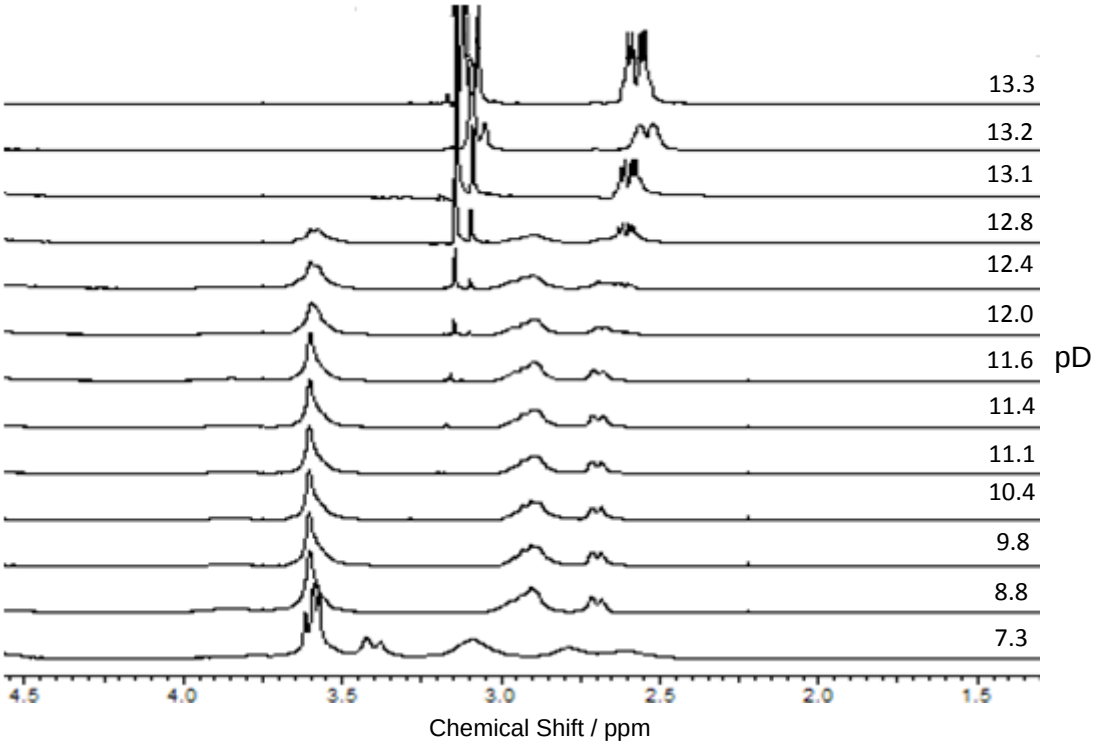

Figure F: ^{1}H-NMR spectra for the effect of pD on the 1:1:1 Th^{IV}:$DTPA^{5-}$:CO_3^{2-} system; $[Th^{IV}]_i$= $[DTPA^{5-}]_i$=$[CO_3^{2-}]_i$ =10 mM.

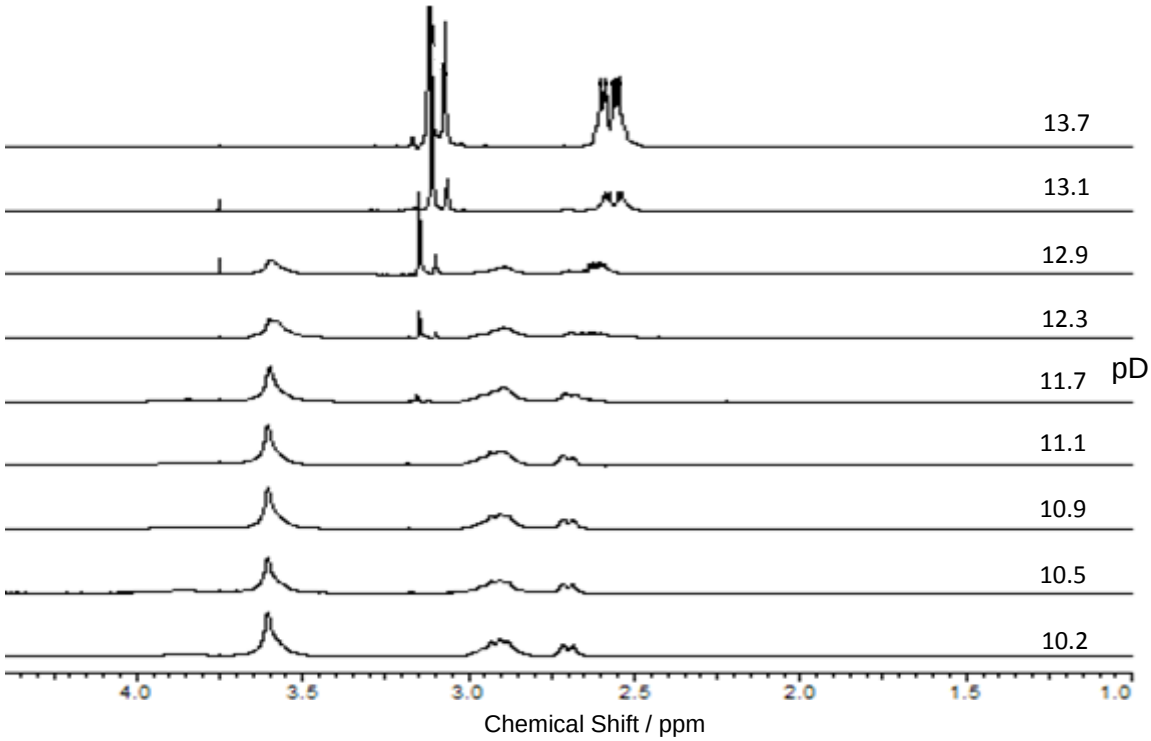

Figure G: ^{1}H-NMR spectra for the effect of pD on the 1:1:2 Th^{IV}:$DTPA^{5-}$:CO_3^{2-} system; $[Th^{IV}]_i$= $[DTPA^{5-}]_i$ =10 mM; $[CO_3^{2-}]_i$ = 20 mM.

Appendix 4

pH	τ / ms
1	30.5
3	60.1
8	57.7
10	61.4
12	60.1
12.3	63.1
12.5	80.9
13	100.7

A

pH	τ / ms
7	58
7.5	60.2
8.5	57.8
9.5	63
10	64.2
10.3	68
10.6	60.8
11	58.5
11.5	61.7
11.7	66.3
12.5	80

B

pH	τ / ms
1	30.5
1.5	31.1
3.5	64.2
5.2	59.5
6	56.1
7	57.7
8.5	57.4
10	64.9
10.5	63.8
12	59.9
12.2	65.9

C

Calculated luminescent lifetimes of: **A)** 1:1 Am^{III}:$DO3A^{3-}$ system;

B) 1:1:1 Am^{III}:$DO3A^{3-}$:CO_3^{2-} system and

C) 1:1:1 Am^{III}:$DO3A^{3-}$:lactate system as a function of pH;

$[Am^{III}]_i$=$[DO3A^{3-}]_i$ =$[carbonate/lactate]_i$ = 4 x 10^{-4} M.